

SAMPLE PREPARATION FOR, AND CURRENT STATUS OF, THE ARGONNE PREMIUM COAL SAMPLE PROGRAM*

Karl S. Vorres
Chemistry Division, Building 211
Argonne National Laboratory
Argonne, IL 60439

ABSTRACT

The Argonne Premium Coal Sample Program includes eight coals (Upper Freeport, Wyodak-Anderson, Illinois #6, Pittsburgh, Pocahontas #3, Utah Blind Canyon, Lewiston-Stockton and Beulah-Zap seams) chosen to provide a range of chemical composition, including sulfur content, maceral content and geographic distribution. One of the purposes is to provide a set of pristine samples for comparison and correlation. They have been collected in ton-sized batches and processed to provide a minimal exposure to oxygen, thoroughly mixed, and packaged in borosilicate glass ampoules containing either 5 grams of -100 mesh or 10 grams of -20 mesh material. This material has been analyzed by a number of laboratories, including a round robin with Commercial Testing and Engineering Co. Further data are being added to an analytical data base as they become available. Over 190 shipments have been made to over 110 different users. Research is currently being carried out in almost every area of coal science with these samples.

* This work was supported by the Office of Basic Energy Sciences, Division of Chemical Sciences, U. S. Department of Energy, under contract number W-31-109-ENG-38.

INTRODUCTION

Goals:

The Premium Coal Sample Program was initiated at the Argonne National Laboratory about five years ago to provide the basic coal research community with a small number of carefully selected, collected, processed packaged and analyzed samples. The techniques of mixing, sealing and storage are intended to provide a large number of uniform samples that will be stable over a long time, and will permit reproducible experiments to be carried out at different times and laboratories.

Selection of Samples:

The coals included in the program were selected to give a range of composition in terms of the carbon, sulfur, hydrogen and oxygen contents. A cluster analysis involving data from over 200 channel samples in the existing Pennsylvania State University database was used to provide eight ranges of composition, from which the chemical composition characteristics of the eight samples were chosen. In addition they were selected to give a range of rank, geographical distribution, and maceral content.

In the order collected, these eight coals are:

#	Seam	Origin	Rank
1	Upper Freeport	PA	MVB
2	Wyodak-Anderson	WY	SUB
3	Illinois #6	IL	HVB
4	Pittsburgh	PA	HVB
5	Pocahontas #3	VA	LVB
6	Utah Blind Canyon	UT	HVB
7	Lewiston-Stockton	WV	HVB
8	Beulah-Zap	ND	LIG

The abbreviations are: LIG = lignite, SUB = subbituminous, HVB = high volatile bituminous, MVB = medium volatile bituminous, LVB = low volatile bituminous.

Collection:

Details of the procedures for collection have been given in earlier reports (1-8). In brief, the samples from underground mines were collected from freshly exposed blocks of coal, the thickness of the seam. Typical samples were about 1 1/2 tons. For thick underground seams (#3,4,5,6,7), the 55 gallon stainless steel drums were taken to the seam face, and representative samples were placed directly into the drums. For the thinner seam (#1) the sample was taken to the surface in double plastic bags. Surface mine samples (#2 and 8) were obtained from core samples.

Processing and Packaging:

At the surface the drums were purged with enough argon to reduce the oxygen content to 100 ppm, and quickly transported in a temperature-controlled semi-trailer to Argonne National Laboratory (ANL) for processing. AT ANL, the drums were weighed, placed into airlocks, purged, the contents were crushed, pulverized to -20 mesh, thoroughly mixed, and the contents were packaged. Half the batch was reground to -100 mesh, and then packaged. Packaging included placing about 80% of the coal in carboys of borosilicate glass for long term storage. The balance went into amber borosilicate glass ampoules of 10 grams of -20 mesh or 5 grams of -100 mesh material. The oxygen content of the packaging facility was maintained below 100 ppm at all times, and was typically about 30 ppm.

CURRENT STATUS

Inventory - Long Term Supply:

The ampoules and carboys are kept in a dark air-conditioned storage room. About 10,000 of the 5 gram ampoules and 5,000 of the 10 gram ampoules were made for each sample. Initially about 120,000 samples were placed in storage with about 550 of the 5 gallon carboys. As shipments deplete the inventory, then carboys can be placed in the packaging facility and additional ampoules filled and sealed to replenish the inventory. The current demand is such that the supply of ampoules should not need replenishing for another 6 years. The Illinois #6 sample is the most frequently requested.

Homogeneity:

Samples were taken during the processing to be irradiated and counted for homogeneity analysis. The results indicate that the samples were well mixed. Additional samples have been sent to a number of laboratories for analysis. Commercial Testing and Engineering Company performed a round robin analysis for the proximate analysis, and also carried out a number of ultimate, ash and other analyses as well.

Stability:

Stability analyses are carried out in two ways. The ampoules are routinely sent to the Analytical Chemistry Laboratory at ANL for gas analyses. The gas inside of the ampoules is analyzed for oxygen, hydrogen, nitrogen, carbon dioxide, methane, and other hydrocarbon gases. The results have indicated that no oxygen is entering the ampoules and the interior gas has a generally stable composition, with some tendency to liberate methane and carbon dioxide. The other stability study involves the gieseler plasticity analysis for the bituminous samples. These samples are sent at half year intervals for continued monitoring.

Analyses:

Other laboratories are encouraged to make the results of their analytical efforts known to the author so that they may be incorporated into a compendium of results for the benefit of all of the sample users. Table 1 gives a listing of the results for the analyses done by CT&E. The modified Parr formula used for the Dry mineral matter free content calculations was:

$$\text{Mineral matter(dry)} = 1.13 \text{ Ash} + 0.47 \text{ Pyritic S(dry)} + 0.50 \text{ Cl (dry)}$$

Other Studies:

This unique set of samples can advantageously be used to carry out a number of studies in a "round-robin" type of effort to help different laboratories compare their results, and develop an understanding of the differences in the coal samples. A study of the NMR characteristics of the samples is being planned, with the results to be shared near the end of 1989.

Shipments:

The acceptance and popularity of the samples may be gauged by the number of shipments, re-ordering and scope of work done with them. At the time of the writing, over 190 shipments had been made. These included over 110 different laboratories and investigators. Several of these have requested four different batches of samples. The shipments have gone approximately about 2/3 to academic institutions, and the rest about evenly divided between industrial and governmentally supported laboratories. About 5% of the shipments have gone to countries other than the U. S. A. The number of ampoules shipped has exceeded 6,000.

USGS Circulars - Geology and Geography:

In addition, the United States Geological Survey, which supervised the collection of the samples, is preparing a series of USGS Circulars, which will summarize the geological and geographical information of general interest about these samples. These may be obtained directly from the USGS.

Newsletter:

A newsletter has been initiated to provide current information of value to all recipients of the samples. The quarterly publication gave the contents of this symposium, and announced the development of a bibliography of references to the use of the Argonne Premium Coal Samples. All recipients of samples are asked to provide references to reports, journal articles and other public information so that this information may be shared with other investigators.

Types of Research Work:

The types of research being done with the samples are about as diverse as the research being done on coal. The symposia that follows will give a representative sample, but certainly does not include all of the work that is being done. The major fields include: structural studies, determination of the functional groups qualitatively and quantitatively in the coal, coalification, pyrolysis, liquefaction and gasification, sulfur removal, new methods of analysis and others.

Symposia:

This symposium is the second in a series devoted to research done with the Argonne Premium Coal Samples. The first, held in New Orleans in September, 1987 had 23 papers on a variety of topics. The organization this year is based on the subject matter of the individual papers. The range of work is such that a number of papers are finding their way into symposia on topics of special interest such as coal liquefaction, and this trend will probably continue.

Future Activities:

The APCSP will continue to provide samples and information about these samples to the users. It is planned to provide a data handbook to give in one document the most frequently requested information. This will include the results of the analytical work that is reported to the author, and special studies which have been arranged to provide for a reasonably complete set of information.

Further, individual studies may be initiated to respond to certain findings of potential interest to the user community. The observation of increased concentrations of methane and carbon dioxide in some of the ampoules led to speculation that anaerobic bacteria may be present with the samples. An effort is underway

to culture bacteria from samples of coal from each of the batches. The results of this effort will be described at a future meeting.

REFERENCES

1. Vorres, K. S., Preprints of the Fuel Chem. Div., Am. Chem. Soc., 32(4) 221-6(1987), *ibid.*, 32(1) 492(1987) (with S. K. Janikowski), 31(3), 304-9(1986) (with S. K. Janikowski), *ibid.*, 30(4), 193-6(1985), *ibid.*, 29(6) 230-3(1984).
2. Vorres, K. S., Proc. , Fourth Annual Pittsburgh Coal Conf., pp. 160-5, Sept 28-Oct. 2, 1987. Univ. of Pittsburgh.
3. Vorres, K. S., 1987 Intl. Conf. on Coal Science, pp. 937-40, Elsevier Science Publishers, BV., Amsterdam, 1987, ed. J. A. Moulijn, H. A. G. Chermin and K. A. Nater.
4. Vorres, K. S., 1985 Intl. Conf. on Coal Science, International Energy Agency, pp 640, October 28-31, Sydney, Australia.
5. Vorres, K. S. SME-AIME Annual Meeting, New York, February 1985, Paper #85-12.
6. Vorres, K. S., J. Coal Quality, 3(4), 31 (1984).
7. Vorres, K. S., Proc. of Workshop on Standards in Biomass for Energy and Chemicals, National Bureau of Standards, Gaithersburg, MD, 1-3 Aug. 1984, pp. 27-33. Ed. T. A. Milne, SERI/CP-234-2506.
8. Anon., Chem. Engr. News, 62(1)24(1984).

ACKNOWLEDGMENTS

The author gratefully acknowledges the support of the Office of Basic Energy Sciences, Division of Chemical Sciences of the U. S. Department of Energy. The efforts of many individuals who contributed at each stage of the program is deeply appreciated. Among these is the glass-blowing done by Joe Gregar.

Table 1. As-received and maf values Calculated from Dry Data from CT&E

Coal	UF	WY	IL	PITT	POC	UT	WV	ND
AR N2O	1.13	28.09	7.97	1.65	0.65	4.63	2.42	32.24
AR Ash	13.03	6.31	14.25	9.10	4.74	4.49	19.36	6.59
AR VM	27.14	32.17	36.86	37.20	18.48	43.72	29.44	30.45
AR S	2.29	0.45	4.45	2.15	0.66	0.59	0.69	0.54
AR Btu	13315	8426	10999	13404	14926	13280	11524	7454
Dry Ash	13.18	8.77	15.48	9.25	4.77	4.71	19.84	9.72
Dry VM	27.45	44.73	40.05	37.82	18.60	45.84	30.17	44.94
Dry S	2.32	0.63	4.83	2.19	0.66	0.62	0.71	0.80
Dry Btu	13467	11717	11951	13629	15024	13925	11810	11001
Dry C	74.23	68.43	65.65	75.50	86.71	76.89	66.20	65.85
Dry H	4.08	4.88	4.23	4.83	4.23	5.49	4.21	4.36
Dry N	1.35	1.02	1.16	1.49	1.27	1.50	1.25	1.04
Dry Cl	0.00	0.03	0.05	0.11	0.19	0.03	0.10	0.04
Dry F	0.00	0.00	0.00	0.00	0.00	0.00	0.00	0.00
Pyritic S	1.77	0.17	2.47	1.32	0.15	0.24	0.16	0.14
Sulfate S	0.00	0.03	0.01	0.01	0.03	0.03	0.03	0.03
Organic S	0.64	0.43	2.01	0.81	0.48	0.35	0.52	0.63
MAF C	85.50	75.01	77.67	83.20	91.05	80.69	82.58	72.94
MAF H	4.70	5.35	5.00	5.32	4.44	5.76	5.25	4.83
MAF N	1.55	1.12	1.37	1.64	1.33	1.57	1.56	1.15
MAF Org S	0.74	0.47	2.38	0.89	0.50	0.37	0.65	0.70
MAF Cl	0.00	0.03	0.06	0.12	0.20	0.03	0.12	0.04
MAF F	0.00	0.00	0.00	0.00	0.00	0.00	0.00	0.00
MAF O	7.51	18.02	13.51	8.83	2.47	11.58	9.83	20.34
MAF Btu	15511	12843	14140	15018	15777	14613	14733	12185

Dmmf values based on modified Parr formulas

Coal	UF	WY	IL	PITT	POC	UT	WV	ND
Dry Ash	13.18	8.77	15.48	9.25	4.77	4.71	19.84	9.72
Dry VM	27.45	44.73	40.05	37.82	18.60	45.84	30.17	44.94
Dry S	2.32	0.63	4.83	2.19	0.66	0.62	0.71	0.80
Dry Btu	13467	11717	11951	13629	15024	13925	11810	11001
MM Parr	15.73	10.00	18.68	11.13	5.56	5.45	22.54	11.07
Dry C	74.23	68.43	65.65	75.50	86.71	76.89	66.20	65.85
Dry H	4.08	4.88	4.23	4.83	4.23	5.49	4.21	4.36
Dry N	1.35	1.02	1.16	1.49	1.27	1.50	1.25	1.04
Dry Cl	0.00	0.03	0.05	0.11	0.19	0.03	0.10	0.04
Dry F	0.00	0.00	0.00	0.00	0.00	0.00	0.00	0.00
Pyritic S	1.77	0.17	2.47	1.32	0.15	0.24	0.16	0.14
Sulfate S	0.00	0.03	0.01	0.01	0.03	0.03	0.03	0.03
Organic S	0.64	0.43	2.01	0.81	0.48	0.35	0.52	0.63
Dmmf C	88.08	76.04	80.73	84.95	91.81	81.32	85.47	74.05
Dmmf H	4.84	5.42	5.20	5.43	4.48	5.81	5.44	4.90
Dmmf N	1.60	1.13	1.43	1.68	1.34	1.59	1.61	1.17
Dmmf Org	0.76	0.48	2.47	0.91	0.51	0.37	0.67	0.71
Dmmf Cl	0.00	0.03	0.06	0.12	0.20	0.03	0.13	0.04
Dmmf F	0.00	0.00	0.00	0.00	0.00	0.00	0.00	0.00
Dmmf O	4.72	16.90	10.11	6.90	1.66	10.88	6.68	19.13
Dmmf Btu	15980	13020	14696	15336	15908	14728	15247	12370

KINETICS OF VACUUM DRYING AND REHYDRATION IN NITROGEN OF COALS FROM THE ARGONNE PREMIUM COAL SAMPLE PROGRAM*

Karl S. Vorres and Roger Kolman
Chemistry Division, Building 211
Argonne National Laboratory
Argonne, IL 60439

ABSTRACT

The kinetics of vacuum drying and rehydration in nitrogen of Wyodak-Anderson subbituminous, and Illinois #6 and Utah Blind Canyon high volatile bituminous coal samples have been studied at room temperature. Some samples were oxidized at room temperature. Several cycles of drying and rehydration were carried out on the same sample. The drying rates depended on particle size and moisture content of the sample. Several different mechanisms of moisture loss and rehydration were indicated by the kinetic data. The mechanism depended on particle size, coal rank, and degree of oxidation.

* This work was supported by the Office of Basic Energy Sciences, Division of Chemical Sciences, U. S. Department of Energy, under contract number W-31-109-ENG-38.

INTRODUCTION

Drying and rehydration of a porous material can give some insight into the surface properties and the internal structure of the material. The rate of moisture removal or replacement will depend upon the coal surface, the macromolecular network of the coal particles and the structure of the pores through which the moisture flows.

An earlier study (1) reported the results of drying and rehydration studies on Illinois #6 Argonne Premium Coal Samples. The work involved different particle sizes and indicated that the mechanisms of drying and rehydration changed, depending on the coal particle size. The samples were fresh and aged, which also affected the results.

In general four mechanisms were observed (1). One involves a diffusion limited process of migration through a uniform barrier, and is observed with a parabolic curve. This is also referred to as Fickian diffusion. A second mechanism, obeying first order kinetics, similar to radioactive decay, would imply that the probability of a given water molecule being removed or adsorbed was a random probability event, and that all surface sites from which the water molecules depart or the water molecules in the sample were apparently equivalent. The third mechanism gives a plot following an adsorption isotherm curve. The mechanism here depends on the degree of surface coverage. A fourth mechanism, sometimes associated with the parabolic curve, is a linear mechanism implying a uniform barrier for diffusion.

The equation for the diffusion through a growing uniform barrier is:

$$W^2 = kt$$

where W is the mass change, k is a rate constant and t is the elapsed time.

The equation for the first order kinetics is:

$$\log W = k t$$

A characteristic half-time or half-life is associated with this reaction such that half the reaction is over in the half life, 3/4 is over in two half lives, 7/8 is over in three half lives etc.

For the adsorption or desorption reaction, the equation is:

$$W = k(t/t + 1)$$

A characteristic half time or half life is also associated with this reaction. The half time is the time for half of the observed change to take place. Then 2/3 of the reaction takes place in two half times, 3/4 takes place in three half times, 4/5 takes place in four half times etc.

The equation for the linear reaction is:

$$W = kt$$

This study extended the earlier work and involved examination of the drying and rehydration behavior of a lower rank Wyodak-Anderson sample, and a similar rank (but lower moisture content) sample from a different coal basin (Utah Blind Canyon seam).

APPARATUS, MATERIAL AND PROCEDURES

The studies were carried out with an Ainsworth recording thermobalance (described earlier (1)). The samples were weighed on a quartz pan and suspended from the balance. A quartz envelope was placed around the sample to control the gaseous environment. A water bath was placed around the sample to provide for temperature control to about 1° C. Initially the gas atmosphere was removed with a vacuum pump for dehydration. After dehydration, the samples were rehydrated by stopping the vacuum pump, backfilling with nitrogen, removing the quartz envelope, inserting an ice cube, re-evacuating to remove air, and backfilling with nitrogen. The ice cube was melted with warm water, and the water bath was replaced. The cycle was repeated by removing the quartz envelope and water, drying the envelope and replacing it and the water bath. From two to four cycles of dehydration and rehydration with the same sample were obtained in this way.

Sample weights varied between 0.100 and 1.112 grams. The weights used were:

IL #6 Block	1.112 grams
IL #6 -20 mesh	0.100 gram
IL #6 -100 mesh	0.239 gram
Wyodak -20 mesh	0.100 gram
UT Blind Canyon -100 mesh	0.346 gram

The data were recorded on chart paper and estimated to the nearest .01 mg. Buoyancy corrections for going between vacuum and atmospheric pressure were made. Due to some difficulties in establishing the initial weight during the conversions from vacuum to moist nitrogen and vice-versa (due to the rapidity of the change and the sensitivity of the sample to the change in conditions) the nature of the initial mass change is considered somewhat uncertain for some of the pulverized samples.

Data were transferred to a Lotus 1-2-3 file and analyzed on an IBM PC-XT microcomputer. Initial plots were generated from the program.

Some of the analytical data on the samples are as follows:

Sample	Moisture	Ash	Carbon (maf)
Wyodak-Anderson	28.09	6.31	75.01
Illinois #6	7.97	14.25	77.67
Utah Blind Canyon	4.63	4.49	80.69

RESULTS

The data for the samples was placed on a common basis of mass change in milligrams per gram of sample. The results for the Illinois #6 sample are given in Figures 1-6 for cycles of dehydration or of rehydration for the block, -20 mesh and -100 mesh material, respectively, at room temperature. Figures 7-8 indicate the data for the Wyodak sample at room temperature, while the Figures 9-10 indicate the data for the Utah Blind Canyon for room temperature. The points represent observed data, and continuous lines represent calculated results using the equations for the mechanisms which gave the best fit to the data. Numbers on the figures refer to the cycle of dehydration or rehydration to which the points correspond.

The mechanisms observed are summarized in Table 1.

DISCUSSION

The dehydration of the Illinois # 6 block followed a set of desorption curves. The amount of water desorbed depended on the amount initially present or returned during the rehydration step. The rehydration #2 was allowed to continue for 3 weeks and indicated that the amount of water which can be adsorbed under those conditions significantly exceeds the ASTM moisture value. The adsorption process is slow and probably would require a number of weeks for a one gram block to reach equilibrium. The desorption mechanism indicates that the rate controlling step involves a loss of moisture from the surface, rather than diffusion from the bulk of the particle to the surface.

The rehydration of the Illinois # 6 block followed a set of parabolic curves, of the type indicating a growing uniform barrier to further diffusion of moisture. This could indicate that the moisture swells the macromolecular network in a manner that uniformly impedes further increase of moisture. The effect of pores for this process is not noticeable.

The dehydration of the -20 mesh material is unique for the samples which have been studied. The initial loss was very low due to the small amount of moisture in the sample at the start. Subsequent runs followed a combination of linear and parabolic segments. The mass change for the initial linear segments increased from cycle 2 to cycle 3. The surface of this sample was oxidized which would provide a number of hydrophilic sites, in contrast to the hydrophobic sites to be expected on pristine samples. The moisture loss is significantly greater than the ASTM moisture value, and a large part takes place in the initial linear segment. This suggests that some moisture may be caught in the interstices of the particles. The ASTM moisture should be the sum of the moisture held in pores and in the macromolecular network. The pore moisture can be approximated by subtracting the amount taken up during the parabolic portion and the final linear part from the ASTM moisture. The amount in excess of the ASTM moisture may approximate the amount held in the interstices between the particles. The interstitial water is expected to be released quickly and following the linear mechanism.

The rehydration of the -20 mesh material was observed to largely follow the adsorption mechanism.

The dehydration of the -100 mesh sample followed the desorption model. The sample had initially been equilibrated with distilled water at room temperature and lost about 11 % moisture. The subsequent rehydration allowed only about 8 % moisture (the ASTM moisture) and that was lost in the following dehydration.

The rehydration curves initially followed an adsorption model and then showed evidence of multilayer formation. However, the subsequent dehydration did not show evidence of separate layers being desorbed.

A comparison of the rates of the reactions showed that the block is the slowest to change mass per gram. The initial rate for the -20 mesh reflects the low initial moisture content of that sample. The intermediate rate was indicated for the -100 mesh material, and the fastest rate for the oxidized -20 mesh material after the initial dehydration. This comparison is valid for both the dehydration and the rehydration mechanisms.

The dehydration data for the Wyodak sample indicated a desorption model.

The rehydration of the Wyodak sample indicated the formation of several layers of moisture following an initial layer of moisture adsorption. Nevertheless, the subsequent dehydration did not show any significant or comparable deviation from the normal desorption curve. The mass loss on the second dehydration indicated that only about 15 % moisture was lost, compared to the 28 % moisture determined by the ASTM method.

The dehydration of the Utah Blind Canyon sample followed the desorption model. The rehydration of the sample also followed the adsorption curve. There was no evidence of multilayer formation.

CONCLUSIONS

The mechanisms of dehydration and rehydration vary depending on the sample size and history. The behavior of an individual particle is best approximated by the block of Illinois #6 which indicated the desorption mechanism for dehydration and the parabolic mechanism or Fickian diffusion for rehydration. In general pristine samples followed an adsorption or desorption mechanism. Aged or oxidized samples showed combinations of linear and parabolic mechanisms which probably reflect a change in the surface properties in going from a hydrophobic behavior for the more pristine to hydrophilic for the more aged or oxidized material. Multilayer adsorption was observed on the lower rank materials which implies that the functional groups present on the surface facilitate this type of phenomenon.

ACKNOWLEDGMENTS

The authors gratefully acknowledge the support of the Office of Basic Energy Sciences, Chemical Sciences Division, and the Argonne National Laboratory Division of Educational Programs. Tim Griswold helped obtain the data and do some of the data reduction. The glassblowing by Joe Gregar was extremely helpful. Useful discussions with Anthony Fraioli are also acknowledged.

REFERENCE

1. Vorres, K. S., Kolman, R. and Griswold, T., Preprints, Fuel Chem. Div., Am. Chem. Soc., 33(2), 333(1988)

TABLE 1.

MECHANISMS FOR THE DEHYDRATION AND REHYDRATION OF COAL SAMPLES.

Sample		Dehydration	Rehydration
Illinois #6	Block	Desorption	Parabolic
	-20 mesh	L - P - L	Adsorption
	-100 mesh	Desorption	Adsorption
Wyodak-Anderson	-20 mesh	Desorption	Adsorption
Utah Blind Canyon	-100 mesh	Desorption	Adsorption

Vacuum Dehydration of IL #6 Coal Block

22 C., IL0012&3, IBDGAL

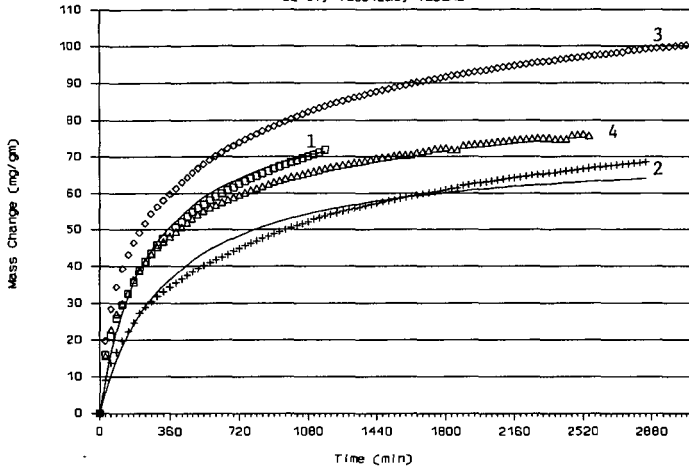


Figure 1.

Rehydration of IL #6 Coal Block

22 C., IL0012R, IBDGAL

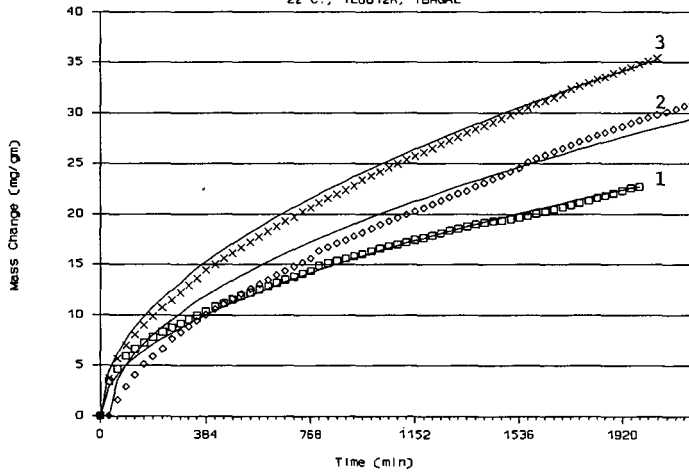


Figure 2.

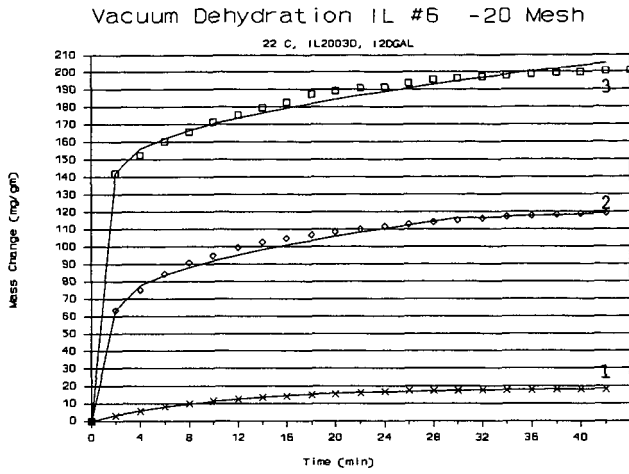


Figure 3.

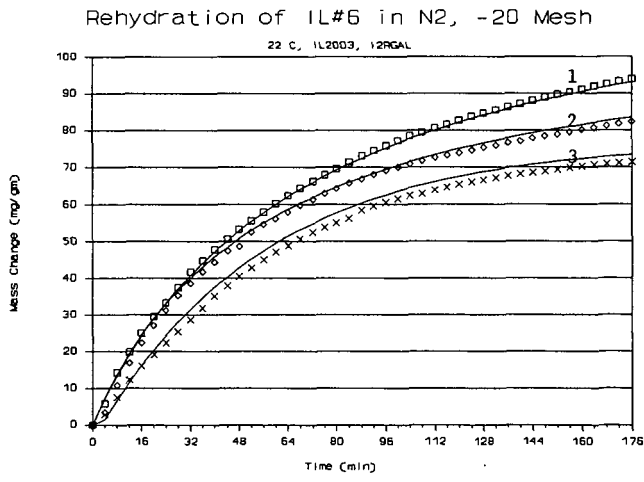


Figure 4.

Vac. Dehydration of IL #6 -100 Mesh

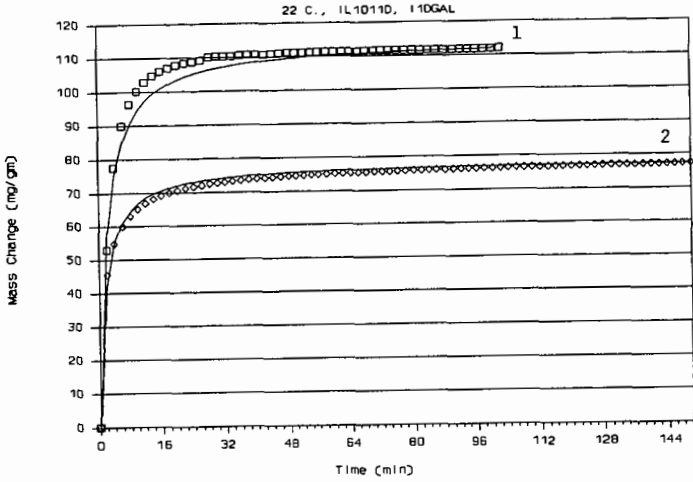


Figure 5.

Rehydration of IL #6 -100 Mesh in N2

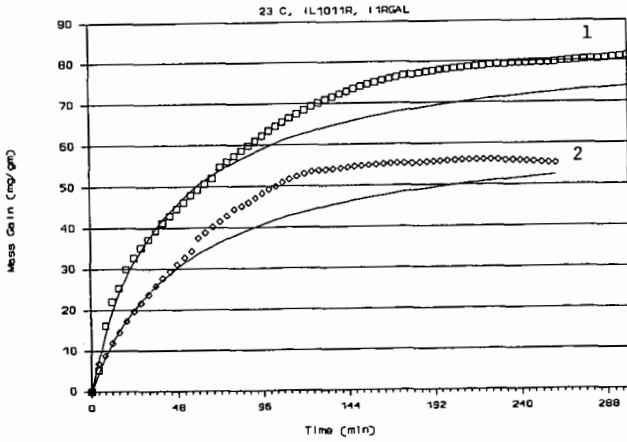


Figure 6.

Vacuum Dehydration of Wyodak -20 mesh

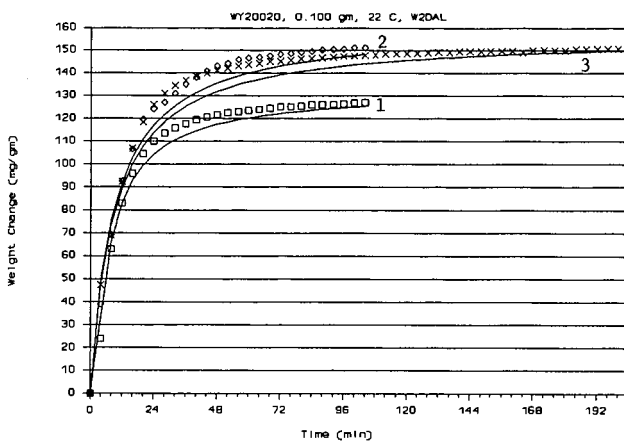


Figure 7.

Rehydration of Wyodak -20 mesh in N2

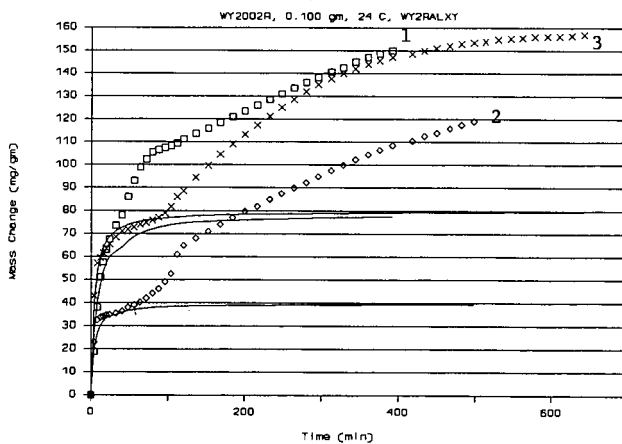


Figure 8.

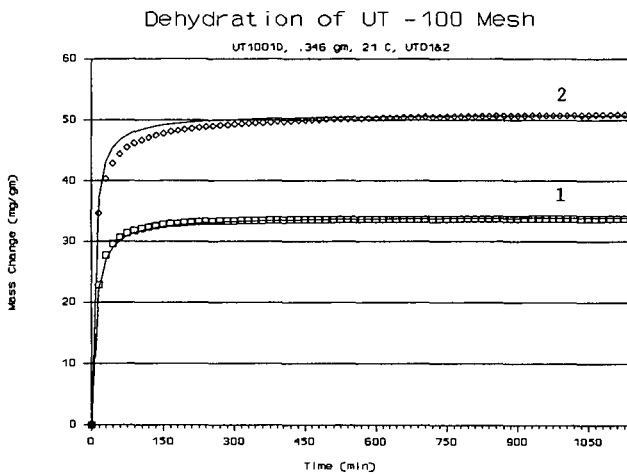


Figure 9.

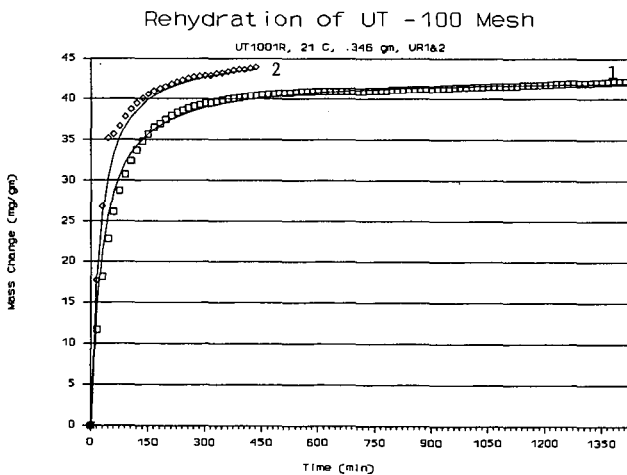


Figure 10.

STRUCTURAL GROUP ANALYSIS OF ARGONNE PREMIUM
COALS BY FTIR SPECTROSCOPY

K.A. Martin
S.S. Chao

Institute of Gas Technology
Chicago, Illinois 60616

INTRODUCTION

Infrared spectroscopy is a well-established method of coal characterization (1-12). Aspects of coal structure such as functional groups and hydrogen-bonding (11) and changes in structure during pyrolysis (6,7) and oxidation (4,5,9,10) have been described through infrared analysis and related to macromolecular processes. In particular, Painter *et. al.* (2), have proposed an FTIR procedure for a fairly exhaustive analysis of coal functional groups. Many of these suggestions are incorporated into the present study for the development of a functional group analysis data base for a set of standard coals.

EXPERIMENTAL

Eight Argonne premium coal samples were studied: Pennsylvania Upper Freeport, Wyodak, Illinois #6, Pittsburgh #8, Pocahontas #3, Utah Blind Canyon, West Virginia Stockton-Lewiston, and Beulah-Zap. Each ampoule of -100 mesh coal was mixed, opened, and the contents dried in a vacuum oven at 40°C for two hours. The dried samples were stored under vacuum until used. Diffuse reflectance infrared (DRIFT) spectra were obtained on neat dried samples with a Nicolet 60SXB FTIR with 500 scans at 4 cm⁻¹ resolution. KBr pellets were also prepared (about 0.3% coal by weight) and spectra collected with 128 scans at 4 cm⁻¹ resolution. Carbon, hydrogen and nitrogen analyses were performed with a LECO CHN-600 analyzer, and oxygen analyses were performed on a Carlo ERBA 1106 elemental analyzer. The low temperature ash of each coal was obtained with 0.5 g sample in an International Plasma Machine 1101B at 130 watts for several days. Another 0.5 g of each coal was acetylated by heating the coal at 100°C in a 2:1 mixture of pyridine and acetic anhydride for eight hours followed by filtering and vacuum drying.

RESULTS AND DISCUSSION

Each of the two sampling methods employed here, DRIFT and KBr pellets, have advantages and drawbacks in coal analysis. DRIFT suffers from a lower signal-to-noise ratio, but is very sensitive to some infrared bands which do not appear well in transmission spectra. Figure 1 compares the C-H stretching region of the Blind Canyon coal from DRIFT and KBr pellet spectra. Absorbance units are used rather than Kubelka-Munk units because the latter result in intensities too weak to resolve well. A weak band at 2732 cm⁻¹ is apparent in the DRIFT spectrum, but barely observed in the transmission spectrum. The relative intensities of the C-H bands also change, with the symmetric and asymmetric CH₃ modes enhanced in the DRIFT spectrum. DRIFT is especially useful because coal can be sampled without an interfering matrix, which is important in determinations of OH and water content. KBr pellets, on the other hand, offer the advantages of a high signal-to-noise ratio and better

control over sample concentration for quantitative work. The strengths of both methods have been exploited in this study.

A common method for determining relative aromatic and aliphatic hydrogen concentrations has been to compare the absorbances or integrated areas of the 3100-3000 and 3000-2800 cm^{-1} regions (2,7). Table 1 gives the results of using conversion factors obtained from model compounds to determine the relative amounts of aliphatic and aromatic hydrogen from the integrated areas of the CH regions. As expected, the ratio of aliphatic to aromatic hydrogen increases as the C/H ratio decreases. A pitfall in this procedure is the assumption of a single average conversion factor for all of the coals. Individual C-H groups have different extinction coefficients and variations in the composition of the aliphatic moiety would affect the average absorption coefficient. Inspection of the asymmetric CH stretch of these coals indicates that the ratio of CH_3 to CH_2 groups increases as the coal rank increases. Also, the second derivative and deconvoluted spectra show that the Beulah-Zap, Wyodak and Blind Canyon coals have very few CH_3 bands, while the other coals have a more diverse composition. In spite of this variation, a single conversion factor applied to all coals should result in a good approximation of the relative abundance of the aliphatic and aromatic hydrogens.

The out-of-plane aromatic CH region, 900-700 cm^{-1} , has three major bands in each of the coal spectra after subtraction of the low-temperature ash spectrum at 870-855 cm^{-1} , 816-812 cm^{-1} , and 754-748 cm^{-1} (Figure 2). These can be assigned to the bending modes of an isolated hydrogen, two adjacent hydrogens, and three or more adjacent hydrogens, respectively. From curve-fitting results, the coals with the highest C/H ratio, Pocahontas and Pennsylvania, have the largest contribution from the band due to lone hydrogen, along with the Illinois and Lewiston-Stockton coals, indicating a higher degree of substitution or cross-linking in these coals. The Wyodak, Blind Canyon and Beulah-Zap coals, with the lowest C/H ratios, have the largest contribution from the 815 cm^{-1} band and a much smaller contribution from the 870 cm^{-1} band, but also fewer aromatic hydrogens overall. This implies a less aromatic structure with less substitution and less cross-linking.

Another facet of aromatic substitution may be the weak band at 2732 cm^{-1} which appears in all but the Wyodak and Beulah-Zap coals. Painter (2) has assigned this as an overtone of methyl groups attached directly to an aromatic ring. The increased intensity of this band as the aromaticity and CH_3 concentration increase supports this assignment. The integrated peak area of this band compared to the total aliphatic CH area can be converted into the percentage of aliphatic hydrogens in methyl groups attached to aromatic rings, using factors obtained from model compounds. The results for the six coals are given in Table 2. These results indicate that over half of the aliphatic hydrogens in the Pocahontas coal are in methyl groups attached to aromatic groups. This leaves few hydrogens which can form methylenic linkages. Blind Canyon coal, on the other hand, has very few hydrogens in this form. This is compatible with the observation that the Blind Canyon coal is less highly substituted.

The prominent band at 1600 cm^{-1} in the spectra of all coals has been attributed to an aromatic ring mode, highly conjugated carbonyls, electron transfer between aromatic planes, to a non-crystalline, non-aromatic graphite-like phase, or to combinations of these (12). Figure 3 shows the spectra of

the eight coals between 1700 and 1500 cm^{-1} after subtraction of the low-temperature ash spectrum. It can be seen that the shape and maxima of the bands shift for the different coals, suggesting a different underlying character. The most intense 1600 cm^{-1} band is found in the Beulah-Zap coal, with the intensity of this band in the other coals decreasing in the same order as the oxygen content decreases. Deconvolution, second derivative and curve-fitted spectra showed that the composition of this band varies. The Wyodak and Beulah-Zap coals have major bands at 1655 and 1562 cm^{-1} , usually assigned to conjugated carbonyls and carboxylate groups (2), but only weak features near 1600 cm^{-1} where the aromatic ring mode is expected. The Pocahontas and Pittsburgh coals, however, have their strongest contribution from a band at 1611 cm^{-1} .

In order to measure the phenolic and alcoholic content of the coals, acetylated derivatives were prepared. The subtracted spectra of the acetylated and initial coals were curve-fit between 1800 and 1500 cm^{-1} . Figure 4 shows the subtracted spectra for the Illinois, Pennsylvania, Wyodak and Pocahontas coals. The bands at 1770, 1740 and 1685 cm^{-1} have been assigned to acetylated phenolic, alkyl OH, and NH groups (2). Conversion factors were obtained from model compounds. Because of the inconsistency in the amine results, only the phenolic and alcoholic results are reported. Table 3 gives the relative abundance of phenolic and alkyl OH groups in the coals. Contrary to Painter's findings (2), this ratio is not very consistent, but increases significantly for the low rank coals. However, this discrepancy could be due to incomplete acetylation of less accessible OH groups.

ACKNOWLEDGMENT

The authors thank Dr. Karl Vorres of Argonne National Laboratory for the coal samples.

REFERENCES

1. J. K. Brown, J. Chem. Soc., 744 (1955).
2. P. Painter, M. Starsinic and M. Coleman, in "Fourier Transform Infrared Spectroscopy", Vol. 4, J. R. Ferraro and L. J. Basile, Eds., Academic Press, Orlando (Fla.), Chap. 5, 1985.
3. S. H. Wang and P. R. Griffiths, Fuel 64, 229 (1985).
4. M. P. Fuller, I. M. Hamadeh, P. R. Griffiths and D. E. Lowenhaupt, Fuel 61, 529 (1982).
5. N. R. Smyrl and E. L. Fuller, in "Coal and Coal Products: Analytical Characterization Techniques", E. L. Fuller, Ed., ACS Symposium Series 205, American Chemical Society, Washington, D.C., Chap. 5, 1982.
6. C. J. Chu, S. A. Cannon, R. H. Hauge and J. L. Margrave, Fuel 65, 1740 (1986).
7. P. R. Solomon, D. G. Hambley and R. M. Carangelo, in "Coal and Coal Products: Analytical Characterization Techniques", E. L. Fuller, Ed., ACS Symposium Series 205, American Chemical Society, Washington, D.C., Chap. 4, 1982.

8. P. C. Painter, S. M. Rimmer, R. W. Snyder and A. Davis, Appl. Spec. 35, 271 (1981).
9. J. S. Gethner, Appl. Spec. 41, 50 (1987).
10. R. Liotta, G. Brons and J. Isaacs, Fuel 62, 781 (1983).
11. P. C. Painter, M. Sobkowiak and J. Youtcheff, Fuel 66, 973 (1987).
12. N. Berkowitz, "An Introduction to Coal Technology", Academic Press, New York, 1979.

RPP/kate2/PF

Table 1. Relative Ratios of the Number of Aliphatic and Aromatic Hydrogens

	<u>Aliphatic Hydrogens/ Aromatic Hydrogens</u>	<u>C/H Ratio</u>
Pocahontas	1.1	20.03
Pennsylvania	2.75	16.54
Lewiston-Stockton	3.9	15.30
Pittsburgh No. 8	5.1	14.99
Illinois No. 6	7.4	14.23
Beulah-Zap	10.9	14.89
Blind Canyon	13.1	13.33
Wyodak	13.8	13.80

Table 2. Concentration of Aliphatic Hydrogens in ϕ -CH₃ Groups

	<u>%</u>
Pocahontas	56.4
Pennsylvania	42.9
Pittsburgh	26.4
Lewiston-Stockton	24.9
Illinois	14.7
Blind Canyon	12.9

Table 3. Ratio of Phenolic to Alkyl OH Groups in Coal

Pocahontas	3.3
Blind Canyon	3.7
Lewiston-Stockton	4.5
Pittsburgh	5.0
Pennsylvania	5.6
Beulah-Zap	9.1
Wyodak	10
Illinois	11

RPP/kate2/PF

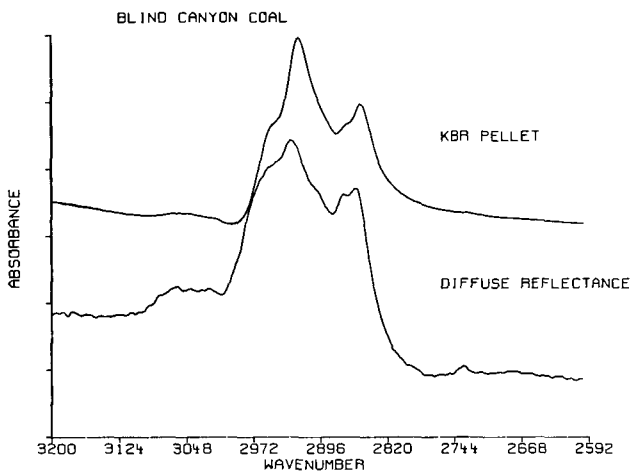


Figure 1. Comparison of KBr pellet and diffuse reflectance spectra of Blind Canyon coal.

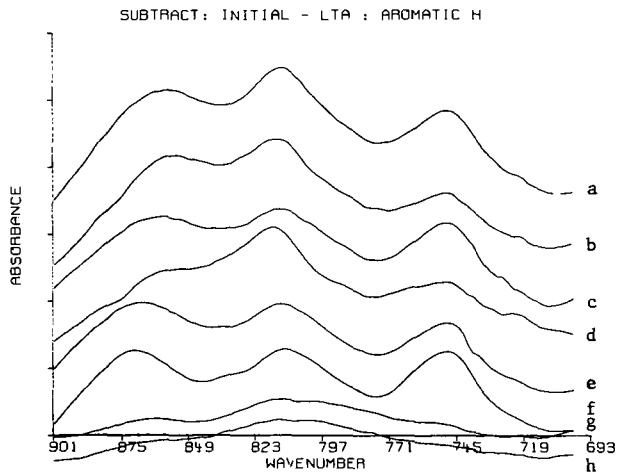


Figure 2. Aromatic hydrogen out-of-plane bending modes (a = Pittsburgh, b = Illinois, c = Lewiston-Stockton, d = Blind Canyon, e = Pennsylvania, f = Pocahontas, g = Wyodak, h = Beulah-Zap).

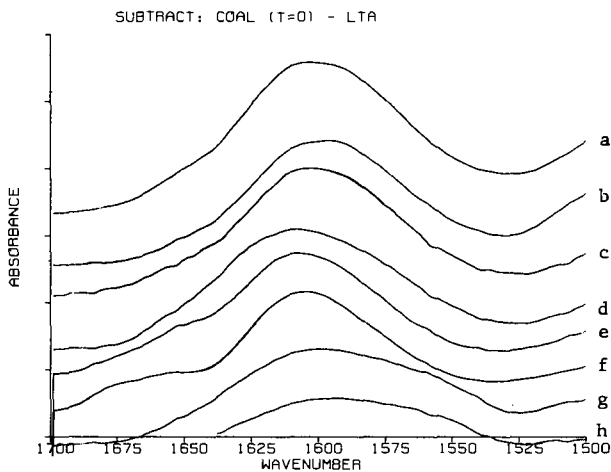


Figure 3. Comparison of 1600 cm^{-1} band for the different coals (a = Pittsburgh, b = Illinois, c = Lewiston-Stockton, d = Blind Canyon, e = Pennsylvania, f = Pocahontas, g = Wyodak, h = Beulah-Zap).

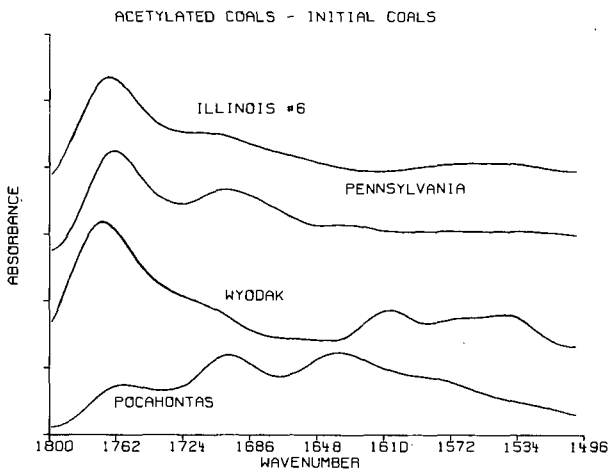


Figure 4. Spectra of Acetylated OH and NH groups for Illinois, Pennsylvania, Wyodak and Pocahontas coals.

SURFACE AND PORE PROPERTIES OF ANL AND PETC COALS.

C. H. Bartholomew, W. E. White, D. Thornock, W. F. Wells, W. C. Hecker, and L. D. Smoot,
Department of Chemical Engineering and Advanced Combustion Engineering Research Center,
Brigham Young University, Provo, Utah 84602

and
D. M. Smith and F. L. Williams
Department of Chemical and Nuclear Engineering
and UNM Powders and Granular Materials Laboratory
University of New Mexico
Albuquerque, New Mexico 87131

ABSTRACT

Surface areas, pore volumes, pore size distributions, and solid densities were measured for three ANL coals (Pittsburgh No. 8, Wyodak, and Beulah Zap Lignite), two PETC coals (Lower Wilcox, and Dietz) and a Utah Scofield coal and for chars derived from these coals. Surface areas were measured using nitrogen and carbon dioxide adsorptions; pore volumes were determined using nitrogen adsorption, mercury porosimetry, and NMR spin-lattice relaxation measurements of samples saturated with water. Solid densities were obtained using helium displacement. The results indicate that chars have larger surface areas and pores relative to coals; large fractions of the internal surfaces of coals are not penetrated by nitrogen molecules but are penetrated by carbon dioxide suggesting that the pores are mostly smaller than 1 nm.

INTRODUCTION

Coals are highly-aged biomaterials (with mineral inclusions) of high surface area and high porosity. These surface properties play an important role in their application as fuels. For example, in pulverized coal combustion the removal of volatile matter and the oxidation of the remaining char are processes the kinetics of which are governed at least in part by diffusion of materials in and out of the pores. Moreover, char oxidation rates depend upon the surface properties of the char, such as total surface area, active surface area and pore structure.

The work reported here is part of an ongoing collaborative study of the surface properties and pore structure of U.S. coals and in particular of a suite of 11 coals selected for comprehensive study by the Advanced Combustion Engineering Research Center (ACERC) of which 8 are ANL coals and 3 are PETC coals [1]. The principal objective is to correlate the surface, pore, and chemical properties of coals and chars with their rates of combustion. Ultimately these correlations will be developed into a computerized mathematical model of char oxidation which relates reactivity with structure [2].

This paper reports surface areas and pore volumes of 6 coals (3 ANL, 2 PETC, and one Utah coal) and of high temperature chars derived from three of these coals. It includes the results of studies of the precision of surface area and pore volume measurements on a given sample and on different samples by different adsorption techniques and by different laboratories. Comparisons are made of the results of this study with those reported in the literature for the same coals and similar chars derived from these coals.

EXPERIMENTAL

Materials. The coals studied are listed in Table 1 according to rank and source.

Table 1
Rank and Source of Coals Studied

<u>Coal Name</u>	<u>Rank</u>	<u>Location</u>	<u>Coal Bank Source</u>
1. Pittsburgh #8	H.V. A Bituminous	Greene Co., PA	ANL
2. Utah Scofield	H.V. C Bituminous	Scofield, UT	Valley Camp Mn
3. Dietz	Subbituminous B	Bighorn Co., MT	PETC
4. Wyodak	Subbituminous C	Gillette, WY	ANL
5. Beulah-Zap	Lignite A	Mercer Co., ND	ANL
6. Lower Wilcox	Lignite A	Titus Co., TX	PETC

Coal Preparation. The parent coals were air-classified and sieved. The lignite coals agglomerate easily and therefore, to facilitate the sieving process, they were first separated into wide size fractions using a cyclone particle classifier. The coal was processed through the separator two times. The first time, the apparatus removed the largest particles which were reground. The reground coal was then fed through the classifier again along with the smaller fraction from the first separation to remove the smallest size fraction. The larger size fraction was then classified using sieve screens to obtain the -200/+230 mesh size fraction. Sieving was performed to collect 200–300 grams of each coal using a RoTap sieve shaker; every fifteen minutes the screens were blown clean. The number of 15-minute periods for completion was greatly dependent on the individual sample, but was generally 4–6. The sieving was considered complete when the percentage passing through the 230 mesh screen remained constant. Both -325/+400 mesh (37–44 μm) and -200/+230 mesh (63–74 μm) size fractions were collected so that the effects of particle size could be studied.

Char Preparation. Details of the char preparation unit are described elsewhere [3]. The apparatus consists of a vibrating annular coal feeder, air/methane delivery system, a flat flame burner, and a cooled probe collection system. The coal feed rate is generally about 30 grams per hour. The flat-flame burner is fabricated from a ceramic monolith support (Cordierite, Corning Glass Works) with 300 square cells per square inch. The monolith is divided into two halves, and glass capillary tubes are inserted in every other hole in every other row. This arrangement gives a flame composed of many diffusion flamelets (at about 2000 K). Flows are controlled by high-accuracy rotameters and pressures are maintained constant by low-pressure line regulators to ensure a stable flame. Typical flow rates (SCFH) are: N₂ feed, 0.632; N₂ quench, 6; methane, 5.867; and air, 59.4. The collection system consists of a water-cooled, nitrogen-quenched probe, a cyclone separator, and a household vacuum. The particle residence time may be changed by varying the height of the collection probe above the burner. The cyclone separator is designed to collect 20 micron particles with greater than 90% efficiency.

Surface Area/Pore Volume Measurements. Total surface areas were measured by means of carbon dioxide adsorption at 273 or 298 K and nitrogen adsorption at 77 K, using either volumetric [4,5] or flow (Quantasorb) adsorption systems. Carbon dioxide adsorption measurements at UNM were conducted at 273 K and three relative pressures using a Quantasorb flow adsorption analyzer, after samples had been outgassed in a dry helium stream at 373 K. CO₂ adsorption measurements at BYU were conducted at 298 K and 3-7 relative pressures using either flow or static, volumetric systems on samples previously outgassed *in vacuo* for 12 hours at 378 K or outgassed in helium at 373 K. In both cases, the data were analyzed using the Dubinin-Polyani (DP) or Dubinin-Radushkevich (DR) equation using an area for the CO₂ molecule of 0.201 nm² based on good agreement between nitrogen adsorption and carbon dioxide adsorption measurements on a graphite carbon [6]. Nitrogen adsorption and desorption experiments were conducted over the relative pressure range of 0.05 to 0.99 at 77 K using

either an Autosorb-1 automated volumetric adsorption analyzer (UNM) or (at BYU) a volumetric adsorption apparatus [4,5]. Samples were outgassed *in vacuo* at either 383 K for three hours (UNM) or 378 K for 12 hours (BYU). Nitrogen isotherms were analyzed using the BET equation and an area for the nitrogen molecule of either 0.162 nm² (BYU) or 0.170 nm² (UNM) to obtain surface areas.

Pore size distributions for pores in the 1-100 nm range were obtained from extended nitrogen isotherms using the Kelvin equation. Mercury intrusion experiments were obtained (at UNM) for selected samples previously outgassed at 383 K *in vacuo* for one hour in the pressure range of 12 to 33,000 psia. The analysis of the mercury intrusion data was complicated by (i) filling of irregular-shaped voids around particles and (ii) sample compression at higher pressures necessary to fill pores smaller than 3 nm diameter [6].

NMR spin-lattice relaxation measurements of pore volume and pore size distribution were performed (at UNM) at 20 MHz and 303 K on samples saturated with water vapor. Coal and char samples were saturated by placing them in a desiccator, evacuating, backfilling with water or salt solution and allowing the samples to equilibrate with the solution vapor at a given pressure. Samples were weighed into 5 mm NMR tubes and a 180°-t-90° spin-lattice relaxation experiment was performed from which pore size distributions for pores of greater than 0.5 nm were extracted [6,7]. The surface-interaction parameter, β , was determined from measurements at different water contents [8]. Helium or "true" densities were obtained by helium pycnometry at UNM.

RESULTS AND DISCUSSION

Surface areas were measured for six coals and three chars while pore volumes, pore size distributions, and densities were also measured for three coals and three chars (two samples of one of the chars). Data obtained at BYU and the University of New Mexico (UNM) are summarized in Tables 2-4 and in Figure 1.

Table 2 summarizes the results of a repeatability study of CO₂ and nitrogen adsorptions on a Utah Scofield coal using a volumetric system to (i) define pretreatment conditions that would lead to removal of adsorbed CO₂ and allow repeatable measurements on the same sample and (ii) define the precision of CO₂ and N₂ adsorption measurements on the same sample and different samples (of about 1 g). The data (Table 2) indicate that immersing the sample cell in boiling water for five minutes, while evacuating, quantitatively removes adsorbed CO₂ and enables the adsorption measurement to be repeated with a high degree of precision (better than 7%). The data (Table 2) also indicate the precision of both CO₂ and N₂ measurements is within 7% on different samples.

Table 3 summarizes results from a similar repeatability study on high temperature Dietz chars using a flow system. They indicate that different runs on the same sample are repeatable to within 1-2% while the precision of measurements on different samples of the same preparation is 7-14% for samples sizes of 25-35 mg from a poorly-mixed preparation and 2-7% for sample sizes of 75-120 mg from a well-mixed sample. Accordingly, it is clear that the precision of surface area measurements by the flow method is significantly greater for samples larger than 50-75 mg and/or is improved by mixing the sample well. These results emphasize the importance of choosing representative samples and of conducting repeat measurements on different samples of the same preparation rather than repeating measurements on the same sample. Comparison of the data for the Dietz A and B preparations (temperature and residence time were nearly the same) indicates that large variations in surface areas (20% for CO₂ and 300% for N₂) can be obtained with only subtle variations in the preparation conditions. Similar variations are observed for Dietz Chars B and C prepared

under nearly the same conditions (Table 4). This emphasizes the need for careful temperature and residence time control in char preparation. Thus, we are presently computerizing our preparation system to enable better reproduction of gas temperature and particle residence time in our preparations.

Table 4 summarizes our measurements of total surface area, pore volume, pore volume distribution and interaction parameters from NMR measurements for the five coals and 3 chars. Wilc Chars 1 and 2 were prepared separately; the preparation of Wilc Char 2 involved a higher residence time and probably a higher degree of burnout; this is confirmed in part by the larger nitrogen BET surface area of Wilc Char 2 relative to Char 1. Wherever possible, measurements were repeated to obtain a measure of experimental precision; the listed limits of error refer to the the standard deviation for a series of 2-5 measurements.

Several significant trends in the data (Table 4) are evident: (i) CO₂ surface areas of coals are generally 50-300 and of chars 2-5 times larger than the corresponding N₂ surface areas, (ii) CO₂ and N₂ surface areas of chars are higher than those of the corresponding coals, and (iii) the fraction of pores having diameters of less than 0.5 nm is significant for both coals and chars. The first of these trends is explained by the ability of the CO₂ to penetrate micropores (of less than about 1 nm diameter) whereas N₂ is unable to penetrate; accordingly it is clear that most of the internal surface area of coals and much of that of these chars consists of micropores having diameters less than 1 nm. The larger measured surface areas of chars relative to coals is explained by a combination of the following factors: (i) the removal of strongly adsorbed molecules or functional groups from the micropores that would otherwise hinder access of CO₂ and N₂, (ii) creation of new micropores during the restructuring process involved in devolatilization, and (iii) creation of greater macroporosity as volatile materials are removed.

The data in Table 4 and Figure 1 indicate that the net result of these factors is to slightly decrease during char production the fraction of pores in the range of 0.5-1 nm, while significantly increasing the fraction of pores in the range of 1 to 10 nm and to increase pore volume measured by either nitrogen or water adsorptions. The data for the Wilc Char provide an exception to this trend; however in this case, the unexpectedly large pore volume of coal may be due to swelling as water is taken up by the lignite structure. A similar effect may also explain the unexpectedly large fraction of pores less than 0.5 nm for Wilc Char 1.

Table 5 compares surface area and pore volume data available in the literature with those determined in this study. The relatively few surface area data available are in fair to good agreement with the data obtained in this study, while the pore volume data are insufficient to enable comparison. The differences in the results from this and other studies are probably explained by differences in the pretreatments of the samples, e.g., the extent of oxidation and outgassing of the sample and by differences in the conditions of adsorption, e.g. the temperature at which CO₂ was adsorbed and the cross-sectional area used in calculating surface areas. This emphasizes the need for development of standard pretreatment conditions and methods of adsorption. To realize that goal additional studies of pretreatment effects, such as that of Deevi and Suuberg, [10], are needed. It is hoped that this continuing study will contribute to that end.

ACKNOWLEDGEMENTS

This work was sponsored by the Advanced Combustion Engineering Research Center (ACERC) and by DOE/PETC (Grant No. DE-FG22-85PC80529). Funds for ACERC are provided by the National Science Foundation, the State of Utah, 24 industrial participants, and the U. S.

Department of Energy. The authors gratefully acknowledge technical assistance by Mr. R. Merrill, Mr. A. Cook, and Mr. S. Simmerman.

REFERENCES

1. K.L. Smith and L. Douglas Smoot, "Selection and Characteristics of Standard ACERC Coals," Report submitted to ACERC, June 1, 1988.
2. L.D. Smoot, C. H. Bartholomew, and D. W. Pershing, "Research Program," Second Annual Report, Advanced Combustion Engineering Research Center, December 31, 1987, pp. 37-45.
3. R. Merrill, C. H. Bartholomew, and W. C. Hecker, "Char Preparation Facility," Char/ACERC-1, Submitted to ACERC, September 18, 1987.
4. C. H. Bartholomew, Quarterly DOE report, FE-1790-1, Aug. 6, 1975.
5. C. H. Bartholomew and R. B. Parnell, *J. Catal.*, **65**, 390 (1980).
6. D.M. Smith, C. L. Glaves, S. B. Ross, and D. L. Stermer, "Surface Area and Pore Structure of Char," Progress Report submitted to ACERC, December 1987.
7. D.P. Gallegos and D. M. Smith, *J. Colloid Interface Sci.*, **122**,143 (1988).
8. C. L. Glaves, P. J. Davis, D. P. Gallegos, and D. M. Smith, "Pore Structure Analysis of Coals via Low Field Spin-Lattice Relaxation Measurements," *Energy and Fuels*, In press.
9. H. Gan, S. P. Handi, and P. L. Walker, Jr., "Nature of the Porosity in American Coals," *Fuel*, **51**, 272 (1972).
10. S. Deevi and E. M. Suuberg, "Physical Changes Accompanying Drying of Western U. S. Lignites," *Fuel* **66**, 454 (1987).
11. D. P. Gallegos, D. M. Smith and D. L. Stermer, "Pore Structure Analysis of American Coals," in Characterization of Porous Solids, eds. Unger, Rouquerol, Sing, and Kral, Elsevier, 1988.
12. N. Y. Nsakala, R. L. Patel, and T. C. Lao, "Combustion Characterization of Coals for Industrial Applications , Final Technical Report, DOE/PC/40267-5 [DE-AC22-81PC40267], March, 1985.

Table 2: Repeatability Data for CO₂^a and N₂^b Adsorptions on a Utah Bituminous Coal (Scofield Mine; Deseret Coal Co.) Obtained in a Static System

Run No.	Procedure	S.A. (m ² /g)	
		CO ₂	N ₂
1.1	Outgassed; CO ₂ adsorption	129.8	
1.2	Cell immersed in boiling water for 5 min.; pumped 2 hr. to <10 ⁻⁴ torr; CO ₂ adsorption	129.3	0
1.3	Same as run #1.2	132.4	
2.1	Same as run #1.1	156.8	
2.2	Same as run #1.2	140.9	
2.3	Same as run #1.2	147.4	0
3.2	Same as run #1.2	150.8	0
3.3	Same as run #1.2	153.8	
3.4	Same as run #1.2	152.7	
4.1 & 4.2	Pumped to <10 ⁻⁴ Torr		1.72, 1.94
4.3	Same as 4.2		1.95
4.4	Same as 4.2		1.96
4.5	Same as 4.2		1.73

^a CO₂ area = 0.201 nm²; P_{CO₂} = Polynomial Fit

^b N₂ area = 0.162 nm²

Table 3: Repeatability Study in a Flow System of CO₂ and N₂ Adsorptions on Dietz Chars^a

Sample ^b	Run No. ^c	CO ₂ SA (m ² /g)	N ₂ SA (m ² /g)
A-1	1		333
	2		325
	4		327
	5		331
	6		<u>324</u>
	ave 5 runs		328 ± 3.9
B-5	5	289	
	6	296	
	7	289	
	8	293	
	9	<u>298</u>	
	ave 5 runs	293 ± 4.1	
A-1		394	328
A-2		381	322
A-3		<u>304</u>	<u>288</u>
	ave of A samples	360 ± 49	313 ± 22
B-4		301	106
B-5		293	89
B-6		293	93
B-7		307	99
B-8		<u>285</u>	<u>99</u>
	ave of B samples	296 ± 7.6	96.0 ± 5.9

a. Prepared in methane flame (gas temperature of 2000 K; residence time of about 10 ms).

b. A and B are different repeat preparations of char; A-1 to A-3 are different samples of Preparation A. A samples were 25-35 mg and not well mixed; B samples were 75-120 mg and well mixed

c. Run numbers and averages of runs are provided for samples A-1 and B-5 only

Table 4: Physical and Surface Properties of ANL, PETC & Other U.S. Coals and Chars

Sample	Surface Area (m ² /g)		Pore Volume (m ³ /g)			β^d , ^e (nm/s)	Fraction of PV <0.5nm ^d	Density of g/cm ³
	CO ₂ ^a	N ₂ ^b	Hg	N ₂ ^c	H ₂ O ^d			
Pitt #8 (-200+230) ^f	119±17	1.3±0.1	0.43	0.012	0.031	20.4	0.35	1.39±0.01
Pitt #8 (-200+230) ^h	117±18							
Pitt #8 Char ^g	155	74.6	-	0.056	0.053	67.1	0.28	-
Wilc (-200+230) ^f	144±7	3.3	0.16	0.033	0.282	487	0.31	1.48±0.01
Wilc (-200+230) ^h	154							
Wilc Char 1 ^f	253±30	60.5	0.61	0.128	0.124	36.3	0.88	2.03±0.09
Wilc Char 1 ^h	242±35	47						
Wilc Char 2 ^g	252	124	-	0.164	0.153	226	0.22	-
Dietz (-200+230) ^g	218	3.0	-	0.012	0.257	260	0.44	-
Dietz Char A	360±49	313±22						
Dietz Char B	298±6.8	97±7.4						
Dietz Char C ^{g,j}	526±20	131	-	0.107	0.110	123	0.27	
Wyodak (-200+230) ⁱ	206	5.0±0.4						
Wyodak (-325+400) ⁱ	208	5.0±0.1						
B-Zap (-200+230) ⁱ	229±50	0.5±0.2						
B-Zap (-325+400) ⁱ	255±62	1.0±0.6						
Ut Scof (-200+230) ⁱ	153±10	1.6±0.05						
Ut Scof (-325+400) ⁱ	144±11	1.9±0.1						

^a Measured at 0° C at UNM using flow system, 25° C at BYU using static system; Calc. from DP Eqn. using CO₂ area of 0.201 nm²/molec. and P_{CO2} = 26,144.7 mm Hg at 0° C.

^b Measured at -196° C; Calc. from BET Eqn. using N₂ area of 0.170 nm²/molec.

^c From extended BET measurements

^d From NMR analysis of adsorbed water

^e Interaction parameter from NMR

^f Measured by Mr. Wayne White at UNM; SA's by flow measurement

^g Measured by UNM personnel; SA's

^h Measured at BYU by flow method

ⁱ Measured at BYU by volumetric method

^j Char C was prepared under conditions very similar to those of Char B

Table 5: Comparison of Multisource Surface Area & Pore Volume Data for ANL and PETC Coals and Chars

Samples	Surface Area (m ² /g)		Pore Vol (cm ³ /g)		Ref.	
	CO ₂	N ₂	Hg	N ₂		
Coals	Pitt #8	119	1.3	0.43	0.012	This study
		141	<1.0	-	-	9
	Wyodak	207	5.0	-	-	This study
B-Zap		308	2.6	-	-	9
		242	0.5-1.0	-	-	This study
		-	2.2-4.6	0.08-0.14	-	10
		268	<1.0	-	-	9
Chars ^a		115	1.2-2.6	-	-	11
	Wilcox (2,000 K) ^b	252	47-124	-	0.16	This study
	Wilcox (1,700 K) ^c	211	191	0.68	-	12

^a Gas temperatures shown in parenthesis

^b Prepared in a methane flat flame burner

^c Prepared in a drop tube furnace at a residence time of about 0.2 sec.

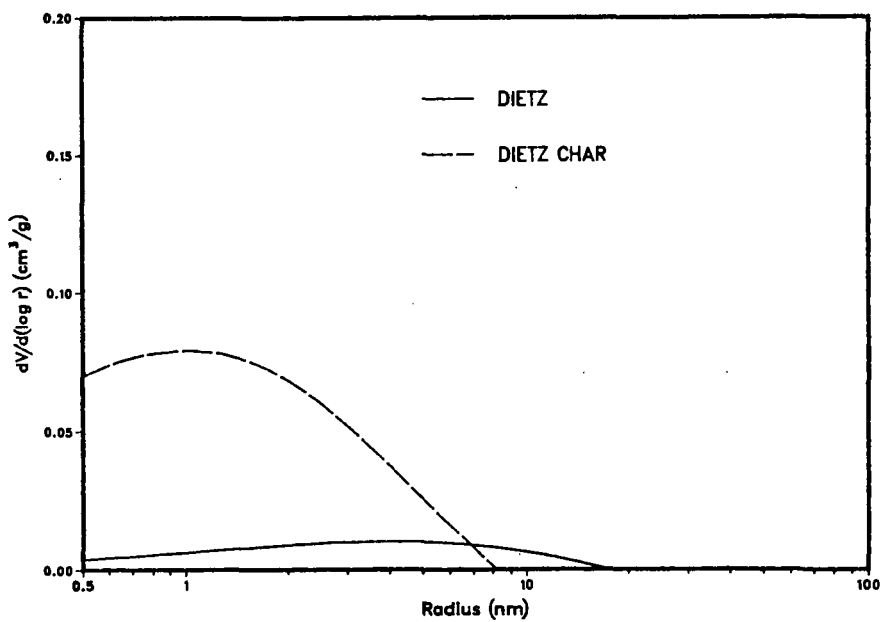
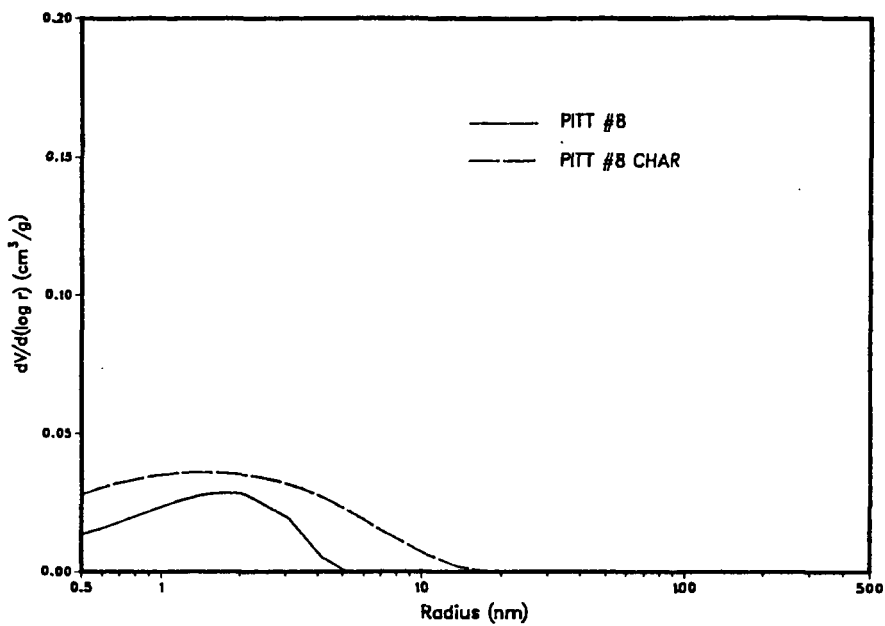


Figure 1. NMR pore volume distributions for two coal/char pairs.

AN EPR STUDY OF PORE ACCESSIBILITY IN ARGONNE PREMIUM COAL SAMPLES

Lalith S. Cooray, Lowell D. Kispert, and Shing K. Wu
Chemistry Department, The University of Alabama
Tuscaloosa, ALabama 35487

INTRODUCTION

We have recently reported (1) an EPR method developed in this lab to determine the pore size and number distribution in high volatile bituminous coal in the presence of a swelling solvent by diffusing nitroxide spin probes of different size, shape and reactivity into the swellable pores of coal samples. The same method has also been shown (2) to be useful in estimating the number distribution of accessible reactive sites containing carboxylic acid, phenol and amine substituents in samples of Mary Lee (A), Black Creek (B), Illinois no. 5 (C) and Illinois no. 6 (D), all high volatile bituminous coal samples by using small size (~0.7 nm radius) spin probes.

It was observed that the distribution of reactive sites varies substantially. For example, the detected acidic and phenolic sites in (B) and (D) (premium coal sample program) exceeded the detected amine site by approximately an order of magnitude. Sample of (B) possessed the greatest number of reactive acidic and phenolic sites of all the coal samples examined. It was also inferred that the ability for the coal pore to hydrogen bond to a spin probe was shown not to be an important process for incorporating spin probes in (A) and (B) and only a slight factor in samples of (C) and (D).

Unfortunately very little independent studies on pore distribution have been reported for coal samples A, B, C and D. Thus it is not possible to verify various conclusions. To remedy this situation, we have expanded our study to include Blind Canyon and Pittsburgh #8 in addition to the Illinois #6 coal samples from the Argonne Premium Coal Sample Program as well as samples from Illinois #6 (PSOC-1354) and New Mexico (PSOC -311) coals wherein comparisons can be made to other studies. For instances, D. Smith and coworkers (3) have studied extensively the pore size distribution for PSOC-311 and PSOC-1354 coals before exposure to solvents by NMR spin-lattice relaxation methods. In addition, small angle neutron scattering studies of Pittsburgh #8 swelled with different solvents have been carried out by Winans and Thiyagarajan (4) while studies by Larsen and Wernett (5) using gas adsorption techniques have permitted some independent measurements of pore accessibility to various solutes in Illinois #6 coal.

This study reports a spin probe - EPR study of pore size distribution, the basic/acidic reactive site distribution, hydrogen bonding site distribution and the effect of a swelling solvent on Blind Canyon, Pittsburgh #8 and Illinois #6 from the Argonne premium coal sample program and Illinois #6 (PSOC-1354) and New Mexico (PSOC-311) from the Penn State Coal Sample Bank at Penn State University.

EXPERIMENTAL

All coal samples were stored and handled under nitrogen or argon. The procedures for preparing (2) the spin probe doped coal samples and analyzing (1,2) the EPR spectra has been described previously. The ash free percentage by weight values for the coal samples obtained from the Argonne Premium Coal Sample Program are as follows: Illinois #6; C(79%), H(5.6%), O(9.7%), and S(5.4%); Pittsburgh #8; C(83%), H(5.8%), O(8%), and S(1.6%); and Blind Canyon; C(79%), H(6.0%), O(13%) and S(0.5%). The proximate and ultimate analysis for PSOC-1354 and PSOC-311 are available from the Penn State Coal Sample Bank at Penn State University. The spin probes (I-IX) were obtained from Molecular Probes, Inc. Junction City, Oregon. The pore size distribution of the coal samples was studied using spin probes I-V while the basic/acid reactive site distribution was examined by using spin probes VI and VII. To differentiate

between hydrogen-bonding to the nitroxyl group and substituents in the swellable pores of the coal, spin probes VIII and IX were used. The effect of a swelling solvent was demonstrated by swelling samples of Pittsburgh #8 coal with toluene, benzene and pyridine. To reduce the sample uncertainty, Professor D. Smith at the University of New Mexico sent his samples of PSOC-311 and PSOC-1354 so that a direct comparison could be made between our results and those he deduced from NMR studies.

RESULTS

Pore Size Distribution

The relative concentration of incorporated spin probes varied among different coal samples and is given in Table I. The relative spin concentration ratio of spin probes I:II:III:IV:V for Illinois #6 (Argonne) and PSOC-1354 (Illinois #6) equals 5.6:15.6:1.3:1.0: 1.9 and 3.5:25.2:1.0:1.0:3:3 respectively. It is clear that both samples have rather similar pore size distribution except that the Illinois #6 (Argonne) coal sample has a greater number of pores with a radius of 0.67-3.4 nm by a factor of 3 to 7. All the coal samples studied show the highest number of cylindrical pores with a diameter of 0.9 nm. However, compared to other samples, Blind Canyon coal has a quite high number of chain-like pore shapes. On the other hand, Pittsburgh #8 coal shows a pore distribution of largely cylindrical type pore shapes. For the coal samples Illinois #6 (Argonne), PSOC-311, and PSOC-1354, the long chain pore (radius = 1.3 nm) occurs the least number of times whereas for Pittsburgh #8 and Blind Canyon coal the long chain pore with a radius of 3.4 nm occurs the least number of times.

The pore structure of PSOC-311 and PSOC-1354 coal samples has been analyzed by Smith et al. (3) using low field NMR spin lattice relaxation measurements. It is known that the spin lattice relaxation time T_1 of H_2O attached to the pore surface differs from the corresponding T_1 for the bulk H_2O . Furthermore, Smith et al. (3) has shown that pore size determination can be deduced from T_1 measurements. Their results show the number of pores in PSOC-1354 with a radius of 0.5-5.0 nm is greater than that found in PSOC-311. In contrast, our studies show just the opposite trend in the presence of a swelling solvent for each spin probe used. This disagreement can be rationalized as follows. The NMR method measures the total volume of pores available in a particular coal sample. However, the spin probe method determines the pore volume that are accessible to a given spin probe upon swelling with a given solvent. On this basis it is possible to deduce that PSOC-1354 coal has more bottleneck pores (unaccessible to spin probes) than the PSOC-311 coal in the presence of toluene.

Recently Small Angle Neutron Scattering (SANS) studies (6) of the pore shapes and sizes of Illinois #6 coal characterize the pore shapes as elongated voids with an average radius of 2.5 nm. Unfortunately the spin probes used in this study are all smaller than this except for V (3.4 nm). Even so the spin probe study indicates a majority of cylindrical and a substantial number of long chain-like pores occur, in reasonable agreement with the SANS data. (6) It has been shown (7) by use of the SANS method that the shape distribution of the micropore and mesopores in unmodified coal do not change when the coal samples in the dry state are suspended in cyclohexane. Toluene, the swelling solvent used in our studies is considered to be a mild swelling solvent and therefore assumed not to significantly change the pore structure. Previous gas adsorption work (5) in Illinois #6 coal samples suggests that coal pores are mostly closed and inaccessible to molecules such as cyclopropane which are not soluble in the coal.

Reactive Site Distribution

The relative acidic/basic reactive site distributions in various samples of coal were determined using spin probes VI and VII. The results are given in Table 2 where the data is normalized to spin probe VI in Pittsburgh #8. The molecular volume of each spin probe is shown within the parenthesis.

The number ratio of pores containing amine groups to those containing acid or phenolic groups is 1:1.2; 1:3.7; 1:5.4; 4.6:1; 1:2.4 for coal samples PSOC-311, PSOC-1354, Illinois #6 (Argonne), Blind Canyon, and Pittsburgh #8 respectively. It is interesting to note that among the data listed in Table 2, only Blind Canyon coal (a low sulfur coal) has more basic sites than acidic acids within the pores defined by spin labels VI and VII. The presence of acidic sites in Illinois #6 has been confirmed by a small angle neutron scattering study (6).

Degree of Hydrogen Bonding in Swellable Pores

The relative spin concentration obtained for spin probes VIII and IX are depicted in Table 3. The volume of each spin probe is given within the parenthesis. It is apparent from the data given in Table 3, that the presence of an additional site for hydrogen bonding slightly benefits the incorporation of spin probes in PSOC-311 and Blind Canyon coal samples. On the contrary, for coal sample PSOC-1354, the presence of additional site for hydrogen bonding is a significant hindrance for spin probe incorporation. Values for Pittsburgh #8 could not be obtained because the EPR spectrum exhibited very poor resolution. Even though the exact reason for this is not understood, it could be due to the failure to collapse sufficient number of pores around the spin probes before being washed away with ethanol.

Pore Distribution Dependence on Swelling Solvent

In Table 4 are presented the changes in the concentration of spin probes I, II and V as Pittsburgh #8 is swelled with toluene, benzene and pyridine. It is to be noted that as the solvent is changed from benzene to pyridine, the number of spherical pores decreases (i.e. spin probe I) while the number of elongated pores increase (spin probe II). Generally, toluene is considered a poor swelling solvent relative to pyridine. Thus the accessible pore volume for those solvents which do not disrupt the original coal structure is significantly reduced over that when a solvent like pyridine is used. These results are in agreement with Winans and Thiyagarajan study (4) using small angle neutron scattering techniques to examine the effect of swelling solvent on pore structure. The results of a mild swelling solvent like benzene was compared to an aggressive swelling solvent (pyridine). The pore structure of Pittsburgh #8 in the presence of benzene was found to be roughly spherical whereas in the presence of pyridine, it was found to be elongated. This very nice agreement with an independent measurement suggests that the spin probe EPR measurements are useful indicators of the behavior of coal pores in the presence of various solvents and measure the relative difference in accessible pores on the molecular level.

CONCLUSION

The spin probe - EPR method showed that as the swelling solvent was changed from benzene to pyridine, the number of spherical pores in Pittsburgh #8 decreased while the number of elongated pores of distinct size increased sharply in agreement with previously reported SANS studies (4). Reasonable agreement was found with independent studies (6) on the average size distribution and the presence of acid character in the accessible pores of Illinois #6. Comparison between NMR data and the pore distribution pattern deduced by the spin-probe EPR method indicates that toluene swelled PSOC-1354 has more bottleneck pores with a radius of less than 5 nm which are not accessible to toluene than PSOC-311.

ACKNOWLEDGMENTS

The authors gratefully acknowledge the U. S. Department of Energy, Pittsburgh Energy Technology Center, University Coal Research Program for support of this research under Grant no. DE-FG22-86PC90502. We wish to thank Professor D. Smith at the University of New Mexico for samples of PSOC-1354 and PSOC - 311 and for numerous discussions.

REFERENCES

1. S. K. Wu and L. D. Kispert, *Fuel*, **64**, 1681 (1985).
2. L. D. Kispert, L. S. Cooray, and S. K. Wu, *Preprints. Div. Fuel Chem., ACS*, **32(4)**, 286 (1987).
3. C. L. Glaves, P. J. Davis, D. P. Gallegos and D. M. Smith, *Energy and Fuel*, in press, 1988.
4. R. E. Winans and P. Thiyagarajan, *Preprints, Div. Fuel Chem., ACS*, **32(4)**, 227 (1987).
5. J. W. Larson and P. C. Wernett, *Preprints. Div. Fuel Chem., ACS*, **32(4)**, 232 (1987).
6. J. S. Gethner, *J. Appl. Phys.*, **59**, 1068 (1986).
7. J. S. Gethner, *Preprints, Div. Fuel Chem., ACS*, **32(1)**, 239 (1987).

Table 1. The relative pore size distribution for spin probes I, II, III, IV, and V (toluene swelling solvent).

Radius ^a Molecular Vol. Sample	I 0.67 nm 143.9 Å ³ Spherical	II 0.90 nm 230.7 Å ³ Cylindrical	III 1.07 308.7 Å ³ Chain	IV 1.3 nm 335.3 Å ³ Long Chain	V 3.4 nm 459.1 Å ³ Long Chain
PSOC-311	48.6	202.6	48.6	7.7	37.7
PSOC-1354	10.2	73.7	2.9	3.0	9.7
ILLINOIS #6	72.3	201.1	17.0	12.8	25.3
BLIND CANYON	15.4	133.0	116.9	70.9	10.3
PITTSBURGH #8	4.0	133.4	1.9	9.3	1.0

(a) Effective radius including Van der Waals nearest approach distance.

Table 2. The relative basic/acid reactive site distributions for spin probes VI and VII (toluene swelling solvent).

Coal Sample	VI (143.6 Å ³) Basic sites	VII (131.5 Å ³) Acid sites
PSOC 311	16.9	21.2
PSOC 1354	1.6	6.1
Illinois #6	3.1	16.9
Blind Canyon	8.8	1.8
Pittsburgh #8	1.0	2.4

Table 3: Relative sites distribution for spin probes VIII and IX (hydrogen-bonding-differences).

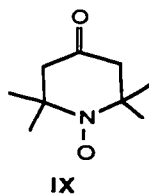
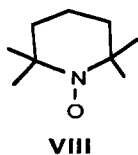
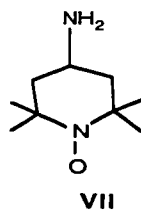
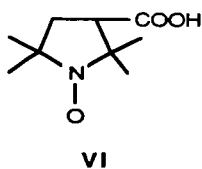
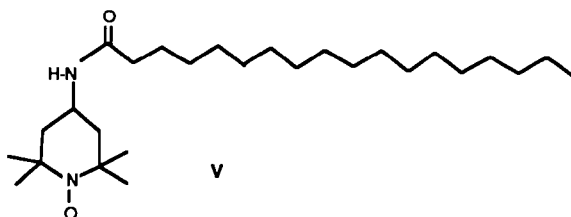
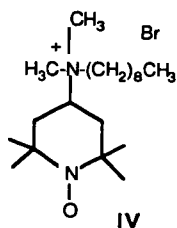
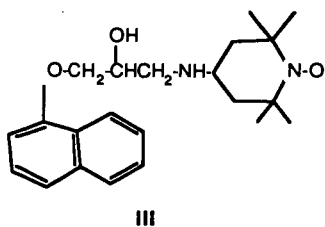
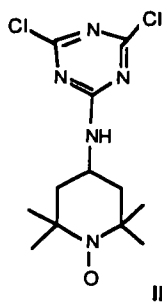
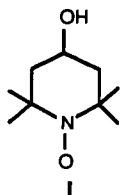
Coal Sample	VIII (138.3 Å ³) (1-H bond site)	IX (138.2 Å ³) (2-H bond sites)
PSOC-311	21.3	37.1
PSOC-1354	25.7	1.0
Illinois #6	3.5	3.7
Blind Canyon	5.7	11.0
Pittsburgh #8	--	---

Table 4. The relative spin probe concentration for probes I, II, III as a function of swelling solvent for Pittsburgh #8 coal.

Spin Probe	Solvent	Spin Probe Concentration Ratio ^a
I (Spherical)	Toluene	4.2
	Benzene	18.8
	Pyridine	1.0
II (Cylindrical)	Toluene	205
	Benzene	348
	Pyridine	2860
V (Long Chain)	Toluene	2.0
	Benzene	5.1
	Pyridine	6.1

(a) normalized to spin probe I in pyridine.

SPIN PROBES I-IX



ANALYSIS OF ARGONNE PREMIUM COAL SAMPLES BY THERMAL METHODS

Fawzy S. Sadek and Sara A. DeBot,
Chemistry Department, Winston-Salem State University,
Martin L. King Blvd., Winston-Salem, N.C. 27110

Thermal methods are used to determine the chemical characteristics of coal as well as its reactivity. Coal grading or ranking is generally based on fixed carbon and volatiles. Percentages of moisture, volatiles, fixed carbon and ash are reported in what is referred to as proximate analysis of coal, coke or fuel materials. ASTM methods can be used to determine each of these values, however, the procedures are time consuming, results are very subjective and the most important value, fixed carbon, is not measured directly. A more reliable and faster method for conducting proximate analysis is thermogravimetry (TG) (1,2). The sample's mass is continuously measured as a function of temperature in a controlled atmosphere and fixed carbon is measured directly as well as the range of medium volatiles and ash.

Coals are further characterized according to heat values, considered by some to be one of their most important properties, especially from a commercial or industrial aspect. Gross calorific value is traditionally determined by ASTM methods which employ various bomb calorimeters (3,4). Although these methods can generate acceptable results, they are also time-consuming, can be dangerous and give only total heat values. Thermogravimetry is an equally accurate technique compared to ASTM procedures, much faster and gives more information about the sample. The calorific value of bituminous coals containing 5-40% volatile matter on dry ash free (DAF) basis can be calculated from proximate analysis data using the Goutal equation (5). Earnest and Fyans (6) developed a modified form of this equation to obtain heat values of anthracitic coals and cokes while Ferguson and Rowe (7) have presented an equation relating calorific values of lignites to their proximate analyses.

A method for calculating heat values from ultimate analysis data has been described by Culmo (8). Percents carbon, hydrogen, nitrogen and sulfur determined by elemental analysis along with TG values of moisture and ash, were used to calculate calorific values from the Dulong equation. Results were reported to be in agreement within $\pm 3\%$ of the ASTM values. Giazzi and Colombo introduced a modification of this equation for calculating gross and net heat values (9).

An alternative method for the direct determination of calorific values of coals by Differential Scanning Calorimetry (DSC) was introduced by Fyans in 1977 (10). This technique measures heat flow as a function of programmable temperature with the total area under the curve being proportional to the heat of combustion. A typical thermocurve for coal shows a two step decomposition with the first peak being the combustion of volatiles and the second relates to fixed carbon. Fyans and

Earnest have reported surprisingly good agreement between the area of the DSC peaks and the ASTM calorific values (10-12).

In recent years the goals of thermal analysis investigations have become more and more quantitative. Unresolved problems associated with DSC, however, have brought results by this method under question. Varhegyi, et.al. (13), showed that DSC curves reveal considerably less energy release than the true reaction heats of oxidation of organic materials and the measured heat is strongly affected by the experimental conditions. To correctly characterize calorific values for volatiles produced in various steps of thermal decomposition as well as the heat of oxidation of the resulting char, they proposed the use of catalysts as aids to combustion at the low temperatures of DSC. In an effort to improve the DSC technique for coal analysis, we have focused on the use of metal oxides as well as the effects of variables related to sample characteristics. Heat values determined by DSC and bomb calorimeters are compared with calculated values from proximate and ultimate analysis.

EXPERIMENTAL SECTION

Apparatus:

Ultimate Analysis of coals by the determination of C/H/N/S was made on the left channel (O/S) of a Carlo Erba Elemental Analyzer Model 1106. A model C-31 Cahn Co. microbalance and IBM computer were interfaced with the instrument. Eager 100 software of Carlo Erba was used for operating the system and data analysis.

The Mettler system used for proximate analysis and drying of coal samples was composed of a TG-50 thermogravimetric unit, M3 microbalance, TC-10A controller TA processor equipped with TA 3000 version 3.1 software attached to an IBM/PC computer for data storage, TA-70 for data processing, RO-80 Swiss printer/plotter for actual time thermocurve printing and Epson HI-80 for printing processed data. A Mettler DSC 20 with measuring cells containing medium sensitivity sensors was used to determine heat values of coal samples directly. Nitrogen used for pyrolysis was purified with a Supelco High Capacity Heated Carrier Gas Purifier, cat.# 2-3802.

Samples and Materials:

The 100 mesh Premium Coal Samples used in this study were supplied by Argonne National Laboratory (ANL). All chemicals used for filling reactors, and consumables for Elemental Analysis were purchased from Carlo Erba Co.. Platinum crucibles with fine platinum mesh lids were used for proximate analysis of coal. Standard 40 μ l aluminum or gold crucibles were utilized in the determination of heat values by DSC. Two equal weight crucibles with lids were selected and a hole of approximately 0.5mm was made in the center of each lid. A 1:1 mole ratio mixture of

magnesium oxide and silver oxide was finely ground in a mortar and stored in a vial shell in a vacuum dessicator until use. Approximately 0.3 to 0.6 mg dried coal was spread evenly in the center of the crucible and from 8 to 12 mg of the additive mixture was placed over the sample. The heat capacity was counterbalanced by putting an amount of the spent additive in the reference crucible equal to 93% of the freshly prepared mixture.

Ultra high purity (99.99% or better) oxygen, nitrogen, helium and argon were purchased from National Specialty Gases, a division of National Welders Supply. Magnesium oxide, lead chromate (Analytical Reagent, Mallinckrodt), silver oxide (Baker and Adamson), praeaseodymium oxide (Alpha Inorganics), calcium oxide, copper oxide (certified ACS, Fisher), and lead dioxide (Fisher) were used as received.

Procedures:

Remixing of coal samples was done according to recommendations of the supplier before the ampoules were opened in a glove box filled with argon gas. Approximately 25 mg of the as received coal was placed in a platinum crucible in the TGA furnace in dry, oxygen free nitrogen for moisture analysis. The temperature was brought to 112°C at a heating rate of 100 °C/min and then held isothermally for 2 min. The evaporation of moisture from each of the seven samples is graphically presented in Fig. 1.

Proximate and ultimate analyses were made on the dried coal samples. Percent moisture and ash were used for calculating results on dry basis as well as moisture and ash free basis (14). Heat values were calculated from proximate analysis data applying the Goutal equation and using in house software. The software calculates the Heat Value (ΔH) as follows: ΔH (cal/gram) = $82C + aV$, where C is % fixed carbon, V is % volatiles and "a" is the Goutal coefficient. The value of "a" is a function of V and is obtained by interpolating known values of "a" at various values of V as derived by Goutal. Elemental analysis percentages were used in the calculation of heat values from the modified Dulong equation (8). Gross and net heat values are printed at the end of each analysis in calorie/gram units. These are changed to BTU/lb for comparison with ASTM bomb calorimeter values.

A procedure for determining heat values by DSC was stored on the TC-10A processor. This included 10°C/min heating rate from room temperature to 600°C. An oxygen flowrate of 20 ml/min was used. Integration of the heat flow during the dynamic experiment gives the heat change in coal directly. The two peak curve was integrated over a baseline starting at 105°C to the end of the run.

RESULTS AND DISCUSSION

Proximate and ultimate analyses of seven bituminous Premium Coal Samples are shown in Table 1. The calculated percentages are

comparable with those reported by ANL. Proximate analysis data made by TG were calculated by the instrument while data listed for ANL/ASTM were derived indirectly from the values of volatiles and ash provided with the samples. ASTM criteria for proximate analysis precision in reproducibility of data between two laboratories or by different methods are met with minor exceptions found in volatile matter of the Illinois #6 sample and percent ash of the Wyodak sample.

In ultimate analysis (14) the four major elements of coal were determined simultaneously on 1.0 to 3.0 milligram samples (Fig.3). The ANL data were made on different aliquot portions. Results are comparable with the exception of Illinois #6 and Blind Canyon carbon percentages and Upper Freeport hydrogen values. The sulfur values show a distinct difference for Illinois #6. In both proximate and ultimate analysis three or four values are compared with each other or with their counterpart made by a standard method. The logical way to compare sample data is to simplify to one numerical value. Mathematical equations to combine each group of data have existed for several decades. Goutal introduced his equation to give the heat value of bituminous coals as a function of percent volatiles and fixed carbon. By applying this equation to calculate heat values of TG data as well as ANL data we arrived at the values shown in Table 1. The average error of the TG heat values relative to ANL data calculated with the same equation is 3.9%. The difference between TG data and bomb calorimeter values is 3.5%. It is worth mentioning that most TG calculated heat values are slightly higher than those determined by the ASTM/bomb calorimeter method. This phenomenon repeats itself with calculated heat values from elemental analysis results. Work with elemental analysis confirmed that a catalyst is needed to insure the complete combustion of carbon in organic compounds regardless of the use of large amounts of oxygen and high temperatures. Oxides of copper, chromium, tungsten, vanadium and others (14) have been used at temperatures up to 1050°C to accomplish the complete oxidation of carbon to carbon dioxide. A comparison of elemental analysis results with those obtained with bomb calorimeters shows an average error of about 1.5% higher which may indicate a more complete combustion of the sample.

Direct determination of heat values by DSC traditionally has produced results 20 to 40 percent lower than those determined by bomb calorimeters. Varhegyi, et. al., proved by mass spectrometry that these low results are due to the formation of carbon monoxide (13). A mixture of cupric oxide and lead chromate was used as a catalyst but the true heat of combustion of the coal samples was not achieved even though the instruments maximum temperature reaches 750 °C. Many commercially available DSC instruments have a maximum of only 600°C and some manufacturers recommend pressurized containers made of either glass or stainless steel and/or pressurized DSC cells, further complicating the situation. It was found that the effects of factors such as heating rate, sample mass and particle size, type and amount of additive, hole size in container lid as well as

oxygen flowrate, are dependent on each other.

Heating metal oxides in an oxygen atmosphere using TG proved that most of the oxides are stable and usually contain the metals in the highest oxidation state (16). Contrary to this statement the TG curves of calcium, magnesium, lead, praseodymium and silver oxides in Fig. 4 show a mass loss. The curves were obtained in an atmosphere of oxygen and at a heating rate of 40 C/min. Dissociation of these oxides with the release of active oxygen appears to be definite. Magnesium oxide and silver oxide release oxygen and dissociate without phase transitions while calcium oxide and praseodymium oxide dissociate with phase transitions. Lead dioxide loses oxygen as shown in Fig. 4 in two steps below 650°C and a third step above 650°C which disturbs the DSC curve in that region.

Magnesium oxide (Fig. 5) was selected as a combustion aid due to its release of oxygen in the region of coal volatile matter to assist in its complete oxidation. In addition, it has been reported that magnesium oxide catalyses the oxidation of carbon monoxide to carbon dioxide (17). Formation of carbon dioxide releases approximately four times the amount of heat as the formation of carbon monoxide from the same amount of carbon. This is basically the reason for the lower heat values measured in unpressurized low temperature DSC. Silver oxide (Fig.5) releases its oxygen relative to the fixed carbon combustion region as shown in Fig. 6. Heat value results determined using the magnesium-silver oxide mixture are listed in Table 1. DSC results are comparable with ASTM values.

CONCLUSIONS

Thermogravimetric and elemental analysis data have been used to derive heat values of Argonne Bituminous Premium Coal Samples. The average error between heat values calculated from proximate analysis data by the classical Goutal Equation and ASTM/bomb calorimeter values was less than 4%. It was found to be less than 2.0% between Ultimate Analysis values calculated by the Dulong Equation. A comparison of heat values obtained directly by conventional low temperature DSC using metal oxide additives shows an average error of 0.5%.

ACKNOWLEDGMENT

We are grateful to Dr. Karl S. Vorres for providing the Argonne National Laboratory Premium Coal Samples. We also acknowledge G. Paul and D. McMorran of Mettler Co. for valuable information concerning the Mettler DSC 20.

LITERATURE CITED

- (1) Sadek, F.S.; Herrell, A.Y. *Thermochimica Acta*, 81 (1984) 297.
- (2) Ottaway, M., *Fuel* 61 (1982) 713.
- (3) "ASTM Designation D2015-85, Annual Book of ASTM Standards, 05.21 (1985).
- (4) "ASTM Designation D3286-85, Annual Book of ASTM Standards, 05.21 (1985).
- (5) Goutal, M. *Compt. Rend.*, 135 (1902) 477.
- (6) Earnest, C.M.; Fyans, R.L. *Thermal Analysis Applications Study #21*, Perkin-Elmer Corp., Norwalk, CT (1977).
- (7) Ferguson, J.A.; Rowe, M.W. *Thermochimica Acta*, 107 (1986) 291.
- (8) Culmo, R.F., *Elemental analysis Application Study #2*, Perkin-Elmer Corp., Norwalk, CT (1977).
- (9) Giazzi, G.; Colombo, B. *The Journal of Coal Quality*, 2 (1982) 26.
- (10) Fyans, R.L., *Thermal Analysis Application Study #21*, Perkin-Elmer Corp., Norwalk, CT, (1977).
- (11) Earnest, C.M., "Analytical Calorimetry" (Johnson, J.F.; Gill, P.S. Eds.) Vol. 5, Plenum Press, New York, (1984), 343.
- (12) Earnest, C.M. *Int. Instrum. Res.*, (1985), 57.
- (13) Varhegyi, G; Szabo, P.; Till, F. *Thermochimica Acta*, 106 (1986) 191.
- (14) Sadek, F.S.; deBot, S.A. "Rapid Automated Methods For Coal Ultimate Analysis" *Proceedings of the 6th International Coal Testing Conference*, (1987) 97.
- (15) "ASTM Designation D3180, Annual Book of ASTM Standards, Vol. 05.05 (1984).
- (16) Wendlandt, W.W. "Thermal Analysis" 3rd Edition John Wiley & Sons, New York (1986) 179.
- (17) Lundsford, J.H.; Jayne, J.P. *Journal of Chemical Physics*, 44 (1966) 1492.

Table 1. COMPARISON OF ARGONNE PREMIUM COAL SAMPLE DATA OBTAINED BY DIFFERENT THERMAL METHODS.

PROXIMATE ANALYSIS*

	TGA (%)			ANL/ASTM (%)		
	Ash	VM	FC	Ash	VM	FC
1. Upper Freeport	13.2	27.6	59.2	13.2	27.5	59.3
2. Wyodak	7.5	45.2	47.3	8.8	44.7	46.5
3. Illinois #6	15.4	36.6	48.0	15.5	40.1	44.4
4. Pittsburgh #8	9.2	36.7	54.1	9.3	37.8	52.9
5. Pocahontas #3	4.3	19.0	76.7	4.8	18.6	76.6
6. Blind Canyon	4.6	45.2	50.2	4.7	45.8	49.5
7. Lewis Stockton	20.0	30.2	49.8	19.8	30.2	50.0

ULTIMATE ANALYSIS*

	ELEMENTAL ANALYSIS (%)				ANL/ASTM (%)			
	C	H	N	S	C	H	N	S
1. Upper Freeport	75.1	4.6	1.5	2.3	74.2	4.1	1.4	2.3
2. Wyodak	67.9	4.9	1.0	0.8	68.4	4.9	1.0	0.6
3. Illinois #6	64.6	4.5	1.2	4.5	65.7	4.2	1.2	4.8
4. Pittsburgh #8	75.0	5.0	1.5	2.4	75.5	4.8	1.5	2.2
5. Pocahontas #3	85.7	4.4	1.2	0.7	86.7	4.2	1.3	0.7
6. Blind Canyon	74.9	5.6	1.5	0.8	76.9	5.5	1.3	0.6
7. Lewis Stockton	66.3	4.3	1.2	0.8	66.2	4.2	1.3	0.7

HEAT VALUES* (BTU/lb)

	CALC. GOUTAL		CALC. DULONG		DIRECT	
	TGA	ANL	E. A.	ANL	DSC	ANL/ASTM
1. Upper Freeport	13535	13537	13701	12874	13611	13467
2. Wyodak	11687	11487	11578	11641	11800	11717
3. Illinois #6	11817	10982	11664	11363	11951	11951
4. Pittsburgh #8	13200	14356	13684	13415	13740	13629
5. Pocahontas #3	16090	14867	15141	15102	15029	15024
6. Blind Canyon	12417	12240	13633	13743	13896	13925
7. Lewis Stockton	12005	12057	11869	11626	11857	11810

* As received, on dry basis.

Figure 1. Drying of ANL Premium Coal Samples by TGA.

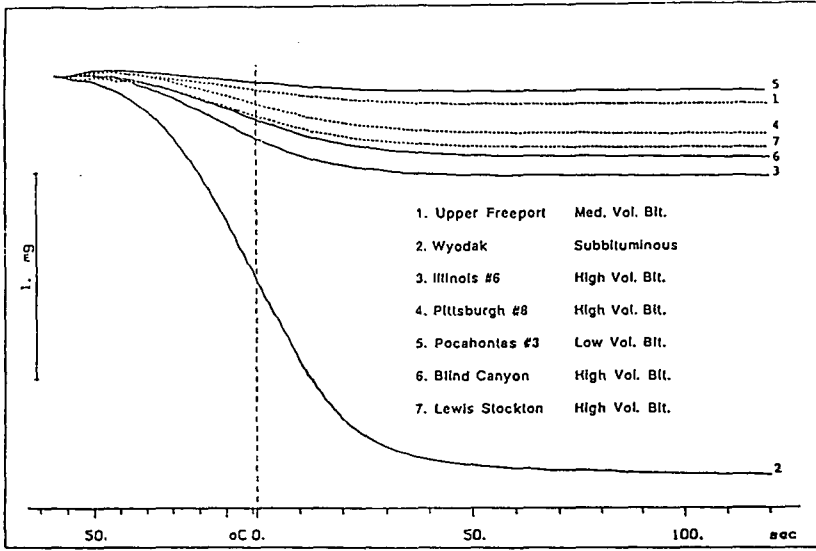


Figure 2. Proximate Analysis of ANL Bituminous Coal on Dry Basis.

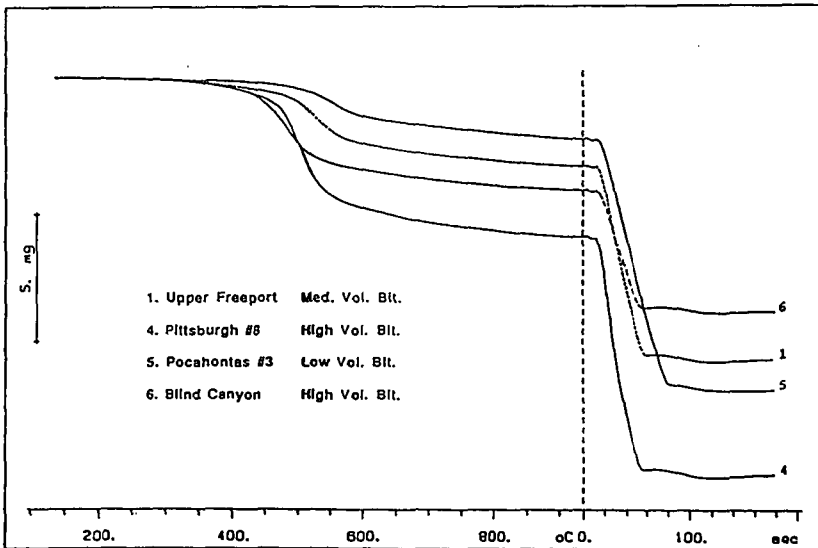
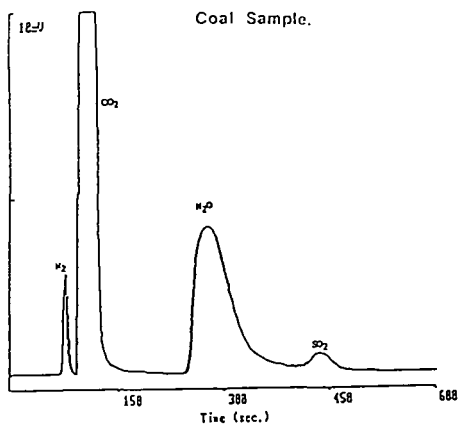


Figure 3. Elemental Analysis of Upper Freeport Coal Sample.



Date : 02-13-1970 Time : 09:32:15 Company name : WSSU
 Sample : 168 COAL 11 AS 15 600 K Type : Unknown
 Sample Weight : 1.8972 Base Line drift (10%) : 12
 Operator : GOR

Ret. T.	Area (10 ⁶ %)	Area 1	Comp. 1	Peak area	
1	77	1.405	1.725122	Nitrogen	
2	97	1267850	82.552	75.67212	Carbon
3	274	238704	15.345	4.764939	Hydrogen
4	434	14091	1.031	1.971164	Sulphur

Carb./Hyd. Area = 5.372648 Carb./Sulph. Area = 78.37535
 Carb./Sulph. Area = 89.03512
 G. M. V. = 7871.641 H. M. V. = 7127.518

Figure 4. Thermocurves of Five Metal Oxides.

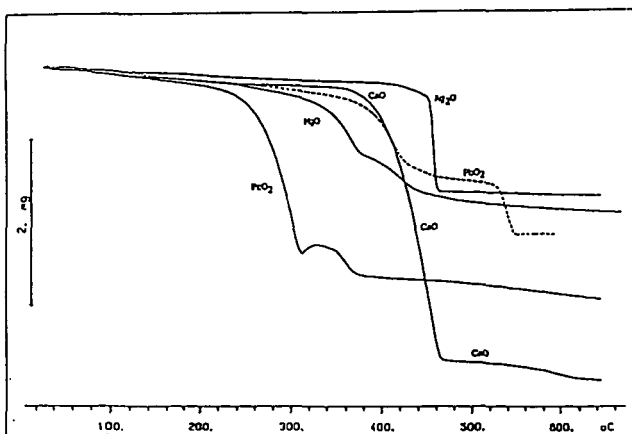


Figure 5. DSC of Magnesium Oxide and Silver Oxide.

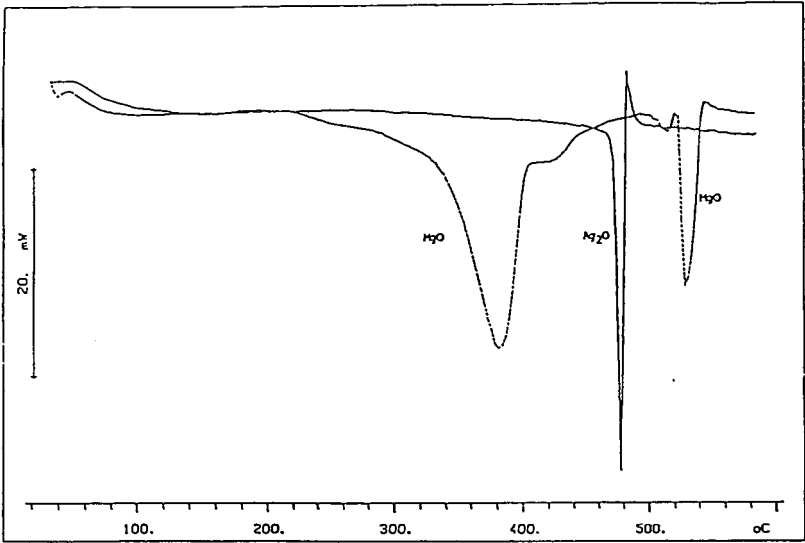
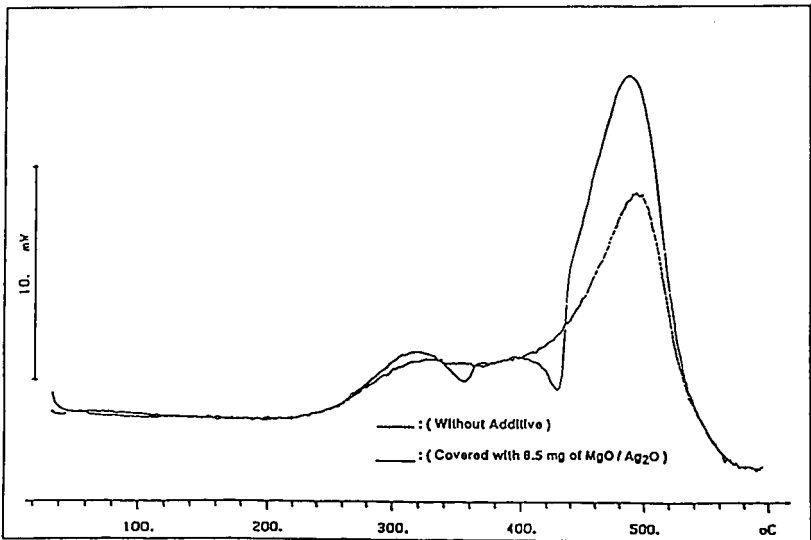


Figure 6. DSC Curves of Pittsburgh #8 Coal Sample at 10° C / min.

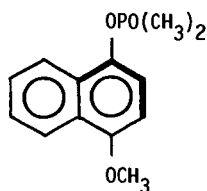


THE DOUBLE CROSS POLARIZATION ^{13}C -NMR EXPERIMENT IN
SOLID FOSSIL FUEL STRUCTURE ANALYSIS

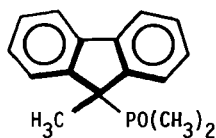
Edward W. Hagaman and Madge C. Woody
Chemistry Division
Oak Ridge National Laboratory
Oak Ridge, Tennessee 37831-6201

The Double Cross Polarization ^{13}C -MAS/NMR experiment has been used to derive a new operational classification of solid fossil fuels based on chemical reactivity^{1,2}. The method requires labeling reactive sites in the organic matrix with a magnetically active isotope not present in the precursor material, and using the local, isolated dipole-dipole interaction between this nucleus and nearby ^{13}C nuclei to detect via cross polarization the carbon centers in the vicinity of the label. The technique is a marriage of chemistry and spectroscopy and the information content of the DCP spectra is defined by both partners.

^1H - ^{13}C - ^{31}P DCP/MAS ^{13}C -NMR spectroscopy has been used to statistically describe phenolic ortho-substitution patterns of coals via their aryl phosphinate or phosphate derivatives, as per model 1. The identification of specific functional group types as the activation source for acidic C-H bonds in these materials has also been effected via the tertiary phosphine oxide derivatives generated from coal carbonions as in model 2. The bold line in these structures indicates the carbon bonding network that is detected by this technique, with signal intensities nominally proportional to the inverse sixth power of the ^{31}P - ^{13}C internuclear distance. The sensitive volume element centered on ^{31}P in which DCP signals are observed is determined by the rate at which the ^{31}P - ^{13}C cross polarization signal accrues, primarily determined by the depolar interaction strength, and the rate at which this signal decays, the ^{13}C rotating frame T_1 . For the ^{31}P - ^{13}C pair, DCP signals are confined to a spherical volume element with a ca. 4 Å radius.



1



2

In these applications of DCP NMR the new, detailed structure and/or reactivity information is realized by detection of carbon resonances one or more bonds removed from the reaction center, but in a volume element of intramolecular dimensions. To the extent that intermolecular contributions to the spectrum are detected, and not recognized as such, the structure/reactivity correlation is weakened.

Direct substitution of phosphorus on the aromatic rings in the organic matrix of the coal is not readily accomplished. This environment potentially can be labeled with fluorine in a selective fashion using newly developed reagents³. The possibility of determining the changes in average ring substitution patterns as a function of chemical treatment or coal diagenesis emerges. Recent developments in the field of DCP ¹³C NMR will be presented.

References

1. Local Structure Evaluation in Solid Organophosphorus Compounds by Double Cross Polarization Carbon-13 Nuclear Magnetic Resonance Spectroscopy. Edward W. Hagaman, submitted for publication.
2. Solid State Nuclear Magnetic Resonance Detection of Reaction Sites in Amorphous, Heterogeneous Organic Matrices. Edward W. Hagaman, submitted for publication.
3. Singh, S., DesMarteau, D. D., Zuberi, S. S., Witz, M., Huang, H.-N. J. Am. Chem. Soc., 1987, 109, 7194-7196.

Acknowledgement

Research sponsored by the Division of Chemical Sciences/Office of Basic Energy Sciences, US Department of Energy under contract DE-AC05-84OR21400 with the Martin Marietta Energy Systems, Inc.

SOLID STATE ^{13}C RELAXATION STUDIES OF COALS

R. E. Botto* and David E. Axelson**

*Chemistry Division, Argonne National Laboratory,
9700 South Cass Avenue, Argonne, IL 60439

**Energy, Mines & Resources Canada, CANMET,
P.O. Box 1280, Devon, Alberta, Canada T0C 1E0

INTRODUCTION

Despite many studies of coal and related fossil fuels, no attempts have been made to systematically correlate changes in the solid state ^{13}C -NMR parameters as a function of static field strength. In particular, questions arise regarding differences in spectral resolution and relaxation parameters. While discrimination among the complex structural components of fossil fuels can be based on relaxation time differences (1), this also necessitates a more intensive study of static field-strength effects if a more complete understanding of coal structure is to be gained.

Carbon-13 spin-lattice relaxation was chosen as the parameter of interest for this study because it represents a "dilute" nuclear spin system, which therefore minimizes spin diffusion interaction among phases. Furthermore, it is not as complicated to interpret as $T_{1\rho}$ measurements, and exhibits a field dependence in the slow motion regime (Figure 1). These studies also comprise part of a more comprehensive on-going evaluation of the Argonne Premium Coal Samples.

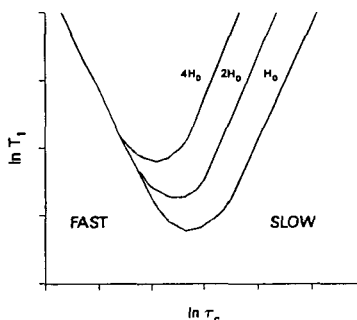


Figure 1. Motional dependence of T_1 with magnetic field.

EXPERIMENTAL

All NMR spectra taken at higher field were obtained on a Bruker CXP-200 spectrometer. Parameters used to acquire data were as follows: spectrometer frequency 50.306 MHz, 3 kHz magic-angle spinning in a boron nitride rotor containing a deuterated polymethylmethacrylate base (exhibiting no ^{13}C background from residual non-deuterated material), dipolar decoupling of 50-60 kHz, 90° pulse width of 4-5 ms, spin temperature alternation of the H-1 pulse, 20 kHz spectral width, 4K data points, 50-75 Hz line broadening, 500-3000 scans/spectrum, ambient temperature, 12 bit digitizer resolution, quadrature detection, both normal and spinning-sideband suppressed spectra (TOSS), recycle delay 3-5 s, contact time 1 ms and 50-80 ms decoupling time. All chemical shifts were reference to TMS via adamantane as a secondary reference.

Spectra taken at lower field at Argonne were obtained at 25.18 MHz using a Bruker CXP-100 spectrometer in the pulse Fourier transform mode with quadrature phase detection. The sample spinners were made of ceramic with an internal volume of 250 μ L and were spun at approximately 4 kHz. Operating parameters in CP experiments included a spectra width of 10 kHz, a 90° proton pulse width of 3.75 μ s (67-kHz proton-decoupling field), an acquisition time of 20 ms, a pulse repetition time of 2s, a contact time of 1.5 ms, and a total accumulation of 1000 transients. In a typical experiment, words of memory were allocated for data acquisition and then increased to 4K (2K real data) by zero filling. Before Fourier transformation of the data, the interferogram was multiplied by a decreasing trapezoidal window function after the first 40 data points. Carbon aromaticities were derived from integrated signal intensities for sp^2 -hybridized (δ 110-160) and sp^3 -hybridized (δ 0-60) carbon absorption bands. For the aromatic carbons, signal intensities of the spinning sidebands were added to the intensity of the centerband. Chemical shifts were referenced to TMS using tetrakis(trimethylsilyl)silane [TKS] as a secondary reference (2).

American coals were obtained from the Argonne Premium Coal Sample Program. For the Canadian coals, homogenized bulk samples representative of the coal deposits from their respective regions were obtained by a bucket auger drill rig. Samples were stored in sealed barrels at low temperatures to minimize long term deterioration. The same samples were used for the NMR measurements on the two instruments to eliminate sample heterogeneity problems for the purposes of this comparison.

RESULTS AND DISCUSSION

Proximate and ultimate analysis of the coals are summarized in Table 1. Apparent aromaticities are given in Table 2 and carbon-13 spin-lattice relaxation measurements are shown in Table 3.

Related studies on proton relaxation at different fields have been reported by Packer et al. (3), Pembleton (4), and Sullivan et al. (5). Dudley and Fyfe (6) discussed carbon relaxation times for a pitch and three Canadian coals. Emphasis was placed on the effects of paramagnetics (including oxygen) in rationalizing the results. Palmer and Maciel (7) reported relaxation parameters for a kerogen concentrate of a Colorado oil shale and Powhatan #5 coal. Aliphatic and aromatic regions exhibited bi-exponential relaxation decay curves for both T_1 and T_2 measurements for the kerogen concentrate. The coal sample was characterized by T_{1C} of 5.8 s for all carbons ($B_0 = 1.4$ T, 21°C). For the kerogen concentrate the effect of the static field strength on the T_{1B} value was also determined. On increasing B_0 from 1.4 T to 4.7 T the proton T_1 increased from about 100 ms to 184 ms. Changing the temperature from ambient to -141C resulted in only a marginal increase in T_1 to 124 ms, whereas the optimum contact time did not change at all.

Figure 2 illustrates the nature of the spectra obtained on a low rank coal (lignite) at the two different field strengths. The 50-MHz CP/MAS spectrum was obtained using sideband suppression (TOSS). No apparent differences in resolution exist under these conditions.

Apparent aromaticities are summarized in Table 2. The average deviation for the ten coals at the two fields is about ± 0.02 units, about equal to the precision

TABLE 1. Ultimate Analysis of Coals.^a

Sample	C	H	N	O	S	A
Beulah-Zap lignite (APCS #8)	72.9	4.83	1.15	20.30	0.70	9.7
Wyodak-Anderson subB (APCS #2)	75.0	5.35	1.12	18.00	0.47	8.8
Herrin hvCB (APCS #3)	77.7	5.00	1.37	13.50	2.38	15.5
Upper Freeport mvB (APCS #1)	85.5	4.70	1.55	13.20	0.74	13.2
Pocahontas lvB (APCS #5)	91.0	4.44	1.33	2.47	0.50	4.2
Ontario lignite	66.9	4.65	0.9	27.23	0.32	4.8
Ardley subB	75.7	4.1	1.2	18.5	0.50	20.0
Smokey Tower subB	75.8	5.1	1.7	16.9	0.50	20.0
Dunvegan hvAB	84.4	5.6	2.1	5.4	2.50	4.4
Gates lvB	93.2	4.63	1.5	0.17	0.50	11.0

^aColumn headings defined as follows: C = % carbon; H = % hydrogen, N = % nitrogen; O = % oxygen; S = % sulfur; A = ash.

TABLE 2. Apparent Carbon Aromaticities of Coals.

Coal	Aromaticity	
	2.3 Tesla CP/MAS	4.7 Tesla TOSS
Beulah-Zap lignite	0.66	0.69
Ontario lignite	0.62	0.61
Wyodak-Anderson subbituminous	0.67	0.63
Ardley subbituminous B	0.74	0.75
Smokey Tower subbituminous A	0.66	0.67
Herrin hvC bituminous	0.72	0.71
Dunvegan hvA bituminous	0.76	0.71
Upper Freeport mv bituminous	0.82	0.81
Pocahontas lv bituminous	0.85	0.86
Gates lv bituminous	0.82	0.82

TABLE 3. Carbon T₁(s) Relaxation in Coals.

Coal	2.3 Tesla		4.7 Tesla	
	Aliphatic	Aromatic	Aliphatic	Aromatic
Beulah-Zap lignite (APCS #8)	0.3 (34%)	0.3 (46%)	0.1 (54%)	0.1 (57%)
	1.7 (66%)	2.4 (54%)	1.9 (46%)	2.0 (43%)
Ontario lignite	0.6 (68%)	0.8 (58%)	0.2 (41%)	0.2 (46%)
	6.7 (32%)	4.7 (42%)	3.3 (59%)	5.0 (54%)
Wyodak-Anderson subbituminous (APCS #2)	0.8 (38%)	0.9 (36%)	0.4 (67%)	0.2 (63%)
	2.1 (62%)	2.2 (64%)	7.5 (33%)	6.0 (37%)
Ardley subbituminous B	---	---	0.6 (45%)	0.7 (46%)
	1.2	1.4	3.0 (55%)	5.2 (54%)
Smokey Tower subbituminous A	0.6 (41%)	0.5 (35%)	0.3 (72%)	0.3 (65%)
	1.2 (59%)	1.6 (65%)	6.1 (28%)	4.5 (35%)
Illinois No. 6 hv bituminous (APCS #3)	1.4 (38%)	3.0 (34%)	0.1 (39%)	0.1 (24%)
	5.5 (62%)	9.9 (65%)	9.2 (61%)	14.7 (76%)
Dunvegan hvA bituminous	3.0 (37%)	6.2 (25%)	0.9 (48%)	---
	5.8 (63%)	13.9 (75%)	22.3 (52%)	25.3
Upper Freeport mv bituminous (APCS #1)	1.2 (60%)	9.0 (9%)	1.5 (38%)	---
	6.9 (40%)	10.2 (91%)	14.8 (62%)	20.6
Pocahontas lv bituminous (APCS #5)	---	4.7 (17%)	0.3 (18%)	0.1 (6%)
	5.6	9.1 (83%)	10.7 (82%)	15.7 (94%)
Gates lv bituminous	---	---	0.4 (38%)	---
	3.5	5.9	9.3 (62%)	15.5

of the aromaticity measurements. The effects of sideband suppression and magic-angle spinning itself on aromaticity measurements of fossil fuels have been discussed previously (8,9). Agreement is reasonably good between aromaticities derived from both normal and sideband suppressed spectra for this series.

More significant deviations in measured aromaticities arise from comparison of values derived from spinning and non-spinning samples (9-12). Line narrowing is found in the strong collision limit ($\omega t \gg 1$) due to effective coherent spatial averaging from magic-angle spinning, as well as in the weak collision limit ($\omega t \ll 1$) due to incoherent averaging from the random molecular motion. In the intermediate regime ($\omega t \approx 1$), where the MAS frequencies are similar to the frequencies associated with the molecular motion of either some or all components of the sample, destructive interference gives rise to severely broadening lines. This phenomenon occurs over a relatively narrow range of spinning frequencies (10,11). A similar destructive interference effect has also been noted between dipolar decoupling frequencies and molecular motion (12). Subject to these considerations, the present data indicate that good agreement can be attained in independent measurements of apparent aromaticities of spinning samples.

The ^{13}C spin-lattice relaxation times (in seconds) and corresponding mass fractions (percentages in brackets) for all samples studied are given in Table 3. Aliphatic and aromatic regions at both field strengths were analyzed separately. Most coals exhibited two-component exponential decays for each region. Differences in relaxation times of these components vary widely (from a factor of about 2 to over 30). Separation of the decays for the more similar relaxation rates gives rise to greater uncertainty in the mass fractions reported, although trends are still discernible as a function of rank.

Figure 3 illustrates one such trend between rank (as denoted by %C) and the ^{13}C T_1 of the long component of the aromatic decay. For the low-rank coals the relaxation time for this fraction is of the order of 2-6 seconds, with the longer relaxation times usually associated with the higher field. Above the 80%C the T_1 difference at the two static field strengths increase significantly for the same sample. In addition, the relaxation times appear to reach a maximum value

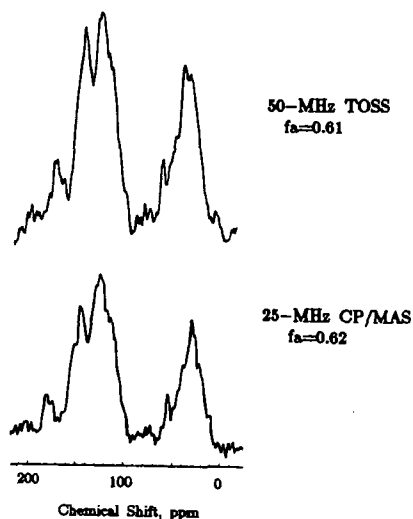


Figure 2. 25- and 50- MHz CP/MAS spectra of Ontario lignite.

at about 85°C. The phenomenon occurs at both fields. A similar trend is observed for the long relaxing component of the aliphatic carbon.

The trends in Figure 3 arise from differences in coal structure that also vary systematically with rank. These compositional variations are reflected in both the field dependence of the measurements and the observation of the maximum. We propose that these data can be related to two general factors: an underlying difference in coal structure as rank increases and the presence of paramagnetic species (oxygen, heavy metal minerals, organic free radicals). In the former case, changes in molecular motion (overall rotational diffusion, local segmental and librational motions) would be manifest as T_1 differences. In the latter instance, paramagnetic species in sufficient quantity could dramatically reduce the T_1 values measured.

A plot of the mass fraction of the long relaxing aromatic component versus %C is shown in Figure 4. At both fields there is a systematic increase in the fraction of species relaxing slowly. This trend may be attributed, in part, to a decrease in the oxygen-rich humic portion of the coals studied with increasing rank. Scatter in mass fraction measurements reflects the relative difficulty of deconvoluting overlapping decays of varying degrees of similarity (and with different signal-to-noise ratios) at the two fields.

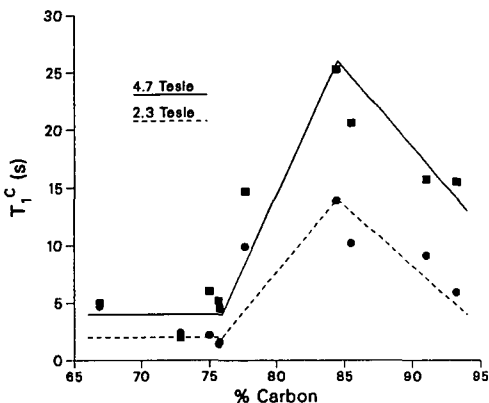


Figure 3. Variation in aromatic carbon relaxation (long) with carbon content of coal.

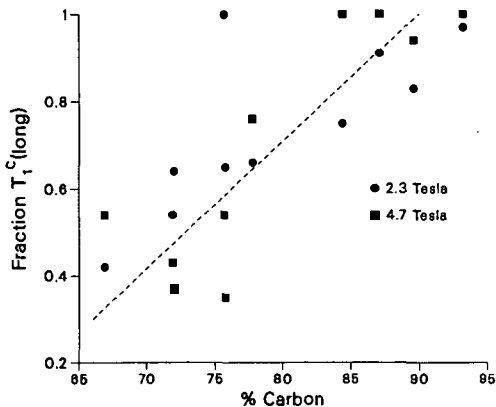


Figure 4. Variation in fraction aromatic T_1^C (long) with carbon content of coal.

As confirmation of the effect of paramagnetic species on our measurements, the Beulah-Zap lignite was treated with a dilute HCl solution to remove iron. The relaxation decay changed significantly as shown in Figure 5. The original two-component decay became a single-exponential decay after treatment, with a concomitant increase in the relaxation time occurring. Atomic absorption data on the HCl washings indicate a significant level of extractable iron in this lignite sample: 1,951 $\mu\text{g Fe/g coal}$. Relaxation discrimination experiments allow the analysis of short and long relaxing components and will be presented.

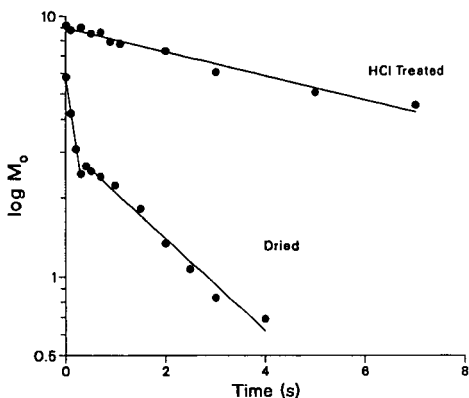


Figure 5. Changes in aromatic carbon T_1 of APCS #8 with acid treatment.

CONCLUSIONS

Spectral resolution is virtually invariant with rank over the static frequency range of 25 to 50 MHz. Although correlations between relaxation times and rank-related parameters are clearly observed at both field strengths, they probably arise from both fundamental changes in coal structure (with increasing degree of coalification) and systematic variations in the nature and extent of paramagnetic species present. The paramagnetic species themselves may represent a combination of stable organic free radicals present in large aromatic ring systems and a distribution of inorganic species, presumably which are chelated to oxygen-rich organic structures (particularly in the low-rank coals). The presence of a maximum in the spin-lattice relaxation time at both fields at 85%C probably reflects these competing interactions.

For the raw, untreated coals there are systematic differences in relaxation times with rank that may be of use in relaxation discrimination experiments.

It remains to be determined how the concentration and exact distribution of paramagnetic species can be quantitatively related to the relaxation rates observed. The rank dependence of these variables is also of ultimate concern for the rationalization of these data.

REFERENCES

1. D. E. Axelson, "Solid State NMR of Fossil Fuels", Multiscience, Montreal, 1985.
2. J. V. Muntean, L. M. Stock, R. E. Botto, J. Magn. Reson., 48, 35 (1988).
3. K. J. Packer, R. K. Harris, A. M. Kenwright, C. E. Snape, Fuel, 62, 999 (1983).
4. R. G. Pembleton, Ph.D. Thesis, Iowa State University, 1978.
5. M. J. Sullivan, N. M. Szeverenyi, G. E. Maciel, "Magnetic Resonance Introduction, Advanced Topics and Applications to Fossil Energy", L. Petrakis, J. P. Fraissard (Eds.), pp. 607-616, D. Reidel Publishing Company, 1984.
6. R. L. Dudley and C. A. Fyfe, Fuel, 61, 651 (1982).
7. A. J. Plamer and G. E. Maciel, Anal. Chem., 54, 2194 (1982).
8. R. E. Botto and R. E. Winans, Fuel, 62, 271 (1983).
9. D. E. Axelson, Fuel, 66, 195-199 (1987).
10. D. Suwelack, W. P. Rothwell, and J. S. Waugh, J. Chem. Phys., 73, 2559 (1980).
11. P. Ollivier and B. C. Gerstein, Carbon, 22, 409 (1984).
12. W. P. Rothwell and J. S. Waugh, J. Chem. Phys., 74, 2721 (1981).

ACKNOWLEDGMENT

This work was performed under the auspices of the Office of Basic Energy Sciences, Division of Chemical Sciences, U.S. Department of Energy, under contract number W-31-109-ENG-38.

THE DETERMINATION OF THE HYDROXYL AND CARBOXYLIC ACID CONTENT OF COAL MACERALS USING COMBINED CHEMICAL AND SPECTROSCOPIC TECHNIQUES

Chol-yoo Choi, John V. Muntean, and Arthur R. Thompson

Chemistry Division, Argonne National Laboratory,
9700 South Cass Avenue, Argonne, IL 60439 and
Department of Chemistry, The University of Chicago,
Chicago, IL 60637

ABSTRACT

Macerals were separated from two high volatile bituminous coals obtained from the Argonne Premium Coal Sample Program and one high volatile bituminous coal from the Pennsylvania State University Coal Sample Bank. A preliminary survey of the nature of these macerals using chemical and spectroscopic techniques are reported. Alkylation using ^{13}C enriched methyl iodide followed by solid ^{13}C NMR analysis were used to determine the concentrations of acidic OH and CH sites in these macerals. The relative quantities of various types of methyl ethers and methyl esters were also estimated from the NMR spectra.

INTRODUCTION

The combined use of alkylation using ^{13}C enriched reagents and solid ^{13}C NMR spectroscopy has been shown to be an effective procedure for the determination of the different types of acidic sites in coals (1-7). Alkylation using tetrabutylammonium hydroxide as base catalyst alkylates the acidic oxygen functional groups in coal such as phenols and carboxylic acids to produce ethers and esters (8). Certain acidic carbon sites in structures such as fluorene, indene, and benzanthrene can also be alkylated under these reaction conditions (3,5). The distinct chemical shift differences of methyls on carbon and oxygen allows the estimation of the relative degree of methylation on oxygen versus carbon. Furthermore, the O-methyl region of the ^{13}C spectra can be resolved into three distinct regions corresponding to the methyl carboxylates, unhindered aryl methyl esters and hindered aryl methyl ethers.

Macerals were separated from three high volatile bituminous coals by density gradient centrifugation (9). The concentration of the various types of hydroxyl and carboxylic acid groups in these macerals as estimated by ^{13}C enriched methylation and solid ^{13}C NMR spectroscopy are reported.

RESULTS AND DISCUSSION

Preliminary Survey. The coals used in this study were obtained from the Pennsylvania State University Coal Sample Bank and the Argonne Premium Coal Sample Program. These were the West Virginia Upper Kittanning seam hvA bituminous coal (PSOC-732), the Utah Blind Canyon seam hvB bituminous coal (APCS-6), and the West Virginia Lewiston-Stockton seam hvA bituminous coal (APCS-7). Maceral groups were separated from these coals using density gradient centrifugation (9). The elemental data for the coals and macerals, which can conveniently be discussed in terms of mole ratios, are shown in Table I. The

H/C values for the macerals follow the order: liptinite > vitrinite > inertinite for the West Virginia Upper Kittanning and the West Virginia Lewiston-Stockton macerals, and resinite > sporinite > vitrinite for the Utah Blind Canyon macerals. Nitrogen is more concentrated in the vitrinites than in the other macerals. The nitrogen content is substantially lower in the Utah Blind Canyon resinite than in the other macerals from this coal, and this finding is in accord with previous reports of other Utah resinites (10,11). The O/C values follow the order: vitrinite - inertinite > liptinite for all the macerals. It should be noted that the oxygen content was calculated by difference from the C, H, N microanalyses. The contributions from sulfur and mineral matter were not taken into consideration even though significant differences in the sulfur content of different maceral types in the same coal have been reported (12-14).

The solid ^{13}C -CP/MAS spectra of the macerals are shown in Figures 1-3. The NMR spectra are scaled to the intensity of the largest signal. The fraction of carbon aromaticity (f_a) in CP/MAS experiments are shown in Table II. Quantitative interpretations of CP/MAS experiments must be made with caution. Recent experiments suggest that f_a values determined by CP/MAS techniques may underestimate the aromatic carbon content of coals and macerals (15).

Hydroxyl and Carboxylic Acid Concentration. The macerals were alkylated with ^{13}C enriched methyl iodide (98% ^{13}C) using tetrabutylammonium hydroxide as the basic catalyst in tetrahydrofuran following Liotta's procedure (8). The degree of alkylation estimated from the elemental data as methyl groups that had been added to each 100 carbon atoms of the maceral group is shown in Table III.

Methylation on carbon occurs to the extent of 10 to 25 percent of the total methyls added to the macerals of the West Virginia Upper Kittanning and Lewiston-Stockton coals. Methylation occurs on carbon to a lesser degree for the macerals of the Utah Blind Canyon coal, as expected for a less mature coal. The observation that less methyls were added on the whole coals rather than the individual macerals of the Utah Blind Canyon and West Virginia Lewiston-Stockton coals may be due to the larger particle size of the whole coals relative to the macerals. Thus, reagent accessibility may be a factor for these alkylations. However, the relative O- vs. C-methylation ratio for the whole coal is similar to that of the vitrinite, which suggests that the alkylatable oxygen and carbon sites are randomly dispersed.

The CP/MAS spectra of the Utah Blind Canyon macerals alkylated with ^{13}C enriched methyl iodide is shown in Figure 4. The O-methylation region of the ^{13}C NMR spectra appear in three distinct regions. The relative contributions of the three regions based on their relative intensities are summarized in Table IV. The most plausible structural elements in methylated coal that give rise to resonances centered at 50 ppm are the methyl carboxylates; centered at 55 ppm are the unhindered aryl ethers; and at 60 ppm are the hindered aryl ethers (16).

Methyl carboxylates represent a major proportion of the O-methylated products of the liptinites from all three coals while little or no methyl carboxylates are detected in the methylated vitrinites or inertinites. The higher concentration of carboxylic acid in liptinites relative to vitrinites have been noted by others using infrared spectroscopy (17-19), but the comparative estimates of the carboxylic acid concentration have not been previously reported for macerals.

The relative intensities of the two resonances centered at 55 ppm and 60 ppm that can be assigned to unhindered methyl ethers and hindered methyl ethers vary between the maceral types. The ratio of hindered methyl ethers to unhindered methyl ethers follow the order: liptinites > vitrinites > inertinites. This is consistent with the notion that this reflects the degree of alkyl substituents on the aromatic structures in these macerals.

ACKNOWLEDGMENTS

We gratefully acknowledge the support of this work by the Office of Basic Energy Sciences, Division of Chemical Sciences, U.S. Department of Energy, under contract number W-31-109-ENG-38. The elemental microanalyses were performed by Steve Newnam of the Analytical Chemistry Laboratory at Argonne National Laboratory. We thank C.A.A. Bloomquist, R.E. Botto, and G.R. Dyrkacz for helpful discussions. This paper is dedicated to the memory of Prof. Peter H. Given.

REFERENCES

1. Liotta, R.; Brons, G. J. Am. Chem. Soc., 1981, 103, 1735-1742.
2. Hagaman, E.W.; Woody, M.C. Fuel, 1982, 61, 53-57.
3. Chambers, R.R., Jr.; Hagaman, E.W.; Woody, M.C.; Smith, K.E.; McKamey, D.R. Fuel, 1985, 64, 1349-1354.
4. Hagaman, E.W.; Chambers, R.R., Jr.; Woody, M.C. Anal. Chem., 1986, 58, 387-394.
5. Botto, R.E.; Choi, C.Y.; Muntean, J.V.; Stock, L.M. Energy Fuels, 1987, 1, 270-360.
6. Hagaman, E.W.; Chambers, R.R., Jr.; Woody, M.C. Energy Fuels, 1987, 1, 352-360.
7. Chambers, R.R., Jr.; Hagaman, E.W.; Woody, M.C. In "Polynuclear Aromatic Compounds"; Ebert, L.B., Ed.; Advances in Chemistry Series 217, American Chemical Society; Washington, D.C. 1988.
8. Liotta, R. Fuel, 1979, 58, 724-728.
9. Dyrkacz, G.R.; Horwitz, E.P. 1982, 61, 3-12.
10. Winans, R.E.; Hayatsu, R.; Scott, R.G.; McBeth, R.L. In "Chemistry and Characterization of Coal Macerals", Winans, R.E.; Crelling, J.C., Eds.; ACS Symposium Series 252, American Chemical Society, Washington, D.C., 1984.
11. Bodily, D.M.; Kopp, V. Prepr. Pap.-Am. Chem. Soc., Div. Fuel Chem. 1987, 32(1), 554-7.
12. Raymond, R., Jr. Proc.-Int. Kohlenwiss. Tag., 1981, 857-862.
13. Dyrkacz, G.R.; Bloomquist, C.A.A.; Ruscic, L. Fuel, 1984, 63, 1367-1373.
14. Tseng, B.H.; Buckentin, M.; Hsieh, K.C.; Wert, C.A.; Dyrkacz, G.R. Fuel, 1986, 65, 385-389.
15. Botto, R.E.; Wilson, R.; Winans, R.E. Energy Fuels, 1987, 1, 173-181.
16. Stock, L.M.; Willis, R.S.; J. Org. Chem., 1985, 50, 3566-3573.
17. Bent, R.; Brown, J.K. Fuel, 1961, 40, 47-56.
18. Allan, J., Ph.D. Dissertation, University of Newcastle upon Tyne, Great Britain, 1975.
19. Dyrkacz, G.R.; Bloomquist, C.A.A.; Solomon, P.R. Fuel, 1984, 63, 536-542.

TABLE I. The Elemental Data of the Macerals Expressed as Molar Ratios.

Maceral Group	H/C	N/C	O/C ^a
<u>West Virginia Upper Kittanning (PSOC-732)</u>			
Whole Coal	0.67	0.015	0.11
Liptinite	0.88	0.012	0.05
Vitrinite	0.71	0.017	0.10
Inertinite	0.56	0.014	0.11
<u>Utah Blind Canyon (APCS-6)</u>			
Whole Coal	0.90	0.016	0.19
Resinite	1.41	0.005	0.05
Sporinite	1.07	0.013	0.13
Vitrinite	0.92	0.016	0.19
<u>West Virginia Lewiston-Stockton (APCS-7)</u>			
Whole Coal	0.75	0.016	0.12
Liptinite	0.97	0.012	0.10
Vitrinite	0.70	0.016	0.13
Inertinite	0.49	0.011	0.12

^aThe oxygen content was determined by difference from the C,H,N microanalyses.

TABLE II. Carbon Aromaticities Estimated by Cross-Polarization NMR.

Maceral Group	f ^a (CP)*
<u>West Virginia Upper Kittanning (PSOC-732)</u>	
Whole Coal	0.78
Liptinite	0.59
Vitrinite	0.79
Inertinite	0.87
<u>Utah Blind Canyon (APCS-6)</u>	
Whole Coal	0.60
Resinite	0.16
Sporinite	0.46
Vitrinite	0.63
<u>West Virginia Lewiston-Stockton (APCS-7)</u>	
Whole Coal	0.74
Liptinite	0.54
Vitrinite	0.76
Inertinite	0.87

*CP Experiments: 2 ms. mix time.

TABLE III. Distribution of Added Methyl Groups as Estimated by Solid ¹³C NMR Spectra.

Maceral Group	Methyl Groups/100°C		
	Total	On Oxygen	On Carbon
<u>West Virginia Upper Kittanning (PSOC-732)</u>			
Whole Coal	4.8	3.8	1.0
Liptinite	6.0	5.0	1.0
Vitrinite	5.2	4.4	0.8
Inertinite	1.6	1.3	0.3
<u>Utah Blind Canyon (APCS-6)</u>			
Whole Coal	1.9	1.8	0.1
Resinite	0.9	0.9	<0.1
Sporinite	2.1	2.0	0.1
Vitrinite	3.1	2.8	0.3
<u>West Virginia Lewiston-Stockton (APCS-7)</u>			
Whole Coal	1.3	1.2	0.1
Liptinite	4.2	3.2	1.0
Vitrinite	3.1	2.8	0.3
Inertinite	2.5	2.0	0.5

TABLE IV. Relative Quantities of Methyl Ethers and Methyl Esters.

Maceral Group	60 ppm	55 ppm	50 ppm
<u>West Virginia Upper Kittanning (PSOC-732)</u>			
Whole Coal	1.1	2.7	0
Liptinite	1.2	2.4	1.4
Vitrinite	1.2	3.2	0
Inertinite	0.2	1.1	0
<u>Utah Blind Canyon (APCS-6)</u>			
Whole Coal	0.7	1.1	0
Resinite	0.3	0.2	0.4
Sporinite	0.9	0.9	0.2
Vitrinite	1.0	1.8	0
<u>West Virginia Lewiston-Stockton (APCS-7)</u>			
Whole Coal	0.4	0.8	0.1
Liptinite	1.5	1.2	0.5
Vitrinite	0.8	1.9	0.1
Inertinite	0.2	1.8	0

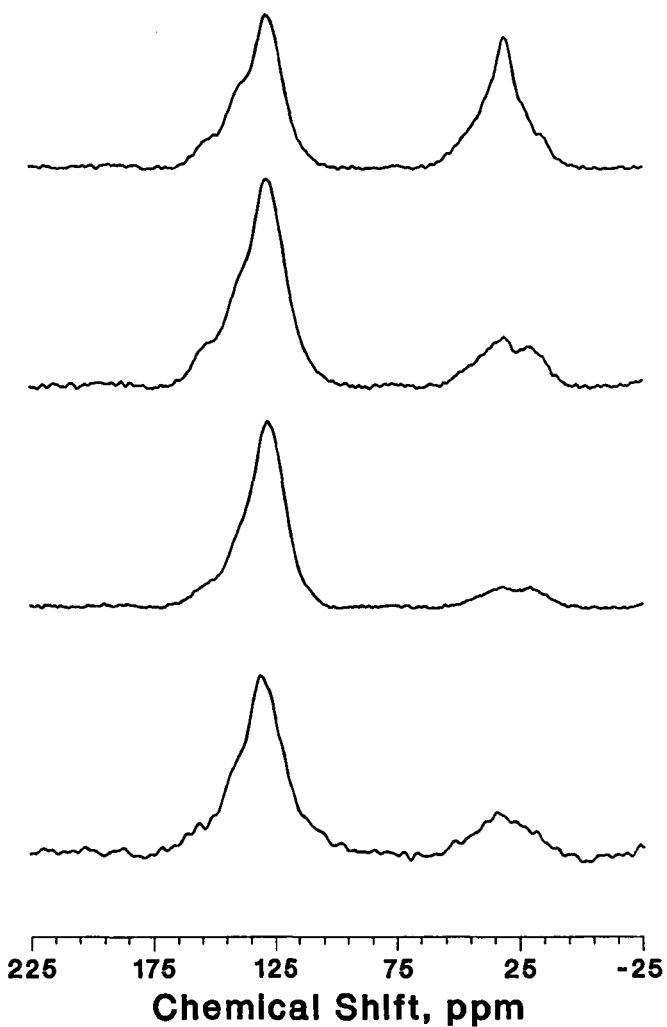


Figure 1. Solid ^{13}C CPMAS spectra of West Virginia Upper Kittanning Coal (PSOC 732). (A) Liptinite; (B) Vitrinite; (C) Inertinite; (D) Whole Coal.

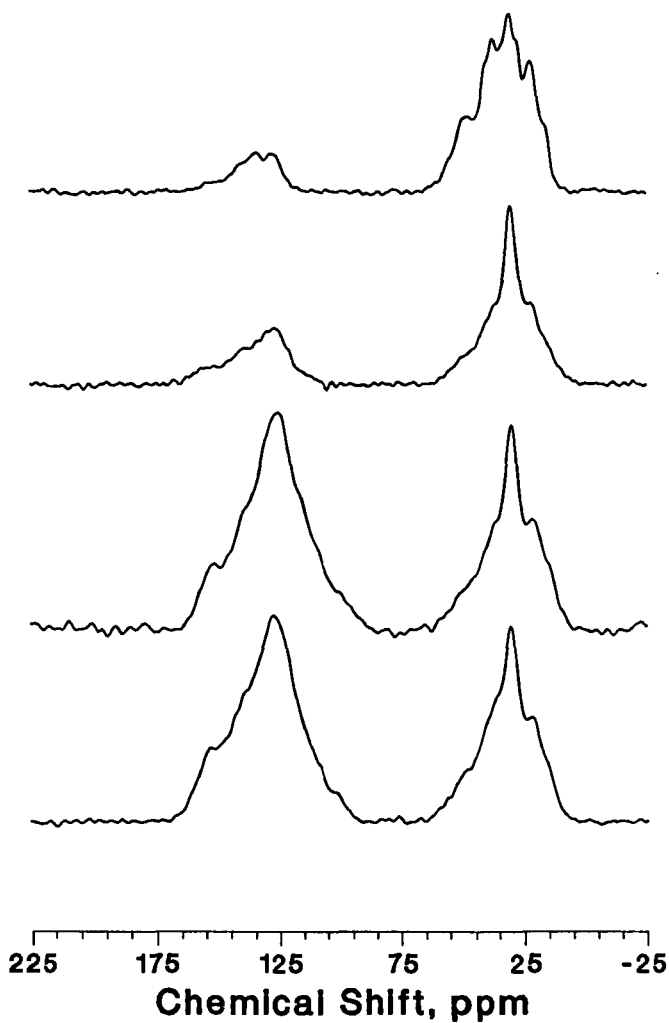


Figure 2. Solid ^{13}C CPMAS spectra of Utah Blind Canyon Coal (APCS #6). (A) Resinite; (B) Sporinite; (C) Vitrinite; (D) Whole Coal.

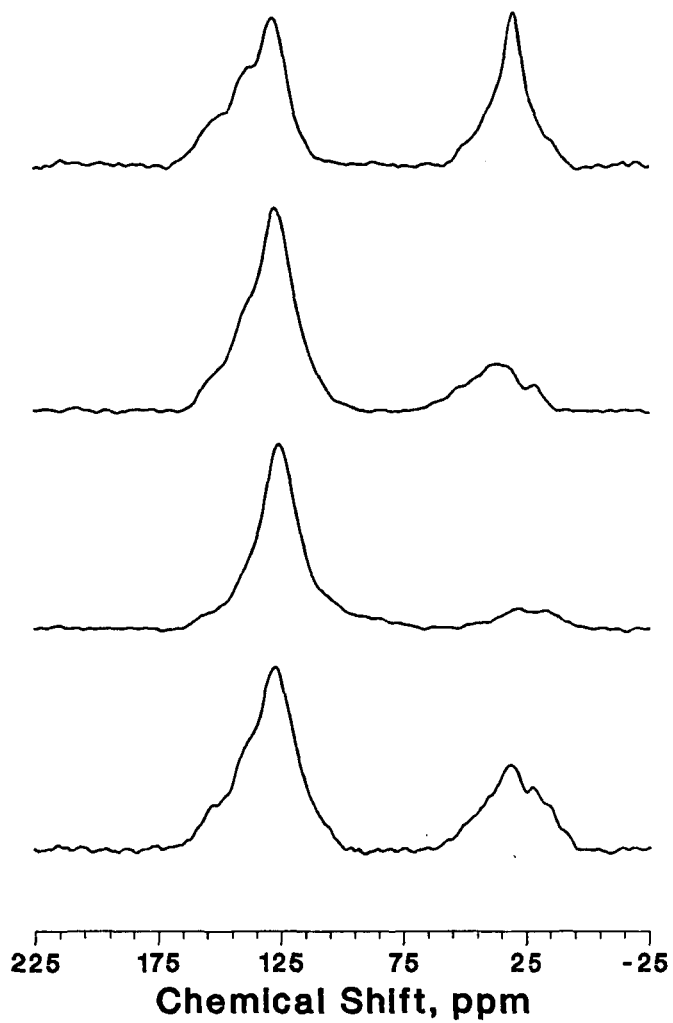


Figure 3. Solid ^{13}C CPMAS spectra of West Virginia Lewiston-Stockton Coal (APCS #7). (A) Liptinite; (B) Vitrinite; (C) Inertinite; (D) Whole Coal.

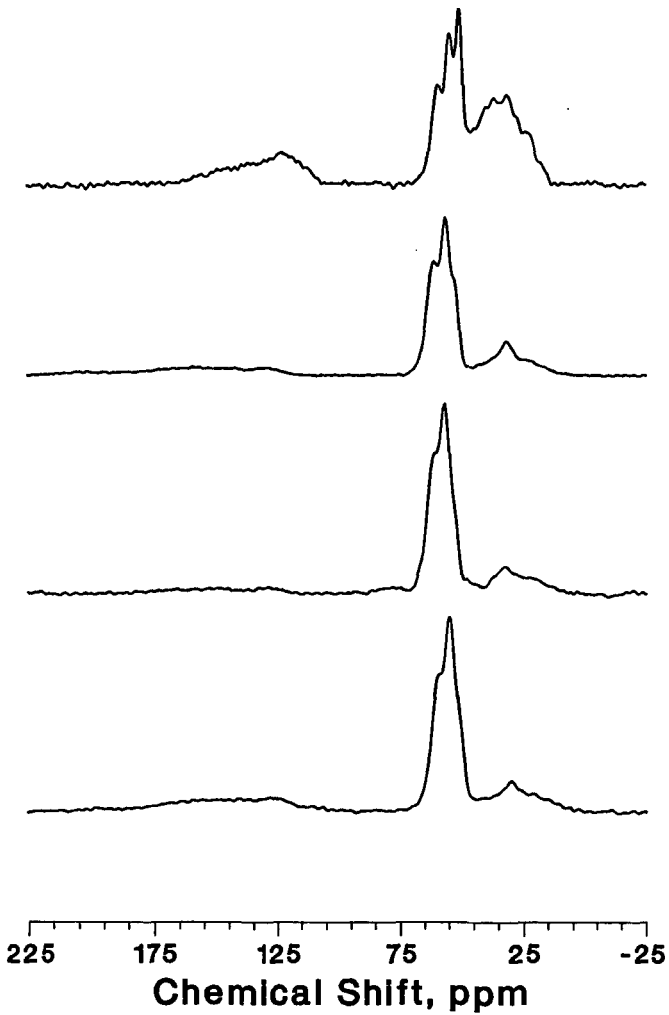


Figure 4. Solid ^{13}C CPMAS spectra of Utah Blind Canyon Coal (APCS #6) methylated with ^{13}C enriched methyl iodide. (A) Resinite; (B) Sporinite; (C) Vitrinite; (D) Whole Coal.

AN INVESTIGATION OF HEATING RATE AND PRESSURE EFFECTS IN COAL PYROLYSIS AND HYDROPYROLYSIS

Jon Gibbins-Matham and Rafael Kandiyoti
Chemical Engineering Department
Imperial College, London SW7 2AZ

INTRODUCTION

The high-pressure wire-mesh apparatus (perhaps best known from work by Anthony^{1,2} and Suuberg^{2,3} at MIT) allows a well-dispersed coal sample to be used, which minimises secondary effects and enables a wide range of heating rates to be applied. Generally, however, the heating rates that have been employed in high-pressure wire-mesh experiments have been limited to about 50 K/s and above by the relatively simple one- or two-stage, fixed-level heating systems that have been used, while the absence of any cooling to prevent reactor components overheating has limited maximum run times to about 30 seconds. In this study it has been possible to extend the investigation of the effects of pressure to heating rates as low as 5 K/s in a wire-mesh apparatus with a computerised feedback temperature control system. Water cooling has also been provided for the parts of the apparatus in contact with the heated sample holder, allowing holding times as long as 200 seconds at 600°C. Preliminary data from the apparatus is presented, showing the effect of heating rate on pyrolysis yields under inert gas pressure and the role of heating rate and holding time at temperature in hydroxyolysis reactions.

SAMPLE PREPARATION

The principal coal used in this study is Pittsburgh No. 8 from the Argonne Premium Coal Sample Program. A single 10 gram sample of -20 mesh coal was used for all experiments. All the sample was ground by hand in air, within about 30 minutes, to pass through a 150 micron sieve and then screened to +100 microns. Some supplementary data is also given for a UK bituminous coal, Linby. This was obtained as washed singles (25 mm sized coal) and was first crushed to approximately 6 mm by hand in air and then ground in a small hammer-mill and sieved to 100-150 microns in a glove-box under nitrogen. The sample used was sealed in a screw-top jar in the glove-box and stored for approximately 18 months in a domestic freezer before use; this had no detectable effect on the pyrolysis yields. Both coal samples were dried overnight under nitrogen at 105°C and stored under flowing nitrogen until required. The analysis of the Linby coal is given in Table I.

EXPERIMENTAL APPARATUS AND METHOD

The high pressure wire-mesh apparatus used in this study is shown in Fig. 1. The wire-mesh sample holder (1) is folded to contain the coal sample between two single layers of 65 micron AISI 304 stainless steel mesh. The sample holder, which also serves as an electrical resistance heater, is held between two electrode/clamps (2 and 3), one of which (3) is sprung to keep the sample holder taut when thermal expansion takes place. Beneath the sample holder is a water-cooled brass plate (4) with a 30 mm diameter hole in it below the working section where the coal sample is spread. A layer of amber mica (5), approximately 0.25 mm thick, electrically insulates the sample holder from the brass plate, while still allowing heat conduction. Another layer of mica (6)

is used to isolate the live electrode (2) which is connected to an insulated terminal (7). Cooling water travels through two hollow support pillars (8) connected to longitudinal holes in the brass plate (4) which communicate in turn with the hollow earthed electrode (3) through two 3.5 mm diameter stainless steel tubes (9), which also act as springs. The base of the pressure vessel (10), the top (11) and the clamping collar (12) are made from 316 stainless steel. The apparatus, with the electrode assembly in position, has been hydraulically tested to 300 bars, giving a 50% safety margin at the maximum pressurising gas cylinder pressure of 200 bars. The gas inlet (13) for helium or hydrogen is a compression fitting sealed with a taper thread in the base. A diffuser (14), consisting of approximately twenty layers of wire-mesh in a brass frame, is provided to break up the jet from the small-bore inlet. Other compression fittings are used for the gas outlet (15) at the top and a pressure tapping (16) in the base.

The regulator on the appropriate gas cylinder is used to set the internal gas pressure in the apparatus. This can be held within about ± 1.5 bars of the desired value, over a range of 20 to 170 bars. The gas flow rate is set by a pressure letdown/flow control valve on the outlet line from the reactor and measured, at atmospheric pressure, by a dry gas meter with an opto-electronic shaft encoder added in-house. By counting the encoder's output pulses on a microcomputer the average flow rate is calculated over ten second intervals.

A sample of 100-150 micron coal is placed in a pre-weighed sample holder which is then stretched between the electrodes. A suction nozzle is used to distribute the coal evenly in an approximately 12 mm diameter circle at the centre of the working section; the suction also serves to remove any particles which can pass through the mesh. The sample holder is then re-weighed to determine the sample size. After the sample holder is replaced in the apparatus two thermocouples are formed, at the edge and centre of the sample respectively, by inserting the thermocouple wires through holes in the mesh. This arrangement avoids distortion of the mesh by welding and, since the short length of mesh between the thermocouple wires is itself part of the thermocouple circuit, unambiguously locates the measuring junction on the surface of the sample holder. Before heating, the system is filled to 100 bars with the working gas and then emptied three times to remove air. The apparatus is then pressurised to the desired value and the flow control valve opened to set the required flow rate of 1 litre/min for every bar of internal pressure. After heating is completed the gas supply is shut off and the internal pressure allowed to come to atmospheric. If hydrogen has been used the apparatus is repressurised to 100 bars with helium and emptied again to avoid the risk of ignition when it is opened. Finally, after the thermocouple wires have been withdrawn, the sample holder is removed and weighed to establish the total volatile yield. Further details of the equipment and experimental methods are given elsewhere for this apparatus⁴ and a very similar wire-mesh reactor for atmospheric pressure and vacuum pyrolysis studies^{5,6}.

When the apparatus was conceived it was hoped to provide a forced sweep of gas through the sample holder, a technique that has been demonstrated successfully in this laboratory for atmospheric pressure operation^{5,6}. This would have given positive removal of the volatiles from the hot zone around the sample holder and allowed tars to be collected in an external trap. Unfortunately, even at 20 bars the cooling effect of gas flowing at only a few cm/s through the sample holder was found to be so intense that uniform temperatures could not be maintained and, because very high power inputs therefore had to be applied, even slight deviations in the local cooling effect could cause severe

overheating and melting of the sample holder material. After extensive trials with various gas flow arrangements the best that could be achieved was to provide a diffuse flow of gas upwards from the base of the vessel at a volumetric flow rate (at the internal pressure) of 1 litre/min. This provides some entrainment of the products and also relieves expansion on heating.

In order to observe the flow patterns and to see whether yields differed from other atmospheric pressure results with a forced sweep gas flow, Linby coal was pyrolysed in helium at atmospheric pressure with the diffuse flow. The high-pressure apparatus was used, but with the steel top replaced by a glass top of similar dimensions. As Fig. 2 shows, the absence of the forced sweep caused only a small reduction in total volatile yields and, since tars could be seen to be recirculated back onto the sample holder by natural convection currents, this reduction was probably due more to secondary re-deposition of the volatiles rather than to a significant increase in the surface mass transfer resistance. Some discolouration of the working section of the sample holder was also observed, which tends to confirm this, but when high pressure hydrogen is used no visible deposit is formed on the sample holder. Any tars which touch the surface apparently crack to form lighter volatiles rather than char. As discussed later, however, a direct test of the effect of sweep velocity at pressure would be desirable.

Even with the diffuse flow regime, heat losses by convection from the sample holder are very large: at 70 bars the power input must be increased approximately five-fold compared to atmospheric pressure operation to hold the temperature steady at the same value and the ratio between convective and other heat losses, which is roughly 1:1 at atmospheric pressure, then rises to about 9:1. With convection so dominant, only slight variations in the gas flow are needed to cause significant (up to about ± 50 K) fluctuations in the local temperature of the sample holder. Although the computer feedback control system can usually hold the average of the readings from the two thermocouples within 20 K or less of the desired value, the instantaneous difference between the individual readings is determined solely by the unsteady physical conditions inside the reactor. Similar fluctuations in temperature at high pressures (measured with a single thermocouple) are reported by Anthony¹, despite the use of an insulated baffle below his sample holder to reduce circulation currents. The temperature fluctuations have a time-scale of the order of 0.2 seconds, so to give reasonably representative time-averages for the peak temperature (rather than a possibly misleading instantaneous value) a significantly longer holding period at peak temperature is generally used. The fluctuations do, however, limit the precision with which the effective transition between a slow-heating stage and a rapid-heating stage can be located, since the control system must be set to start rapid heating when the instantaneous control temperature (i.e., the average of the two thermocouple readings) reaches a specified value.

RESULTS AND DISCUSSION

In order to give the effect of hydrogen pressure on primary coal pyrolysis reactions the greatest possible weighting compared to char hydrogasification reactions a peak temperature of 600°C is used in most of the results presented here. Atmospheric-pressure data obtained in this laboratory for Pittsburgh No. 8^{3,6} and Linby⁴ coals suggest that, for holding times in excess of about 5 seconds, this temperature is high enough for the bulk of the thermally-induced primary breakdown reactions to run to completion. A longer hold time,

10 seconds, was chosen to allow for a possible increase in resistance to volatile transport at elevated pressure, and as Fig. 3 for Linby coal shows, even at 100 bars this appears to give an adequate margin for thermally initiated breakdown reactions. As data presented below (Fig. 7) shows, the hydrogasification reactions carry on for a much longer period. With the standard conditions selected, the effect of heating rate on pyrolysis yields for Pittsburgh No. 8 in hydrogen and helium at 70 bars (1000 psig) was investigated. The results (presented in Fig. 4) showed that at 70 bars the yields in helium appear to be unchanged or to decrease slightly, while yields in hydrogen show a very pronounced fall, from about 52% of the daf sample at 5 K/s to around 47% at 1000 K/s.

Although more data over a range of temperatures and pressures, as well as at lower heating rates, is required to allow firm conclusions to be drawn, the level or slight downward trend with increased heating rate in helium at 70 bars is of interest because previous studies in this laboratory^{5,6} have shown an opposite effect of heating rate in helium at atmospheric pressure, with tar being the main product affected. It was suspected at the time (partly because vacuum pyrolysis showed an even greater sensitivity to heating rate) that tar transport was being enhanced due to the greater sample plasticity and more rapid outward flow of volatiles at high heating rates. While observations suggest that plasticity, if anything, increases with pressure, the volume of the volatile products and hence the rapidity of their outward flow must be reduced by the applied pressure, which may account for the observed equality between fast and slow heating at 70 bars in inert gas.

In addition, the helium results can be regarded as a base-line for the hydrolysis data, showing the purely physical effect of the applied gas pressure. The yield at 5 K/s must then reflect a greater degree of chemical interaction between the hydrogen and the coal, but it cannot be deduced from Fig. 4 whether this is due to hydrogen promoting yields during the initial, rapid volatile release stage of pyrolysis or simply more char gasification occurring in the longer time available (ie. during heating, since hold times are identical) at the slower heating rate.

To investigate the temperature range over which hydrogen was enhancing yields at 5 K/s, two-stage heating was used. The sample holder was heated at 5 K/s to the required intermediate temperature and then immediately heated at 1000 K/s to 600°C and held there for 10 seconds. The results, shown in Fig. 5, suggest that varying the heating rate between 5 K/s and 1000 K/s will have no effect below about 500°C. As discussed earlier, precise resolution of the intermediate temperature is difficult, but it appears likely that there is a gradual transition to the higher yield above 500°C. If the effect had been observed at lower temperatures, before significant amounts of volatiles were evolved, it might have been possible to rule out hydrogasification reactions, but Fig. 6 shows that appreciable amounts of devolatilisation will have taken place by 500°C even at 1000 K/s and differentiation between enhanced primary pyrolysis and hydrogasification is therefore not feasible.

To attempt to distinguish between a possible beneficial effect of a lower heating rate in the later stages of the initial, rapid pyrolysis reactions and more extensive char gasification in the extra 20 seconds available between 500°C and 600°C, the total volatile yields as a function of holding time after 5 K/s and 1000 K/s heating were measured. If it was simply that extra time for hydrogasification is available at 5 K/s then presumably this difference would become less significant at longer holding times and the two sets of data would

converge to the same asymptotic value. In fact, as Fig. 7 shows, while the differences do become less significant at longer hold times, even when yields superficially seem to have reached an asymptotic value at 200 seconds there is still an offset of about 2% of the daf sample.

It is tempting to ascribe the additional 2% of material that apparently can be volatilised by reducing the heating rate from 1000 K/s to 5 K/s to increased interaction between hydrogen and the pyrolysing mass; stabilisation of the heavy tar precursors remaining as the melt start to coke could be a feasible mechanism. The magnitude of the difference is, however, well within the likely experimental scatter and a more detailed study would be needed to allow such a definite conclusion. It would also be possible to explain the apparent trends if slower heating produced a more reactive char, unless the extra products could be analysed and shown not to be able to come from char gasification reactions; more detailed product distribution data, including tar/liquid yields, would be needed for this.

Finally, in all the experiments some coked residue from fluid material that had been evolved from the coal particles could be seen. This was much more noticeable for runs in helium, when globules of charred liquid residue covered large areas of the outer faces of the mesh adjacent to the sample. Hydrogen appears to be giving a higher volatile yield as a result of chemical removal of some of this material, probably before charring takes place. While a sweep flow has been shown to be relatively unimportant at atmospheric pressure and flow rates up to 0.3 m/s, the visible availability of un-removed liquid material suggests that a gas sweep, perhaps at a higher flow, might be able to increase volatile yields by promoting evaporation and possibly entrainment.

ACKNOWLEDGEMENTS

The authors are grateful to many colleagues in the Chemical Engineering Department for assistance with this project, particularly to Dr. G. Saville, Mr. R. King and Mr. T. Meredith for their contributions to the mechanical design and construction of the apparatus and to Mr. R. Wood for the electrical components. The sample of Linby coal was supplied by British Coal, Coal Research Establishment. Financial support was provided by the UK Science and Engineering Research Council under grants GR/B/58962 and GR/D/06582.

REFERENCES

1. Anthony, D. B., Sc.D thesis, MIT, 1974.
2. Howard, J. B., Ch.12 in Chemistry of Coal Utilization, 2nd Supp., (Ed. Elliott, M. A.), Wiley, NY, 1981.
3. Suuberg, E. M., Sc.D thesis, MIT, 1977.
4. Gibbins-Matham, J. R., Ph.D thesis, Imperial College, 1988 (in preparation).
5. Gibbins-Matham, J. R. & Kandiyoti, R., ACS DFC Prepr. 32(4), 1987, 318-323.
6. Gibbins-Matham, J. R. & Kandiyoti, R., Energy & Fuels (accepted for publication).

TABLE I Linby Coal: Proximate and Ultimate Analyses

----- % dry basis -----							
VM	FC	Ash	C	H	O	N	S
36	60	4.0	77.8	5.1	10.1	1.6	1.4

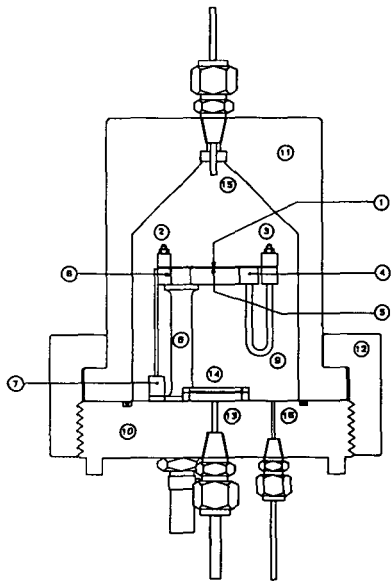


Fig. 1 High pressure wire-mesh apparatus.

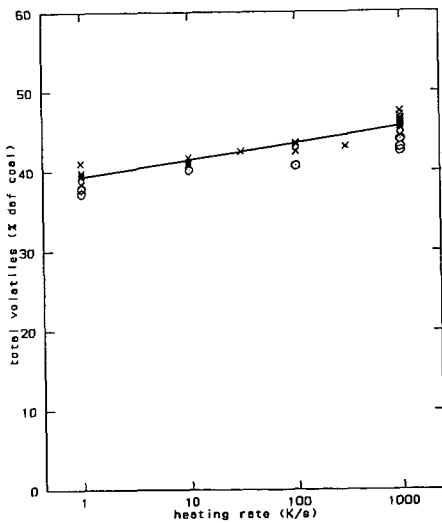


Fig. 2 Effect of 'diffuse flow' regime on total volatile yields from Linby coal heated to 700 deg.C with 30 seconds hold, in helium at 1.2 bars.
x, D.1-0.3 m/s sweep.
O, diffuse flow.

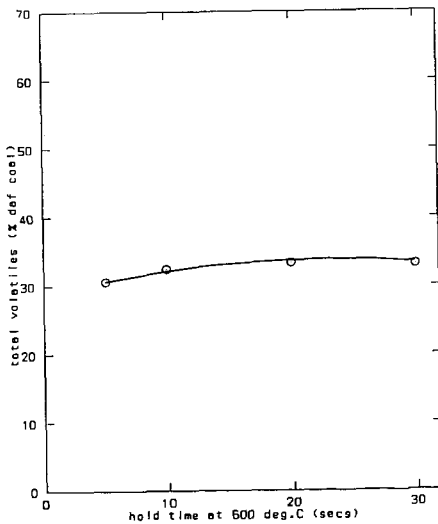


Fig. 3 Effect of hold time at 600 deg.C on volatile yields from Linby coal heated at 625 K/s in helium at 100 bars, diffuse flow.

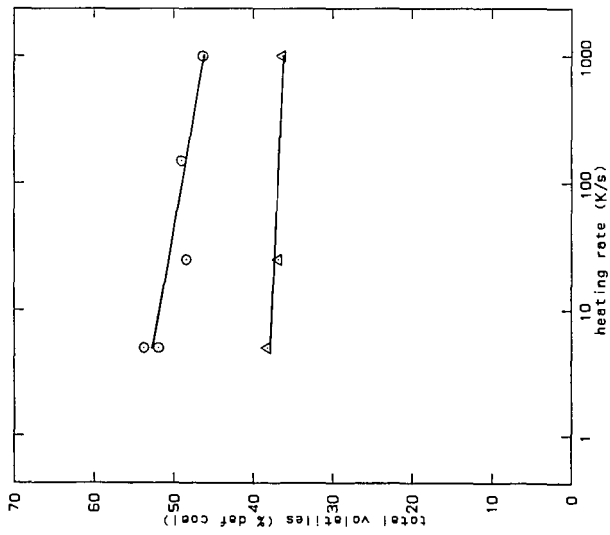


Fig. 4 Effect of heating rate on total volatile yields from Pittsburgh #8 at 70 bars with diffuse flow.
 O, 600 deg.C, 10 s hold, hydrogen.
 Δ, 600 deg.C, 10 s hold, helium.

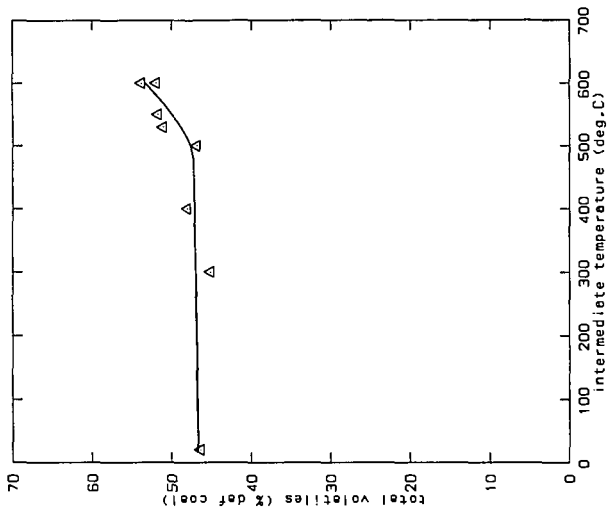


Fig. 5 Effect of intermediate temperature between 5 K/s and 1000 K/s heating on total volatile yields from Pittsburgh #8 in hydrogen at 70 bars.
 Final temperature 600 deg.C, hold time 10 s.

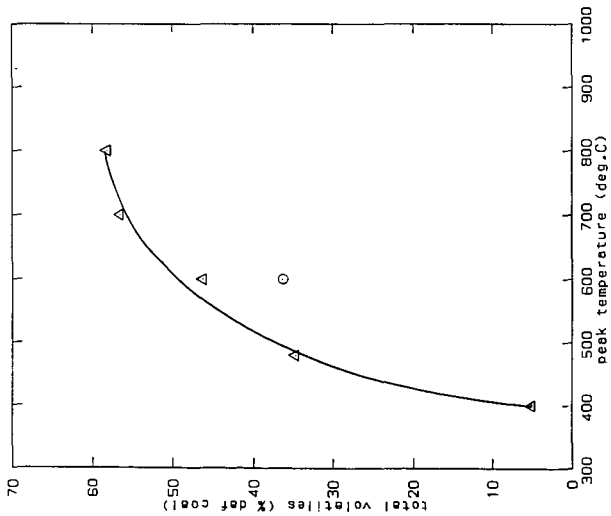


Fig. 6 Effect of peak temperature on total volatile yields from Pittsburgh #8 at 70 bars.
 Δ , 1000 K/s, 10 s hold, hydrogen, diffuse flow.
 \circ , 1000 K/s, 10 s hold, helium, diffuse flow.

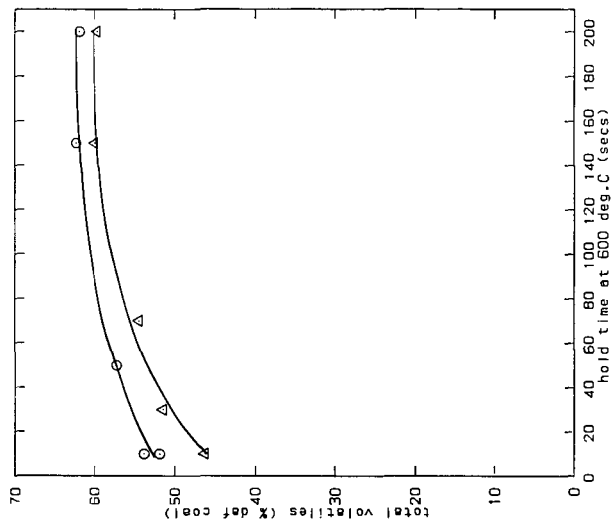


Fig. 7 Effect of hold time at 600 deg.C on total volatile yields from Pittsburgh #8 in hydrogen at 70 bars with diffuse flow.
 Δ , 1000 K/s heating; \circ , 5 K/s heating.

SIMULTANEOUS THERMOGRAVIMETRIC AND MASS SPECTROMETRIC OBSERVATIONS ON VACUUM PYROLYSIS OF ARGONNE PCSP COALS

Yongseung Yun and Henk L.C. Meuzelaar
Center for Micro Analysis & Reaction Chemistry, University of Utah
Salt Lake City, Utah 84112

ABSTRACT

The most serious limitations of many coal gasification and liquefaction models are due to the lack of reliable char and total volatiles yield data, of accurate kinetic parameters, and of reliable data on the composition of the total volatiles in the initial devolatilization step. Consequently, a vacuum thermogravimetry/mass spectrometry (TG/MS) system consisting of a Mettler TA1 Thermoanalyzer and a Finnigan MAT 3200 quadrupole mass filter was built to obtain accurate quantitative and qualitative data on coal devolatilization processes at heating rates in the 10^{-2} - 10^0 K/s range. Hundreds of mass spectra can be obtained during a single TG run, thereby providing detailed information about the concentration of various devolatilization products as a function of temperature while continuously recording the sample weight loss. Moreover, factor analysis-based methods enable deconvolution of overlapping trends and numerical extraction of chemical component spectra. TG/MS results on four Argonne PCSP coals are discussed.

INTRODUCTION

Previous mass spectrometric studies of coal devolatilization phenomena in our laboratory [1, 2, 3] have focussed on the use of Curie-point pyrolysis mass spectrometry (Py-MS) techniques using heating rates in the 10^2 - 10^4 K/s range. This enabled Chakravarty *et al.* [1] to identify at least four structural components with distinct kinetic profiles in an ANL-PCSP Pittsburgh #8 coal: (1) a relatively minor vacuum distillate fraction consisting primarily of alkylsubstituted one- and two-ring aromatic hydrocarbons; (2) a sporinite-like fraction consisting of branched and/or alicyclic hydrocarbon components; (3) a cutinite- or alginite-like polymethylenic component; and (4) a vitrinite-like component consisting primarily of alkylsubstituted hydroxyaromatic and aromatic moieties. Attention was drawn to the fact that only the two aliphatic components appeared to exhibit a simple depolymerization behavior consistent with the idea of a first-order unimolecular decomposition reaction. The vacuum distillate component was thought to be more appropriately described by a reaction order between 0 and 1, whereas the vitrinite-like component appeared to behave like a char-forming thermoset, and thus, should be described by a reaction order considerably greater than 1. Attempts to obtain more accurate kinetic parameters, however, were only partially successful due to the very short reaction times involved (approx. 8 s) and the significant broadening of the product evolution profiles by diffusion processes between the pyrolysis zone and the ionization region.

In order to overcome this problem we decided to build a vacuum thermogravimetry/mass spectrometry (TG/MS) system capable of precisely controlling heating rates in the 10^{-2} - 10^0 K/s range while providing accurate temperature and weight loss information and simultaneously recording the evolution profiles of gas and tar products.

Vacuum TG/MS experiments with coals have been reported previously by Ohrback *et al.* [4, 5]. However, in the experiments reported here we were especially interested in using the set of eight standard coals available from the Argonne National Laboratory Premium Coal Sample Program (ANL-PCSP) in order to enable direct comparison with TG/FTIR experiments performed by Serio *et al.* [6], as well as to enable reproduction of our experiments by other researchers. Moreover, since most of our extensive Py-MS data on U.S. coals [7, 8, 9] has been obtained under low voltage (approx. 12-14 eV) electron ionization conditions, we wanted to perform the TG/MS analyses under comparable ionization conditions.

Finally, an important goal of the experiments reported here was to use sophisticated multivariate analysis techniques, as developed by Windig *et al.* [10], in order to deconvolute overlapping trends in the TG/MS data and to identify the underlying chemical components.

At the time of writing, only 4 of the 8 ANL-PCSP coals have been analyzed and a full report of the results on all 8 coals will be published elsewhere.

EXPERIMENTAL

Four ANL ampule samples (Pittsburgh #8 (-100 mesh), Illinois #6 (-100 mesh), Wyodak (-20 mesh), Beulah-Zap (-100 mesh)) were employed in vacuum TG/MS runs and the ultimate analysis data of the samples were described elsewhere [11]. The TG/MS system (Figure 1) consists of a Mettler TA1 Thermoanalyzer directly interfaced to a small Finnigan MAT 3200 quadupole mass filter. Pyrolysis was performed directly in front of the ion source of the mass spectrometer in order to prevent recombination reactions and/or secondary decomposition of reactive compounds as well as to minimize the loss of polar compounds through condensation. A turbomolecular pump (Balzers TPU 050) was used for evacuating the MS chamber up to 4×10^{-7} torr in 7-8 minutes. In addition, two diffusion pumps were employed to maintain a pressure of less than 1×10^{-4} torr in the TG balance chamber. Moreover, the LN₂ cold trap in Figure 1 was used to guarantee a low background signal level in the mass spectra. A detailed description of time-resolved Curie-point pyrolysis MS (TR Py-MS) can be found elsewhere [2].

Sample aliquots of approximately 4-5 mg were heated under vacuum ($3-6 \times 10^{-7}$ torr) while the temperature was increased from ambient to 700°C at 25°C/min. MS conditions were as follows: electron impact energy 14 eV, mass range scanned m/z 33 to 193 (m/z 48-193 for Pittsburgh #8 seam coal), total number of scans 80, and total scan time 27 minutes. Each spectrum scanned was stored separately in the memory of an IBM 9000 computer.

Factor analysis was employed to deconvolute overlapping time trends and to numerically extract the chemical component spectra. In order to give all the variables an equal contribution, factor analysis was done on the correlation around the origin matrix. Deconvolution was performed by using a combination of pure mass [12, 13] and variance diagram (WARDIA) [10, 14] techniques.

RESULTS AND DISCUSSION

The time-integrated low voltage mass spectra of Pittsburgh coal obtained by TG/MS and by TR Py-MS are highly similar with regard to type and relative abundance of the pyrolysis products (as shown in Figure 2) in spite of a

factor 3×10^2 difference in heating rate and a factor 2×10^2 difference in sample size, as well as differences in pyrolysis technique, ion source, quadrupole, etc. In fact, since Curie-point Py-MS patterns obtained at heating rates of 6×10^4 K/s and 1×10^2 K/s are highly similar too (not shown here), we can conclude that the mechanisms of primary coal devolatilization reactions appear to be independent of heating rate over at least five orders of magnitude (10^{-1} - 10^4 K/s range).

The main differences between the TG/MS and TR Py-MS data on Pittsburgh #8 coal in Figure 1 appear to be the much larger SO_2^+ and HSSH^+ signals (due to the higher end temperature of the TG/MS system; similar SO_2 increases can be seen when using higher temperature Curie-point wires), and the somewhat increased dihydroxybenzene. The dihydroxybenzene intensities in the TR Py-MS spectrum can be increased by preheating the pyrolysis chamber. Hydroaromatics (e.g. tetralins) tend to form relatively late during the devolatilization process, therefore the higher end temperatures explain their increased abundance in the TG/MS spectrum.

The sharp evolution profile and the constant evolution temperature of SO_2 , as illustrated in Figure 3, offer exciting possibilities for controlling the final distribution of sulfur between the char and the gas phase (e.g., in low temperature gasification and/or liquefaction processes). However, we do not see the very early SO_2 components shown by Serio *et al.* [6] in TG/FTIR. Possibly, the FTIR signal shows interference from a different compound.

Four factors were employed to deconvolute overlapping trends in total ion count profiles from TG/MS. The eigenvalues and variances explained by the first six factors are illustrated in Table 1, showing that the first four factors can explain approx. 98% of total variance for each coal. Our deconvoluted data provide a strong indication for the presence of two kinetically distinct pyrolysis regimes (under our TG conditions at approx. 370-380°C and at 420-440°C, respectively). Whereas each of these regimes may indeed be relatively independent of rank as suggested by Serio *et al.* [6], the "vitrinitic component" (m/z 124/138) appears to shift from the lower to the higher temperature regime with increasing rank. The aliphatic hydrocarbon component always pyrolyzes in the higher regime. The following hypothesis for these observations would be possible: the two temperature regimes represent ether bridges (or other weak bonds) and methylenic bridges, respectively. In liptinites such as alginites or cutinites methylenic bridges are present from the beginning (and thus already in low rank coals). In vitrinitic macerals derived from lignin-like structures the initial bridges are primarily ether type. With increasing rank these are "replaced" by methylenic bridges (or perhaps lost through CO elimination with consequent formation of new methylenic cross-links).

The rank dependent shift in the ratio of aromatic vs. terpenoid (isoprenoid) structure reported by Blazso *et al.* [15] was also confirmed by our findings (disappearance of m/z 191 component, appearance of m/z 156 component).

The rank dependent appearance of the "oil formation" window in high volatile A and B bituminous coal [1] is evident in Pittsburgh #8 coal. Perhaps this could be called "geothermal pyrolysis". However, the relatively aromatic oil formed does not appear to contain many polymethylenic moieties (contrary to the suggestion by Serio *et al.* [6]). Also the term "guest molecules" is an obvious misnomer. These are not "guests" but "offspring" (sons or

daughters). The TG/DTG curves (only shown DTG curve in this preprint) show only very small quantities of these vacuum distillable components. This can be explained as follows: assume that the total amount is only a few percent of dry coal weight and that the total tar yield is approx. 20%, then (e.g., 30% gas, 40% char, 10% ash) the vacuum distillable "bitumen" could still be as much as approx. 10% of the tar.

Although SO₂ evolution appears to coincide with the end of the main tar formation phase (and/or onset of the char formation process) neither the origin nor the mechanistic significance of the SO₂ evolution are entirely clear at present.

It should be pointed out here that the charring stage is strongly underrepresented in our study due to the limited lower mass range ($\geq m/z$ 34) and the low voltage EI conditions (low MW pyrolysis products tend to have higher ionization potentials). Further TG/MS runs are planned to investigate low MW pyrolysis products.

ACKNOWLEDGEMENTS

This work was sponsored by the Advanced Combustion Engineering Research Center. Funds for this Center are received from the National Science Foundation, the State of Utah, 23 participants and the U.S. Department of Energy.

REFERENCES

1. Chakravarty, T., H.L.C. Meuzelaar, W. Windig and G.R. Hill, ACS Preprints (Div. of Fuel Chem.), 32(3) 1988, 211-216.
2. Jakab, E., W. Windig, and H.L.C. Meuzelaar, Energy and Fuels, 1(2), 1987, 161-167.
3. Jakab, R., B. Hoesterey, W. Windig, G.R. Hill and H.L.C. Meuzelaar, Fuel, 67, 1988, 73-79.
4. Ohrback, K.H. and A. Kettrup, ACS Preprints (Div. of Fuel Chem.), 29(2), 1984, 12-19.
5. Ohrback, K.H., A. Kettrup and G. Radhoff, J. of Analytical and Applied Pyrolysis, 8, 1985, 195-199.
6. Serio, M.A., P.R. Solomon and R.M. Carangelo, ACS Preprints (Div. of Fuel Chem.), 33(2), 1988, 295-309.
7. Meuzelaar, H.L.C., A.M. Harper, G.R. Hill and P.H. Given, Fuel, 63, 1984, 640-652.
8. Harper, A.M., H.L.C. Meuzelaar and P.H. Given, Fuel, 63, 1984, 793-802.
9. Metcalf, G.S., W. Windig, G.R. Hill and H.L.C. Meuzelaar, Int. J. of Coal Geology, 7, 1987, 245-268.
10. Windig, W. and H.L.C. Meuzelaar, Anal. Chem., 56, 1984, 2297-2303.
11. Vorres, K.S., ACS Preprints (Div. of Fuel Chem.), 32(4), 1987, 221-226.
12. Knorr, F.J. and J.H. Futrell, Anal. Chem., 51, 1979, 1236-1241.
13. Malinowski, E.R. and D.G. Howery, Factor Analysis in Chemistry, John Wiley & Sons, 1980, New York.
14. Windig, W., E. Jakab, J.M. Richards, and H.L.C. Meuzelaar, Anal. Chem., 59, 1987, 317-323.
15. Balzso, M., T. Szekely, F. Till, G. Varhegyi, E. Jakab and P. Szabo, J. of Analytical & Applied Pyrolysis, 8, 1985, 255-269.

TABLE 1
 VARIANCE EXPLAINED BY THE FIRST SIX FACTORS OBTAINED BY PRINCIPAL COMPONENT
 ANALYSIS OF THE CORRELATION AROUND-THE-ORIGIN MATRIX FOR EACH TG/MS DATA SET

Factor Number	Pittsburgh #8		Illinois #6		Wyodak		Beulah-Zap	
	Eigen-value	% variance	Eigen-value	% variance	Eigen-value	% variance	Eigen-value	% variance
1	119.99	87.27	138.07	88.29	135.92	87.39	129.53	84.32
2	7.02	5.11	8.33	5.33	8.92	5.74	12.46	8.11
3	5.07	3.68	4.43	2.83	5.29	3.40	6.66	4.33
4	2.43	1.77	3.47	2.22	2.99	1.90	2.83	1.85
5	1.74	1.27	1.38	0.88	1.48	0.95	1.31	0.85
6	1.23	0.90	0.71	0.46	0.92	0.59	0.83	0.54

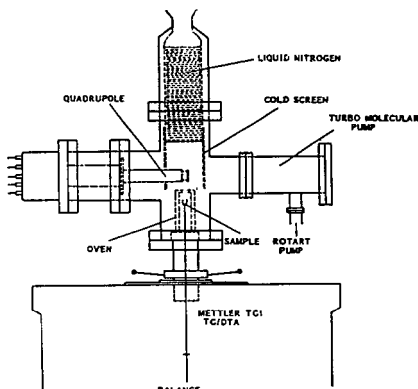


Figure 1. Schematic diagram of vacuum TG/MS system, based on the combination of a Mettler TA1 TG/DTA system and a Finnigan MAT 3200 mass spectrometer with specifically designed vacuum housing.

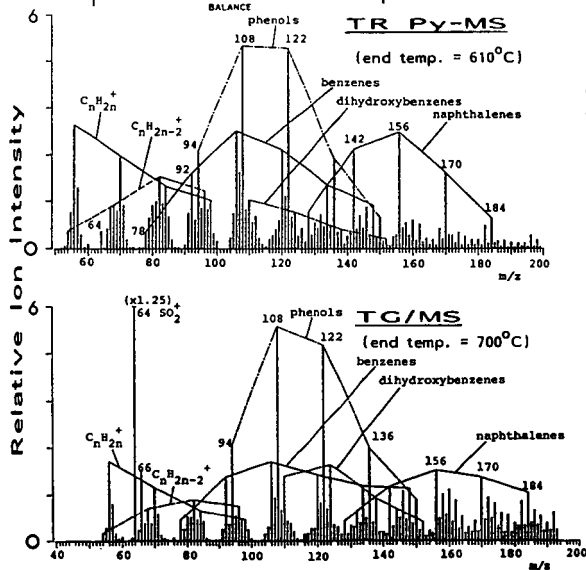


Figure 2. Time-integrated spectrum obtained by summing all 41 (TR Py-MS), 80 (TG/MS) spectra scanned on Pittsburgh #8.

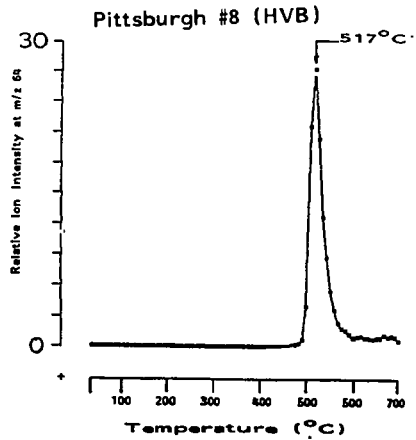
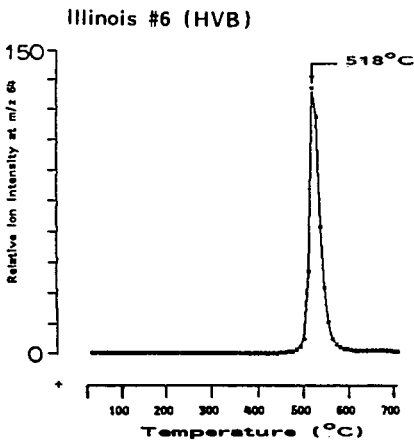
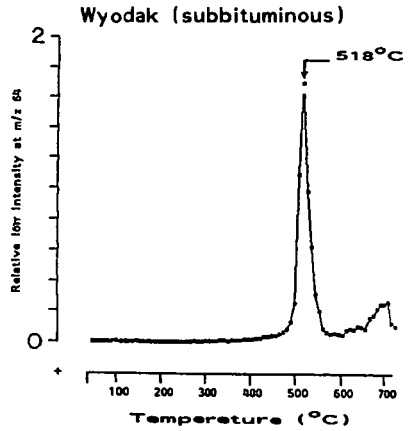
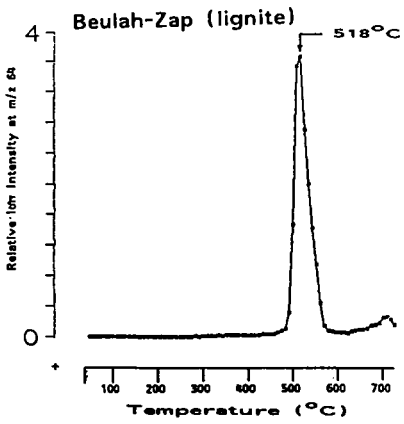


Figure 3. Evolution profiles of m/z 64 (SO_2^+) for four ANL-PCSP coals. Note the similar evolution profile and maximum evolution temperature independent of rank.

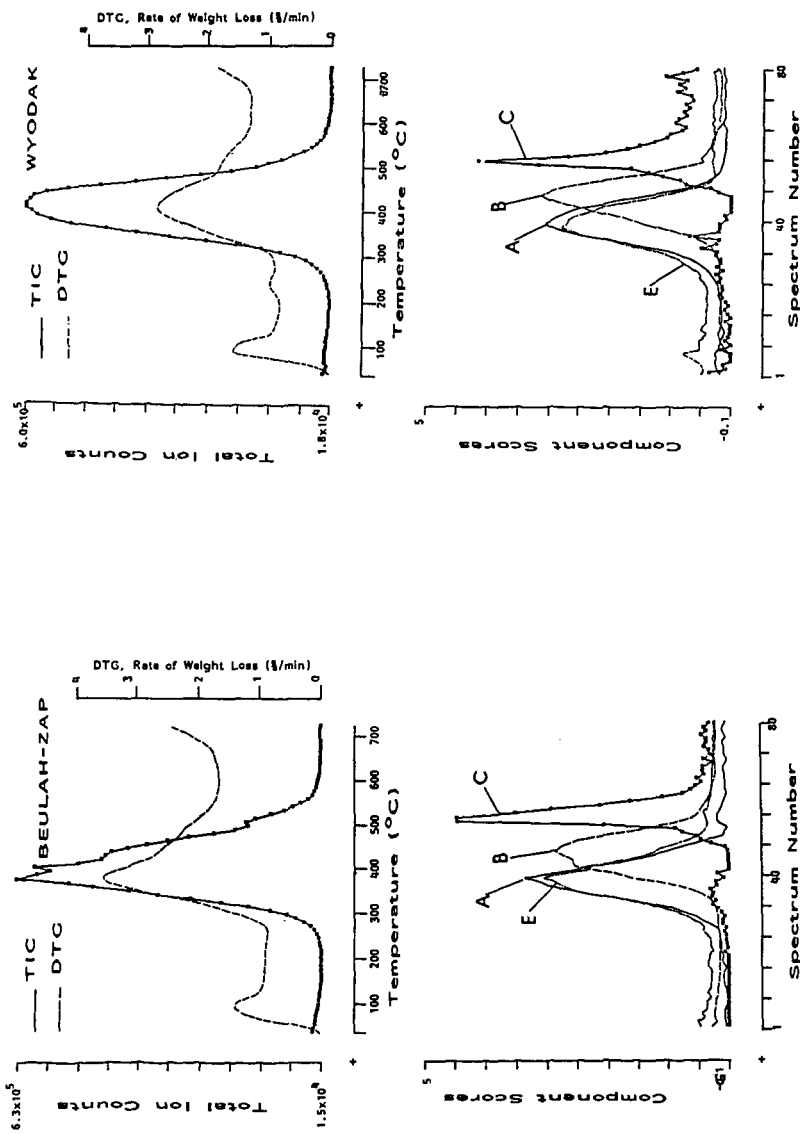


Figure 4. TIC, DTG profiles with temperature and the corresponding deconvoluted components (A,B,C,E) for Wyodak, Beulah-Zap coals. The numerically extracted ("deconvoluted") spectra of each component are shown in Figure 6. Mainly component A consists of dihydroxybenzenes, component B aliphatics + phenols, component C SO₂, component E terpenoid fragments.

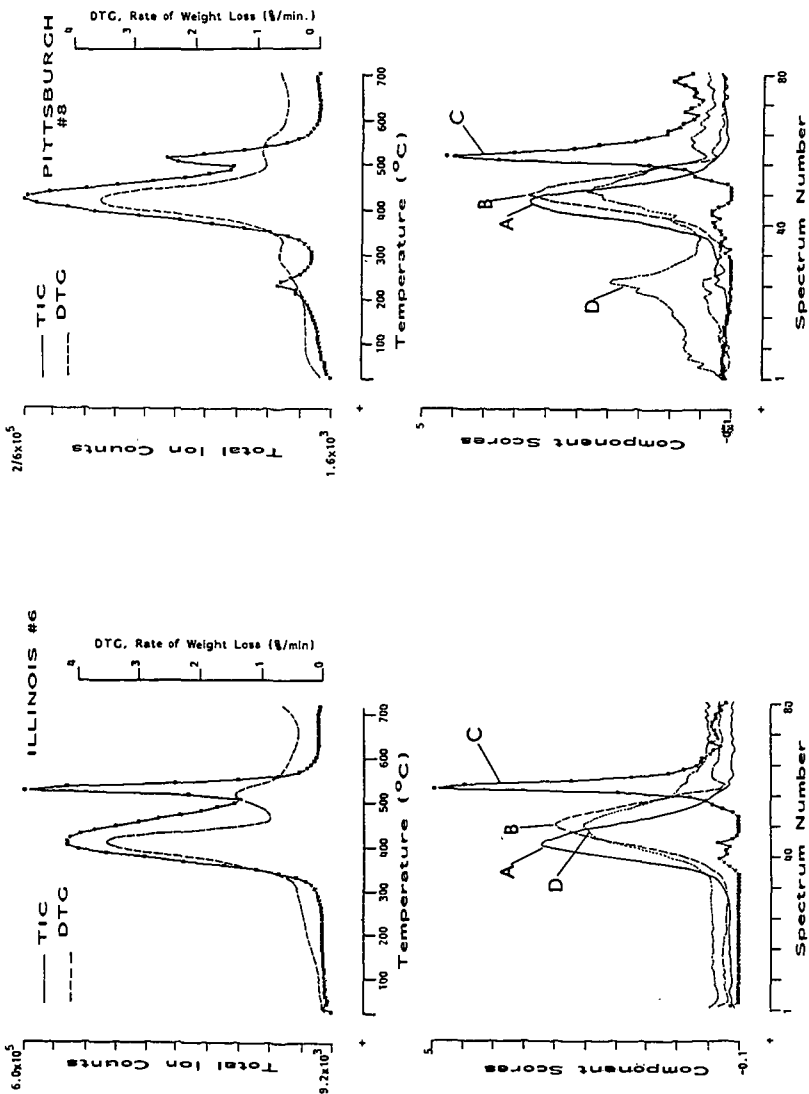


Figure 5. TIC, DTC profiles with temperature and the corresponding deconvoluted components (A, B, C, D) for Illinois #6, Pittsburgh #8 coals. The numerically extracted ("deconvoluted") spectra of each component are shown in Figure 7. Mainly component A consists of dihydroxybenzenes, component B aliphatics + phenols, component C SO_2 , component D bitumen (benzenes + naphthalenes).

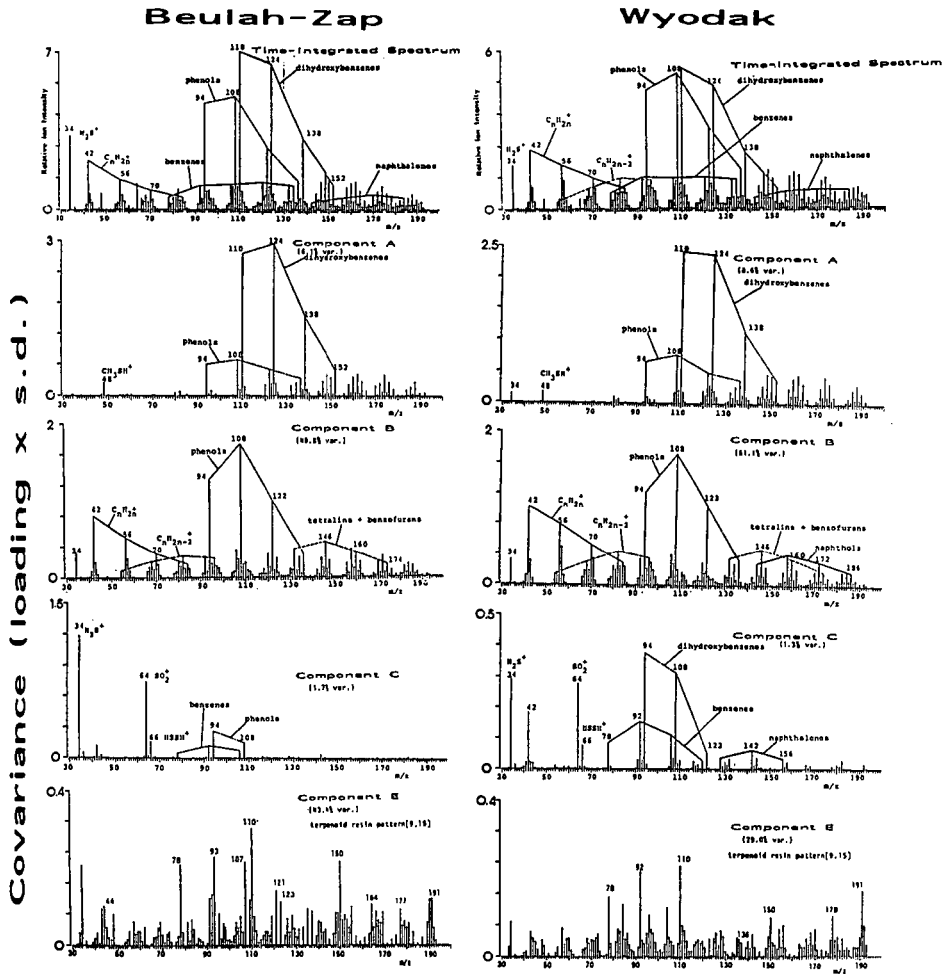


Figure 6. Time-integrated spectra obtained by summing all 80 spectra scanned during TG/MS runs and numerically extracted ("deconvoluted") spectra of the four components shown in Figure 4 for Beulah-Zap and Wyodak coals.

Illinois #6

Pittsburgh #8

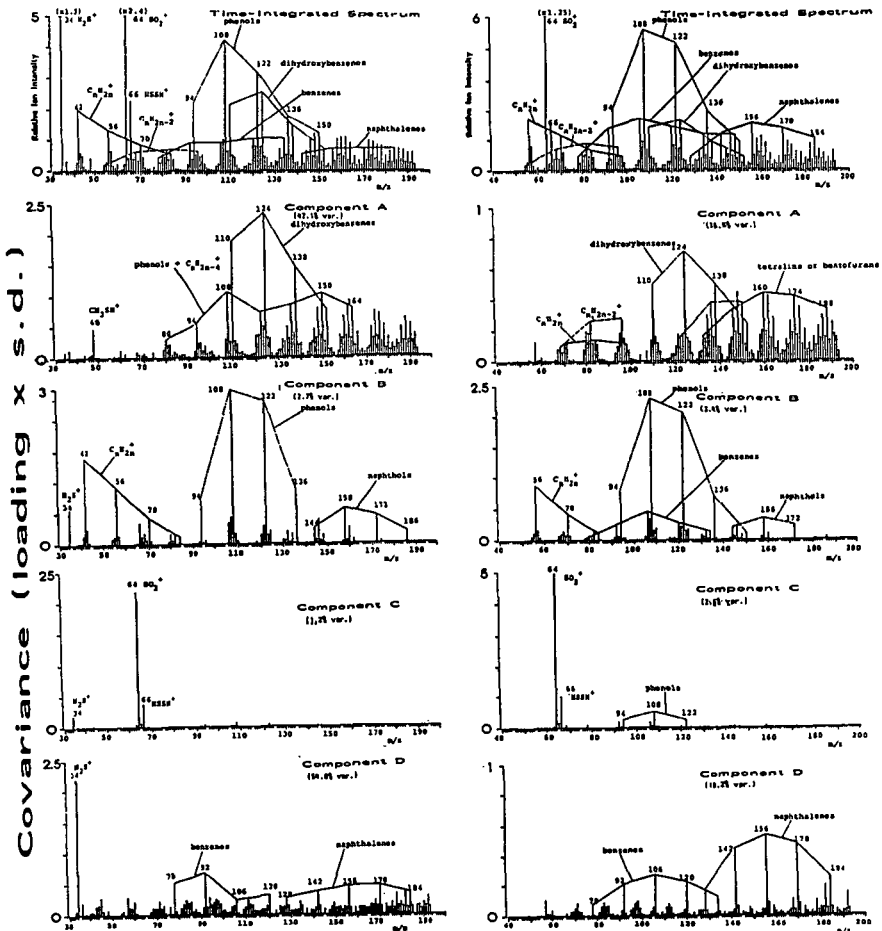


Figure 7. Time-integrated spectra obtained by summing all 80 spectra scanned during TG/MS runs and numerically extracted ("deconvoluted") spectra of the four components shown in Figure 5 for Illinois #6 and Pittsburgh #8 coals.

CHARACTERIZATION OF THE ARGONNE PREMIUM COAL SAMPLES BY PYROLYSIS HIGH RESOLUTION MASS SPECTROMETRY

Randall E. Winans, Robert L. McBeth and Paul H. Neill
Chemistry Division, Argonne National Laboratory, Argonne, IL 60439

INTRODUCTION

The complete set of Argonne Premium Coal Samples have been characterized using Pyrolysis High Resolution Mass Spectrometry (PyHRMS). A major objective in the study is to examine differences in the heteroatom (oxygen, sulfur and nitrogen) containing molecules as a function of rank of the coals. Operating in the high resolution mode makes it possible to directly separate these species from each other and from the hydrocarbon molecules. In addition, many molecules, which can not be observed with gas chromatography by virtue of their size or polarity, can be observed with this method.

We have applied PyHRMS to characterization of separated coal macerals and coal degradation products.¹⁻³ There are many papers on low resolution PyMS applied to coals^{4,5} and one applied to these premium coals.⁶ The PyMS approach can provide very detailed information on the molecules which are released in vacuum pyrolysis, however the probability of secondary reactions is a consideration and all interpretation must be made with this fact in mind. This approach yields more specific molecular data than any other method. A problem with low resolution PyMS is that in many if not most cases there may be several ions present with the same nominal mass but with different chemical compositions. This problem is eliminated by using an high resolution spectrometer which may scan more slowly, but will resolve peaks which overlapped at lower resolution and yield more information.

EXPERIMENTAL

The samples have been obtained from the Argonne Premium Coal Sample Program and the preparation of the samples has been described.⁷ The appropriate elemental analysis for the samples is presented in Table 1. A second set of samples was obtained by extracting the original coals in refluxing pyridine under a nitrogen atmosphere. The residue was washed with dilute aqueous HCl and with methanol and dried *in vacuo* at 60°C.

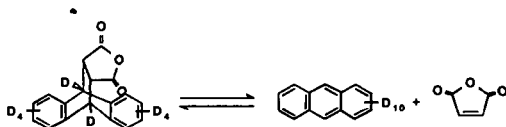
TABLE 1. Elemental Analysis for the Fresh Coal Samples.

Sample	Name	%C(maf)	Per 100 Carbons				Ash
			H	N	S	O	
1	Upper Freeport mvB	85.5	66.0	1.55	0.32	6.59	13.20
2	Wyodak-Anderson SubB	75.0	85.6	1.28	0.23	18.00	8.77
3	Herrin hvCB	77.7	77.2	1.51	1.15	13.03	15.50
4	Pittsburgh hvAB	83.2	76.7	1.69	0.40	7.96	9.25
5	Pocahontas lvB	91.0	58.5	1.25	0.21	2.04	4.23
6	Blind Canyon hvBB	80.7	85.7	1.67	0.17	10.78	4.71
7	Stockton-Lewiston hvAB	82.6	76.3	1.62	0.30	8.93	19.80
8	Beulah-Zap Lignite	72.9	79.5	1.35	0.36	20.88	9.72

Both sets of samples, fresh coal and extract residue, were pyrolysed under the same conditions, in an all glass heated inlet system (AGHS), rapidly to 600°C. The inlet system was designed in this laboratory to use a quartz pyrolysis probe fitted with a platinum grid which was heated by a computer controlled DC power supply. The inlet system was thermostated at 300°C and a silicon-carbide leak metered the sample into the mass spectrometer. An internal standard has been used which was the Diels-Alder adduct of D¹⁰-anthracene and maleic anhydride prepared from the two reactants in refluxing p-xylene. The spectrometer, a Kratos MS-50, was operated at 40,000 dynamic resolving power scanning at 100 sec/decade, with an EI source set at 70 eV. The resulting data (10 scans) were averaged and sorted according to heteroatom content and hydrogen deficiency (Z number = number of double bonds + rings).

RESULTS AND DISCUSSION

The internal standard is very important for comparing the results of the PyMS between the different rank coals. It allows a more quantitative comparison, while ideally not participating in any secondary reactions. Our standard appears to function very well. The Diels-Alder product shown below undergoes a thermally induced retro-reaction very cleanly at approximately 300°C to yield D¹⁰-anthracene quantitatively. In the precise mass measurement mode it is easy to separate this ion from the coal pyrolysis products. All of the data presented in this paper have been normalized to this standard. Since this standard is



released at a lower temperature than the coal pyrolysis there is no evidence for deuterium scrambling. The peaks resulting from the standard are excluded from the final averaged spectra and from the Z number and heteroatom analysis. In the analysis the following heteroatoms or combination of heteroatoms were searched for: none, oxygen, two oxygens, three oxygens, sulfur, two sulfurs, sulfur-oxygen, sulfur-nitrogen, and nitrogen. Typically, peaks accounting for greater than 90% of the total ion current can be assigned reasonable formula. This approach has been used to characterize petroleum and coal liquids and has recently been described in detail.⁸

A typical averaged spectra is shown in Figure 1 for the fresh Illinois Herrin Seam coal (APCS #3). Note that there are a significant number of peaks at m/z ratios greater than 200, which is characteristic for all the high volatile bituminous coals. Hydrocarbons are usually found in the 400 region which can be attributed to molecules derived from pentacyclic triterpenoids. This is especially true in the Utah coal (APCS #6) which is rich in liptinites. Most of these types of molecules are extractable, which is seen in the loss of these high mass peaks in the pyridine extracted Utah coal.

The effect of pyridine extraction on the distribution of pyrolysis products is very rank dependent. There is very little difference between raw and extracted coals for those of higher rank such as the low volatile bituminous coal, while

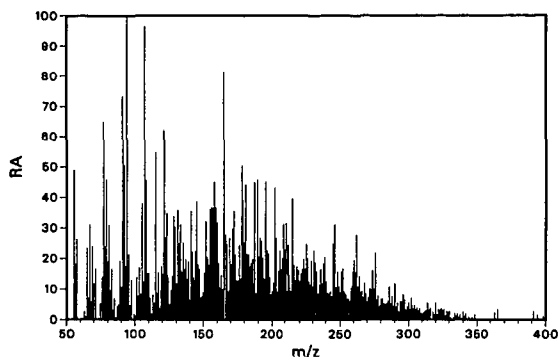


Figure 1. Averaged mass spectra for the fresh Herrin Seam coal (APCS #3), [RA = relative abundance].

an increased yield of pyrolysis products and a greater variety of molecules is found for the lower rank coals which have been extracted. The results for the subbituminous coal are shown in Figure 2. Also, note that the higher mass peaks (>200) are more abundant in the extracted sample. This effect may be simply due to the fact that the low rank coals contain a significant amount of water.

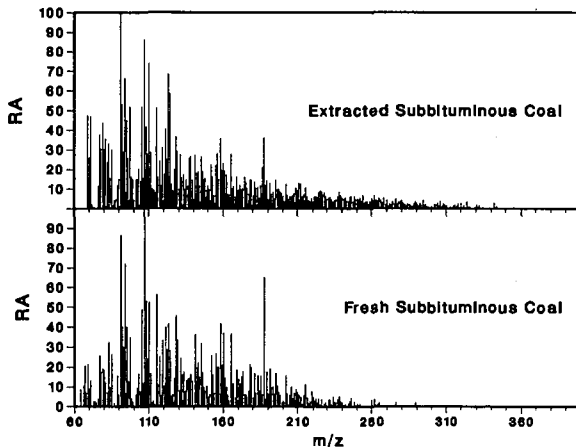


Figure 2. Comparison between averaged mass spectra for fresh and extracted subbituminous coal (APCS #2).

The analysis of the as received sample indicated 28% moisture for the subbituminous coal. The pyridine extraction will effectively remove this water and the sample was vacuum dried. The effect of vacuum drying on the fresh samples is being explored.

The oxygen content of these coals greatly varies from 20% in the lignite down to 2.5% in the lv bituminous. However, the relative yields of oxygen containing species in the pyrolysis product does not change as much as one would

expect based on this variation in oxygen content. There is a decrease with rank which can be seen in the adjacent Figure 3. Also, species with two oxygens are almost absent in the higher rank coals, the mv and lv bituminous ranks. It is known that for lignite and subbituminous coals significant amounts of the oxygen is lost as CO and CO₂.⁹ However, it may be possible that in the higher rank coals the pyrolysis products are enriched in the oxygen containing molecules while the residue is depleted compared to the original oxygen content. These coals have not been exposed to atmospheric oxygen making it unlikely that these oxygen containing aromatics were formed from surface oxidation.

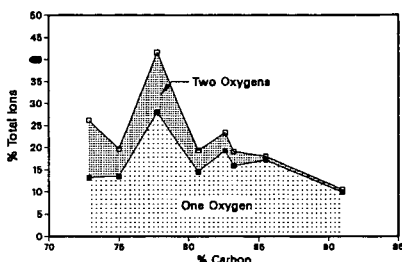


Figure 3. Variation in the oxygen containing products as a function of carbon content presented in a stacked plot.

Although the total amount of oxygen-containing species in the products does not change dramatically with rank, the types of molecules that are seen do change with rank. As can be seen in the adjacent Figure 4, the amount of ions in single ring aromatics (Z=4) decreases with increasing rank while the larger heteroaromatics such as dibenzofuran (Z=9) and naphthobenzofuran (Z=12) are more prevalent in the higher rank coals. These compounds are likely assignments for a combination of these Z numbers and the carbon number for the first peak seen in the series with one oxygen. For example, while hydroxyfluorene has a Z number of 9, the parent molecule has a carbon count of 13 which is one greater than dibenzofuran. Presently, a method is being used to help to distinguish between hydroxylated aromatics and both aryl ethers and annellated furans by modifying the acidic hydroxyls prior to pyrolysis.² With the Pocahontas low volatile bituminous coal, molecules with a single oxygen were observed at up to Z=19 with significant abundances at up to Z=17. With the lignite coal the maximum hydrogen deficiency observed was 12.

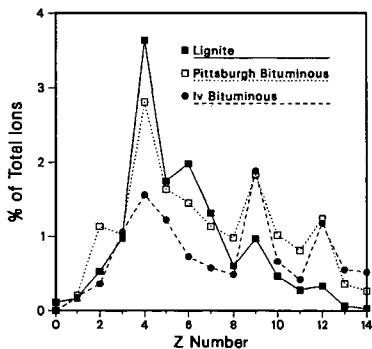


Figure 4. Distribution of molecules which contain one oxygen as a function of hydrogen deficiency for three coals.

Examination of the data from molecules containing a single sulfur yielded two very interesting results for the higher rank coals. Data from the very sulfur-rich Illinois Herrin Seam coal are compared to those from the low volatile bituminous coal in Figure 5. First, the yield of sulfur in the low volatile coal seems to be enhanced in comparison to the original amount of sulfur in the coal. The hv bituminous coal has five times as much, 'organic' sulfur in it as the low volatile coal. The yield of H_2S is probably much larger for the Herrin Seam coal. Second, in the Pocahontas coal small amounts of thiophene (Z=3) and dibenzothiophene (Z=9) are observed. These species along with benzothiophene and naphthobenzothiophene are typical sulfur heterocyclics found in coal liquefaction products^{10,11} and coal extracts.^{11,12} However, in duplicate experiment for both the fresh and extracted sample, the most abundant class of sulfur compounds had a Z number of 10 as is seen in Figure 5 and a carbon number of 14 for the parent molecule in the series. This result was also observed in the Upper Freeport mv bituminous coal. Selected peaks for the Herrin coal and the Pocahontas low volatile coal are shown in

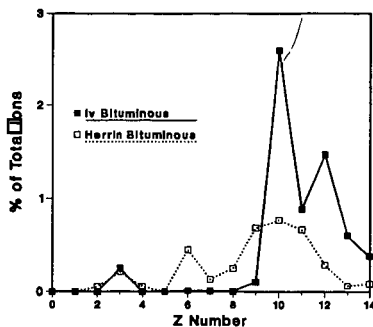


Figure 5. Distribution of species containing a single sulfur atom for two of the fresh coals.

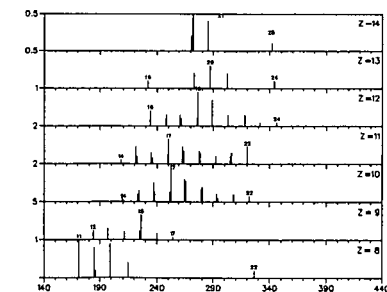


Figure 6. Selected ion peaks containing one sulfur from Z = 8 - 14 for the Herrin seam coal.

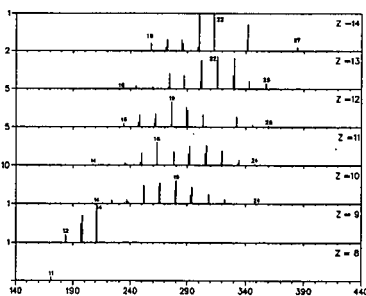


Figure 7. Selected ion peaks with one sulfur for Z = 8 - 14 for the Pocahontas low volatile coal (APCS #5).

Figures 6 and 7. Note that in both these plots the relative abundances for each subplot will vary since they are automatically scaled. The numbers on each plot represent the carbon number for the adjacent peak. In Figure 7 the most abundant peak has 19 carbons and a hydrogen deficiency of 10. A possible structure which would fit this data is alkylated phenylbenzothiophene. Phenylthiophenes have been identified in the extracts of Wyoming coal (PSOC-521).¹¹ The position of the phenyl group would determine if fragmentation would result in benzothiophene fragment peaks which are not seen in the high rank coal. The benzothiophene

fragment is observed if the phenyl were on the thiophene ring.¹³ Another possibility, although it seems less likely, is an addition of a 5-member ring to dibenzothiophene which one would expect to be converted to an indene type structure in the pyrolysis. The results are being investigated further using PyGCMS for these high rank coals.

SUMMARY

Extraction of the coals yielded variable results ranging from enhanced pyrolysis yield from the low rank coals to no difference for the very high rank coal. It was shown that this approach is useful for examining the distribution of heteroatom containing molecules which are produced in the vacuum pyrolysis. It is interesting to note that these species appear to be enriched in the products produced from the higher rank coals.

ACKNOWLEDGMENTS

This work was performed under the auspices of the Office of Basic Energy Sciences, Division of Chemical Sciences, U.S. Department of Energy, under contract number W-31-109-ENG-38. The AGHIS and probe were constructed by J. Gregar in the ANL Chemistry Division.

REFERENCES

1. Winans, R.E.; Hayatsu, R.; Scott, R.G.; McBeth, R.L. In *Chemistry and Characterization of Coal Macerals*; Winans, R.E.; Crelling, J.C., Eds.; ACS Symposium Series No. 252; American Chemical Society: Washington, D.C. 1984; pp. 137-155.
2. Winans, R.E.; Scott, R.G.; Neill, P.H.; Dyrkacz, G.R.; Hayatsu, R. *Fuel Proc. Tech.* 1986 12, 77-88.
3. Winans, R.E.; Hayatsu, R.; McBeth, R.L.; Scott, R.G.; Botto, R.E., *Preprints, Div. Fuel Chem., ACS 1988, 33(1)*, 407-414.
4. Melcalf, G.S.; Windig, W.; Hill, G.R.; Meuzelaar, H.L.C. *Int. J. Coal Geol.* 1987, 1, 245-268.
5. van Graas, G.; de Leeuw, J.W.; Schenk, P.A. In *Advances in Organic Geochemistry 1979*; Douglas, A.G.; Maxwell, J.R., Eds.; Pergamon Press: Oxford, 1980; pp. 485-493.
6. Yun, Y.; Hoesterey, B.L.; Meuzelaar, H.L.C.; Hill, G.R., *Preprints, Div. Fuel Chem., ACS 1987, 32(4)*, 301-308.
7. Vorres, K.S.; Janikowski, S.K., *Preprints, Div. Fuel Chem., ACS 1987, 32(1)*, 492-499.
8. Schmidt, C.E.; Sprecher, R.F.; Batts, B.D. *Anal. Chem.* 1987, 59, 2027.
9. Serio, M.A.; Solomon, P.R.; Yu, Z.Z.; Deshpande, G.V.; Hamblen, D.G., *Preprints, Div. Fuel Chem., ACS 1988, 33(3)*, 91-101.
10. Nishioka, M.; Lee, M.L.; Castle, R.N. *Fuel* 1986, 65, 390-396.
11. Nishioka, M. *Energy Fuels* 1988, 2, 214-219.
12. White, C.M.; Douglas, L.J.; Perry, M.B.; Schmidt, C.E. *Energy Fuels* 1987, 1, 222-226.
13. Blatt, H.; Brophy, J.J.; Colman, L.J.; Tairyck, W.T. *Aust. J. Chem.* 1976, 29, 883-890.

PYROLYSIS MODELING OF THE ARGONNE PREMIUM COALS

M.A. Serio, P.R. Solomon, Z.Z. Yu, G.V. Deshpande, and D.G. Hamblen

Advanced Fuel Research, Inc., 87 Church Street, East Hartford, CT 06108 USA

INTRODUCTION

The establishment of the Argonne Premium Sample Bank (1) provides a good opportunity to test a recently developed "general" model of coal devolatilization (2-4). The model, which is called "FG-DVC", combines a functional group model for gas evolution (FG) and a statistical model for tar formation (DVC). It assumes that the kinetics of functional group decomposition are independent of coal type, but that the amounts do vary with coal type (5-7). The rank dependence of the tar yield, tar molecular weight distribution, extract yields, and viscosity are explained by the rank dependence of CO₂ yields according to this model (2,8). The early evolution of CO₂ in low rank coals appears to lead to crosslinking at low temperatures and hence thermosetting behavior, low tar yields, and low extract yields (8).

The validation of the FG-DVC model was previously done for two coals, North Dakota lignite and Pittsburgh Seam bituminous (2). The Argonne Premium Sample set provides six more coals and different samples of these same two coals for comparison. In order to compare with data over a wide range of conditions, pyrolysis experiments were done in three different reactor systems, as described below.

EXPERIMENTAL

Coal Properties - Elemental and ultimate analysis data are given for the eight Argonne coals in Table 1. This information was obtained either from Reference 1 or directly from Karl Vorres. The values were normalized to equal 100%. Note that the coals have been numbered in descending rank order based on carbon content. This is a different numbering system than the Argonne sample designations.

Reactors - The reactors used included a thermogravimetric analyzer (TG) with evolved gas analysis by Fourier Transform Infrared (FT-IR) spectroscopy. The TG-FTIR apparatus is offered commercially by Bomem, Inc. under the name TG/Plus. The TG/Plus couples a Dupont 951 TGA with a Bomem Michelson 100 FT-IR spectrometer. The details of the TG-FTIR apparatus can be found in several publications (6,9,10). Under the present work, approximately 35 mg of the -100 mesh fraction of each coal sample was heated at 30°C/min, first to 150°C for drying, and then to 900°C for pyrolysis.

The entrained flow reactor (EFR) has been described previously in other papers (7,11). The experiments were done at a single injector/collector separation of 24" at three different temperatures (700, 1100, and 1400°C). The heating rate in this system is approximately 5000°C/s and the total residence time is approximately 0.5 s.

The molecular weight distribution of tar evolved during pyrolysis at 0.05°C/s under vacuum to 450 or 500°C was determined by Field Ionization Mass Spectrometry (FIMS) at SRI International. The apparatus has been described by St. John et al. (12). The total weight loss under these conditions was also determined.

A summary of the experimental conditions is given in Table 2. The TG-FTIR and FIMS experiment were done with the -100 mesh ampoules, while the EFR experiments were done with bulk samples supplied by Karl Vorres.

RESULTS AND DISCUSSION

Experimental Data - The experimental results for these coals from the TG-FTIR have been presented in a previous paper (6). These data showed some variations (e.g., 15°C for CH₄, 60°C for tar, 60-90°C for most oxygenates) in the peak temperatures for the maximum evolution rate, particularly in the case of oxygenated volatiles. The variations in the peak temperatures for the various species are consistent with results from an earlier programmed pyrolysis experiment on ten coals (5). However, for each species, the variation in the peak temperature with rank is small relative to a) the width of the peak; b) the variations among species; c) the variations among experiments with significantly different heating rates; d) the typical variations in the data of different investigators for the same species from the same coal. In view of the relative insensitivity of individual species kinetics when compared to these factors, the FG-DVC model assumption of rank independent rates appears sound. The corollary conclusion that the principal variation of pyrolysis behavior with rank is due to variations in the concentration of functional groups and hence, the amount of each pyrolysis product is also unchanged. These conclusions are supported by the ability of the FG-DVC model, which incorporates these assumptions, to fit pyrolysis data for a wide range of coal types over a wide range of conditions, as discussed below.

The complete set of data for the EFR experiments has been given in DOE reports (13). The data for the three temperatures for a high rank (Pocahontas) and low rank (Wyodak) coal are shown in Figs. 1 and 2, respectively. The Wyodak coal shows a significantly higher volatile yield (lower char yield) which can be accounted for by higher yields of oxygenated volatiles. Both coals show the influence of secondary cracking reactions above 700°C and secondary gasification reactions above 1100°C. At 1400°C, the products are close to thermodynamic equilibrium in both cases and consist primarily of char, CO, and H₂. Models have been developed to describe secondary reactions (7), but these have not been included in the version of the model used here, except for the tar cracking which is part of the standard FG model used for reactors where the tar is not quenched (2,7). Consequently, we do not show model predictions for the 1400°C EFR experiments which are dominated by these effects.

Determination of Parameters for the FG-DVC Model - The FG-DVC model contains several parameters, some of which depend on the coal and one which depends on the experiment type. The large number of parameters has been criticized by some. However, it should be pointed out that the model is able to predict a large number of pyrolysis phenomena such as the yields of individual gas species, the yields of tar and char, the tar molecular weight distribution, the crosslink density and the viscosity. The model also accounts for the variation of these quantities with temperature, heating rate, residence time, and pressure in a manner that agrees well with experiment. The details of the model inputs and a sensitivity analysis are included in a recent paper (2).

The first step is to obtain elemental analysis data for C, H, N, O, and S. This is needed to construct a coal composition file. The next step is to determine the amounts of the individual functional group (FG) pools (CO₂-extra loose, CO₂-loose, CO₂-tight, CH₄-loose, etc). This requires data from at least two standard pyrolysis experiments. The first is a slow heating pyrolysis

experiment, like the TG-FTIR experiment, which can provide good quantitative gas yields and differential evolution curves. This type of experiment is best able to resolve the individual loose, tight, etc. pools for a given gas, especially when both the integral and differential curves are compared with the model predictions. The values of the FG pools so determined are checked against a second pyrolysis experiment done at high heating rates, such as the EFR 1100°C data. The pools are adjusted to simultaneously fit the low and high heating rate experiments. This usually involves a series of iterations.

This procedure has been followed for the eight Argonne coals and the results are shown in Fig. 3 for the major FG pools, which are CH₄, CO₂, H₂O, and CO. These values have not yet been fully optimized and may change slightly in the future, but give good agreement with experiment except in the case of H₂O where the data are scattered. The oxygenated species show a systematic increase with decreasing rank. The amount of CH₄ goes through a maximum in the medium rank coals, as do other hydrocarbon species such as tar (see below).

Once the functional group pools have been established to allow a good match between the integral and/or differential yield curves for two pyrolysis experiments, the input parameters for the DVC (tar formation) part of the model are determined. The first step is to adjust the average oligomer length to match the coal extract yield. The next step is to adjust the number of unbreakable bridges ("hard" bonds) between monomer clusters to fit the experimentally observed tar yields for the same low and high heating rate experiments used to calibrate the functional group pools. The relationships between these input quantities and the experimentally measured quantities are shown in Figs. 4 and 5. The extract yield data (which were obtained from Professor Milton Lee at Brigham Young University) and the average oligomer length are inversely correlated. The same is true of the number of hard bonds and the tar yield. Again, these values have not been fully optimized and are subject to change.

Other parameters which go into the tar formation model are the average monomer molecular weight (M_{avg}) and the average molecular weight between crosslinks (M_c). The value of M_c is interpolated from the literature data of Nelson (14). We eventually plan to use literature data for M_{avg} as well. However, the size of the average cluster varies significantly among different research groups and the reported rank variations are not systematic or clearly understood. Currently, we are using a value of 256 for all the coals except the Pocahontas where a value of 506 is used. The significantly higher average cluster size for the Pocahontas compared to the others is supported by the calculations of Gerstein et al. (15) based on NMR, FT-IR and elemental analysis data obtained for a number of coals.

The last important parameter to be selected is the value of ΔP , which is the average pressure difference between the ambient and the particle's interior during pyrolysis. This parameter is used in the internal transport model. The choice of ΔP has a significant effect on tar yield and the tar molecular weight distribution for non-softening coals under most conditions except high pressure. For fluid coals, a value of $\Delta P = 0$ is a good approximation for pressures of one atm or higher. The sensitivity of the model to the choice of ΔP is discussed in a recent paper (2). This is the only parameter in the model which is adjusted for each type of experiment. The original FG model also had a fitting parameter, X_0 , which was used to match the final tar yield to account for differences in particle size, heating rate, bed depth and reactor geometry (2). While it can be said that we have traded one adjustable parameter, X_0 , in the FG model for

another, ΔP , in the FG-DVC model, this is not exactly true as the latter model is much richer in its ability to predict a variety of pyrolysis events. The values of ΔP are more restricted than X_0 and have a more fundamental basis that it is related to the coal's viscosity.

The use of the FG-DVC model involves several constraints: 1) Where experimental data are available on the starting coal, such as for the molecular weight between crosslinks (M_c), the extract yield, or the elemental analysis, they are used as inputs. Additional information will be incorporated as it becomes available. 2) The kinetic parameters for the evolution of the FG group pools are assumed to be invariant with coal type. 3) The amounts of the FG pools are constrained to fit data from experiments at very low (0.5°C/s) and very high (5000°C/s) heating rates. This results in a model which is very robust in its ability to fit pyrolysis data over a wide range of conditions. It is also true that when enough coals have been studied, a detailed calibration of the model may not be needed and perhaps the elemental analysis, the particle size and the reactor conditions will be sufficient.

Comparison of Model with Experimental Data - The model is compared with experimental data from the three reactors in Figs. 6 and 7. Except for H_2O , the agreement of the model is generally quite good over a wide range of extents of pyrolysis and for what is a wide range of coal types. A comparison is made between the tar molecular weight measured by FIMS and the predicted values in Fig. 8. The model predicts rank dependent phenomena, such as the steep drop off in the distribution for the low rank coal due to crosslinking events (2,8).

CONCLUSIONS

The conclusions for this work are as follows:

- The pyrolysis kinetic data for this series of coals support the assumption of relative rank insensitivity, as does the ability of the model to fit the data using rank independent rates.
- There is a systematic variation in the amounts of individual pyrolysis gases with rank. The oxygenates (CO , CO_2 , H_2O) are highest for the low rank coals while the hydrocarbons are highest for the medium rank coals.
- There is a systematic variation in the tar yield and tar molecular weight distribution with rank. The tar yield is highest for medium rank coals. The mean of the tar average molecular weight distribution is highest for the high rank coals. The drop-off in the tar molecular weight distribution is greatest for low rank coals.
- The rank dependent phenomena are well described by the FG-DVC model over a wide range of experimental conditions.

ACKNOWLEDGEMENTS

This work was supported under DOE Contract No. DE-AC21-86MC23075 through the Morgantown Energy Technology Center. Justin L. Beeson is the Project Manager. Karl Vorres supplied bulk samples of the Argonne coals for the EFR experiments.

REFERENCES

1. Vorres, K.S., ACS Fuel Chem Div. Preprints, **32**(4), 221 (1987).
2. Solomon, P.R., Hamblen, D.G., Carangelo, R.M., Serio, M.A. and Deshpande, G.V., "A General Model of Coal Devolatilization", accepted for publication, Energy and Fuel, (1988).
3. Solomon, P.R., Hamblen, D.G., Carangelo, R.M., Serio, M.A. and Deshpande, G.V., ACS Fuel Div. Preprint, **32**(3), 83 (1987).
4. Solomon, P.R., Hamblen, D.G., Carangelo, R.M., Serio, M.A. and Deshpande, G.V., Combustion and Flame, **71**, 137 (1988).
5. Solomon, P.R. and Hamblen, D.G., Prog. Energy Combust. Sci., **9**, 323 (1983).
6. Serio, M.A., Solomon, P.R., and Carangelo, R.M., ACS Div. of Fuel Chem. Preprints, **33**, (2), 295, (1988).
7. Serio, M.A., Hamblen, D.G., Markham, J.R., and Solomon, P.R., Energy and Fuels, **1**, 138, (1987).
8. Deshpande, G.V., Solomon, P.R., and Serio, M.A., ACS Div. of Fuel Chem. Preprints, **33**, (2), 310, (1988).
9. Carangelo, R.M., Solomon, P.R. and Gerson, D.J., Fuel, **66**, 960 (1987).
10. Whelan, J.K., Solomon, P.R., Deshpande, G.V., and Carangelo, R.M., Energy and Fuels, **2**, 65, (1988).
11. Solomon, P.R., Hamblen, D.G., Carangelo, R.M., and Krause, J.L., 19th Symposium (Int) on Combustion, The Combustion Institute, Pittsburgh, PA, 1139, (1982).
12. St. John, G.A., Buttrill, Jr., S.E. and Anbar, M., ACS Symposium Series, **71**, 223 (1978).
13. Solomon, P.R., Hamblen, D.G., Serio, M.A., Smoot, L.D. and Brewster, S., "Measurement and Modeling of Advanced Coal Conversion", First Annual Report DOE/METC Contract #DE-AC21-86MC23075 (1987).
14. Nelson, J.R., Fuel, **62**, 112 (1983).
15. Gerstein, B., Murphy, P.D. and Ryan, L.M., Coal Structure, (R.A. Meyers, Ed.) Chapter 4, Academic Press, New York (1982).

Table 1- Elemental Analysis of Argonne Premium Coal Samples.

	% daf Basis					As-Received	
	C	H	O	N	S	% Dry Basis	Moisture Basis
1. Pocahontas	90	4.7	3	1.3	1.0	5	0.6
2. Upper Freeport	84	5.0	7	1.5	2.5	13	1.1
3. Pittsburgh #8	82	5.8	8.8	1.6	1.8	9	1.6
4. Lewiston-Stockton	81	5.5	11	1.6	0.8	20	2.4
5. Utah Blind Canyon	79	6.0	13	1.6	0.5	5	4.6
6. Illinois #6	76	5.7	10	1.4	6.4	16	8.0
7. Wyodak	74	5.1	19	1.1	0.4	8	28.1
8. Beulah-Zap	72	5.2	21	1.1	0.8	6	32.2

Table 2 - Experimental Conditions

Reactor	Temperature (°C)	Heating Rate °C/s	Hold Time s	Pressure atm
TG-FTIR	900	0.5	0	1
EFR	700, 1100, 1400	5000	0.5	1
FIMS	500	0.05	0	0

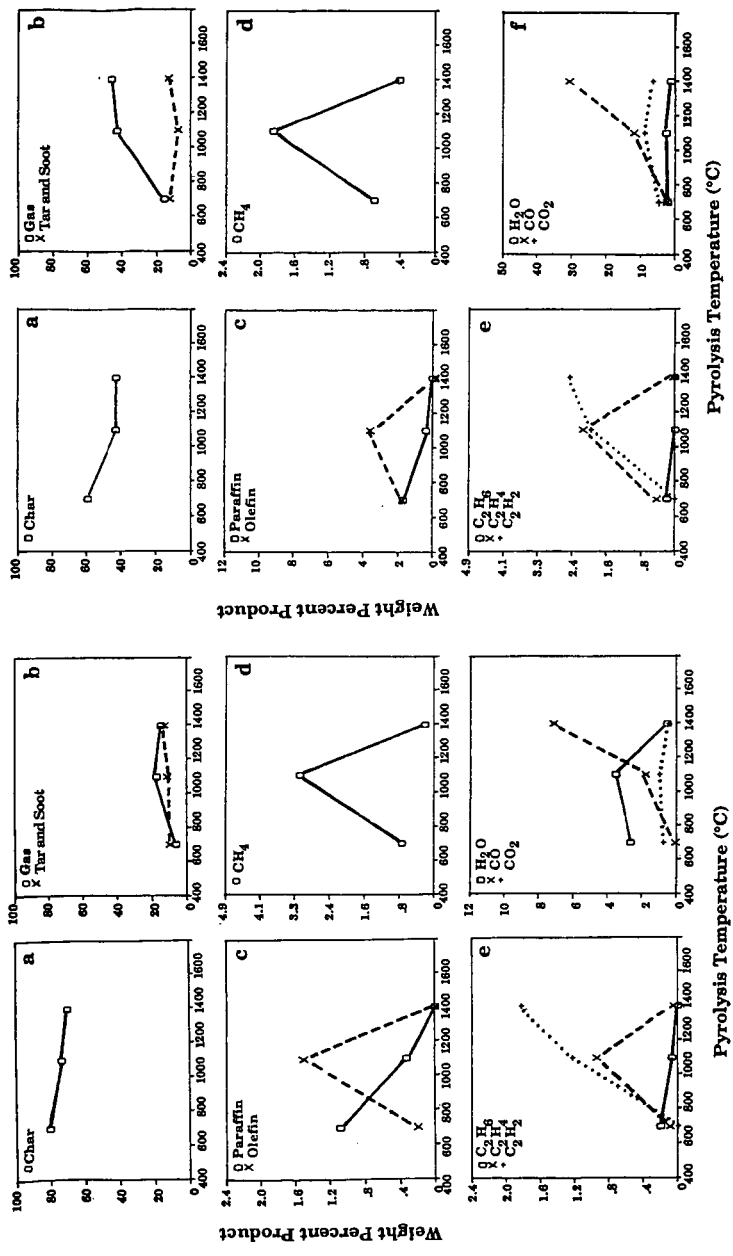


Figure 1. Pyrolysis Results for Pocahontas Bituminous Coal, 200 x 325 mesh, in the Entrained Flow Reactor. The Solid, Dashed and Dotted Lines are used to connect the Data and are not Model Predictions.

Figure 2. Pyrolysis Results for Wyodak Subbituminous Coal, 200 x 325 mesh, in the Entrained Flow Reactor. The Solid, Dashed and Dotted Lines are used to connect the Data and are not Model Predictions.

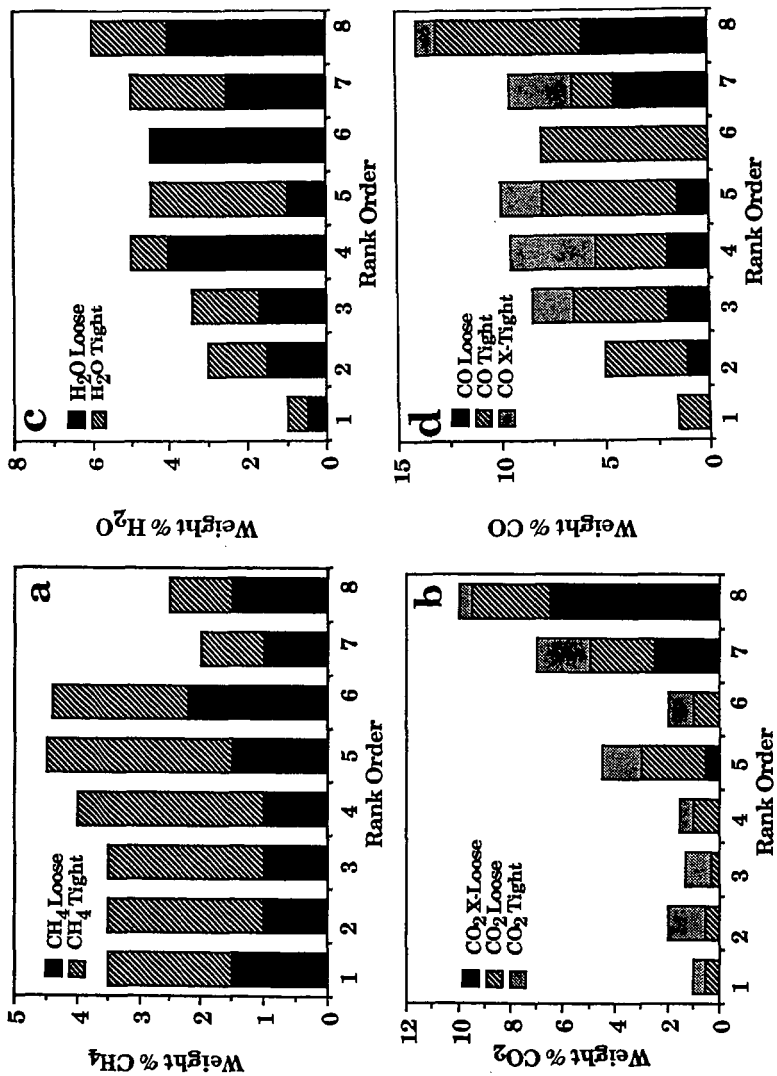


Figure 3. Variation of Functional Group Pools with Rank Order.

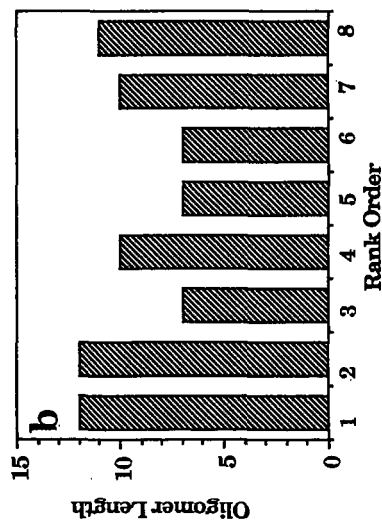
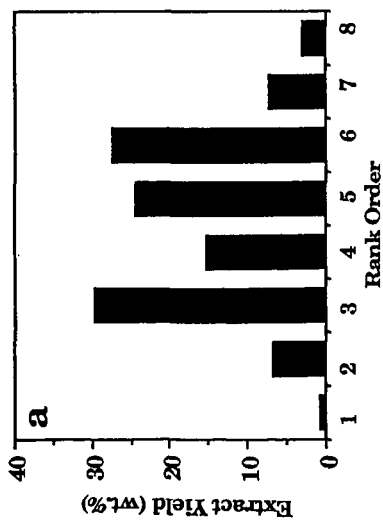


Figure 4. Variation of Extract Yield and Oligomer Length with Rank Order.

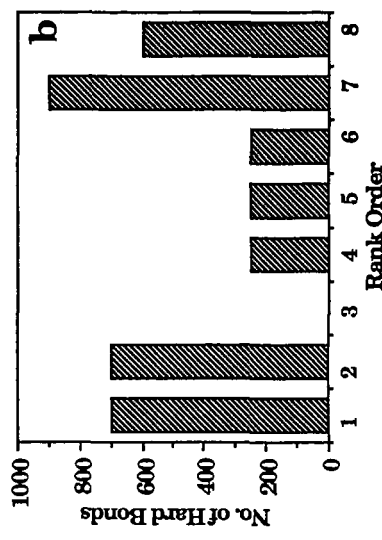
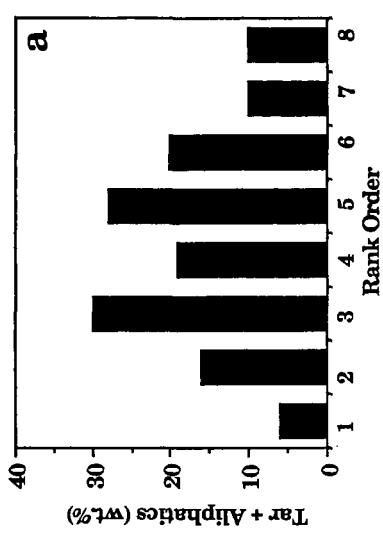


Figure 5. Variation of Tar Yield from TG-FTIR Experiment and Number of Hard Bonds with Rank Order.

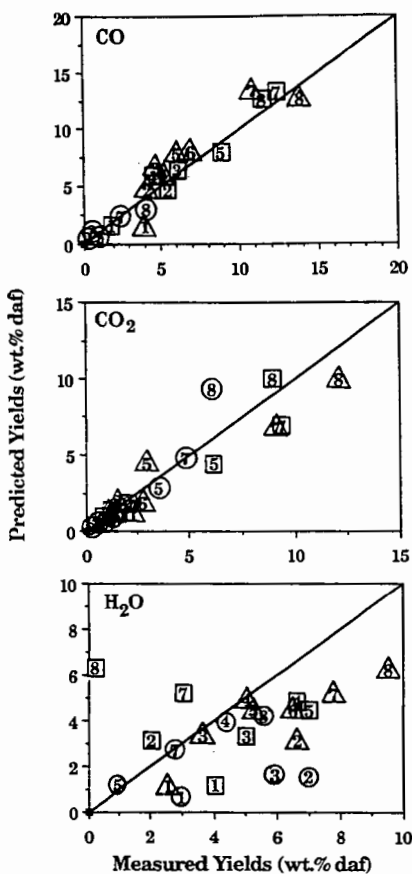


Figure 6. Comparison of Model Predictions with Data for the Yields of Oxygenated Species. The Numbers Refer to the Coal Type. The Symbols Around the Numbers Refer to the Reactor Type. ○ - EFR, 700°C; □ - EFR, 1100°C; △ - TG-FTIR; No Symbol - FIMS.

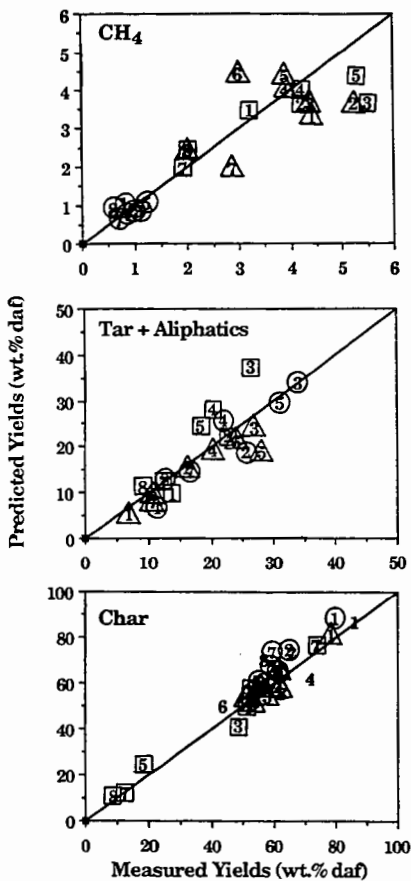


Figure 7. Comparison of Model Predictions with Data for CH₄, Tar Plus Aliphatics, and Char. The Numbers Refer to the Coal Type. The Symbols Around the Numbers Refer to the Reactor Type. ○ - EFR, 700°C; □ - EFR, 1100°C; △ - TG-FTIR; No Symbol - FIMS.

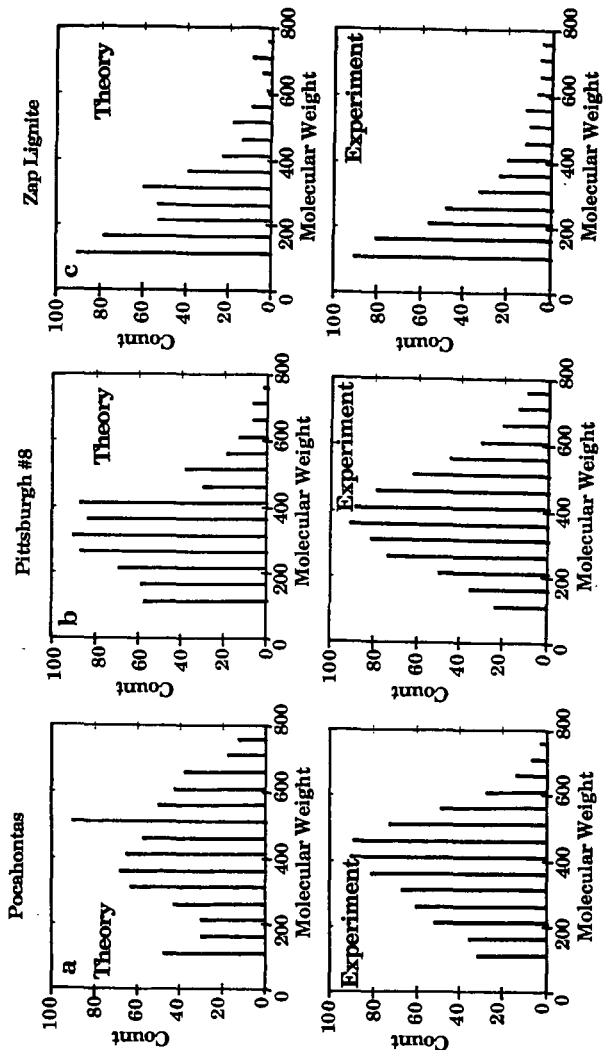


Figure 8. Comparison of Measured and Predicted Tar Molecular Weight Distributions.

THERMOCHEMICAL COMPARISON OF ARGONNE PREMIUM COAL SAMPLES WITH MODEL SOLID ACIDS.

by

Edward M. Arnett*
Brenda J. Hutchinson
Michael Gumkowski
Qitao Liu

Department of Chemistry
Duke University
Durham, North Carolina 27706

Abstract

This presentation will be a summary of results acquired over the last five years using the heats of interaction of a series of bases with various solid acids as a means for classifying them. A sulfonic acid resin provides a solid model for Brønsted acidity. Silica is a model solid for hydrogen bonding interactions and several grades of graphitized carbon black are an excellent model for van der Waals/dispersion force interactions. Heats of interaction of the series of bases with several types of Argonne premium coals will be compared with those for the model solids and will serve as a means for coal classification.

INTRODUCTION

Thermochemical methods based on various types of calorimetry are a powerful tool for comparing acid-base interactions both in homogeneous and heterogeneous systems. Previous reports from this laboratory have described the thermochemical method for comparing solid acids with their homogeneous analogues in response to interactions with a variety of basic liquids. We have attempted to find appropriate solid prototypes for Brønsted acidity (1), hydrogen-bonding acidity (2), and dispersion force interactions (3). These could be used as standards for comparison in classifying more complex solid acids such as coals.

Much of the recent literature on the thermochemistry of adsorption onto coals has focused on their interactions with water or alkanols so that pre-treatment conditions could be examined with respect to their influence on the resulting heat of interaction (4-7). Some studies have examined other types of interacting compounds, such as amines, pyridines, and alkanes (8-12).

The present report compares six carefully classified coals from the Argonne National Laboratory Premium Coal bank by two calorimetric methods (heats of immersion and thermometric titration) using a series of twelve solvents chosen especially to bring out the differences between Brønsted acidity, hydrogen-bonding and dispersion force interactions (13).

RESULTS

Heats of immersion of the six premium coal samples, three coals from a previous study and two prototype solids (Dowex, silica) into twelve carefully chosen solvents at 75° are listed in Table I. Also listed in Table I are the heats of adsorption of the bases with Carboxpack F. The values reported are averages of two or three measurements, along with the standard deviation.

DISCUSSION

An important goal of this project is to see whether acid-base interactions of complex solids such as coals can be characterized thermochemically in the same manner which has been successful for characterizing acid-base interactions of homogeneous systems. A number of years ago, we demonstrated that there was a clear difference between the thermochemical order for interaction of a series of bases with the strong Brønsted acid, fluorosulfuric acid, as compared with the hydrogen-bonding acid, *p*-fluorophenol (14,15). The twelve basic solvents listed in Table I were chosen primarily to discriminate between surface sites which form hydrogen-bonds and those which are capable of Brønsted acid interactions. For example, dimethyl sulfoxide is a strong hydrogen-bond acceptor although it is a relatively weak proton acceptor from Brønsted acids in solution (15).

Comparison of Premium Coals with Each Other. Heats of immersion data for six coals listed in Table I were subjected to linear correlation analysis. By heat of immersion, the greatest similarity is between Illinois #6 and Pittsburgh #8 and between Wyodak and N. Dakota lignite. The biggest difference is between Pittsburgh #8 and Pocahontas #3.

Comparison with Earlier Work. The premium Wyodak coal sample (taken from the Gillette strip-mine) may be compared to the four year old sample of Wyoming Rawhide coal obtained from Exxon and kept dry under nitrogen. Comparison of heats of immersion in ten solvents (see Table I) gives a correlation coefficient of 0.96. A similar correlation for the Exxon sample of Illinois #6 as compared to the Argonne Premium, using only six bases, has an *r* value of 0.97. Finally, with a sample of only five bases, correlation of the old data for Texas Big Brown lignite with the Premium sample of North Dakota lignite gives an *r* value of 0.97.

Comparison with Standard Solid Acids. Heats of immersion of Dowex sulfonic acid resin, the prototype Brønsted acid, and of silica, the prototype solid hydrogen-bonding acid, can be compared with heats of immersion of the five premium coals using data for ten bases: pyridine, dimethyl sulfoxide, 4-methylpyridine, toluene, cyclohexanone, 2,6-dimethylpyridine, 2,4,6-trimethylpyridine, *n*-butylamine, propylene carbonate and *n*-hexylamine as shown by the correlations in Table II.

It is clear that by themselves neither Dowex, silica, or graphitized carbon black provide good models for the interaction of basic liquids with these coals. When two parameter equations are used to include contributions from both Brønsted acidity and hydrogen-bonding, there is considerable improvement. As might be expected, the introduction of yet another correlation parameter for dispersion forces improves things even more. Recent work in this laboratory indicates that Carbo-pack F[®], graphitized carbon black, is a better model than graphite for non-specific physical adsorption. Regression equations using heats of immersion of Dowex, silica and van't Hoff heats of adsorption determined by gas chromatography on Carbo-pack F as parameters to describe the heats of immersion of five premium coals in ten liquids are also shown in Table II.

The percentage contributions of Brønsted acidity (Dowex), hydrogen bonding (Silica), and dispersion force interactions (Carbo-pack) to the heats of immersion for each coal in ten bases were determined by the method of Swain and Lupton. It is interesting to see the variation of these contributions from one type of coal to another and the relatively large role of hydrogen-bonding. This supports the proposal of Larsen (16) for the role of this type of interaction to the swelling and solubilization of coal. This treatment has the advantage of expressing the results of three types of actions that are presumed to affect an interaction (such as that between a solid and liquid) in percentage terms. However, its shortcoming is that the results are assumed to be completely

determined by these actions, that is, they add up to 100%, which in turn implies that a perfect fit should be obtained with three parameters. This is clearly far from the case.

Table II shows that our fundamental strategy of trying to dissect the interactions of a complex solid, such as a coal, with a series of solvents into contributions that are modeled by prototype "simpler" solids has had only modest success.

Finally, it may be asked whether accessibility or acid properties are strongly affected by the surface areas of the coals. These have been determined by BET analysis and when the results are compared with heats of immersion or titrametric heats there is no indication that surface area is a significant factor. This behavior is very different from heats of immersion of silicas in the same bases where surface area plays a key role (2). In all probability the difference lies in the fact that coals are readily swollen and penetrated by the basic solvents so that eventually most acid sites are reached in the open cross-linked gel network. In contrast silica is a relatively undeformable solid.

References

1. Arnett, E.M.; Haaksma, R.A.; Chawla, B.; Healy, M.H., J. Am. Chem. Soc. 1986, 108, 4888.
2. Arnett, E.M.; and Cassidy, K.F., Reviews of Chemical Intermediates, 1988, 9, 27.
3. Arnett, E.M.; Hutchinson, B.J.; Healy, M.H., J. Am. Chem. Soc. (In press.)
4. Fuller, E.L., Jr., J. Coll. Interf. Sci., 1980, 75, 577.
5. Senkan, S.M.; Fuller, E.L., Jr., Fuel, 1979, 58, 729.
6. Glanville, J.O.; Newcomb, K.L.; and Wightman, J.P., Fuel, 1986, 65, 485.
7. Phillips, K.M.; Glanville, J.O.; and Wightman, J.P., Colloids and Surfaces, 1986, 21, 1.
8. Brooks, D.; Finch, A.; Gardner, P.J.; Harington, R., Fuel, 1986, 65, 1750.
9. Larsen, J.W.; and Knemmerle, E.W., Fuel, 1978, 57, 59.
10. Glanville, J.O.; Wightman, J.P., Fuel, 1980, 59, 557.
11. Larsen, J.W.; Kennard, L.; and Kuemmerle, E.W., Fuel, 1978, 57, 309.
12. Chawla, B., Arnett, E.M., J. Org. Chem. 1984, 49, 3054.
13. Gumkowski, M.; Liu, Q.; Arnett, E.M., Energy and Fuels, 1988, 2, 0. (In press)
14. Arnett, E.M.; Quirk, R.P.; Larsen, J.W., J. Am. Chem. Soc., 1970, 92, 3977.
15. Arnett, E.M.; Mitchell, E.J.; Murty, T.S.S.R., J. Am. Chem. Soc. 1974, 96, 3875.
16. Larsen, J.W.; Green, T.K; Kovac, J., J. Org. Chem. 1985, 50 4729.

Table II. Regression of Premium Coal Immersion Values Against Those for Dowex and Silica and Carbopack-F for Ten Bases (see Table I).

(10 Bases as listed in Table I).

$$\Delta H_{\text{Wyodak}} = -10.833 - 0.754\Delta H_{\text{Dowex}} + 4.440\Delta H_{\text{silica}} - 7.218\Delta H_{\text{Carbopack-F}}$$

$$r = 0.962; r_{\text{Dowex}} = -.546; r_{\text{silica}} = 0.886; r_{\text{Carbopack-F}} = 0.468$$

$$\Delta H_{\text{Ill. #6}} = 61.806 - 0.312\Delta H_{\text{Dowex}} + 3.625\Delta H_{\text{silica}} + 1.126\Delta H_{\text{Carbopack-F}}$$

$$r = 0.947; r_{\text{Dowex}} = 0.662; r_{\text{silica}} = 0.942; r_{\text{Carbopack-F}} = 0.078$$

$$\Delta H_{\text{Pitts. #8}} = 29.867 - 0.366\Delta H_{\text{Dowex}} + 2.821\Delta H_{\text{silica}} - 1.197\Delta H_{\text{Carbopack-F}}$$

$$r = 0.946; r_{\text{Dowex}} = 0.618; r_{\text{silica}} = 0.934; r_{\text{Carbopack-F}} = 0.235$$

$$\Delta H_{\text{Pocah. #3}} = -5.084 - 0.085\Delta H_{\text{Dowex}} + 0.202\Delta H_{\text{silica}} - 0.519\Delta H_{\text{Carbopack-F}}$$

$$r = 0.658; r_{\text{Dowex}} = 0.156; r_{\text{silica}} = 0.466; r_{\text{Carbopack-F}} = 0.453$$

$$\Delta H_{\text{N.Dakota}} = -52.691 - 0.905\Delta H_{\text{Dowex}} + 3.481\Delta H_{\text{silica}} - 9.556\Delta H_{\text{Carbopack-F}}$$

$$r = 0.893; r_{\text{Dowex}} = 0.375; r_{\text{silica}} = 0.715; r_{\text{Carbopack-F}} = 0.596$$

DETERMINATION OF PHENOLIC STRUCTURES IN LOW RANK COALS: ELUCIDATION OF TRANSFORMATION PROCESSES OF LIGNIN AT THE EARLY STAGE OF COALIFICATION

R. Hayatsu, R. L. McBeth, R. G. Scott, and R. E. Winans

Chemistry Division, Argonne National Laboratory,
9700 South Cass Avenue, Argonne, IL 60439

INTRODUCTION

Because lignin is considered to be a major precursor of coal vitrinite, chemical alteration studies of lignin structure are important for elucidating coalification processes as well as for understanding the chemical structure of vitrinite. Many investigators have attempted to elucidate the chemical processes in the coalification lignin. For example, Wayman et al. (1) have reported that a 100-million-year-old conifer consists of lignin-like material which is about one-third demethylated. Extensive cleavage of lignin ether linkages was also observed. Recently, based on ^{13}C NMR study, Hatcher (2) has concluded that the defunctionalization reactions of lignin-derived aromatic structures occur sequentially during coalification. A similar pathway has been suggested by Wilson (3). From a comparative NMR study of [$\beta\text{-}^{13}\text{C}$]lignin and its coalified products, Botto (4) has suggested that transformation of lignin is initiated by the heterolytic bond cleavage of labile β -aryl ether groups.

The present study continues our investigation of transformation processes of plant organic material to coal during early stages of coalification. To understand alteration of phenolic structures in lignin, and natural and synthetic coals have been characterized by using two-step depolymerization procedure of alkaline hydrolysis followed by silver oxide oxidation. In parallel experiments, lignin model compounds and a polymer have been transformed using thermal catalytic reaction conditions that mimic natural catagenetic metamorphism.

EXPERIMENTAL

Samples. The elemental compositions are presented in Table 1. Prior to the oxidations, all coal samples were exhaustively extracted with benzene-methanol (3:1) and CHCl_3 under reflux, and these were demineralized with HCl-HF at room temperature. A softwood lignin was isolated from pine.

Alkaline Hydrolysis. Each sample (0.5-1.0 g) was hydrolyzed with 12% NaOH aq. solution in an autoclave at 180°C for 4 hours. The air in the autoclave was replaced by nitrogen. The yields of alkaline hydrolyzed fractions from all samples are shown in Table 1. The soluble hydrolyzed fraction (after acidity) consists of humic acid-like material (soluble in alkali only but not HCl and organic solvents) and small molecules (soluble in organic solvents); dried at 60°C under vacuum.

Oxidation. Each alkaline hydrolyzed fraction was methylated with dimethyl- d_6 sulfate (5) before oxidation. A methylated- d_3 sample (0.3 ~ 0.4 g) was oxidized with alkaline silver oxide (freshly prepared 6 g of Ag_2O and 60 ml of 16% NaOH

TABLE 1. Elemental and Maceral Compositions of Samples.

No.	Sample	Elemental Composition per 100 Carbons	Soluble ^a	Insoluble ^b	Loss (by difference)
1	Victorian Brown Coal (Pale Lithotype)	$C_{100}H_{89}O_{34}N_{0.5}S_{0.2}$	64.3	28.7	7.0
2	Beulah-Zap Lignite (APCS #8)	$C_{100}H_{80}O_{21}N_{1.4}S_{0.4}$	57.5	28.5	14.0
3	Wyodak-Anderson Subbituminous (APCS #2)	$C_{100}H_{86}O_{18}N_{1.3}S_{0.2}$	53.0	31.4	15.6
4	Illinois #6 seam hvC Bituminous (APCS #3)	$C_{100}H_{77}O_{13}N_{1.5}S_1$	12.7	79.9	7.4
5	Blind Canyon hvB Bituminous (APCS #6)	$C_{100}H_{88}O_{11}N_{1.7}S_{0.2}$	32.7	58.8	8.5
6	Upper Freeport mv Bituminous (APCS #1)	$C_{100}H_{86}O_{6.8}N_{1.8}S_{0.3}$	8.6	84.5	6.9
L	Lignin	$C_{100}H_{108}O_{33}$	69.3	22.0	8.7
SY	Synthetic Coal	$C_{100}H_{86}O_{23}N_{1.2}S_{0.3}$	54.4	29.3	16.3

^aThe soluble, in experimental hydrolyzed fraction (after acidity) consists of humic acid-like material (soluble in alkali only but not HCl and organic solvents) and small molecules (soluble in organic solvents); dried at 60°C under vacuum.

^bInsoluble residue was determined after washing with HCl, H₂O and organic solvents, dried at 80°C under vacuum.

aqueous solution) at 80°C for 10 hours. After filtration, the reaction mixture was acidified with 10% HCl, concentrated, and extracted with benzene-methanol (3:1) and ether-methanol (3:1). Finally the solvent extractable material was esterified with diazomethane for GCMS analysis.

Thermal Catalytic Reaction. As shown in Table 2, six lignin model compounds and a polymer were used. Each sample (0.5 g) and montmorillonite K-10 (Aldrich Chemical Co.) were placed in a 25 x 2 cm i.d. glass tube. After evacuation, the tube was sealed and then heated at 150°C for two weeks. After the reaction, the mixture was extracted with refluxing benzene-methanol (3:1) and then CHCl₃.

In general, phenolic groups are strongly adsorbed on the surface of clay minerals. Therefore, it is necessary to treat the reaction mixture with 6N-HCl (reflux for 6 hrs.) before extraction with organic solvent. The solvent insoluble residue was treated with concentrated HCl-HF (1:1) at room temperature to remove the clay. A synthetic coal was prepared by heating a mixture of lignin, amino acids and K-10 at 150°C for two months (6-7).

Characterization and Identification Procedures. The analytical procedures used in this study have been described in detail previously (5,7-8).

RESULTS AND DISCUSSION

We have found that the alkaline hydrolysis effectively solubilizes lignin and low rank coals. The most likely mechanism of solubilization is the cleavage of ether linkages except aryl methyl and diaryl ethers. As expected, high oxygen containing samples (L, No. 1-3 and SY in Table 1) were hydrolyzed appreciably and produced significant amounts of solubilized materials.

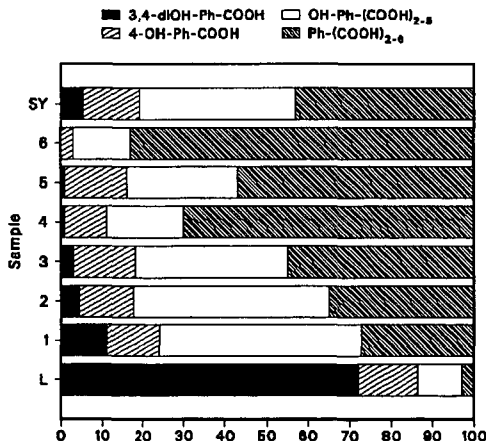
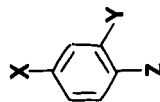


Figure 1. Relative abundances of the phenolic- and benzene-carboxylic acids obtained from silver oxide oxidation of alkaline solubilized materials; determined by GCMS as methyl esters.

TABLE 2. Summary of the Thermal Catalytic Reaction of Lignin Models.

Run	Model			Yield of Product wt%		Soluble Products (GCMS Analysis)	
	X	Y	Z	Soluble	Insoluble Polymers	Major	Minor
1	CH ₂ OH	OME	OH	38	42	C ₁₋₃ alkyl-catechols	dimers
2	O-nBu	H	H	53	10	C ₁₋₇ alkyl-phenols	dimers, trimers
3	OCD ₃	H	{CH-CH ₂ } _n	27	61	C ₁₋₃ alkyl, CD ₃ -phenols	dimers
4	OCH ₂ Ph	H	H	45	41	hydroxyl-diphenylmethanes	dimers
5	H	OH	OCH ₂ Ph	63	16	benzylcatechols	dimers, trimers
6	CH ₂ OCH ₂ Ph	H	H	42	37	C ₁₋₂ alkyl-diphenylmethanes	triphenylalkanes
7	OPh	H	H	79	13	starting material	monomeric and dimeric phenols

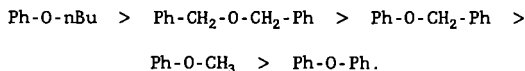


A summary of the silver oxide oxidation products from d_3 -methylated solubilized materials is shown in Fig. 1. The yields are 63-89 wt%. The major product from oxidation of lignin is 3-methoxy-4-methoxy- d_3 -benzoic acid. This result is in excellent agreement with the latest softwood lignin model (9) and other oxidation studies (e.g. 10). On the other hand, the oxidation of coal samples shows much smaller yields of dimethoxybenzoic acid. The GCMS analyses of coal oxidation products indicated that the concentration of 3,4-dimethoxy- d_6 derivative is much higher than that of 3-methoxy-4-methoxy- d_3 compound which is lignin's major product; $(OCD_3)_2/OCD_3OCH_3$ ratios are 0.16 for lignin and 4.7 - 7.5 for coal samples.

Most informative was the identification of large amounts of phenol-polycarboxylic and benzene-polycarboxylic acids in the oxidation products of low rank coals (Nos. 1-3). These acids are found in very little or negligible concentration in the oxidation products of lignin or slightly altered lignin. These observations apparently show that phenolic structures in lignin are considerably changed even at early stages of coalification.

With increasing rank (HV bituminous coals), the yield of phenolic acids decreases; benzenecarboxylic acids become the most abundant products. Polynuclear aromatics such as naphthalene carboxylic acids have also been found as minor products.

As shown by the results of thermal catalytic reactions of lignin models in Table 2, it is apparent that the reactions proceed by intra- and inter-molecular rearrangements of ethers. Aryl methyl and aryl butyl ethers (runs 1-3) rearrange to alkyl phenols; benzyl ethers were found to be converted to diphenylmethane derivatives through cleavage of ether linkages and benzylation. The reactivity of ethers under the reaction conditions used in this study are shown to increase in the following series:



These results imply that ether linkages in lignin structures (benzyl aryl type ethers; β -O-4, α -O-4 and γ -O-4) are labile and readily cleaved with accompanying intra- and inter-molecular rearrangements at early stages of coalification. Botto has observed (4) the occurrence of such rearrangement reactions from ^{13}C NMR studies of [β - ^{13}C] lignin samples coalified by the thermal catalytic reactions.

In this and previous (6-7) studies, we have also found that the oxidation results of synthetic coals obtained from lignin closely resemble those of the oxidation of samples No. 1 and 2 (Fig. 1), and other coals and vitrinites (6-7). Both natural and synthetic coals produce phenolic- and benzene-polycarboxylic acids as major oxidation products.

An important problem has been understanding how phenolic structures in lignin are altered to benzene and other aromatic structures such as naphthalene and tetralin. In our preliminary studies, we have found that phenols and phenyl ethers undergo catalytic hydrogen transfer reactions with terpenoids found in

low rank coals and sedimentary rocks. The terpenoids are apparently acting as hydrogen donors. These reactions are believed to be catalyzed by clay minerals.

One of our experiments indicates that the reaction of p-hydroxy-polystyrene and d-limonene in the presence of montmorillonite K-10 produce alkyl benzenes and p-cymene together with alkyl phenols. Such hydrogen transfer reactions may reveal the processes by which benzene rings are formed at the expense of lignin-phenols. It is considered that somewhat transformed lignin may also contain hydrogen donors such as hydroaromatics. Indeed, Botto has suggested (4) formation of hydroaromatic structures such as dihydrofurans during coalification of lignin. Detailed results for this study will be reported.

SUMMARY

The present study indicates that natural alteration processes from lignin to low rank coal are highly diverse and involve many types of organic reactions. Among them are clay catalyzed intra/inter-molecular rearrangement, hydrogen transfer and transalkylation reactions (11-14) which occur simultaneously rather than sequentially.

ACKNOWLEDGMENT

This work was performed under the auspices of the Office of Basic Energy Sciences, Division of Chemical Sciences, U.S. Department of Energy, under contract number W-31-109-ENG-38.

REFERENCES

1. M. Wayman, M. R. Azhar and Z. Koran, Wood Fiber, **3**, 153 (1971).
2. P. G. Hatcher, Energy & Fuels, **2**, 48 (1988).
3. M. A. Wilson, "NMR Techniques and Applications in Geochemistry and Soil Chemistry", Pergamon Press, p. (1987).
4. R. E. Botto, Energy & Fuels, **1**, 228 (1987).
5. R. Hayatsu, R. G. Scott and R. E. Winans, In "Oxidation in Organic Chemistry" Part D, Academic Press, p. 279 (1982).
6. R. Hayatsu, R. L. McBeth, R. G. Scott, R. E. Botto and R. E. Winans, Org. Geochem., **6**, 463 (1984).
7. R. Hayatsu, R. E. Botto, R. G. Scott, R. L. McBeth and R. E. Winans, Fuel, **65**, 821 (1986).
8. R. Hayatsu, R. E. Botto, R. L. McBeth, R. G. Scott and R. E. Winans, Energy & Fuels, submitted.
9. A. Sakakibara, Wood Sci. Technol. **14**, 89 (1980).
10. N. Morohoshi and W. G. Glasser, Wood Sci. Technol., **13**, 165 (1979).
11. R. M. Roberts and A. A. Khalaf, "Friedel-Crafts Alkylation Chemistry", Marcel Dekker, (1984).
12. P. Laszlo (Ed.), "Preparative Chemistry Using Supported Reagents", Part VIII, Academic Press, (1987).
13. T. P. Goldstein, Am. Assoc. Petrol. Geol. Bull., **67**, 152 (1983).
14. P. Laszlo, Acc. Chem. Res., **19**, 121 (1986); Science, **235**, 1473 (1987).

THE DESULFURIZATION OF COAL AND MODEL COAL COMPOUNDS IN AMBIENT TEMPERATURE MOLTEN SALTS

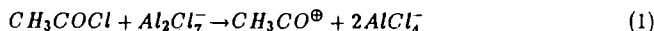
David S. Newman, Ellen M. Kurt, and Denguan Chen
Department of Chemistry
Bowling Green State University
Bowling Green, Ohio 43403

ABSTRACT

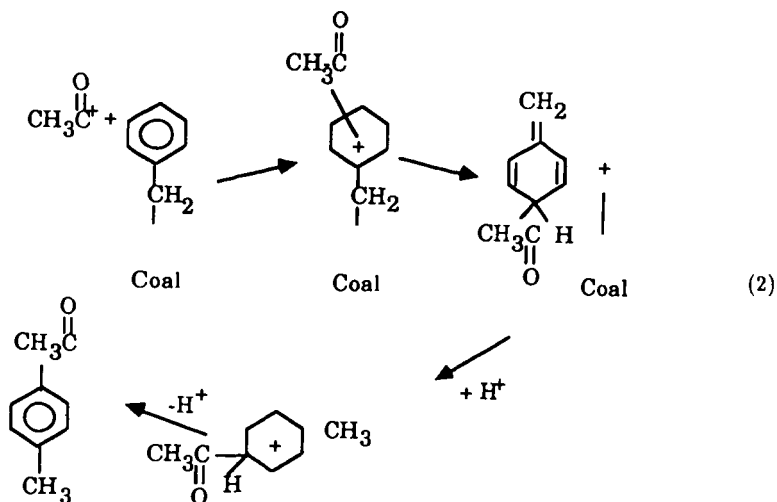
An ambient temperature molten salt, $C_5H_5N^+ \cdot Al_2Cl_7^-$ (pyridinium heptachloroaluminate) containing dissolved $CdCl_2$ was used as the reaction medium and catalyst for the acylation and concomitant desulfurization of IL #6 coal and several model coal compounds. The reactions were done at 40°C and 1 at. pressure and, in the case of the model compounds, products were identified and mechanisms proposed.

INTRODUCTION

Gaseous byproducts of the combustion of coal are the major contributors to acid rain. Since a gradual change from a primarily petroleum-based economy to a coal-based economy is virtually inevitable, cleaning, liquefying, gasifying, and generally modifying coal have become major goals of chemistry and chemical engineering. Ideally, coal should be modified by means of chemical scission reactions which remove designated portions of the coal or break specific chemical bonds via a known mechanism. Moreover, these scission reactions should occur at ambient temperature and atmospheric pressure so that unwanted side reactions occur at a minimal rate. To this end we have developed a series of Friedel-Crafts acylations and alkylations that take place in the ambient temperature molten salt $C_5H_5N^+ Al_2Cl_7^-$ (pyridinium heptachloroaluminate). (1,2,3,4) For Example, we found that F-C alkylation of PSOC 244 high sulfur coal increased its solubility in a 3:1 benzene/methanol solution approximately five fold relative to the untreated demineralized coal. (1,2) We also found that acylating IL #6 coal with acetyl chloride in this medium increased its solubility in 3:1 benz/methanol by about a factor of five. (3,4) The increased solubility is caused by hydrogen ions breaking the methylene chains holding the sub units of the coal macromolecule together. The mechanism for the acylation and accompanying depolymerization is most likely: (3,5,6)



followed by:



The proton then reacts with AlCl_4^- :

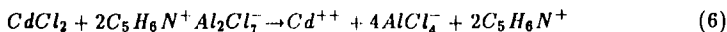


Both AlCl_3 and HCl have been identified as reaction products. The net reaction is



In 1980 Mobley and Bell found that ZnCl_2 catalyzed the removal of sulfur from the model coal compounds dibenzyl sulfide and tetrahydrothiophene and a variety of solid sulfides were identified. The net result of the ZnCl_2 -model compound interaction was the breaking of the aliphatic -C-S bond in each of the model compounds. (7) The ZnCl_2 had little effect on aromatic C-S bonds in thiophene and diphenyl thiophene. The mechanism suggested by Mobley and Bell for the catalytic reaction is somewhat similar to the mechanism for the F-C acylation or alkylation of coal or model compounds in pyridinium heptachloroaluminate. Since CdCl_2 is more soluble in this melt, (8) and also has a great affinity for sulfur, we

decided to dissolve CdCl_2 in the heptachloroaluminate melt. The dissolution reaction is probably,



The $\text{C}_5\text{H}_6\text{NAl}_2\text{Cl}_7$ acts as an acid and the CdCl_2 acts as a base. We then used the Cd^{++} containing melt as both catalyst and reaction medium for the removal of sulfur from model compounds and from coal. We also thought that the scission of C-C- and C-S bonds, as well as the formation of sulfides, would be facilitated by the F-C reactions and by the aluminum ion which forms an extremely stable sulfide. Hydrogen ions, arising from a variety of sources, would also be expected to facilitate the formation of H_2S .

The F-C experimental conditions were similar to those used in earlier studies. (2,3,4)

RESULTS AND DISCUSSION

Reactions of Model Coal Compounds

1. Dibenzyl Sulfide

Dibenzyl sulfide (0.0041 moles) was dissolved in 0.1143 moles of pyridinium heptachloroaluminate to which 0.0071 moles of acetyl chloride and 0.0027 moles of CdCl_2 were added. The mole fraction of CdCl_2 in the slurry was 0.022. The reaction was allowed to proceed under N_2 for 20 hours at 40°C whereupon it was quenched with water. The inorganic compounds $\text{HCl}(\text{g})$, $\text{H}_2\text{S}(\text{g})$ and $\text{AlCl}_3(\text{g})$ were isolated and identified as reaction products. The organic reaction products tentatively identified by GC/MS are listed in Table 1 in order of abundance.

In addition to the compounds listed in Table I, unidentifiable polymeric material was obtained. A second mixture with different concentrations (melt, 0.1200 moles; dibenzyl sulfide, 0.0076 moles; acetyl chloride, 0.0615 moles; CdCl_2 , 0.0081 moles) was allowed to react under N_2 for 20 hours at 40°C . The same products, in different proportions, were identified.

Some of the original cadmium was found in the aqueous layer, and some was incorporated into a black precipitate which formed during the reaction. It is not clear what percentage of the model compound's C-S bonds were broken, but our estimate is that approximately half were cleaved under the reaction conditions used. We think that if reaction conditions were optimized for sulfur removal, all of the C-S bonds in dibenzyl sulfide could be broken.

2. Thiophene

Thiophene (0.0106 moles) was allowed to react with acetyl chloride (0.0625) moles in the Cd^{++} containing melt. $\text{H}_2\text{S}(\text{g})$ was identified along with $\text{HCl}(\text{g})$ and $\text{AlCl}_3(\text{g})$. A yellow filtrate was collected upon filtration of the quenched reaction products. A solid precipitate formed which consisted of brownish-white crystals and a few black crystals. Both Cd and Al were found in the precipitate, as well as some polymeric material that could not be identified. The yellow liquid contained unreacted thiophene, acylated thiophene, and several species which have not been identified yet. Since the H_2S and probably the Cd and Al found in the precipitate arose from a reaction of the thiophene with the melt, aromatic C-S bonds had to have been broken! This was not found to occur with ZnCl_2 even though the reaction conditions were much harsher (250°C , 10 atm pressure). (7)

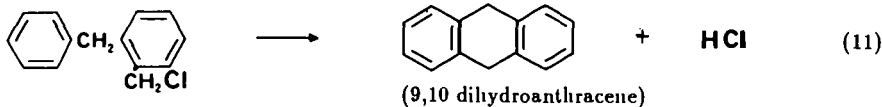
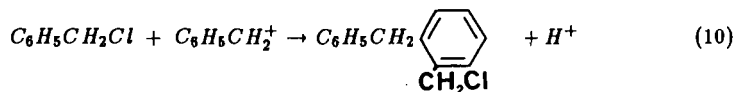
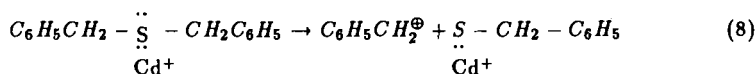
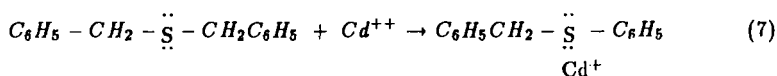
3. Dibenzothiophene

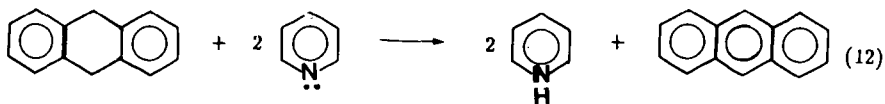
Dibenzothiophene did not react to a measurable degree under the previously described experimental conditions.

II. IL #6 Coal

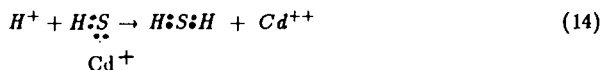
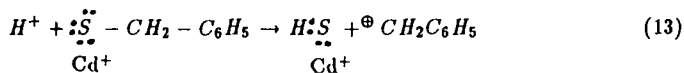
A 1 g sample of HF/HCl demineralized IL #6 coal (batch # I.D. 301.00135) was slurried in 50 ml of Cd^{++} containing heptachloroaluminate molten salt to which 1 g of acetyl chloride was added. The reaction was allowed to continue for 16 hours under nitrogen atmosphere. The procedure is similar to that used in earlier studies. (1,2,3) The coal's solubility was then measured in 3:1 benz/methanol and found to be 11.7%. A small quantity of H_2S was identified as a reaction product of the F-C acylation by allowing the N_2 carrier gas to pass through an aqueous $CdCl_2$ solution and observing the precipitation of CdS . The total sulfur content of the insoluble and soluble portions of the coal were analyzed and compared with the sulfur content of the original demineralized coal. The difference between the sulfur content of the reacted and original coal is assumed to have formed H_2S . The data are shown in Table II. The sulfur containing compounds formed during the reaction will be identified where possible and the results reported at a later date.

The formation of anthracene or phenanthrene from dibenzyl sulfide is perhaps the most unexpected aspect of the model coal compound study. A plausible mechanism that fits all of the data is the following:





In order to substantiate this mechanism, benzyl chloride was added to the melt and allowed to react for 20 hours at 40°C. GC/MS of the precipitate gave the same spectrum as authentic anthracene alone. To establish the presence of 9,10 dihydroanthracene as an intermediate in the reaction, authentic dihydroanthracene was added to the neat melt and allowed to react for 20 hours at 40°C. GC/MS of the precipitate showed the same spectrum as anthracene alone did. The mechanism for H₂S formation is probably as follows:



The Cd⁺⁺ thus serves as a catalyst for the reaction. Al⁺³ also reacts very strongly with sulfur and its role in the desulfurization mechanism is currently under investigation.

CONCLUSION

The extremely mild conditions used for the solubilization and desulfurization of coal and model coal compounds indicate that the molten salt may be an extremely useful medium for coal chemistry. If the soluble coal compounds can be identified, the nature of the sulfur containing fragments of the coal macromolecule can also be determined with some degree of assurance because their structure is the same as, or at least mechanistically related to their structure, in the original coal. Furthermore, if reaction conditions are optimized, a very high percentage of a coal's sulfur can be removed at room temperature and atmospheric pressure.

ACKNOWLEDGMENT

We would like to thank the Alumni Undergraduate Research Program at Bowling Green State University and the Research Challenge Program of the State of Ohio for their support. We would also like to thank the Premium Coal Sample Program at Argonne National Laboratory for contributing the coal samples.

LIST OF REFERENCES

1. D. S. Newman, R. E. Winans, "Proceedings of the Third International Symposium on Molten Salts," G. Mamantov, M. Blander, G. P. Smith, Editors, The Electrochemical Society Softbound Series, p. 425, Pennington, NJ, 1981.
2. D. S. Newman, R. E. Winans, R. L. McBeth, *J. Electrochem. Soc.* **131**, 1079 (1984).
3. D. S. Newman, T. H. Kinstle, G. Thambo, "Proceedings of the Joint International Symposium on Molten Salts," G. Mamantov, M. Blander *et al.* Eds., The Electrochemical Society, Pennington, NJ 1987, p. 991-1001.
4. D. S. Newman, T. H. Kinstle, G. Thambo, R. E. Winans, R. Hayatsu, R. L. McBeth, "Energy and Fuels," submitted for publication, 1988.
5. J. A. Boon, J. A. Levisky, J. L. Pflug, J. S. Wilkes, *J. Org. Chem.* **51**, 480 (1986).
6. J. A. Boon, S. W. Lander, J. A. Levisky, J. L. Pflug, L. M. Skizynecki-Cooke, J. S. Wilkes, "Proceedings of the Joint International Symposium on Molten Salts," G. Mamantov, M. Blander *et al.* Eds., The Electrochemical Society, Pennington, NJ 1987, p. 979-990.
7. D. P. Mobley and A. T. Bell, *Fuel* **59**, 507 (1980).
8. R. R. Rhinebarger, Ph.D. Thesis, Michigan State University (1986).

Table I. Organic Reaction Products of Dibenzyl Sulfide at 40°C

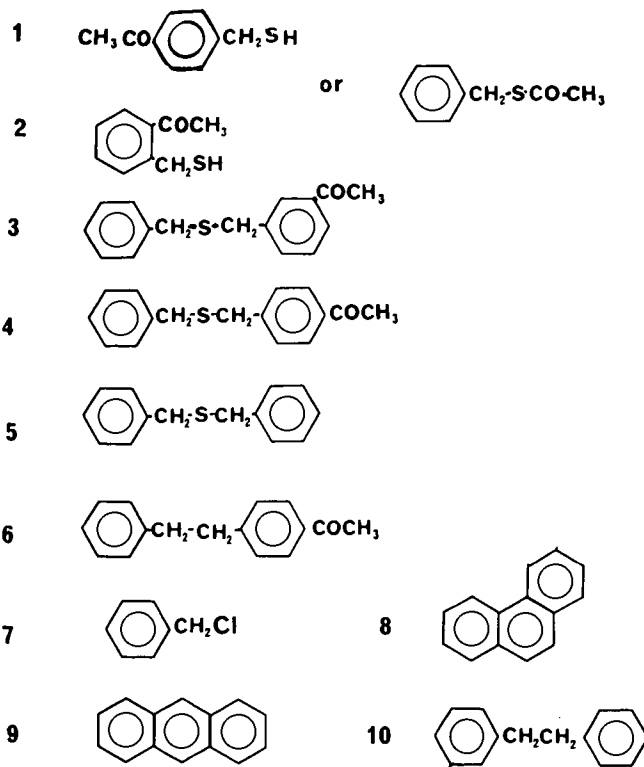


Table II. Weight Percent Sulfur in Coal Samples

Original Coal	Insoluble Portion	Soluble Portion
4.57	3.37	2.42

This page intentionally left blank

THE EFFICIENT, LARGE SCALE SEPARATION OF COAL MACERALS

Gary R. Dyrkacz and C.A.A. Bloomquist

Chemistry Division, Argonne National Laboratory,
9700 South Cass Avenue, Argonne, IL 60439

INTRODUCTION

For fundamental work on the chemical structure of coal, one of the first tasks that should be performed on a coal sample is to ensure that it is as homogeneous as is currently possible. This should require, at the very least, a petrographic analysis, and in many cases a subsequent separation to regulate the quality of the maceral or maceral group, even if the coal sample is optically monomaceral. Dyrkacz et al. have shown that even "pure" vitrinite shows a density distribution, which is, in part, related to differences in chemistry within the vitrinite maceral group.¹⁻³ However, despite the probability that experimental data may suffer from poorly characterized coal samples, it is not traditional practice to be concerned with the maceral separation of coal. The primary reason for this is that maceral separation is considered to be tedious and time-consuming. There is some truth in this statement, but the underlying question which should be asked is what is more important, the credibility and general applicability of the research data, or the additional time required to do a physical separation.

In our continuing efforts in the area of maceral separation, we have recognized the need for a process to supply relatively large amounts of macerals as rapidly as possible. Earlier we reported some initial work using combined sink/float and density gradient centrifugation (DGC) or continuous flow centrifugation and DGC.⁴ These early results indicated that continuous flow separation was somewhat effective, but beset with equipment specific difficulties.

Nevertheless, there are several notable advantages in using continuous flow centrifugation for maceral separation. First, the coal particles can be in a highly dilute suspension, which reduces particle-particle interactions. Second, large amounts of material can be separated; the major limitation being the capacity of the rotor. Third, the separation efficiency is higher. Unlike batch sink/float centrifuge operations, there are less cross-contamination problems with removal of the light and heavy particles, since the light phase is continuously removed. Lastly, the separation is fast. To produce an equivalent amount of purified coal material, much less manipulation is necessary to achieve separation compared to batch sink/float.

With all of these advantages in mind, we have again turned our investigations to continuous flow centrifugation for maceral separations. However, this time we are using a centrifuge specifically designed for such work. We report here our initial investigations on the separation of the maceral groups from Lewiston-Stockton coal from the Argonne Premium Coal Sample Program (APCS-7).

EXPERIMENTAL

Coal Pre-treatment. The APCS-7 coal (-100 mesh) was ground to 1-2 microns average particle size using a Fluid Energy Mill (Sturtevant). The coal was then demineralized using HCl and HF as we have previously reported.⁵

Continuous Flow Centrifugation Procedure. A continuous flow centrifuge (CEPA-LE Laboratory centrifuge, Carl Padberg Zentrifugenbau GmbH; U.S. supplier: New Brunswick Scientific Co., Inc.) with a model "K" clarifier rotor was used for the work reported here. A Sharples model T-1, (PenWalt Corp.), with a 1-H clarifier rotor was also used for some early work. Rotor speed was measured with a Xenon strobe lamp and maintained at 37000 ± 2000 rpm. A peristaltic pump (Masterflex, Model 7520-00, Cole-Parmer) was used to pump the coal slurry through the spinning rotor at a flow rate of 160 mL/min. Before the coal slurry was fed into the rotor, clear solution was used to fill the rotor. Clear solution was also used after the separation to ensure that all the floating coal had been removed. The rotor effluent and deposit were filtered, washed with water, dried and weighed. When the rotor was stopped, fluid that remaining in the spinning rotor drained out. This material was collected and analyzed separately.

DGC Monitoring of the Continuous Flow Separation. Aliquots of the three fractions: effluent (float), deposit (sink) and rotor liquid, derived from the continuous flow centrifuge separation were analyzed by the analytical density gradient centrifugation procedures of ref. [5].

RESULTS

The continuous flow centrifuge that we employed is commonly used for separation of biological materials, such as the harvesting of cells or other biological particulates. This centrifuge is a much simpler design than we used previously.⁴ The heart of the centrifuge is the rotor which consists of a simple rotating hollow cylinder which narrows to an open tube at the bottom and has holes drilled perpendicular to the main axis for the fluid to exit at the top. The expelled effluent is retained by an encircling collector ring. Fluid is injected into the rotor at the bottom through a nozzle centered in a lower bearing assembly. A series of radial vanes within the bottom of the rotor help accelerate the fluid to the rotor velocity. From this description, it is obvious that the CFC process is not truly continuous, since once the rotor deposit nearly fills the rotor, operation must be suspended long enough to empty the rotor. However, this represents only a minor inconvenience when compared to the manipulations involved in a sink/float centrifuge separation.

The coal sample that was chosen for our investigations was the Lewiston-Stockton coal (APCS-7) from West Virginia. This coal is reported to have a high proportion of all three maceral groups. Our own petrographic analysis shows this coal to contain 11.5% liptinite, 72.8% vitrinite and 15.6% inertinite.

There are two ways to analyze the efficiency of the continuous flow procedure. One of the more common approaches is to petrographically analyze the samples generated in the CFC separation. However, we know that the maceral groups have particle density distributions that naturally overlap each other.² Thus, the presence of more than one maceral type in a sink or float fraction does not necessarily translate to a bad separation. Since petrographic analysis is not

able to make such fine distinctions, we chose to use density gradient centrifugation (DGC) to determine the true state of the separated material.

To effectively use DGC, it is first necessary to obtain the density distribution of the unseparated coal. Figure 1 represents the separation and maceral analysis of a two gram sample of APCS-7 coal, using a CsCl/Brij-35 aqueous gradient. This maceral distribution pattern is consistent with other coals of similar rank.^{2,4}

Two CFC separations were done on APCS-7 using separate samples. The density cuts were made at 1.232 and 1.332 g cm⁻³ using CsCl/Brij-35 aqueous solutions. From Figure 1, these densities are near the density points where equal amounts of either liptinite/vitrinite or vitrinite/inertinite particles should be present. The concentration of coal in the feed slurry was 40 g/L. This amount is not the highest slurry concentration that can be used, but instead represents a conservative experiment to demonstrate the separation. However, even this slurry concentration is still much higher than we would recommend for optimum resolution in simple sink/float maceral separations.

Once the separations were completed, the coal in each fraction was isolated by filtration, washed, dried and weighed. Figure 2 represents the sum of all the observations for these two individual separations. The data on the sink/float fractions, as we have already indicated, were derived from analytical DGC on very small amounts (2 mg) of each fraction. The vertical bars on the plots represent the densities of the solutions. Following any particular density distribution of a sink or float fraction (lower two plots), anything passing the vertical line represents cross-contamination. As can be seen some of the fractions are better than 90% disengaged. This result approaches the limit of analytical DGC to probe the CFC separation, since there is some unavoidable maceral band spreading which can give the false impression of contamination. On the other hand, there are some fractions which show substantial cross-contamination. The liptinite/vitrinite+inertinite separation shows a strong bimodal distribution in the float fraction, as does the sink fraction in the liptinite+vitrinite/inertinite separation.

The curves in the lower two plots of Figure 2 oversimplify a more complicated experimental reality, which more critically explains the reason for some fractions showing poorer maceral resolution. The sink data in Figure 2 are actually composed of two separate fractions. Three fractions are actually collected from each run: the float, which exits the rotor during the run, the sink, which is the deposit on the rotor wall, and a third portion, which is obtained from the solution left in the rotor when the run is completed. This additional fraction is collected once the velocity of the rotor decreases below a certain limit. The centrifugal force becomes too low to retain the fluid, and it drains out the bottom of the rotor. It is the sum of this material and the material deposited on the rotor wall, which is shown in Figure 2. Figures 3 and 4 show all three fractions from both density cuts. Each density distribution curve has been normalized to the highest absorbance value (roughly proportional to mass). Notice that all the fractions labeled as sink (material on rotor wall) are actually well separated. The fraction labeled as rotor drainage (Rtr. Drng.) exhibits a high degree of cross-contamination in both runs. Table 1 provides the separation data on the purity of the fractions; the data is derived by integrating the analytical DGC results before and after the solution density cut line shown in either Figures 2 or 3. Without the inclusion of the rotor drainage material (which can account for approximately 50% of the sink material

collected), the material deposited on the rotor wall shows excellent resolution from float material.

We have attributed the behavior of this rotor drainage fraction to the sum of several processes:

1. When the solution in the rotor drains out at the end of the run, some of the material from the rotor wall is unavoidably carried away in this process. At this time we cannot say how much. The level of contamination with sink material may be high because in our tests relatively small amounts of coal (20 grams) are being separated and are being deposited in a narrow area of the rotor.
2. The coal particles have a range of particle size from about 0.5 to 6 microns. The very fine particles may not have time to separate during their passage through the rotor and may be held up in the rotor.
3. Some of the material cannot be separated because it is at or very close to the same density as the solution density.

We have examined several of the float contaminations in our sink fractions under the microscope, and indeed have found that finer material is present in much higher concentration than in the feed. In the case of the liptinite/vitrinite+inertinite separation in Figure 3 the float fraction also shows a large contamination peak. We have determined that the high density peak is due to the presence of extremely fine particles (< 1 micron). This fact suggests that the high density peak does not represent the true amount of material. We have observed previously that fine particles may give rise to a much larger absorbance than larger particles due to greater scattering. The purity in this case should be considered as a minimum enrichment.

DISCUSSION

We believe that the separation of macerals by continuous flow centrifugation offers a simple technique for the large scale separation of macerals. With relatively little cost (~ \$10K), it provides an opportunity for obtaining quite pure maceral fractions. Although we have not completely worked out all the nuances of this separation system, we believe that the problems we have indicated can be minimized to pose only minor inconvenience.

We cannot say that this system completely bypasses the disagreeable tedium or time involved in separating macerals, nor will it by itself overcome the mental inertia required to make maceral separation an accepted necessary fact in fundamental coal science. However, we find our particular brand of continuous flow centrifugation is considerably faster than sink/float separation, can provide a good quality product with even one separation cycle, and permits the handling of more material than a conventional sink/float centrifuge separation.

ACKNOWLEDGMENTS

This work was performed under the auspices of the Office of Basic Energy Sciences, Division of Chemical Sciences, U.S. Department of Energy, under contract W-31-109-ENG-38.

REFERENCES

1. Dyrkacz, G.R., Bloomquist, C.A.A., and Ruscic, L., Fuel, **63**, 1166-1173 (1984).
2. Dyrkacz, G.R., Bloomquist, C.A.A., and Ruscic, L., Fuel, **63**, 1367-1373.
3. Dyrkacz, G.R., Bloomquist, C.A.A., Ruscic, L. and Crelling J., to be published.
4. Dyrkacz, G.R., Bloomquist, C.A.A., and Horwitz, E.P., Sep. Sci. Tech., **16**, 1571-1588 (1981).
5. Dyrkacz, G.R., and Horwitz, E.P., Fuel, **61**, 3-12 (1982).

TABLE 1. Analysis of Continuous Flow Centrifugation Separation by Analytical Density Gradient Centrifugation.

Percent Purity of Fraction from DGC			
Float	Rotor Drainage	Rotor Deposit	Total Sink
Cut Density = 1.232 g cm ⁻³			
47.9	95.7	99.6	98.6
Cut Density = 1.332 g cm ⁻³			
97.4	59.3	97.6	79.4

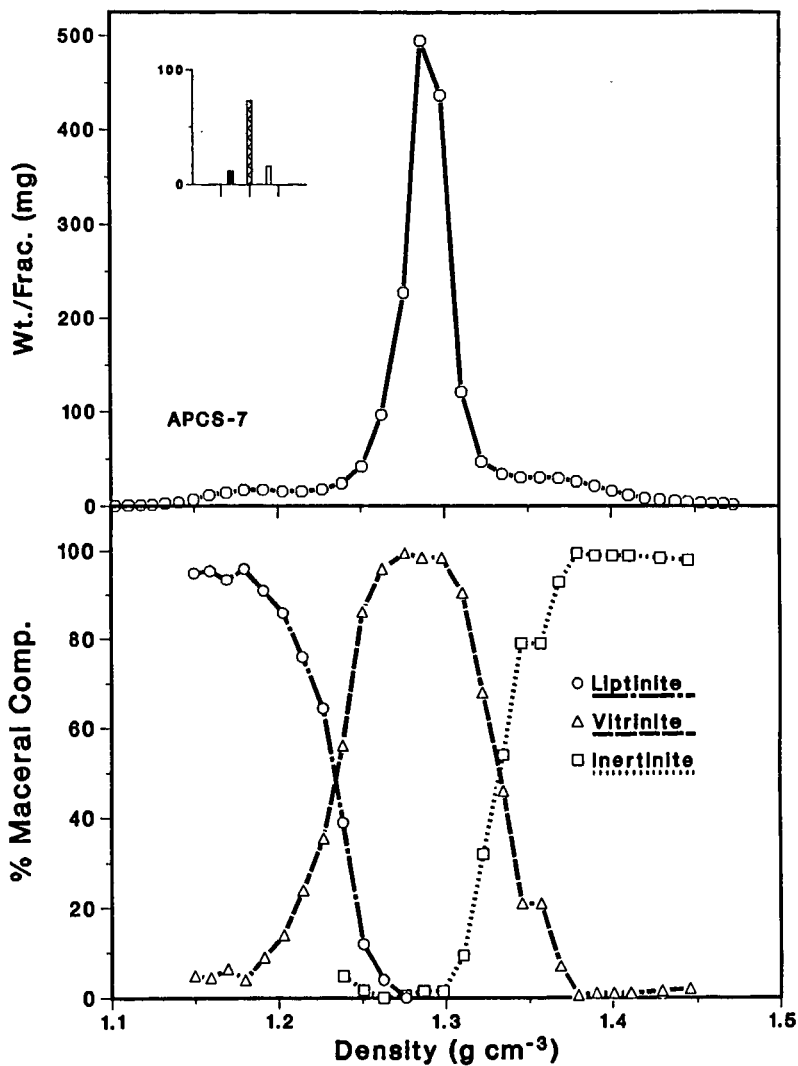


Figure 1. Maceral density distribution of APCS-7 coal obtained by DGC. Lower plot is the maceral analysis of selected density fractions. All densities are at 25°C.

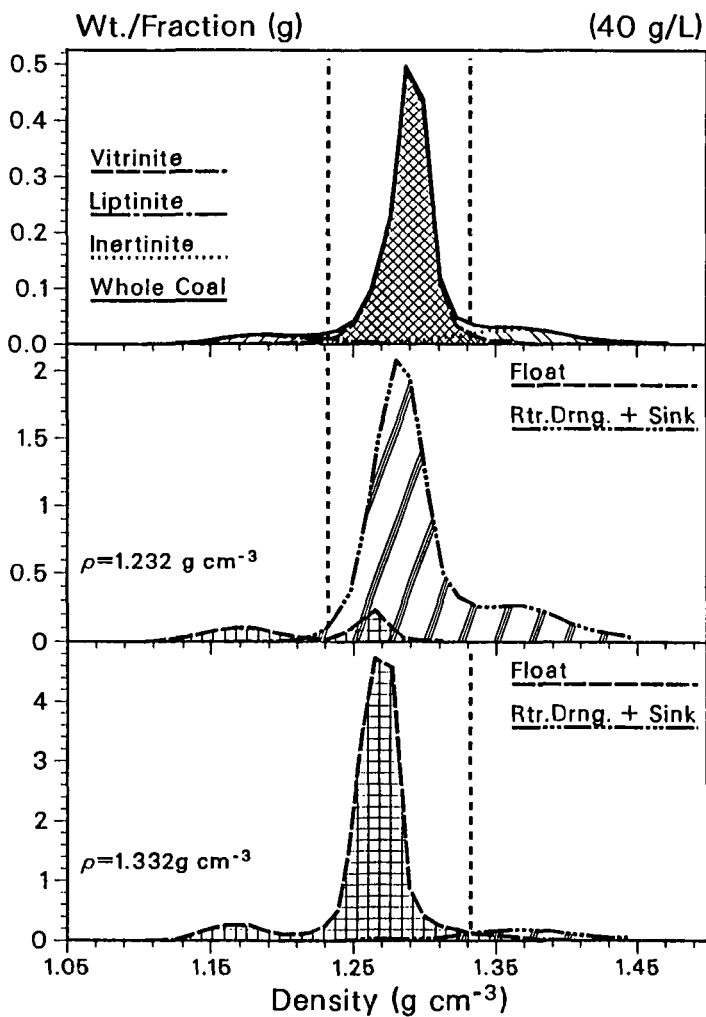


Figure 2. Top: Maceral density distributions of APCS-7 showing the actual weight distribution of each maceral group. Middle: DGC separations of float and sink CFC fractions for removing liptinite from vitrinite + inertinite. Bottom: DGC separations of float and sink CFC fractions for removing vitrinite + liptinite from inertinite. Absorbance is roughly proportional to weight.

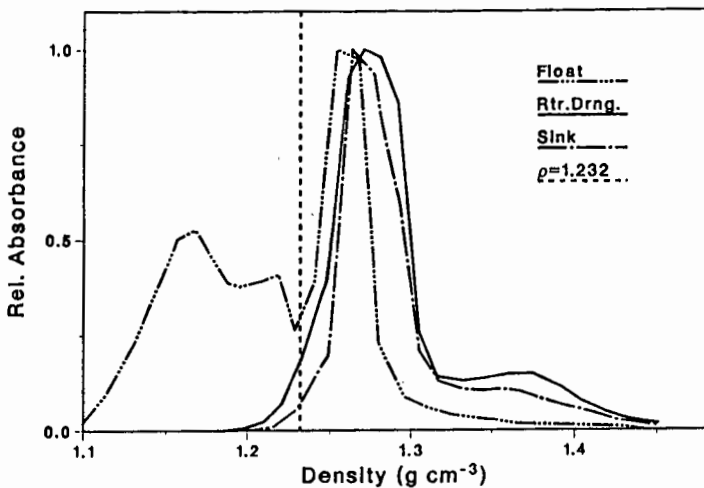


Figure 3. Detailed DGC pattern for the three collected CFC fractions for liptinite removal. All distributions have been normalized to the highest peak in each individual fraction.

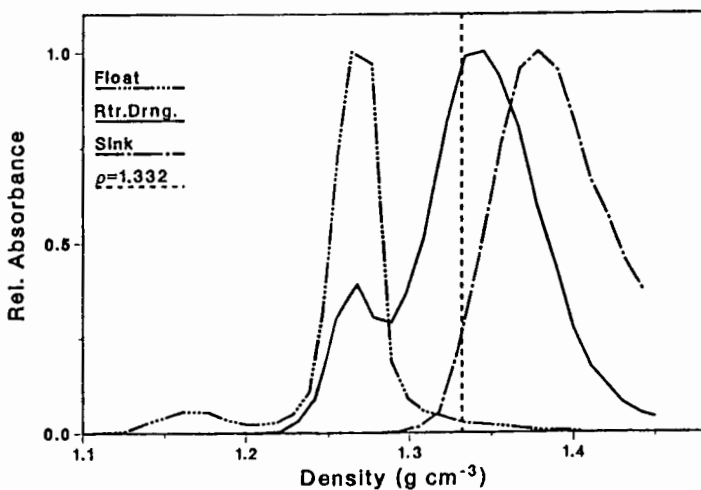


Figure 4. Detailed DGC pattern for the three collected CFC fractions in inertinite removal. All distributions have been normalized to the highest peak in each individual fraction.

WEATHERING STUDY OF ARGONNE PREMIUM COAL SAMPLES
BY FTIR AND MOSSBAUER SPECTROSCOPY

K.A. Martin
S.S. Chao

Institute of Gas Technology
Chicago, Illinois 60616

INTRODUCTION

A considerable number of infrared studies have been done on the low-temperature oxidation of coal with conflicting results. Because the reactions occurring in coal are dependent on a number of factors such as coal rank, particle size, temperature and humidity, a consensus on the oxidation mechanism(s) has not been achieved. Oxidation has been found to produce ethers (1-4), carboxyl groups (2-6), and OH functionalities (5). The formation of a peroxide is generally considered to be the major pathway for the production of new oxygen-containing groups, while at the same time a decrease in the aliphatic CH stretching region is observed (1,5) corresponding to dehydrogenation. The present study is an attempt to use FTIR to follow the effects of mild weathering conditions on a series of standard coal samples. In one part of the study, the room temperature desorption of moisture from these coals was followed using diffuse reflectance spectroscopy (DRIFT), and in the other part, the coals were weathered at room temperature in water-saturated air and sampled at intervals over a three month period for FTIR and Mössbauer analysis.

EXPERIMENTAL

Eight Argonne premium coal samples (-100 mesh) were studied: Pennsylvania Upper Freeport, Wyodak, Illinois #6, Pittsburgh #8, Pocahontas #3, Utah Blind Canyon, West Virginia Stockton-Lewiston, and Beulah-Zap. After thorough mixing, each ampoule of PCSP coal was opened and about 300 mg of the neat sample was transferred to a DRIFT sample cup and enclosed in an environmental chamber in a stream of dry air (2 ml/sec). Infrared spectra were collected at intervals over an eight hour period and again after 24 hours with a Nicolet 60SXB FTIR using 300 scans at 4 cm^{-1} resolution. The same dried KBr reference was used for each series of spectra and, because difference spectra were obtained, the KBr did not contribute to the absorption in the OH region.

For the longer-term study, a second vial of the coal was opened and the coal transferred to a large petri dish which was placed in a large dessicator (without dessicant) through which water-saturated air at 22°C was flowed at a rate of approximately 1 ml/sec. Portions of the coal were removed at intervals of 0, 1, 4, 24, and 48 hours, 1 week, and 1 and 3 months. These samples were dried in a vacuum oven at 40°C for two hours to halt the weathering process and stored under vacuum prior to analysis. Each sample was divided into different portions for infrared, Mössbauer and elemental analysis. Another 0.5 g of the original coal was removed to make the low-temperature ash (International Plasma Machine 1101B, 130 Watts for several days). DRIFT spectra were obtained on the neat coal sample with an environmental chamber for the non-weathered coal and without an environmental chamber for all DRIFT samples. Transmission spectra were obtained on KBr

pellets (about 0.3% coal by weight). All spectra were collected at 4 cm^{-1} resolution using 500 scans for the DRIFT spectra and 128 scans on the KBr pellets. Samples for Mössbauer analysis were prepared by grinding 0.3-0.6 g of the coal with 0.8 g of SOMAR blend, an organic binding agent, and pressing the samples into 32 mm diameter pellets. Mössbauer spectra were obtained on a Ranger Scientific MS-900 spectrometer at room temperature for 1-3 days. Carbon, hydrogen and nitrogen analyses were performed with a LECO CHN-600 analyzer, and oxygen analyses were performed with a Carlo ERBA 1106 elemental analyzer.

RESULTS AND DISCUSSION

Moisture Desorption

The desorption of water from the fresh coal samples was followed by DRIFT in the region $3800\text{-}2800\text{ cm}^{-1}$. DRIFT is especially useful for this type of study because it eliminates the error associated with water which may be trapped in a KBr pellet. This method has been used previously to study water desorption at elevated temperatures (7). The decrease in the integrated area of the OH region from the fresh coal to the vacuum-dried coal can be directly related to the moisture content determined by a separate procedure. In this case, absorbance units were used rather than the Kubelka-Munk units normally used for DRIFT spectra with good results. Table 1 gives the moisture contents of the initial coals and the moisture contents remaining after 1/2 hour and 8 hours of exposure to a stream of dry air at room temperature. Eight hours was found to be sufficient to remove over 90% of the moisture in all but the Illinois and Pittsburgh coals. Between one-third to one-half of the water was removed within the first half-hour of drying with the rate of desorption proportional to the initial moisture level. Spectral subtraction revealed no other changes in the spectrum other than a negative band near 1640 cm^{-1} as water was removed.

Weathering

Weathering under humid conditions over a longer period of time showed other changes in the OH region. DRIFT spectra of the vacuum-dried coals show an increase in the OH band over periods of 1 week and 1 month (Figure 1) with the largest increases found in the Pittsburgh, Illinois, Beulah-Zap and Blind Canyon coals and the least increase in the Pocahontas coal. Simultaneously, a slight increase in absorption centered around 1100 cm^{-1} is observed in all of the KBr pellet coal spectra after 1 week and after 1 month of weathering. An increase in this region after weathering is usually attributed to ethers but may also be due to alcohol groups. Other increases were apparent in the carbonyl region $1800\text{-}1500\text{ cm}^{-1}$ after 1 month (Figure 2). A weak band at 1710 cm^{-1} , not very apparent in the compressed spectra of Figure 2, appears in the subtraction spectra of the Pocahontas and Wyodak coals. All of the coals show an increase near $1660\text{-}1630\text{ cm}^{-1}$, which may be due to highly hydrogen-bonded carbonyls or to water bending modes from water of hydration which is not removed by vacuum. All of the coals except Pennsylvania and Pocahontas show a slight increase in the region $1560\text{-}1540\text{ cm}^{-1}$, which may arise from the formation of carboxylate groups.

In contrast to previous studies which found ether formation the dominant reaction under low temperature oxidation conditions (1-2), these results indicate the formation of an OH group, from either a hydroxyl functionality or water of hydration. This formation is only slightly dependent on coal rank, as the Pennsylvania and Pocahontas coals form the least amount of OH, but the other coals form OH in a manner independent of rank. The formation of ether groups and/or alcohol groups is indicated by the increase near 1100 cm^{-1} . The new bands near 1650 cm^{-1} may be due to water or to a shift in carboxyl group frequency due to increased hydrogen bonding, as might occur with the formation of OH groups, or to oxidation to new carbonyl groups. Carboxylate groups appear to form for all but the highest rank coals. In conclusion, new functional groups are formed on coal after weathering under humid conditions at room temperature for as little as 1 week. These include carboxylate groups on all but the Pennsylvania and Pocahontas coals, carbonyl groups on the Pocahontas and Wyodak coals, and chemisorbed water, alcoholic or ether groups.

ACKNOWLEDGMENT

The authors thank Dr. Karl Vorres of Argonne National Laboratory for the coal samples.

REFERENCES

1. R. Liotta, G. Brons and J. Isaacs, Fuel **62**, 781 (1983).
2. J. S. Gethner, Appl. Spec. **41**, 50 (1987).
3. G. P. Huffman, F. E. Huggins, G. R. Dunmyre, A. J. Pignocco and M. C. Lin, Fuel **64**, 849 (1985).
4. D. C. Cronauer, R. G. Ruberto, R. G. Jenkins, A. Davis, P. C. Painter, D. S. Hoover, M. E. Starsinic and D. Schlyer, Fuel **62**, 1124 (1983).
5. A. G. Pandolfo, R. B. Johns, P. D. Nichols and D. C. White, ACS Preprints, Division of Fuel Chemistry **32**, 171 (1987).
6. B. M. Lynch, L. I. Lancaster and J. A. MacPhee, ACS Preprints, Division of Fuel Chemistry **32**, 139 (1987).
7. N. R. Smyrl and E. L. Fuller, in "Coal and Coal Products: Analytical Characterization Techniques", E. L. Fuller, Ed., ACS Symposium Series 205, American Chemical Society, Washington, D.C., Chap. 5, 1982.

kate

Table 1. Moisture Content of Coals After Room Temperature Air-Drying

	Initial Moisture, %	Moisture Remaining After 1/2 Hour, %	Moisture Remaining After 8 Hours, %
Pocahontas	0.84	0.42	0
Pennsylvania	1.41	1.01	0
Pittsburgh	2.54	1.31	0.32
Lewiston-Stockton	2.70	1.69	0.27
Blind Canyon	5.04	2.38	0
Illinois	8.65	5.83	1.41
Wyodak	24.23*	15.00	0.24
Beulah-Zap	32.84*	25.45	0.92

*From PCSP provided data.

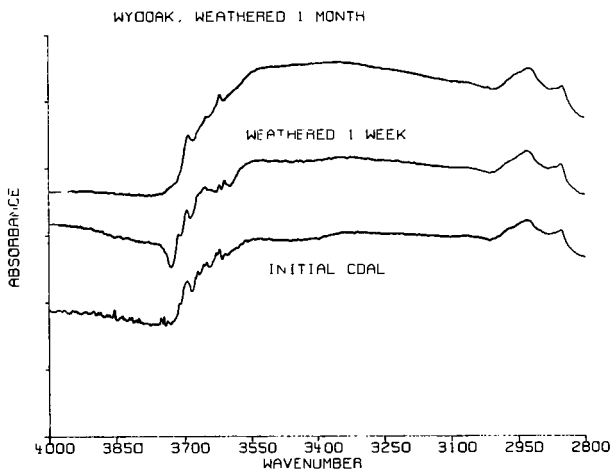


Figure 1. Increase in OH region over one month (Wyodak coal).

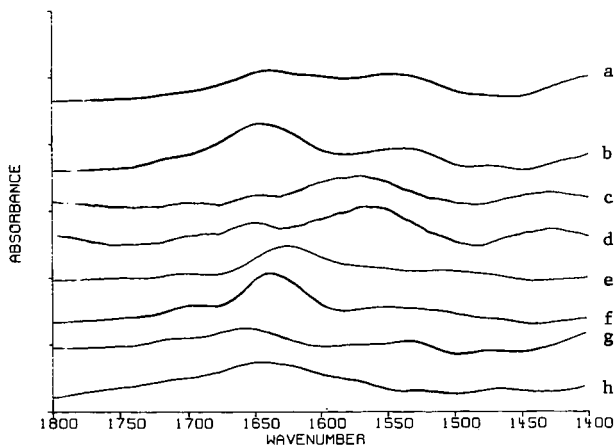


Figure 2. Change in carbonyl region over one month (a = Pittsburgh, b = Illinois, c = Lewiston-Stockton, d = Blind Canyon, e = Pennsylvania, f = Pocahontas, g = Wyodak, h = Beulah-Zap).

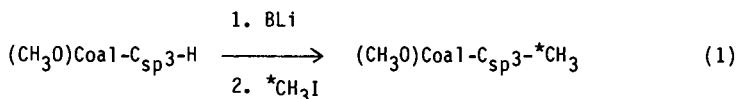
THE IMPORTANCE OF DIPHENYLMETHANE-LIKE STRUCTURAL UNITS
IN AN ARGONNE PREMIUM COAL SAMPLE*

R. Rife Chambers, Jr., E. W. Hagaman and M. C. Woody
Chemistry Division
Oak Ridge National Laboratory
Oak Ridge, Tennessee 37831-6197

INTRODUCTION

The development and application of chemical and spectroscopic techniques for the purpose of evaluating the acidic O-H and C-H sites in coal has received much attention recently (1-8). In general, these studies have relied on the ability of bases to abstract acidic protons from O-H and C-H sites to generate coal anions. These anions can then be alkylated with a variety of reagents which includes alkyl halides (2,5), alkyl tosylates (4) and alkyl sulfates (6,8). The resultant coal derivatives can be studied by using a combination of chemical and spectroscopic probes such as Soxhlet extractability (2,5), pyrolytic behavior (9) and ^{13}C NMR (2,6,7,8).

Our approach (3,6,8) for characterizing the acidic C-H bonds in coal is to treat O-methyl coal with a series of indicator bases, BLi, followed by methylation with C-13,14 double labelled methyl iodide, equation (1).



*C = 13,14C

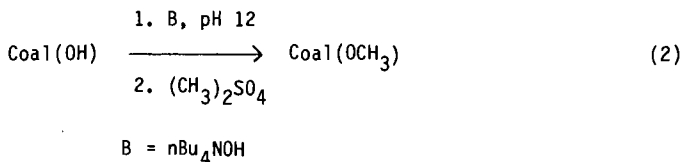
By varying the identity of BLi, and thus the pK_a of the conjugate acid BH, it is possible to evaluate the number of C-H bonds as a function of pK_a . The bases we have used thus far, 9-phenylfluorenyllithium (pK_a , 18.5 (10)), fluorenyllithium (pK_a , 22 (10)) and trityllithium (pK_a , 31 (10)), have allowed us to evaluate the distribution of acidic C-H sites within the three pK_a ranges: $12 < \text{pK}_a < 18.5$, $18.5 < \text{pK}_a < 22$, and $22 < \text{pK}_a < 31$. The application of this approach to two bituminous coals, namely Illinois No. 6 hvCb and PSOC 1197 lvb, led to the discovery of a significant concentration of acidic C-H sites with $18.5 < \text{pK}_a < 22$ which was interpreted as evidence for fluorene-like structural units in coal (6,8).

This approach to coal structure analysis is limited to the evaluation of acidic C-H sites with $\text{pK}_a < 31$. Furthermore, it was shown that PhCH₂Ph (pK_a , 33(11)), the prototypical diarylmethane, is not alkylated to a significant extent upon treatment with trityllithium and methyl iodide (12). For these reasons, we have developed approaches for the evaluation of acidic C-H sites with $31 < \text{pK}_a < 33$. In this article, we illustrate these approaches using Upper Freeport mvb (APCS number 1) as the coal.

*Research sponsored by the Division of Chemical Sciences/Office of Basic Energy Sciences, U.S. Department of Energy under contract DE-AC05-84OR21400 with the Martin Marietta Energy Systems, Inc.

RESULTS AND DISCUSSION

The Upper Freeport coal, empirical formula $C_{100}H_{76}S_{10}O_3$, was O-methylated at pH 12 by using tetrabutylammonium hydroxide as base and natural abundance dimethyl sulfate as previously reported (8), equation (2).



Parallel experiments in which ^{14}C -dimethyl sulfate was employed as the methylating agent established that no more than 0.4 O-methyl groups per 100 coal carbons are formed under these conditions.

The first approach to evaluate the C-H sites with $31 < pK_a < 33$ relies on a comparison of the relative reactivity of the O-methyl coal towards alkylation with base and $^{13,14}\text{CH}_3\text{I}$, where the pK_a of the conjugate acid of the base equals 31 or 33. This was done using trityllithium (pK_a , 31 (10)) and diphenylmethyl-lithium (pK_a , 33 (11)) as the bases. Carbon-14 combustion analysis (13) was used to evaluate the number of methyls introduced with the two bases as a function of the number of repetitive treatments with base and methyl iodide. The data, as shown in Table 1, demonstrate the requirement for a minimum of three multiple treatments to achieve exhaustive methylation. This result parallels our earlier observations on the C-alkylation of O-methyl Illinois No. 6 (3) and O-methyl PSOC 1197 (6,8). This chemical property can be interpreted as evidence for the methylation of structural units which contain multiple acidic C-H bonds such as the methylene group, $-\text{CH}_2-$. The calculation of the number of acidic C-H bonds with $31 < pK_a < 33$ is done by making the difference: number of methyls added with diphenylmethyl-lithium minus number of methyls added with triphenylmethyl-lithium. For O-methyl Upper Freeport, this calculation yields $0.5 \pm 0.2/100$ coal C when the first treatment values are used and $1.1 \pm 0.3/100$ coal C after three treatments.

A second approach was also used to evaluate the number of C-H sites with $31 < pK_a < 33$. This involves the exhaustive methylation of all acidic C-H sites with $pK_a < 31$ followed by methylation using diphenylmethyl-lithium and $^{13,14}\text{CH}_3\text{I}$. Alkylation of the acidic sites with $pK_a < 31$ was accomplished by treating O-methyl Upper Freeport with trityllithium and natural abundance methyl iodide a total of six repetitive treatments. Subsequent methylation of this coal derivative with diphenylmethyl-lithium and $^{13,14}\text{CH}_3\text{I}$ followed by ^{14}C combustion analysis yielded a value of 0.9 C-H sites/100 coal C (1 treatment only). Further work is in progress to determine whether this value increases as a result of multiple treatments.

These preliminary data from the two complementary approaches indicate that diarylmethylene units, ArCH_2Ar , and substituted analogs such as ArC(H)RAR which have C-H sites with $31 < pK_a < 33$ are important structural entities in the Upper Freeport coal. Considering only the first treatment data from each approach

where multiple alkylation at $-CH_2-$ groups is assumed to be negligible, then the number of these structural types can be estimated as 0.5 - 0.9 per 100 coal carbons.

REFERENCES

1. L. M. Stock, Coal Science, 1, 161 (1982).
2. (a) R. Liotta, Fuel, 58, 724 (1979). (b) R. Liotta, K. Rose, and E. Hippo, J. Org. Chem., 46, 277 (1981). (c) R. Liotta and G. Brons, J. Am. Chem. Soc., 103, 1735 (1981).
3. R. R. Chambers, Jr., E. W. Hagaman, M. C. Woody, K. E. Smith, and D. R. McKamey, Fuel, 64, 1349 (1985).
4. M. Ettinger, R. Nardin, S. R. Mahassay, and L. M. Stock, J. Org. Chem., 51, 2840 (1986).
5. N. Mallya and L. M. Stock, Fuel, 65, 736 (1986).
6. E. W. Hagaman, R. R. Chambers, Jr., and M. C. Woody, Energy and Fuels, 1, 352 (1987).
7. R. E. Botto, C. Choi, J. V. Muntean, and L. M. Stock, Energy and Fuels, 1, 270 (1987).
8. R. R. Chambers, Jr., E. W. Hagaman, and M. C. Woody, ACS Advances in Chemistry Series No. 217, 'Polynuclear Aromatic Compounds', L. B. Ebert, Ed., 255 (1988).
9. G. R. Rose, R. F. Zabransky, L. M. Stock, C. Huang, V. R. Srinivas and K. Tse, Fuel, 63, 1339 (1984).
10. D. A. Bors, M. J. Kaufman, and A. Streitwieser, Jr., J. Am Chem. Soc., 107, 6975 (1985).
11. A. Streitwieser, Jr., E. R. Vorpapel, and C. Chen, J. Am. Chem. Soc., 107, 6970 (1985).
12. R. R. Chambers, Jr., E. W. Hagaman, and M. C. Woody, Fuel, 65, 895 (1986).
13. V. F. Raaen, G. A. Ropp, and H. P. Raaen, 'Carbon-14', McGraw-Hill: New York, 1968, Chapter 11.

Table 1. C-Methylation of O-Methyl Upper Freeport by using BLi and $^{13,14}\text{CH}_3\text{I}$ in THF at 0°C

Base, BLi (pK_a , BH)	Treatment No.	No. $^{14}\text{CH}_3/100$ Coal C
trityllithium (31)	1	0.61 ± 0.06
	2	0.90 ± 0.09
	3	1.1 ± 0.1
diphenylmethylithium (33)	1	1.1 ± 0.1
	2	1.8 ± 0.2
	3	2.2 ± 0.2

ADVANCES AND NEW DIRECTIONS IN DIRECT LIQUEFACTION

S. N. Rao, Burns and Roe Services Corporation
P. O. Box 18288, Pittsburgh, PA 15236

H. D. Schindler, SAIC International
One Sears Drive, Paramers, NJ 07652

G. V. McGurl, U. S. Dept. of Energy
Pittsburgh Energy Technology Center, Pittsburgh, PA 15236

1.0 INTRODUCTION

With advances in single stage processes such as H-Coal, EDS and SRC, and refining and upgrading of coal liquids by Chevron and UOP, the direct liquefaction process has continuously evolved to the present two-stage catalytic configuration, which produces the highest liquid yield and product quality of any process worldwide.

The Two Stage Liquefaction (TSL) process has been successfully applied to bituminous and subbituminous coals, overcoming problems associated with earlier processes. But, potential for additional improvement is recognized in several areas:

- o Cleaning coal prior to liquefaction.
- o Low temperature and pressure preconditioning of feed coal.
- o Novel catalysts development to arrest regressive reactions and improve hydrotreatment and cracking reactions.
- o Improvement in hydrocarbon value recovery and reduced energy rejection by alternate bottoms processing techniques.

In this paper, after discussing briefly the history of liquefaction and development of the TSL process, present potential areas for research and development are presented.

2.0 BACKGROUND

During the 1970's, four single stage processes (SRC-I, SRC-II, H-Coal and EDS) received substantial interest. Two of these, SRC-I and SRC-II, primarily involved thermal liquefaction and hydrogenation reactions. Others utilized catalytic reactions as well. The liquids from these processes needed substantial upgrading to obtain marketable products (1). The common features and drawbacks of these processes are:

- o 90% or better coal conversion is obtained but, reaction severity is high (820-860°F temperature, 1500-3000 psi pressure and 20-60 minutes residence time).
- o Distillate yields are about 50% of MAF coal, which are low relative to recent developments.

- o Hydrogen utilization is good but, efficiency is low due to high yields of hydrocarbon gases.

Attempts to improve the distillate yields and reduce reaction severity resulted in the development of two stage liquefaction (TSL) processes.

3.0 INTEGRATED TWO STAGE LIQUEFACTION (ITSL)

A. Early Studies

In late 1970's several thermal coal dissolution investigations concluded that coal conversion is essentially complete in an extremely short residence time of 1-2 minutes. The investigations also observed that higher hydrotreatment temperature and residence times resulted in increased yield of hydrocarbon gases. About the same time, at Wilsonville (Runs 145-146), increased importance of liquid phase hydrogen transfer in liquefaction was observed. Combining these observations Lummus developed the ITSL process.

B. Lummus ITSL

The Lummus ITSL process, tested in a 500 lbs per day PDU, consists of a short contact time (SCT) coal dissolution first stage followed by a LC-Fining catalytic hydrotreater as a second stage. Based on petroleum background, Lummus introduced Antisolvent Deashing (ASDA) equipment between the two stages.

The SCT reactor operated at shorter residence times (2-3 min.) and low pressures (500-1000 psi), while maintaining coal conversions above 90% MAF. The hydrocarbon gas yields were low and hydrogen utilization efficiency was high. Distillate yields were significantly better than the single stage processes. The SCT resid was reactive not only for conversion to distillate but also for heteroatom removal. The ITSL process also showed that the ashy recycle is not detrimental to catalyst activity and that a lighter and more desirable product (-650°F) can be made with little loss in hydrogen efficiency.

C. Wilsonville ITSL

Scale-up of the ITSL process to 6 tons/day (24 times) was performed at Wilsonville. A H-Oil ebullated bed hydrotreater (in place of the LC-Fining unit) and a Kerr-McGee Critical Solvent Deashing (CSD) unit for ash removal (in place of ASDA) were utilized. In spite of the retrogressive reactions in the CSD that lowered the coal conversion from 92 to 88% and the high organic rejection with the ash concentrate stream, a distillate yield of about 54% was obtained.

Wilsonville increased the distillate yield to 62% by placing the de-asher after the second stage (after vacuum distillation) which had no detrimental effect on the catalytic activity in the second stage reactor. With this reconfigured ITSL (RITSL) operation, retrogressive

reactions were limited and good operability with on-stream time of more than 95% was demonstrated. This RITSL operation showed that deashing prior to second-stage hydrotreatment was not necessary.

To further reduce retrogressive reactions by minimizing holding time between the reactors (first and second stage) and to eliminate pressure let down and repressuring, the two reactors were operated in a close coupled ITSL (CCITSL) mode. In this operation, all the first stage gases (CO, H₂S, H₂O etc.) and light oil were removed prior to second stage. There was no significant impact on catalyst activity and there was no discernable loss in performance relative to ITSL (yields, allowable space velocities, etc.). However, more rigorous analysis at a consistent set of conditions is necessary to verify the improvement of CCITSL over RITSL.

4.0 CATALYTIC TWO-STAGE LIQUEFACTION (CTSL)

A. HRI CTSL (1984 - Present)

In CTSL, the first stage temperature was lowered to 750°F to more closely balance hydrogenation and cracking rates, and to allow the recycle solvent to be hydrogenated *in situ* to facilitate hydrogen transfer during coal dissolution. The second stage was operated at higher temperature (820-830°F) to promote resid hydrocracking and generation of an aromatic solvent, which is then hydrogenated in the first stage (see Figure 1). The lower first stage temperature provides better overall management of hydrogen consumption, with hydrocarbon gas yields reduced by about 50 percent. Higher distillate yields were attained by the reduction of resid in the rejected ash-concentrated stream and the subsequent conversion of that recovered resid to distillates.

A pressure filter reduces resid concentration in the reject stream (filter cake) below 45-50 percent. This change signalled the end of the "hydrogen balanced" process and showed that overall liquefaction economics improve if the process maximizes distillate yield and produces hydrogen by natural gas reforming or by coal gasification.

A third change by HRI was in the use of NiMo catalyst. The H-Coal process had used a cobalt-molybdenum (CoMo)-on-alumina catalyst (American Cyanamid 1442B), which is used in petroleum applications. In coal liquefaction, hydrogenation of solvent must occur first, before the aromatic molecules can thermally crack. The catalyst must hydrogenate large molecules which determine the rate at which resid is converted. The (NiMo) catalyst has a bimodal pore distribution with larger micropores, 115-125 Å, which allows easier diffusion, as opposed to 60-70 Å for H-Coal catalyst, and the nickel promoter is also more active for hydrogenation than cobalt.

The latest reported results with Illinois No. 6 coal show a 78 percent distillate yield (Table 1). Hydrogen efficiency is over 10 pounds of distillate per pound of hydrogen reacted. In addition, the two catalytic reaction stages produce a liquid with low heteroatom concentrations and a high H/C ratio.

B. Wilsonville CTSL (1986-Present)

The most significant differences at Wilsonville are the reactor temperatures. As in ITSL, most of the thermal cracking takes place in the first reactor and solvent hydrogenation is in the second reactor. Therefore, the first reactor is at the higher temperature (800-820°F), while the second reactor is kept slightly lower at 795°F. Other reaction conditions are similar to HRI CTSL, including the catalyst type. The distillate yields are about the same, i.e. 78% MAF Coal. Wilsonville deashes by CSD, and steady improvement has reduced organic rejection to 8-15 percent, about the same as achieved by HRI.

C. Evolution of Liquefaction Technology

Substantial improvements in liquefaction processes and catalysts associated with these processes have taken place. The yields and quality of liquids have improved substantially. History of process development improvements are shown in Table 1. Yields of distillates have increased from 41% to 78% (5 barrels/ton of MAF bituminous coal). Quality is comparable to or better than No. 2 Fuel Oil with good hydrogen content and very low heteroatom content.

5.0 FUTURE RESEARCH AND DEVELOPMENT

The overall goal of coal liquefaction R&D is to develop technology to produce marketable liquids economically (\$25/Bbl by 1995). This requires scientific and engineering knowledge based on:

- o Improved processes to provide product selectivity and quality, increased liquid yields per ton of coal and improved thermal efficiency--involves current as well as novel catalysts and processes.
- o Improved plant operability and onstream factors by process and component development.
- o Reduction of Capital and Operating costs by optimization and integration of R&D improvement.

Brief descriptions of significant areas follow:

A. Preconversion and Regressive Reactions

The preceding discussion placed emphasis on process improvements, principally on the coal dissolution and resid upgrading reactions. This requires a better understanding of coal conversion chemistry.

The term "first reactor" is a misnomer, because there is strong evidence that the coal has undergone considerable reaction before entering that vessel (2). Coals have been found to undergo changes at temperatures as low as 200°C. Suuberg (3) has measured the evolution of carbon dioxide from low rank coals at low temperatures and Solomon (4) has related this gas evolution to cross-linking, which reduces coal reactivity thereafter. The onset of swelling has been measured at 200°C, with completion at about 500°C (4), again an indication of cross-linking. Derbyshire has shown that soaking coal at temperatures below 400°C increases yield of toluene solubles, presumably as the result of increased hydrogen transfer from the solvent (5). Recently, with liquid-phase transfer, 85 percent conversion of sub-bituminous coal and 91 percent conversion of bituminous coal (to quinoline-solubles) in about 30 seconds at 425°C (6) was reported. These findings show that coal has already reacted in the preheater, and in all likelihood, the coal (or coal liquid), in the reactor may be less reactive and must have necessitated high severity reaction conditions to undo the damage that took place during heat-up.

More information on the mechanism of these preconversion reactions and their impact on process yields and product quality are required. The effects of time, temperature, solvent quality, and catalyst-dispersed or soluble-on the kinetics of coal dissolution below 400°C and on the structure of the liquid product must be quantified. Process developers will utilize this information to modify preheat conditions to supply a more reactive feed to the first reactor. The anticipated benefits are increased coal conversion, increased reactivity of coal liquids, smaller reactors, moderating reaction conditions and better hydrogen efficiency. A more reactive feed should also improve catalyst activity in both stages.

B. Hydrotreatment and Cracking Reactions

Process development has emphasized resid conversion and liquid yield, but how is conversion achieved? Unlike petroleum resid, which cracks thermally to smaller molecules, which are then hydrogenated, coal resid must first be hydrogenated before cracking can occur. Hydrogenation is catalytic, while the cracking reactions may be either thermal or catalytic. Little is known about the kinetics of these reactions, and this work has the potential to improve on current TSL performance.

Catalyst activity for conversion falls to about 20 percent of its initial value in a few days. Sandia has related most of the catalyst deactivation to carbon laydown on the catalyst and the inhibiting effects of certain nitrogen compounds in the coal liquids (7). Others point to phenols as a source of deactivation (8). The mechanism of deactivation is not understood. With additional information, improved catalysts and regeneration may be possible.

A better understanding of the kinetics of these reactions could greatly improve process economics or even cause a major modification of the process. Lummus Crest, Inc. (LCI) found that resid hydrogenation is rapid at 450°C (9) therefore, most of the second stage reactor volume is required for conversion, which might be by thermal cracking. Increasing the cracking functionality of the catalyst could significantly reduce reactor volume.

In addition to investigating the kinetics of resid hydrogenation/cracking, additional information is needed on kinetics of hydrogenating heavy distillate (650°F+), and hydrogen transfer rates from solvent to coal and from distillate to resid. This latter point is of great importance in the preheater reactions just discussed. The benefits of soaking at low temperature may be related to relative rates of thermal cracking and hydrogen transfer at 200-400°C. Therefore, this temperature range must be included in the kinetic study of hydrogenation and cracking.

C. Integration of Coal Beneficiation and Cleaning

The quality and quantity of resid (or organic) rejected is a function of ash composition in the coal. Removal of ash by coal beneficiation has been a fairly standard practice and interest in deep cleaning to remove pyritic sulfur has increased substantially in the last decade. This has resulted in significant advances, such as:

- o Heavy media cyclone cleaning
- o Oil agglomeration
- o Microbubble flotation
- o Molten caustic cleaning

Intuitively, reduced ash content reduces organic rejection and facilitates liquefaction and hydrotreating by reduced corrosion and erosion. However, reduced pyrites and sulfur may decrease the catalytic activity. As a result, benefits of beneficiation and cleaning were uncertain and liquefaction units operated with standard coal beneficiation used for power plants (10% ash).

Recent coal agglomeration work by Consol, Alberta Research Council and PETC, and liquefaction data from PETC, HRI and Wilsonville operations have shown the advantages of deep coal cleaning (about 5% ash). Liquid yields increased by 5% and energy rejection was reduced. Corresponding economic benefits were noted by Mitre.

There are many unanswered questions:

- o What are the liquefaction characteristics of cleaned coal?
- o Can selective coal cleaning improve the process substantially.

- o Should the coal be cleaned to an ash content of 1%, 2% ash or 5%? What limits this ash content - coal cleaning process or liquefaction process?
- o How do we integrate? With bottoms? With heavy distillates?
- o What are the implications of integration on liquefaction reactions, hydrotreating reactions and coal cleaning?
- o Which coal cleaning process is more attractive economically and under what conditions?

Future R&D should provide answers to some of the above.

D. Alternate Liquid/Solid Separation System

The Wilsonville PDU employs the CSD developed for the SRC-1 process and HRI uses pressure filtration because the feed is lighter and less viscous than deasher feeds of just a few years ago. Both CSD and filtration achieve high recovery of resid, but are expensive to install and operate. As a result, comparative economics of alternate systems and alternate processes are required to achieve even better results at lower cost.

Recently, a fluid coking study (10) showed that over 60 percent of the toluene solubles in the deasher feed is recoverable as coker distillate. This is also expensive, but Mitre has estimated that it has economic advantages over CSD (11). Additionally, the coker distillate is highly aromatic and analyses by Consol have shown that, after hydrogenation, it is capable of effecting higher coal conversion than recycle solvents currently being used (12). Therefore, coking is being investigated, not only as a viable alternative approach to liquid/solid separation, but as a possible source of improved coal reactivity.

Should deep cleaning of coal become an integral step of direct liquefaction, the solids rejected will be only about 9 percent of MAF coal, and solids removal by vacuum distillation may become attractive. Total organics rejected in the vacuum tower bottoms would be only about 11 percent (less than 15 percent by CSD). Most of the bottoms will be recycled to the solvent tank and a small purge stream will remove ash, possibly by coal beneficiation. This alternate liquid/solid separation scheme is dependent on improvements elsewhere in the process and corresponding follow-up R&D, process integration and economic evaluation are required.

E. Systems Integration Schemes

Research to improve direct liquefaction technology must take into account the integrated nature of the process. A change made in any component in the process will impact others. Therefore, the entire

system, its technical viability and overall economics, must be considered as process improvements occur. For example, the alternative liquid/solid separation discussed earlier (Figure 2) uses a vacuum tower as the means of liquid/solid separation and may result in many process changes:

- o The composition of the recycle solvent will be changed (ratio of solvent/resid/solids);
- o The vacuum tower bottom may be fed to coal beneficiation to recover more organics;
- o The vacuum tower overhead may be the agglomerating oil for beneficiation;
- o The vacuum tower bottoms may be fed to a coker to recover coker distillate, and the coker distillate may be hydrogenated in the second stage.
- o The hydrogenated coker distillate may leave as product or may be recycled as solvent. Its effect on solvent quality is, as yet, unknown.

Similarly, the investigation of preconversion reactions may well result in changes that may effect the entire process and a similar systems approach will be necessary. Even changes in catalyst or reaction conditions must be viewed in terms of its impact on overall operability and economics of the process. Coordinated R&D with systems integration schemes are required.

F. Integration and Optimization

The direct liquefaction section is part of a larger plant. Some of the other areas that must be considered include:

- o Hydrogen production and purification
- o Coal preparation and handling
- o Waste processing and disposal
- o Refining and upgrading of coal liquids to marketable products

The first three areas constitute a large fraction of the cost of a liquefaction plant and R&D to improve these operations could greatly improve the overall economics of liquefaction.

Hydrogen production is always a potentially fruitful topic for research because of the cost of the hydrogen plant. Should hydrogen be made by gasification of CSD or vacuum tower bottoms, or by gasification of coal, or by reforming of natural gas? Whichever is selected will effect the entire plant. The effect of carbon monoxide on cata-

lyst activity is still not clear. Research is needed in that area. If CO has no inhibiting effect on catalyst activity, the hydrogen plant can be simplified. Conversely, the economic incentive of a less expensive hydrogen plant may be the impetus to develop such a CO-resistant hydrotreating catalyst. What are the requirements for recycle gas purification? How can they be integrated and optimized?

Similarly, it is to be expected that the use of coals different than those tested to date may require process modifications to achieve optimum yields. These coals may require different liquefaction processing or coal preparation. Weathering and oxidation effects on reactivity may have to be investigated.

The refining of coal liquids has received relatively little attention, even though this is the step that makes the marketable products that are the ultimate goal of the plant. Chevron (1) has already shown that a heavy distillable coal liquid is difficult to refine. This finding directed efforts to the production of a lighter (-650°F) coal liquid, which has been achieved successfully. However, further integration with the utilities and refiners may lead to other process modifications in order to make coal liquids more valuable, either as a refinery feed or as marketable products.

6.0 CONCLUSIONS AND RECOMMENDATIONS

The current CTSL process is the best direct liquefaction process in the world. It produces the highest yield of liquid product, having the highest quality-- and it does this at a lower cost per barrel than previous processes. Significant improvements, however, are attainable and are needed to be competitive with crude oil prices (\$25/bbl). These will come from research on the fundamentals of coal liquefaction and on process modifications. All research must be performed with an understanding of the effect it will have on the entire process. The most promising areas for future research are in preconversion chemistry and retrograde reactions, hydrogenation and cracking reactions, coal preparation, and solids rejection. Many of these programs are already in progress. The results are expected to provide a better understanding of liquefaction and foster a new generation of more economic and efficient direct liquefaction technology.

REFERENCES

1. Chevron Research Co., Refining and Upgrading of Synfuels from Coal and Oil Shales by Advanced Catalytic Processes, DOE Reports: DOE/ET/10532 - T11, T17, T19, T23, T25, T27
2. The Lummus Co., Integrated Two Stage Liquefaction, DOE Report 14804-Q10.
3. Suuberg, E.M., Unger, P.E., and Larson, J.W., ACS Division of Fuel Chem., Preprints 30 (4), 291 (1985).

4. Deshpande, G.V., Solomon, P.R., and Serio, M.A., "Crosslinking Reactions in Coal Pyrolysis" presented at ACS Toronto Meeting, June 1988.
5. Derbyshire, F.J., Davis, A., Epstein, M., Stansberry, P., Fuel 65, 1233-1240 (1986).
6. Lummus Crest Inc., Research of Coal Liquefaction Co-Processing, DOE Report PC70042-TF.
7. Stephens, H.P. Stohl, F.V., ACS Division of Petroleum Chemistry, Preprints 30 (3), 465-472 (Sept. 1985).
8. Moroni, E.C., Proceedings - 1987 International Conference on Coal Science, Maastricht, the Netherlands, Elsevier, pp. 351-354 (1987).
9. Lummus Crest Inc., Integrated Two Stage Liquefaction, DOE Report PC50021-Q11.
10. Lummus Crest Inc., Alternate Vacuum Bottoms Processing, Final Report for DOE Contract DE-AC22-87PC79338.
11. The Mitre Corporation, Assessing the Economic Impact of the Two Stage Liquefaction Process Improvements, Direct Liquefaction Contractors' Review Meeting, Pittsburgh, PA, October 6-8, 1987.
12. Winschel, R.A., and Burke, F.P., Recycle Oils From Fluid Coking of Coal Liquefaction Bottoms, ACS National Meeting, Los Angeles, CA, Sept. 1988.

**Table 1. CTSL DEMONSTRATION RUN COMPARISON WITH H-COAL
(ILLINOIS NO. 6 COAL)**

Process	H-Coal (PDU-5)	CTSL Run No.	
		(227-20)	(227-47)
YIELDS, Wt% MAF			
C ₁ -C ₄	11.3	6.6	8.6
C ₅ -390°F	22.3	18.2	19.7
390-650°F	20.5	32.6	36.0
650-975°F	8.2	16.4	22.2 ¹
975°F+ Oil	20.8	12.6	2.7 ¹
HYDROGEN CONSUMPTION	6.1	6.3	7.3
COAL CONVERSION, Wt% MAF	93.7	94.8	96.8
975°F+ CONVERSION, Wt% MAF	72.9	82.2	94. ¹
C₅-975°F, Wt% MAF	51.0	67.2	77.9 ^{1, 2}
HYDROGEN EFFICIENCY	8.4	10.7	10.7
C₅- DISTILLATE PRODUCT QUALITY			
EP, °F	975	975	750
°API	20.2	23.5	27.6
% Hydrogen	10.63	11.19	11.73
% Nitrogen	0.49	0.33	0.25
% Sulfur	0.2	0.05	0.01
BBL/TON	3.3	4.1	5.0

¹750°F Distillate end point.

²Coal contained 5.8% ash.

NOTE: All data at catalyst age representative of typical commercial replacement rates.

**Table 2 HISTORY OF PROCESS DEVELOPMENT AND PERFORMANCE
FOR BITUMINOUS COAL LIQUEFACTION**

Process	Configuration	Distillate (wt% MAF coal)	Yield (bbt/t MAF coal)	Distillate Quality (gravity °API)	Nonhydrocarbon (wt%)		
					S	O	N
SRC II (1982)	One-stage, noncatalytic	41	2.4	12.3	0.33	2.33	1.0
H-Coal (1982)	One-stage, catalytic	52	3.3	20.2*	0.20	1.0	0.50
Wilsonville (1985), RITSL	Integrated two-stage, thermal-catalytic	62	3.8	20.2**	0.23	1.9	0.25
Wilsonville (1986), CTSL	Integrated close- coupled two-stage catalytic-catalytic	70	4.5	26.8**	0.11	<1	0.16
Wilsonville (1987), CTSL	Integrated close- coupled two-stage low-ash coal	78	5.0	+	+	+	+
HRI, CTSL (1987)	Catalytic-catalytic	78	5.0	27.6	0.01	-	0.25

*Light product distribution, with over 30% of product in gasoline boiling range; less than heavy turbine fuel.

**Higher boiling point distribution, with 20% of product in gasoline fraction and over 40% turbine fuel range.

*API and elemental analysis data unavailable at this time.

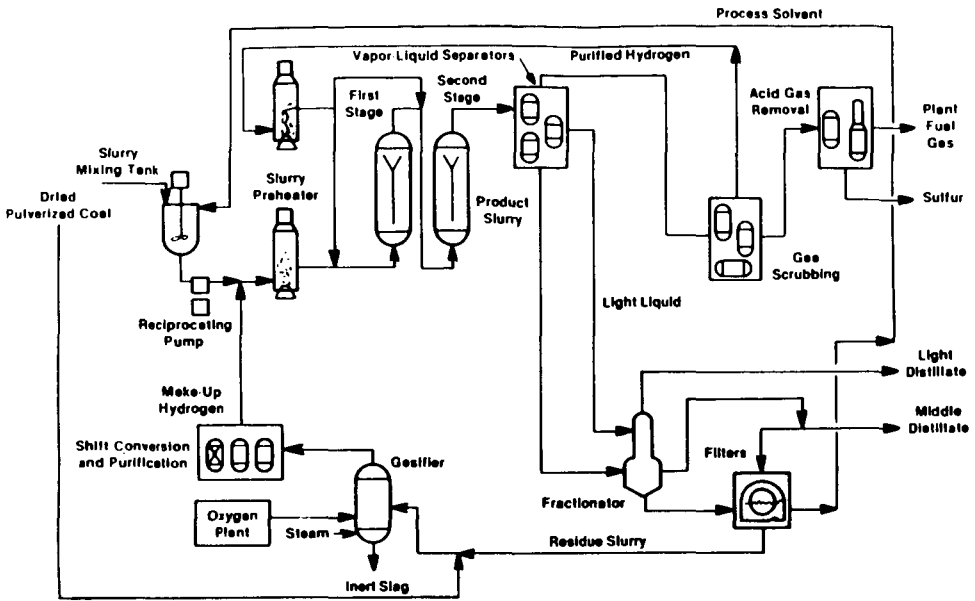


FIGURE 1. HRI CATALYTIC TWO-STAGE LIQUEFACTION

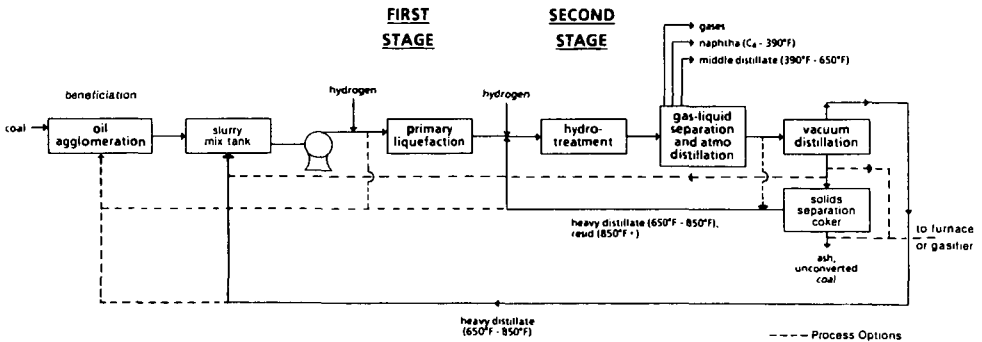


Figure 2. Process Options with Beneficiation and Coking.

No./13,005

TWO-STAGE COAL LIQUEFACTION PROCESS DEVELOPMENTS AT WILSONVILLE

J. M. Lee, O. L. Davies, T. E. Pinkston and J. R. Gough
Catalytic, Inc., Wilsonville, AL 35186

INTRODUCTION

The Advanced Coal Liquefaction R & D Facility at Wilsonville, Alabama has been operating for over 14 years to develop alternate technologies for producing low cost fuels. A recently completed close-coupled integrated (CC-ITSL) processing mode was an important development in the Wilsonville program for making clean distillate fuels. In the CC-ITSL mode the two reactors were directly coupled without any pressure letdown. Interstage cooling was done only to the extent required to control the second reactor temperature. Such close-coupled operation should offer several process benefits such as increased overall thermal efficiency, reduced potential for retrogressive reactions which may take place in the absence of hydrogen at longer residence times, and improved product quality.

This paper is focused on two-stage coal liquefaction process performance with close-coupled reactors. Results are presented for two runs: Run 253 and Run 254. Run 253 processed high ash Illinois No. 6 coal and used Shell 317 1/20" trilobe bimodal catalyst in both reactors. Product yield and product quality data are discussed. Catalyst performance comparisons for Shell 317 (Run 253) and Amocat 1A and 1C (Run 251-I and Run 252) are made in terms of distillate yields, catalyst deactivation and catalyst replacement rates.

Run 254 processed low ash Ohio No. 6 coal and used Shell 317 1/20" trilobe bimodal catalyst in both reactors. The effects on process performance of the low ash feed coal, high resid recycle, high second stage reaction temperature and high space velocity are presented. The effect of the coal type on the distillate yield is discussed in comparisons of Illinois No. 6 and Ohio No. 6 coals. The first stage catalyst equilibrium activity level is discussed. Catalyst performance data at different second stage reaction temperatures are presented in terms of catalyst deactivation and catalyst replacement rates. Optimum and cascading catalyst requirements are discussed.

Catalyst properties used in the close-coupled integrated runs (Run 250-254) are listed in Table 1. Catalyst performance in the close-coupled configuration has been extensively studied and reported in the previous EPRI and DOE contractors' conferences (1,2,3,4). Relative process economics evaluations (5), configuration effects on process performance (6) and developments of ITSL models (7) were reported elsewhere.

PROCESS DESCRIPTION

A block flow diagram of the catalytic-catalytic CC-ITSL process is shown in Figure 1. The process consists of a slurry preparation step and two catalytic reaction stages followed by hydrotreated solvent recovery and critical solvent deashing systems. The system was integrated by the recycle of CSO (Critical Solvent Deashing) resid, hydrotreated solvent, and low-pressure flash bottoms containing ash, unconverted coal, hydrotreated resid, and hydrotreated solvent. Solids recycle allowed an increased concentration of solids in the CSD feed and hence a lower CSD feed rate. The solvent recovery system consists of atmospheric flash and vacuum flash equipment. The recycle distillate was fractionated in a vacuum tower to reduce the light ends (650°F- fraction) in the recycle solvent.

RUN 253 RESULTS

Catalyst Activity and Deactivation

Run 253 was the first CC-ITSL run with a significantly extended operation of catalyst addition to the first stage (2 lb/ton MF coal). The operation time with the catalyst addition was about 27 days. The impact of the catalyst addition was very significant. The C₄+ distillate yield is approximately higher by 21 wt % MAF coal at 3000 lb resid + CI/lb catalyst of the second stage catalyst age, compared to the yield linearly extrapolated from the batch deactivation data.

A slight decline of the slope indicates that 2 lb/ton addition is not sufficient at 385 MF lb/hr coal feed rate to maintain catalyst activity to achieve the "all-distillate" product slate with 69 wt % MAF C₄+ distillate. This observation is further substantiated in the catalyst requirement data for the resid extinction mode. Using the estimated catalyst activity data approximately 4.0 lb/ton catalyst addition is projected for the "all-distillate" product slate with a 69 wt % distillate yield. At 480 MF lb/hr high coal feed rate, the catalyst requirement is doubled to 8.1 lb/ton (Table 2).

These higher catalyst requirements for Run 253 with Shell 317 catalyst (approximately 2 to 3 times higher than those for Run 251-I and 252 with Amocat 1A and 1C catalysts) (Tables 2 and 3) were attributed to less catalyst charges in both reactors by 12 wt % and lower TSL catalyst activity as compared in Figures 2 and 3. Shell 317 catalysts for Run 253B showed a lower C₄+ distillate yield by 10 wt % MAF coal at a similar catalyst volume basis and by 3 wt % MAF at the same catalyst weight basis (Figure 2), compared to Amocat 1A/1C catalysts used in Run 251-IC. In addition, Amocat 1C/1C catalysts for Run 252B showed a higher C₄+ distillate yield by 5 wt % MAF coal at a similar catalyst volume and the same catalyst weight basis, compared to Amocat 1A/1C catalysts used in Run 251-ID and IE (Figure 3).

Each stage catalyst activity was much different from TSL catalyst activity trends discussed before; Run 253 Shell 317 catalyst activity was lower in the first stage and higher in the second stage reactor, compared to Run 251-I and 252 Amocat 1A and 1C catalysts. Run 253 Shell 317 catalyst deactivation rates for both reactors appeared to be very similar to those for Runs 251-I and 252 Amocat 1A and 1C catalysts (2,3).

Catalyst selectivities in TSL hydrogenation and heteroatom removal were discussed and compared in Run 253 Report (8). Selectivities were studied with relation to TSL hydrogen consumption, which is an indication of TSL process severity. Run 253 with Shell 317 and Run 252 with Amocat 1C catalyst showed slightly higher selectivities for the potential liquid yield (C₄+ resid) production by 1 to 3 wt % MAF coal, compared to Run 251-I with Amocat 1A and 1C catalysts. This was primarily attributed to less C₁-C₃ gas make. Overall heteroatom (N, S, O) removal was similar for all three runs. However, Run 253 with Shell 317 and Run 252 with Amocat 1C catalyst showed higher nitrogen removal activity. Analyses of aged Shell 317 catalysts used for Run 253 indicated the first stage as a guard bed by removing catalyst deactivation and poison material before going to the second stage. The second stage aged catalyst showed lower carbon deposits by 6 wt % of catalyst than the first stage and a higher hydrogenation activity value by 50 (m moles of hydrogen consumed) in hydrogenation of naphthalene. This guard bed effect was also commonly observed with other catalysts such as Amocat 1A and 1C used for Run 251-I and Run 252 (2,3).

Product Quality

Run 253 product quality data are listed in Table 4. During Run 253 the recycle distillate was fractionated in a vacuum column to reduce the light ends in the recycle solvent. The naphtha and distillate yields were about the same in all the periods (C, E and F). The gas-oil yield was the lowest in the concentrated coal slurry test. Other than this there were no major differences in product quality among various Run 253 tests. Preliminary laboratory analyses of distillate products indicated a significant reduction of the distillate product end point, by 30 to 80°F. This was achieved by increasing the recycle of 650°F+ by 8 wt % in the recycle process solvent (from 89 to 97 wt %).

RUN 254 RESULTS

Run 254 processed low ash Ohio No. 6 coal in a catalytic-catalytic close-coupled configuration. Unwashed high ash Ohio coal with about 10-12 wt % ash was used for the startup process solvent equilibration at 500 MF lb/hr coal feed rate. Low ash Ohio coal with 6 wt % ash was prepared by washing the run-of-the-mine coal with heavy media. During the operation with 40 wt % resid level, the "all-distillate" product slate could not be achieved because of high potential distillate (C₄+ resid) yields, 76-78 wt % MAF coal, and high excess resid yields, 8-10 wt % MAF processing the low ash Ohio No. 6 coal. In order to achieve one of the run objectives of the resid extinction, it was recognized that a higher catalyst activity level is required, since Ohio No. 6 coal apparently has lower resid conversion activity than Illinois No. 6 coal. The higher level of resid recycle could also improve significantly resid conversion, as observed in the previous runs (8,9), that is, 0.3 wt % MAF coal distillate yield increase per 1 wt % resid content increase in the recycle process solvent.

Low Ash Ohio No. 6 Coal

Advantages of the low ash Ohio No. 6 coal with 6 wt % as opposed to the high ash with 10 wt % are threefold as shown in Tables 5 and 6; (1) an increase of the potential liquid yield (C₄+ resid) by 6 wt % MAF coal, (2) an increase of coal conversion by 3 wt % MAF coal, and (3) a decrease of organic rejection by 8 wt % MAF coal. The increase of coal conversion is probably due to removal of less reactive

coal components such as inertinites by cleaning with heavy media (10). The low UC yield with the low ash coal reduced the organic rejection and consequently increased the potential liquid yield. The ratio of the organic rejection to the UC yield was 2.68, same for both periods, which indicates that the UC yield is a primary variable affecting the organic rejection.

Effect of Second Stage Reaction Temperature

The effect of the second stage reaction temperature change from 760°F to 790°F was studied during periods 254C-D and 254F-G. The observed C₄+ distillate yield increase due to the temperature increase was very significant, about 11 wt % MAF coal during 254C-D. The hydrogen consumption was also increased in a relatively small degree from 6.1 to 6.7 wt % MAF, which gives a significantly better hydrogen efficiency at 790°F (10.3 vs 9.5 lb C₄+ dist/lb H₂ consumed). C₁-C₃ gas make and organic rejection were similar for both periods. The C₄+ distillate yield response during 254F-G due to the second stage reaction temperature change from 760°F to 790°F was 8 to 9 wt % MAF coal, which is slightly lower than that during 254C-D.

Activation energy for the second stage catalyst was calculated based on the C₄+ distillate response during 254C-D. The activation energy was approximately 43,300-53,750 Btu/lb mole for the second stage reaction temperature range of 760°F to 790°F. A similar value of 47,800 Btu/lb-mole was also observed during 254F-G for the periods at a higher level of resid recycle about 50 wt %. This activation energy processing Ohio No. 6 coal is slightly higher than that processing Illinois No. 6 coal (42,300 Btu/lb mole for the temperature range of 720°F to 770°F) (11).

The effect of the second stage reaction temperature change from 790°F to 810°F was studied during period 254J-K. The estimated C₄+ distillate response due to the second stage reaction temperature change by 20°F was 6 wt % MAF coal, which corresponds to the activation energy 69,000 Btu/lb mole for the temperature range of 790°F to 810°F. This activation energy is much higher than that observed for the temperature range of 760°F to 790°F (47,800 Btu/lb mole).

The high second stage reaction temperature at 810°F (254K) lowers hydrogen efficiency and distillate selectivity by producing more C₁-C₃ gas make (2 wt % MAF coal), compared to at 790°F (254J).

Effect of High Resid Recycle

Very careful experimentation for periods 254G-H was conducted to evaluate the effect of 50 wt % resid recycle in the recycle process solvent on process performance. Period 254D was selected for comparisons with 40 wt % resid recycle. Significant advantages of the 50 wt % high resid recycle are found in process performance improvements; (1) 6 wt % MAF coal increase in the C₄+ distillate yield and (2) a higher hydrogen efficiency (11.1 vs 10.3 lb C₄+ dist/lb H₂ consumed). C₁-C₃ gas make and organic rejection were similar for both periods. The "all-distillate" product slate became possible for period 254G-H with more resid conversion through higher recycle of the reactive resid. The C₄+ distillate increase was slightly higher than the projected (5 wt % MAF). The economic impact in the commercial plant design will be slightly compensated due to the higher resid recycle by 40% and the higher slurry rate by 10%, although the production rate of the distillate is increased by about 9%.

During period 254G the C₄+ distillate yield was 78 wt % MAF coal, the highest ever observed at Wilsonville, the lowest organic rejection 7 wt % MAF (254I), and the highest coal conversion 97 wt % MAF. The hydrogen efficiency was very high, 11.3 lb C₄+ dist/lb H₂ consumed. This highly improved distillate production can be achieved by a moderate catalyst addition below 5 lb/ton of MF coal. Three main reasons can be attributed to these excellent process achievements; (1) high coal conversion activity of the low ash Ohio coal, (2) high distillate selectivity at 790°F of the second stage reaction temperature, and (3) high recycle of the reactive resid.

Effect of Space Velocity

Three different coal feed rates, 440, 365 and 300 MF lb/hr were studied during periods 254H, I and J. The first stage catalyst ages were similar approaching the equilibrium catalyst age of 610 lb MF coal/lb catalyst due to the catalyst addition at 3 lb/ton of MF coal, while the second stage catalyst ages were different, gradually increasing, due to the batch mode of operation. The C₄+ distillate yield was 72 wt % MAF coal at 365 MF lb/hr coal feed rate (254H) and increased to 76 wt % MAF at 300 MF lb/hr (254I) and then significantly decreased to 64 wt % MAF at 440 MF lb/hr (254J). The response for 300 MF lb/hr (254I) was relatively smaller than the expected (4 wt % vs 8 wt %). This was due to the catalyst activity decline in the second stage at a low coal feed rate. Similar observations were made during Run 253 processing Illinois No. 6 coal. Catalyst requirements for 440 MF lb/hr will be high, not desirably for the practical operation, more than 5 lb/ton of MF coal, which is suggesting the operation at a higher second stage temperature than 790°F.

The effect of the coal feed rate decrease from 440 to 375 MF lb/hr at 810°F of the second stage reaction temperature was studied during period 254K-L. The estimated C₄+ distillate response due to the coal feed rate change was 8 wt % MAF coal. C₁-C₃ gas make and organic rejection were similar for both periods. Catalyst requirements for 440 MF lb/hr is estimated to be below 5 lb/ton of MF coal (Table 7), much less than at 790°F of the second stage reaction temperature. This was due to the high second stage catalyst activity at 810°F (Figure 6).

Catalyst Activity and Deactivation

Two-stage catalyst activity was compared in Figure 4, based on C₄+ distillate yield trend data. Ohio No. 6 coal with both high (254B) and low (254C) ash contents significantly reduced the C₄+ distillate yield by 7 wt % MAF coal in the batch mode of operation, compared to Illinois No. 6 coal with a high ash content (253D). In addition, in comparisons of 254D and 253EFG Ohio No. 6 coal required a higher catalyst addition (3 vs 2 lb/ton of MF coal) and a higher second stage reaction temperature (790°F vs 760°F) for a similar C₄+ distillate yield (70 wt % MAF coal). These indicate that Ohio No. 6 coal has lower resid conversion activity than Illinois No. 6 coal. Run 254B in the batch operation processing Ohio No. 6 coal showed a similar two-stage catalyst deactivation rate to that for Run 253D processing Illinois No. 6 coal.

Catalyst activity trends for Run 254 operation with a high level of resid recycle (50 wt %) were analyzed for the two-stage system, first stage and second stage, based on two-stage resid make and resid + UC conversion. The first stage equilibrium activity level with 3 lb/ton of MF coal catalyst addition was achieved at the catalyst age near to 550 lb MF coal/lb catalyst (calculated equilibrium age = 610 lb MF coal/lb catalyst), as illustrated in Figure 5. The first stage catalyst ages,

550 and 610 lb MF coal/lb catalyst, are corresponding to the second stage catalyst ages, 2000 and 3000 lb resid + CI/lb catalyst, respectively. In Figure 5 the measured first stage catalyst activity values with the catalyst addition are very close to the theoretically calculated by using the estimated batch deactivation data, which confirms that the first stage batch catalyst activity data in Figure 6 are reasonable for further catalyst requirement calculations.

Because of the continuous catalyst addition in the first stage, the two-stage catalyst deactivation rate was gradually decreased and became primarily dependent on the second stage deactivation rate. Figure 6 shows a graphical presentation of differences in the second stage catalyst activity at different reaction temperatures, 760°F, 790°F and 810°F. Second stage reaction temperature increases from 760°F to 790°F, and further to 810°F significantly increased catalyst activity levels, although the second stage deactivation rate for 810°F was significantly higher (but for 790°F, slightly higher) than for 760°F. At the same reactor temperature of 810°F for both stages, the second stage catalyst activity was higher than that of the first stage and the second stage catalyst deactivation rate was lower. These observations at 810°F of the second stage reaction temperature need to be substantiated because of limited data points at high catalyst ages (1600-2100 lb MF coal/lb catalyst of second stage catalyst ages).

Catalyst requirements at 790°F of the second stage reaction temperature were 3.1 to 4.6 lb/ton of MF coal to achieve the "all-distillate" product slate (77 wt % MAF coal C₄+ distillate yield) for 300 to 370 MF lb/hr coal feed rates (Table 7). Effects of the 810°F of the high second stage reaction temperature on catalyst performance were very substantial (Table 7 and Figure 7): (1) increased coal throughput, (2) increased catalyst activity, (3) lower catalyst requirements and (4) lower distillate selectivity (C₄+ distillate yield decreased to 74 wt % MAF coal because of a high C₁-C₃ gas make) (Figure 8).

Optimum Catalyst Requirements and Cascading

Catalyst replacement rates reported in Table 7 and Figure 7 were calculated, assuming to achieve each stage performance experimentally measured at the Wilsonville pilot plant. Considering the significant differences in each stage catalyst activity due to different reaction temperatures employed for CC-ITSL configuration studies, one might visualize that there would be an optimum catalyst requirement for a fixed coal feed rate with resid extinction only by shifting each stage catalyst requirement loading. For instance, Figure 9 presents graphically optimum catalyst requirements for 300 and 370 MF lb/hr coal feed rates. The variable selected as X-coordinate is the first stage resid + UC conversion. The plots are simply showing that the optimum catalyst requirement is not only a function of the coal feed rate but also of the first stage resid + UC conversion. In addition the operation range for the optimum is very narrow within 1 to 3 wt % variation of the first stage resid + UC conversion. Data in Figure 9 were generated without considering catalyst residual activities and based on 77 wt % C₄+ distillate yield with resid extinction. Organic rejection was assumed to be 8 wt % MAF coal. Operating conditions were 810°F first stage temperature, 790°F second stage temperature, 2.3 solvent/coal ratio, 50 wt % resid and 12 wt % CI in the recycle process solvent.

Other interesting points can be made from plots in Figure 9, that is, (1) catalyst cascading is practically possible with a possible reduction of catalyst addition about 1 to 2 lb/ton of MF coal (this saving can be considered as maximum) and (2) Wilsonville plant experimentations were conducted at operating conditions of optimum catalyst requirements (Run 254I and GH).

Four different cases were studied for optimum catalyst requirements and cascading possibility. Results were generated with considering catalyst residual activities and are summarized below. The catalyst addition for the cascading is listed for the range of interest. The actual amount is dependent on the cascading catalyst activity, which needs to be experimentally determined. The upper limit has only theoretical meaning for an equal amount of the catalyst addition for both stages with zero cascading catalyst activity. This upper limit shows a higher catalyst addition than the optimum.

Case	<u>1</u>	<u>2</u>	<u>3</u>	<u>4</u>
Base data	<u>254I</u>	<u>254GH</u>	<u>254L</u>	<u>254K</u>
Coal feed, MF lb/hr	300	370	375	440
Second stage T, °F	790	790	810	810
C ₄ + dist with resid extinction wt % MAF coal	77	77	74	73
<u>Catalyst addition</u> lb/ton of MF coal				
<u>experimentally measured</u>				
<u>first stage</u>	2.4	3.3	3.3	3.8
<u>second stage</u>	0.7	1.3	0.2	0.7
<u>total</u>	<u>3.1</u>	<u>4.6</u>	<u>3.5</u>	<u>4.5</u>
<u>optimum</u>				
<u>first stage</u>	2.4	3.3	0.3	1.1
<u>second stage</u>	0.5	1.0	1.2	1.8
<u>total</u>	<u>2.9</u>	<u>4.3</u>	<u>1.5</u>	<u>2.9</u>
<u>cascading</u>				
<u>first stage</u>	1.8	2.6	0.9	1.6
<u>second stage</u>	1.8	2.6	0.9	1.6
<u>total</u>	<u>1.8-3.6</u>	<u>2.6-5.2</u>	<u>0.9-1.8</u>	<u>1.6-3.2</u>

As already pointed out, in Cases 1 and 2 at 790°F of the second stage reaction temperature, optimum catalyst requirements only improve slightly about 0.2-0.3 lb/ton of MF coal, since Wilsonville pilot plant data were generated near at the optimum operating conditions. Another significant improvement can be made by doing cascading from the second stage to the first stage reactor, potentially reducing the catalyst requirement by 1.1 to 1.7 lb/ton of MF coal.

Very unusual striking results were revealed for the operation at 810°F of the second stage reaction temperature. Optimum calculations are suggesting that Wilsonville plant experimentations were not conducted at operating conditions of

optimum catalyst requirements (Run 254L and K) and therefore, if operated at optimum, catalyst savings will be about 1.6 to 2.0 lb/ton of MF coal. Additional reduction of catalyst addition can be made by 0.6 to 1.3 lb/ton of MF coal by doing catalyst cascading (this can be considered as a maximum potential). These observations need to be substantiated by further experiments at young catalyst ages, which data are not available at the present time. The assumption made for the second stage catalyst activity at 810°F should be further investigated and experimentally proved, before making definite conclusions of significant process performance achievements at 810°F of the second stage reaction temperature.

A significant advantage of 810°F of the second stage reaction temperature as opposed to 790°F lies in an increase of the coal throughput by 47% and the C₄+ distillate production rate by 40% (Cases 1 and 4). Optimum catalyst requirements for both Case 1 and 4 were same, 2.9 lb/ton of MF coal. These process performance improvements will impact tremendously the process economic valuation for commercialization and reduce significantly the selling price of the distillate product, if other critical variables in the economic evaluation are similarly affecting the results for both cases.

SUMMARY

Several noteworthy accomplishments in 1987/88 are listed below:

- (1) Successful operations processing Illinois No. 6 and Ohio No. 6 coals were demonstrated by using Shell 317 catalyst in the close-coupled ITSL catalytic-catalytic configuration.
- (2) Interstage separation was eliminated, resulting in significant reduction in capital costs.
- (3) Best process performance was achieved processing low ash Ohio No. 6 coal with 78 wt % MAF coal distillate yield, 97 wt % coal conversion and 7 wt % organic rejection.
- (4) High second stage reaction temperatures, 790°F and 810°F, were investigated, resulting in significantly increased coal throughput and distillate production due to high catalyst activity and low catalyst requirements.
- (5) The increased reactive resid recycle improved the distillate production.
- (6) The increased gas-oil recycle produced lighter and better quality distillates.
- (7) The close-coupled ITSL process data-base was significantly expanded for processing bituminous coals.
- (8) The process economics was significantly improved for future commercialization of the coal liquefaction process.

ACKNOWLEDGEMENTS

This work was supported by the U.S. Department of Energy under Contract DE-AC22-82PC50041, and the Electric Power Research Institute under Contract RP1234-1-2, and was managed by the Southern Company Services, Inc. The authors also gratefully appreciate the assistance of Mr. Harvey Crean, the graphic arts department personnel in Philadelphia, PA, Ms. Mary Peoples, Ms. Joyce Spearman and Mr. George Jau. Mr. William R. Hollenack is greatly acknowledged for his various helpful suggestions in preparation of this paper.

REFERENCES

1. C. W. Lamb, J. M. Lee and R. V. Nalitham. "Two-Stage Coal Liquefaction Process Performance with Close-Coupled Reactors in Wilsonville." Proceedings of the Eleventh Annual EPRI Clean Liquid and Solid Fuels Conference, May 1986.
2. R. V. Nalitham, J. M. Lee and C. W. Lamb. "Recent Liquefaction Developments at Wilsonville Plant With Close-Coupled Reactors." Proceedings of the Twelfth Annual EPRI Conference on Fuel Science, May 1987.
3. R. V. Nalitham, J. M. Lee and W. R. Hollenack. "Catalytic-Catalytic Close-Coupled Liquefaction Process Development at Wilsonville Plant." Proceedings of DOE Direct Liquefaction Contractors' Review Meeting, October 1987.
4. R. V. Nalitham, J. M. Lee, C. W. Lamb and T. W. Johnson. "Two-Stage Coal Liquefaction Process Performance With Close-Coupled Reactors." Fuel Processing Technology, Vol. 17, 1987, pp. 13-27.
5. J. R. Gough, W. R. Hollenack, C. W. Lamb and R. V. Nalitham. "Wilsonville Process Studies and Engineering Evaluation of Improved Options." Proceedings of the Eleventh Annual EPRI Clean Liquid and Solid Fuels Conference, May 1986.
6. Catalytic, Inc., Topical Report. "The Effect of Integration Configurations on Two Stage Coal Liquefaction Process Yields and Performance." DOE Contract No. DE-AC22-82PC50041, EPRI Contract No. RP1234-1-2, Document No. DOE/PC/50041-82. Report to be published.
7. Catalytic, Inc. Topical Report. "Development of a Simulation Model for Bituminous Coal Liquefaction in the Integrated Process at Wilsonville." DOE Contract No. DE-AC22-82PC50041, EPRI Contract No. RP1234-1-2, Document No. DOE/PC/50041-89.
8. Catalytic, Inc. Technical Progress Report. "Run 253 With Illinois No. 6 Coal." DOE Contract No. DE-AC22-82PC50041, EPRI Contract No. RP1234-1-2, Document No. DOE/PC/50041. Report to be published.
9. Catalytic, Inc. Technical Progress Report. "Run 247 With Illinois No. 6 Coal." DOE Contract No. DE-AC22-82PC50041, EPRI Contract No. RP1234-1-2, Document No. DOE/PC/50041-63.
10. R. P. Anderson, B. F. Alexander, C. H. Wright and J. Freel. "Effect of Coal Cleaning on the Short Contact Time Liquefaction of Illinois No. 6 Coal." Fuel, Vol. 64, November, 1985, pp. 1558-1563.
11. Catalytic, Inc. Technical Progress Report. "Run 251 - Part I With Illinois No. 6 Coal and Part II and III With Wyodak Coal." DOE Contract No. DE-AC22-82PC50041, EPRI Contract No. RP1234-1-2, Document No. DOE/PC/50041-88.

Table 1

Wilsonville CC-ITSL catalyst properties

catalyst RUN(e)	Shell 324 250,251	Amocat 1C 250-252	Amocat 1A 251	Shell 317 253,264
shape	(----- cylindrical -----)			trilobe
size	1/32"	(----- 1/16" -----)		1/20"
Ni (wt %)	2.7	2.3		2.7
Co			2.5	
Mo	13.2	10.4	9.8	11.6
surface area, m ² /g	185	190	235	235
pore volume, cc/g	0.48	0.85	0.80	0.75
pore size distribution	unimodal	(----- bimodal -----)		
compacted bulk density, lb/ft ³	54	42	41	36

Table 2. Shell 317 Trilobe Catalyst Replacement Rates

run no.	253D	253B
coal feed (mf lb/hr)	385	480
WHSV (hr ⁻¹)	3.9	5.1
second stage reactor temperature (°F)	760	760
TSL C4+ distillate (% maf coal)	69	68
catalyst addition (lb/ton mf coal)	4.0	8.1

Table 3. Amocat 1A and 1C Catalyst Replacement Rates

run no.	251-IE	251-ID	251-1C	252C
catalyst (1st/2nd stage)	1A/1C	1A/1C	1A/1C	1C/1C
coal feed (mf lb/hr)	300	385	480	385
WHSV (hr ⁻¹)	2.7	3.4	4.2	3.5
second stage reactor temperature (°F)	760	760	760	760
TSL C4+ distillate (% maf coal)	70	70	70	70
catalyst addition (lb/ton mf coal)	0.9	1.6	3.0	1.2

Table 4. Run 253 - Distillate Product Properties

distillation cut	%MAF ¹	elemental (wt%)					*API
		C	H	N ²	S	O (diff)	
Run 253C (40% coal slurry)							
naphtha (IBP-350°F)	19.9	84.80	14.94	0.02	0.06	0.18	46.7
distillate (350-650°F)	27.3	87.74	12.03	0.11	0.01	0.11	18.9
gas oil (650°F+)	18.2	88.84	10.83	0.29	0.01	0.23	5.6
Run 253E (no separator)							
naphtha (IBP-350°F)	14.6	85.35	14.45	0.04	0.07	0.00	44.1
distillate (350-650°F)	26.2	87.97	11.61	0.15	0.05	0.02	17.5
gas oil (650°F+)	27.0	89.57	9.97	0.37	0.02	0.10	2.9
Run 253F (ground catalyst & no separator)							
naphtha (IBP-350°F)	14.7	85.58	14.21	0.03	0.02	0.16	43.8
distillate (350-650°F)	22.4	87.83	11.71	0.13	0.01	0.32	18.1
gas oil (650°F+)	28.5	89.54	10.07	0.34	0.02	0.03	3.8

¹by simulated distillation on GC

*nitrogen by Kjeldahl

Table 5

run no.	TSL operating conditions	
	254B	254CD
first stage		
catalyst replacement (lb/ton MF coal)	none	3
average reactor temperature (°F)	(-----810-----)	(-----)
inlet hydrogen partial pressure (psf)	(-----2600-----)	(-----)
coal feed rate (lb/hr MF)	385	370
space velocity (lb feed/hr-lb cat)	(-----3.9-----)	(-----)
solvent-to-coal ratio	(-----2.0-----)	(-----)
solvent resid content (wt%)	(-----40-----)	(-----)
solvent C1 content (wt%)	(-----12-----)	(-----)
catalyst age [lb (resid + C1)/lb cat]	850-1300	1150-1200
(lb MF coal/lb cat)	400-650	550-800
second stage		
average reactor temperature (°F)	760	760/790
space velocity (lb feed/hr-lb cat)	(-----3.7-----)	(-----)
feed resid content (wt%)	(-----41-----)	(-----)
catalyst age [lb (resid + C1)/lb cat]	600-900	1100-1450
(lb MF coal/lb cat)	400-600	700-950

Table 6

run no.	TSL yield structures	
	254B	254CD
10% vs 6% coal ash		
potential liquid yield		
C ₄ + resid (% maf coal)	70	76
coal conversion (% maf coal)	94	97
energy content of feed coal rejected to ash conc. (%)	18	9
organics rejected to ash conc. (% maf coal)	18	8

Table 7. Shell 317 Trilobe Catalyst Replacement Rates

run no.	254I	254GH	254L	254K
coal feed (mf lb/hr)	300	370	375	440
WHSV (hr ⁻¹)	3.5	4.3	4.3	5.1
second stage reactor temperature (°F)	790	790	810	810
TSL C4+ distillate (% mf coal)	77	77	74	73
catalyst addition (lb/ton mf coal)	3.1	4.6	3.5	4.5

Figure 1

**CC-ITSL with solids recycle
catalytic-catalytic
close-coupled mode**

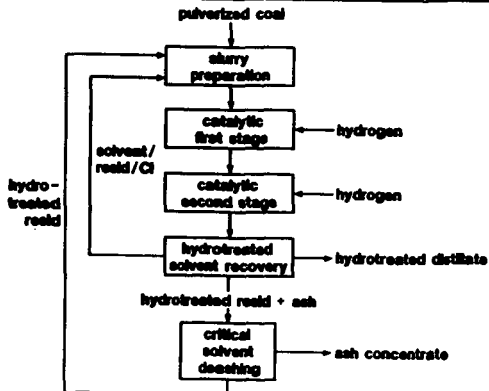


Figure 2. Amocat 1A/1C vs Shell 317 Catalyst

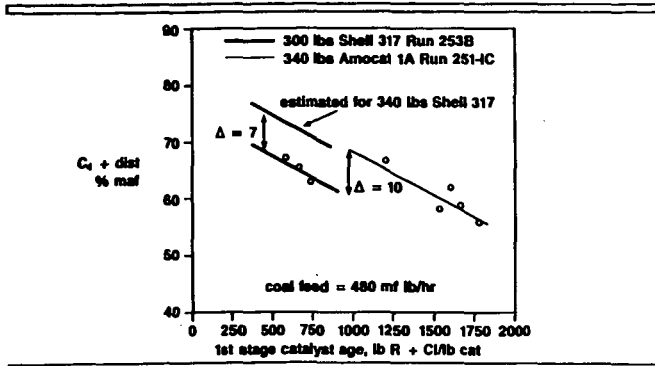


Figure 3. Amocat 1A/1C vs Amocat 1C/1C Catalyst

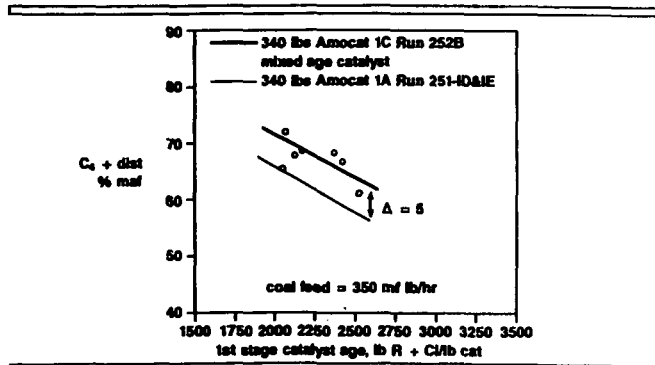


Figure 4. Illinois No. 6 vs Ohio No. 6 Coal

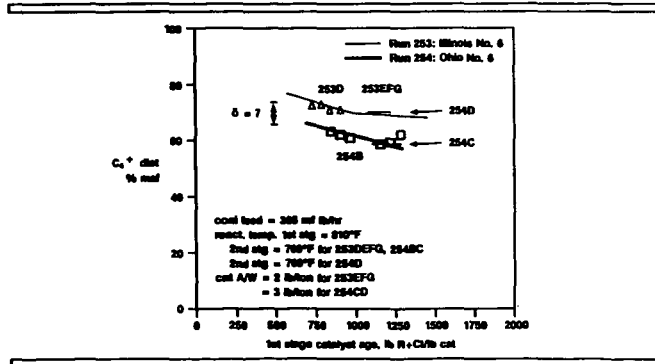
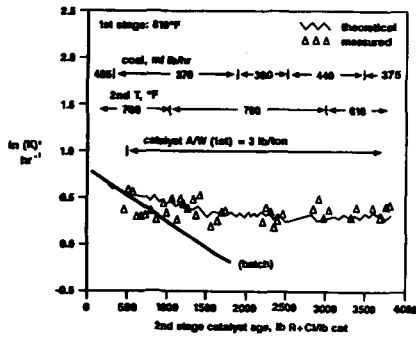


Figure 5

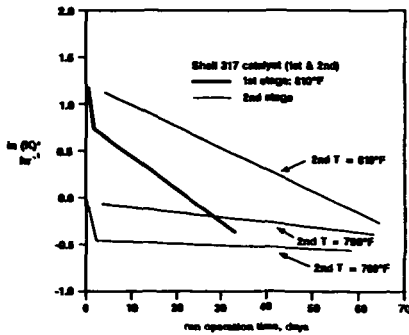
RUN 254 first stage Shell 317 aging with catalyst addition



* (meald + UC) conversion rate constant

Figure 6

catalyst aging - RUN 254



* (meald + UC) conversion rate constant

Figure 7. Run 254 - Catalyst Replacement vs 2nd Stage Temperature

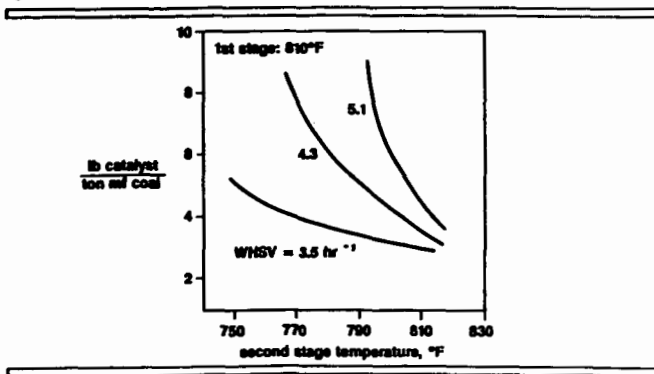


Figure 8. Run 254 - Distillate Selectivity vs 2nd Stage Temperature

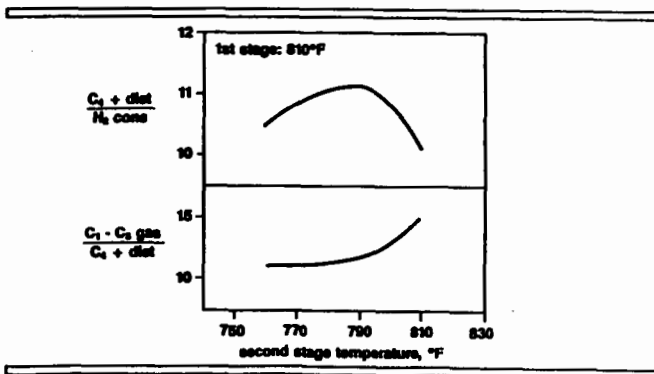
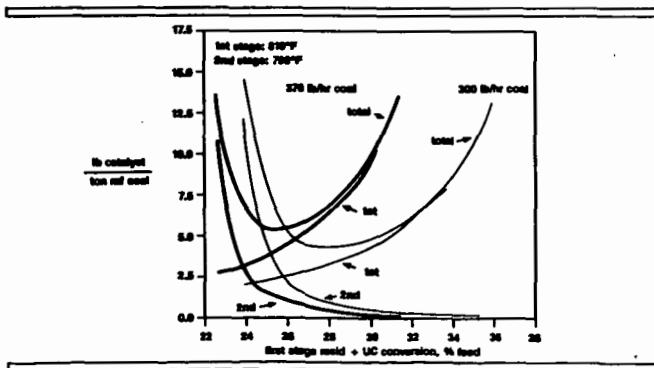


Figure 9. Run 254 - Optimum Catalyst Replacement Rate



.

**PROGRESS IN DIRECT COAL LIQUEFACTION:
THE ECONOMIC PERSPECTIVE**

David Gray and Glen Tomlinson
The MITRE Corporation
Civil Systems Division
7525 Colshire Drive
McLean, VA 22102

ABSTRACT

The economic impact of demonstrated and projected improvements in two-stage direct coal liquefaction processes are evaluated. The computerized methodology employed estimates the quantity and quality of products from a 30,000 ton/day commercial scale plant, based on input test data. Steam, hydrogen and fuel gas balances are determined. Capital and operating costs are then estimated, and the required selling price of raw liquid products is determined by conventional discounted cash flow (DCF) analysis. Product quality is quantified by computing the cost of upgrading the raw products to motor gasoline.

Improvements in two-stage processing since the early demonstration of the Lummus Integrated Two-stage (ITSL) process in 1980 are shown to reduce the required initial selling price (RISP) of gasoline from coal liquids by about 16 percent. Further process improvements, which offer the potential for an additional 16 percent RISP reduction, are identified.

This report also compares the economics of two-stage processing with earlier studies of the H-Coal, Exxon Donor Solvent and Lummus ITSL processes. The high costs of coal liquids found in these earlier studies are explained and revised costs for these earlier plants using a common financial and technical basis are determined.

INTRODUCTION

Two-stage coal liquefaction research and development efforts have yielded significant increases in distillate quantity and quality over the last few years. The Lummus Integrated Two-stage Liquefaction (ITSL) process experience⁽¹⁾ showed that high yields of good quality coal liquids can be produced from bituminous coals using a combination of short contact time (SCT) thermal processing, anti-solvent deashing and LC-Fining* of deashed coal extract. Since then the concept has undergone several modifications.

At the Wilsonville Advanced Coal Liquefaction R&D Facility⁽²⁾, both the thermal processing and the hydrotreating have generally been of longer duration than at Lummus. The critical solvent deashing system⁽³⁾ has been more efficient at recovering coal extract and has thus rejected less soluble material than the Lummus anti-solvent process.⁽⁴⁾ The ITSL concept itself, where the thermal first stage and catalytic second stage have been separated by the deashing step, has been modified so that the topped thermal effluent is hydrotreated before deashing. This configuration is called the Reconfigured ITSL (RITSL) mode of operation.⁽⁵⁾ More recently the RITSL mode has been modified so that the first and second stage reactors are directly coupled together and the entire thermal effluent is

* Registered Trade Mark of Lummus-Cities Service hydrorefining process.

hydrotreated. This is the close-coupled operation (CC-ITSL). A vent separator is often used between the two-stages to let down the first stage products. In even more recent tests a portion of the ash-containing effluent from the hydrotreater is recycled to the first stage, the so called ash-recycle mode.⁽⁸⁾ Catalytic-catalytic configurations have also been tested at Wilsonville.⁽⁶⁾

The overall objective of these modifications in two-stage processing is to increase the yield of high quality distillate while reducing the cost of production.

Sandia National Laboratories, which is supported by the U.S. Department of Energy under contract DE-AC04-76DP00789, has contracted MITRE to develop a method to quantify the impact of these modifications on the cost of coal liquids. In response, MITRE has developed a computerized coal liquefaction cost model that simulates the technical and economic performances of conceptual commercial scale coal liquefaction plants that incorporate the research and development improvements under study at Wilsonville.

METHODOLOGY

Introduction

The analysis methodology employed in the coal liquefaction cost model has been developed over the past several years. The objective of the methodology is to estimate the outputs and required selling price of products from a conceptual commercial scale plant. During 1986, the methodology was refined and computerized to permit rapid evaluation of the impact of variations in process performance on the required selling price of product liquids. The model is programmed in LOTUS 1-2-3 (Issue 2) and can be readily modified and expanded as refinements in the analysis methodology are developed. The paragraphs below present a brief overview of the analysis methodology. A more complete description may be found in reference (7).

Commercial Plant Output

Product outputs, product quality, and the flows to primary process units in the liquefaction plant are determined from experimental test data. The data may be directly scaled to the selected commercial size based on moisture ash free (MAF) coal throughput. (Postulated results may of course be substituted for test data in order to determine the potential economic impact of speculative process improvements.) The model is designed to make certain data adjustments if desired. In most runs, the data are adjusted to reflect operation with no net output of resid (+850°F residual material). When this adjustment is made in the model, the space velocity (hence capacity) of the hydrotreater is adjusted to the level required to achieve the desired resid conversion.

The resid adjustment provision of the program is also used when there are changes in the resid available to be converted because of assumed changes in the quantity of resid rejected with process solids (for example variations in deasher performance). The conversion factors for the resid are averages of several actual sets of data obtained during the Wilsonville operations.

Auxiliary Processes

The bottoms rejected from the liquefaction plant are gasified to produce

hydrogen. Additional coal is gasified when bottoms are not adequate to meet hydrogen requirements. Texaco gasification is assumed. Steam driven air separation equipment is used to produce oxygen for gasification. The model performs preliminary steam and fuel gas balances in order to obtain a thermally balanced plant and to determine the required capacities for auxiliary equipment. A coal fired steam plant with flue gas desulfurization is used to superheat steam produced from in-plant heat recovery, and to produce and superheat any additional steam required.

Cost Analyses

Preliminary designs of commercial plants employing two-stage liquefaction were prepared by UOP/SDC in 1981 under DOE contract^(8,9). These designs are used as the baseline for estimating capital and operating costs in the MITRE model. The UOP/SDC studies considered both Non-integrated Two-stage Liquefaction (NTSL)⁽⁸⁾, and Integrated Two-stage Liquefaction (ITSL)⁽⁹⁾ configurations, and thus encompassed the major process elements of a wide variety of two-stage plant configurations.

The total erected costs (TEC) of process equipment required in the plant being analyzed are estimated by comparing the capacity required to the capacity of similar units in the baseline design. A 0.7 scale factor is used. Thus

$$\text{TEC (unit)} = \text{TEC baseline unit} \times \left(\frac{\text{unit capacity}}{\text{baseline capacity}} \right)^{0.7} \times \text{INF}^*$$

Analyses of Required Selling Prices

The required selling price per barrel of raw product is computed by dividing the annual costs by the annual output in barrels. Annual costs are the sum of net operating costs and capital recovery costs. The program computes capital recovery costs by multiplying the required capital by an input capital recovery factor. The capital recovery factor for any specific set of financial assumptions is calculated by discounted cash flow (DCF) analysis in a separate program. The baseline economic assumptions used in the study are 25% equity, 15% DCF, 3% inflation, 34% tax rate, 8% interest on debt, and a 5 year construction period. These assumptions result in a capital recovery factor of 0.167.

There are substantial differences in the quality of products produced by direct liquefaction processes in terms of boiling range, hydrogen content and heteroatoms. These characteristics necessarily influence the degree to which the product must be further processed to produce specification fuels. We have accounted for differences in product quality by estimating the cost of additional processing required to produce a standard heteroatom free 40 API gravity product (e.g., "hydrotreated product") or unleaded motor gasoline.

The value of the syncrude relative to petroleum crude (equivalent crude value) is determined by computing the cost of crude that would permit gasoline to be processed and sold at the same price as the gasoline from syncrude.

RESULTS AND DISCUSSION

Table 1 summarizes the results of using the coal liquefaction cost model. The table shows economic and technical data for four conceptual commercial * INF accounts for inflation between the year the UOP/SDC design was developed and the year 1986 (INF = 1.125).

two-stage plants processing Illinois #6 coal. The baseline plant (Lummus ITSL) can produce raw liquid product for \$41.52/barrel (1986 dollars), which is equivalent to crude selling for \$35.82/barrel. Wilsonville run 244-B data, which was obtained using the integrated two-stage liquefaction configuration, can produce product at an equivalent crude value of \$35.36/barrel, i.e. very similar to the Lummus results. However, the close-coupled configuration run 250-D shows a significant reduction in product cost. The final column in Table 1 shows results obtained using data from Wilsonville run 250-G, which is a close-coupled run with ash-recycle. Again this shows a further decrease in product cost. Raw product cost reductions of about 16 percent have been realized in going from Lummus ITSL to the ash-recycle close-coupled Wilsonville configuration. This product cost decrease is brought about by the combination of a significant yield improvement (26 percent increase on a raw product basis) and only a slight increase in capital required to obtain that gain (about 5 percent capital increase). Therefore, it is estimated that raw coal liquids could be produced for approximately \$35/barrel; this is equivalent to crude oil at about \$30/barrel.

As an R&D guidance tool, the model can also be used to estimate potential savings in required selling prices that could be realized if certain potential process improvements were incorporated into the system. Potential improvements include using cleaned coal and eliminating the deashing system, increasing coal slurry concentration, and improving catalyst activity, selectivity and life. The model predicts that an additional cumulative reduction in required selling price of products of approximately 16 percent is possible by incorporating all of the above improvements into the current ash-recycle Wilsonville two-stage configuration processing Illinois #6 coal. Table 2 shows that these additional cost reductions result in production of coal liquids for about \$29/barrel, which is equivalent to crude at about \$25/barrel.

Table 3 summarizes earlier direct coal liquefaction economic studies undertaken by Bechtel⁽¹⁰⁾, Exxon⁽¹¹⁾ and UOP/SDC^(8,9) for the H-Coal, Exxon Donor Solvent and Lummus ITSL processes respectively. Direct comparisons are not meaningful, however, because of the differences in plant scale, economic factors, and other assumptions. The earlier studies were made during a period of high inflation and high capital return expectations, and the analysts assumed a continuation of high inflation through the construction period. In order to separate the impact of improved technology from the overriding impact of changes in economic conditions, the earlier technologies were re-evaluated using the our model. The required selling prices computed by the model thus reflect the same costing methodology, plant scale and economic assumptions used in the analysis of the advanced two-stage system.

The results are shown in Table 4. Required selling prices are shown for raw liquefaction products, and for products after hydrotreatment to a consistent standard of quality. The latter prices are more meaningful for comparative purposes, since they reflect the large differences in the quality of the single and two-stage products. On this basis, required selling prices have been reduced from about \$49 to about \$36.60 per barrel, which represents a savings of about 25%.

CONCLUSIONS

Over the past decade continued research in the production of liquid fuels from coal has substantially increased both the quantity and the quality of distillate from a ton of coal. This increase of distillate, which amounts to approximately 35 percent, has resulted in a significant real decrease in the cost of liquid products

from coal of about 25%. Continued research is expected to further reduce the cost of coal liquids.

ACKNOWLEDGEMENT

This work was funded by Sandia National Laboratories, which is supported by the U. S. Department of Energy under contract DE-AC04-76DP00789.

REFERENCES

- (1) Schindler, H.D. and J. Chen, Integrated Two-stage Liquefaction, Final Technical Report Volume I, PC50021-Q11, prepared for U.S. Department of Energy by Lummus Crest and Cities Service R&D Company, July 1985.
- (2) Catalytic Inc., The Wilsonville Advanced Coal Liquefaction Research and Development Facility Technical Progress Report Run 244 with Illinois No. 6 Coal, DOE/PC/50041-34, prepared for U.S. Department of Energy, May 1984.
- (3) ElSawy, Abdel, D. Gray and G.C. Tomlinson, Critical Evaluation of Solvent Deashing of Coal Liquids, Volume II: Kerr-McGee Critical Solvent Deashing Process, MTR83W42, McLean VA: The MITRE Corporation, November 1983.
- (4) ElSawy, Abdel and M.B. Neuworth, Critical Evaluation of Solvent Deashing of Coal Liquids, Volume I: CE-Lummus Antisolvent Deashing Process, MTR83W42, McLean, VA: The MITRE Corporation, June 1983.
- (5) Catalytic Inc., The Wilsonville Advanced Coal Liquefaction Research and Development Facility Technical Progress Report, Run 250 with Illinois No. 6 Coal, DOE/PC/50041-Draft, prepared for U.S. Department of Energy, 1986.
- (6) Catalytic Inc., The Wilsonville Advanced Coal Liquefaction Research and Development Facility, Technical Progress Report, Run 251 with Illinois No. 6 Coal Part II and III With Wy Oil and Coal, DOE/PC/50041-Draft, prepared for U.S. Department of Energy, 1987.
- (7) Gray, D. and G. Tomlinson, "Assessing The Economic Impact of Two-Stage Liquefaction Process Improvements," WP87W00215, McLean, VA: The MITRE Corporation, April 1988.
- (8) Schachtschneider, A.B., R.N. Dinapoli, C.S. Yin, W.F. Chorba, and J.R. Schulze, Conceptual Design of Commercial Integrated Two-Stage Coal Liquefaction Facility, Report No. WD-TR-81/014-003, prepared for U.S. Department of Energy by UOP/SDC, June 1981.
- (9) Schachtschneider, A.B. et al., Conceptual Design of Commercial Two-stage Coal Liquefaction Facility, Report No. WD-TR-81/014-002, prepared for U.S. DOE by UOP/SDC, April 1981.
- (10) Ashland Synthetic Fuels Inc. and Airco Energy Company. The Breckinridge Project Initial Effort. Report. X. No. DE-FC05-800R, 20717. Prepared for the Synthetic Fuels Corporation, 1981.
- (11) Epperly, W.R., EDS Coal Liquefaction Process Development, Phase V. EDS Wyoming Coal Bottoms Recycle Study Design - Main Report. DOE/ET/10069-T33. Prepared for the U.S. Department of Energy by Exxon Research and Engineering Company, March 1983.

TABLE 1
 CONCEPTUAL COMMERCIAL PLANT SUMMARY DATA
 FOR ILLINOIS #6 COAL FEEDSTOCK

	<u>LUNMUS ITSL</u>	<u>244-B ITSL</u>	<u>250-D CC-RITSL</u>	<u>250-G-RAR</u>
<u>Economic Data (Million \$)</u>				
Plant Capital Cost	4,418	4,859	4,670	4,658
Coal Cost	271	290	314	330
Other Operating Cost	337	389	380	374
Byproduct Credit	79	69	126	150
Hydrotreating Cost	227	330	190	209
Total Operating Cost	756	939	758	762
<u>Plant Coal Requirements TPD (AR)</u>				
Coal to Liquefaction	33,232	33,232	33,232	33,232
Coal to Steam Plant	2,564	1,980	2,433	2,626
Coal to Gasification Plant	371	3,441	6,276	8,162
Total Coal to Plant	36,166	38,652	41,941	44,019
<u>Plant Product Outputs (BPD)</u>				
Raw Product	92,400	106,900	112,200	116,900
Hydrotreated Product	103,800	122,800	124,400	127,700
Gasoline	111,100	131,400	133,100	136,600
<u>Required Selling Price (\$/Bbl)</u>				
Raw Product	41.52	40.27	36.40	34.52
Hydrotreated Product	43.61	43.21	37.46	36.56
Gasoline	45.75	45.26	40.07	39.30
<u>Equivalent Crude Value (\$/Bbl)</u>	35.82	35.36	30.40	29.66

TABLE 2
 CUMULATIVE POTENTIAL IMPROVEMENTS SUMMARY FOR CONCEPTUAL
 COMMERCIAL PLANTS PROCESSING ILLINOIS #6 COAL

	BASE CASE		CATALYST		CATALYST		CLEAN COAL		SLURRY COAL	
	250 G		ACTIVITY	SELECTIVITY	LIFE	NO DEASHER	36 PERCENT		36 PERCENT	
			DOUBLED	IMPROVED	DOUBLED					
<u>Economic Data (Million \$)</u>										
Plant Capital Cost	4,659	4,528	4,510	4,501	4,619	4,457				
Coal Cost	330	330	330	330	376	376				
Other Operating Cost	374	369	368	348	395	395				
Byproduct Credit	151	151	57	57	88	88				
Hydrotreating Cost	209	209	169	149	174	174				
Total Operating Cost	762	757	790	770	857	857				
<u>Plant Coal Requirements TPD (AR)</u>										
Coal to Liquefaction	33,232	33,232	33,232	33,232	33,596	35,596				
Coal to Steam Plant	2,630	2,630	2,630	2,630	3,075	3,075				
Coal to Gasification Plant	8,162	8,162	8,162	8,162	11,574	11,576				
Total Coal to Plant	44,023	44,023	44,023	44,023	50,245	50,245				
<u>Plant Product Outputs (BPD)</u>										
Raw Product	116,851	116,851	128,672	128,672	147,663	147,663				
Hydrotreated Product	127,663	127,663	135,270	135,270	155,500	155,500				
Gasoline	136,599	136,599	144,739	144,739	166,385	166,385				
<u>Required Selling Price (\$/Bbl)</u>										
Raw Product	34.52	33.81	32.83	32.34	29.85	29.14				
Hydrotreated Product	36.56	35.91	34.57	34.10	31.73	31.07				
Gasoline	39.30	38.69	37.64	37.20	34.98	34.36				
<u>Equivalent Crude Value (\$/Bbl)</u>										
	29.66	29.08	28.07	27.66	25.53	24.94				

TABLE 3
REQUIRED SELLING PRICES FROM PUBLISHED STUDY DESIGNS

PROCESS	H-COAL	H-COAL	EDS	ITSL
DATA SOURCE	BECHTEL	BECHTEL	EXXON	UOP/SDC
DEBT/EQUITY RATIO	0/100	52/48	0/100	75/25
<u>Required Selling Price</u>				
<u>(\$/Barrel)</u>				
1981 Dollars	\$ 57	\$ 36	\$ 53	\$ 43
Start-Up Year Dollars	\$ 90	\$ 57	\$121	\$ 69
(Year)	(1988)	(1988)	(1993)	(1986)
<u>Financial Assumptions</u>				
Return on equity	15.0%	15.0%	15.0%	26.0%
Interest Rate	NA	10.8%	NA	17.0%
<u>Inflation Rates</u>				
Construction costs	8.5%	8.5%	7.5%	10.0%
Operating Costs	6.0%	6.0%	7.0%	10.0%
Product Value	6.7%	6.7%	9.0%	10.0%

TABLE 4
REQUIRED SELLING PRICE OF PRODUCTS \$/BARREL (\$1986)
(ILLINOIS #6 COAL)

	<u>SINGLE-STAGE</u>		<u>TWO-STAGE</u>	
	<u>PROCESSES</u>		<u>PROCESSES</u>	
	EDS	H-COAL	ITSL	CURRENT
Raw Product	\$43.58	\$42.35	\$41.52	\$34.52
Hydrotreated Product	\$49.18	\$48.80	\$43.61	\$36.56

RECYCLE OILS FROM FLUID COKING OF COAL LIQUEFACTION BOTTOMS

R. A. Winschel
F. P. Burke

CONSOLIDATION COAL COMPANY
Research & Development
4000 Brownsville Road
Library, PA 15129

ABSTRACT

A series of nine fluid-coker tars, produced by Lummus-Crest, Inc., from coal liquefaction vacuum bottoms, was characterized to evaluate their use as liquefaction recycle oils. The primary variables in the coking tests were temperature (1000 to 1200°F) and coker feedstock source. The properties of the tars are principally influenced by the coking temperature. Those produced at higher temperature are more aromatic and contain less hydrogen, and are principally unsubstituted and methyl-substituted condensed aromatic compounds. The tars produced at 1000°F are expected to be poor hydrogen donor solvents, whereas those produced at 1200°F are not expected to be hydrogen donor solvents. However, a 1200°F tar was readily hydrotreated to produce a good to excellent donor solvent. Based on these results, it would appear that tars produced from fluid coking of liquefaction vacuum bottoms can be recycled to a catalytic liquefaction reactor to produce additional liquids without adversely affecting process performance.

INTRODUCTION

In the development of processes for the direct liquefaction of coal, the efficient removal of solids from the product has proven to be particularly difficult. Many techniques have been tested and used, including filtration, hydrocyclones, vacuum distillation, Critical Solvent Deashing and antisolvent deashing; however, no truly satisfactory means has been developed. All suffer from high product rejection, high cost or serious engineering difficulties. An alternate method, fluid coking of vacuum bottoms, is being explored by Lummus-Crest, Inc., under subcontract to Burns and Roe Services Corp. through U.S. DOE Contract DE-AC22-84PC72571. The recently completed Lummus experimental program included ten tests in which five different samples of coal liquefaction vacuum bottoms were coked in a 20g/hr (nominal) continuous stirred coking unit (CSCU). The CSCU was used to simulate true fluid coking. The range of operating conditions used in the CSCU tests was chosen based on earlier tests (1,2) with a batch coker. Operating conditions for the CSCU tests are shown in Table 1, as reported by Lummus (3). Ranges of product yields (3) from the ten tests (on a wt % of total product basis) were as follows: gases, 5 to 18; coker distillate, 30 to 81; coke plus ash, 14 to 59. On an ash-free product basis, coke yields (3) ranged from 11 to 52 wt %. Details of the coker tests, the equipment and product yields appear elsewhere (3). The vacuum bottoms that were coked were originally produced in the Advanced Coal Liquefaction Test Facility at Wilsonville, Alabama, and at the Catalytic Two-Stage Liquefaction (CTSL) continuous bench unit, which is operated by Hydrocarbon Research Inc. (HRI) in Lawrenceville, New Jersey. The vacuum bottoms were produced from

Ohio 6, Illinois 6 and Wyodak coals. In the conceptual integration of liquefaction and fluid coking, the coker tars would be processed in the liquefaction plant, ultimately to produce additional distillate products. The tars could be introduced to the liquefaction plant as part of the recycle solvent or as a second stream entering a second-stage reactor. The coke would be gasified to produce hydrogen, burned for power or landfilled.

The coker tars may be quite dissimilar to typical liquefaction oils. If used as a significant part of the recycle oil, the donor-solvent quality of that stream could be altered. Moreover, the ease with which the coker tars can be hydrotreated to finished products is unknown. The objectives of the work reported here are: 1) to characterize the coker tars, 2) to evaluate their properties as donor solvents, and 3) to explore the potential of hydrotreating to improve their characteristics as products and as donor solvents.

EXPERIMENTAL

MATERIAL

Nine coker "distillates" were obtained from Lummus. Lummus uses the term "coker distillate" to describe these materials; however, since they are largely non-distillable, the term "coker tar" will be used here. The feedstock and operating conditions used to produce each of the coker tars are shown in Table 1 (3). Lummus' program consisted of ten tests, but no product was provided from Run CSCU-11. In some cases, the samples we received were total liquid products (TLP). In other cases we received the 650°F⁺ portion from a true boiling point distillation of the TLP. Typically, the 650°F⁺ portion accounted for about 97% of the TLP (4).

ANALYSES

C, H, N and S were determined on the tars with Leco CHN-600 and SC-32 instruments. There was some difficulty obtaining samples containing representative quantities of ash for the CHN-600 instrument and, as a result, C, H, and N results may contain more uncertainty than usual. Ash was determined on the whole samples. The samples were filtered through Whatman #42 filter paper with freshly distilled tetrahydrofuran (THF). The filter cake was dried, weighed and ashed to determine the ash and insoluble organic matter (IOM) content, and to confirm the ash content. The filtrate was rotary evaporated to dryness to remove the THF and to determine the mass of solubles. Complete removal of THF was verified by proton nuclear magnetic resonance (¹H-NMR) spectroscopy. ¹H-NMR spectra were obtained in CDCl₃ solution as previously reported (5). Spectra were obtained on each whole sample and on several of the THF-soluble portions. There was no significant difference between the spectra of the two types of samples. The ¹H-NMR solvent, CDCl₃, dissolved almost, but not quite the entire THF-soluble sample. This did not appreciably affect the ¹H-NMR spectra since spectra obtained on the whole sample in C₅D₅N were essentially the same as the spectra of the THF solubles in CDCl₃. Phenolic -OH contents were determined on the THF solubles by the previously reported Fourier-transform infrared spectroscopic method (6). Gas chromatography/mass spectrometry (GC/MS) analyses were performed by the previously reported method (7).

HYDROTREATING

A sample of the coker tar from Run CSCU-1 (5g) was hydrotreated (750°F, 60 min) in a 45 mL shaking microautoclave in the presence of 5g of

Amocat 1A catalyst and 1600 psig H₂ (cold). The total H₂ charged was about 0.34 g. Its initial pressure at 750°F would be about 3700 psig. The micro-autoclave was agitated at 1000 half-inch strokes/min. The catalyst was supplied by Hydrocarbon Research, Inc., and was removed from the first-stage reactor early in Run O-1 of their Catalytic Two-Stage Liquefaction program. The product was freed of solids and analyzed as described above. The overall recovery of charged material (excluding gases) was 97.8 wt %. The THF-soluble hydrotreated product accounted for 88.5 wt % of the feed, or 101.9 wt % of the THF-solubles in the feed.

DISCUSSION

CHARACTERISTICS OF COKER TAR

The elemental analyses and ash and IOM contents of the coker tars are shown in Table 2. Table 3 shows the proton distributions of the chloroform solubles and the concentrations of phenolic -OH in the THF solubles. All the coker tars contained substantial quantities of ash and IOM. The ash appeared to be a mixture of coal ash and alumina particles that reported with the tars through entrainment. It appears that the alumina "seed" used as the bed in the coker (3) was the source of the alumina particles in the coker tar ash. The IOM in the coker tars may have also originated from entrainment, though some portion of it may derive from retrogressive reactions among the tar components.

The characteristics of the hydrocarbon portion of the tars are clearly influenced heavily by coking temperature. Averages (\pm std dev) of selected properties are shown below as a function of temperature.

Coking T, °F	wt %, ash free		Proton Types, % in CDCl ₃ Solution		
	C	H	Aromatic	Cyclic Beta	Paraffinic
1000	91.2 \pm 0.4	6.6 \pm 0.5	36.8 \pm 7.5	12.2 \pm 2.7	25.0 \pm 0.5
1100	91.8 \pm 0.4	5.0 \pm 0.3	53.2 \pm 2.3	6.7 \pm 0.8	12.4 \pm 0.2
1200	94.8 \pm 0.4	4.6 \pm 0.1	68.0 \pm 1.6	3.1 \pm 0.3	4.7 \pm 0.8

Aromatic protons consist of the sum of condensed and uncondensed aromatic protons. Paraffinic protons consist of the sum of alkyl beta plus gamma protons. Cyclic beta protons provide an indication of the donatable (hydroaromatic) hydrogen content. Though Lummus did not use a complete factorial experimental design, the above table clearly demonstrates that the properties of the hydrocarbon portion of the tar are most affected by coking temperature. With increasing coking temperature, the tars became much more aromatic and contained much lower concentrations of hydroaromatic, paraffinic and total hydrogen. Over the range tested, the other variables had a less significant impact on the properties of the hydrocarbon portion of the tars.

In fluid coking, material can report to the tar product through a combination of cracking and devolatilization. Additional material is carried out of the coker by simple steam distillation and entrainment. The characteristics of the tars indicate that the former mechanism is relatively more important at 1200°F and that the latter mechanisms are relatively more important at 1000°F. However, cracking reactions are important even at 1000°F, as evidenced by the proton distributions of, for example, the feedstock and tar product from CSCU Run 8. Though the exact feedstock used in Run CSCU-8 was not available for analysis, numerous other second-stage vacuum bottoms samples from Wilsonville Run 254 were analyzed (8). Ranges of their properties are shown below.

Proton Type	Proton Distributions, %	
	Vacuum Resid, Range From Wilsonville Run 254	Run CSCU-8 Coker Tar
Aromatic	22.4 - 35.4	42.1
Cyclic Beta	14.1 - 18.2	10.3
Paraffinic	20.5 - 32.6	21.4

The lower concentrations of paraffinic and cyclic beta protons in the tars produced at 1200°F indicate that pyrolysis reactions have cracked most of the alkyl substituents longer than methyl from the aromatic nuclei.

In contrast to the hydrocarbon moieties, the heteroatom contents and phenolic -OH concentrations in the tars show no clear temperature dependence and may primarily reflect the characteristics of the liquefaction bottoms used as the coker feed.

EVALUATION OF TARS AS DONOR SOLVENTS

Conceptually, the coker tars could be introduced to the liquefaction plant as a portion of the recycle oil. If the tars were to comprise a significant portion of the recycle oil, their properties as donor solvents could be important to the performance of the overall process.

None of the tars was directly tested for donor solvent quality. However, a previously developed correlation (5) between proton distributions and donor solvent quality was used for their evaluation. The original correlation was developed for distillate coal liquefaction recycle oils. Though the correlation was not developed for coker tars, it should provide a good indication of their donor solvent quality. The solvent quality index shown in Table 3 was calculated from Equation 4 of Reference 5. These data are summarized below by coking temperature.

<u>Coker Temp., °F</u>	<u>Calculated Solvent Quality Index</u>
1000	74.0 ±7.4
1100	67.4 ±6.9
1200	52.5 ±4.1

With increasing coker temperature, donor solvent quality is substantially reduced. Based on our experience in evaluating solvent quality, we would conclude that the tars produced at 1000°F are poor donors, those produced at 1100°F are even poorer donors and those produced at 1200°F are essentially non-donors.

In those situations in which donor solvent properties are important, for example in a non-catalytic first-stage reactor, it would be expected that the tars would deleteriously affect liquefaction performance if used as a substantial portion of the recycle oil. Of course, any deleterious effect would be reduced as the tar became a smaller portion of the recycle oil. In catalytic liquefaction, such as the H-Coal or catalytic two-stage liquefaction processes, the solvent quality of the recycle oil may be less important. If the tars can be rapidly hydrogenated to produce hydroaromatics (donors), then they may actually improve the donor solvent quality in the reactor inventory. The low concentration of alkyl groups longer than methyl would be beneficial to the donor solvent quality of the hydrogenated tars.

HYDROTREATING OF COKER TAR

All advanced liquefaction processes being developed employ at least one catalytic reactor to maximize distillate production by converting the solubilized coal to distillable products. If fluid coking is to be successfully combined with liquefaction, it must be possible to hydroprocess the coker tars to produce suitable products and an acceptable recycle oil. If the tars are refractory to hydrotreating, coking will provide very little additional liquids yield to the liquefaction process.

One experiment was performed with a coker tar produced at 1200°F to explore the potential of hydrotreating to upgrade the coker tar. Procedural details are presented in the Experimental section. Analyses of the feed and product are presented in Table 4. The data show that even this simple batch hydrotreating was quite successful in hydrogenating the coker tar and removing heteroatoms. ¹H-NMR spectra of the feed coker tar and the hydrotreated product, which are shown in Figures 1A and 1B, respectively, show that a substantial portion of the aromatics were converted to hydroaromatics. The calculated solvent quality index (5) increased from 51.3 to 85.9, i.e., the tar was converted from an essentially non-donor solvent to a high quality solvent.

GC/MS analyses were performed on both materials. Only the portion boiling below about 500°C was detected by the procedure used. The only identified components in the coker tar were four-ring condensed aromatics containing 0 to 2 alkyl carbons (most alkylation was methyl and dimethyl). The hydrotreated product contained compounds with a range of from two to six rings, most of which were partially hydrogenated and contained 2 or fewer alkyl carbons. Examples include methyl tetralins, octahydrophenanthrene, decahydrophyrene and tetrahydrochrysene, all of which are good donors.

ACKNOWLEDGMENT

This program was conceived in conjunction with R. Rao (Burns & Roe), H. Schindler (SAIC), E. Moroni (DOE) and N. Stavropoulos and H. Riegel (Lummus). Their contributions are gratefully acknowledged. The coker tars were supplied by N. Stavropoulos of Lummus. The catalyst was supplied by J. B. McLean of Hydrocarbon Research, Inc. Phenol determinations were performed by G. A. Robbins of Consol. This work was funded by the U.S. Department of Energy under Contract No. DE-AC22-84PC70018.

REFERENCES

1. Riegel, H. and Stavropoulos, N., "Batch Bench Coking Under Fluid Coking Conditions", report to Burns and Roe Services Corp. under U.S. DOE Contract No. DE-AC22-84PC72571, Subtask 3.01 (FY87), August 1987.
2. Stavropoulos, N., Riegel, H. and Suci, D., "Coking of Coal Liquefaction Bottoms, Batch Bench Coking Tests", presented at the DOE Direct Liquefaction Contractors' Review Meeting, Pittsburgh, Pennsylvania, October 1987.
3. Riegel, H., Stavropoulos, N. and Strangio, V., "Continuous Coking Tests Under Fluid Coking Conditions", draft report to Burns and Roe Services Corp. under U.S. DOE Contract No. DE-AC22-84PC72571, Subtask 3.01, March 29, 1988.

REFERENCES (Continued)

4. Stavropoulos, N., personal communication to R. A. Winschel, February 19, 1988.
5. Winschel, R. A., Robbins, G. A. and Burke, F. P., Fuel 1986, 65, 526-32.
6. Burke, F. P., Winschel, R. A. and Robbins, G. A., "Recycle Slurry Oil Characterization - Final Report", DOE Contract DE-AC22-80PC30027, March 1985.
7. Winschel, R. A., Robbins, G. A. and Burke, F. P., "Coal Liquefaction Process Solvent Characterization and Evaluation - Technical Progress Report for April 1 through July 31, 1987", DOE Contract No. DE-AC22-84PC70018, February 1988.
8. Winschel, R. A., Robbins, G. A. and Burke, F.P., "Coal Liquefaction Process Solvent Characterization and Evaluation, Status Report for March 1988", DOE Contract No. DE-AC22-84PC70018, April 15, 1988.

/Is

TABLE 1
 COKER FEEDSTOCKS AND OPERATING CONDITIONS (3)

CSCU Run	Vacuum Bottoms Feedstock Source			Operating Conditions				
				T, °F	P, psig	Inject Steam to Feed, wt Ratio	Approx. Res. Time, sec.	
	Coal	Plant (Run No.)	Sample				Liquid	Vapor
8	Ohio 6	W'ville (254)	3587	1000	10	0.40	7.7	4.0
11	Ohio 6	W'ville (254)	3587	1100	10	0.40	7.9	4.3
9	Ohio 6	W'ville (254)	3587	1200	10	0.40	7.3	3.6
1	Ohio 6	W'ville (254)	3587	1200	2	0.31	8.2	5.2
2	Ill. 6	W'ville (250-D,E)	3567	1200	10	0.28	10.2	5.9
4	Ill. 6	W'ville (250-D,E)	3567	1200	10	0.33	7.8	4.6
12	Ill. 6	W'ville (253)	3584	1100	10	0.40	7.4	3.9
7	Ill. 6	HRI (1-25)	3576	1000	10	0.35	9.6	5.8
6	Ill. 6	HRI (1-25)	3576	1200	10	0.37	8.4	5.5
13	Wyodak	W'ville (251)	3566	1100	10	0.4	7.4	3.9

TABLE 2
 ANALYSES OF COKER TARS

Sample	wt %, Ash Free					wt %, As Determined	
	C	H	N	S	O (diff)	Ash	IOM
CSCU-8, TLP	91.0	6.3	1.0	0.1	1.6	2.5	0.6
CSCU-9, TLP	92.1	4.7	1.0	0.2	2.0	4.7	4.0
CSCU-1, 650°F ⁺	95.0	4.7	1.1	0.2	-1.0	10.7	6.9
CSCU-2, 650°F ⁺	94.3	4.5	1.2	0.2	-0.2	9.8	8.8
CSCU-4, 650°F ⁺	94.9	4.6	1.0	0.2	-0.7	12.7	8.2
CSCU-12, TLP	91.3	5.3	1.0	0.3	2.1	4.4	3.3
CSCU-7, 650°F ⁺	91.5	7.0	0.6	<0.1	0.9	1.2	1.0
CSCU-6, 650°F ⁺	95.1	4.7	0.9	0.1	-0.8	19.0	7.3
CSCU-13, TLP	92.0	4.9	1.0	0.7	1.6	26.9	13.6

TABLE 3
 PROTON DISTRIBUTIONS AND PHENOLIC -OH CONCENTRATIONS OF COKER TARS

Sample	Proton Distributions, %							Conc. of Phenolic -OH in THF-Sols., meq/g	Calculated Solvent Quality Index
	Cond Arom	Uncond Arom	Cyclic Alpha	Alkyl Alpha	Cyclic Beta	Alkyl Beta	Gamma		
	CSCU-8, TLP	28.2	13.9	12.7	13.5	10.3	14.1	7.3	0.65
CSCU-9, TLP	54.7	10.9	14.9	10.7	3.5	3.5	1.8	0.60	59.3
CSCU-1, 650°F ⁺	57.6	11.1	13.6	10.9	2.7	3.2	1.0	0.53	51.7
CSCU-2, 650°F ⁺	54.8	12.4	12.2	11.6	3.3	3.7	2.1	0.53	49.5
CSCU-4, 650°F ⁺	56.7	11.9	13.6	11.0	3.0	2.4	1.4	0.51	52.8
CSCU-12, TLP	41.2	10.3	16.6	12.3	7.3	7.8	4.4	0.64	72.3
CSCU-7, 650°F ⁺	25.6	5.9	16.1	9.6	14.1	19.3	9.4	0.23	79.2
CSCU-6, 650°F ⁺	60.0	9.9	12.9	10.3	2.8	2.8	1.4	0.30	49.1
CSCU-13, TLP	42.6	12.2	13.5	13.1	6.1	9.0	3.5	0.52	62.6

TABLE 4
HYDROTREATING RESULTS

<u>Analysis, wt % Ash Free</u>	<u>Feed (CSCU-1) (a)</u>	<u>THF Soluble Hydro Product</u>
C	92.3	91.7
H	5.1	6.7
N	1.3	0.9
O (Diff)	1.2	0.6
S	0.2	<0.1
<u>Conc. of Phenolic -OH in THF Solubles, meq/g</u>	0.55	0.31
<u>H-Aromaticity of CDCl₃ Solubles, %</u>	68	41

(a) This is a different sample of the 650°F⁺ fraction from Run CSCU-1 than appears in Tables 2 and 3. Differences in analytical data from Tables 2 and 3 may be real or may reflect uncertainty.

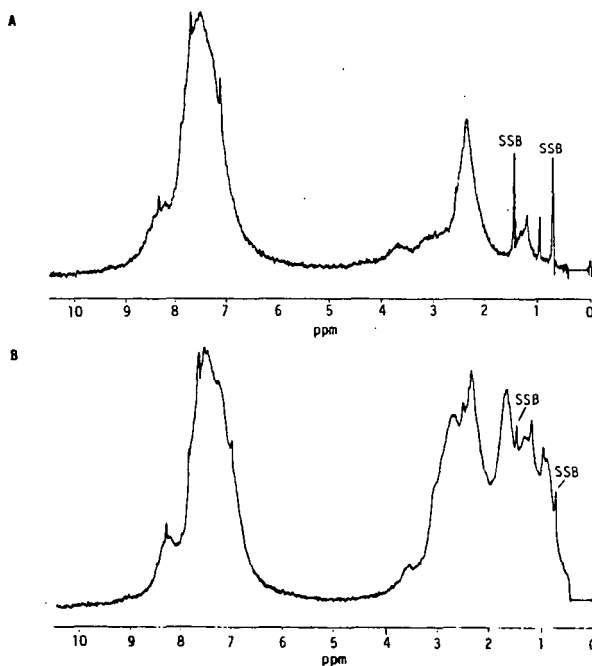


Figure 1. ¹H-NMR Spectra in CDCl₃ of A) Coker Tar from Run CSCU-1 and B) of Hydrotreated Product (SSB = Spinning Side Bands).

CATALYSIS IN DIRECT COAL LIQUEFACTION : STATUS AND DIRECTIONS FOR RESEARCH

Frank Derbyshire
Sutcliffe Speakman Carbons Limited
Guest Street, Leigh, Lancashire, U.K.

The economic viability and operability of processes to convert coals to useful liquid products is contingent upon the development and application of effective catalysts. New and improved catalysts can lead to more favourable process economics by increasing the rate of conversion and the selectivity to the desired products and by allowing operation at reduced temperatures and pressures.

The processes of primary coal dissolution and coal liquids upgrading are distinguished. The status and limitations of catalysts used to promote these reactions are discussed together with approaches which could lead to the development of improved and novel catalysts.

INTRODUCTION

The production of distillate fuels and chemicals from coal has never been economical in a free market economy. The principal factors which contribute to the high cost of coal-derived liquids are the large amounts of hydrogen which must be added to remove heteroatoms and to convert material containing about 5 wt% hydrogen to products with between 12 to 14 wt% hydrogen, the severe reaction conditions (temperature and pressure) and the relatively low rates of conversion which are experienced.

In spite of these limitations there are valid reasons for pursuing research and development in coal liquefaction. Practically every future energy scenario envisions the development of indigenous fossil fuel resources to supplement and replace materials derived from petroleum crudes. In the short term, situations could arise whereby the supplies of imported crudes to oil-poor industrialised nations are restricted and, in the long term, world petroleum reserves will be eventually be depleted.

As has occurred in the development of the petroleum processing and chemical industries, the route to significant improvements in liquefaction processing lies in the successful development and application of suitable catalyst systems. In this paper some of the more salient aspects of liquefaction catalysts are reviewed in terms of the limitations of our present understanding and approaches which could lead to improved and novel developments. Reference is made to a much more extensive critical review which the author has recently completed for the International Energy Agency under the sponsorship of the United States Department of Energy (1). A companion review on catalysis in syngas conversion has also been prepared by Alex Mills (2).

The recognition that liquefaction takes place in two loosely-defined stages, consisting of coal dissolution followed by upgrading of the solubilised products, has led to the concept of two-stage process configurations. The progression from a single, noncatalytic process to a catalytic - catalytic two stage process is summarised in Table 1 (3). The adoption of a fully catalytic process has led to increases in coal throughput and in the yield and quality of distillate products. In addition, since the construction of the first commercial-scale plants in Germany there has been appreciable progress in lowering operating severity and improving the selectivity to liquid products,

Table 2. Nevertheless there is still a pressing need for innovations which can lead to further gains in process performance and operability. The distinction between the processes of dissolution and upgrading provides a convenient division between dispersed and supported catalysts. While there are exceptions, the former have been applied primarily to promote the process of coal dissolution and the latter to upgrading the solubilised coal liquids. These catalysts cannot really be used interchangeably. It is unlikely that dispersed catalysts could realise the selectivity which is possible with supported catalysts; restricted access to the reaction surface of supported catalysts precludes their being able to directly influence the reactions of coals and high molecular weight coal derived products.

SUPPORTED CATALYSTS

The catalysts which have been applied to coal liquids upgrading comprise a combination of the metals Co, Ni, Mo and W, together with promotional additives, distributed over a porous support of alumina or silica-alumina. The catalysts must be sulphided in order to attain their active form. These catalysts are used extensively in petroleum refining and evolved from catalysts which were originally developed for hydroprocessing distillate coal liquids. No concerted attempts have been made to adapt them for hydroprocessing high boiling coal liquids. Research efforts have focused mainly on catalyst screening and evaluation and little attention has been given to investigating novel formulations.

One of the important conclusions emanating from a long program of research by Sullivan and co-workers at the Chevron Research Company (4, 5) is that coal liquids can be adequately hydroprocessed over conventional catalysts provided that the end-point does not exceed about 370°C. The presence of higher boiling materials is deleterious to catalyst life which is shortened by the formation of carbonaceous deposits, the adsorption of basic compounds and the deposition of metals. These effects are considerably more pronounced in the presence of non-distillable coal-derived materials. Under these conditions and during continuous processing there is a rapid and massive reduction in catalyst activity during the first 30 to 50 hours on stream, due principally to the deposition of carbonaceous materials which effect a drastic reduction in surface area. Subsequent loss in activity is more gradual and is attributed to the accumulation of metals. Other contributory causes are the loss of active metals and sintering. Substantial research has been conducted at the Sandia National Laboratories and the Pittsburgh Energy Technology Center to investigate the causes and mechanisms of deactivation (see reference 1). The deposition of carbon is generally attributed to the adsorption and reaction on catalyst acid sites of species such as polycondensed aromatics and heteroatom-containing compounds.

It is concluded that the existing generation of supported catalysts cannot adequately meet the exacting requirements for upgrading primary coal liquids. Two prospective approaches to resolving this problem are indicated. The first involves the development of new supported catalysts which are less susceptible to deactivation by the mechanisms discussed. Avenues for research are considered in reference (1). The second approach is to produce materials which are more amenable to upgrading over supported catalysts through effective catalytic control of the process of coal dissolution. While both of these strategies are considered to be important priorities for future research, the remainder of this paper will be given to a discussion of dissolution catalysis.

It is considered that successful research in this area could have an immediate impact on liquefaction process development.

DISSOLUTION CATALYSTS

Although many catalysts have been examined in fundamental studies, large scale investigations have been primarily concerned with two groups of catalyst materials; metal sulphides and acid catalysts. The sulphides of metals such as Mo and Fe are believed to function as hydrogenation catalysts while metal halides like $ZnCl_2$ promote bond cleavage by an ionic mechanism. In both cases, effective control of the dissolution process requires intimate contact between the catalyst and coal. In turn, this means that the used catalyst is associated with the solid reaction products, which complicates its recovery. For this reason, low cost has been a priority in catalyst selection as it allows use on a once-through basis. This has limited the choice of candidate catalyst materials. The development of technologies for catalyst recovery could alleviate the cost constraint and have a major influence on broadening the resource base for the selection of catalysts.

It is also true to state that research on catalytic coal dissolution has been retarded by the persistent and misguided belief that catalysts cannot influence the reactions whereby the solid coal feed is converted to soluble products.

Sulphide Catalysts

For most metals, the thermodynamically stable form under liquefaction conditions is a sulphide or mixture of sulphides. Fortunately, a number of sulphided metals are active catalysts for coal dissolution. A water or oil-soluble catalyst precursor is normally introduced to the coal or coal-solvent slurry in a manner intended to disperse it efficiently. The sulphided catalyst is subsequently produced by the in-situ reaction of the precursor with sources of sulphur. For a given metal, the catalyst activity will be a function of its dispersion and the stoichiometry of the sulphide phase.

Dispersion is very difficult to quantify. It is always described qualitatively and inferred from experimental data. Logically, it will be dependent upon the precursor composition and the mode of its addition. There is a need to develop methods to quantitatively assess catalyst dispersion. Without this information, there is no means to distinguish effects due to differences in dispersion from those caused by changes in other parameters.

The kinetics of formation of the active phase will be determined by the dispersion and composition of the catalyst precursor and the availability of sulphur-containing species. This reaction is of some relevance since, if the rate is slow, the initial and critical reactions within the coal matrix may be thermally controlled, despite the ostensible presence of catalyst.

Increasing the partial pressure of H_2S will promote precursor conversion and can have an important influence on catalyst activity. In the presence of added pyrrhotite, increasing the H_2S partial pressure has been shown to enhance the hydrocracking of diphenylether and diphenylmethane (6). Research on upgrading petroleum feedstocks with unsupported vanadium catalysts showed that the catalyst activity passed through a maximum between 10-25 mole percent H_2S (7). Studies with supported catalysts have demonstrated that increasing the partial pressure of H_2S accelerates the rate of

hydrodenitrogenation (8-11). One explanation of these phenomena is that the H₂S partial pressure serves both to maintain the catalyst in its sulphided state and to control its stoichiometry. However, it has also been found that H₂S alone can promote cracking reactions and its direct participation in hydrogenolysis reactions may well contribute to the effects observed in the presence of catalysts.

Some thoughts are presented here concerning the mechanisms by which sulphide catalysts may promote coal dissolution. Indisputably, they promote hydrogenation of the coal. It is also probable that they provide several other functions although, as yet, there have been no clear indications of these.

McMillen (12-14), and earlier Vernon (15), have described a mechanism by which the addition of H-atoms to the ipso positions of linkages to aromatic systems can induce bond cleavage. Free H atoms could be made available from one of several sources including the catalytic dissociation of molecular hydrogen. However, even at high levels of dispersion, a large proportion of the catalyst centres must be distant in molecular dimensions from the bonds which are broken. The facility with which hydrogen is known to move through the structure of coals suggest that it should be able to diffuse from the sites where it is generated by a spill-over mechanism, Figure 1. Thus the catalyst can be viewed as a means to inject H-atoms into the coal or the coal-solvent mixture and thereby increase the pool of available hydrogen. This hydrogen will be available for aromatic hydrogenation, the promotion of bond cleavage reactions and radical stabilisation.

In the proposed mechanism, the catalyst does not participate directly in bond cleavage which is dependent upon the level of thermal energy input. This could explain why, for a given coal, different catalysts have been found to show evidence of liquefaction activity over the same range of temperature, Figure 2 (16). The threshold temperature will depend upon the types and distribution of connecting linkages and is expected to differ from coal to coal and to show a systematic change with coal rank.

The effectiveness of the catalyst can be strongly influenced by the presence and composition of a liquefaction solvent. While space precludes an extended discussion of this subject, it seems that those solvent characteristics which have been found to be desirable in 'thermal' liquefaction also hold for catalytic coal conversion. The solvent can provide additional routes for the transport of H-atoms produced by the catalytic dissociation of H₂. The presence of polycondensed aromatics in the solvent has been found to be particularly advantageous (see reference 1).

The possibility that there exists a temperature threshold, below which hydrogenation catalysts have little effect on liquid yields places a lower limit on the temperatures required for liquefaction. However this constraint need not hinder the development of more effective catalysts.

Catalysts with higher activities for dissociating molecular hydrogen will increase the availability of hydrogen atoms and may make it possible to operate at more elevated temperatures (thereby increasing the rate of conversion) while suppressing condensation reactions. Reductions in operating pressure may also be realised. A number of single metals and metal compounds which possess the desired attributes have been excluded from research programs because of their

cost. The scope of fundamental research should not be restricted by such considerations. Until the extent of any potential benefits are determined experimentally, judgements of economic viability can only be subjective.

Although catalytic hydrogenation does not appear to significantly enhance the yield of product liquids below a certain temperature range, it has been shown that reaction at lower temperatures can effect structural modifications to the coal which are advantageous to the production of liquids upon subsequent high-temperature reaction (17,18). The influence of the catalyst can thus be augmented by reacting the coal in successive stages of increasing temperature.

Perhaps the most promising approach to the development of novel catalysts lies in research into multicomponent systems which, in comparison to work on single metals, are essentially unexplored. There are good reasons to anticipate that synergistic effects will lead to exciting discoveries. Synergism has been reported for Fe - Mo catalysts (19). It is supposed that the two metals provide complementary functions which results in non-additive behaviour. A further example of this is given below. The use of a second component could also reduce catalyst cost if the concentration of a more expensive component can be reduced.

Acid Catalysts

Acid catalysts can promote the cleavage of the linkages which connect coal structural units and crack the structures which comprise these units. Several of the catalysts of interest for coal dissolution are metal halides, such as $ZnCl_2$, which possess a low melting point and develop significant vapour pressure at sub-pyrolysis temperatures. This facilitates their penetration and dispersion in the coal matrix. Cracking reactions proceed by an ionic mechanism in which protonation of the reactants is the initial and rate - limiting step. The driving force is the strength of the acid. By using stronger acid catalysts the rate of reaction can be accelerated and the reaction temperature can be reduced.

Process development research conducted by Zielke and co-workers at the Consolidation Coal Company in the 1960s and 1970s demonstrated that it is possible to liquefy coals at fast rates of throughput and with high selectivity to gasoline-range products, using a zinc chloride catalyst. The disadvantages were (i) that the use of massive concentrations of $ZnCl_2$ necessitated the development of techniques for catalyst recovery and (ii) that the corrosive nature of the catalyst created problems in plant construction and operation (see reference 1).

It is possible that many of these technical difficulties could be resolved. However, there is a further problem relating to the process chemistry. In general, acid catalysts do not promote hydrogenation. As a consequence of their inability to adequately stabilise the cracked products, cracking reactions are accompanied by condensation reactions leading to the production of high molecular weight materials. A possible solution is to introduce a second component which can provide a hydrogenation function, Table 3 (20). As discussed above, there are indications that research into multicomponent catalyst formulations can lead to improved control of the reaction chemistry of coal conversion. In this case, it could bring the more desirable features of acid catalysis closer to practical realisation.

References

1. Derbyshire, F J (1988) Catalysis in coal liquefaction: new directions for research.
IEA Coal Research, London, UK (in press)
2. Mills, G A (1988) Catalysts for fuels from syngas.
IEA Coal Research, London, UK (in press)
3. Weber W, Stewart N (1987) Direct coal hydroliquefaction.
EPRI Journal: 12(1); 40-41
4. Sullivan R F (1986) Transportation fuels from two-stage liquefaction products.
American Chemical Society, Division of Fuel Chemistry, Preprints; 31(4); 280-293
5. Sullivan R F, Frumkin H A (1986) Refining coal liquids: where we stand.
American Chemical Society, Division of Fuel Chemistry, Preprints; 31(2); 325-339
6. Sweeny P G, Stenberg V I, Hei R D, Montano P A (1987) Hydrocracking of diphenyl ether and diphenylmethane in the presence of iron sulphides and hydrogen sulphide.
Fuel: 66; 532-541 (1987)
7. Gatsis J G (1975) Catalytic conversion of hydrocarbon mixtures.
US Patent 3,915,842; 6 pp (28 Oct 1975)
8. Hirschon A S, Laine R M (1985) Catalytic hydrodenitrogenation of an SRC II coal liquid: effect of hydrogen sulphide.
Fuel; 64; 868-872
9. Satterfield C N, Gueltekin S (1981) Effect of hydrogen sulfide on the catalytic hydrodenitrogenation of quinoline.
I&EC Process Design & Development; 20; 62-68
10. Yang S H and Satterfield C N (1983) Some effects of sulfiding of a NiMo/Al₂O₃ catalyst on its activity for hydrodenitrogenation of quinoline.
Journal of Catalysis; 81, 168-178
11. Yang S H, Satterfield C N (1984) Catalytic hydrodenitrogenation of quinoline in a trickle-bed reactor. Effect of hydrogen sulfide.
I&EC Process Design & Development; 23; 20-25
12. McMillen D F, Malhotra R, Chang S-J, Nigenda S E (1985) Solvent radical mediated hydrogenolysis in coal liquefaction.
In: Proceedings - 1985 International Conference on Coal Science, Sydney, NSW, Australia, Pergamon Press pp 91-94
13. McMillen D F, Malhotra R, Hum G P, Chang S-J (1987) Hydrogen-transfer-promoted bond scission initiated by coal fragments.
Journal of Energy and Fuels; 1; 193-198

14. McMillen D F, Malhotra R, Chang S-J, Nigenda S E (1985) Hydrogenolysis in coal liquefaction and pyrolysis: the relative importance of solvent radicals and free hydrogen atoms.
American Chemical Society, Division of Fuel Chemistry, Preprints; 30 (4); 297-307
15. Vernon L W (1980) Free radical chemistry of coal liquefaction: role of molecular hydrogen.
Fuel; 59; 102-106
16. Charcosset H, Bacaud R, Besson M, Jeunet A, Nickel B, Oberson M (1986) On the chemical effects of catalysts in the direct liquefaction of coal.
Fuel Processing Technology; 12; 189-201
17. Derbyshire F J, Davis A, Epstein M, Stansberry P (1986) Temperature-staged catalytic coal liquefaction.
Fuel; 65; 1233-1240
18. Bolton C, Riemer C, Snape C E, Derbyshire F J, Terrer M-T (1988) Effect of low temperature catalytic hydrogenation on pyrolysis and hydroxyrolysis of a bituminous coal.
Fuel; (in press)
19. Garg D, Givens E N (1983) Relative activity of transition metal catalysts in coal liquefaction.
American Chemical Society, Division of Fuel Chemistry, Preprints; 28 (5); 200-209
20. Mobley D P, Bell A T (1980) Hydrogenolysis of dibenzyl ether using zinc chloride-metal co-catalyst systems.
Journal of Catalysis; 64; 494-496

Table 1 - History of Process Development and Performance for Bituminous Coal Liquefaction

	<u>Configuration</u>			
	Single stage noncatalytic (1982)	Single stage catalytic (1982)	Two stage noncatalytic/catalytic (1985)	Two stage catalytic/catalytic (1986)
Distillate (wt% coal maf)	41	52	62	70
Distillate quality/gravity °API	12.3	20.2	20.2	26.8
Nonhydrocarbons (wt%)				
S	0.33	0.20	0.23	0.11
O	2.33	1.0	1.9	<1
N	1.0	0.50	0.25	0.16

Source: Weber and Stewart, 1987 (3)

Table 2 - Impact of Catalysis on Process Conditions and Selectivity

<u>Process</u>	<u>Temp oC</u>	<u>Pressure MPa</u>	<u>Liquid/gas ratio</u>
Single Stage			
I G Farben	480	30-70	2.4
Ruhrkohle	475	30	2.3
H-coal	450	12	4.0
Two Stage (noncatalytic/catalytic)			
British Coal	400-425	20	4.8
Lummus	410-460	18	10.8
Two Stage (catalytic/catalytic)			
HRI	400-440	17	12.0

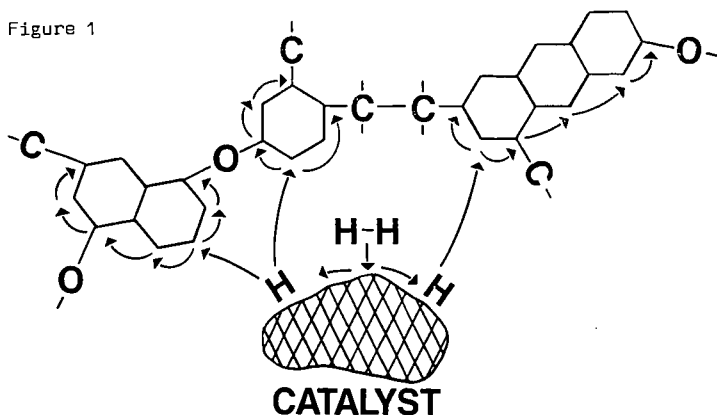
Source: various

Table 3 - Effect of hydrogenation component on ZnCl₂ - catalysed cracking of dibenzylther

Catalyst	% Ether Conversion	% Yield	
		Toluene	Insoluble Resin
None	3.8	1.4	-
ZnCl ₂	100.0	3.9	97.0
Ni	38.2	19.5	2.5
Ni+ZnCl ₂	96.5	65.6	6.0

Source: Mobley and Bell, 1980 (20)

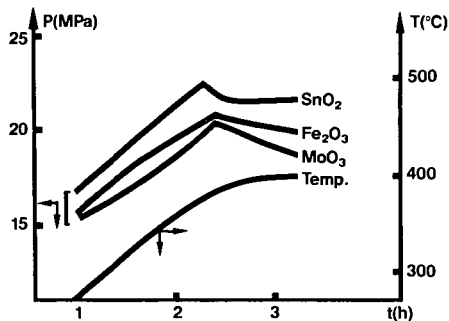
Figure 1



**DISTRIBUTION OF H-ATOMS BY
HYDROGEN SPILLOVER**

*Produced by catalytic dissociation of H₂.
H-Atoms induce bond cleavage and stabilise radicals.*

Figure 2



**EVIDENCE FOR EXISTENCE OF A
THRESHOLD TEMPERATURE IN
CATALYTIC COAL LIQUEFACTION**

**(BITUMINOUS COAL: TETRALIN: CATALYST =
40: 95: 0.8; HEATING RATE 3°C/MIN)**

H. Charcosset and others (1986), Fuel Processing Technology, 12, 189-201

DIRECT COAL LIQUEFACTION: DISTINCTION BETWEEN REACTANTS
AND CATALYSTS

ENE0 C. MORONI

U.S. department of Energy, FE-231 GTN, Washington, D.C. 20545

INTRODUCTION

An extensive research and development program on disposable catalysts and slurry catalysis was supported by the Fossil Energy Office of the U.S. Department of Energy (DOE) during the period 1978-82. Actually, prior to 1978, a project of similar nature was carried out for several years, at a low priority effort, at the U.S. Department of Interior, Bureau of Mines laboratories which is now known as the Pittsburgh Energy Technology Center (PETC).

Although numerous slurry-phase catalysts were tested in this program, two metals, iron and molybdenum, in their sulfided form, were singled out as the most promising candidates for scale-up processing.

In 1982, Gray and Neuworth (1) and in 1983, Davidson (2) have made comprehensive reviews on the role of iron sulfides on coal liquefaction, and, up to the present, there has been a continuing level of activity in this area. Iron and molybdenum sulfides catalysts were amply covered in a very recent comprehensive and critical review on catalysis in direct coal by Derbyshire (3). This excellent review provides a current state of knowledge of all form of catalysis which are potentially of interest from a practical standpoint, in addition to give valuable new directions for research in this area.

Garg and Givens (4) have shown evidences of synergism for an Iron-Molybdenum catalyst in which mixed catalyst has a definite advantage over each individual metal preforming. Similarly Gatsis (5) uncovered a distinct synergism occurring for an Iron-Vanadium catalyst which permits the partial replacement of the expensive Vanadium with the low cost Iron, with no loss of the catalytic activity level.

The aforementioned references report that iron sulfides catalysts exhibit consistently lower hydrogenation activity than either the molybdenum or the vanadium sulfides. Various explanations were attributed to the low catalytic activity of the iron sulfides, such as the very low surface area and the variable catalytically active iron sulfides forms found in pyrites, the precursors present in the mineral matter of most coals.

This paper, presently in the form of a communication to be complemented by the oral presentation and to be expanded for publication in Energy and Fuels, intends to provide evidences that the active forms of iron sulfides have a different function than the other metal sulfides, the function of being reactants and catalysts.

An additional objective of this paper, in conjunction with a series of papers presented by this author in recent years (6), is to stimulate the research community, dedicated to coal liquefaction fundamentals, to undertake a more systematic research approach to discriminate the critical reactions from the numerous ones occurring particularly the lower temperature range, which, in turn, profoundly affect the subsequent reactions occurring at the higher temperatures.

INITIAL STAGES OF COAL LIQUEFACTION

This author (7) has stressed the importance of reactions involving heteroatom-containing compounds in coal dissolution and subsequent coal liquid upgrading. of the three major heteroatoms present in coal, the most abundant is the oxygen, and, particularly when it is in the form of carboxylic and phenolic species, it seems to dominate the reactions occurring in the initial stages of liquefaction. Except for the low-rank coals, in which the carboxylics are converted at the temperature range of 250-300°C, with the observed loss of CO₂, the phenolic chemistry appears to dominate the reactions occurring in the 280-350°C temperature range, for coals of all ranks, except, perhaps, for the low-oxygen german's hard coal. In particular, the phenols are the major contributors for the regressive reactions, causing the high viscosity of coal liquids and increasing the difficulty of upgrading and refining, and, as discover in recent work, the promoters for catalyst deactivation. Lemberston et al.(8) tested a sulfided nickel-molybdenum on alumina catalyst for the hydrogenation/hydrocracking of a mixture of phenanthrene, carbazole and 1-naphtol, and discovered that the catalyst maintain its activity in the presence of the phenanthrene-carbazole mixture, but it is strongly deactivated when 1-naphtol is added to that mixture. This experimental evidence of catalyst deactivation promoted by the phenols confirms the intuitive thoughts emerged some ten years ago

from the experimental data provided by Suntech (9) by which the removal of the phenols from a SRC II distillate solvent caused a seven-fold increase in the kinetics of nitrogen removal by catalytic hydrogenation. At a later date, Garg et al. (10) used a defunctionalized solvent in which most of the phenols and nitrogen compounds were removed from a SRC I process solvent, and obtained high conversion and oil yield with only 0.2-0.5 weight percent addition of pyrite to the coal/solvent slurry. When the untreated solvent was used for comparison, addition of 3-5 percent pyrite was required to obtain the same conversion and oil yield.

The obvious thought, derived from this data, was that a large portion of the active iron sulfide reacted with the oxygen moieties with the loss of catalytic activity, and, only the excess pyrite functioned as the actual catalyst. To prove this point, the work of Montano (11) indicated a strong affinity of an active iron sulfide surface towards oxygen in which the carbon-oxygen bonds are broken even from very stable aromatic ethers to generate aromatic hydrocarbon and catalytically inactive forms of iron sulfate or oxide.

The removal of oxygen moieties from coals, in the initial and subsequent stages of liquefaction, by the reaction with inexpensive iron sulfides, whose precursors happened to have the good fortune of being the most abundant components of the mineral matter in coal, ought to be considered highly desirable from the economic and technological point of view.

CONCLUSIVE REMARKS

Derbyshire (3), in his review on catalysis for coal liquefaction, questioned the modest progress obtain in catalytic liquefaction, particularly when research in this field has been conducted for half a century. Absence of a realistic model coal structure, and, of a clear understanding of the reaction chemistry and, the cyclic nature of interest in research of coal liquefaction were the main reasons for the impediment of progress in catalysis, according to Derbyshire.

The data and thoughts presented in this communication seem to complement Derbyshire's assessment, in that the scarce progress in catalytic liquefaction is due to the fact that catalyst activity is more dependent on the feed composition in contact with the catalyst than on the catalyst formulation. Preconversion treatments to remove first the active oxygen species is necessary prior to submit coal-derived extracts to supported catalysts for further conversion to environmentally acceptable fuels.

This suggests that the research approach in coal liquefaction ought to be systematic because there is the likelihood of significant complex relationships between coal structure, reaction mechanisms, thermodynamics, analytical chemistry, kinetics and, finally, catalyst selection.

REFERENCES

1. D. Gray and M. Neuworth, Disposable Catalysts in Coal Liquefaction: The Effect of Iron Sulfides. The MITRE Corp./DOE Contract 10280 WP-81W427, September, 1981
2. R. Davidson, Mineral Effects in Coal Conversion, ICTIS/TR 22, London, UK, IEA Coal Research, 1983.
3. F. Derbyshire, Catalysis in Direct Liquefaction: New Direction for Research. IEA Coal Research. In press.
4. D. Garg and E. Givens, Relative Activity of Transition Metal Catalysts in Coal Liquefaction. ACS Fuels Chemistry Preprints. 28, 5, 200-209, 1983.
5. J. Gatsis, Allied Chemicals.- Private Communication.
6. E. Moroni, Origins and Reactions of Alkyls and Alkanes in Direct Coal Liquefaction. ACS Fuels Chemistry Preprints. 33, 1, 384- 86, 1988.
7. E. Moroni, Coal Liquefaction and Upgrading Benefit from Heteroatom Removal. Proceedings of the 1987 International Conference on Coal Science. Maastricht, The Netherland, October 26-39, 1987, 351, and references therein.
8. J. Lemberon, M Touzeyidio and M. Guisnet, Effect of an Acid Catalyst on the Activity of a Sulfided Catalyst for Hydroconversion of Model Compounds. GRECO Hydroconversion and Pyrolysis of Coal. Poitiers, France, Sept. 10-11, 1987.
9. E. Hollstein et al., Coal Conversion to Distillate Fuels. Suntech, Inc./DOE Contract 10592, Final Report, 34, 1982.
10. D. Garg et al., Effect of Solvent Modification on Coal Liquefaction APCI/DOE Contract 50003-38, Final Report, 1985.
11. P. Montano and A. Bommannavar, J. Molecular Catalysis, 20, 393, 1983.

COPROCESSING OF COAL WITH HIGH METAL CONTENT RESIDS
Timothy J. Miller, Sudhir V. Panvelker, Irving Wender, and John W. Tiemey
University of Pittsburgh, Pittsburgh, PA 15261
Yatish T. Shah
University of Tulsa, Tulsa, OK 74114
Gerald Huffman
University of Kentucky, Lexington, KY 40506

INTRODUCTION

The energy industry will have to consider alternative sources for the production of liquid fuels in view of the rapid depletion of conventional light oil reserves. Several processes are being developed for upgrading heavy crudes and bottom-of-the-barrel residual oils.^(1,2) The heavy oils contain large amounts of metals which interfere with catalytic upgrading to clean distillates by acting as catalyst poisons. In the 1970s, several direct liquefaction processes were developed to produce liquid fuels from coal. One of the drawbacks of these processes is the fact that it is necessary to recycle a significant amount of product oil to slurry feed coal. This leads to increased plant complexity and higher production costs. Coprocessing, where coal is liquefied in a once-through mode in a heavy oil slurrying medium, may form a bridge between the existing petroleum-refining technology and the syntuels industry of the future. Besides producing light products from coal as well as from heavy oil, it can accomplish a high degree of demetallation of oil, by rejecting the metals to the solid residue.

The composition of coal-derived recycle solvents is very different from that of heavy oils. The former are highly aromatic and hydroaromatic while the latter are mostly paraffinic and naphthenic. Thus, it should be expected that coal conversion in a heavy oil, in general, would be less than in a coal-derived solvent in the absence of a catalyst. However, it is possible to achieve a high degree of conversion by proper choice of host oil, operating conditions, or by pretreating the host oil before it is used for liquefaction. Yan and Espenscheid have reported that 90% conversion of Illinois No. 6 coal to pyridine-solubles was achieved by liquefying the coal in bottoms from a fluid catalytic cracking unit without using any catalyst⁽³⁾ as this solvent was highly aromatic. Similar high conversions have been reported by researchers using catalysts.⁽⁴⁻⁶⁾ Curtis et al. have reported that petroleum residua are deficient in labile hydrogen; however, if a catalyst is used under hydrogen atmosphere, coprocessing can proceed with fairly high conversions.⁽⁷⁾ It is possible to increase the liquefying efficacy of a residuum by its prior hydrocracking, or by adding external hydrogen donors.⁽⁸⁾

This paper presents the results of thermal (with no added catalyst) coprocessing of Illinois No. 6 (hvBb) coal with Maya (650°F+) ATB residual oil and with whole Boscan crude. The relationship between reaction conditions and coal conversion and product selectivity has been studied. The removal of vanadium during coprocessing has been investigated. The results on heteroatom removal reactions have also been presented as the amount of heteroatoms in petroleum is often correlated with that of metals.⁽⁹⁾

EXPERIMENTAL

Tables 1 and 2 show analyses of Illinois No. 6 coal and the host oils respectively. A few experiments were made using a coal-like char and an activated carbon (NUCHAR). The char was synthesized in this laboratory from cellulose. All liquefaction experiments were conducted using a horizontal 20 ml microreactor. Typically the reactor was loaded with 8-10 g of reactants along with four 2 mm stainless steel balls as a mixing aid. It was pressurized with hydrogen to 6.9 MPa (1000 psig) at ambient temperature. The reactor was then brought to the desired reaction temperature by immersing it in a heated fluidized sand-bath. The reactor was shaken horizontally (five one-inch displacements per second) to ensure adequate mixing. The desired temperature was attained within 3-4 minutes and this was taken as zero time. At the end of the desired reaction time, the reactor was removed from the sand bath and cooled with water. The products were removed by washing the reactor with tetrahydrofuran (THF). Almost all the runs were made in duplicate.

The reaction products were classified as THF-insolubles (also referred to as coke), asphaltenes, and oils based on their solubility behavior. Asphaltenes were defined as product soluble in THF but insoluble in pentane; oils (often called maltenes) were defined as products soluble in pentane. The vanadium content of samples was determined using inductively coupled plasma (ICP).

RESULTS AND DISCUSSION

COAL CONVERSION AND PRODUCT DISTRIBUTION

Illinois No. 6 coal was liquefied in the Maya ATB at temperatures between 410^o-450^oC using various coal-to-solvent ratios. Figure 1 shows the effect of coal concentration on coke yields at 425^oC. The coke (THF-insolubles) yields comprise unreacted organic matter from the coal along with its inorganic matter and the high molecular weight materials produced during the reaction. At short reaction times (<15 minutes), there was a decrease in the coke yields due to partial dissolution of coal. Part of the coal might have liquefied (breakdown of the macromolecular coal structure) under hydrogen pressure at 425^oC. Perhaps the dissolution was also due to the extraction of a so-called mobile (trapped) phase from the coal. Some covalent bonds such as C-C, C-O, and C-S bonds which form the linkages in the macromolecular coal structure can be cleaved at 425^oC to form reactive free radicals. A portion of these free radicals can be quenched with molecular hydrogen at high hydrogen pressures or with the hydrogen transferred from the solvent. As mentioned earlier, heavy oils, relative to recycle solvents, are deficient in hydroaromatic hydrogen - the type of hydrogen which can be easily transferred. Table 3 shows the amount of "transferable" hydrogen present in the Maya ATB, the Boscan ATB and, for the purpose of comparison, from two coal liquids.⁽¹⁰⁾ (Note that the table shows the transferable hydrogen from the Boscan ATB, whereas the whole crude was used in the experiments in our study. However the data in Table 3 do provide a valid comparison, as the Boscan crude is very heavy and the difference between the the whole crude and the ATB is small.) Table 3 shows that the heavy oils contain very little transferable hydrogen as compared to coal liquids. As a result, it should be expected that coal-derived and resid-derived free radicals would tend to form heavier products such as coke once the transferable hydrogen is consumed.

As shown in Figure 1, the coke yields increased with an increase in the coal concentration in the feed. The higher coke yields are due to the increase in the rates of coking in addition to the higher amounts of THF-insolubles originally present in the feed. The rate of coke formation varied with coal concentration as apparent from the difference in the slopes of the coking curves (at longer reaction times) in Figure 1. Coal concentrations below 25 wt.% showed a negligible increase in the rate of coking over the rate of thermal coking of the Maya ATB alone. However, the rate of coking was significantly higher for 40 wt.% coal concentration. The results can be attributed to the limited supply of transferable hydrogen available in the resid and the higher demand for hydrogen imposed by the high coal concentrations.

It is not possible to calculate the actual coal conversion (to THF-solubles) as the THF-insolubles contain the unconverted coal plus the coke formed from the liquefied coal and also from the resid. However, one can use the "net" coal conversion as an approximate measure of liquefaction. The net coal conversion is a measure of the effective contribution of coal to THF-solubles and can be calculated from the yield of THF-insolubles during coprocessing after subtracting from it the amount of coke formed from the processing of resid alone under identical conditions. Figure 2 shows net coal conversion in the Maya ATB as a function of coal concentration in the coprocessing feed. The net coal conversion showed a maxima relative to the reaction time. At higher reaction times, the net coal conversion decreased due to retrogressive reactions. The decrease was more pronounced for higher coal concentrations. Similar trends were obtained when the Boscan crude was used in place of the Maya ATB. As said earlier, the Boscan crude showed a greater tendency to coke. Figure 3 shows net coal conversion obtained with the Boscan crude. The net coal conversion was slightly lower with the Boscan crude. The effect of coal concentration in the feed on the net coal conversion can be seen from Figures 2 and 3. At long reaction times, net coal conversions with the Maya ATB were higher for higher coal concentrations. This is understandable as a high coal concentration leads to increased hydrogen demand and, if the supply is limited, to increased retrogressive reactions. However, at shorter reaction times with the Maya ATB, net coal conversion for 40 wt.% coal concentration was higher than for 25 wt.% coal concentration. The net conversion for 10 wt.% coal with the Maya ATB was intermediate between those for 25 wt.% and 40 wt.% coal concentrations. Obviously, the data are too scattered to draw a statistically valid inference. Most of the converted coal formed asphaltenes on a net basis and very little oils were generated.

The increased occurrence of retrogressive reactions, when the demand for hydrogen outpaces the limited supply of the transferable hydrogen in the resid, was also apparent when the liquefaction temperature was varied. The effect of temperature on the net coal conversion is illustrated in Figure 4. At high

temperatures, the net coal conversion fell sharply (the yield of coke rose) for reaction times greater than 10 minutes due to high demand for hydrogen. The maximum conversion at 450°C was much lower than that at 410°C and at 425°C.

DEMETALLATION OF HEAVY OILS

The coprocessing of coal and heavy oils was accompanied by significant demetallation of the heavy oil. The metals present in the asphaltenes and the oils were transferred to the solids formed during coprocessing. The Maya ATB contained 400 ppm of vanadium. A significant amount of this metal content was rejected along with the coke when the resid was processed by itself; however, the demetallation was significantly higher when the resid was processed along with coal. The results are shown in Figure 5. When the resid was processed without any coal, 65% of the vanadium present in the feed was transferred to the coke, whereas 89% of the vanadium was transferred to the coke when the feed contained 40 wt.% coal. The overall demetallation of the oils (maltenes) was relatively easier than that of the asphaltenes fraction.

The Boscan crude contained 1100 ppm of vanadium. The results on demetallation of the Boscan crude are shown in Figure 6. The results are similar to those on the Maya ATB. Although the Boscan crude contained much more vanadium, the amount of vanadium removed with coke was similar to that from the Maya ATB on a percentage basis. With a feed containing 25 wt.% coal and 75 wt.% Boscan crude, 84% of the total vanadium was rejected to coke.

In order to understand the mechanism of demetallation in coprocessing, a few samples of the feedstock, THF-solubles, THF-insolubles, pentane-solubles, and pentane-insolubles were analyzed using X-ray absorption fine structure (EXAFS) spectroscopy using facilities at Stanford University. X-ray absorption near-edge spectra (XANES) of all the samples were very similar and matched that of a vanadyl porphyrin (tetraphenylporphyrin) standard. Although these results are insufficient to identify precisely the type of vanadium compounds present, it can be concluded that the removal of vanadium along with the solids formed is not due to any change in the nature of bonding of vanadium. Vanadium remains chiefly in organometallic complexes very similar to the original porphyrins. This is contrary to that found in catalytic hydrodemetallation where vanadium on adsorption on a catalyst is converted to an inorganic form.⁽¹¹⁾ The samples studied here were obtained on noncatalytic coprocessing at 425°C and at 1000 psi (measured at ambient temperature) hydrogen pressure. It is possible, of course, to have different behavior under more severe conditions or when a hydrogenation catalyst is present.

There are several potential pathways by which the demetallation might have occurred. The metal-containing components might have been adsorbed on the surface of coke. It is also possible that such compounds might have been trapped in the coke matrix during its formation. The third possibility is that the metal components became chemical constituents of the coke. If either of the latter two routes is valid, then the extent of demetallation would depend upon the amount of coke produced during the reaction. If the demetallation occurs through adsorption, the extent of demetallation would not only depend upon the amount of coke produced but could also depend upon the amount of unconverted coal present in the system. Several experiments were made to shed light on the mechanism of demetallation using chars made from cellulose and also using activated carbon in place of coal.

Cellulose when heated to high temperatures (330°C-475°C) in an inert atmosphere yields chars whose elemental analysis and infrared spectra resemble those of coal.⁽¹²⁾ Chars can be liquefied similar to coal. When a feed containing 90 wt.% Maya ATB and 10 wt.% of a char made from cellulose at 415°C-425°C and under 5.2 MPa nitrogen pressure was coprocessed at 425°C, 80% of the vanadium content was rejected along with coke after one hour reaction time. Under similar conditions, 69% of the vanadium was removed using 10 wt.% coal. It was further observed that the liquefaction and the demetallation behavior of char and its IR spectrum were dependent upon the conditions under which it was synthesized. It can be concluded that the demetallation is dependent upon the chemical nature of the liquefying substance. Since the char did not contain inorganics, the inorganic matter in coal is not responsible for the observed demetallation. Activated carbon in place of coal was equally effective in removing metals. There was no decrease in the yields of THF-insolubles at any reaction time indicating that as expected, the activated carbon, unlike coal, did not liquefy. The net amount of coke produced was higher relative to the processing of the Maya ATB alone. Thus, it is not clear if the demetallation observed with the activated carbon was due to the adsorption of the metal compounds on the activated carbon or it was due to the coke formed during the reaction.

Although the mechanism of demetallation is not clear from this series of experiments, it is possible to make some observations. It is unlikely that demetallation occurs due to the trapping of metal-containing compounds in the coke matrix as it forms, since only a small amount of coke formed can cause large amount of demetallation. In the early stages of coprocessing, when the yield of coke decreases due to the liquefaction of coal, the demetallation is seen to proceed at a rapid rate. This indicates that the demetallation is dependent not on the amount of coke present in the system (which includes the unreacted coal and the coke formed) but rather on the amount of coke formed during the reaction. Thus, physical adsorption of metal-containing compounds on coal is not likely the main mechanism of demetallation. Yan has studied the use of inorganic solids to demetallate heavy oils.⁽¹³⁾ The extent of demetallation was found to be strongly dependent upon the processing temperature. At 700°F (371°C), metal removal was very small. The demetallation increased rapidly as the temperature was increased to 800°F (427°C). The amount of demetallation was independent of the surface area of the solids at higher temperatures. In a recent paper, Audeh and Yan reported that very low levels of demetallation are observed when an adsorbent such as silica gel is used in place of coal under the conditions of low coking.⁽¹⁴⁾ This again indicates that adsorption is not the main mechanism of demetallation although it may be a contributing factor.

Demetallation through chemical reactions is a probable occurrence. It is known that the cokes produced from petroleum resids or coal liquids are anisotropic in nature.⁽¹⁵⁾ The transformation of isotropic resid into anisotropic coke occurs via an intermediate anisotropic nematic liquid-crystal phase. The nematic liquid crystals consist of lamellar constituent molecules stacked parallel to each other. The coking process involves continuous polymerization of the constituent molecules of the liquid-crystal phase eventually forming a solid semicoke. The intermediate phase between the starting isotropic liquid and the solid semicoke is called mesophase. Large molecules containing planar regions tend to form mesophase. The asphaltenic molecules present in resids can form mesophase very easily. It has been reported that metals tend to concentrate in mesophase.⁽¹⁶⁾ The organometallic structures found in petroleum are planar or have planar regions and hence are probably capable of forming mesophase. It is reasonable to expect that such structures would participate in the polymerization process leading to the formation of coke. It should be pointed out that such condensation need not involve any change in the nature of vanadium bonding. The formation of mesophase is initiated when the concentration of mesophase precursors reaches a threshold level. The enhanced demetallation in the presence of coal is perhaps due to the introduction of components (such as coal-derived asphaltenes) which participate in the process. Recent report that addition of deashed SRC (which is a liquid at the coprocessing temperatures) can demetallate heavy oils⁽¹⁰⁾ support this hypothesis. Another cause for the enhanced demetallation may be the interaction between mesophase and solid surfaces. Solid coal particles may increase the amount of mesophase formed.⁽¹⁷⁾ It has been observed in this laboratory, using a high-pressure and high-temperature microscope, that the presence of solids aids in the crystallization of mesophase under typical coprocessing conditions. The solid surface may act as a depository for condensed products.

HETEROATOM REMOVAL

Illinois No. 6 coal contained 2.98 wt.% sulfur and 0.67 wt.% nitrogen, while the Maya ATB contained 4.6 wt.% sulfur and 0.48 wt.% nitrogen. The amount of heteroatoms in the THF-solubles decreased on coprocessing. Treating 10:90 and 25:75 coal-to-resid feeds for one hour at 425°C removed 40-50% of the sulfur present in the resid to the coke and the product gas. A 35% sulfur removal was observed processing the Maya ATB alone under the same conditions. Similar observations were made on nitrogen removal. 55% of the nitrogen present in the feed was removed when 25:75 coal-to-resid ratio was used compared to 8% removal observed when the Maya ATB was processed alone. The results can be attributed to the association between heteroatoms and metals.

CONCLUSIONS

Illinois No. 6 bituminous coal was coprocessed with Maya ATB (650°F+) and with whole Boscan crude under thermal, non-catalytic conditions. Retrogressive reactions hinder production of THF-solubles when the demand for hydrogen increases as when the temperature is high or when the feed contains a high concentration of coal. Coprocessing results in a significant level of demetallation and heteroatom removal as these compounds are removed with the product coke. It is thus possible to achieve over 85% removal of vanadium. Very high levels of demetallation can also be achieved using char or activated carbon in place of coal.

ACKNOWLEDGEMENTS

This work was supported by a grant from the U.S. Department of Energy (DE-FC-22 85PC80009). We are grateful to Pittsburgh Energy Technology Center for assistance in the experimental work.

REFERENCES

1. Schultze, B., and Hoffman, B., *Hydrocarbon Proc.*, Vol. 63, 75(1984).
2. Speight, J. G., *Ann. Rev. Energy*, Vol. 11, 253(1986).
3. Yan, T. Y., and Espenscheid, W. F., *Fuel Proc. Tech.*, Vol. 7, 121(1983).
4. Kelly, J., Fouda, S., Rahimi, P., and Ikura, P., "CANMET Coprocessing: A Status Report", *Syn. Fuels Res. Lab. Div. Rep. ERP/ERL 85-52*, 1984.
5. Shinn, J. H., Dahlberg, A. J., Kuehler, C. W., and Rosenthal, J. W., Paper Presented at the 9th Annual EPRI Contractors' Meeting, Palo Alto, CA, 1984.
6. Moschopedis, S., Hawkins, R., and Speight, J., *Fuel Proc. Tech.*, Vol. 5, 213(1982).
7. Curtis, C. W., Tsai, K. J., and Guin, J. A., Paper Presented at the Symposium on New Chemistry of Heavy Ends, Chicago, IL, 1985.
8. Curtis, C. W., Tsai, K. J., and Guin, J. A., *Fuel Proc. Tech.*, Vol. 16, 71(1987).
9. Boduszynski, M. M., *Energy and Fuels*, Vol.1, 2(1987).
10. Cugini, A. V., Lett, R. G., and Wender, I., *ACS Div. Fuel Chem. Prep.*, Vol. 33, No. 1, 71(1988).
11. Wei, J., "Toward the Design of Hydrodemetallation Catalysts", in "Catalyst Design: Progress and Perspective", ed. by L. Hegedus, Wiley, New York, NY, 1987.
12. Friedel, R. A., Queiser, J. A., and Retcofsky, H. L., *J. Phys. Chem.*, Vol. 74, 908(1970)
13. Yan, T., *I&EC Proc. Des. Dev.*, Vol. 23, 415(1984).
14. Audeh, C. A., and Yan, T., *I&EC Research*, Vol. 26, 2419(1987).
15. Marsh, H., and Walker, P. L., Jr., "The Formation of Graphitizable Carbon via Mesophase: Chemical and Kinetic Considerations", in "Chemistry and Physics of Carbon", ed. by P. L. Walker, Jr., and P. A. Thrower, Vol. 15, Marcel Dekker, New York, NY, 1979, pp. 229-286.
16. Imura, T., Yamada, Y., Honda, H., Kitajima, E., and Tsuchitani, M., *Sekiyu Gakkai Shi (J. Jap. Petrol. Inst.)*, Vol. 18, 776(1975), CA 87:120993u.
17. Tillmans, H., Pietzka, G., and Pauls, H., *Fuel*, Vol. 57, 171(1978).

TABLE 1
ANALYSES OF ILLINOIS NO. 6 COAL

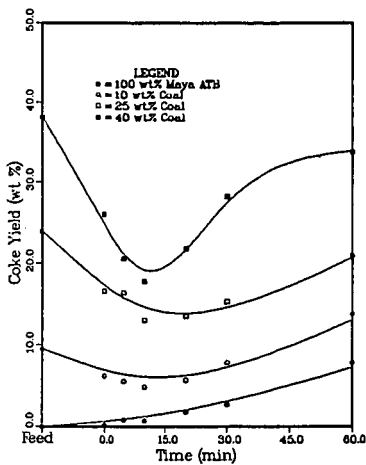
<u>PROXIMATE ANALYSIS (wt.%)</u>		<u>ULTIMATE ANALYSIS (wt.%)</u>	
Moisture	4.24	Hydrogen	5.04
Volatile Matter	36.93	Carbon	67.18
Fixed Carbon	48.18	Nitrogen	0.89
Ash	10.56	Sulfur	2.98
		Oxygen	13.26
		Ash	10.56

TABLE 2
ANALYSIS OF MAYA (650°F+) ATB RESID AND BOSCAN CRUDE

	<u>MAYA ATB</u>	<u>BOSCAN CRUDE</u>
Gravity (°API)	8.8	10.0
H/C Atomic Ratio	1.52	1.55
S (wt.%)	4.60	5.30
N (wt.%)	0.48	0.60
V (ppm)	400	1100
Ni (ppm)	78	100

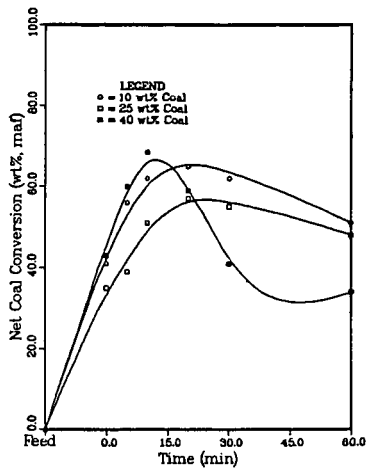
TABLE 3
TRANSFERABLE HYDROGEN IN RESIDS AND COAL LIQUIDS(10)

	TRANSFERABLE HYDROGEN	
	(mmol/g)	(% of total H)
Maya (650°F+)	2.1	4
Boscan (650°F+)	1.9	4
Wilsonville VTB	3.7	11
Wilsonville ITSL Solvent	7.5	16



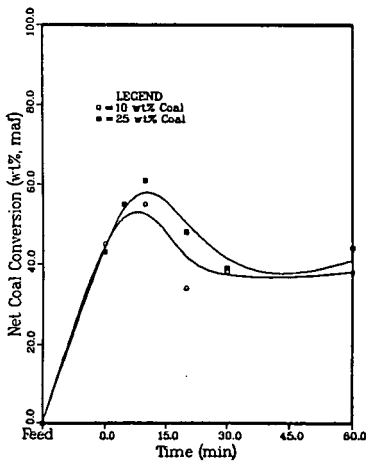
EFFECT OF COAL CONCENTRATION ON COKE YIELDS FROM MAYA ATB AT 425 C

Figure 1



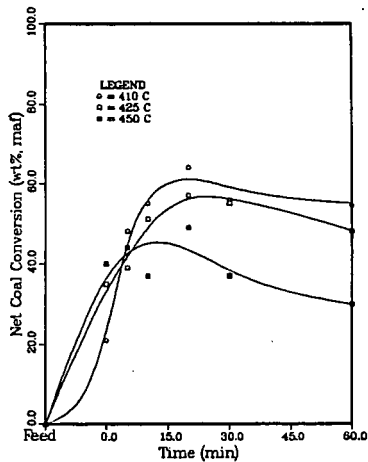
EFFECT OF COAL CONCENTRATION ON COAL CONVERSION IN MAYA ATB AT 425 C

Figure 2



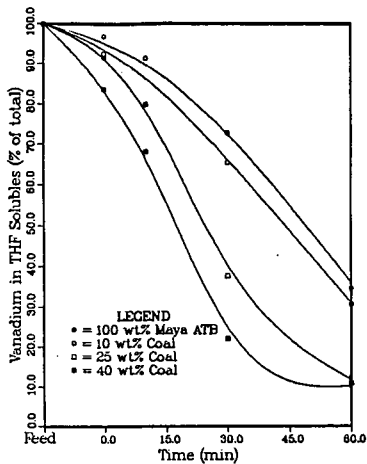
EFFECT OF COAL CONCENTRATION ON COAL CONVERSION IN BOSCAN CRUDE AT 425 C

Figure 3



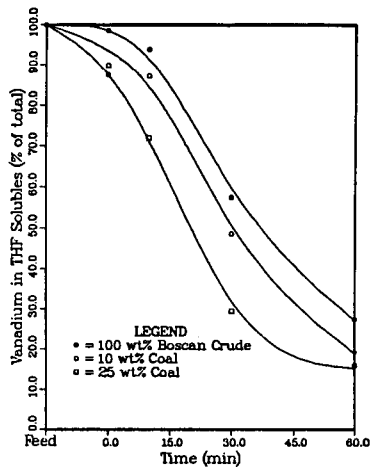
EFFECT OF TEMPERATURE ON NET COAL CONVERSION IN MAYA ATB AND 25 WT% COAL

Figure 4



EFFECT OF COAL CONCENTRATION ON REMOVAL OF VANADIUM FROM MAYA ATB AT 425 C

Figure 5



EFFECT OF COAL CONCENTRATION ON REMOVAL OF VANADIUM FROM BOSCAN CRUDE AT 425 C

Figure 6

STUDIES OF DEACTIVATING SPECIES
ON COAL LIQUEFACTION CATALYSTS*

Frances V. Stohl

Sandia National Laboratories, Albuquerque, NM 87185

Ripu Malhotra

SRI International, Menlo Park, CA 94025

INTRODUCTION

Previous studies (1,2) of catalyst samples from laboratory experiments with model compounds and coal-derived hydrotreater feeds from the Wilsonville Advanced Coal Liquefaction R&D Facility have shown that most deactivation is due to hydrotreating strongly basic heterocyclic nitrogen compounds. For example, hydrotreating nitrogen polycyclic aromatic compounds, separated from a hydrotreater feed from Wilsonville run 247, caused a 95% loss of the catalyst's hydrogenation (HYD) activity within a 2 h run. This activity loss was much greater than obtained by hydrotreating the whole hydrotreater feed or the other chemical classes of compounds (aliphatics, neutral polycyclic aromatic compounds, hydroxy polycyclic aromatic hydrocarbons) that made up the feed. Hydrotreating model compounds representative of the different types of nitrogen compounds present in coal liquids, including strongly basic compounds (quinoline, pyridine, acridine), a weakly basic compound (indole), and a neutral compound (carbazole), showed that the strongly basic compounds caused greater deactivation than the other compounds. Losses of about 75% of the HYD activity were observed by hydrotreating the strongly basic compounds in 2 h reactions, compared with a 50% loss for indole and a 24% loss for carbazole.

Quinoline hydrotreating studies (3) were performed to determine the effects of process conditions on deactivation caused by hydrotreating strongly basic nitrogen compounds. The reactions were carried out at two times (5 min, 2 h) and two temperatures (300°C, 400°C). The results showed that the deactivation was the same in all cases. Gas chromatographic (GC) analyses of the liquid products from these runs demonstrated that increasing reaction severity yielded more unidentified compounds (i.e., compounds that were not part of the reported quinoline hydrodenitrogenation (HDN) reaction scheme (4)). At the lowest reaction severity condition (300°C, 5 min), 19% of the liquid product consisted of unidentified compounds, whereas at the highest severity condition (400°C, 120 min) 86% was unidentified. At low severity, only 2% of the nitrogen was removed, as determined by liquid product analyses, whereas at high severity 18% was removed. A comparison of the amount of nitrogen remaining in the liquid product from the high severity reaction with gas chromatographic analyses of the liquid product showed that most of the remaining nitrogen was present in compounds that were formed by side reactions.

The ultimate objectives of the catalyst deactivation work reported here are to determine how the deactivation due to hydrotreating strongly basic nitrogen compounds occurs on the catalyst surface and to identify the compounds that cause the deactivation. The work reported here is aimed at evaluating the usefulness of Field Ionization Mass Spectrometry (FIMS) analyses for our catalyst deactivation studies. Results of the application of FIMS techniques to characterize the compounds volatilized from the aged catalysts and the liquid

* This work was supported by the U.S. Dept. of Energy at Sandia National Laboratories under contract DE-AC04-76DP00789.

products of our quinoline HDN experiments are described. The results are compared to those obtained for catalysts used at Wilsonville. The field emission method employed in FIMS is a mild, yet efficient, ionization that exclusively produces molecular ions from most chemical compounds. Thus the mass spectra of complex mixtures are not complicated by the presence of large numbers of peaks associated with molecular fragments. FIMS thus provides molecular profiles of samples. It has been used in the characterization of both petroleum and coal derived-materials (5-7). The relative ionization efficiencies of many different classes of organic compounds analyzed by FIMS are very similar, varying by only a factor of two (8).

EXPERIMENTAL PROCEDURES

FIMS results are reported for aged catalysts from Wilsonville runs 246 and 247 and for catalysts and products from quinoline hydrotreating experiments (3).

Materials

The catalyst used both for processing coal at Wilsonville and for the laboratory hydrotreating experiments was Shell 324M, which contains 12.4 wt% Mo and 2.8 wt% Ni on an alumina support, in the form of extrudates measuring about 0.8 mm in diameter and 4 mm in length. Prior to use in the laboratory experiments, the catalyst was presulfided with a 10 mol% H₂S/H₂ mixture at 400°C and atmospheric pressure for 2 h. Before analysis, all aged catalyst samples were Soxhlet extracted with tetrahydrofuran, to remove as much soluble material as possible, and then dried overnight at 100°C under vacuum.

Wilsonville Catalysts

Two catalyst samples from each of two Wilsonville runs were analyzed by FIMS. The run 246 samples had catalyst ages of 36 and 592 lb resid/lb catalyst and the run 247 catalysts had ages of 28 and 546 lb resid/lb catalyst. Catalyst age was determined from the amount of resid, which is nondistillable material at 600°F and 0.1 mm Hg, in the Wilsonville hydrotreater feed. Activity test results and characterization results of these Wilsonville samples have been reported previously (9).

Run 246 processed subbituminous Wyodak coal using the Double-Integrated Two-Stage Liquefaction (DITSL) mode up to a catalyst age of about 300 lb resid/lb catalyst and the Integrated Two-Stage Liquefaction (ITSL) mode for the remainder of the run. Deashing was performed between the two stages. In the DITSL mode, only the light thermal resid from the deasher went to the hydrotreater, whereas in the ITSL mode all the deashed material went to the hydrotreater. The temperatures in this run ranged from about 320°C to 340°C.

Run 247 processed Illinois #6 coal in the Reconfigured Integrated Two-Stage Liquefaction mode. In this mode, the deashing occurs after the second stage so that all the material from the first stage goes to the hydrotreater. The run temperatures ranged from 350°C to 375°C.

Quinoline Hydrotreating Experiments

Each hydrotreating experiment was performed in a 26 cc batch microreactor with 1200 psig H₂ cold charge pressure. Runs were made for either 5 minutes or 2 hours at either 300°C or 400°C. Experiments were performed with 1.5 g of model compound and 0.5 g presulfided catalyst. Activity test results and characterization results for the aged catalysts from these reactions have been reported previously (3).

FIMS Analysis

FIMS uses a field emission device to ionize the constituents of the vapor

released from a sample when it is heated in an evacuated chamber. The ions are separated by mass in a magnetic sector mass spectrometer. The field ionization mass spectrometer at SRI International, which was used in this study, consists of an activated tantalum foil field source interfaced with a 60° magnetic sector mass analyzer and a PDP 11/23 computer for data acquisition and analysis. A single catalyst pellet or about 50 mg of liquid product was placed in a sample holder and introduced into the mass spectrometer through a heatable direct-insertion probe. Spectra were collected by scanning the spectrometer repeatedly over the 50 to 800 amu range while the sample was gradually heated. The heating range for the catalyst samples was about 25°C to 450°C, whereas the liquid products were heated from about -60°C to 350°C.

RESULTS

Wilsonville Catalysts

Results of the FIMS analyses on the run 246 catalysts (Figure 1 and Table 1) show that the average molecular weights of the volatile species increase with catalyst age; the weight average molecular weight increases from 256 to 278. In addition, the number of peaks increases from 382 to 465 with age. Analyses of the molecular weights show that at least 49% of the peaks are due to nitrogen compounds; compounds with an odd number of nitrogen atoms have odd numbered molecular weights (10). Although there are approximately an equal number of odd and even mass peaks, 60% of the total ion intensity is present in the odd molecular weight peaks. The nine highest intensity peaks from the 36 lb resid/lb catalyst sample and 16 out of the highest 24 peaks are due to nitrogen compounds. In the higher aged catalyst, the highest 14 peaks and 22 out of the highest 24 peaks are due to nitrogen containing compounds.

The FIMS analyses of the two catalyst samples from run 247 (Figure 2 and Table 1) show similar trends to those observed for the run 246 catalysts. The weight average molecular weights increase with catalyst age. The increases are about 24% for these catalysts as compared to about 8% for the run 246 catalysts. About 48% of the peaks in the spectra from the run 247 samples have odd numbered molecular weights. The total number of peaks also increases with catalyst age. About 52% of the total ion intensity in the 28 lb resid/lb catalyst sample and 47% in the 546 lb resid/lb catalyst sample are due to nitrogen compounds. For the 28 lb resid/lb catalyst sample, the highest 6 peaks and 18 out of the highest 24 peaks are due to nitrogen compounds. The higher aged sample from run 247 had 13 nitrogen compounds out of the 24 compounds with the highest peaks.

There is also evidence for the presence of many alkylated compounds in all four of the Wilsonville catalyst spectra. For example, in the 36 lb resid/lb catalyst sample, each peak in the series 216, 230, 244, 258, 272, 286, 300 and 314 differs from the next peak by 14 mass units suggesting that the compounds yielding these spectra differ by one CH₂ group. This series is also present in the other three spectra, although the number of compounds in the series and the intensities of the peaks vary. In addition, there are many other series, with peaks differing by 14 mass units, that suggest the presence of additional alkylated compounds.

Catalysts from Quinoline Experiments

Results of the FIMS analyses on the catalysts from the quinoline hydrotreating experiments (Figure 3 and Table 1) show that the number of peaks obtained increases with both reaction time and temperature. The volatile material from the catalyst used in the 300°C 5 minute reaction has an average molecular weight comparable to that of quinoline (129), although FIMS spectra of

the volatile material from all the other catalysts have higher average molecular weights than either quinoline or the highest molecular weight compound reported in the quinoline HDN reaction scheme (4) (propylcyclohexylamine, 141). The spectrum for the volatile material from the catalyst from the 300°C 5 minute reaction shows that about 68% of the total ion intensity is due to quinoline. The spectrum of the catalyst from the 300°C 120 minute reaction also shows quinoline as a major peak, but has an additional major peak with a molecular weight of 202. The compound causing this peak and the origin of this compound are unknown. The catalysts from the two 400°C reactions each have the same major peaks, although the intensities are different. The only identifiable peak, based on the quinoline HDN reaction scheme, out of the highest 8 peaks in these patterns is that due to quinoline.

Liquid Products from Quinoline Experiments

The spectra obtained from the liquid products (Figure 4) from the quinoline HDN reactions are very different from those obtained from the catalysts. There are many more peaks present in the product spectra than in the spectra of the material volatilized from the catalyst; about half of the peaks in each product spectrum are due to nitrogen compounds. The average molecular weights of the products are also much higher than for the volatile species from the catalyst samples. The spectrum of the product from the 300°C 5 minute reaction has one major peak with a molecular weight of 133 that makes up about 64% of the total ion intensity. This peak is due to tetrahydroquinoline (THQ), 1,2,3,4- THQ, 5,6,7,8-THQ or both. This spectrum is different than that obtained from the catalyst used in this reaction, which had quinoline as the major peak and only a very small amount of THQ. The spectrum from the 300°C 120 minute reaction product also has 133 as the highest peak, but in addition it has a significant peak at 266 and a peak at 399 indicating the presence of THQ dimers and trimers. There is a small peak at 135, which is the molecular weight of o-propylaniline (OPA). The spectrum of the product from the 400°C 5 minute reaction also shows the presence of THQ as the major peak and a peak due to the THQ dimer. There's a larger quinoline peak in this pattern than observed in the 300°C product spectra; this is reasonable since hydrogenation occurs more readily at the lower temperature. The product spectrum from the 400°C 120 minute reaction has 624 peaks with at least 70% of the total ion intensity due to nitrogen compounds. The highest intensity peak in this pattern is at a mass of 135, which is probably due primarily to OPA. There is also evidence in this spectrum of the presence of alkylated species. The series of peaks 129, 143, 157, 171 and 185 indicate the presence of alkylated quinoline compounds. The series 93, 107, 121, 135, 149 and 163 also suggests the presence of alkylated species.

DISCUSSION

The results of the FIMS analyses of the Wilsonville catalysts indicate that some nitrogen compounds are preferentially adsorbed on the catalyst. An analysis of a hydrotreater feed from run 247 (11) has shown that the maximum amount of nitrogen compounds in the hydrotreater feed would be approximately 17%, whereas about 50% of the compounds volatilized from the catalysts are nitrogen compounds. This preferential adsorption of nitrogen compounds is not surprising since many nitrogen compounds are basic compounds that would be readily adsorbed on acidic catalyst sites. These results do suggest, in agreement with previous studies (1,2), that nitrogen compounds are the precursors of the compounds responsible for catalyst deactivation. The increase in the average molecular weights of the volatile compounds with catalyst age could be due to several factors: retrogressive reactions occurring on the catalyst surface (due to either time at temperature in the Wilsonville run or

the desorption procedure in the FIMS analyses), or changes in the hydrotreater feed as the run progresses. Hydrotreater feeds, withdrawn from the pilot plant at the same times as the catalyst withdrawals, were not available for FIMS analyses.

Analyses of spectra taken of catalysts from HDN reactions with quinoline are a little easier to interpret than spectra of Wilsonville catalysts because the reactor feed is known and the HDN reaction scheme has been reported (4). Therefore, it is possible to identify some of the peaks in the FIMS spectra and to ascertain which expected peaks are not present.

Results of studies of the Wilsonville catalysts and the quinoline hydrotreating catalysts suggest that FIMS is a very useful technique for helping identify compounds adsorbed on catalysts during reaction. Based on the results of these studies, we have identified several blank and baseline analyses that should be performed in order to elucidate the significance of the analyzed compounds in regard to either studying reaction mechanisms or determining deactivation mechanisms. First, quinoline and several other compounds that are part of the HDN reaction scheme should be adsorbed on the catalyst at room temperature and the samples then analyzed by FIMS to determine if other compounds are formed catalytically in the desorption step of the analysis. Although changes in compounds have not been found to be a problem with liquid samples, this could be a problem on a catalyst surface when high temperatures are present. Second, analyses should be performed on ground -200 mesh catalysts so that diffusional limitations in the catalyst are minimized. Identification of individual compounds in the FIMS spectra is imprecise because of the limited information available for each peak. Attempts to correlate volatilization temperature to compound properties (such as adsorption energy) have not been effective with catalyst samples because of the wide temperature range over which each compound is volatilized. This could be related to the catalyst's effective diffusivity in addition to the compounds properties. If diffusional limitations are minimized, compounds should be volatilized over a smaller temperature range than occurs with extrudates. The volatilization temperature might then be useful in helping identify the compound. Third, FIMS analyses should be repeated on several catalyst pellets from a given hydrotreating reaction. This would not only indicate the reproducibility of the analysis of catalysts, but would also give sufficient catalyst for both elemental analyses (so that the amount of volatile material could be determined) and activity testing (so that the impact of the volatile material on activity could be evaluated). Finally, catalyst samples and hydrotreater feeds removed from the Wilsonville facility at the same time should be analyzed to determine interactions between the feed and catalyst.

The results of the analyses of the liquid products provide information about the effects of reaction conditions on the product. The liquids are completely volatilized in the FIMS analyses so that all compounds are analyzed. In addition, results of the FIMS analyses have been compared to previous quantitative GC analyses of the liquid products from these hydrotreating reactions. For the product from the 300°C 5 minute reaction, GC analysis gave about 5 wt% quinoline, 76 wt% THQ, and 19 wt% unknown compounds (i.e. compounds that are not part of the HDN reaction scheme), and FIMS gave 3 % quinoline, 70 % THQ, and 27 % unknown compounds. The results of these two analyses are in good agreement; the agreement between the GC and FIMS analyses of the liquid products from the other three reactions at the more severe reaction conditions were equally good. These results indicate, in agreement with previous studies, that there are no chemical changes in the samples due to the FIMS analysis. FIMS analysis gives additional information about the compounds that cannot be obtained with GC alone.

CONCLUSIONS

The results of this study indicate that FIMS analyses are useful for characterizing changes that occur in the feed during hydrotreating. Potential changes that can be quantified include molecular weight distributions, number of compounds and types of compounds. If FIMS analyses are combined with other analytical techniques such as Fourier transform infrared spectroscopy and GC/mass spectrometry, it should be possible to identify many of the compounds in the reaction products. Results of studies of the compounds volatilized from aged catalysts also suggest that FIMS is potentially useful for determining catalytic reaction mechanisms and for studying catalyst deactivation. Additional experiments are being carried out to clarify the interpretation of these results.

REFERENCES

1. Stohl, F. V. and H. P. Stephens, ACS Division of Fuel Chemistry Preprints 31(4), 251-6, 1986.
2. Stohl, F. V., Proceedings DOE Direct Liquefaction Contractors' Review Meeting, October 20-22, 1986, p.124-131.
3. Stohl, F. V., ACS Division of Fuel Chemistry Preprints 32(3), 325- 31, 1987.
4. Satterfield, C. N. and S. H. Yang, Ind. Eng. Chem. Process Des. Dev. 23, 11-19, 1984.
5. Boduszynski, M. M., Energy and Fuels 1, 2-11, 1987.
6. Boduszynski, M. M., R.J. Hurtubise, T. W. Allen and H. F. Silver, Fuel 65, 223-34, 1986.
7. Boduszynski, M. M., R. J. Hurtubise, T. W. Allen and H. F. Silver, Anal. Chem. 55, 232-41, 1983.
8. St. John, G. A., S. E. Buttrill Jr., and M. Anbar, in Organic Chemistry of Coal, J. Larsen, ed., ACS Symp. Ser. 71, 1978, p.223.
9. Stohl, F. V. and H. P. Stephens, Ind. Eng. Chem. Research 26, 2466-73, 1987.
10. Whitehurst, D. D., S. E. Buttrill Jr., F. J. Derbyshire, M. Farcasiu, G.A. Odoerfer and L. R. Rudnick, Fuel 61(10), 994-1006, 1982.
11. Stohl, F. V. Unpublished results.

Table 1. FIMS data for the catalyst and product samples

Wilsonville Catalysts

	<u>Catalyst Age</u>	<u>Wt Av MW*</u>	<u>% Odd MW Intensity</u>	<u>Number of Peaks</u>	<u>% Odd MW Peaks</u>
Run 246	36	255.7	59.5	382	48.9
	592	277.5	60.2	465	49.2
Run 247	28	247.5	51.9	401	48.4
	546	304.4	46.5	424	46.7

Quinoline HDN Catalysts

<u>Reaction Conditions</u>	<u>Wt Av MW</u>	<u>% Odd MW Intensity</u>	<u>Number of Peaks</u>	<u>% Odd MW Peaks</u>
300°C, 5 min	131.5	81.2	41	51.2
300°C, 120 min	173.6	48.7	60	40.0
400°C, 5 min	174.0	52.4	146	34.2
400°C, 120 min	166.7	52.2	343	45.8

Quinoline HDN Product

<u>Reaction Conditions</u>	<u>Wt Av MW</u>	<u>% Odd MW Intensity</u>	<u>Number of Peaks</u>	<u>% Odd MW Peaks</u>
300°C, 5 min	201.9	75.8	182	55.5
300°C, 120 min	275.6	55.6	344	52.2
400°C, 5 min	287.7	59.2	560	49.7
400°C, 120 min	295.2	70.3	624	50.0

* Average molecular weight

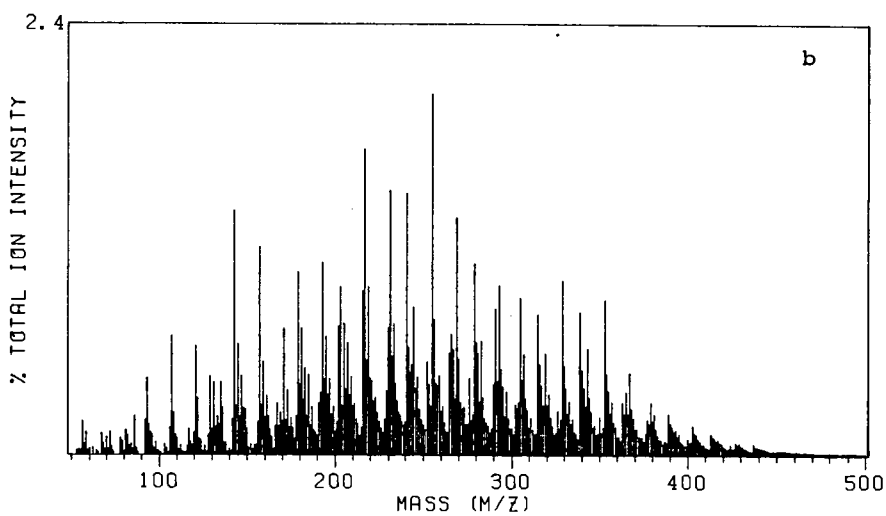
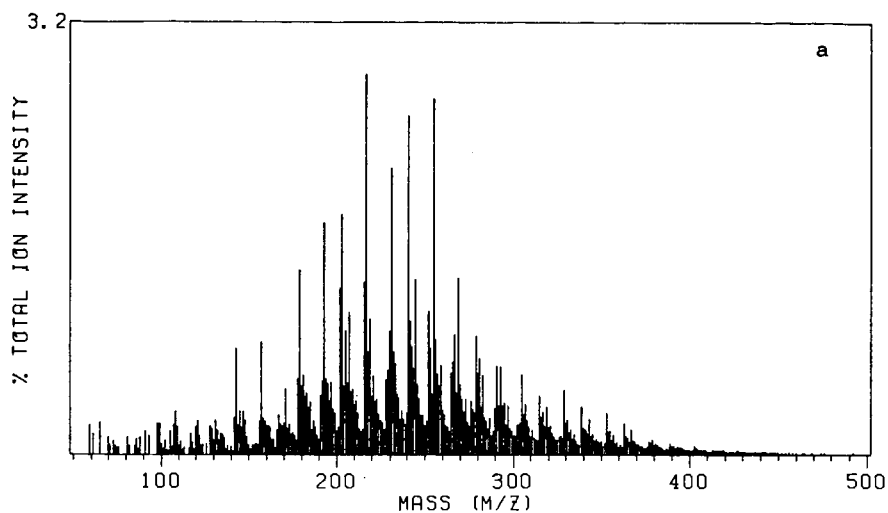


Figure 1. FIMS spectra of Wilsonville run 246 catalysts.
 a - Catalyst age of 36 lb resid/lb catalyst;
 b - Catalyst age of 592 lb resid/lb catalyst.

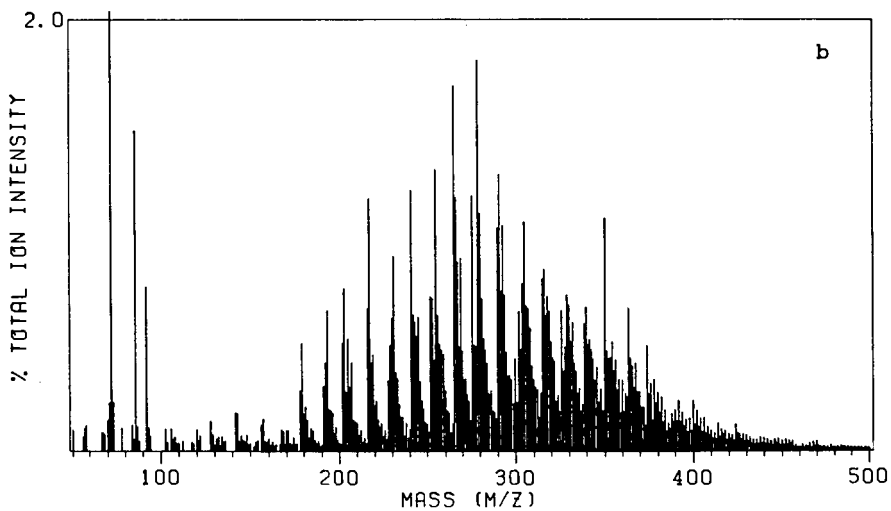
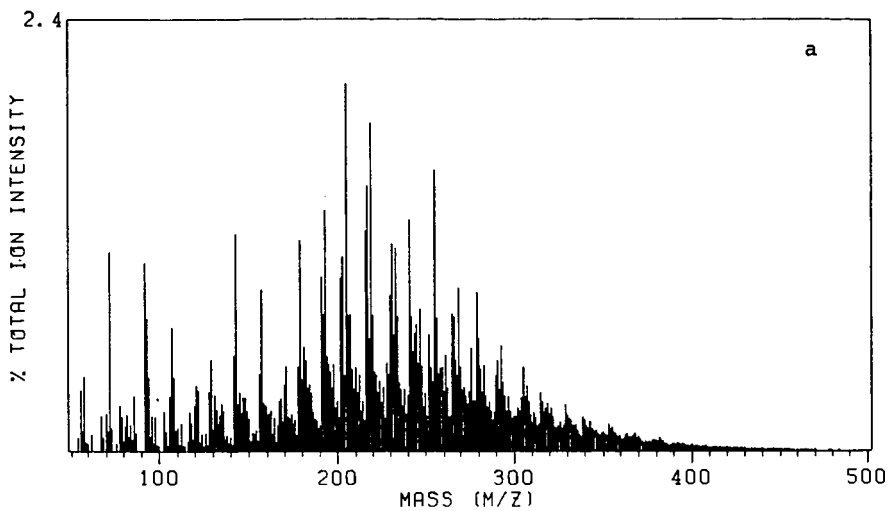


Figure 2. FIMS spectra of Wilsonville run 247 catalysts.
a - Catalyst age of 28 lb resid/lb catalyst.
b - 546 lb resid/lb catalyst.

Figure 3. FIMS spectra of quinoline HDN catalysts.

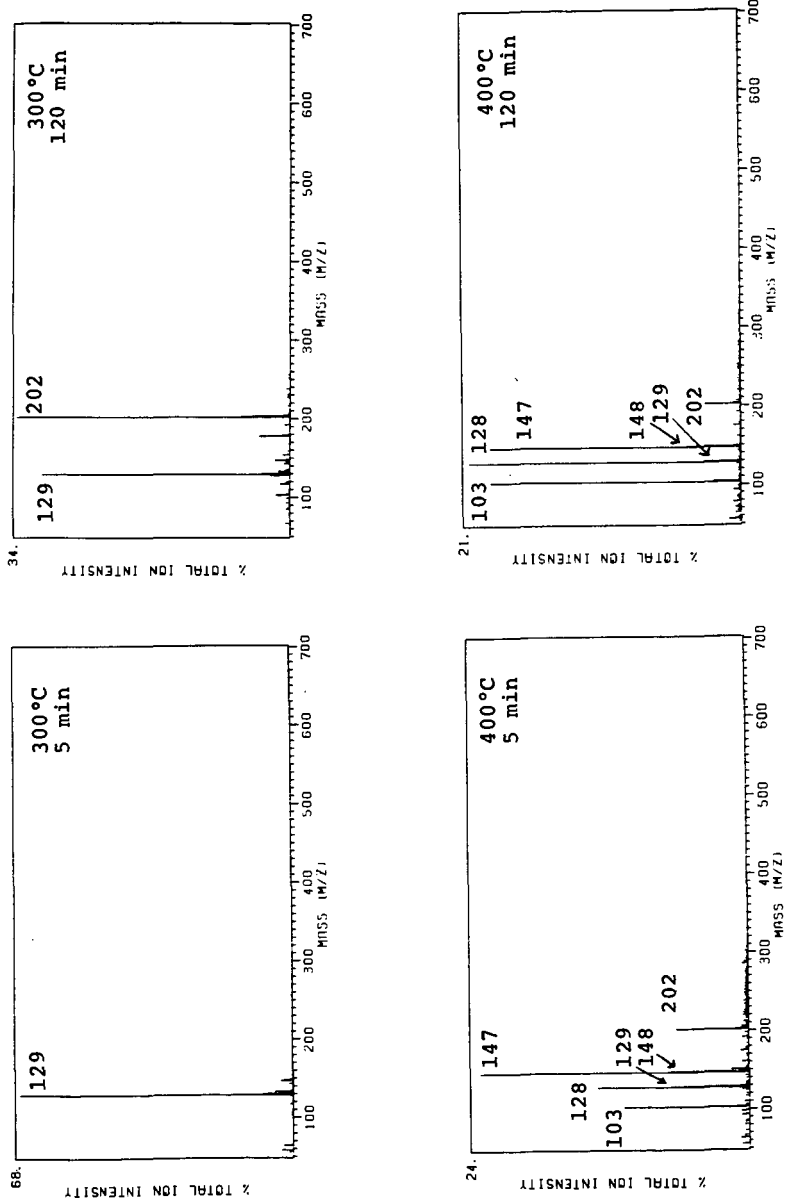
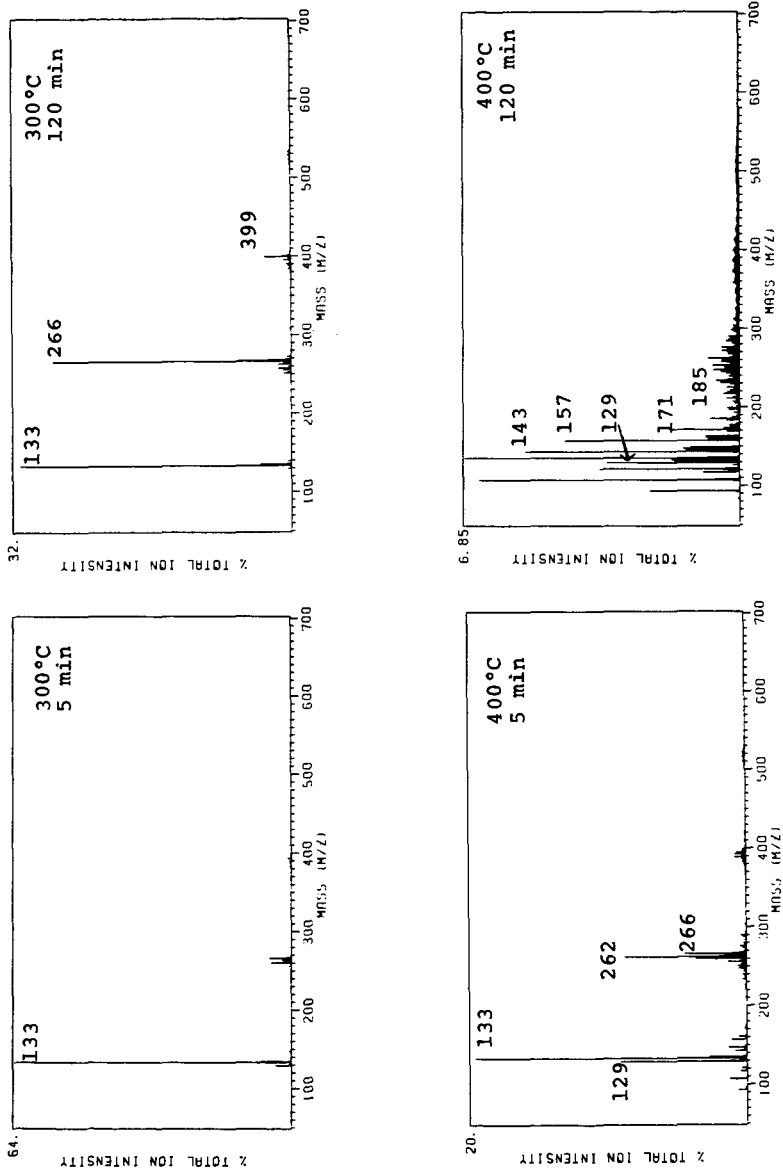


Figure 4. FIMS spectra of liquid products from quinoline HDN reactions.



Nitrogen Base Poisoning of NiMo Liquefaction Catalysts: A Kinetic Study

Bruce D. Adkins, Diane R. Milburn and Burtron H. Davis

Kentucky Energy Cabinet Laboratory
P. O. Box 13015, Iron Works Pike
Lexington, Kentucky 40512

INTRODUCTION

A mechanistic model has been proposed to explain coking on hydrotreating catalysts from four process configurations of the Wilsonville, AL coal liquefaction pilot plant (ref. 1). This model, which utilizes reversible adsorption of nitrogen bases on acid sites, and irreversible poisoning of these sites by sodium, can explain all of the trends seen in the elemental compositions of the catalysts used in six pilot plant runs spanning four process configurations, two coals and two catalysts. The model, presented here for Bronsted acid sites, is:



where CH represents an acid site capable of chemisorbing either one nitrogen base molecule or one sodium atom and BH represents another type of site capable of reacting with sodium but not the nitrogen base. NB_L represents a group of nitrogen bases associated with distillate solvent or light thermal resid (LTR) from the Critical Solvent Deashing unit (CSD) and having a lower average molecular weight than NB_H , which represents basic nitrogen compounds having a higher average molecular weight, associated with the thermal resid stream (TR) from the CSD. $\text{C}^-(\text{NB}_L\text{H})^+$ and $\text{C}^-(\text{NB}_H\text{H})^+$ are the acid-base adducts formed on the catalyst surface. ANa is the sodium present in coal ash, and CNa and BNa are the Na-exchanged acid sites. The essence of this mechanism is that NB_L , NB_H , and Na can exchange on the catalyst surface.

In considering the proposed exchanges, the question of overall rate control must be addressed. A simple kinetic analysis is presented in an attempt to determine whether adsorption, k_a , or desorption, k_d , is controlling these exchanges.

Kinetic Analysis

For an exchange between species "1" and "2", illustrated in reactions (1) and (2) or in (2) and (3):

$$\ln \frac{1 - k_1^* \theta_1}{1 - k_1^* \theta_1^0} = k_2^* t \quad (5)$$

where

$$k_1^* = \frac{k_{a1} + k_{d2}k_a^*}{k_a^* k_{d2}}$$

$$k_2^* = \frac{k_{d1} + k_{d2}k_a^*}{1 + k_a^*}$$

and

$$k_a^* = \frac{k_{a1}[1]}{k_{a2}[2]} = \text{"Adsorption selectivity"}$$

where k_a 's represent first-order adsorption rate constants, k_d 's represent first-order desorption rate constants, θ_1 is the fractional surface coverage of species "1" at any time, and θ_1^0 is the initial surface coverage of "1". Pseudosaturation throughout the exchange is assumed in equation (5), such that $\theta_1 + \theta_2 = 1$.

Solving for the three specific reactions proposed in the model, we obtain for the exchange of NB_L-NB_H shown in reactions (1) and (2):

$$\ln(1 - k_{1,NB_H-NB_L}^* \theta_{NB_H}) = -k_{2,NB_H-NB_L}^* t \quad (6)$$

where:

$$\theta_1 = \theta_{NB_H}$$

$$\theta_{NB_H}^0 = 0$$

$$k_{1,NB_H-NB_L}^* = \frac{k_{d,NB_H} + k_{a,NB_H-NB_L}^* k_{d,NB_L}}{k_{a,NB_H-NB_L}^* k_{d,NB_L}}$$

$$k_{2,NB_H-NB_L}^* = \frac{k_{d,NB_H} + k_{a,NB_H-NB_L}^*}{1 + k_{a,NB_H-NB_L}^*}$$

$$k_{a,NB_H-NB_L}^* = \frac{k_{a,NB_H}[NB_H]}{k_{a,NB_L}[NB_L]}$$

The exchange shown in equations (2) and (3), of NB_H and Na yields:

$$\ln = \frac{1 - k_{1,NB_H-Na}^* \theta_{NB_H}}{1 - k_{1,NB_H-Na}^*} \quad (7)$$

where:

$$\theta_1 = \theta_{NB_H}$$

$$\theta_{NB_H}^0 = 1$$

$$k_{1, NB_H-Na}^* = \frac{k_{d, NB_H} + k_{a, NB_H-Na}^* k_{d, Na}}{k_{a, NB_H-Na}^* k_{d, Na}}$$

$$k_{2, NB_H-Na}^* = \frac{k_{d, NB_H} + k_{a, NB_H-Na}^* k_{d, Na}}{1 + k_{a, NB_H-Na}^*}$$

$$k_{a, NB_H-Na}^* = \frac{k_{a, NB_H} [NB_H]}{k_{a, Na} [ANa]}$$

The form of equation (7) is troublesome if $k_{d, Na} \ll k_{d, NB_H}$. For irreversible sodium chemisorption, a better form is:

$$\ln \theta_{NB_H} = -k_{d, NB_H-Na}^* t \quad (8)$$

where:

$$k_{d, NB_H-Na}^* = \frac{k_{d, NB_H}}{1 + k_{a, NB_H-Na}^*}$$

I. Kinetics Calculated from Process Data

Carbon, nitrogen and sodium analyses were used to solve equations (6) through (8) for the various runs examined (ref. 1). Full coverage of NB_L is determined by the carbon content at saturation in the DITSL runs, which is reached very early in the run, and full coverage of NB_H is estimated by extrapolating the RITSL carbon data to 0% Na. θ_{NB_H} is then:

$$\theta_{NB_H} = \frac{C - C_{NB_L}}{C_{NB_H} - C_{NB_L}} \quad (9)$$

where C represents % carbon, C_{NB_L} is the % carbon present at saturation of NB_L , and C_{NB_H} is the % carbon present at full coverage of NB_H . An example of the fit for this exchange is shown in Figure 1a.

Nitrogen analyses are used in solving for the NB_H -Na exchange, making the analyses easier and more certain by eliminating the assumption that all carbon on the catalyst is present in the form of chemisorbed basic nitrogen. A sample of the fit of equation (8) to these data is shown in Figure 1b. Difficulties were encountered attempting to fit eqn. (7), which suggested the irreversible case (eqn. 8) be used instead.

The results obtained by fitting the model to the data allow examination of the two factors controlling the overall rate exchanges on the catalyst: rate(s) of nitrogen base desorption (k_d 's) and the adsorption selectivity for the two competing species (k_a^*). The relationships for limiting cases in the NB_L-NB_H exchange are shown in Table 1, and for the NB_H-Na exchange in Table 2.

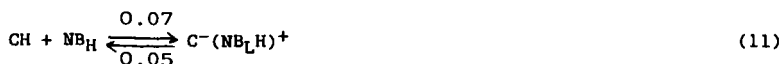
II. Kinetics of Laboratory Desorption of Nitrogen Bases

Laboratory experiments were conducted using a CSTR to test the critical assumption that the nitrogen bases desorb from the catalyst. In two separate experiments blends of DITSL catalysts, still in the original process oil, were placed in the reactor extracted in flowing THF at 120°C, the gently stirred in tetralin feed at 250°C and 2000 psi for three weeks. Samples were taken, twice weekly, after cooling and depressurizing the reactor. Analyses of the catalyst showed a decrease in both nitrogen (from 0.45% to a fairly stable 0.15%) and carbon for the first two weeks, after which time a non-nitrogen containing coke formation was seen, probably tetralin derived carbon on the acid sites exposed by base desorption. A value of 0.04 day⁻¹ was obtained for $k_{d,NB}$, which is in good agreement with the values from Tables 1 and 2, considering the effects of the non-nitrogen containing coke have been ignored. However, re-adsorption of nitrogen bases cannot be ruled out as the concentration of desorbed based present in the reactor could have been as high as 200 to 500 ppm at any time.

III. Comparison with Kinetics of Nitrogen Base Poisoning of Cracking Catalysts

Extensive literature exists on nitrogen base and alkali poisoning of cracking catalysts (e.g., ref. 2). Much less information is available on the poisoning of acidic hydrotreating catalysts, such as Shell 324. We can use cracking catalyst measurements in an attempt to rationalize the kinetic measurements obtained from process and laboratory data. However, the acidity of Shell 324 is likely to be different from that of silica-alumina cracking catalysts.

One of the earliest of these studies was performed by Mills, et al. (ref. 3) in which they studied the adsorption of quinoline on silica/alumina cracking catalysts at 315°C and several pressures. They identified two distinct kinetic regions in the desorption curve, corresponding to what they termed a rapidly desorbing "physisorbed" species, followed by a much slower "chemisorbed" species. Much later Kittrell, et al. (ref. 4) calculated rate constants from these data and suggested that the adsorption and desorption rates for the more rapidly desorbed quinoline should be used to predict reversible nitrogen poisoning of cracking catalysts. The numbers he obtained were approximately $k_a = 200 \text{ day}^{-1}$, $k_d = 150 \text{ day}^{-1}$. An attempt to obtain order-of-magnitude consistency between Kittrell et al.'s rate constants and our measurements yields the following relative rates:





Thus, if k_a and k_d of the NB_L group (which is estimated to have an overall stoichiometry very similar to that of quinoline) are as large as 200 day^{-1} and 150 day^{-1} respectively, a large kinetic difference in the NB_L and NB_H species is indicated. It would be highly speculative at this point to assume that these are the two species observed in reference 3. The main inconsistency with this picture is the rapid saturation of NB_L and NB_H on fresh sulfided catalyst beds that is clearly seen in DITSL and RITSL data.

Next let us assume that the nitrogen bases adsorb rapidly, but is very slow to desorb, analogous to the second species proposed by Mills et al., and using our CSTR measurement of $k_d = 0.05 \text{ day}^{-1}$. Fitting the calculations to our model for this case yields:



This ranking accommodates the rapid saturation of RITSL and DITSL with NB_H and NB_L .

IV. Gravimetric Vapor Phase Experiments

The questions raised in this kinetic study can only be answered by kinetic measurements using a differential flow reactor adsorption and desorption. Thus, a high pressure gravimetric reactor system, shown schematically in Figure 2, has been constructed. This will allow us to measure the adsorption and subsequent desorption of several nitrogen compounds at different pressures, and determine their kinetic rate constants. The ability to introduce hydrogen should also shed light on the HDN performance of this catalysts.

ACKNOWLEDGMENT

This work was supported by the Commonwealth of Kentucky, Kentucky Energy Cabinet and DOE Contract No. DE-FC-22-85PC80009 as part of the Consortium for Fossil Fuel Liquefaction Science (administered by the University of Kentucky).

REFERENCES

1. D. R. Milburn, B. D. Adkins and B. H. Davis, ACS Div. Fuel Preprints, **33** (2), 380 (1988).
2. T. F. Degnan and M. Farcasiu, U.S. Patent No. 4,550,090, October 29, 1985.
3. G. A. Mills, E. R. Boedeker and A. G. Oblad, J. Am. Chem. Soc., **72**, 1554, (1950).
4. J. R. Kittrell, P. S. Tam and J. W. Eldridge, Hyd. Proc., **63** (1985).

Table I.
Kinetic Analyses of NB_L-NB_H Exchanges

Limiting Case—
Preferential
Chemisorption

NB_H (day^{-1}) ($k_s^*, NB_H, NB_L \gg 1$)	$k_d, NB_L \approx 0.1$	$k_d, NB_L \approx 0.1$
NB_L (day^{-1}) ($k_s^*, NB_H, NB_L \ll 1$)	$k_d, NB_L, k_s^*, NB_H, NB_L \approx 0.1$	$k_d, NB_L, k_s^*, NB_H, NB_L \approx 0.1$

Table II.
Kinetic Analyses of NB_H-Na Exchanges

	Wyodak-Shell 324M	Illinois #6-Shell 324M	Illinois #6-Amocat 1C (No Ash Recycle)	Illinois #6-Amocat 1C (Ash Recycle)
Limiting Case— Preferential Chemisorption				
NB_H (day^{-1}) ($k_s^*, Na, NB_H \ll 1$)	$k_d, NB_H, k_s^*, Na, NB_H \approx 0.02$	$k_d, NB_H, k_s^*, Na, NB_H \approx 0.006$	$k_d, NB_H, k_s^*, Na, NB_H \approx 0.006$	$k_d, NB_H, k_s^*, Na, NB_H \approx 0.02$
Na (day^{-1}) ($k_s^*, Na, NB_H \gg 1$)	$k_d, NB_H \approx 0.02$	$k_d, NB_H \approx 0.006$	$k_d, NB_H \approx 0.006$	$k_d, NB_H \approx 0.02$

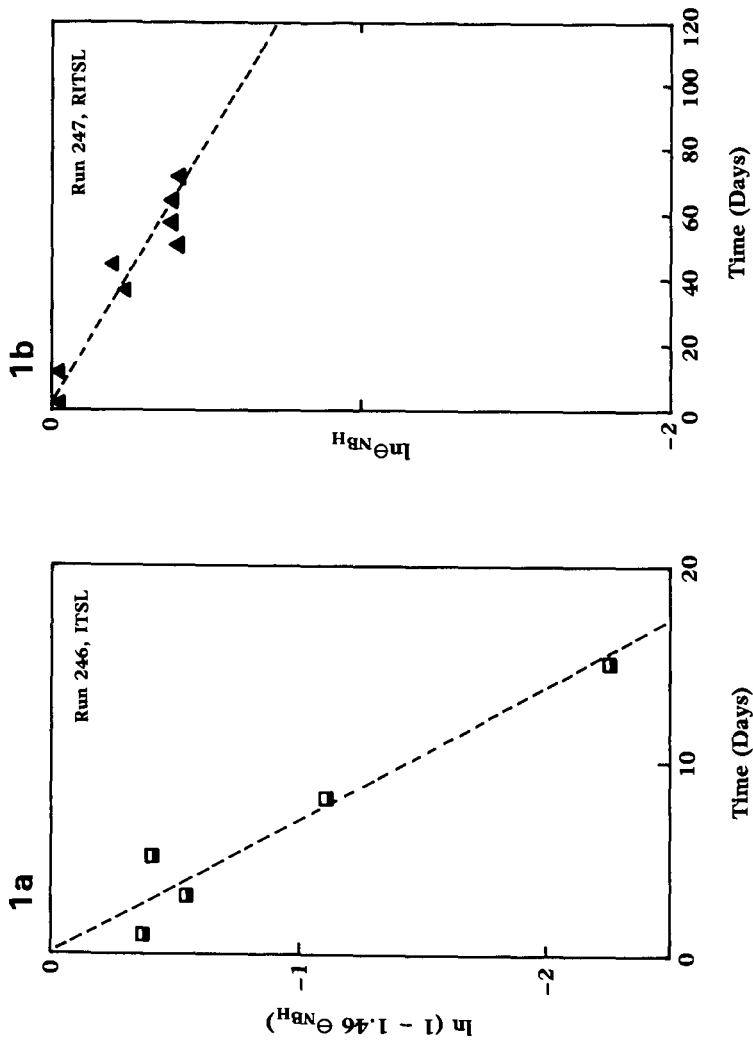


Figure 1a. Process data for the NB_L - NB_H exchange fitted to equation (6).
 Figure 1b. Data from the NB_H -Na exchange fitted to equation (8).

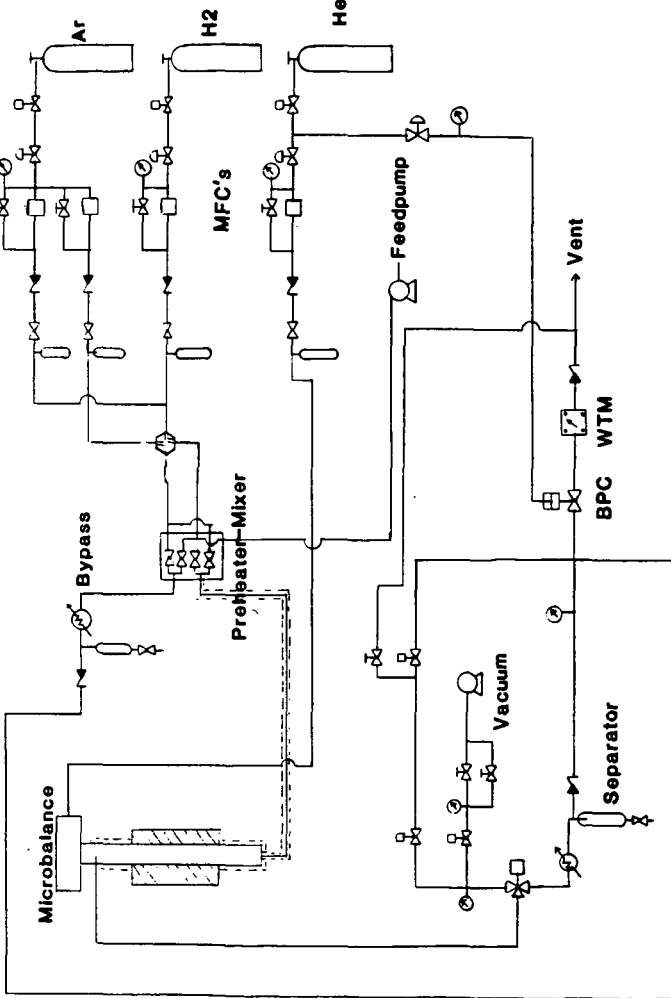


Figure 2. Schematic diagram of the high pressure gravimetric reactor system.

EFFECT OF PORE STRUCTURE ON CATALYTIC COAL LIQUEFACTION

Young-Woo Rhee, James A. Guin, Christine W. Curtis

Auburn University
Department of Chemical Engineering
Auburn University, AL 36849

Introduction

Considerable evidence for pore diffusional limitations in coal liquefaction has been reported in the literature (1-10). In this research catalysts having different pore structures were prepared using two methods, impregnation and coextrusion. The pore structures were controlled either by a sintering technique or by using combustible fibers (7). The initial activity of prepared catalysts was evaluated in coal liquefaction reactions with tetralin solvent. A model describing the relation between catalyst surface area and catalyst activity was developed by assuming 1) that every pore perfectly communicates and has a cylindrical shape, 2) that the pellet catalyst has a simple bimodal pore size distribution and 3) that a single first-order reaction occurs in the diffusion controlled region. For simplicity, reactant molecular size also was assumed to be uniform.

Experimental Section

Catalyst Preparation. Catalysts were prepared using Catapal alumina (Vista Chemical Co.) and cellulose fiber (Avicel) using techniques similar to those used by Tischer (7). Ni and Mo were added by two methods: incipient wetness following calcination or prior to the extrusion process itself (coextrusion). Catalysts were presulfided prior to use. Catalysts were evaluated in 3/16 inch pellet form. The powder prepared by grinding the 3/16 inch pellets was also evaluated.

Catalyst Characterization. To measure the pore size distribution and apparent density of the extrudates, a Quantachrome Autoscan-33 porosimeter equipped with the Autoscan data reduction system was used. The maximum intrusion pressure of mercury was 33,000 psig, which corresponds to ca. 64 angstroms in pore diameter. Surface areas were obtained from a Quantasorb system using the multipoint BET method. Apparent density, macropore diameter and macropore volume of each catalyst were calculated from the mercury porosimeter data. True density, micropore diameter and total pore volume were obtained from a combination of pycnometer (water displacement), BET, and Hg porosimetry methods.

Coal Liquefaction. A horizontal welded tubing bomb microreactor of ca. 45 cc volume was used with the following reactants: 3 g Illinois #6 coal, 10 g tetralin, 1 g catalyst, and 1250 psig (cold) H₂. The reactor was agitated at 425 °C for 60 min in a fluidized bed sand bath. Liquefaction products were classified as gases, oils (pentane soluble), asphaltenes (benzene soluble), preasphaltenes (soluble in a mixture of 10 vol.% methanol and 90 vol.% methylene chloride), and IOM (insoluble organic matter). Solubility fractions were expressed on a solvent-free basis.

Results and Discussion

Characterization of Catalyst Pore Structure. Physical properties of laboratory prepared catalysts and supports are given in Table 1. A macropore is defined as a pore whose diameter exceeds 500 angstroms. Average pore diameters are calculated from the pore volume and BET surface area data by assuming cylindrical pores. Table 1 shows that the pore size distributions of unimodal 3/16" catalyst supports are dependent on the calcining temperature. As the calcining temperature increases, apparent density and average micropore diameter become larger, and surface area is reduced. This phenomenon results from a destruction of some micropores and reconstruction of macropores by a sintering process. Data for support D in Table 1 indicate that most micropores are destroyed and reoriented at high temperatures. Also, as shown in Table 1, the combustible fiber loading directly increases macropore volume and average macropore diameter.

Coal-Tetralin Reaction System. Catalysts shown in Table 1 were used in tetralin-coal reactions using both 3/16 inch pellets and their powder. The powder form of the catalysts, as shown in Table 2, gave the highest activity, indicating diffusional restrictions in the pellets. As shown in Table 2, calcining temperature had a direct effect on catalyst activity as evidenced by pentane-soluble oil yield. If the activity of the pellet catalysts is plotted versus the surface area, a maximal point in the catalyst activity exists. This interesting phenomenon results from a competition between the effective diffusivity and surface area. In a typical catalytic reaction of small molecules, an increase of surface area generally enhances catalyst activity. However, in a reaction of large molecules this increase can reduce the catalyst activity because of diffusional hindrance in the micropores. Thus, catalyst G, having the highest surface area of the unimodal catalysts, does not yield the most pentane soluble oils, due to the very small pore size and the hindered diffusion through these pores.

One way to increase pore accessibility without significantly reducing specific catalyst surface area is to introduce macropores. Using the technique of combustible fibers, we produced macroporous catalysts J, K, and L having high surface areas of 250-300 m²/g. When compared to unimodal catalysts, the bimodal catalysts (J and K in Table 3) give an oils fraction slightly greater than the best unimodal catalyst (I) in Table 2. An increase of fiber loading from 20 to 40 wt% has little additional effect on the activity.

Development of Model. In order to analyze the above results we developed a catalyst model similar to that of Froment and Bischoff (11), i.e. a parallel pore cross linked model with perfectly communicating pores.

For a first order irreversible diffusion controlled catalytic reaction the reaction rate per pellet volume is

$$\begin{aligned} r_v &= k C_s \eta \\ &= k C_s / \phi \\ &= S_x (k D_e)^{1/2} C_s / V_p \\ &= (S_x k_s^2 / V_p) (S_v D_e)^{1/2} C_s \end{aligned} \quad (1)$$

where S_v is the surface area per pellet volume, and D_e is the effective diffusivity.

From a material balance in a batch reactor, we obtain

$$-\frac{d(C_s)}{dt} = r_v V_{cat} = r_g W_{cat} = (r_v / \rho_c) W_{cat} \quad (2)$$

Solving eqs (1) and (2) together we obtain

$$\ln(C_s / C_{s0}) = -k' t \quad (3)$$

where k' is expressed as follows,

$$k' = \frac{S_x k_s^{1/2}}{V_p} \frac{V_{cat}}{(S_v D_e)^{1/2}} \quad (4)$$

or

$$k' = \frac{S_x k_s^{1/2}}{V_p} \frac{W_{cat}}{(S_g D_e / \rho_c)^{1/2}} \quad (5)$$

Equations 4 and 5 are useful for comparing catalyst activity in terms of physical properties such as porosity, density, pore sizes and pellet morphology. Equations (4) and (5) are most convenient when performing reactions using a constant catalyst volume or weight, respectively. In either case the first two terms remain constant if the catalyst shape and the amount of solvent are the same in each reaction.

As a very simple catalyst pore structure model, we adopt a model having only two sizes of cylindrical pores, denoted by radii R_1 and R_2 . Define the total porosity, $\epsilon = \epsilon_1 + \epsilon_2$, where ϵ_1 and ϵ_2 are void fractions of micro (R_1)- and macro (R_2)-pores.

From the definition,

$$\begin{aligned} S_v &= \text{surface area of pores / volume of pellet} \\ S_v &= 2 (\epsilon_1/R_1 + \epsilon_2/R_2) \end{aligned} \quad (6)$$

Introducing dimensionless variables $\lambda_i = R_m/R_i$ where R_m is the reactant molecule size (radius),

$$S_v = (2 \epsilon/R_m) [(\epsilon_1/\epsilon) \lambda_1 + (\epsilon_2/\epsilon) \lambda_2] \quad (7)$$

$$S_g = (2 \epsilon/R_m/\rho_s) [(\epsilon_1/\epsilon) \lambda_1 + (\epsilon_2/\epsilon) \lambda_2]/(1 - \epsilon) \quad (8)$$

In a dimensionless form,

$$\langle S_v \rangle = \epsilon [(\epsilon_1/\epsilon) \lambda_1 + (\epsilon_2/\epsilon) \lambda_2] \quad (9)$$

$$\langle S_g \rangle = \epsilon/(1 - \epsilon) [(\epsilon_1/\epsilon) \lambda_1 + (\epsilon_2/\epsilon) \lambda_2] \quad (10)$$

In the hindered diffusion regime, the effective diffusivity D_e is

$$D_e = (\epsilon D_m / \tau) [(\epsilon_1 / \epsilon) K_{R1} K_{P1} + (\epsilon_2 / \epsilon) K_{R2} K_{P2}] \quad (11)$$

where the frictional resistance, K_{Ri} and partition factor, K_{Pi} are expressed as follows (12).

$$K_{Ri} = 1 - 2.104 \lambda_i + 2.09 \lambda_i^3 - 0.95 \lambda_i^5 \quad (12)$$

$$K_{Pi} = (1 - \lambda_i)^2 \quad (13)$$

Equation 11 assumes the tortuosity τ is not a function of pore size.

In a dimensionless form,

$$\langle D_e \rangle = \epsilon [(\epsilon_1 / \epsilon) K_{R1} K_{P1} + (\epsilon_2 / \epsilon) K_{R2} K_{P2}] \quad (14)$$

Define k_v and k_g from equations 4 and 5 as follows:

$$k_v = (S_v D_e)^{1/2} \quad (15)$$

$$k_g = (S_g D_e / \rho_c)^{1/2} \quad (16)$$

In a dimensionless form,

$$\langle k_v \rangle = \langle S_v \rangle^{1/2} \langle D_e \rangle^{1/2} \quad (17)$$

$$\langle k_g \rangle = \langle k_v \rangle / (1 - \epsilon) \quad (18)$$

Substituting equations 9 and 15 into equations 17 and 18 gives

$$\langle k_v \rangle = \epsilon [(\lambda_1 \epsilon_1 / \epsilon + \lambda_2 \epsilon_2 / \epsilon) \times (\epsilon_1 / \epsilon K_{R1} K_{P1} + \epsilon_2 / \epsilon K_{R2} K_{P2})]^{1/2} \quad (19)$$

$$\langle k_g \rangle = \epsilon / (1 - \epsilon) [(\lambda_1 \epsilon_1 / \epsilon + \lambda_2 \epsilon_2 / \epsilon) \times (\epsilon_1 / \epsilon K_{R1} K_{P1} + \epsilon_2 / \epsilon K_{R2} K_{P2})]^{1/2} \quad (20)$$

where $0 \leq \lambda_1 \leq 1$.

Model Application. The batch reactions conducted in this work were performed with constant catalyst weight and thus eq (20) is most useful for activity comparison. The major difficulty with direct application of eq (20) is that the reactant molecule radius R_m is unknown and, of course, has a wide distribution in coal reactions. To circumvent this problem, we utilize the fact that for a unimodal catalyst ($\epsilon_2=0$), eq (20) has a maximum at $\lambda_1=0.18$ (12). This fact, together with the data of Table 2 showing an optimal micropore size of ca. 85 angstroms (catalyst I), can be used to define an approximate R_m of 15 angstroms. With this assumed value of R_m , $\langle k_g \rangle$ can be computed from eq (20) using the catalyst properties in Table 1. The results of these calculations are given in Table 4.

Comparison of $\langle k_g \rangle$ values with pentane soluble oils yield as given in Table 4 shows reasonable qualitative agreement, in view of the many approximations

made, e.g. first order reaction, single molecule size, etc. The bimodal catalysts have a slightly higher activity in terms of oils yield, however, the effect is not great. Model calculations indicate that a major advantage of the bimodal catalysts may appear later during catalyst deactivation when pore sizes are reduced due to coke and metal deposits, and reactant diffusion becomes more hindered compared to the fresh catalysts.

Nomenclature

C_s	Reactant concentration, mole/cm ³
D_e	Effective diffusivity, cm ² /s
D_m	Molecular bulk diffusivity, cm ² /s
k	Reaction rate constant in equation 1, 1/s
k'	Reaction rate constant defined in equations 4 and 5, 1/s
k_g	Reaction rate constant defined in equation 16, cm ^{7/2} /g/s ^{1/2} .
K_p	Steric coefficient defined in equation 13
K_r	Frictional drag coefficient defined in equation 12
k_s	Surface reaction rate constant, cm/s
k_v	Reaction rate constant defined in equation 15, cm ² /(g-s) ^{1/2}
R	Pore radius, cm
r_g	Reaction rate based on catalyst weight, mole/g-cc
R_m	molecule radius, cm
r_v	Reaction rate based on catalyst volume, mole/cc-s
S_g	Surface area per unit catalyst weight, cm ² /g
S_v	Surface area per unit catalyst volume, 1/cm
S_x	External surface area of pellet, cm ² /g
V	Pore volume
V_p	Pellet volume, cc/g
V_{cat}	Catalyst volume per unit volume of liquid in reactor
W_{cat}	Catalyst weight per unit volume of liquid in reactor

Greek Letters

ϵ	Porosity
λ	Ratio of molecule radius to pore radius
ρ_c	Pellet density, g/cc
ρ_s	Catalyst solid density, g/cc
r	Tortuosity
ϕ	Thiele modulus
η	Effectiveness factor

Subscripts

1	micropore
2	macropore
o	initial
t	total

Symbol

< >	dimensionless group
-----	---------------------

Acknowledgement: This work was supported by the U.S. Department of Energy as research conducted by the Consortium for Fossil Fuel Liquefaction Science under Contract No. UK-RF-42181687.

References

1. Ho, P. N., and Weller, S. W., Fuel Processing Technol., 4, 21 (1981).
2. Curtis, C. W., Guin, J. A., Kamajian, B. L., and Moody, T. E., Fuel Processing Technol., 12, 111 (1986).
3. Curtis, C. W., Tsai, K. J., and Guin, J. A., Ind. Eng. Chem. Research, 26, 12 (1987).
4. Alpert, S. B., Wolk, R. H., Maruhnic, P. and Chervenak, M. C., U.S. Patent 3,630,888 (Dec. 1971).
5. Shimada, H., Kurita, M., Sato, T., Yoshimura, Y., Kawakami, T., Yoshitomi, S., and Nishijima, A., Bull. Chem. Soc. Jpn., 57, 2000 (1984).
6. Tischer, R. E., Narain, N. K., Stiegel, G. J., and Cillo, D. L., J. Cat., 95, 406 (1985).
7. Tischer, R. E., J. Cat., 72, 255 (1981).
8. Nalitham, R. V., Lee, J. M., Lamb, C. W., and Johnson, T. W., Fuel Processing Technol., 17, 13 (1987).
9. Shimura, M. Shiroto, Y., and Takeuchi, C., Ind. Eng. Chem. Fundam., 25, 330 (1986).
10. Guin, J. A., Tsai, K. J., and Curtis, C. W., Ind. Eng. Chem. Process Des. Dev., 25, 515 (1986).
11. Froment, G. F. and Bischoff, K. B., "Chemical Reactor Analysis and Design," Wiley, New York, 1979.
12. Ruckenstein, E. and Tsai, M.C. AIChE.J. 27 697 (1981).

Table 1. Physical Properties of Catalysts

Catalyst Name	Calcining Condition (°C-hrs)	V _t (cc/g)		V ₁ (cc/g)	V ₂ (cc/g)	S _g (m ² /g)		ρ _c (g/cc)	ρ _s (g/cc)	d ₁ (angstroms)	d ₂
		Hg	H ₂ O			Hg	BET				
<u>3/16" Supports used for Impregnation</u>											
A	500 - 16	.43	.45	.45	a	240	220	1.30	3.09	81	a
B	750 - 16	.44	.43	.43	a	203	161	1.29	2.86	106	a
C	1000 - 16	.37	.34	.34	a	113	97	1.50	3.09	142	a
D	1200 - 16	.19	.20	.01	.19	5	3	1.98	3.32	500	1832
<u>Coextruded 3/16" Catalyst: no fiber</u>											
G	500 - 16	.03	.40	.39	a	11	287	1.47	3.50	55	a
I	580 - 16	.31	.42	.42	a	172	197	1.49	3.95	85	a
<u>Coextruded 3/16" Catalyst: 20 wt% fiber</u>											
J	500 - 16	.30	.47	.41	.06	98	301	1.29	3.27	56	1560
<u>Coextruded 3/16" Catalyst: 40 wt% fiber</u>											
K	500 - 16	.62	.80	.40	.40	110	272	.90	3.19	61	2348
L	580 - 16	.73	.81	.42	.39	156	258	.90	3.33	66	2253

Note: V_t: total pore volume measured by Hg or H₂O intrusion
V₁: micropore volume from V_t(H₂O) - V₂
V₂: macropore volume obtained from Hg porosimeter
S_g: specific surface area by Hg porosimeter or BET analysis
ρ_c: apparent density by Hg displacement
ρ_s: true density obtained from H₂O pycnometry
d₁: average micropore diameter 4V₁/BET micropore area
d₂: average macropore diameter 4V₂/Hg macropore area
a: no macropores

Table 2. Effect of Calcining Temperature on Product Distribution

Catalyst Name	Catalyst Shape	Sintering Temperature (°C)	Product Distribution (wt.%)				Coal Conversion (wt%)	
			Gases	Oils	Asphaltenes	Pre/Asphaltenes	IOM	
None	----	----	7	33	36	17	7	94
G	Pellets	500	6	41	23	14	16	84
	Powder	500	5	72	8	5	10	89
I	Pellets	580	6	53	20	9	12	88
	Powder	580	6	78	6	4	6	94
<u>Impregnated on support C</u>								
	pellets	1000	7	47	24	11	11	88
	powder	1000	6	73	13	4	4	95
<u>Impregnated on support D</u>								
	pellets	1200	6	34	36	15	9	90

Table 3. Effect of Fiber Loading on Product Distribution

Catalyst Name	Fiber Loading (wt%)	Catalyst Shape	Product Distribution (wt.%)				IOM	Coal Conversion (wt%)
			Gases	Oils	Asphaltenes	Pre/Asphaltenes		
G	0	Pellets	6	41	23	14	16	84
		Powder	4	72	9	5	10	89
J	20	Pellets	5	55	19	9	12	87
		Powder	4	77	6	5	8	91
K	40	Pellets	6	57	16	8	13	87
		Powder	4	76	6	5	9	91

Table 4. Comparison of Model Catalyst Activity and Experimental Oil Yields

Catalyst	λ_1	λ_2	ϵ_1	ϵ_2	$\langle S_g \rangle$	$\langle k_g \rangle$	Oils Yield (wt%)
C	.11	a	.52	a	.119	.281	47
D	.03	.0082	.03	.37	.007	.065	34
G	.27	a	.58	a	.373	.360	41
I	.18	a	.62	a	.294	.452	53
J	.27	.0096	.54	.07	.376	.442	55
K	.25	.0064	.36	.36	.330	.730	57

Note: a) Catalyst contains no macropores.

HONDO ASPHALTENE DIFFUSION IN MICROPOROUS TRACK-ETCHED MEMBRANES

By

R.C. Sane and T.T. Tsotsis, Department of
Chemical Engineering, University of Southern California
Los Angeles, CA 90089

and

I.A. Webster, UNOCAL Science and Technology Division
Unocal Corporation
P.O. Box 76, Brea, California 92621

1. ABSTRACT

The configurational diffusion of asphaltenes isolated from Hondo crude has been examined. Diffusion studies were performed with track-etched membranes with pore diameters in the range 100A to 4000A. The asphaltene is perceived as a lumped compound, containing a molecular weight range of heteroatomic species. The asphaltene does not diffuse as a single species, but may delaminate before diffusion. We report on the interesting phenomenon of the Hondo asphaltenes' vanadium fragments diffusing in 100A pores more rapidly, than the same asphaltenes' nickel fragments. This phenomenon is shown to be consistent with some previously reported conjectures on the relative distribution of nickel and vanadium within the asphaltene micelle.

2. INTRODUCTION

During the refining of heavy oils, contaminants such as nickel, vanadium and nitrogen must be catalytically removed from the oil. In hydroprocessing the nitrogen is reduced to ammonia, while the nickel and vanadium deposit as sulfides within the pores of the catalyst. Better HDM catalyst design mandates a greater understanding of the diffusion of an oil's metallorganics in the catalyst. Most HDM reactions are strongly diffusion limited at commercial process conditions as evidenced by the rinded nickel and vanadium intra-catalyst pellet metal profiles measured by electron microprobe.

A large fraction of a resid's heteroatoms are complexed in the solubility class called asphaltenes. Asphaltenes are polyaromatic sheet-like structures of large size and molecular weight.

In an attempt to mimic the diffusive transport of whole oil asphaltenes within a catalyst's pores, we have investigated the diffusion of an asphaltene, dissolved in pure xylene, through porous membranes with a range of pore sizes. Our results clearly indicate:

- The lumped compound nature of asphaltenes i.e. they are a solubility class, and as such are comprised of a spectrum of molecular types, each exhibiting a different diffusion coefficient.
- Hindered diffusion of asphaltenes is an important transport mechanism in resid upgrading catalysts.
- The asphaltene exclusion principle operates at low pore diameters.

3. EXPERIMENTAL

Asphaltenes were isolated by n-pentane extraction from Hondo California crude oil. The crystalline like asphaltene powder was redissolved in xylenes to form a 5 weight percent asphaltene model feedstock. Diffusion experiments were conducted in a custom built stainless steel, agitated Wicke-Kallenbach type diffusion cell (1,2). The temperature was controlled at 45°C. The cell's two compartments were separated by polycarbonate membranes (PCM), whose pore size ranged from 100A to 4000A over the entire experimental sequence. The PCMs were purchased from from Nuclepore Corporation, Pleasanton, CA. PCMs are thought to simulate the porous structure of a catalyst, but in a highly idealized sense, since all tortuosity effects have been removed.

The experimental plan is outlined in Figure 1. The strategy was to use a single charge of the asphaltene solution in an experiment where the membrane pore diameter was initially held low i.e. at 100A. The batch-batch diffusion experiment was then monitored by removing samples for analysis from the low concentration (LC), initially pure xylene, side of the membrane.

After a predetermined time the experiment was temporarily suspended and the membrane changed to a larger pore diameter (in the sequence 150A, 300A and 4000A). Simultaneous with each membrane change the LC side has recharged with fresh xylene. The key point, however, is that the original asphaltene solution charge was carried through the entire experiment (Fig. 1), and permitted to lose asphaltene solute by successively recontacting it with pure xylene across increasing membrane pore diameters.

This experimental protocol permits us to examine the relative diffusion rates of the variously sized species which constitute an asphaltene.

Analysis of the LC side samples was performed by X-ray fluorescence for sulfur, nickel and vanadium, and by size exclusion chromatography (SEC) for molecular weight distributions. SEC data will be reported elsewhere.

4. RESULTS and DISCUSSION

The data from the diffusion of Hondo asphaltenes across the range of pore diameters (100-4000A) tested, is depicted in Figs 2 to 4. Sulfur, vanadium and nickel concentrations on the LC side of the membranes are shown as a function of time.

This raw data has been manipulated to generate Fig 5 where the relative initial slope for each species (S,V,Ni) at each pore diameter has been plotted. In addition, Fig 6 is an expanded view of the low time results for nickel and vanadium through the 100A membrane.

This data permits us to form the following evaluation:

- HINDERED TRANSPORT. By following the n-pentane asphaltene isolation procedure, we isolated an oil solubility class, comprised of a spectrum of molecular types and sizes. In this communication we infer little about asphaltene structure but note that it is an ongoing endeavor of our work to reconstruct asphaltene macrostructure from asphaltene diffusion studies. Figures 2 to 4 demonstrate the hindered nature of the transport of asphaltenes in a typical upgrading catalysts' sized pores. The data in these Figures also strongly suggests that small pores could exclude larger asphaltenic fragments.
- DISTRIBUTION OF HETEROATOMS IN ASPHALTENE FRAGMENTS. A semi-quantitative assessment of the data can be made from Fig. 5 which depicts initial slopes of the concentration versus time data as a function of membrane pore diameter.

With respect to each of the three diffusing asphaltene heteroatoms, sulfur, nickel, and vanadium we note:

-Sulfur appears evenly distributed among the various asphaltene sub-fragments, as evidenced by the almost proportional increase in initial transport rate with pore diameter.

-Nickel seems to be concentrated in species with sizes between 150A and 300A since the increase in relative transport rates between these pore diameters is a factor of 8, whereas the increase

between 300A and 4000A is only by a factor of 1.4.

-Vanadium seems to be concentrated with smaller fragments as indicated by the steady increase in vanadium transport rates only up to the 300A pore diameter.

• LOCATION OF METAL COMPOUNDS WITHIN HONDO ASPHALTENE MICELLE.

Figure 6 depicts our initial LC side data for nickel and vanadium diffusing in 100A pores. The interesting observation is that at low times vanadium species cross the membranes while nickel species are excluded. This finding has important implications in residuum hydroprocessing catalyst design. Perhaps vanadium could be selectively removed from the oil by judiciously engineering the catalyst pore size to exclude nickel fragments. The results of Fig. 6 suggest two things:

-The vanadium atoms are complexed in organometallic fragments which are physically smaller than the asphaltene's nickel fragments, or,

-Within the asphaltene micelle the vanadium species are more concentrated on the periphery of the asphaltene micelle, than the nickel species. As the asphaltene may "onion-skin delaminate" prior to diffusion, more rapid transport of the vanadium species would be expected.

The latter explanation is consistent with the work of Larson and Beuther (3) who, from reactivity studies, suggested that the vanadium to nickel ratio is higher on the edge of an asphaltene, than in the asphaltene core.

This demonstrates how it may be possible to infer some information on asphaltene structure from basic diffusivity data.

5. CONCLUSIONS

In summary, we have examined the diffusion of n-pentane isolated asphaltenes from Hondo crude across porous membranes containing molecularly sized pores (Fig. 1) and conclude:

- asphaltanes can be viewed as a lumped compound containing a range of molecular weights.
- diffusion is hindered, and depends strongly on the relative size of asphaltene fragment size and pore diameter. (Figs. 2 to 4)

- Sulfur, nickel, and vanadium heteroatoms may concentrate in different molecular size ranges. (Fig. 5)
- With 100A sized pores, initial diffusion data showed permeation of vanadium, but not nickel (Fig. 6). From this observation, we made some inferences on catalyst design and asphaltene structure.

6. REFERENCES

1. Sane, R. C., Webster, I.A., and Tsotsis, T. T. "A study of asphaltene diffusion through unimodal porous membranes", Paper No. 14f presented at AIChE Annual Meeting, New York, New York, November 1987. Paper available through the Engineering Societies Library, United Engineering Center, 345 East 47th Street, New York, NY 10017.
2. Sane, R. C., Webster, I. A. and Tsotsis, T. T. in "Catalysis, 1987", Proc. 10th North American Meeting of the Catalysis Society, J. W. Ward (Editor), May 1987, San Diego, California, Pub. Elsevier, 1988.
3. Larson, O. A. and Beuther, H., "Processing aspects of vanadium and nickel in crude oils", PREPRINTS Div. Pet. Chem., ACS, 11 (2), 595 (1966).

FIGURE 2: Low concentration side sulfur concentrations

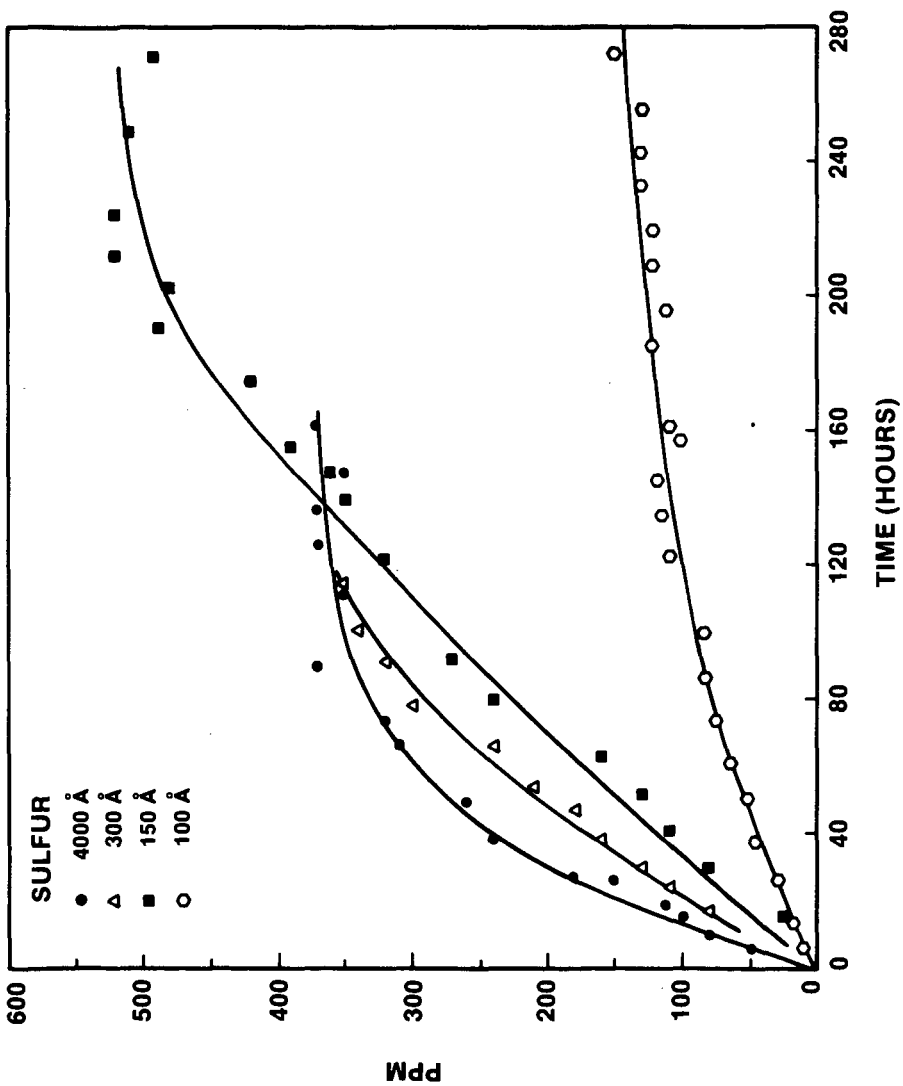


FIGURE 3: Low concentration side vanadium concentrations

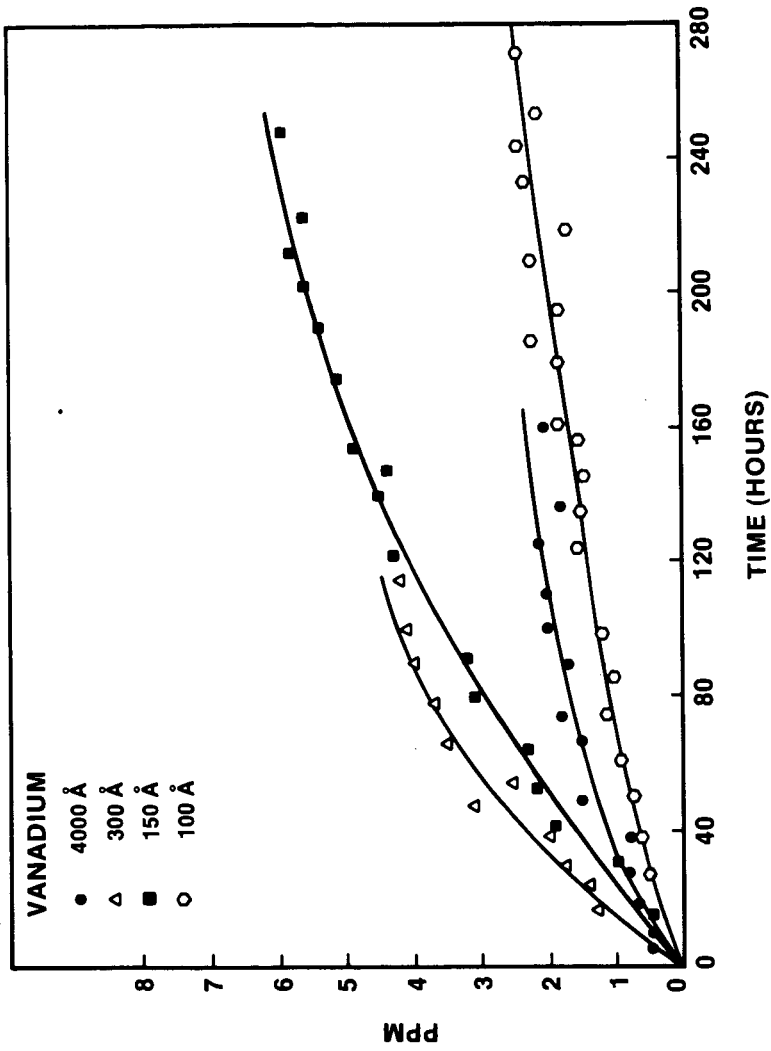


FIGURE 4: Low concentration side nickel concentrations

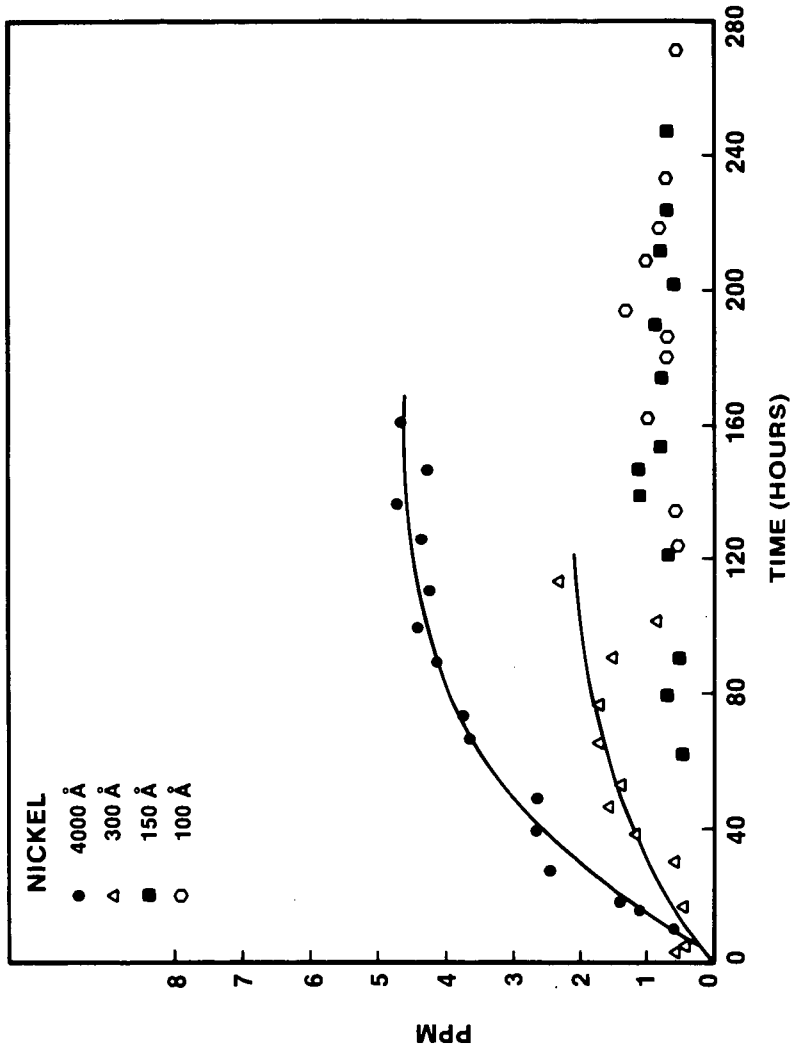


FIGURE 5
RELATIVE INITIAL TRANSPORT RATES (PPM/HOUR)

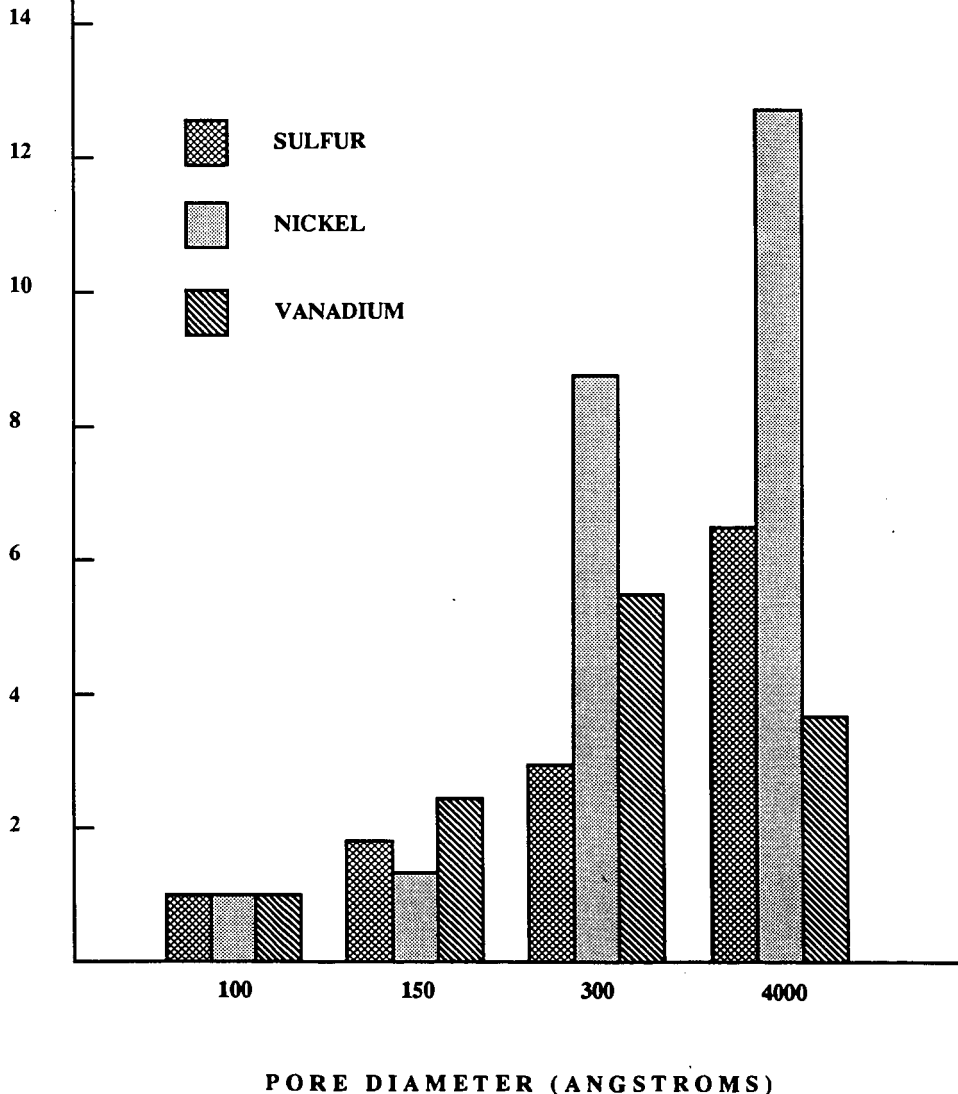
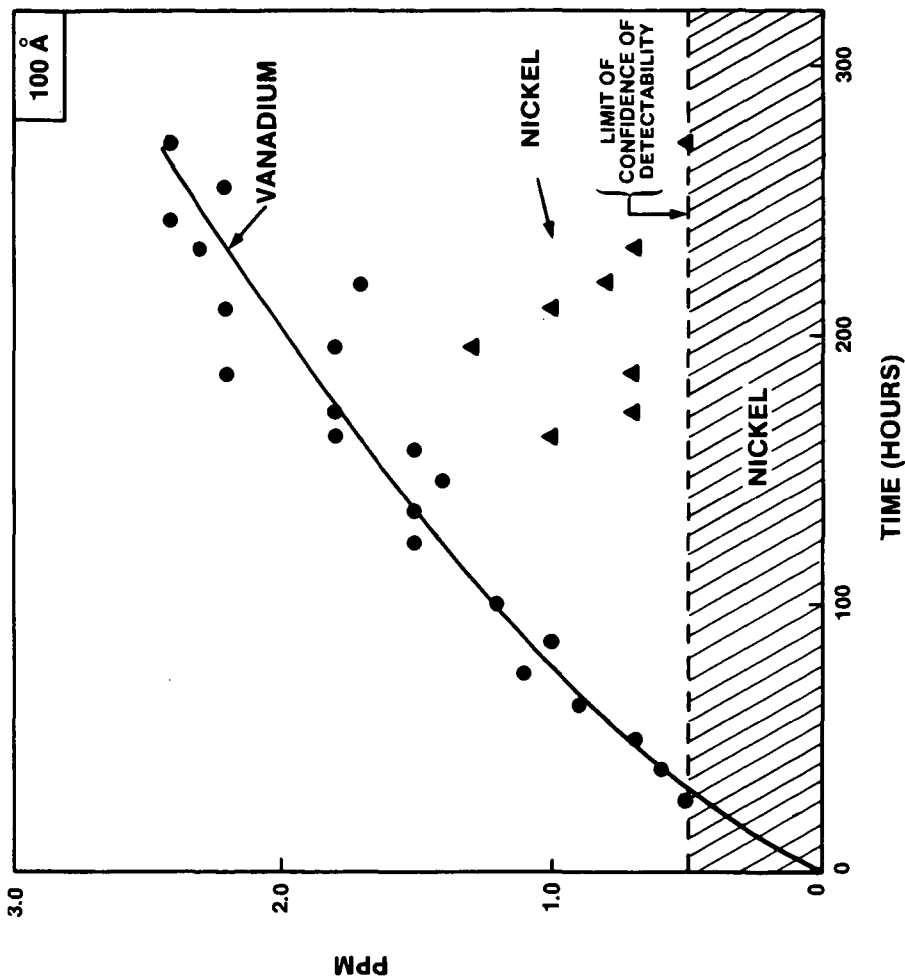


FIGURE 6: Low concentration side nickel and vanadium concentrations for 100A pore diameter membrane



Deactivation of a Hydrogenation Catalyst: Importance of Mass Transfer

Arthur R. Tarrer, Hyon H. Yoon, Vinay P. Wagh
Chemical Engineering Department, Auburn University, AL 36849

Introduction

Over the past few years, a study for a private company has been ongoing at Auburn in parallel with its coal liquefaction program, that involves the development of a hydrogenation process using feedstocks that can be derived from coal. For economic reasons this hydrogenation process had to be done at low severity conditions, i.e., at low temperatures ($\sim 100^{\circ}\text{C}$) and at low hydrogen partial pressures (~ 100 to 200 psi.). It was found that the hydrogenation could be done in the required low pressure and temperature ranges only after a variety of design and operational changes had been made to increase hydrogen gas/liquid mass transfer rates. A new hydrogenation reactor design was developed for the purpose of facilitating hydrogen gas/liquid mass transfer, such that gas compression requirements and gas (VOC) emissions could be kept a minimum.

In this research project, as in coal liquefaction processes, the need exists to reduce process severity by minimizing hydrogen partial pressure requirements. Reducing hydrogen partial pressures can change the relative rates of different reactions (condensation versus hydrogenation) and can result in catalyst deactivation and low conversions. The relative roles that gas/liquid mass transfer and transport mechanisms play in this is important. Design and operational changes can be made, as were done in the above work, to increase mass transfer rates and overcome limitations caused by the mass transfer. Whereas, limitations caused by kinetics, can be overcome by using a more active and selective catalyst. In reducing process severity, mass transfer related parameters and kinetic activity related parameters (e.g., catalyst activity/selectivity) must be changed simultaneously.

In the following discussion, first it will be shown that both a reduction in hydrogen partial pressure and an increase in temperature for the hydrogenation of a heavy coal-derived fraction (SRC) lead to catalyst deactivation. This reaction data for model compound hydrogenation at high severity conditions and at low severity conditions will be presented. In so doing, the responses in catalyst activity/deactivation to changes in kinetic and mass transfer parameters will be examined. A comparison will then be made between the observed responses and governing mechanisms at high severity conditions, and some conclusions will be drawn regarding the importance of mass-transfer parameters--particularly gas/liquid mass transfer--in maintenance of catalyst activity at low severity conditions.

Effect of Hydrogen Partial Pressure and Temperature on Catalyst Activity/Deactivation

Coking is generally accepted to be the chief cause of catalyst deactivation during the hydrogenation of coal liquids. Like any other reaction, coking reactions proceed at a faster rate and to a greater extent at elevated temperatures. The effect of reaction temperature on deactivation rate has been studied here by measuring the activity of a hydrogenation catalyst (Shell 324 Ni-Mo-Al₂O₃) deactivated at different temperatures while hydrogenating a coal liquid (SRC fraction). Naphthalene hydrogenation activity is used here as an indicator of catalyst activity (1) and is given in terms of percent hydrogenation of the naphthalene. Percent hydrogenation (or catalyst activity) is plotted versus the coal liquid (SRC) hydrogenation temperature in Figure 1. As to be expected, present hydrogenation decreases rapidly with increasing temperature.

The effect of hydrogen partial pressure on the extent of deactivation is studied similarly by charging a microreactor with hydrogen at different pressures at room temperature. Naphthalene hydrogenation activity is plotted against reactor charge pressure in Figure 2. The plot shows that percent hydrogenation decreased as the hydrogen pressure in the reactor was decreased.

The above observation--that catalyst was deactivated to a greater extent at reduced hydrogen pressures--agrees with the findings reported for hydrotreating petroleum residue. Sie (2) found that the steady-state carbon level on a catalyst depends on the hydrogen partial pressure in the reactor; an approximate inverse linear relationship between these two parameters was observed. Similarly, in aromatizing cyclohexane, Ruderhausen and Watson (3) observed a linear relationship between the amount of carbon deposition and hydrogen partial pressure. Donath (4) observed that decalin splitting activity for a WS₂ catalyst was decreased considerably at lower pressures. A decrease in hydrogen partial pressure may cause a decrease in the amount of adsorbed hydrogen on the catalyst surface, due to lower mass transfer rates or because the dissolved hydrogen concentration in the reactant is lower, as will be discussed later. As a result, there would probably be an increase in the rate of condensation over that of hydrogenation. This would cause more coke formation at the lower hydrogen pressures.

High Severity Hydrogenation Studies

In this section, naphthalene hydrogenation is used as a model reaction to demonstrate the relative importance of kinetic and mass-transfer parameters on catalyst activity/deactivation. It is to be shown that under high severity conditions, for certain catalysts, naphthalene hydrogenation follows an apparent first-order kinetics, depending on both naphthalene concentration and dissolved hydrogen concentration (i.e., hydrogen partial pressure). Also, gas-liquid mass transfer does not appear to have any significant influence on hydrogenation rates, and no significant deactivation appears to occur for this model reaction as long as the sulfide state of the catalyst is maintained.

A series of naphthalene hydrogenations were done in a microreactor at different hydrogen partial pressures. During hydrogenation, it was assumed that the hydrogen pressure was maintained constant at the mean value of the initial hydrogen pressure and the hydrogen pressure recorded at the end of the

reaction. Figure 3 gives a first-order plot relating hydrogen partial pressure to naphthalene conversion, x . Apparently, naphthalene rates vary with hydrogen partial pressure (thus, dissolved hydrogen concentration) in a first-order manner, under these conditions. The intrinsic rate constant, k , obtained from the slope of the figure for naphthalene hydrogenation on a presulfided CoMo/Al₂O₃ catalyst at 380°C has a value of 4.5242×10^{-3} g liquid/(g catalyst min. psia of H₂).

The reaction parameter used most often to evaluate the relative importance of gas-liquid mass transfer is agitation rate. Varying the agitation rate changes the observed reaction rate only when gas/liquid mass transfer is at least partially rate controlling (5). A plot of naphthalene conversion versus agitation rate is shown in Figure 4. A microreactor was used here. In the absence of steel balls, given by curve 1, the effect of agitation on conversion was marginal up to 500 cpm; however, there was a sudden increase in the conversion in the agitation range 500-550 cpm, and further increase in agitation had no significant effect on conversion which remained constant at about 40 percent. It should be noted that the drop in conversion in the low agitation range (<500 cpm) may be due to poor catalyst dispersion (6). Obviously, in the higher agitation range (>500 cpm), as was used in collecting the deactivation data with coal liquids shown earlier, Figure 1, gas/liquid mass transfer does not appear to be controlling (7).

Catalyst deactivation rate during naphthalene hydrogenation was evaluated by performing successive hydrogenations with a presulfided catalyst in the absence of CS₂ and in its presence. The catalyst activity in terms of percent hydrogenation is given in Figure 5. Since hydrogen was consumed in the hydrogenolysis of CS₂, the amount of hydrogen in the reaction vessel had to be increased in order to maintain the amount of hydrogen available to the reaction at a level equivalent to those reactions without CS₂. In the CS₂ reactions, the percent of excess hydrogen was 1340%, as compared to 1400% without CS₂. The amount of CS₂ added was equivalent to five times the amount used ordinarily to sulfide shell 324 NiMo catalyst.

Apparently, the activity of the catalyst remained essentially constant in all the reaction cycles, with and without CS₂ added. The sulfur content of aged catalysts was measured after the final naphthalene hydrogenation in the successive reaction series. The fresh presulfided catalyst, presulfided/no CS₂ catalyst, and presulfided/CS₂ catalyst had sulfur contents of 8%, 7%, and 7.6% respectively. The presulfided/no CS₂ catalyst as well as the presulfided/CS₂ catalyst had a slightly lower sulfur content compared to that of the fresh presulfided catalyst. Also, the presulfided/no CS₂ catalyst had a slightly less wt.% sulfur than the presulfided/CS₂ catalyst. However, the activity of the presulfided catalyst was nearly the same in the presence as well as in the absence of CS₂. It should be noted that the amount of bulk sulfur may not be a true indication of the extent of sulfiding. In summary, the data show that no significant catalyst deactivation occurred under the reaction conditions used here.

Low Severity Hydrogenation Studies

In all of the above hydrogenations, the reaction severity was relatively high (temp. >300°C, pres. > 800 psi H₂). The hydrogenations to be considered in the following section were those done for a private company and were at

relatively low severity conditions. Here, again using model reactants (naphthalene and *o*-methyl styrene), it will be shown that gas/liquid mass transfer must be considered, because of the high catalyst activity. High catalyst activities are required here in order to attain high conversions under the low severity hydrogenation conditions. A comparison will be made between activities observed with a reactor having poor mass transfer characteristics and one having good mass transfer characteristics. By altering the reactor having poor mass transfer characteristics and making appropriate changes, activities are shown to improve and under these conditions--at which mass transfer becomes no longer controlling--no appreciable catalyst deactivation will be shown to occur.

Hydrogenation of naphthalene was performed at 90°C and 100 psi of H₂ at 25°C in a microreactor (Table 1). Six weight percent catalyst loading of Raney nickel 2800 was used. After 15 min of reaction naphthalene conversion was 100% to tetralin; no significant decalin formation was observed. Assuming first-order kinetics with respect to naphthalene concentration, the kinetic rate constant was about 0.8 min⁻¹ based on 15 min. of hydrogenation required to attain 100% conversion.

To study the influence of gas/liquid mass transfer on low severity naphthalene hydrogenation, a different type of reactor--a 300 cc. autoclave--was used. The gas/liquid mass transfer rates in this autoclave were known to be poorer than that in the microreactor used in the above studies. Figure 6 gives a plot of the mass transfer parameters $k_L a$ versus the mixing parameter, M . These values were obtained using sulfite oxidation. The maximum $k_L a$ values in the bubble column, the stirred tank, and the microreactor (TMBR) were 0.1, 0.25, and 3.8 s⁻¹, respectively. Coefficients as high as 0.15 and 0.5 s⁻¹ have been reported in literature in bubble columns, and stirred vessels (Van't Riet, 1979), respectively, but none approached the value obtained here for the microreactor (TMBR). From Figure 6 it is observed that the gas-liquid mass transfer rate in the TMBR was roughly an order of magnitude greater than in the autoclave and the bubble column reactors (7).

A comparison is made in Table 2 between the naphthalene conversion observed in the microreactor (TMBR) and that in the 300 cc autoclave. In general, while performing the hydrogenation in the autoclave, a steady state catalyst activity could not be obtained. The reproducibility of the reaction rates was consequently poor. This was observed to be true also for low severity *o*-methyl styrene (AMS) hydrogenation at low severity conditions using a relatively high activity catalyst. With AMS, in the microreactor as well as the autoclave, the reaction rate was observed to increase with increased agitation, indicating that mass transfer resistances were the controlling factors (Table 3).

The following changes were made to improve the gas/liquid mass transfer rates in the autoclave: 1) baffles were installed 2) the hydrogen partial pressure was increased (100 to 600 psi) 3) toluene was used instead of hexadecane to reduce the reaction mixture viscosity 4) the maximum stirring rate (2800 rpm) was used. Once these changes were made, the naphthalene conversion was the same in the autoclave as it was in the microreactor. A series of hydrogenations were also made in the autoclave to evaluate catalyst deactivation (Figure 7). Under these conditions of high mass transfer rates, no significant catalyst deactivation was observed.

Summary

Catalyst deactivation was observed to occur while hydrogenating coal liquids under high severity conditions. The rate of catalyst deactivation increased as the hydrogen partial pressure was reduced and as the reaction temperature was increased. For the model reactant naphthalene, however, under high severity conditions, no catalyst deactivation was observed to occur; gas/liquid mass transfer was not controlling; and the hydrogenation appeared to be kinetically controlled having a first-order dependency on dissolved hydrogen concentration (i.e. hydrogen partial pressure) and on naphthalene concentration. Under low severity conditions when a higher activity catalyst was required, on the other hand, mass transfer was observed to be controlling factor both for naphthalene and AMS hydrogenation. Also, with high mass transfer rates no significant catalyst deactivation was observed, but with low mass transfer rates significant catalyst deactivation was observed.

The implications of these observations are that mass transfer as well as kinetic related parameters must be addressed in searching for lower severity coal liquefaction processes. The observed catalyst deactivation with coal liquid hydrogenation cannot be attributed solely to kinetics--catalyst selectivity etc. Poor hydrogen mass transfer could have been a major factor in causing the observed deactivation, even though, for the model reactant naphthalene, mass transfer was not observed to be limiting. Many of the coal liquefaction reactions have higher hydrogenation rates than does naphthalene, and when the hydrogen transport mechanism is not able to meet these higher rate demands, deactivation can occur. To achieve lower severity conditions, higher activity catalysts are needed as was true here with naphthalene, and for higher activity catalysts, higher gas/liquid mass transfer rates are required to minimize deactivation. Higher mass transfer rates can be achieved as was shown here for naphthalene hydrogenation through reactor design changes and appropriate operational changes. In the study done for the private company referred to here, a novel reactor design was developed for their specific purpose.

References

1. Nalitham, R. V., "Parameters and Kinetic Studies on Deactivation and Regeneration of Hydrotreating Catalysts in Solvent Refined Coal Upgrading Process and an Evaluation of the Liquid Vaporization Effects on Hydrotreater Performance." Dissertation, Auburn University, 1983.
2. Sie, S. T., "Catalyst Deactivation," Proceedings of the International Symposium, Elsevier Scientific Publishing Company, New York, NY, 557 (1980).
3. Rudershausen, C. G., and Watson, C. C., Chem. Eng. Sci., 3, 110 (1954).
4. Donath, E. E., Advances in Catalysis, Vol. VIII, Academic Press, New York, NY, 239 (1956).
5. Roberts, G. W., "The Influence of Mass and Heat Transfer on the Performance of Heterogeneous Catalysis in Gas/Liquid/Solid System." In Catalysis in Organic Synthesis, Academic Press, N.Y. (1976).
6. Shah, D. M., "Solvent Effects in Naphthalene Hydrogenation and Benzo thiophene HDS and Studies of Delayed Catalyst Contacting in Single Stage Coal Liquefaction." Thesis, Auburn University, (1982).
7. Gollakota, S. V., "An Investigation of Mass Transfer Phenomena in Coal Liquefaction: Assessment of Resistances and Reactor Types." Dissertation, Auburn University, (1984).

Table 1. Conversion of Naphthalene to Tetralin Using Raney Nickel 2800 and Different Reaction Times (Microreactor)

Reaction time, min	Conversion of Naphthalene to Tetralin, area %
5	31
15	100
30	100
60	100
90	100

Reaction Mixture:

Naphthalene - 0.3 g
 Tetralin - 2.7 g
 Raney Nickel - 0.1 g

Reaction Conditions:

Temperature - 90°C
 H₂ Pressure - 100 psi at 25°C
 Reactor Volume - 45 cc
 Agitation - 860 cpm

1st Order Reaction Rate, $k = 0.8 \text{ min}^{-1}$, based on 15 minute reaction time.

Table 2. Comparison Between Naphthalene Conversion in Microreactor with High Mass Transfer Rates and in 300 cc Autoclave with Low Mass Transfer Rates.

Reaction Time, min	Reactor Type	Conversion of Naphthalene, area %
15	Microreactor	100
60	Autoclave	65

Reaction conditions were the same as those shown in Table 1.

Table 3. Molar Reaction Rates in Alpha-Methyl Styrene Hydrogenation

RPM	Autoclave r, g-moles/hr.lit.	CPM	TBMR r, g-moles/hr.lit.
650	0.025	400	0.75
1050	0.3	600	0.9
1650	0.74	800	1.15
2150	0.84	1000	1.5
		1200	1.75

Experimental Conditions:

Temperature - 20°C
 Catalyst loading - 13.1 g/l (TBMR)
 - 6.6 g/l (Autoclave)

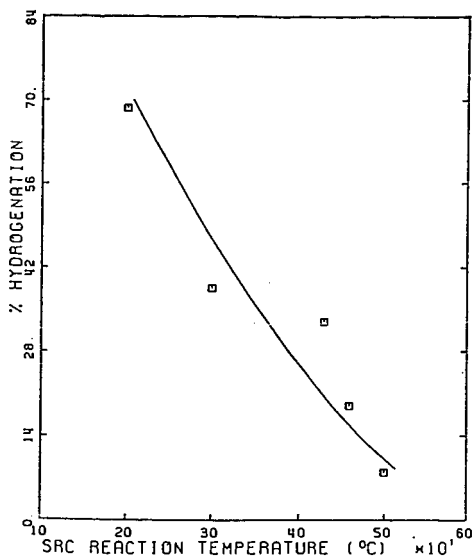


Figure 1. Effect of SRC Reaction Temperature on Catalyst Deactivation (NiMo/Al₂O₃). (1)

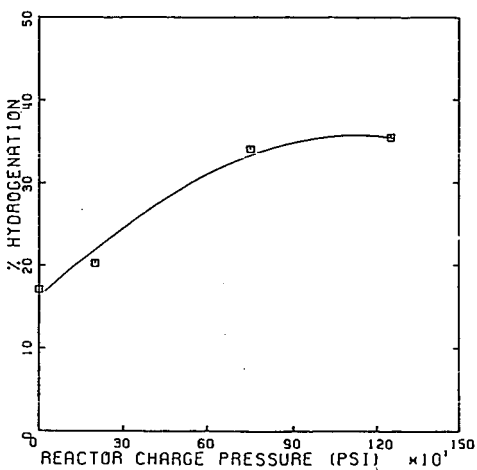


Figure 2. Effect of Hydrogen Pressure on Catalyst Deactivation (NiMo/Al₂O₃). (1)

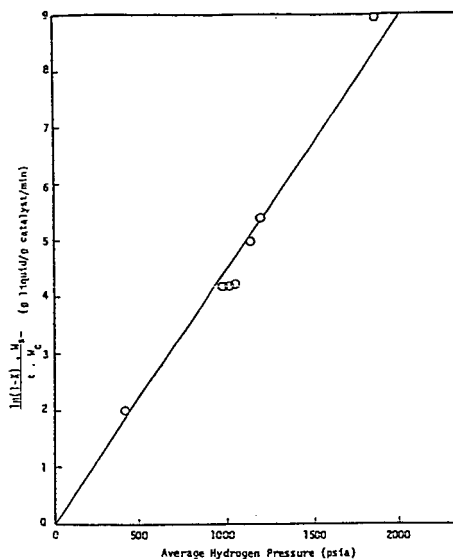


Figure 3. Effect of Hydrogen Pressure on Naphthalene Reaction Rate (CoMo/ Al_2O_3). (6)

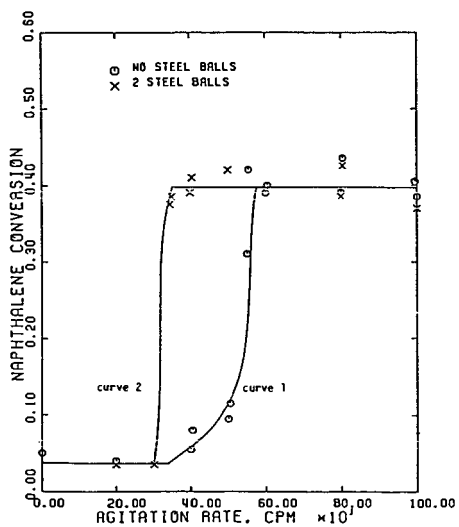


Figure 4. Naphthalene Conversion to Tetralin as a Function of Agitation Rate (CoMo/ Al_2O_3). (7)

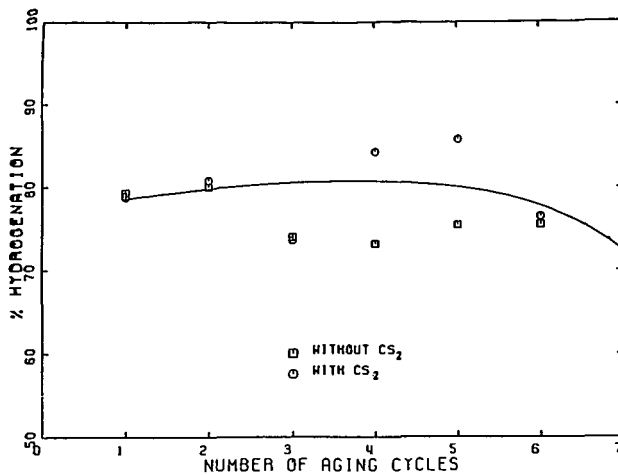


Figure 5. Comparison of the Activity of the Presulfided Catalyst in Successive Naphthalene Hydrogenation Reactions with/without the Addition of CS₂ (NiMo/Al₂O₃). (1)

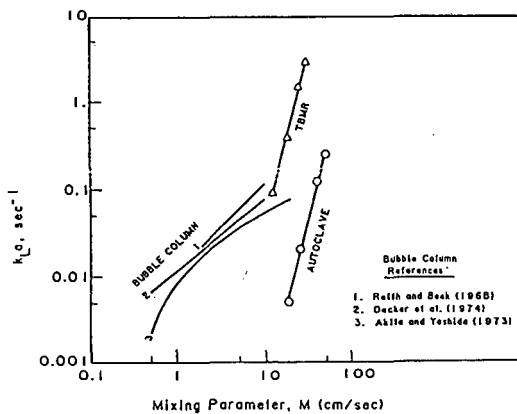


Figure 6. Comparison of $k_{L,a}$ in different Reactor Types. (7)

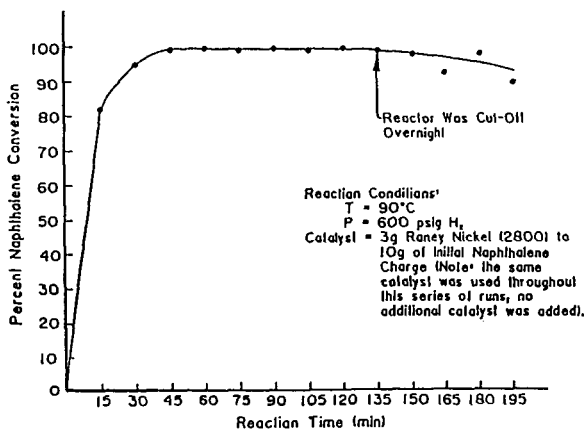


Figure 7. First Series, Batch Hydrogenation of Naphthalene to Tetralin in a 300 cc Autoclave.

SPECTROSCOPIC STUDY OF CATALYSIS BY ZINC CHLORIDE OF COAL DEPOLYMERIZATION

H. Paul Wang, J.-P. Wann, and Edward M. Eyring

Department of Chemistry, University of Utah
Salt Lake City, Utah 84112

ABSTRACT

Diffuse reflectance infrared spectroscopy was used to monitor in situ reactions which ether groups undergo during the depolymerization of ZnCl_2 -impregnated Wyodak coal at elevated temperatures. Subtraction procedures were used to obtain difference spectra that revealed small changes in IR band intensity between 2000 and 1000 cm^{-1} . Evidence was obtained indicating that the ZnCl_2 -impregnated coal samples could be depolymerized in an inert argon atmosphere. However, the degree of the cleavage of ether linkages catalyzed by ZnCl_2 in an inert atmosphere is about 30 % of that in a high pressure hydrogen atmosphere (68 atm). The effect of solvent on impregnation of ZnCl_2 in coal samples was also studied. A higher degree of cleavage of what appears to be a phenyl ether linkage was found for ZnCl_2 -impregnated coal prepared in methanol compared to similar preparations in water and in acetone.

INTRODUCTION

It is believed that ether oxygen plays an important role in linking the macromolecular units in coal. Wachowska and Pawlak [1] have indicated that ether groups represent the main linkages between aromatic clusters. Early works have shown that a catalyst such as ZnCl_2 will promote the liquefaction of coal at temperatures below those at which pyrolysis can occur [2]. Mobley and Bell [3] noted that ZnCl_2 may catalyze the cleavage of ether linkages and thereby promote a reduction in molecular weight.

The average chemical properties of coal have been widely studied using infrared spectroscopy. Recent improvements in the infrared techniques make it possible to measure the infrared spectra of coal powders in situ with the diffuse reflectance method. The present work was undertaken to determine the extent to which the cleavage of ether linkages is catalyzed by ZnCl_2 . We have also applied this method to the study of the effect of solvent on impregnation of ZnCl_2 in coal samples.

EXPERIMENTAL

Reagent grade $ZnCl_2$ (used as received) was impregnated on the THF preextracted Wyodak Coal from different solvent media such as methanol, water, and acetone. The $ZnCl_2$ -impregnated coal samples (25% by weight of extracted Wyodak Coal) was then dried at 353 K overnight. Hydrotreatment of the coal samples were done in a tubing bomb reactor in high pressure hydrogen (68 atm) at 635 K.

Infrared spectra were recorded on a Digilab FT-IR spectrometer (FTS-40). For all spectra reported, a 64-scan data accumulation was obtained at a resolution of 4 cm^{-1} . In order to observe small changes in band intensity, subtraction procedures were used to obtain difference spectra that more effectively compare spectra measured under various conditions. Almost identical base lines for infrared spectra measurements were also obtainable which facilitated calculation of the small spectroscopic changes between different samples using the subtraction method.

About 50 mg of each coal sample was dried at 373 K for one hour in the flowing argon (30 ml/min.) in a controlled environmental chamber (Spectra Tech Inc., Model No.0030-025) which was designed for diffuse reflectance infrared spectroscopy (DRIFTS) at elevated temperatures. In situ infrared spectra of coal samples were measured at temperatures ranging up to 723 K.

RESULTS AND DISCUSSION

It is expected that the presence of the $ZnCl_2$ catalyst during coal liquefaction may accelerate the cleavage of ether linkages (depolymerization) in the coal matrix. The C-O stretching vibrations between 1265 and 1000 cm^{-1} [4] were investigated using in situ infrared spectroscopy. Figure 1 shows the difference infrared spectra obtained at three different temperatures in an inert argon atmosphere. Each spectrum is the difference between the infrared spectra obtained from the original and the $ZnCl_2$ -impregnated (from acetone media) coal samples. The negative features between 1265 and 1000 cm^{-1} in Figure 1 indicate that the cleavage of ether linkages (depolymerization) was catalyzed by $ZnCl_2$. The fact that the depolymerization occurred at a temperature as low as 493 K suggests the possibility of a low-temperature coal liquefaction process catalyzed by $ZnCl_2$. It should be noted that pyrolysis may occur at temperatures higher than 630 K. Furthermore, the negative features between 1350 and 1500 cm^{-1} are in part due to CH_2 and CH_3 bending [4]. The negative feature occurring near 1740 cm^{-1} is present because of the C=O stretching groups [4]. The present work focuses on the study of C-O stretchings in the infrared spectra measured since the formation of C-O bonding is not expected at our reaction conditions.

Generally, the objective of the pyrolysis of coal is to improve the tar/oil yield at the expense of char and gas formation. Thus it is important to study the redistribution of

the hydrogen available within the coal mass and the effect of the hydrotreatment on the depolymerization of coal. The depolymerization of coal samples was investigated in the presence of externally added hydrogen (68 atm). The comparison for the spectra of the depolymerization at 590 K between hydrotreated (573 K and 68 atm hydrogen) and non-hydrotreated coal samples (ZnCl₂ impregnated from acetone) is shown in Figure 2. Difference infrared spectra are used to reveal the net changes in the C-O stretching region. These spectra indicate that the degree of cleavage of ether linkages catalyzed by ZnCl₂ in an inert atmosphere is about 30% of that in a high pressure hydrogen atmosphere (68 atm).

The effect of solvent media used in the ZnCl₂ impregnation on depolymerization of coal samples is shown in Figure 3. The difference spectra were calculated by subtraction of the infrared spectrum of original coal measured at 590 K in the flowing argon from those of ZnCl₂-impregnated coal samples prepared in media such as water, acetone, and methanol. A high degree of cleavage of what appears to be a phenyl ether linkage Ph-O-CH₂-R (~1030 cm⁻¹) was found for ZnCl₂-impregnated coal prepared in methanol compared to similar preparations in water and in acetone. It seems that the dispersion of ZnCl₂ in the coal matrix depends on the media used in impregnation of the catalyst. Thus one should not underestimate the effect of the interactions between solvent media and functional groups of coal on the catalytic depolymerization process.

SUMMARY

The following conclusions have been reached on the basis of this work.

1. The subtraction routines used to obtain difference spectra can reveal small changes in the highly complex infrared spectra of coal.
2. ZnCl₂-impregnated coal samples could be partially depolymerized in an inert argon gas atmosphere.
3. The degree of cleavage of ether linkages catalyzed by ZnCl₂ in an inert atmosphere is about 30% of that in a high pressure hydrogen atmosphere.
4. A higher selectivity in cleavage of a phenyl ether linkage was found for ZnCl₂-impregnated coal prepared in methanol compared to similar preparations in water and acetone.

ACKNOWLEDGEMENTS

Financial support by the U. S. Department of Energy, Fossil Energy Division, through the Consortium for Fossil Fuel Liquefaction Science, Contract No. UKRF-4-21033-86-24, is gratefully acknowledged.

REFERENCES

1. H. Wachowska and W. Pawlak, Fuel, 1977, 56, 422.
2. R. E. Wood and W. H. Wiser, Ind. Eng. Chem., Proc. Design Dev., 1976, 15, 144.
3. D. P. Mobley and A. T. Bell, Fuel, 1979, 58, 661.
4. N. E. Cooke, O. M. Fuller, and R. P. Gaikwad, Fuel, 1986, 65, 1254.

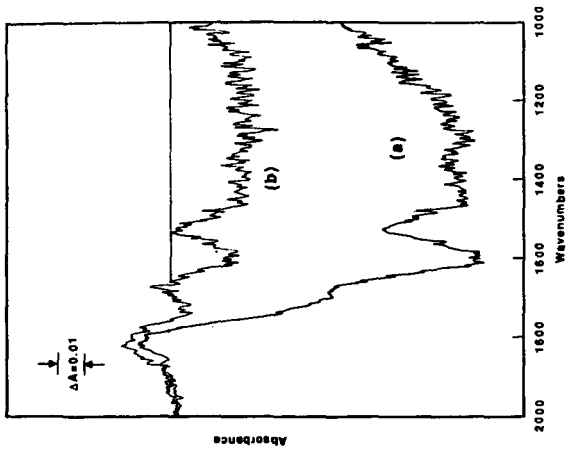


Figure 2
Effect of Hydrotreatment on coal depolymerization.
Difference spectra between original and hydrotreated (a)
and non-hydrotreated (b) $ZnCl_2$ -impregnated coal samples.

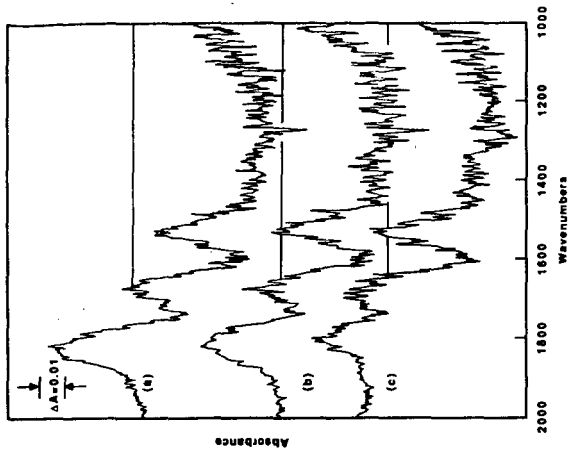


Figure 1
Infrared difference spectra for coal depolymerization
catalyzed by $ZnCl_2$. Difference spectra measured
between original and $ZnCl_2$ -impregnated wyodak coal at
(a) 675 K, (b) 590 K, and (c) 493 K.

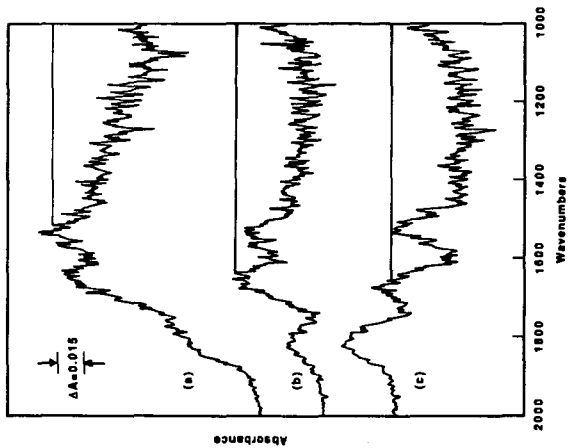


Figure 3
Effect of solvent media used in impregnation of ZnCl₂ in coal samples on the coal depolymerization. Difference spectra between original and ZnCl₂-impregnated coal (a) in methanol, (b) in water, and (c) in acetone.

CORRELATION OF BITUMINOUS COAL HYDROLIQUEFACTION ACTIVATION ENERGY WITH FUNDAMENTAL COAL CHEMICAL PROPERTIES

S.-C Shin, R.M. Baldwin*, and R.L. Miller
Chemical Engineering and Petroleum Refining Dept.
Colorado School of Mines

ABSTRACT

The rate and extent of direct coal hydroliquefaction for 5 bituminous coals from the Argonne Premium Sample Bank have been measured. Data were obtained in batch microautoclave tubing bomb reactors at three temperatures (375, 400, 425 °C) and 5 residence times (3, 5, 10, 15, 40 minutes) in 1-methylnaphthalene vehicle under a hydrogen blanket. Data on rate of conversion of coal to THF and toluene solubles were modeled with a simple reversible rate expression, and activation energies for conversion to each solvent solubility class determined.

Data on carbon and proton distribution in the coals were obtained by ^1H -NMR (Combined Rotational and Multiple Pulse Spectroscopy) and ^{13}C -NMR (CPMAS/Dipolar Dephasing). A strong correlation of activation energy with the aliphatic hydrogen content of the coal was found for conversion to THF solubles. Toluene solubles activation energies were found to be highly correlated ($R^2 > 90\%$) with total oxygen, and protonated aliphatic carbon. ^{13}C -NMR data indicated a high degree of correlation between protonated aliphatic carbon and total oxygen for only the bituminous coals from the Argonne suite, suggesting the importance of etheric oxygen in crosslinking structures for determination of bituminous coal reactivity.

Introduction

The relationship between coal chemical and structural features and coal reactivity has been the subject of considerable research for well over 70 years, dating from the original observations of Bergius (1) regarding the influence of carbon content on hydroliquefaction yield. Early studies of the influence of coal properties on coal reactivity were focused on an attempt to find a single parameter or group of parameters capable of correlating physical, chemical, and geochemical properties with the degree of conversion to some solvent soluble products under a fixed set of reaction conditions (2-8). Given et al. (9-12) developed multiparameter statistical correlations for coal reactivity for an extensive suite of U.S. coals. These correlations were partitioned according to the geographical location of the coal in order to increase the significance of the relationships. Other researchers have attempted to correlate coal hydroliquefaction reactivity with the mineral matter in coal, most notably pyrite, and other physical and chemical properties (13-18). Neavel (19) and Furlong et al. (20) introduced the concept of using reaction rate as a reactivity parameter while Shin et al (21) attempted to combine reaction rate and reaction extent into a single reactivity parameter which could then be correlated to coal properties. Gutmann (22) correlated reaction rate constants with the sulfur content of lignite coals. Other reactivity

relationships based on information from instrumental techniques such as pyrolysis/mass spectrometry have been developed by Baldwin et al. (23).

All of the above attempts to relate coal liquefaction reactivity to coal properties have suffered from two severe limitations. First, the parameters employed as reactivity definitions have generally fallen into two categories: 1) reactivity as defined by a point-yield definition at fixed time and temperature (e.g. toluene solubles at 60 minutes, 450 °C) or; 2) reactivity as defined by a reaction profile with time at fixed temperature. While both of these "traditionally" used reactivity definitions can be correlated with liquefaction reactivity, the correlations developed are not truly universal in that they may not hold at different time and/or temperature levels. This point is demonstrated conclusively below. The second major limitation of prior studies is that the correlations have not been developed in terms of fundamental structural and chemical properties of coal. In many cases, derived coal properties such as volatile matter, fixed carbon, rank, heating value, etc. have been used as the independent variables in multi-parameter statistical models. As pointed out by Neavel (24), such correlations are of limited significance.

The above discussion highlights the need for a reactivity parameter that is independent of both time and temperature, yet which can be correlated with basic coal chemical properties. Further, detailed knowledge of the chemical structure of coal is needed so that the reactivity correlations developed have some significance in terms of the chemistry of the liquefaction process. We have attempted to address both of these problem areas by using activation energy as a reactivity definition, and by exploring the use of structural information from two new NMR techniques (¹H-NMR/CRAMPS and ¹³C-NMR/CPMAS with dipolar dephasing) which do permit determination of fundamental chemical structural features important in coal liquefaction reactivity.

Experimental

Five bituminous coals from the Argonne Premium coal collection were liquefied in 1-methylnaphthalene vehicle. Characterization data for the Argonne coals are shown in Tables 1 and 2. Experimental runs were carried out in batch tubing bomb microautoclave reactors at 375, 400, and 425 °C, and at 3, 5, 10, 15, and 40 minute residence times. All runs were performed in a hydrogen atmosphere under a cold pressure of 6.2 MPa. Data on the rate and extent of coal conversion to THF and toluene solubles were collected using a standard solvent fractionation procedure. Further details concerning experimental methods have been reported elsewhere (25).

The experimental program consisted of two phases. During the first phase, an examination of the effect of vehicle on the measured liquefaction reactivities was carried out using 3 aromatic compounds (1-methylnaphthalene, naphthalene, and phenanthrene). The second phase of the project concerned

measurement of the data, kinetic modeling, and correlation with coal properties.

Proton NMR data for the Argonne coals was obtained from the National Science Foundation Regional Center for NMR at Colorado State University, utilizing the technique of Combined Rotational and Multiple Pulse Spectroscopy (CRAMPS). Basic data on the proton distribution in these coals are shown in Table 3. Information on the carbon distribution via dipolar dephasing of ^{13}C -NMR data was obtained from Dr. R.L. Pugmire at the University of Utah, and these data are presented in Table 4.

Discussion of Results

Effect of Vehicle on Liquefaction Reactivity In order to properly evaluate and compare the inherent reactivities of different coals, a non-hydrogen donor liquefaction vehicle was required so that reactivity differences between similar coals within a given rank or sub-rank could be magnified. The first phase of this experimental program was thus concerned with an evaluation of the effect of three aromatic vehicles on relative reactivities. Liquefaction experiments were performed on the 5 Argonne bituminous coals in 1-methylnaphthalene (1-MN), naphthalene, and phenanthrene, and the relative reactivities of these coals assessed by toluene conversion at 5 and 40 minutes. Figure 1 presents the results of the 40 minute runs. These data clearly indicate that the relative reactivities are independent of choice of vehicle, and that conversions in 1-methylnaphthalene are equivalent to the other two aromatic vehicles. Data from the 5 minute runs led to similar conclusions. Because of the added ease of operation afforded by 1-MN, this material was utilized as the liquefaction vehicle in all subsequent experiments.

Rate Data and Modeling Rate data for conversion of the Argonne coals to THF and toluene solubles were measured. Reproducibility of the data was checked by performing duplicate experiments on the Illinois #6 coal. Various kinetic models were investigated for purposes of data fitting, including the following:

- first-order irreversible
- first-order reversible
- second-order irreversible
- second-order reversible
- first order (forward)/second order (reverse)
- Anthony-Howard model (26)

Rate data from the liquefaction experiments were fit to each of these models for all 5 coals, and model discrimination performed using a goodness-of-fit (R^2) criterion. Statistical results from data fitting indicated that the best model overall from among these candidates was the first/second reversible model. The analysis of variance from regression modeling of the Illinois #6 coal (the replicated data set) gave very low values for the pure error mean square, indicating that the data were highly reproducible. A parity plot for toluene solubles conversion for Illinois #6 coal and the first/second-order reversible kinetic model is shown in Figure 2. As can be seen, the model provides a satisfactory descriptive expression for the data being observed.

Traditional Correlations As mentioned above, the traditional parameters that have been used for coal liquefaction reactivity correlations are point-yield conversion and a kinetic rate constant. We thus began our correlational efforts by exploring similar types of relationships. Figure 3 presents three correlations using the point-yield reactivity definition. Here, conversion to toluene solubles at 5 minutes is used as the yield parameter. As shown, a very strong correlation ($R^2=98\%$) exists between toluene conversion at 5 minutes and 425°C and total oxygen plus total carbon in the coal. However if this same correlation is extended to a different time (40 minutes) at the same temperature, a much weaker correlation ($R^2=61\%$) results. If the temperature is changed to 375°C while time is held constant (5 minutes), essentially no correlation ($R^2=0$) exists. Figure 4 shows the same sort of effect, but using a kinetic constant (from the first/second model) as the reactivity parameter. A very strong correlation is found at 425°C between the rate constant for conversion to THF solubles and the total carbon content of the coal ($R^2=94$). Since the rate constant is time independent, this is a valid reactivity parameter as long as the temperature is not altered. However, if the temperature is reduced to 400 and then to 375°C , the same correlation weakens significantly and then disappears, with R^2 falling to 54% and 12% respectively at the lower temperatures. This graphically illustrates the inadequacy of both of these "traditional" reactivity parameters, which are either time and/or temperature dependent.

The above discussion demonstrates the need for a reactivity parameter that is time and temperature independent. This leads logically to consideration of activation energy as a fundamental reactivity parameter, since:

- activation energy includes temperature effects;
- activation energy should reflect more closely the chemical nature of the parent coals;
- activation energy is obtained by measuring time and temperature effects, but the result is time and temperature independent.

Activation Energy Correlation Intuitively, the behavior noted above might be interpreted as a shift in the controlling mechanism for the liquefaction reaction, with one type of chemical functionality dominating the reaction at one set of conditions. This would be accompanied by a gradual shift to different reaction pathways and hence different chemical functionalities at other temperatures and times. This concept of a distribution of reaction pathways was the basis for the development of the Anthony-Howard model (26). However, when this expression was applied to our rate data little variation in the derived activation energies between the different coals was found. A strong dependency of the derived activation energies with coal type was found, however, for the first/second rate model. These data are presented in Table 5. Exceedingly good fits to the expected Arrhenius temperature dependency were found for the toluene and THF rate constants, as indicated by the

coefficients of determination (R^2) in Table 5. It is important to recognize that these activation energies are not fundamental parameters, but the large differences in activation energies found for these 5 coals suggest that this parameter should be useful as a relative reactivity indicator.

Before initiating correlation of reactivity with coal properties, it is important to determine which of the coal characteristics available are independent parameters, and which are highly correlated with other characteristics and thus are simply derived properties. Eight coal characteristics, including basic data from proximate and ultimate analysis along with the proton NMR (CRAMPS) information, were first investigated in this manner. Volatile matter and total carbon were found to be strongly correlated with aliphatic carbon content, while total carbon was found to be highly correlated with carbon aromaticity. Total sulfur, ash, and aromatic (and hence aliphatic) hydrogen content of the coal were found not to be related with any of the other properties of the coal.

Table 6 presents the results of correlation of the liquefaction activation energies for the 5 bituminous coals with the independent coal properties. The activation energy for coal conversion to toluene solubles was found to be strongly ($R^2=93\%$) correlated with the total oxygen content of the coal, while the activation energy for conversion to THF solubles was found to be highly correlated ($R^2=95\%$) with aliphatic hydrogen content. These correlations are shown graphically in Figures 5 and 6. Correlation of activation energies for conversion to toluene and THF solubles were not found to be highly correlated with any of the other coal properties in Table 6, suggesting that the relationships found between reactivity and these two coal properties are unique.

Data from the ^{13}C -NMR were next investigated, and simple single-parameter correlations of these properties with THF and toluene activation energies attempted. Intercorrelations between the various ^{13}C -NMR properties and other coal characteristics were first investigated in a manner similar to the above. The only intercorrelation found from this data set was for total oxygen and protonated aliphatic carbon (sp^3 -hybridized and CH or CH_2). The correlation between these two parameters for the 6 Argonne bituminous coals (including Blind Canyon) was almost 99%, however when the data for the subbituminous and lignite coals was added, the correlation no longer held. These data are shown graphically in Figure 7. This finding may have strong implications with respect to coal structure, and the differences in reactivity found between low rank and high rank coals in general. The activation energy for conversion to toluene solubles was found to be very highly correlated ($R^2=93\%$) with protonated aliphatic carbon. No other correlations of coal properties from the ^{13}C -NMR data and toluene or THF activation energies were found.

The strong intercorrelation found between protonated aliphatic

carbon and total oxygen for the 6 bituminous Argonne coals can be interpreted structurally in terms of etheric groups in the cross-linking structures between aromatic clusters. While based on a rather limited data set, this relationship and the correlation found between total oxygen and toluene activation energy would seem to suggest that the carbon-oxygen bonds in crosslinking structures are of extreme importance in determining coal reactivity. Data from the ^{13}C -NMR also provides an estimate of the relative abundance of etheric carbon-oxygen structures (All-O in Table 4). However, when this parameter is correlated with the toluene activation energy a less than adequate ($R^2=77\%$) relationship is found as shown in Figure 8. One coal (Stockton) in this data set represents a significant outlier, and if this coal is removed from the regression, the adequacy of the relationship improves to 97%. Due to the limited number of coals in this study, these observations and conclusions must be treated as tentative at this time. Further research on a wider suite of bituminous coals is needed.

Acknowledgements

This research was supported by the U.S. Department of Energy under grant no. DE-FG22-85PC80907. The authors would also like to acknowledge the contributions of Dr. Ronald J. Pugmire and his group at the University of Utah (^{13}C -NMR data) and Dr. Charles Bronnmann at the NSF Regional Center for NMR (^1H -NMR data) at Colorado State University. Dr. Shin would like to express his gratitude to the Ministry of Energy and Resources, Seoul, Korea.

References Cited

1. Berguis, F., Jour. Gasbeleucht. (1912), 54
2. Francis, W., FUEL (1932), 11, 171
3. Petrick, A.J., Gaigher, B., and Groenewoud, P., Jour. Chem. Met. Min. Soc. South Africa (1937), 38
4. Wright, C.C., and Sprunk, G.C., Penn State College Min. Ind. Exp. Sta. Bull. (1939), 28
5. Fisher, C.H., Sprunk, G.C., Eisner, A., Clarke, L., Fein, M.L., and Storch, H.H., FUEL (1940), 19, 132
6. Shatwell, H.G., and Graham, J.L., FUEL (1925), 4, 25
7. Horton, L., Williams, F.A., and King, J.G., Dept. Sci. and Ind. Res. (1936), Fuel Research Tech. Paper 42
8. Fisher, C.H., Sprunk, G.C., Eisner, A., O'Donnell, H.J., Clarke, L., and Storch, H.H., U.S. Bureau of Mines (1942), Tech. Paper 642
9. Given, P.H., Cronauer, D.C., Spackman, W., Lovell, H.L., Davis, A., and Biswas, B., FUEL (1975), 54, 34
10. _____, FUEL (1975), 54, 40
11. Abdel-Baset, M.B., Yarzab, R.F., and Given, P.H., FUEL (1978), 57, 89
12. Yarzab, R.F., Given, P.H., Spackman, W., and Davis, A., FUEL (1980), 59, 81
13. Mori, K., Taniguchi, M., Kawashima, A., Okuma, O., and Takahashi, T., ACS Div. Fuel Chem. Preprints (1979), 24, no. 2
14. Durie, R.A., ACS Div. Fuel Chem. Preprints (1979), 24, no. 2

15. Gray, D., Barrass, G., Jezko, J., and Kershaw, J.R., FUEL (1980), 59, 146
16. Mukherjee, D.K., and Chowdhury, P.B., FUEL (1976), 55
17. Guin, J.A., Tarrer, A.R., Prather, J.W., and Johnson, D.R., Ind. Eng. Chem. Proc. Des. and Devel. (1978), 17, 118
18. Gray, D., FUEL (1978), 57
19. Neavel, R.C., FUEL (1976), 55, 237
20. Furlong, M.W., Baldwin, R.M., and Bain, R.L., FUEL (1982), 61
21. Shin, S-C., Baldwin, R.M., and Miller, R.L., Energy and Fuels (1987), 1, 377
22. Gutmann, M., Radeck, D., Konig, M., and Kell, G., Proc. Int. Conf. Coal Science (1987), 187
23. Baldwin, R.M., Durfee, S.L., and Voorhees, K.W., Fuel Proc. Tech. (1987), 15, 281
24. Neavel, R.C., FUEL (1986), 65, 312
25. Shin, S-C., M.S. Thesis no. T-3267 (1988), Arthur Lakes Library, Colorado School of Mines
26. Anthony, D.B., and Howard, J.B., AIChE Jour. (1976), 22, 625

Table 1. Characterization Data of Argonne Premium Coals
(Elemental & Proximate Analysis)

Coal Seam	State	Rank	Elemental Analysis*				Proximate Analysis**		
			C	H	O	Stot	Ash	V.M	F.C
Illinois #6	IL	HVB	77	5.7	10	5.4	14.8	35.4	44.7
Pittsburgh #8	PA	HVB	83	5.8	9	1.6	9.7	34.9	53.6
Lewiston-Stockton	WV	HVB	81	5.5	11	0.6	20.1	28.6	49.4
Upper Freeport	PA	MVB	87	5.5	4	2.8	13.1	25.1	60.7
Pocahontas #3	VA	LVB	91	4.7	3	0.9	5.3	17.1	77.1

* All the values are given based on wt % (d.a.f basis), except for sulphur which is in dry wt %. These data furnished by Argonne National Laboratory, Argonne, Illinois.

** All the values are given based on as received basis (wt %). These data measured by Huffman Laboratories, Inc., Golden, Colorado

Table 2. Characterization Data of Argonne Premium Coals
(Carbon-13 N.M.R and Proton N.M.R)

Coal Seam	State	Rank	Carbon-13 N.M.R.*		Proton N.M.R. **			
			C-tot	C-arom	C-alip	H-tot	H-arom	C-alip
Illinois #6	IL	HVB	6.42	4.42	2.00	5.7	2.74	2.96
Pittsburgh #8	PA	HVB	6.92	5.17	1.75	5.8	2.21	3.59
Lewiston-Stockton	WV	HVB	6.75	5.00	1.75	5.5	1.68	3.82
Upper Freeport	PA	MVB	7.25	5.92	1.33	5.5	2.10	3.40
Pocahontas #3	VA	LVB	7.58	6.75	0.83	4.7	2.57	2.13

* All the values based on moisture and ash-free atomic basis (wt % divided by m.w of carbon). Aromaticity data measured by Utah University using C-NMR (CPMAS). These data were furnished by Dr. Ronald Pugmire.

** All the values based on moisture and ash-free atomic basis (wt % divided by m.w of hydrogen). Proton NMR data measured by NSF Regional NMR Center (Colorado State University, Fort Collins, Colorado) using H-NMR (CRAMPS).

Table 3. Aliphatic and Aromatic Hydrogen Contents of
Argonne Coals: Proton-NMR (CRAMPS)

coal	aromatic H (%)	aliphatic H (%)
Illinois #6	48.0	52.0
Pittsburgh #8	38.1	61.9
Stockton	30.6	69.4
Upper Freeport	38.2	61.8
Pocahontas	54.6	45.4

Proton spectra obtained at a proton Larmor frequency of 187 MHz using a BR-24 pulse sequence. The 90 pulse width was 1.1 us and the cycle time of 36 tau was 108 us. Samples were spun at the magic angle at a nominal rate of 2 KHz.

Spectra measured by the National Science Foundation Regional NMR Center, Colorado State University, Fort Collins, Co.

Table 4. Carbon Structural Distribution of the Argonne Coals

	Illi #6	Pitt #8	Stockton	Upper F. Pocahontas
Aliphatic-total(SP3)	28%	28%	25%	19%
Ali-H	18	13	18	8
Ali-N	10	15	7	11
(Ali-O)	(5)	(3)	(4)	(2)
Aromatic-total(SP2)	72%	72%	75%	81%
Aro-Ring	72	72	75	81
Aro-R-H	26	27	27	28
Aro-R-N	46	45	48	53
Aro-R-N-P	6	6	5	4
(Aro-R-N-A	18	17	21	20
Aro-R-N-B	22	22	22	29
Aro-Carbonyl	0	0	0	0

Ali-H=fraction of total carbon that is sp³-hybridized and CH or CH₂.
 Ali-N=sp³-hybridized and CH₃ or nonprotonated, Ali-O=sp³-hybridized and bonded to oxygen. Aro-R-H=sp²-hybridized and protonated.
 Aro-R-N=sp²-hybridized and nonprotonated, Aro-R-N-P=sp²-hybridized and phenolic or phenolic ether, Aro-R-N-A=sp²-hybridized and alkylated, Aro-R-N-B=sp²-hybridized and at a bridgehead position.

Data on carbon distribution obtained from Dr. R.J. Pugmire, University of Utah.

Table 5. Activation Energies of 5 Bituminous Argonne Coal

Coal Seam	Toluene solubles		THF solubles	
	E (Kcal/m)	R-Square (%)	E (Kcal/m)	R-Square (%)
Illinois #6	20.9	99.8	17.5	99.5
Pittsburgh #8	15.5	95.2	24.5	96.3
Lewiston-Stockton	26.8	94.3	29.5	98.3
Upper Freeport	9.9	97.0	20.1	99.3
Pocahontas #3	4.3	100	7.5	98.3

Table 6. Correlation of Activation Energy with Coal Properties

o Adjusted Coefficient of Determination (%)

Coal Property	Activation Energy (toluene solubles)	Activation Energy (THF solubles)
C-aliphatic	64.8	32.0
C-aromatic	67.9	21.9
H-total	23.8	42.4
H-aliphatic	32.5	95.1 -----
O-total	93.2 -----	36.2
S-total	0.0	0.0
Ash	72.8	37.1
H-tot/C-tot	50.7	29.2
O-tot/C-tot	91.6	29.9
O-tot + C-tot	27.4	0.0

Figure 1. Solvent Effect on Reactivity Ranking
(Reaction Time: 40 min)

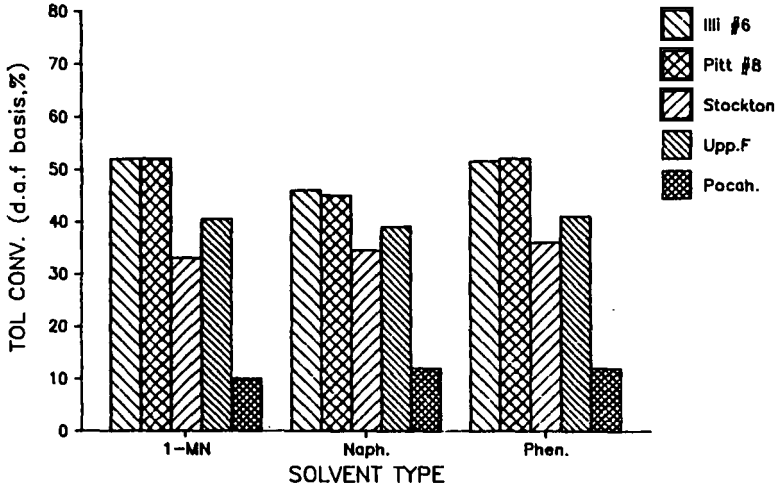


Figure 2. Parity Plot (toluene solubles)

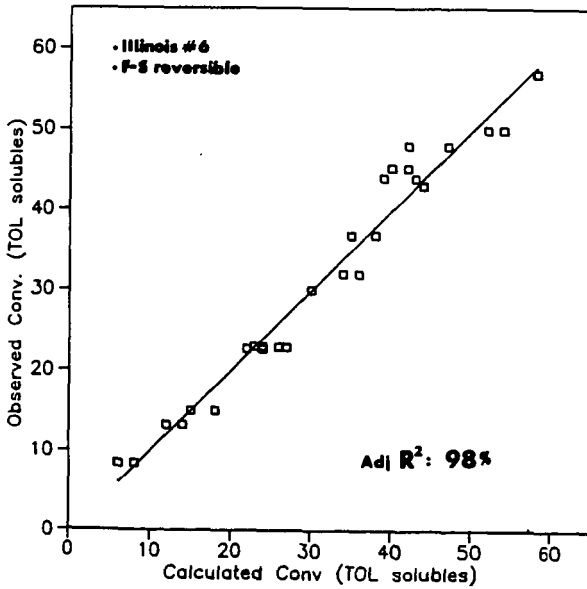


Figure 3. Example I

Point-Yield Reactivity vs. Total C+O

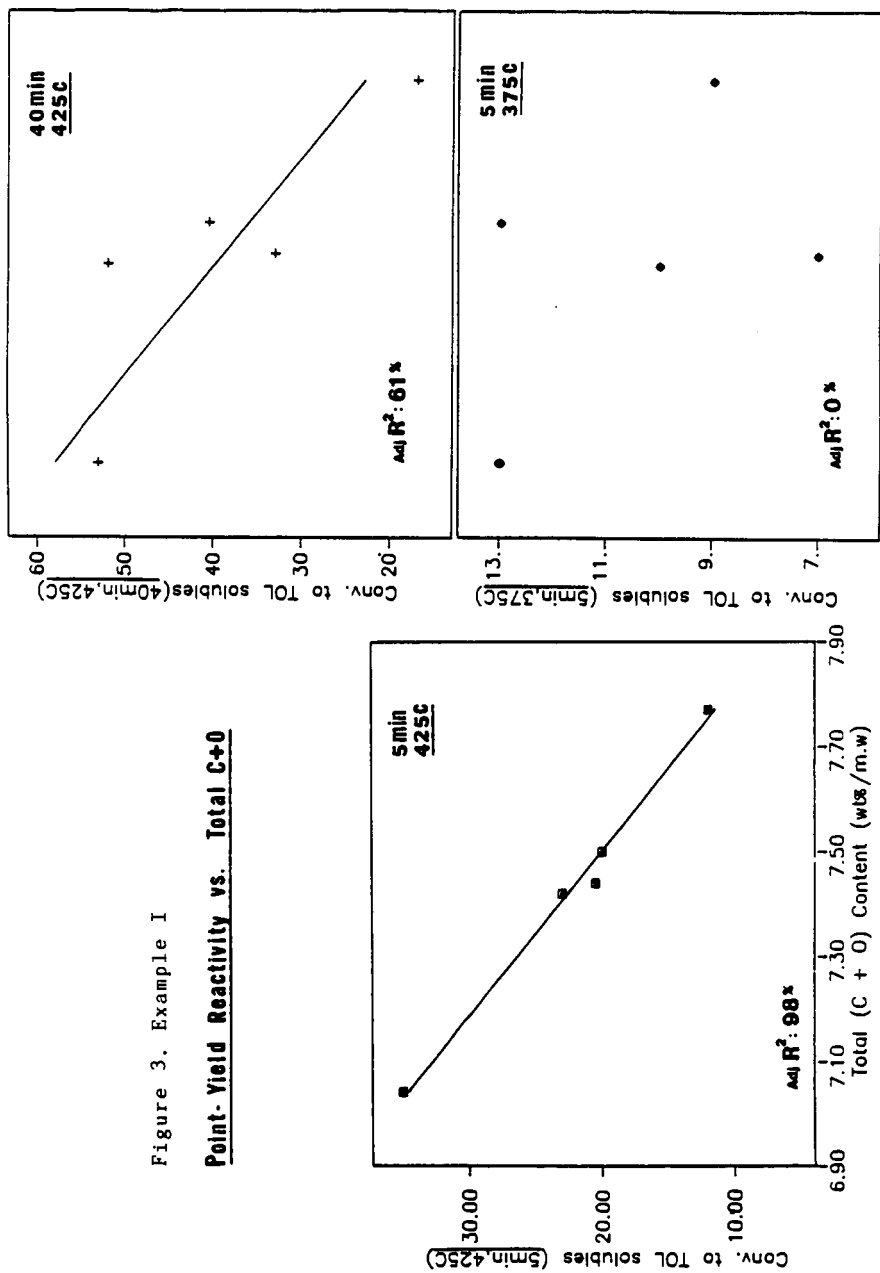


Figure 4. Example II
Kinetic Constant vs. Total Carbon

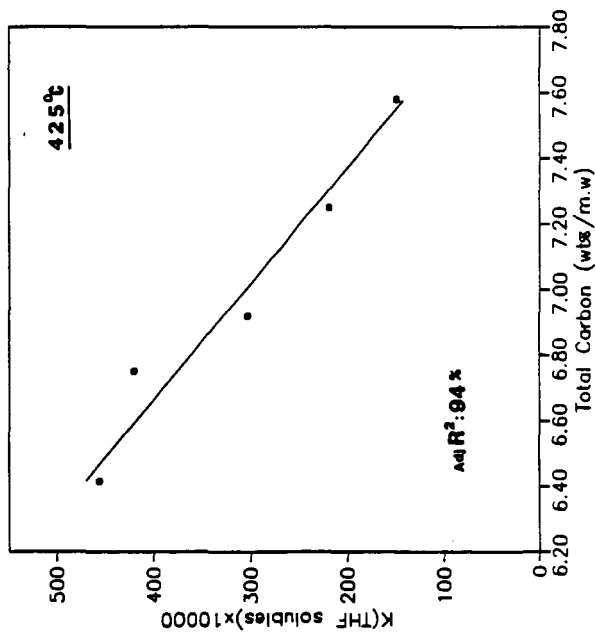
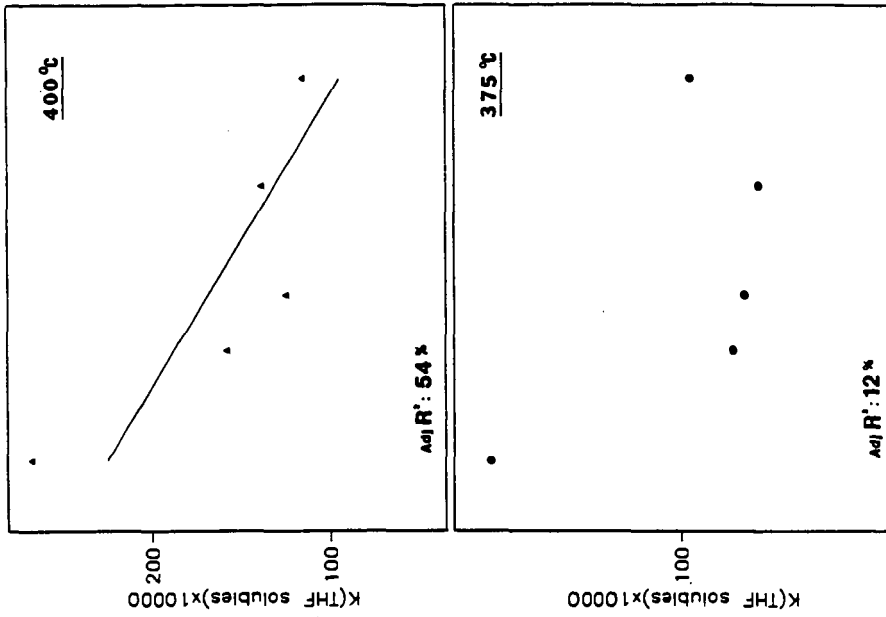


Figure 5. Correlation of Activation Energy (toluene solubles) vs. Oxygen Content

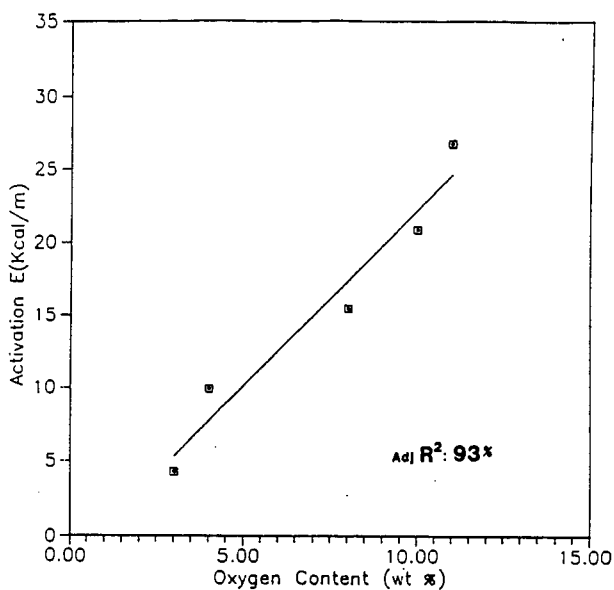


Figure 6. Correlation of Activation Energy (THF solubles) vs. Aliphatic Hydrogen

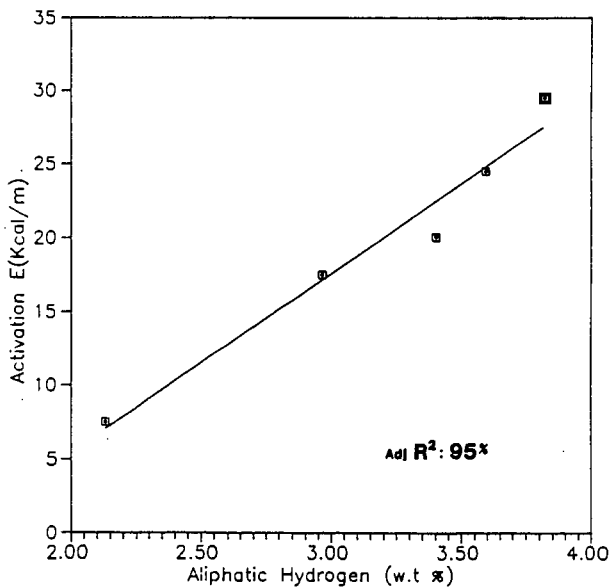


Figure 7. Interrelationship between Total Oxygen and Linking Aliphatic Carbon Content

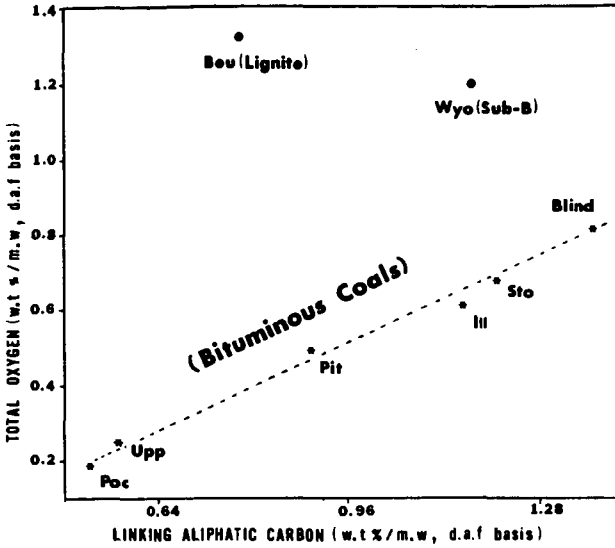
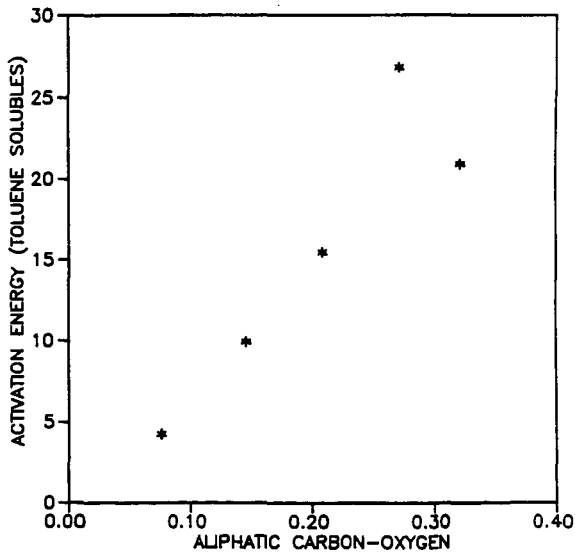


Figure 8. Correlation of Activation Energy (toluene solubles) vs. Aliphatic Carbon-Oxygen



COAL STRUCTURE AND BEHAVIOR--INTERFACIAL CHEMISTRY IN COAL

David S. Ross, Albert S. Hirschon, and Thomas K. Green
SRI International, Menlo Park, California 94025

Introduction and Background

A model for the organic phase of coal recently suggested by Shinn is shown in Figure 1 (1). This model is based on a reconstruction of the parent structure of an Illinois No. 6 coal following a thorough evaluation of reported product data from various liquefaction processes. The model structure contains 11% oxygen, with about 35% of the total O present as ether oxygen. This ether fraction is the same as the value we established in recent work on the fate of oxygen in an Illinois No. 6 coal during thermolysis and conversion (2).

Insofar as it presents an organic network of linked aromatic units, the model is similar to others presented earlier, as summarized by Davidson (3a) and Gray and Shah (3b). However, the Shinn model is closely tied to more recent evidence from liquefaction and analytical studies and as such is the most realistic picture of the organic phase available. Like earlier models, this model is limited to the organic components in coal and ignores the mineral phase. Shinn acknowledges that avoiding the heterogeneous aspect of coal structure precludes a full understanding of its structure and therefore its behavior.

This point is key to the discussion here, as is emphasized by the fact that the structure in Figure 1 is not consistent with some facts on coal behavior recently uncovered by us and others. We submit as a working hypothesis that the reactive centers in coal include and may be dominated by substantial interfacial regions common to both the organic and mineral phases. The focus of our attention is not the catalytic effects of mineral matter in coal conversion to liquids or gases, which have been investigated during the past three decades (4) or longer, but rather the chemistry at the organic/mineral boundary specifically.

While most inorganic material in coal is present in a discrete mineral phase over a range of sizes, from large crystallites to micron-size grains (5), Mraw, et al. demonstrated the presence of very small clay inclusions down to 10 nm in size (6). They speculated that the fine grain size corresponds to a very high surface area, which in turn could play a role in the chemistry of coal. More recently, Allen and VanderSande reported even smaller, ultrafine mineral material, estimating abundance of up to 15% of the full mineral assay (7). Their technique required comparison of pairs of x-ray spectra of respectively a particle and the organic matrix 1-2 particle diameters away for comparison. As is seen in Figure 2, while the particle in question clearly is rich in titanium, both spectra, in particular that from the organic matrix, show aluminum and silicon. It would thus appear that the organic phase includes clay inclusions with characteristic sizes extending below their 2 nm resolution limit, perhaps extending to collections of hundreds of atoms. The result would be an organic/mineral interface of enormous extent.

This picture of an integrated structure could be tied with the recent findings that are otherwise unreconcilable with conventional structures. Towne, et al. found that the addition of water to conventional H-donor media substantially increased the

extent of liquefaction (10). Brandes and Graff found that hydrothermal treatment activated coal for subsequent mild gasification (11a,b). Perhaps the most striking aspect of this work was the finding that their brief pretreatment changed the swelling characteristics of the coal so that water itself became a swelling agent. Bienkowski et al. have reported a beneficial effect on liquefaction (12) in line with some of our work, where aqueous pretreatment activates the coal toward subsequent liquefaction (13).

Results

In an attempt to evaluate the importance of interfacial chemistry to coal behavior, we have conducted studies at 400°C with both H₂O and D₂O, using both Illinois No. 6 coal (PSOC 1098) and pure organic compounds. We were directed to this approach through accounts in the geochemical literature, in which considerable attention is paid to kerogen/mineral interactions tied to petroleum production (14,15).

Figure 3 summarizes our effort, and virtually none of the material presented here is consistent with the organic structures depicted in Figure 1. We found that while coal recovered from simple hydrothermal treatment in D₂O/N₂ for 20 minutes under nitrogen contained more than 90% of the starting carbon, 30% of the starting hydrogen and about half the starting oxygen were lost. Our account of the anomalous O-loss has recently appeared (2). These losses could not be accounted for by CO₂ and light hydrocarbon evolution. Of the remaining protium in the product, 53% had been exchanged for deuterium. The product had been subjected to back-exchange in H₂O at mild conditions to convert the phenolic hydrogen to protium, so the large levels of exchange were strictly for hydrogen bonded to carbon.

In other runs the coal was converted to products that were 50-60% toluene soluble (TS) by replacing the N₂ with CO. The D-fractions for both TS and toluene insoluble (TI) fractions (back-exchanged) were 53% and 59% respectively, or a composite value essentially the same as that for the produce from the N₂ run. Thus, the conversion chemistry operated on the material that had undergone isotope exchange rapidly and prior to conversion to the TS fraction, a very useful finding since structural factors subsequently developed from NMR work for the TS fraction could then be tied to the original structure with some confidence.

¹H NMR studies on the TS fractions from parallel H₂O and D₂O runs revealed little exchange for the β- and γ-alkyl hydrogens in the coal. About 57% of the aromatic protium was exchanged, a result in accord with the known phenolic exchange chemistry under these conditions (16) and consistent with the known phenolic content of the coal and the structure in Figure 1. For the benzyl hydrogen, however, the result was striking. We found that fully 76% of the benzyl hydrogens in the TS fraction were replaced by deuterium in the 20-minute treatment.

These findings can be compared with those from work with work under the same conditions with pure organic materials. At 20 minutes in D₂O we found no trace of exchange for benzene, toluene, or bibenzyl. Indeed, we had to extend the period to 1200 minutes to observe the introduction of deuterium into the benzylic positions in bibenzyl and the toluene derived from it, while benzene and toluene themselves were still virtually unexchanged after this extended period.

Thus, the benzyl-protium exchange rate in coal is roughly 100 times faster than that for bibenzyl and considerably faster than that for toluene. This result can be translated to suggest that the thermal generation of free radical sites in the coal

operates at a rate two to three orders of magnitude greater than that for bibenzyl. However no feature in the organic structures proposed for coal can generate such a flux of reactive free radicals by a wide margin. Indeed, we are aware of no chemistry for structures such as that in Figure 1 which can accommodate our findings for both the H and O components of the organic phase.

Discussion

Accordingly, we are led to consider a scenario in which the chemistry involves significant reactions at the organic/mineral interface. Two accounts from areas outside coal chemistry lend support to our view. The first is geochemical work on the origins of petroleum by Hoering (17). The results and rationale are rather detailed, and they are discussed fully in Appendix A. In summary, Hoering reports anomalous incorporation of deuterium into hydrocarbons released from shale-bound kerogen upon hydrothermal pyrolysis in D_2O that we view as reconciled only through action directly at the kerogen/shale interface. The parallel to our results with coal is compelling and suggests similarity in both chemical structure and chemistry.

The second occurs in research tied to work in highway degradation, as reported by Ensley and coworkers (18a,b). Prepared bitumen/clay interface samples were studied and showed a distinct interphase volumes with a striated structure, were disrupted by water, and were most likely regions rich in H-bonding between the polar fractions of the bitumen and the mineral surface. At present, little is known about the specific chemical speciation within the region (19). The disruptive action of water seen here is that we suggest plays a role in the beneficial effects of water pretreatment observed for coal, and can act as a probe into coal structure.

Our findings could have considerable impact on both fundamental coal chemistry and the practical aspects of coal use. The potential effects on the understanding of coal behavior derive from the fact that clays are known to inhibit free radical reactions. For example, the free radical polymerization of methyl methacrylate is fully suppressed in the presence of montmorillonite, even at temperatures as high as $100^\circ C$ (20). Given the presence of a variety of clays in the mineral phase in coals, this striking factor raises the question of the significance of free radical chemistry generally in coal and supports the view put forward in this proposal that the overall structure of coal, including the nature of its reactive centers, can be viewed from a new perspective.

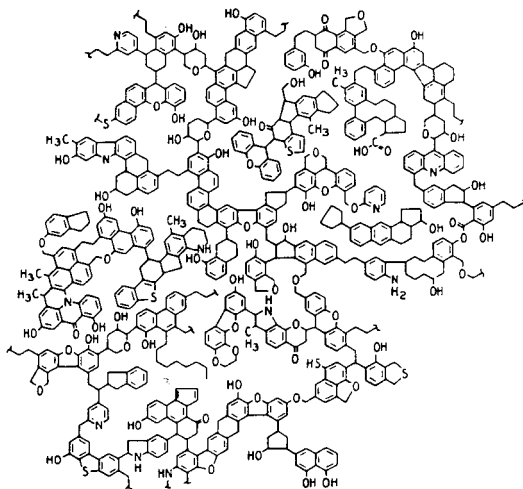
The implications for practical ends can also be noted. We can presume that the polar, heteroatom-containing portions of the organic phase migrate over geologic time to the mineral surfaces, resulting in heterogeneous distribution of the N- and S-containing components within the organic phase, concentrated around the mineral microinclusions. Just such a slanted distribution has been noted for the organic material removal from Green River shale (21). Thus, properly conducted hydrothermal pretreatment or microbial/enzymatic delamination at the mineral/organic interface could lead to separation of heteroatom components and mineral material.

Finally, geochemical studies on the role of the mineral matrix in the pyrolysis of petroleum yielding kerogen show that hydrocarbon retention and char formation correlates with the clay content of the matrix (22). Increased clay levels lead to greater carbonization. By extension, we suggest that the presence of ultrafine clay inclusions in coal contribute to the retrogressive chemistry operative during liquefaction and mild gasification and indeed may be the major factor in such action.

REFERENCES

1. J. H. Shinn, *Fuel*, 63 (9), 1187-1196 (1984).
2. D. S. Ross, T. K. Green, R. Mansani, and G. P. Hum, *Energy and Fuels*, 1, 292-294 (1987).
3. a. R. M. Davidson, "Molecular Structure of Coal, Report No. ICTIS/TR 08, IEA Coal Research, London, 1980.
b. J. A. Gray and Y. T. Shah, in Reaction Engineering in Direct Coal Liquefaction, Y. T. Shah, Ed., Addison-Wesley Publishing Co., Reading, Mass., 1981, pp. 24-101.
4. R. M. Davidson, "Mineral Effect in Coal Conversion," Report No. ICTS/TR22, IEA Coal Research, London, 1983.
5. R. C. Neavel in Chemistry of Coal Utilization, Second Supplementary Volume, M. A. Elliott, ed., Wiley-Interscience/John Wiley and Sons, New York, 1981, pp. 121-122.
6. S. C. Mraw, J. P. DeNeufville, H. Freund, Z. Baset, M. L. Gorbaty, and F. J. Wright, in Coal Science, Vol. 2, J. Larsen, M. Gorbaty, and I. Wender, Eds., Academic Press, New York, 1983, pp. 1-26.
7. R. M. Allen and J. B. VanderSande, *Fuel*, 63, 24-29 (1984).
8. A. Meyer, D. Farin, and D. Avnir, *J. Am. Chem. Soc.*, 108, 7897-7905 (1986).
9. a. B. K. G. Theng, The Chemistry of Clay-Organic Reactions, John Wiley and Sons, New York, NY, 1974.
b. C. Breen, J. Adams, and C. Riebel, *Clays and Clay Minerals*, 33 275-284 (1985).
10. S. Towne, Y. Shah, G. Holder, G. Deshpande, and D. Cronauer, *Fuel*, 64, 883-889 (1985).
11. a. S. D. Brandes and R. A. Graff, *Am. Chem. Soc. Div. of Fuel Chemistry Preprints*, 32 (3), 385-393, (1987).
b. R. A. Graff and S. D. Brandes, *Energy and Fuels*, 1, 84-88 (1987).
12. P. R. Bienkowski, R. Narayan, R. A. Greenkorn, and K-C Chao, *Ind. Eng. Chem. Res.*, 26, 202-205 (1987).
13. D. S. Ross, T-C. Miin, and A. S. Hirschon, unpublished results.
14. M. Tarafa, J. Hunt, and I. Ericsson, *J. Geochem. Expl.*, 18, 75-85 (1983).
15. J. Espitalie, K. Makadi, and J. Trichet, *Org. Geochem.*, 6, 365-382, (1984).
16. I. F. Tupitsyn and V. I. Komarov, *Reakts. Sposobn. Org. Soedin.*, 6, 616-626 (1969).

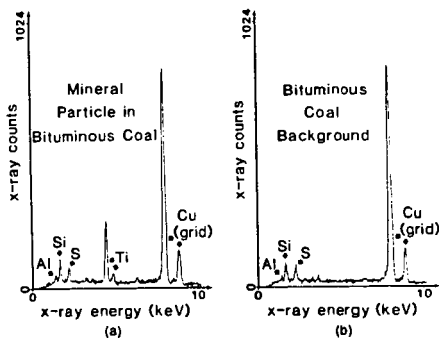
17. T. Hoering, *Org. Geochem.*, 5 (4), 267-278 (1984).
18. a. E. Ensley, H. Plancher, R. Robertson, and J. Petersen, *J. Chem. Ed.*, 55 (10), 655-658, (1978).
b. E. Ensley, *J. Appl. Chem. Biotechnol.*, 25, 671-682 (1975).
19. J. Peterson, personal communication.
20. Reference 9, p. 271.
21. J. McKay and M. Blanche, *Liq. Fuels Techn.* 3 (4), 489-521.
22. J. Espitalie, M. Medac, and B. Tissot, *AAPG Bulletin*, 64, 59-66 (1980).



SOURCE: J. H. Shinn, *Reactive Model of Coal Structure*, *Fuel* 63, 1190 (1984).

RA-320583-331

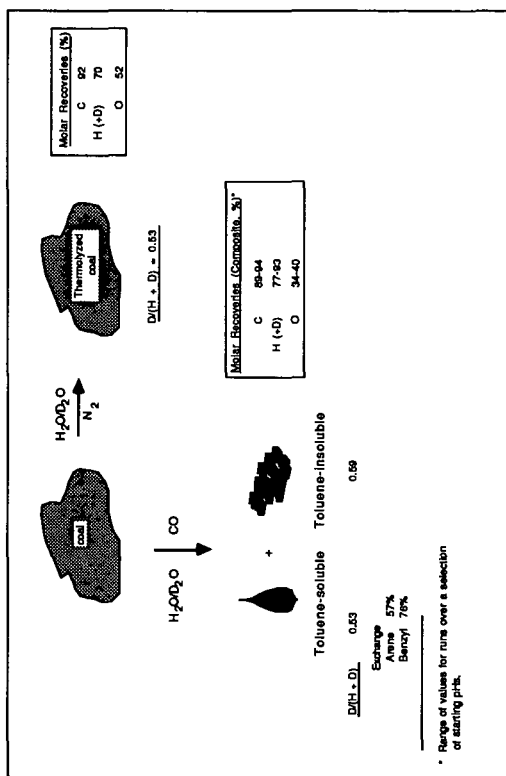
Figure 1. Model of bituminous coal structure.



SOURCE: R. M. Allen and J. B. VanderSande, *Analysis of Sub-Micron Coal Mineral Matter*, *Fuel* 63, 27 (1984)

RA-320583-332

Figure 2. Examples of x-ray spectra from bituminous sample.



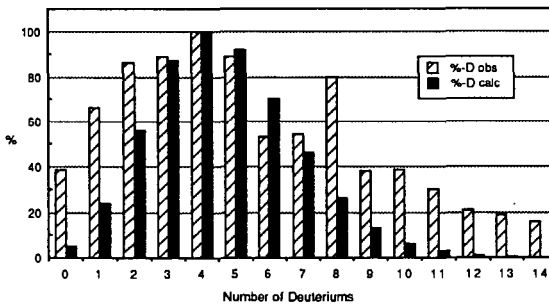
RA-20868-33

Figure 3. Coal studies at 400°C/20 min.

APPENDIX A

GEOCHEMICAL SUPPORT FOR THE PROPOSED COAL MODEL

Our proposition of a significant and reactive mineral/organic interface in coal is supported by a somewhat parallel set of results developed in research into petroleum formation by Hoering, who reported on pyrolyses of samples of previously extracted Messel shale (1). The pyrolyses were conducted in D_2O at $330^\circ C/3$ days, and they generated a series of saturated hydrocarbons resembling natural petroleum. The hydrocarbons were extensively deuterated. A portion of the product was a series of n-alkanes in the range of 14-30 carbon atoms, with each alkane containing distributions of isomers with 0 to more than 14 deuterium atoms. The maximum deuterium substitution was in the 4-6 range as shown in Figure A-1 for the C_{18} product, a profile representative of the entire suite of isolated alkanes.



Source: T. C. Hoering, *Org. Geochem.*, 5, 267-278 (1984).

Figure A-1. Deuterium distribution.

The distribution is broad, with the D_0 case nearly 40% of the D_4 material, and significant deuteration continues out to beyond D_{14} . The author ruled out the presence of preexisting, trapped alkanes, since in that case undeuterated product would have dominated the samples. Moreover, in control experiments in which the shale was purposefully spiked with an n-alkane, it was recovered virtually entirely untagged. The purposeful addition of a terminal n-alkene resulted in the recovery of about half the corresponding alkane, a curious result suggesting the presence of reducing chemistry, but with the product containing only small quantities of deuterium.

Thus, both preexisting alkanes or olefin precursors can be eliminated as origins of the multilabeled n-alkanes. Also ruled out on the basis of the deuterium isotope

distribution is their formation from thermal production of the corresponding n-alkyl radicals through kerogen pyrolysis, followed by a successive deuterium attachment chain. The distribution expected from such a process can be estimated by numerical simulation of sequential exchange, ignoring isotope effects which would be insignificant at these temperatures. The result, adjusted so that the maximum substitution is at C₄, is presented in Figure A-1, and it is considerably more narrow than the one observed, with the bulk of the substitution falling between C₂ and C₇. The calculated D₀ level is only about 10% of that observed, and virtually no substitution is expected beyond C₁₁.

The calculated profile is firm and applies to any sequential exchange mechanism which the rate is the same for all steps. Thus the considerably broader distribution observed in Hoering's data dictates either several different mechanisms operating in parallel, an unlikely proposition, or different precursors for each isotope isomer. We adopt the latter view here.

We suggest that alkane precursors exist at the mineral surface, attached to the surface over several points. Theng has discussed a similar situation for the adsorption of linear polymers on clay (2). D₂O then engages in some chemistry yet to be uncovered, releasing the alkane and creating a C-D bond at the point of attachment. The reducing chemistry noted for the case of the consumed alkene could play a significant role.

We propose, by extension, a similar scheme for coal. We envision mineral/organic attachment at the portions of the coal structure leading to benzylic positions following hydrothermal treatment.

REFERENCES

1. T. C. Hoering, *Org. Geochem.*, 5 (4), 267-278 (1984).
2. B. Theng, *Clays and Clay Minerals*, 30, 1-10 (1982).

AMPHOTERIC REACTIONS OF SUPERCRITICAL WATER WITH COAL MODELS

Akiko K. Horiuchi¹, Howard T. Fish¹ and Michael A. Mikita^{2*}

¹Department of Chemistry, University of Colorado at Denver
Denver, Colorado 80204

²Department of Chemistry, California State University Bakersfield
Bakersfield, California 93311

INTRODUCTION

For the past several years this laboratory has been studying water assisted coal liquefaction. Initial experiments were designed to determine whether water could replace all or part of the donor solvent in coal liquefaction [1]. More recent work has focused upon the chemical reactions of coal models in supercritical water [2].

In summary of our experiments with coal [1], high conversions of Illinois No. 6 (River King Mine) bituminous coal were obtained in minireactor experiments at modest temperatures with little or no hydrogen-donor solvents.

The use of water in liquefaction has also been studied by others. When used in combination with carbon monoxide and a suitable catalyst, water was a source of hydrogen for the reduction of coal [3,4]. Liquefaction under carbon monoxide, without an organic solvent, has also been carried out with slurries composed of coal and either water or aqueous base [5,6]. In some cases, water served to carry dissolved metal salts used as homogeneous catalysts as well as acting as the liquefaction medium [7]. In comparison with conventional organic liquefaction solvents, water is quite effective when used in combination with H₂S, in particular under synthesis gas rather than hydrogen [8]. Aqueous liquefaction using impregnated catalysts has also been combined with supercritical water distillation to separate the oil and asphaltene from the coal char residue [9]. The simple treatment of coal with supercritical water in the absence of hydrogen or catalysts renders a substantial portion of the treated coal extractable by tetrahydrofuran [10]. From these extraction studies, it is apparent that water is able to assist the diffusion and dispersion of liquefaction products and reactants.

In addition to these roles, water may directly participate as a reactant in the thermolytic chemistry of certain model compounds. In the presence of water, dibenzyl ether decomposes at 374°C by both pyrolytic and hydrolytic pathways [11]. The removal of nitrogen from heterocyclic compounds, such as isoquinoline, is accelerated in the presence of supercritical water [12]. Most recently, it was suggested

* Author to whom correspondence should be addressed.

that in the presence of supercritical water the hydrolysis of coal models proceeds through a transition state that is more polar than the reactants [13].

Taken together, these studies indicate that under various conditions, supercritical water may act as a good liquefaction medium, dissolve or extract coal-derived liquid products, promote the cleavage of certain bonds likely to be found in coal, provide hydrogen through the water-gas shift reaction, and possibly assist the contacting of coal with catalysts or hydrogen.

For the past year our efforts have centered upon the study of two distinct coal model compound systems with water under liquefaction conditions. This research is intended to further evaluate the chemical role of water above its critical temperature in the conversion of coal to a liquefaction product.

EXPERIMENTAL

Commercially available reagents were used without further purification. Bibenzyl (Aldrich), benzyl phenyl ether (TCI), and hydroquinone monobenzyl ether (Fluka) were analyzed for purity by gc/ms prior to use. All other models were synthesized from the commercially available substituted benzyl halides, with the exception of 2-bromo-p-toluic acetate which was synthesized from the reaction of diazomethane with 2-bromo-p-toluic acid. Reaction of the benzyl halides with triethylphosphite afforded the phosphonates which were in turn coupled via Wittig reaction with benzaldehyde or benzyl-ether-protected salicylaldehyde to form the substituted stilbenes and protected o-hydroxystilbenes respectively. Hydrogenation of the stilbenes over Pd/C afforded the desired products.

A five minireactor system [14] at the Pittsburgh Energy Technology Center was employed for all reactions with the bibenzyls. The bibenzyls (2.6 mmol) were reacted in the presence of 4.3 mL H₂O and/or D₂O solutions containing 2 mL n-pentanol as an internal standard per 93.4 mL H₂O or 100 mL D₂O. The reactors were purged with N₂ then submerged into a fluidized sand bath at 400 °C for 3 hours. The pressure of the reactants was not measured directly; using van der Waal's equation the partial pressure of water was estimated at 4290 psi. The density of the supercritical water was 0.10 g/mL. Once cooled, the reactors were washed several times with 5 mL dichloromethane. The resulting heterogeneous solutions were agitated for several days. Each organic layer was analyzed on DB1 capillary column using an HP #5790A gc and a HP #5970A MSD.

In the study of the benzyl phenyl ethers, 0.5 mmol of each model was reacted with 2.9 mL H₂O or D₂O (0.16 mmol) at 400 °C for forty minutes using a Parr # 4704 22 cc minireactor. The estimated pressure and water density in these reactions was 5900 psi and 0.13 g/cc. An internal standard was not employed in these studies and molecular oxygen was not excluded. Analysis was identical to that described above with the substitution of ether for CH₂Cl₂.

DISCUSSION

In the first study, a Hammett series of substituted bibenzyls and o-hydroxy bibenzyls were synthesized via Wittig reaction with subsequent hydrogenation. The substituents synthesized were p-NH₂, p-t-Bu, p-CH₃, H, m-CF₃, and p-CH₃O₂C.

Not surprisingly, thermolysis pathways dominated the observed products from these preliminary reactions of the substituted bibenzyls. Both the thermolysis products and recovered starting materials were observed to undergo deuterium exchange. The major products from all reactions with the bibenzyls and o-hydroxybibenzyls, along with the maximum number of deuterium incorporated into each, are compiled in Table 1.

With the simple bibenzyls, electron donating substituents were observed to enhance D-substitution into the recovered starting materials. D-exchange may be envisioned by either radical or ionic pathways as illustrated in Scheme 1. Ionic route B would be stabilized by electron donating groups, but alcohol products would be expected and these have not been observed. Ionic route C forms carbanion intermediates, hence electron withdrawing groups would be expected to stabilize the intermediates. Electrophilic aromatic substitution, illustrated via route A, would agree with the observed substituent effects, since electron donating groups would be expected to stabilize the intermediate arenium ions.

In the case of p-carboxylic acid methyl ester bibenzyl, demethylation and decarboxylation predominated with a deuterium substitution pattern suggestive of an ionic decarboxylation.

Comparison of the conversions of the o-hydroxy substituted bibenzyls in H₂O and D₂O suggested a primary isotope effect. This is an intriguing observation considering that thermolysis pathways again predominated.

The o-hydroxy bibenzyls exhibited more extensive deuterium exchange than with the simple bibenzyls, presumably due to the enhanced H(D)-atom transfer ability of the phenolic-H(D). The tautomerization pathway [15] contributed significantly to the product distribution with the o-hydroxy bibenzyls. The production of substituted ethylbenzenes also exhibited a

primary isotope effect suggesting that tautomerization is rate limiting.

2-Ethyl-4-substituted biphenyl ethers were also observed in some cases, presumably through the rearrangement of the respective substituted *o*-hydroxybibenzyls (Scheme 2.).

Cyclization of *p*-NH₂-, *p*-CH₃-, and *H*- *o*-hydroxy substituted bibenzyls to dibenz[b,f]dihydrooxepane was also observed. Two possible mechanisms for these transformations are illustrated in Scheme 3.

In our other preliminary study, benzyl phenyl ether (BPE) reactions pathways were complicated by the presence of molecular oxygen. For example, in addition to the thermolysis products phenol and toluene, autooxidation product benzaldehyde was also observed. Significant amounts of benzylalcohol and *o*-benzyl phenol were also produced. Both products can be explained through ionic reactions with water, although the former may also result from autooxidation.

Hydroquinone monobenzyl ether (HQMBE) also exhibited the expected thermolysis products hydroquinone and toluene, as well as the autooxidation product benzaldehyde. The tautomeric pathway was also important as evidenced by the significant production of benzylalcohol. The observed formation of catechol monobenzyl ether (CMBE) may also be simply explained by the recombination of phenoxy and benzoxy radicals, both requiring tautomerization for their generation. The deuterium substitution pattern of CMBE, however, suggests a fascinating mechanistic alternative. CMBE from reaction in D₂O exhibited its parent ion at 203 *m/e*, an increase of three from unsubstituted CMBE. Recovered HQMBE exhibited its parent at 201 *m/e*, indicating only one deuterium substitution. If the methylene protons were responsible for the additional exchange in CMBE, similar D-substitution patterns would be expected for both HQMBE and CMBE.

Two successive nucleophilic aromatic substitutions of D₂O with HQMBE would account for the observed substitution pattern. The first substitution would give resorcinol monobenzyl ether, followed by a more facile second to yield the thermodynamically preferred CMBE. This possibility is illustrated in Scheme 4.

The impact of these preliminary model compound studies toward an understanding of the organic chemical reactions of coal in supercritical water is striking. The observation that electron donating substituents favored D-exchange with the substituted bibenzyls supports our earlier suggestion [2] that electrophilic aromatic substitution by a proton for suitable aryl substituents is a possible alternative reaction pathway for coal in the presence of water. Even more dramatic is the possibility of nucleophilic aromatic substitution with water as suggested by the production and D-substitution pattern of CMBE. Such a reaction would be

consistent with the observed production of phenols during liquefaction.

The heterogeneous nature of coal requires that we view liquefaction as mechanistically complex. The results of this preliminary study suggest that the unique amphoteric character of water may present coal with reaction pathways unavailable under traditional liquefaction conditions.

ACKNOWLEDGMENTS

The minireactor expertise of Henry Davis is gratefully recognized, as is the encouragement and advice of Brad Bockrath. Financial support from the DOE (DE-FG22-85PC81544) and Oak Ridge Associated Universities is acknowledged.

REFERENCES

1. Blaustein, B.C.; Davis, H.M.; Friedman, S.; Illig, E.G.; Mikita, M.A. Am. Chem. Soc. Div. Fuel Chem. Preprints 1985, 30(2), 359.; Mikita, M.A. Bockrath, B.C.; Davis, H.M.; Friedman, S.; Illig, E.G. Energy Fuels 1988 (in press).
2. Mikita, M.A.; Fish, H.T. Am. Chem. Soc. Div. Fuel Chem. Preprints 1986, 31 (4), 56; Horiuchi, A.K. M.S. Thesis, University of Colorado at Denver, January, 1988; Fish, H.T. B.A. Honors Thesis, University of Colorado at Denver, December, 1987.
3. Appell, H.R.; Wender, I.; Miller, R.D. Chem. Ind. 1969, 1703.
4. Appell, H.R. Energy 1976, 1, 24.
5. Ross, D.S.; Blessing, J.E. Fuel 1978, 57, 379.
6. Ross, D.S.; Blessing, J.E.; Nguyen, Q.C.; Hum, G.P. Fuel 1984, 63, 1206.
7. Ross, D.S.; Nguyen, Q.C.; Hum, G.P. Fuel 1984, 63, 1211.
8. Stenberg, V.I.; Hei, R.D.; Sweeney, P.G.; Nowok, J. Am. Chem. Soc. Div. Fuel Chem. Preprints 1984, 29(5), 63.
9. Barton, P. Ind. Eng. Chem., Process Des. Dev. 1983, 22, 589.
10. Deshpande, G.V.; Holder, G.D.; Bishop, A.A.; Gopal, J.; Wender, I. Fuel 1984, 63, 956.
11. Townsend, S.H.; Klein, M.T. Fuel 1985, 64, 635.
12. Hoser, T.J.; Tiffany, D.M.; Li, Z.; McCarville, M.E.; Houghton, M.E. Fuel 1986, 65, 827.
13. Townsend, S.H.; Abraham, M.A.; Huppert, G.L.; Klein, M.T.; Paspek, S.C. Ind. Eng. Chem. Res. 1988, 27, 143.
14. Anderson, R. R.; Bockrath, B. C. Fuel 1984, 63, 329.
15. McMillan, D.F.; Orgier, W.C.; Ross, D.C. J. Org. Chem. 1981, 46, 3322.



Table 1. Major Products from the Reaction of Supercritical Water with

products	OH		X-C ₆ H ₄ -CH ₂ -CH ₂ -C ₆ H ₄ -R		X-C ₆ H ₄ -CH ₂ -CH ₂ -C ₆ H ₄ -R		X-C ₆ H ₄ -CH ₂ -CH ₂ -C ₆ H ₄ -R		starting materials		rearranged compound		epicis compound		high m. wt. compounds		
	OH	H	OH	H	OH	H	OH	H	OH	H	OH	H	OH	H	OH	H	
NH ₂	H ₂ O	0.22 ⁽¹⁾	-	0.16	-	0.56	-	0.062	-	0.84	-	Y	-	OB	-	OB	-
	D ₂ O	ND	ND	ND	0.21 ^{3D}	ND	0.12 ^{6D}	ND	1.44 ^{5D}	-	ND	ND	ND	OB	ND	OB	ND
CH ₃	H ₂ O	0.12	-	0.15	-	0.27	-	0.36	-	0.80	-	OB	-	OB	-	OB	-
	D ₂ O	ND	ND	ND	ND	ND	ND	0.053 ^{3D}	-	1.85 ^{6D}	-	DB	ND	OB	ND	OB	-
H	H ₂ O	0.009	-	0.08	-	0.10	-	0.32	-	1.01	-	OB	-	OB	-	ND	-
	D ₂ O	0.062 ^{3D}	ND	0.026 ^{4D}	ND	0.23 ^{6D}	0.13 ^{3D}	0.15 ^{3D}	0.13 ⁽²⁾	1.51 ^{7D}	2.39 ^{3D}	OB	ND	OB	OB	ND	ND
m-CF ₃	H ₂ O	ND	-	0.017	-	0.014	-	0.10	-	1.14	-	OB	-	ND	-	OB	-
	D ₂ O	ND	ND	ND	ND	0.069 ^{6D}	0.16 ^{2D}	0.053 ^{3D}	0.064 ^{2D}	1.34 ^{5D}	1.83 ^{2D}	OB	ND	ND	ND	OB	OB
CH ₃ O ₂ C	H ₂ O	ND	-	ND	-	0.13	-	0.083 ^(-3D)	-	-	-	ND	-	ND	-	OB	-
	D ₂ O	ND	ND	ND	ND	0.047 ^{6D}	0.18 ^{6D}	0.056 ^{5D}	0.14 ^(-3D)	0.021 ^(-3D)	0.13 ^{1D}	ND	ND	ND	ND	OB	ND

(1) The numbers are the ratios of pentanol/product, measured by the area under the GC peaks. ND: not detected. number D: the number of possible deuteriums incorporated. OB: observed. (2) experimental value x 1/2

Table 2. Products from the Reaction of Supercritical Water with Benzyl Phenyl Ether and Hydroquinone Monobenzyl Ether¹

From Benzyl Phenyl Ether

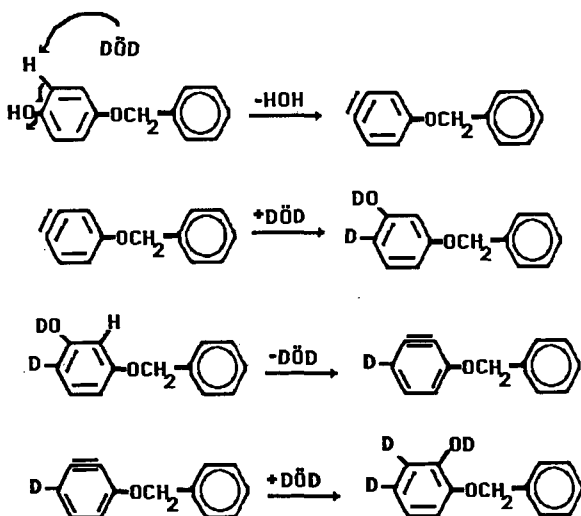
recovered BPE
phenol
benzaldehyde
benzylalcohol
o- or p- benzyl phenol
toluene

From Hydroquinone Monobenzyl Ether

recovered HQMBE
catechol monobenzyl ether
benzylalcohol
p-cresol
benzaldehyde
toluene

¹ Products are listed in the order of abundance as estimated from gc/ms. Quantitative experiments are in progress with these models.

Scheme 4. Suggested Mechanism for the Formation of Catechol Monobenzyl Ether



ADDITIVE EFFECTS OF SOLVENT REFINED COAL FRACTIONS AND
NITROGEN-CONTAINING AROMATIC COMPOUNDS ON THE
HYDROGENOLYSIS OF THE DIARYLMETHANE

Yoshio KAMIYA, Seiya KOYANAGI, and Shigeru FUTAMURA
Department of Reaction Chemistry, Faculty of Engineering, The
University of Tokyo, 7-3-1, Hongo, Bunkyo-ku, Tokyo, Japan 113

INTRODUCTION

The authors have already reported that solvent refined coal (SRC) promotes the hydrogenation of aromatic compounds in tetralin [1]. Further investigation has revealed that SRC not only donates its inherent hydrogen but mediates the hydrogen transfer from tetralin to the diarylmethane [2]. The structural analysis of SRC was monitored, and some imino linkages in SRC were suggested to be the possible moiety shuttling hydrogen.

This paper intended to clarify the action mechanism of SRC in hydrogen transfer reactions and presented the SRC-mimetic hydrogenolysis of the diarylmethane.

EXPERIMENTAL

Materials

The diarylmethanes were synthesized according to the method described in the previous paper [3]. The additives and the solvents were commercially purchased and purified if necessary by the conventional methods. The SRC's were prepared from Miike (C, 84.5%, H, 6.1%), Akabira (C, 83.4%, H, 6.2%), and Yallourn (C, 67.4%, H, 5.9%) coals as follows: each coal (20 g) was reacted in tetralin (60 ml) at 400 °C at 9.0 MPa of hydrogen for 30 min. The reaction mixtures were subjected to Soxhlet extraction for 15 h using tetrahydrofuran (THF) as solvent. The residues obtained in the reduced distillation (3 mmHg, at 250°C, for 1 h) of the THF extracts were used as SRC in the hydrogenolysis of the diarylmethane. Column chromatographic separation of SRC derived from Miike Coal, which would be designated only as SRC unless otherwise noted, was carried out by eluting ether-MeOH (98:2 v/v) (SRC-1, 54 wt%), THF (SRC-2, 38 wt%), and pyridine (SRC-3, 8 wt%). Table 1 shows the elemental analyses of the SRC's.

Hydrogenolysis of the diarylmethane

Prescribed amounts of a diarylmethane, a hydrogen donor solvent, and an additive were put into a 90 ml stainless, magnetically stirred autoclave. After being pressurized by 2.0 MPa of hydrogen, the autoclave was heated up to the reaction temperature and maintained during the prescribed period of time. After the reaction, the autoclave was cooled to room temperature by an electric fan.

Product analysis

The products were identified by GC-MS. Quantitative analysis of the products recovered with THF was carried out by GC. Structural change of SRC was monitored by means of ¹H- and ¹³C-NMR, GPC, and elemental analysis.

RESULTS AND DISCUSSION

Solvent-dependent additive effect of SRC

As Table 2 shows, addition of SRC promotes the hydrogenolysis of di(1-naphthyl)methane. The additive effect does not seem to depend on SRC origin, reflecting their similar chemical compositions [4], but it is greatly affected by the hydrogen donatability of solvent. On addition of Yallourn or Akabira SRC (0.40 g), about a two-fold larger conversion of di(1-naphthyl)methane is obtained in tetralin than in 1-methylnaphthalene, respectively.

The additive effect of recovered SRC is also solvent dependent (Table 3). In tetralin, recovered SRC and raw SRC show the comparable additive effect and the similar conversion of tetralin is obtained. Under the reaction conditions, the rearrangement of tetralin to 1-methylindan also occurred and the molar ratio of 1-methylindan/naphthalene was 3.05 in the absence of SRC. This ratio decreased to 0.86-1.10 in the presence of SRC. These facts suggest that the initial transfer of α -hydrogen in tetralin would occur more selectively in the presence of SRC since 1-methylindan is derived only from 2-tetralyl radical and isomerization of 1- and 2-tetralyl radicals is negligible [5]. Recovered SRC, which was partly dehydrogenated in the first reaction, showed the comparable promoting effect compared with raw SRC. This fact suggests that hydrogen shuttling could occur on the dehydrogenated moiety in the recovered SRC. On the other hand, in 1-methylnaphthalene, a modest conversion of 9-benzylphenanthrene is obtained in the presence or absence of recovered SRC, suggesting that almost no hydrogen transfer proceeds from 1-methylnaphthalene or decalin to dehydrogenated SRC.

Tables 4 and 5 show that the conversion of di(1-naphthyl)methane does not necessarily correlate with the amount of H_{α} in the fractionated SRC. The weight ratio of hydrogen consumed in the hydrogenolysis of di(1-naphthyl)methane/ H_{α} lost from SRC falls on 1.8-5.7, which reinforces that some bondings in dehydrogenated SRC act as a hydrogen shuttler rather than a hydrogen donor as shown in Scheme 1.

Structural analysis of SRC

Figure 1 shows the GPC profiles of the raw and recovered SRC's. Basically, similar molecular size distributions were obtained before and after the reactions for all the SRC's although the structures sensitive to light at 260 nm grew for SRC-3 after the reaction. These findings indicate that decomposition and condensation of SRC are negligible under the reaction conditions. Thus, the recovered SRC was analyzed by ^{13}C -NMR in order to detect the chemical structures shuttling hydrogen in dehydrogenated SRC. Figure 2 shows the ^{13}C -NMR spectrum of the recovered SRC soluble in THF. The carbon atoms at 139 and 154 ppm can be assigned to the azomethine carbons and the carbons at the ipso-positions in phenolics.

This finding urged us to investigate into the hydrogen shuttling

abilities of 3-ring azaaromatic compounds, which have been sparsely documented in the literature. They were also compared with the hydrogen shuttling abilities of some aromatic hydrocarbons.

Hydrogen shuttling effect of some azaaromatics

As Table 6 shows, the hydrogenolysis of 9-benzylphenanthrene is remarkably promoted on adding acridine or phenanthridine. However, 1- and 4-azaphenanthrenes are less effective additives.

These facts can be interpreted on the basis of the hydrogen accepting abilities of these hydrogen shuttlers. It has been reported in our previous paper [3] that the superdelocalizability gives a good measure to estimate the reactivity of the diarylmethane toward hydrogenolysis, and the quantum chemical data in Table 7 also indicate that phenanthridine and acridine are more hydrogen accepting than quinoline, 1-azaphenanthrene, and 4-azaphenanthrene (eqs. (1) and (5) in Fig. 3).

The other factor controlling the effectiveness of the shuttler is the hydrogen releasing ability of the hydroaromatic radical derived from the hydrogen transfer to the azaaromatic compound. If the hydroaromatic radical is more susceptible to further hydrogenation (eqs. (3) and (7)) rather than to hydrogen donation to 9-benzylphenanthrene (eqs. (2) and (6)), considerable amounts of hydrogen from tetralin is consumed in vain to afford the dihydro-derivatives of the shuttlers. The perhydro-derivatives of the azaaromatics are considered to show the lower hydrogen donatability than the hydroaromatic radicals. Direct and indirect overhydrogenation reactions of the shuttler such as disproportionation of these dihydro-derivatives formed in eqs. (3) and (7) are undesirable to promote the smooth hydrogen shuttling.

The azaaromatics used in this study showed the different reactivities toward hydrogenation of their own aromatic nuclei. In the tetralin-acridine system, 87% of acridine was converted to afford 9,10-dihydroacridine and 1,2,3,4-tetrahydroacridine in 18 and 60% selectivities, respectively. As for the tetralin-quinoline system, 52% of quinoline was converted to 1,2,3,4- and 5,6,7,8-tetrahydroquinolines in 69% combined selectivity. On the other hand, in the tetralin-phenanthridine system, the phenanthridine conversion was not more than 10% and 5,6-dihydrophenanthridine was formed in 60% selectivity. Therefore, there is no correlation between the 9-benzylphenanthrene conversion and the amounts of the perhydro-azaaromatics formed during the reactions.

These facts reveal that phenanthridine could act as an effective hydrogen shuttler since overhydrogenation of phenanthridine and adduction of phenanthridine derived compounds into the hydrogenolysates from 9-benzylphenanthrene occur only to a small extent, contrasting with the cases of quinoline-1,2,3,4-tetrahydroquinoline mixtures [6-8].

CONCLUSION

We have shown that SRC and phenanthridine are effective hydrogen shuttlers. The effectiveness of phenanthridine can be ascribed to its facile hydrogen shuttling ability and higher stability under the reaction conditions.

REFERENCES

1. Y. Kamiya, H. Ohta, A. Fukushima, M. Aizawa, and T. Mizuki, Proc., Int. Conf. on Coal Science, Pittsburgh, p. 195 (1983).
2. S. Koyanagi, S. Futamura, and Y. Kamiya, Proc., Conf. on Coal Science, Fukuoka, p. 206 (1987).
3. S. Futamura, S. Koyanagi, and Y. Kamiya, Fuel, in press.
4. Y. Kamiya, J. Fuel Soc. Jpn., 57, 12 (1978).
5. J. A. Franz and D. M. Camaioni, Fuel, 59, 803 (1980).
6. R. I. McNeil, D. C. Young, and D. C. Cronauer, Fuel, 62, 806 (1983).
7. J. W. Hellgeth, L. T. Taylor, and A. M. Squires, Proc., Int. Conf. on Coal Science, Pittsburgh, p. 172 (1983).
8. F. J. Derbyshire, G. A. Odoerfer, and D. D. Whitehurst, Fuel, 63, 56 (1984).

Table 1 Elemental Analyses of the Fractionated Miike SRC's.

	SRC raw	SRC-1	SRC-2	SRC-3
Eluent		Ether-Methanol	THF	Pyridine
Weight %		54	38	8

C	86.9%	87.6 %	87.1%	78.3 %
H	5.8	5.9	6.0	5.6
N	1.2	1.1	1.1	1.7
O(diff.)	5.9	5.4	5.8	11.5
Ash	0.23			2.9
H/C	0.80	0.81	0.83	0.86

Table 2 Additive Effect of SRC on the Hydrogenolysis of Di(1-naphthyl)methane (DNM).

SRC (Amount/g)	Conv. of DNM	Yield of 1-MN	Solvent (Conv.)	Sel. of 1-MI
None	8%	6%	Tet(8%)	47%
Yallourn(0.1)	13	9	Tet(8)	38
Akabira (0.1)	12	9	Tet(8)	40
Yallourn(0.4)	38	19	Tet(12)	26
Akabira (0.4)	38	20	Tet(12)	26
Miike (0.4)	36	19	Tet(16)	27

None	5		1-MN(0.3)	
Yallourn(0.1)	9		1-MN(3)	
Akabira (0.1)	6		1-MN(2)	
Yallourn(0.4)	17		1-MN(6)	
Akabira (0.4)	20		1-MN(7)	

DNM 7.5 mmol, solvent 75 mmol, 460°C, initial hydrogen pressure 2.0 MPa, 30 min.
 Yallourn SRC (C, 83.3%, H, 6.0%), Akabira SRC (C, 86.2%, H, 6.3%), 1-MN = 1-Methylnaphthalene, Tet = Tetralin, 1-MI = 1-Methylindan.

Table 3 Additive Effect of the SRC's Derived from Miike Coal on the Hydrogenolysis of 9-Benzylphenanthrene (9-BP).

Solvent	Additive	Conv. of 9-BP	Selectivities of			Conv. of Solv.	Select. of	
			Tol	Phen	DHP		MI	NpH
Tetralin	none	19%	71%	70%	13%	13%	61%	20%
Tetralin	raw SRC	52	83	88	11	20	38	44
Tetralin	recovered SRC	42	86	75	11	18	44	40
Decalin	none	17	-	75	Nd	7		
Decalin	raw SRC	35	-	90	3	7		
Decalin	recovered SRC	20	-	77	Nd	7		

9-BP 7.5 mmol, solvent 75 mmol, SRC 0.4 g, 430°C, initial hydrogen pressure 2.0 MPa, 5 h.

Tol = Toluene, Phen = Phenanthrene, DHP = 9,10-Dihydrophenanthrene, MI = 1-Methylindan, NpH = Naphthalene. Nd = Not detected.

Table 4 Additive Effect of the Fractionated SRC's Derived from Miike Coal on the Hydrogenolysis of Di(1-naphthyl)methane.

Additive SRC	Conv. of DNM	Yield of 1-MN	Conv. of Tet	Select. of MI
none	8%	6%	8%	47%
SRC raw	36	19	16	27
SRC-1	49	33	16	26
SRC-2	41	19	17	26
SRC-3	30	25	10	26

DNM 7.5 mmol, tetralin 75 mmol, SRC 0.4 g, 460°C, initial hydrogen pressure 2.0 MPa, 30 min.

Table 5 Amounts of Hydrogens Bonded to α -Position on the Aromatic Ring in 0.4g of the SRC Derived from Miike Coal.

	H α /mg in Original SRC A	H α /mg in Recovered SRC B	Consumed H α /mg A - B	Amounts of Hydrogen Needed in the Hydrogenolysis of DNM/mg
SRC raw	7.83	4.83	3.00	5.40
SRC-1	7.83	4.92	2.91	6.15
SRC-2	5.92	4.74	1.18	4.95
SRC-3	3.60	3.02	0.58	3.30

Table 6 Hydrogen-shuttling effect of the azaaromatics in the hydrogenolysis of 9-benzylphenanthrene (9-BP).

Additive (mmol)	Conv. of 9-BP(mol%)	Selectivities(mol%)			Tetralin conv. (mol%)	Select.(mol%)	
		Tol	Phen	DHP		1-MI	NpH
None	19	71	70	11	13	61	20
Quinoline (7.5)	22	76	73	9	19	47	36
1-Azaphenanthrene(7.5)	23	71	a)	8	18	50	27
4-Azaphenanthrene(7.5)	23	69	72	7	17	52	28
Phenanthridine (3.3)	25	74	74	9	20	47	34
Phenanthridine (7.5)	33	65	73	7	23	43	39
Phenanthridine (15.0)	36	72	76	8	26	33	44
Phenanthridine (22.5)	37	70	75	8	28	38	43
Acridine (7.5)	40	76	79	b)	25	37	53

9-BP 7.5 mmol, tetralin 75 mmol, reaction temperature 430°C, initial hydrogen pressure 2.0 MPa, reaction time 5 h.

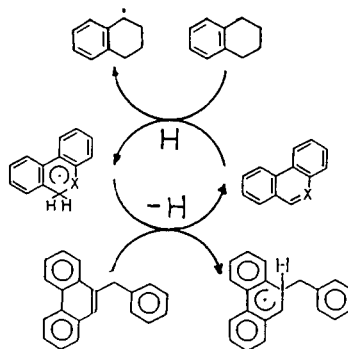
a) Not calculated owing to the inseparability of phenanthrene and the perhydro-derivatives of 1-azaphenanthrene.

b) Not calculated owing to the inseparability of DHP and the tetra- and octahydroacridines.

Table 7 Superdelocalizability values (Sr(R))^{a)} of some azaaromatics.

Aromatic compounds	Sr(R) (position)
Quinoline	1.0527 (4-)
	1.0059 (5-)
Phenanthridine	0.9905 (8-)
	1.1045 (6-)
	0.9993 (7-)
1-Azaphenanthrene	0.9936 (5-)
	1.0214 (4-)
4-Azaphenanthrene	1.0009 (5-)
	1.0151 (5-)
	0.9926 (6-)
Acridine	1.4732 (9-)
	1.2738 (10-)
	1.0564 (4-)
9-Benzylphenanthrene	0.9803 (9-)

a) Superdelocalizability values toward radical reactions, which were calculated according to the Simple Hückel Theory.



Scheme 1 Hydrogen Shuttling Cycle.

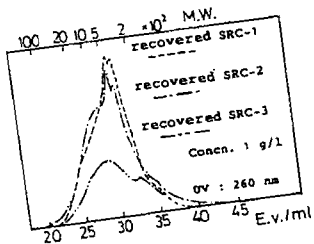
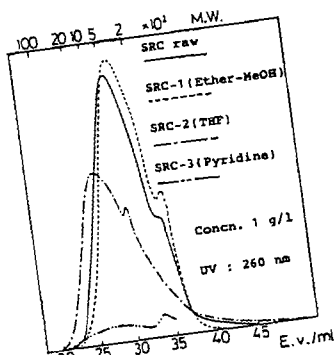


Fig. 1 GPC Profiles of the SRC's.

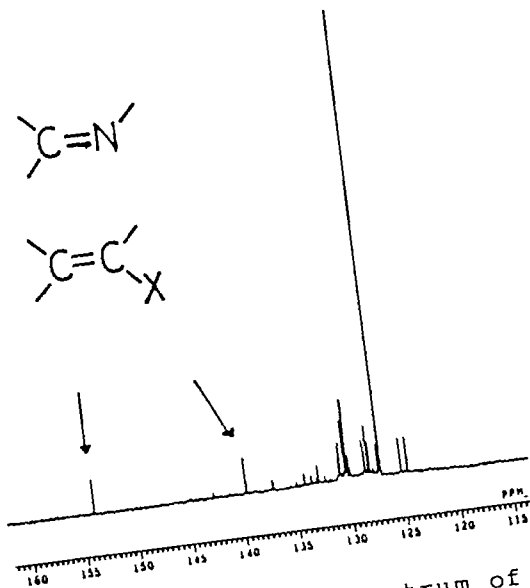
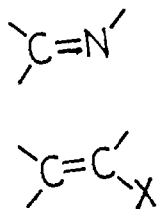
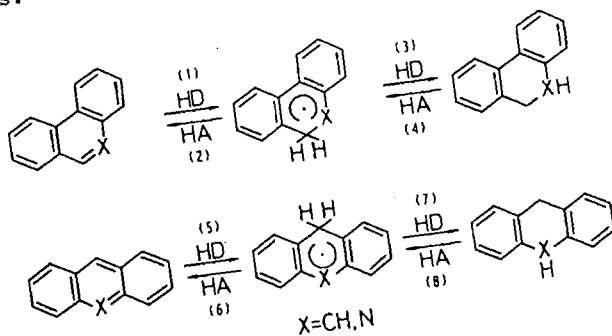


Fig. 2 ^{13}C -NMR Spectrum of the Recovered SRC Soluble in THF-d_8 .



HD=Hydrogen donor
HA=Hydrogen acceptor

Fig. 3 Hydrogen Transfer Processes where the 3-ring Aromatic Compounds and Their Dihydro-derivatives are Involved.

COAL GEL CHEMISTRY 2. COAL LIQUIFACTION BY BINARY SOLVENT SYSTEM

Testuo Aida, Motohiko Satoh, Yasuhumi Shimoura, Masayuki Fujii

Department of Industrial Chemistry
Faculty of Engineering
Kinki University in Kyushu
11-6 Kayanomori, Iizuka, Fukuoka 820, JAPAN

INTRODUCTION

Although the importance of the accessibility of hydrogen donor solvents like a tetralin into coal matrix has long been emphasizing to the primary coal liquifaction of coal(1), not many efforts have been devoted to the study on the penetration mechanism of penetrants into coal, and developing practical devices of improving the accessibility.

Recently, we developed a new method for accurately measuring both the dynamic and equilibrium solvent swelling behaviors of coal(2), and revealed that the coal behaved as a molecular sieve which discriminated among molecules diffusing into the pore system of coal on the basis of size, shape and functionality.

Based on our observations, tetralin is one of the penetrants which show significantly low degree of penetration rate into coal matrix, probably because of its steric hindrance. Meanwhile during the investigation of the synergistic effect on the solvent swelling of coal in the binary solvent system, of which one component was more less bulky than other, we also found that the steric requirement of coal could be released by forming "Coal Gel" under such condition.

Here we report the results of the study on the improvement of the accessibility of hydrogen donor like a tetralin into coal matrix, and the primary liquifaction of coal by using binary solvent systems.

EXPERIMENTAL

The swelling measurements were carried out as described into previous paper (2). Coal, Illinois #6, used in thses studies were from the Ames Laboratory Coal Library. Prior to use, the coal was ground, sized, dried at 110°C overnight under vacuum and stored under nitrogen atmosphere. The solvents were distilled by ordinary procedures before use.

The coal liquifaction were carried out by using a stainless steel tubing micro-autoclave(8.0ml capacity). A typical coal liquifaction procedure is as follows: Coal(500mg; 50-60 mesh) and solvent(3.0ml) were taken into the auto-clave with a stainless ball. After a nitrogen gas was bubbled through the mixture, it was heated for 2 hours in an electric oven maintaining temperature at 370 °C, which was shaken for 3 minutes with 30 minutes intervals. After the re- action, the autoclave was cooled at room temperature, and carefully opened. The content was washed out with 50ml of distilled pyridine, and the mixture was immersed in an ultrasonic cleaning bath for 2 hours. Then it was filtered through 3 μ m Millipore-filter.

RESULT AND DISSCUSSION

1. Swelling of Illinois #6 Coal in Hydrocarbons

Table 1 shows the swelling data of Illinois #6 coal obtained with hydro- carbon solvents.

These data clearly indicate that there is a steric component to the swell- ing rate for solvent penetration of the coal matrix, for example, in the branch- ed isomer, that is, in iso-propylbenzene the coal swelled aproximately 9 times slower than in n-isomer. On this point of view, it seems to be quite understand- able that t-butylbenzene or tetralin are belonging to the slowest group of the penetrants. Actually, the molecular model of tetralin shows that the saturated ring system in this molecule makes a significant steric barrier upon the planer aromatic ring system.

2. Swelling of Illinois #6 Coal in Binary solvent System

Figure 2 shows the Illinois #6 coal in benzene / tetralin solvent system. There is a obvious synergistic effect on the equilibrium swelling ratio (Q-value) which means that the addition of certain amount of benzene to tetralin can make a significant increase of tetralin in the coal matrix in terms of the quantity and the penetration rate. As we reported previously (3), in this case also, the relative concentrations of each components, benzene and tetralin, in the supernatant of the coal-solvent mixture was varied through swelling, that is, the concentration of benzene was sharply decreased at the initial stage of swelling and then maintained almost constant value which was a little below the initial concentration.

These observations clearly indicate that less bulky benzene molecule penetrated predominantly into coal matrix, and formed so-called "Coal Gel" which will not possess such rigid steric requirement as the raw coal.

Table 2 shows the equilibrium swelling ratio (Q-value) obtained various solvent systems. It is obvious that the net volume of tetralin in the coal matrix in the binary solvent systems are significantly increased compared to tetralin alone.

3. Coal Liquifaction by Binary Solvent System

Figure 2 shows the pyridine solubles obtained from the liquifaction by the various binary solvent systems, in which the results by tetralin and THQ (1,2,3,4-Tetrahydroquinoline) are also illustrated.

Here, some arguments may come to the penetration mechanism at the liquifaction temperature, 370°C, and the swelling measurement temperature, 21°C.

However the results shown in this Figure strongly suggest that the enhancements of the yields of the liquifaction of coal were caused by the improvement of the accessibility of hydrogen donor like tetralin.

A curious phenomenon was also observed in the case of pyridine / tetralin system in which the addition of pyridine seemed to have induced a negative

effect on the coal liquifaction. It is quite interesting contrast to our common understandings that pyridine was one of the best solvents in the coal chemistry, i.e., extraction or swelling.

ACKNOWLEDGEMENTS

We wish to thank Professors Toshihisa Maeshima and Masakuni Yoshihara for their useful discussions and encouragements.

REFERENCES

1. M. B. Neuworth, D. Gray, "Fundamental Aspects of Primary Coal Liquifaction", Contractor Report, SAN85-7211, 1985
2. T. Aida T. G. Squires, Prepr. Pap.-Am. Chem. Soc., Div. Fuel Chem., 30, 95 (1985)
3. T. Aida, Y. Shimoura, M. Fujii, T. G. Squires, M. Yoshihara, T. Maeshima, Prepr. Pap.-Am. Chem. Soc., Div. Fuel Chem., Previous paper presented at this meeting (1988)

Table 1. Swelling Behaviors of Illinois #6 Coal in Hydrocarbons ^{a)}

Hydrocarbons	Q-Value ^{b)}	V _{Ret.} ^{c)}
n-Pentane	1.022	0.8
Benzene	1.046	1.0 ^{d)}
Ethylbenzene	1.038	4.0
n-Propylbenzene	1.024	17.0
i-Propylbenzene	1.008	153
t-Butylbenzene	1.003	> 10 ³
Tetralin	1.003	> 10 ³

a) 100-200 mesh, measured at 21 °C

b) After one month

c) Rate Retardation Factor : $V_i(\text{benzene}) / V_i(\text{hydrocarbome})$

d) $V_i = 2.73 \times 10^{-4} \text{ min.}^{-1}$

Table 2. Swelling of Illinois #6 Coal in Binary Solvent System ^{a)}

Solvent System	Q - Value ^{b)}
Tetralin	1.003
n-Pentane	1.022
n-Pentane / Tetralin ^{c)}	1.025
Benzene	1.046
Benzene / Tetralin ^{c)}	1.030
Methanol	1.323
Methanol / Tetralin ^{c)}	1.110
Pyridine	2.734
Pyridine / Tetralin ^{c)}	1.482
NMPDN ^{d)}	3.063
NMPDN ^{d)} / Tetralin ^{c)}	1.625

a) Coal: 100-200 mesh, measured at 21°C

b) After one month

c) Solvent / Tetralin (1 : 2 vol.)

d) N-Methylpyrrolidinone

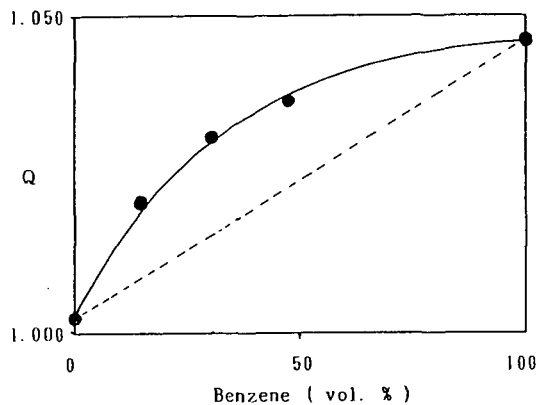


Figure 1 Swelling of Illinois #6 Coal in Benzene / Tetralin System (Coal: 100-200 mesh, 21 °C)

Solvent System	Pyridine Soluble (%, dmmf)		
	0	50	100
Tetralin		43	
THQ ^{a)}			93
n-Pentane / Tetralin ^{b)}		74	
Benzene / Tetralin ^{b)}		71	
Methanol / Tetralin ^{b)}			83
Pyridine / Tetralin ^{b)}		10	
NMPDN ^{c)} / Tetralin ^{b)}			92

- a) 1,2,3,4.-Tetrahydroquinoline
- b) Solvent / Tetralin (1:2 vol.)
- c) N-Methylpyrrolidinone

Figure 2. Coal Liquifaction (Coal : 50-60 mesh, 370 °C, 2 hrs.)

STUDIES OF COAL PYROLYSIS AND COAL
EXTRACTION USING IN-SITU ESR SPECTROSCOPY

Mohindar S. Seehra
Physics Department, West Virginia University
Morgantown, West Virginia 26506

ABSTRACT

Important features of recent results on the pyrolysis and solvent extraction of American coals (H/C between 0.55 and 0.81) using in-situ ESR spectroscopy are presented. In the pyrolysis studies, the temperature variation of the free radical density between 25°C and 650°C establishes the presence of four distinct stages in about a dozen coals studied. Extraction of the coals with N-Methyl Pyrrolidone shows an inverse correlation between percentage extraction and room temperature free radical density. Significance of these results is discussed.

INTRODUCTION

Electron spin resonance (ESR) due to free radicals in coals was discovered in 1954 [1,2]. Since then, some correlations between the ESR parameters of the free radicals in coals and various properties of coals (such as rank [3], heteroatom content [4], liquefaction [5] and coking behavior [6]) have been reported. Recently we developed a heated gas-flow system in which in-situ ESR spectroscopy of samples could be carried out between room temperature and 650°C. This apparatus has been used to study pyrolysis behavior of about a dozen American coals with atomic H/C varying between 0.55 and 0.81. One of the most significant results of this study is the discovery of four distinct temperature regions in these coals from the temperature variation of the free radical density [7-9]. Following this work, Fowler et al [10] have confirmed the presence of similar regions in some British coals. Although some explanations have been advanced for these regions in earlier studies [7-10], additional discussion on these temperature regions or stages as well as some details of the high-temperature apparatus used in this work, are presented in this paper. We also examine the use and limitations of ESR in the studies of the extraction and de-ashing of coals with N-Methyl pyrrolidone (NMP), a subject of considerable current interest [11,12].

THE HIGH TEMPERATURE CAVITY SYSTEM

A block diagram of the high-temperature microwave cavity system used for the in-situ ESR studies for temperatures to 650°C is shown in Fig. 1. All parts with prefix 'WG' are made of quartz and they were obtained from Wilmad Glass Co. The system uses a flowing nitrogen gas passing over a heater (powered by a Variac) to heat the sample located in a TE₁₀₂ mode cavity. To obtain various temperatures, first the voltage in the Variac is adjusted. Additional control is provided by adjusting the gas pressure and flow rate. Temperature stability of ±1°C was obtainable in the whole temperature range studied. Because of the isolation provided by the quartz dewar, the external temperature of the TE₁₀₂ cavity, even at 650°C sample temperature, did not exceed 50°C. Since a thermocouple cannot be placed inside the cavity next to the sample during an ESR experiment, a separate experiment was carried out to calibrate the thermocouple placed at the sample position, but without making ESR measurements. Finally, a screw is used (Fig. 1) to keep the microwave coupling to the cavity constant at different sample temperatures. Further details of this apparatus are given elsewhere [13]. Details of the other experimental procedures are given in our earlier publications [7-9].

RESULTS AND DISCUSSION

A typical variation of the free radical density N_s with temperature for a representative coal (Matewan coal with $H/C \approx 0.71$) is shown in Fig. 2. The data is from Ref. 9 and it shows the four distinct temperature regions mentioned above in the Introduction. In region 1 ($\sim 25^\circ$ - 250°C) and in region 3 ($\sim 400^\circ$ - 600°C), the spin concentration N_s increases with increasing temperatures whereas in region 2 (250° - 400°C) and region 4 ($>600^\circ\text{C}$), N_s decreases with increasing temperatures. Although the locations of these regions or stages differ slightly from coal to coal on the temperature scale and relative changes in N_s with temperature are also different for different coals, the qualitative features of the variation of N_s noted above are the same for all of about dozen coals studied in our work [7-9]. Recent work of Fowler et al [10] on some British coals have yielded similar variations for N_s even though their experiments were done under slightly different conditions viz. flowing N_2 gas through the samples versus evacuated samples in our case. Note that N_s represents the spin density corrected for the Curie variation [7-10].

As an aid to interpret the results, we show in Fig. 2b the schematic variation of the CO_2 internal surface area as a function of the charring temperature for a bituminous coal (Saline County, Illinois) [14] and in Fig. 2c the temperature variation of the sample weight for a British coal [10]. Although the results in Figs. 2a, 2b and 2c are for different coals, sufficient evidence exists [7-10,14] that qualitatively features of these curves are the same for different coals. It is evident from Fig. 2 that these different measurements all point to the distinct temperature stages first highlighted in our ESR work [7]. We now critically examine the nature of these distinct stages.

The average activation energies, evaluated for stage 1 assuming Arrhenius variation is ≈ 4 kcal/mol. Since the magnitude is much smaller than that necessary for bond fission [3,15], stage 1 probably corresponds to the decomposition of the substituted groups, resulting in the release of CO_2 , CO and H_2O [7,15]. Some decrease in the weight of the samples observed in this region supports this finding. Fowler et al [10] have noted that increase of N_s in their samples may partly be due to desorption of oxygen. However this cannot be the case in our samples because our samples were evacuated and vacuum sealed prior to experiments.

The decrease in N_s with increasing temperatures in stage 2 is perhaps one of the more interesting results of these recent studies. Several mechanisms could contribute to a decrease in N_s :

- a. Recombination of free radicals by thermally activated mobility within the pore network;
- b. Previously stable radicals become very reactive, become short-lived and hence are not observed;
- c. Quenching of radicals by internally transferred hydrogen; and
- d. Decrease in the surface area leading to the blocking of the pore network and recombination.

It is noted that there is no significant loss in the sample weight in this region so that some kind of quenching or recombination of the radicals is most likely the cause for the decrease of N_s . We tend to disfavor explanation b since if this was the mechanism, a broadening of the ESR lines should be observed. This certainly is not the case [9]. Explanations a and d are related and they receive strong support from the observed decrease in the surface area

(Fig. 2b and Ref. 14). It is noted that stage 2 is observed even in treated samples [10] and in residues and extracts after treatment with NMP [12] although the location of the peaks and valleys are affected by the treatment. Swelling of coals which is observed in many coals in this temperature range is partially due to release of gases such as H_2 and may cause the observed decrease in the internal surface area. H_2 gas is known to quench the free radicals [16]. Thus it is very likely that explanations a, c, and d are simultaneously operative in stage 2, perhaps at different levels in different coals.

In stage 3, the sharp decrease in the sample weight accompanied by the sharp increase in N_s has been interpreted to be due to breaking and rearrangement of the aromatic rings of the coal structure. The activation energies determined from the temperature dependence of N_s are in the range of 15 kcal/mol [9]. These energies are sufficient for bond fission [3,15]. The fact that the volatiles in this stage contain free radicals further supports this interpretation [17]. In stage 4, the decrease in N_s is most likely to be recombination of free radicals and formation of chars.

The use of ESR spectroscopy in coals treated with solvents such as NMP [12] has led to considerable understanding of the mechanism of coal extraction with these solvents. There is strong evidence that treatment with NMP extracts exinites and to a lesser degree vitrinites present in coal samples whereas the inertinites and ash are left in the residue [12]. This conclusion is partly based on the observation of the inverse correlation between N_s and percent extraction as exinites have lower free radical density [12].

CONCLUDING REMARKS

In this paper we have discussed some of the recent results obtained with in-situ ESR spectroscopy on coal pyrolysis and coal extraction. Although many interesting results have been obtained and we have now the capability of measuring ESR due to free radicals at high temperatures at time intervals of one minute or so, the short-lived free radicals are not observed by the steady-state ESR spectroscopy. The next advance in this area is likely to come from an understanding of the role of short-lived free radicals in coal conversion processes.

ACKNOWLEDGEMENTS

The author thanks C. W. Kruse for bringing Ref. 14 to his attention. Technical assistance of S. E. Mullins and B. Ghosh is acknowledged. This work was supported in part by a grant from the U.S. Department of Energy through the Consortium for Fossil Fuels Liquefaction Science, G. Huffman, Director.

REFERENCES

1. D.J.E. Ingram, J.G. Tapley, R. Jackman, R.L. Bond, and A.R. Murnaghan, *Nature (London)* 174, 797 (1954).
2. J.J. Uebersfeld. *J. Phys. Radium* 15, 126 (1954).
3. H.L. Retcofsky, J.M. Stark and R.A. Friedel, *Anal. Chem.* 40, 1699 (1968).
4. H.L. Retcofsky, M.R. Hough, M.M. Maguire and R.B. Clarkson in 'Coal Structure', (Eds. M.L. Gorbaty and K. Ouchi) *Am. Chem. Soc. Advances in Chem. Series*, 192, 1981.
5. L. Petrakis and D.W. Grandy, 'Free Radicals in Coals and Synthetic Fuels' (Elsevier, 1983).
6. M. Sakawa, T. Uno, and Y. Hara, *Fuel* 62, 585 (1983).
7. M.S. Seehra, B. Ghosh, and S.E. Mullins, *Fuel* 65, 1315 (1986).
8. B. Ghosh and M.S. Seehra, 'Proc. Third Annual Pittsburgh Coal Conf. 1986 (Pittsburgh Coal Conf. MEMS, One Northgate Square, Greensburg, PA 15601) pp. 704-716.
9. M.S. Seehra and B. Ghosh, *J. Anal. Appl. Pyrolysis* 13, 209 (1988).
10. T.G. Fowler, K.D. Bartle, and R. Kandiyoti, *Fuel* 66, 1407 (1987).
11. K. Renganathan, J.W. Zondlo, E.A. Mintz, P. Kneisl, and A.H. Stiller, *Fuel Process. Tech.* (in press).
12. M.S. Seehra, B. Ghosh, J.W. Zondlo, and E. Mintz, *Fuel Process. Tech.* (in press).
13. S.E. Mullins, M.S. Thesis, West Virginia University, 1987 entitled 'A High Temperature Electron Spin Resonance Cavity System and Coal Pyrolysis Studies'.
14. C.W. Kruse and N.F. Shimp, *Coal Processing Tech.* 7, 124 (1981).
15. G.R. Gavalas, 'Coal Pyrolysis', Elsevier 1982.
16. G. Srinivasan and M.S. Seehra, *Fuel* 61, 1249 (1982); *ibid* 62, 792 (1983).
17. C.J. Chu, R.H. Hauge, and J.L. Margrave, *Am. Chem. Soc. Div. Fuel Chem. Prepr.* p. 87 (1986).

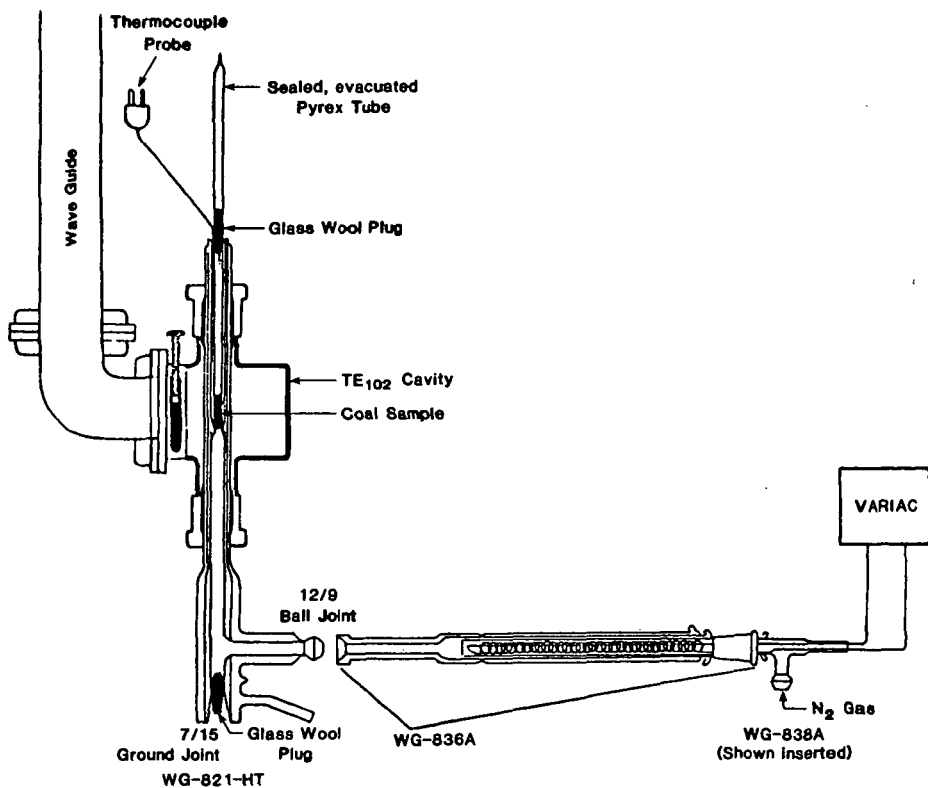


Fig. 1. A block diagram of the high-temperature microwave cavity system for in-situ ESR studies to 650°C with $\pm 1^\circ\text{C}$ stability. Components labelled with prefix 'WG' are made of quartz and they were obtained from Wilmad Glass Co. (see text for details).

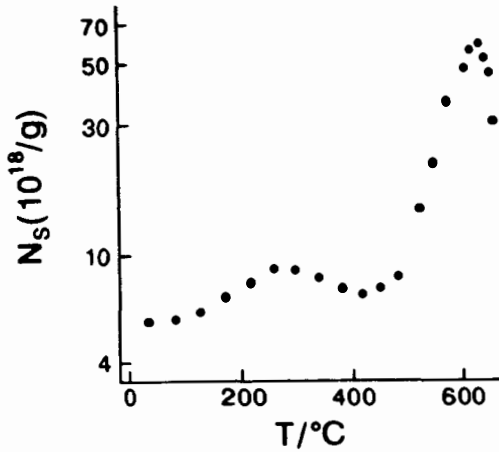


Fig. 2a. Free radical density N_s vs temperature for Matewan coal (Based on Ref. 9).

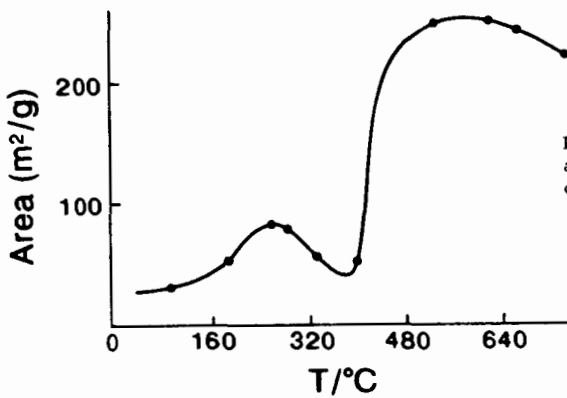


Fig. 2b. Internal CO₂ surface area vs temperature for a coal (Based on Ref. 14).

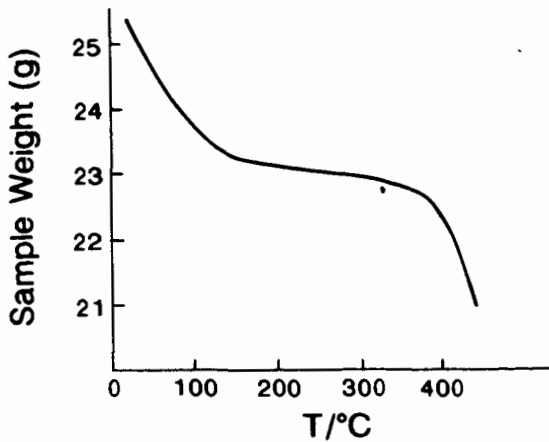


Fig. 2c. Sample weight vs temperature for a British coal (Based on Ref. 10).

THE IMPACT OF LIQUEFACTION SOLVENT COMPOSITION ON HYDROGEN UTILIZATION EFFICIENCY

Ripudaman Malhotra and Donald F. McMillen,

Department of Chemical Kinetics,
SRI International, Menlo Park, CA 94025

INTRODUCTION

Hydrogen utilization efficiency in coal liquefaction is important not only because of the direct cost of H_2 , but more particularly because of the cost of the high pressure equipment that is required to hydrogenate solvent and coal structures even in the presence of catalysts. The effects of solvent composition on H-utilization efficiency would most readily be obtained from batch autoclave studies, where solvent composition can most easily be treated as an independent variable. However, such data are scarce because the rate of coal conversion is often the primary, if not the only, observable addressed.

In previous mechanistic work directed at understanding the modes of bond scission available for relevant coal structures, we observed experimentally that the selectivity and efficiency with which donatable hydrogen is used to cleave aryl-alkyl linkages in coal surrogates is highly dependent on the degree of hydrogenation of the donor (1-3). The observed variations in efficiency were well reproduced by a mechanistic numerical model incorporating the various competing H-transfer processes (3). The basic trend elaborated by the model is that an increase in the level of polycyclic aromatic hydrocarbon in the solvent can increase the efficiency of H-utilization markedly, at a minor expense in H-transfer rate. Conversely, solvents which are very low in the fully aromatic PCAH component tend to transfer hydrogen faster, but do it less discriminately, such that a much smaller fraction of the hydrogen transferred goes to produce hydrogenolysis, and more goes to simple ring hydrogenation. At that time we proposed that this trend in efficiency could have substantial implications for actual coal liquefaction, but we had no obvious examples at hand to cleanly support this assertion. The recent results of Mochida and coworkers (4) provide a very clear illustration of the relevance of our earlier projections. This demonstration of relevance includes the premise on which these conclusions were based, namely that H-transfer-induced bond scission plays a substantial role in coal liquefaction. In this paper we discuss Mochida's results in light of our earlier findings, and elaborate on the interactive effects of the H-donor and acceptor components of liquefaction solvents.

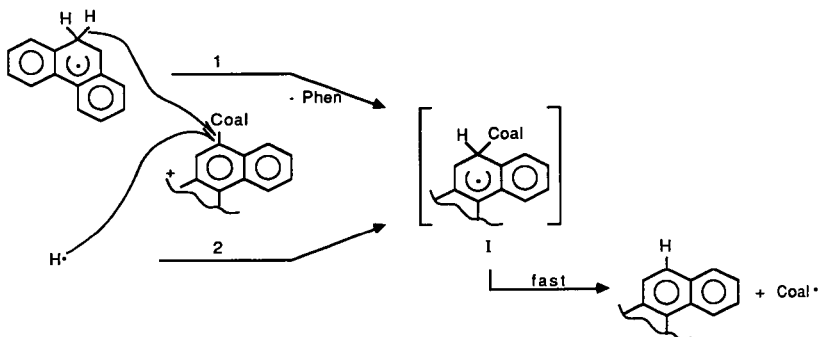
RESULTS AND DISCUSSION

Mochida et al. recently described the liquefaction of an Australian brown coal in tetrahydrofluoranthene (THFL), a donor solvent, containing varying amounts of fluoranthene (FL), a non donor (4). Their results show that although the conversion rates decrease as FL is added to the reaction mixture, the selectivity to oils (vs. gases) goes up somewhat, and the efficiency of H-utilization for oil production increases substantially. In Table 1 are shown the yields reported by Mochida for conversion in two media: 100% THFL and in a mixture of 75% THFL and 25% FL. In each case, the values shown are those reported at the time of maximum oil yield.

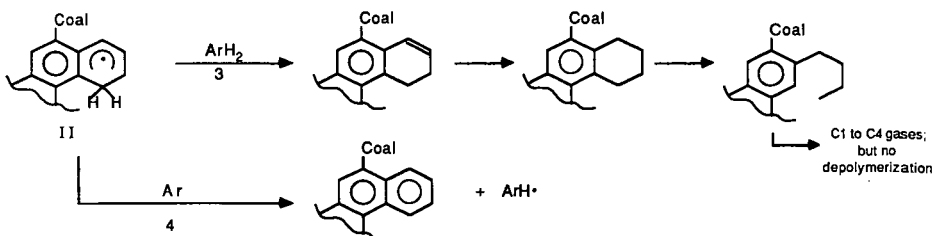
Replacement of 25% of the donor THFL with an equal amount of the non donor FL in the starting solvent increases the oil yield by five percentage points at the "expense"

of the gas yield. Substantially more pronounced is the impact of FL addition on the H-utilization efficiency (the ratio of oil produced to THFL consumed). As Table 1 shows, this value increases by 60%.

The origin of this change in efficiency cannot be understood without understanding the modes of H-transfer that lead to hydrogenolysis and/or hydrogenation. For this purpose, it is necessary to review some of our earlier findings. First, we can make the general statement that a shift in the utilization of hydroaromatic hydrogen could not occur without there being a shift in the mode of H-transfer. Specifically, if the addition of free H-atoms to positions on aromatic clusters bearing linkages (Reaction 1) were not in competition with the recently elucidated (1,2,5,6) radical hydrogen-transfer process (Reaction 2), there would be no basis for such a shift.



In Figure 1, we show previously presented (3) experimentally observed and numerically modeled H-utilization efficiency data for dinaphthylmethane cleavage. The reactions depicting the efficiency-determining competition in H-transfer processes are shown below:



It is not sufficient to consider merely the manner of formation of the ipso-substituted cyclohexadienyl radical I, because this intermediate, once formed at coal conversion temperatures, has an extremely short lifetime before elimination of virtually any linkage (as Coal·). In other words, cleavage will result no matter how I was formed.

Efficiency is determined by what happens to all of the radical species produced by H-transfer to positions not bearing linkages, II. When the concentration (and effectiveness) of polycyclic aromatic hydrocarbons that can act as hydrogen acceptors, transferring H-atoms back from non-ipso radicals, is low, then the non-ipso radicals are more likely to abstract a second hydrogen (e.g., from hydroaromatic in an "over hydrogenated" solvent). This dihydro intermediate is very reactive and will quickly be reduced to a tetrahydro intermediate. The tetrahydro intermediate can then receive additional hydrogens to open the aliphatic ring and crack off the 4-carbon chain as light hydrocarbons. In the example shown, this would mean that 6 or more hydrogens were consumed and no linkages were broken.

In contrast, when the concentration of H-acceptors is sufficient, the otherwise wastefully transferred hydrogen is recovered from the non-ipso radicals by the bimolecular RHT process, regenerating the hydrogen carrier radicals ArH^{\cdot} , so that the hydrogen transfer activity is maintained and there can be another chance at transfer to an ipso position. Ideally, this could result in having the only irreversible H-transfer being that to positions bearing linkages. In fact, the observed and computed hydrogen utilization efficiencies shown in Figure 1 indicate that, at least in the model system, a utilization efficiency approaching 90 to 100% can be achieved by merely adjusting the degree of hydrogenation.

When the original model compound studies were performed several years ago, we were surprised to observe that not only did the rate of hydroaromatic consumption go down when the solvent initially contained a significant amount of the respective aromatic, but that the absolute amount of hydroaromatic remaining at various reaction times could actually be larger when starting with less!

The final point to be recalled from our earlier studies is (as mentioned above) that the increase in H-utilization efficiency is achieved at some expense in terms of reaction rate. In the case of the data in Figure 1, when the efficiency showed a six-fold increase from 15% to 90%, the cleavage rate declined by about 60%. Closer examination of Mochida's data, as discussed below, shows that all of these trends are observed in the real coal liquefaction system.

Figure 2 shows the gas, oil, asphaltene, preasphaltene, and residue yields observed by Mochida as a function of time, when the starting solvent contained no fluoranthene, and when it contained 25% fluoranthene (4). In the 0% FL case, the oil yield develops faster, and the residue disappears more quickly, but in the 25% FL case, the more slowly developing oil yield reaches a 8% higher value at its maximum (which is at 30 min rather than 10 min), and the gas yield is only about 2/3 of that produced when the starting solvent is 100% THFL. This moderate advantage that results from starting with 25% FL becomes quite marked when the ratio of oil yield to THFL consumption is computed, revealing, as shown above in Table 1, a 60% increase in H-utilization efficiency.

The evolution of the solvent composition for these same two cases also shows the curious trend that there is equal or greater THFL remaining when the starting solvent contained less. For example, at 20 minutes the THFL concentration in the recovered solvent is 30% when starting with pure THFL and 35% when the starting with only 75% THFL. The extent of crossover is small and could easily be assigned to experimental scatter, were it not for the fact that similar crossovers were also observed in our studies. The faster THFL decline is associated with a greater rate of production of perhydrofluoranthene. Thus in Mochida's case, as in our earlier model system studies, the absence of a significant initial concentration of PCAH allows multiple H-transfers and full reduction of some of the hydroaromatic species; one can infer that similar reduction without cleavage, followed by ring opening and gas production, are also occurring within the coal structures themselves.

A year ago, we presented a similar explanation (7) for excessive gas production when high temperature excursions occurred during coal hydrolysis as reported by Gorbaty and Maa (8). In this case the effectiveness of the PCAH systems as H-acceptors evidently decreased as a result of increasing temperature, thereby allowing greater ring reduction and ring opening. The chemistry we proposed was criticized as being excessively speculative. We find it gratifying to note that in the present case, careful analysis by Mochida of the recovered liquefaction solvents provides direct evidence for the anticipated wasteful reduction of aromatic systems.

Finally, we wish to suggest that the trend in H-utilization efficiency noted here is not merely a fortuitous result of scattered behavior. In an earlier publication, Mochida et al. described in less detail the liquefaction of three subbituminous coals in the fluoranthene solvent system (9). For two of the coals, a decrease in the starting THFL content from 100% to 67% resulted in an oils plus asphaltenes yield decrease of only 3%. Although THFL consumption was not detailed, given that the decreases in THFL consumption found in the more recent studies on brown coals were generally on the order of 40 to 45%, it can be presumed that in the case of subituminous coals too, the decrease in THFL consumption was much more than 3%. Thus, a trend in H-utilization efficiency similar to that observed for the brown coal probably also occurred for the subbituminous coals. Despite the fact that concern with conversion rate has tended to overshadow consideration of H-utilization efficiencies, other examples undoubtedly exist. For example, Derbyshire et al. earlier reported increased conversions in tetralin/pyrene mixtures as compared to pure tetralin (10). Although they did not report the consumptions of hydroaromatic, it once again is very likely that consumption decreased upon addition of pyrene. Similarly, more recent results of Cassidy et al (11) showing a substantial increase in absolute oil yields upon partial replacement of tetralin with pyrene probably also reflect increased H-utilization efficiency. Thus, we anticipate that a more thorough examination of the literature will provide many other examples.

We recognize that the apparent advantage of lower THFL concentration cannot be expected to transfer unchanged from the batch autoclave to continuous units. For example, the somewhat longer time required for disappearance of the THF-insoluble residue in the 75% THFL case (Figure 2b) could have a detrimental impact under large-scale continuous processing conditions, where persistence of an insoluble phase in the preheater could exacerbate coking on heat-transfer surfaces.

SUMMARY

The recent results of Mochida and coworkers, showing that modest decreases in conversion rate are accompanied by very substantial increases in hydroaromatic hydrogen utilization efficiency when 25% of the hydroaromatic in the starting solvent is replaced by the corresponding aromatic, provide significant confirmation of projections we had made earlier. These predictions were based on the premise that solvent-mediated hydrogenolysis of strong bonds plays an important role in coal liquefaction, and they required an understanding of the role of competitive H-transfer processes in these hydrogenolyses.

ACKNOWLEDGEMENT: Support for this work by the Pittsburgh Energy Technology Center, U.S. Department of Energy, under Contract No. DE-FG22-86PC90908 is gratefully acknowledged.

REFERENCES

1. McMillen, D. F.; Malhotra, R.; Chang, S.-J.; Nigenda, S. E., Am. Chem. Soc., Div. Fuel Chem. Prep., 1985, 30(4), 297.
2. McMillen, D. F.; Malhotra, R.; Hum, G. P.; Chang, S.-J., Energy and Fuels, 1987, 1, 193.
3. McMillen, D. F., Malhotra, R.; Nigenda, S. E., "Solvent-Mediated Hydrogenolysis in Coal Liquefaction," Final Report, Contract No. DE-FG22-84PC70810, Pittsburgh Energy Technology Center, U.S. Department of Energy, July 1987, p. 36.
4. Mochida, I.; Yufu, A.; Sakanishi, K.; Korai, Y., Fuel, 1988, 67, 114.
5. McMillen, D. F.; Malhotra, R.; Chang, S.-J., Fleming, R. H.; Ogier, W. C.; Nigenda, S. E., Fuel, 1987, 66, 1611.
6. Billmers, R.; Griffith, L. L.; Stein, S. E., J. Phys. Chem. 1986, 90, 383.
7. McMillen, D. F.; Malhotra, R.; Nigenda, S. E., Am. Chem. Soc., Div. Fuel Chem. Prep., 1987, 32(3), 180.
8. Gorbaty, M. L.; Maa, P. S., Am. Chem. Soc., Div. Fuel Chem. Prep., 1986, 31(4), 5.
9. Mochida, I.; Kishino, M.; Sakanishi, K.; Korai, Y.; Takahashi, R., Energy and Fuels, 1987, 1, 343.
10. Derbyshire, F. J.; Varghese P.; Whitehurst, D. D., Fuel, 1982, 61, 859.
11. Cassidy, P. J.; Grint, A., Jackson, W. R.; Larkins, F. P.; Louey, M. B.; Rash D.; Watkins, I. D., Proceedings of the International Conference on Coal Science, Elsevier, 1987, p. 223.

Table 1

EFFECT OF REPLACEMENT OF PART OF TETRAHYDROFLUORANTHENE (H-DONOR) BY
FLUORANTHENE (NON-DONOR) ON EFFICIENCY OF H-UTILIZATION AND SELECTIVITY TO OILS

THFL Content	PRODUCT YIELD*	
	100%	75%
Gas	18	13
Oil	63	68
Asph.	13	14
PA + Res.	6	5
Oil Yield	1.1	1.7
THFL Consumption	1.1	1.7

* Optimal yield for coal conversion at
450°C/N₂/Solvent:Coal 3:1

Data from Mochida, 1988

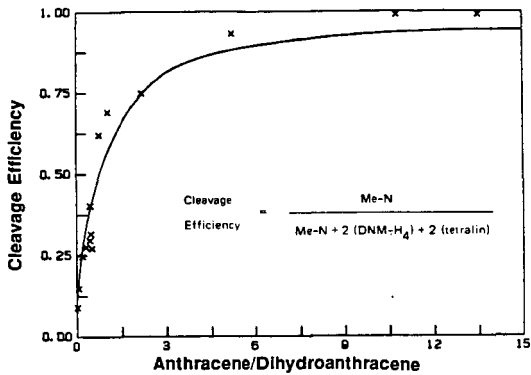


Figure 1. Experimental and Computed cleavage efficiency as a function of aromatic/hydroaromatic ratio

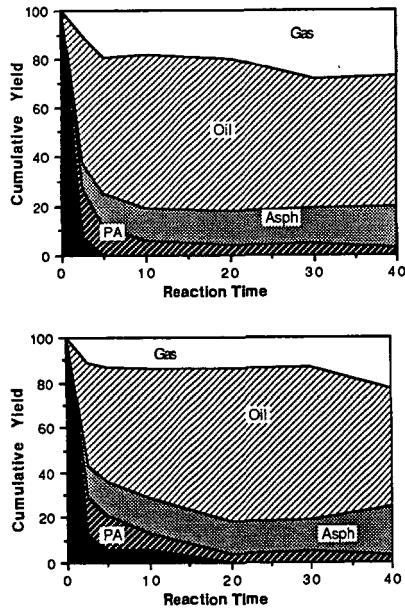


Figure 2. Product yields from conversion of an Australian Brown Coal In (a) 100% tetrahydrofluoranthene, and (b) a 75/25 mixture of tetrahydrofluoranthene and fluoranthene.

Data from Mochida, 1988

INVESTIGATION OF LIQUEFACTION MECHANISMS USING MOLECULAR PROBES

B.C. Bockrath, K.T. Schroeder, and M.R. Smith*

U.S. Department of Energy
Pittsburgh Energy Technology Center
Pittsburgh, PA 15236

*Chemistry Department
Bethany College
Bethany, WV 26032

INTRODUCTION

The mechanisms of coal liquefaction have been investigated using 1,3-dimethylnaphthalene and decalin as molecular probes. These two pure compounds have been added to various mixtures composed of a coal, a liquefaction solvent, and a high molecular weight alkane. In all cases, the amount of the probes added to the reaction mixture of coal, solvent, and alkane is small enough that the probes themselves are unlikely to perturb the reaction chemistry to a measurable degree.

The mixtures were heated in small autoclaves to liquefaction conditions, and the products recovered for analysis by quantitative gas chromatography. From the analysis of the products from the added probes, it is possible to draw conclusions about the relative amount and kind of intermediates that were created by the liquefaction conditions. For example, cis-decalin is transformed to the equilibrium mixture of the cis-and trans-isomers by the abstraction of hydrogen from either tertiary position by a free radical (1,2). The extent to which the equilibrium has gone to completion is then a measure of the exposure of decalin to radicals of sufficient reactivity to abstract the tertiary hydrogen. In the case of 1,3-dimethylnaphthalene, it is the monomethyl products that are of particular interest. Dealkylation of aromatic compounds is known to proceed under liquefaction conditions by the attack of free hydrogen atoms (3,4) or by the transfer of a hydrogen atom from a reactive donor (5). The total amount of demethylation is then a measure of the exposure of 1,3-dimethylnaphthalene to the total of free hydrogen atoms plus hydrogen atom donors. The use of the 1,3-isomer also allows the selectivity of the attack of hydrogen atoms to be measured. Loss of the methyl group from the 1-position leaves 2-methylnaphthalene as the product, whereas loss of the methyl group from the 3-position leaves the 1-methylnaphthalene as the product. The ratio of these easily separated isomers is then a measure of the weighted average of the selectivities of the entire population of hydrogen atom donors to which the probe is exposed.

In the present application of this approach, it is of particular interest to probe the effect of using petroleum residua as the liquefaction solvent in conjunction with coal. A combination of coal and resid was selected that has previously been used at the Pittsburgh Energy Technology Center for detailed evaluation of coprocessing schemes (6). The results

described below show that the interaction of coal and residua may lead to a reaction environment wherein the exposure of the probes to free radicals is enhanced over that expected based on additive behavior alone. The addition of coal, in particular, also has a very large influence on the selectivity of demethylation of dimethylnaphthalene.

EXPERIMENTAL

The 8-gram reaction mixtures contained 2.5% cis-decalin, 2.5% 1,3-dimethylnaphthalene, 0-20% Illinois No. 6 coal, 0-20% Maya atmospheric tower bottoms (ATB), and 57-95% n-octacosane or n-dotriacontane as solvent. The 40-mL reactors were pressurized to 1200 psig with hydrogen, heated to 425°C within 5-6 minutes by plunging them into a preheated fluidized sand bath, and held at temperature for 15, 60, or 180 minutes. The reaction products were washed from the reactors with tetrahydrofuran, and the soluble products were analyzed by quantitative capillary gas chromatography using internal standards. Selected samples were analyzed by GC/MS. The proximate and ultimate analyses of the coal and ATB are given in Table 1.

RESULTS AND DISCUSSION

The isomerization of cis-decalin is initiated by the free radical abstraction of the tertiary bridgehead hydrogen. Subsequent hydrogen transfer to the near planar radical intermediate leads to a mixture of cis- and trans-decalin. Thus, decalin can be used as a probe for radical activity in general, since its isomerization is initiated by any radical capable of abstracting the tertiary hydrogen. Since the isomerization is reversible, the ratio of decalin isomers eventually approaches its equilibrium value. If the rates of isomerization are constant over time, the rate of approach to equilibrium can be described by the expression for first-order reversible reactions

$$\ln \left(\frac{A_0 - A_e}{A - A_e} \right) = kt \quad (1)$$

where A_0 is the initial mole percent of cis-decalin, A_e is the equilibrium mole percent, A is the mole percent at time t , and k is the pseudo-first-order rate constant. Added radical sources will increase the pseudo-first-order rate constant and thus increase the rate of equilibration. Furthermore, if the added source provides over time a stable concentration of radicals of constant reactivity, the rate of equilibration should be well fit by Equation 1. To test this supposition, the extent of equilibration was measured after 15, 60, and 180 minutes without an additive and with either coal or petroleum residuum.

The time dependence of the decalin isomerizations is shown in Figure 1. The linear regression results are given in Table 2. The value of A_e was calculated by extrapolating the results of Schucker (7) to 425°C. The expected equilibrium ratio is 5.0, or about 83% trans-decalin. The large effect of added Illinois No. 6 coal is evident even at 15 minutes. The increase in the rate constant is striking; it becomes 50% larger when 10% coal is added. Both the ATB and the coal give good straight-line relationships. Thus, first-order reversible kinetics is a good approxima-

tion to the actual rate, and the efficiency of the hydrogen abstraction is not changing appreciably with time. This indicates that a steady-state radical activity is reached early in the reaction and maintained.

Of the benefits claimed for coprocessing, the synergism between the coal and residua leading to higher conversions for the mixtures than for either alone is especially intriguing (6). A chemical basis for this activity was sought in the total radical activity as measured by the cis-decalin isomerization. To accurately predict the expected activity of mixtures of coal and residua, the influences of coal concentration and ATB concentration on the extent of equilibration at 60 minutes were determined independently. These results, plotted as a function of the weight fraction squared, are shown in Figure 2. The dependence on concentration squared was determined empirically; considerable curvature was apparent when linear correlations with concentration were attempted. Linear regression analysis for the coal data gave

$$\ln \left(\frac{A_0 - A_e}{A - A_e} \right) = 0.32 + 24.9 [\text{Coal}]^2 \quad (2)$$

where A_0 , A_e , and A are as defined in Equation 1. The regression analysis of the ATB data gives

$$\ln \left(\frac{A_0 - A_e}{A - A_e} \right) = 0.30 + 13.1 [\text{ATB}]^2 \quad (3)$$

Both sets of data should, and do, share a common intercept.

Equations 2 and 3 define the dependence of the extent of decalin equilibration in the presence of only ATB or only coal. If there is no interaction between the coal and ATB, then the total isomerization will be given by the sum of the contributions of the coal, ATB, and background. Thus, Equation 4 should predict the extent of decalin isomerization after 60 minutes if no synergism or inhibition is present.

$$\ln \left(\frac{A_0 - A_e}{A - A_e} \right) = 0.31 + 13.1 [\text{ATB}]^2 + 24.9 [\text{Coal}]^2 \quad (4)$$

The 0.31 in this equation is the average of the intercepts of Equations 2 and 3.

A parity plot of experimental data and the predicted results is shown in Figure 3. The open circles represent the data already presented in Figure 2 for the ATB and coal in the absence of one another, which were used to derive the Equation 4. The solid circles represent the data obtained from experiments using mixtures of coal and ATB. At low total concentrations, no difference between the experimental and the predicted extent of isomerization is seen. At moderate concentrations, a significant increase in the extent of isomerization above that predicted by the sum of individual effects becomes apparent. An enhanced steady-state activity is attained for these mixtures of Maya ATB and Illinois coal. The synergism observed in the conversion of the coal and ATB (6) may be related to the enhanced radical activity displayed by these mixtures.

The isomerization of decalin is a non-specific indicator of free radical activity, since any radical of sufficient energy can abstract the tertiary hydrogen. In contrast to this probe for overall activity, the demethylation of 1,3-dimethylnaphthalene is specific for hydrogen atom activity.

The free radical hydrocracking of 1,3-dimethylnaphthalene (DMN) proceeds via the attachment of a hydrogen atom to the position ipso to a methyl group. Subsequent loss of methyl radical leads to either 1- or 2-methylnaphthalene. The yield of the monomethylnaphthalenes is an indicator of the extent of hydrocracking activity. Additionally, the ratio of the products is a measure of the selectivity of the ipso substitution.

In the presence of added coal or ATB, the percent yield of methyl-naphthalenes increases. The change in the 1-methylnaphthalene (1-MN) yield with increasing additive is small at most, while the yield of 2-methylnaphthalene (2-MN) increases with added ATB or coal. The net effect on the selectivity of DMN hydrocracking is shown in Figure 4.

While the total yields of monomethylnaphthalenes provide an estimation of the hydrocracking activity, the ratio of the 2-MN to the 1-MN provides a sensitive measure of the selectivity of the hydrocracking reactions. Selectivity differences indicate a common intermediate does not predominate in all cases. McMillen et al. (5) have shown in studies of model compounds that the selectivity of attack at the 1- and 2-positions of naphthalene may vary according to the hydrogen atom donor responsible for the attack. The most reactive and least selective intermediate is the hydrogen atom itself. Hydrogen atoms are formed as the result of radical hydrogen abstraction from gas phase hydrogen (3). Hydrogen atoms react with suitable acceptors, such as aromatic hydrocarbons, to form sigma complexes. Hydrogen transfer from these complexes is less exothermic and hence more selective than direct attack by hydrogen atoms. In the present experiments, hydrogen atoms may form more selective hydrogen atom donors by attachment to aromatic species in the coal or ATB. In addition to providing hydrogen atom acceptors, the aromatic and hydroaromatic species in the coal and ATB could interact to form the intermediate sigma complexes directly. The disproportionation of dihydroanthracene and anthracene to form hydroanthracenyl radicals is an example of this type of reaction (8). Thus, the selectivity of the hydrocracking reactions can be altered by several means in the presence of coal or ATB.

The results in Figure 4 are particularly interesting for the case of mixtures of coal and ATB. The bottom two curves show the effect of each additive in the absence of the other. The top two curves show the effect of increasing either coal or ATB in the presence of a constant amount of the other. As the concentration of ATB is increased in the absence of coal (bottom curve), the selectivity increases in a nearly linear fashion. This effect is more pronounced in the presence of coal. The efficiency of the coal in altering the selectivity of the hydrocracking is much greater than that of the ATB. Only 5% coal is needed to achieve the same selectivity as 20% ATB.

Surprisingly, selectivities in the mixtures are higher than in either component separately. A limiting value around 7.5 is approached at the highest levels of addition. These preliminary data are insufficient to determine whether the selectivity produced by addition of still higher levels of coal by itself would approach the same limiting value. However, it now appears that the combination of the ATB with the coal enhances the approach of the selectivity to this value. Thus, as revealed by this probe, the nature of the hydrogen atom intermediates becomes more dominated by coal or coal products as ATB is mixed into the systems.

CONCLUSIONS

Selected organic compounds can be used to probe the types of reactions occurring during the coprocessing of coal with petroleum residua. By combining the results from both the decalin isomerization and the dimethylnaphthalene cracking, a fuller description of the nature of the free radical activity during coprocessing can be achieved. As measured by the equilibration of decalin, the total radical activity remains fairly constant with time. This total activity is increased with added coal or ATB, and thus these additives can be viewed as functioning as free radical initiators. Some portion of this total activity results in hydrocracking reactions. The selectivity of these hydrogen atom or mediated hydrogen atom reactions is strongly influenced by coal and to a lesser degree by ATB. The total radical activity is greater than expected from a simple additivity of effects, while the selectivity of the demethylation of dimethylnaphthalene is more strongly mediated by coal when ATB is also present. Work to determine if these effects can be seen for other coals and residua is under way.

REFERENCES

1. Bockrath, B.C.; Illig, E.; Schroeder, K.T.; Miller, R.D. Process Mineralogy; Hausen, D.M.; Park, W.C., Eds.; The Metallurgical Society of AIME: New York, 1981; 493-513.
2. Bockrath, B.C.; Schroeder, K.T. ACS Symposium Ser. 1981, 169, 191-200.
3. Vernon, L.W. Fuel 1980, 59, 102-106.
4. Bockrath, B.C.; Schroeder, K.T.; Keldsen, G.L. Proceedings, International Conference on Coal Science, 1985, Pergamon Press: Sidney, Australia, 1985, 83-86.
5. McMillen, D.F.; Malhotra, R.; Hum, G.P.; Chang, S-J. Energy Fuels 1987, 1, 193-198.
6. Cugini, A; Lett, R.G.; Wender, I. Prepr. Pap.-Am. Chem. Soc., Div. Fuel Chem. 1988, 33(1), 71-88.
7. Schucker, R.C. J. Chem. Eng. Data 1981, 26, 239-241.
8. Stein, S.E. ACS Symposium Ser. 1981, 169, 97-129.

Table 1. Analyses of Coal and Residua

	<u>Illinois No. 6</u>	<u>Maya ATB</u>
<u>Proximate Analysis, wt%</u> (As Received)		
Moisture	11.52	<0.03
Volatile Matter	34.04	----
Fixed Carbon	44.78	----
Ash	9.66	0.06
<u>Ultimate Analysis, wt%</u> (As Received)		
Carbon	61.57	84.2
Hydrogen	5.53	11.9
Nitrogen	0.83	0.29
Sulfur	2.47	3.0
Oxygen (Indirect)	19.94	0.55
Ash	9.66	0.06

Table 2. Linear Regression Results for the Time Dependence of the Decalin Isomerization

<u>Additive</u>	<u>Slope x 1000</u> <u>(Min.⁻¹)</u>	<u>Y-Intercept</u>	<u>R²</u>
None	6.87	-0.09	0.991
10% Maya ATB	6.98	0.00	0.999
10% Illinois No. 6 Coal	10.66	0.01	0.990

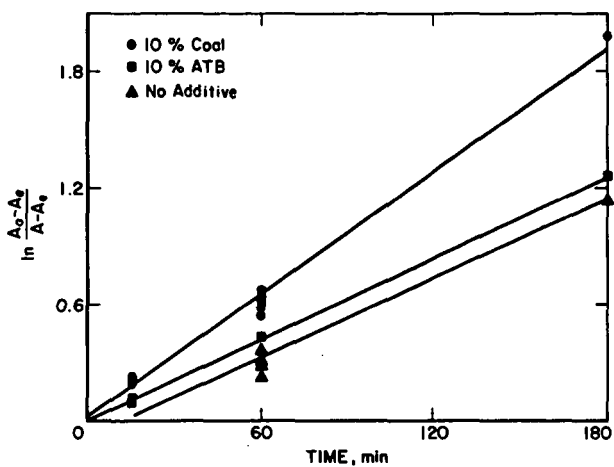


Figure 1. First Order Reversible Kinetics for the Decalin Isomerization.

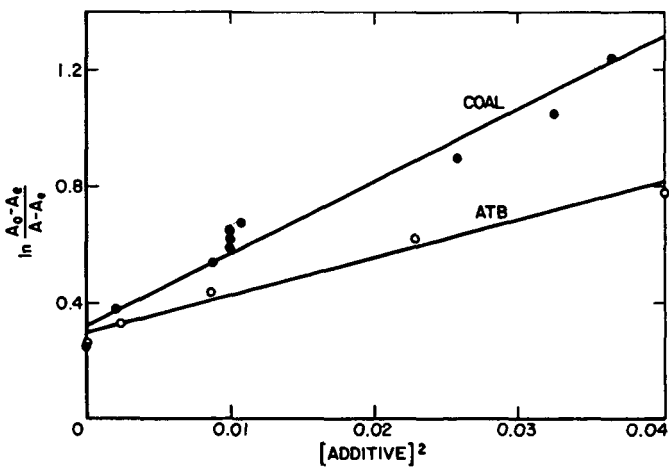


Figure 2. Effect of Coal and ATB on the Rate of the Isomerization of Decalin.

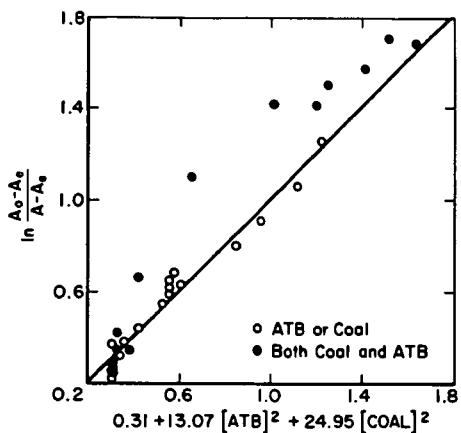


Figure 3. Parity Plot for the isomerization of Decalin.

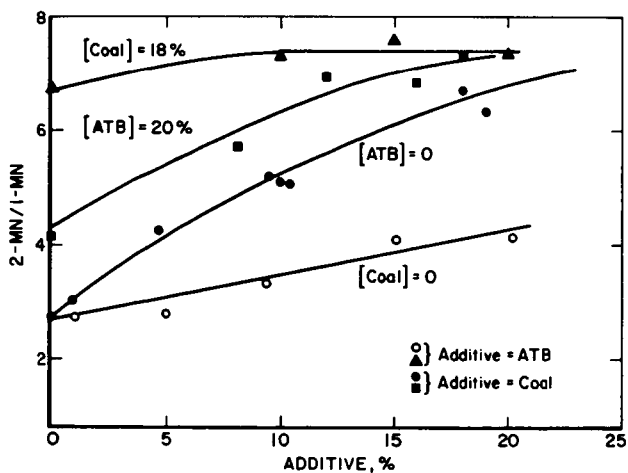


Figure 4. Effects of Coal and ATB on the Hydrocracking Selectivity.

Coal Liquefaction: Impact of Alkyl Substitution in Naphthalene Model Solvents

R. A. Keogh, B. Chawla, K.-J. Tsai and B. H. Davis
Kentucky Energy Cabinet Laboratory
P.O. Box 13015, Iron Works Pike
Lexington, Kentucky 40512

ABSTRACT

The solvent 1-methylnaphthalene has a unique ability of being able to effect the use of gaseous hydrogen during coal conversion. This unique characteristic is not universal; rather it is exhibited only for about one-third of the eastern and western Kentucky coals examined in this study. With these exceptional coals, 1-methylnaphthalene may be as, and sometimes even more, effective than tetralin in converting coal to pyridine soluble products.

INTRODUCTION

One of the features of a process solvent that is believed to be important is the amount of donatable hydrogen that is present in the form of hydroaromatic compounds. Neavel (1), for example, shows that, in the initial stages of the liquefaction of an Illinois high-volatile C bituminous coal, the conversion to pyridine solubles is similar in tetralin, a good hydrogen donor solvent, and in naphthalene, a solvent without donatable hydroaromatic hydrogens. Only after a few minutes does one see a significant difference in the overall conversion. With tetralin, a conversion of greater than 90% is attained rapidly, and this remains constant during the next 100 minutes of residence time (Figure 1a). When naphthalene is the solvent, the early conversion reaches ca. 85% but rapidly declines during the next 40 minutes of residence time to a level below 40% conversion (Figure 1b). Neavel's data dramatically emphasize a concept that has developed over the years as it relates to the need for donatable hydrogen in a liquefaction solvent that inhibits retrograde reactions.

For studies in microreactors, a convenient way to vary the amount of hydrogen donor is to use a model solvent containing tetralin and naphthalene. 1-Methylnaphthalene, a liquid at room temperature, is frequently used instead of naphthalene, a solid at room temperature since this makes the experimental procedure for sample removal and analysis easier. Naphthalene and 1-methylnaphthalene could be interchanged, on a molar basis, without altering the amount donatable hydrogen and, presumably, without altering the conversion for a solvent with a particular donatable hydrogen content.

For example, Pina et al. (2) found that the conversion of a western Kentucky coal was essentially constant as the fraction of 1-methylnaphthalene was increased up to 0.8 to 0.9 range; as the amount of donatable hydrogen was further decreased by increasing the amount of 1-methylnaphthalene a dramatic, rapid decrease in coal conversion was observed. Derbyshire and Whitehurst (3) made a similar observation for the conversion of a Belle Ayr sub-bituminous coal in a mixture of tetralin with 2-methylnaphthalene or pyridine; in this case, a lower concentration of the nondonor methylnaphthalene was required to

cause a decrease in conversion. Chiba et al. (4) have obtained conversion data with 1-methylnaphthalene-tetralin and a Yallourn coal that are intermediate to that of the above two studies. Maa et al. (5) reported that EXXON Research & Engineering Company had developed a solvent-quality index (SQI) to characterize the ability of recycle solvents to effect coal conversion and that, for some coals, below a critical value of SQI, the liquid yields and coal conversions decreased sharply. Furthermore, for the three coals reported, two coals, an Illinois No. 6 bituminous and Wyodak sub-bituminous, showed a much stronger sensitivity to SQI than did a West Virginia Ireland Mine bituminous coal. The implication of the data presented in this study is that all coals do not respond in the same manner to a given SQI.

For some Kentucky coals, a higher conversion may be obtained in a pure 1-methylnaphthalene solvent than in a tetralin. These data indicate that the amount of donatable hydrogen required for a "good" solvent is dependent upon the coal. In view of the expanding use of 1-methylnaphthalene as a model solvent (e.g., Ref. 6) to provide solvents of varying amounts of donatable hydrogen, some of these results are described in this report.

EXPERIMENTAL

The coal samples were collected from the working face of the mine and stored under argon prior to analysis and liquefaction. Chemical and petrographic analyses of the coals are given in Table 1. The coals were ground to -100 mesh, stored under argon and dried prior to the liquefaction experiments.

The liquefaction experiments were conducted in a 50 ml microautoclave reactor. The reactor charge was typically 5 g of coal and 7.5 g of model solvent. The reactor was pressurized with the appropriate gas (H_2 or N_2) to 800 psig at ambient temperature. The reactor was immersed in a heated fluidized sand bath for the desired reaction time. Typically, the time required to reach a reaction temperature of $385^\circ C$ was two minutes, or less. Mixing of the reactor charge was facilitated by a 1/4" steel ball in the reactor. The reactor was vertically shaken (1" amplitude) at a rate of 400 cpm. At the end of the liquefaction experiment, the reactor was immersed in a cold fluidized sand bath to quickly cool to less than $100^\circ C$ in less than two minutes to quench the reactions.

Once the reactor has reached ambient temperature, the product gases were collected in a sample bomb for g.c. analysis. The remaining products were quantitatively washed from the reactor with benzene into a Soxhlet thimble. The sample was extracted with benzene until the solution was clear or a pale yellow. From the benzene solubles, the asphaltene fraction was separated from the oil fraction by precipitation of the asphaltenes with pentane. The preasphaltene fraction was obtained by a Soxhlet extraction of the benzene insolubles with pyridine. Conversions were obtained by subtracting the weight percent pyridine insolubles (maf basis) from 100%.

The extraction solvents were HPLC grade and obtained from Burdick and Jackson. The liquefaction model solvents were used as received from Aldrich Chemical Co.

RESULTS AND DISCUSSION

An eastern and western Kentucky coal were converted in tetralin or 1-methylnaphthalene solvent using a reaction time of 15 minutes, a temperature of 385°C and either a hydrogen or nitrogen atmosphere (Figure 2). The data clearly show that molecular hydrogen is utilized in the liquefaction of both coals when 1-methylnaphthalene is the solvent. When tetralin was employed as the solvent, similar conversions were obtained when the reactor vessel was pressurized with either hydrogen or nitrogen. However, when 1-methylnaphthalene was used as the solvent for either coal, the conversion in the hydrogen atmosphere was about double the conversion in a nitrogen atmosphere. Thus, the 1-methylnaphthalene is effecting the utilization of gaseous hydrogen to produce higher conversions. Even more surprising is the observation that, in a hydrogen atmosphere, the 1-methylnaphthalene is as effective as a solvent as tetralin for coal conversion.

The observation that equal conversions are obtained using 1-methylnaphthalene and tetralin as liquefaction solvents does not apply for all coals. Even when a hydrogen atmosphere is used, the expected lower conversions are obtained for ca. 60% of the eastern Kentucky coal samples in Figure 3 (see reference 7 for coal analysis); i.e., the conversion when tetralin is utilized is appreciably higher than when 1-methylnaphthalene is the solvent. The data in Figure 3 indicate that equivalent conversions are obtained for those special coals in both solvents (which span the entire range of conversions). Therefore, this phenomena is not restricted to a set of coals with high or low reactivities. From the data, it may be concluded that some unique coal property, or properties, are responsible for this observation. Similar results have been obtained with western Kentucky coals.

The time dependence of conversions in the two solvents are shown in Figure 4 for a western Kentucky #9 Alston coal. The same conversion is obtained for either nitrogen or hydrogen atmosphere at 15 and 30 minutes with the tetralin solvent. A very different result is obtained with the 1-methylnaphthalene solvent. With this latter solvent and a hydrogen atmosphere, the conversions up to 30 minutes are clearly greater than when tetralin was employed. In addition, the conversions, when a nitrogen atmosphere was used instead of hydrogen, were lower (ca. 30%) and did not increase with longer reaction times. With 1-methylnaphthalene and hydrogen, the conversion at 60 minutes was the same as when tetralin was used as the solvent. Therefore, in addition to the surprising fact that the conversion of the western Kentucky #9 coal is initially greater in the 1-methylnaphthalene solvent, it does not appear that the retrograde reactions, as shown in Figure 1b, have made a measurable contribution in lowering conversions, even after 60 minutes. Again, the data clearly show that 1-methylnaphthalene is able to effect gaseous hydrogen usage and, with this particular coal, appears to be able to provide the hydrogen needed for conversion to pyridine solubles even more effectively than tetralin.

The data in Figure 5 indicate the effect of alkyl substitutions in aromatic and hydroaromatic rings on the conversions obtained for a Western Kentucky #9 and Eastern Kentucky Peach Orchard coal. The conversions obtained by these two coals, using naphthalene as the solvent, are lower than those obtained when tetralin was employed as the liquefaction solvent; this is anticipated from previous reports. Liquefaction of the two coals using 2-methylnaphthalene as a solvent produce significantly lower conversions when

compared to those obtained in 1-methylnaphthalene. However, the conversions in 2-methylnaphthalene are essentially the same as those observed for the liquefaction of the coals in naphthalene. One explanation for the above data may be the physical state of the model solvents employed. Naphthalene and 2-methylnaphthalene are solids at room temperature while 1-methylnaphthalene is a liquid. Poor mixing during the initial stages of liquefaction using the solid model solvents could be a factor in the lower conversions observed using these compounds. However, this does not appear to be the case as shown by the data in Figure 6. With the two solid liquefaction solvents, 2-methylnaphthalene and 2,3-dimethylnaphthalene, the microautoclave was preheated to a temperature slightly above the melting point of the solvent and mixed prior to immersion in the sand bath to obtain the reaction temperature. As shown by the data in Figure 6, the conversions, within experimental error, are the same regardless of the physical state of the model solvent prior to heating to reaction temperature.

Dihydronaphthalene is a more effective solvent than tetralin, and this has been observed frequently (e.g. Ref. 8). In fact, Virk et al. (8) propose that Woodward-Hoffmann rules apply so that 1,2-dihydronaphthalene will be more effective for transferring hydrogen to phenanthrene type structures while 1,4-dihydronaphthalene will be more effective for hydrogen transfer to anthracene compounds. These authors present data to show that, at 400°C and 30 minutes reaction time, 1,2-dihydronaphthalene provides essentially the same conversion as tetralin, and the conversion of in these two solvents is about twice that obtained in naphthalene (ca 70 vs. 30%). However, the conversion in 1,4-dihydronaphthalene is greater than in tetralin (81 vs. 70%). Our data differ from since the conversion in 1,2-dihydronaphthalene is much greater than in tetralin (Figure 5).

It is surprising that both methyltetralins used in this study produce significantly higher conversions of these two coals when compared to the results obtained using tetralin. In fact, the two methyltetralin compounds produce as high a conversion as 1,2-dihydronaphthalene does. One could argue that in 1-methyltetralin the tertiary hydrogen provides a relatively weak C-H bond, and this could provide a lower activation energy reaction pathway for hydrogen transfer. However, this argument does not apply for 5-methyltetralin.

At this time, we have no ready explanation how the 1-methyl substituent promotes the use of gaseous hydrogen so much more effectively than does the 2-methyl substituted naphthalene during coal conversion. Likewise, the effect must be specific since 1-ethylnaphthalene does not appear to be a better solvent than the unsubstituted solvent, naphthalene (Figure 5). The coal properties in Table 1 do not provide a ready explanation as to why some coals have equivalent or better conversion, thorough utilization of gaseous hydrogen, in the 1-methylnaphthalene case when compared to the tetralin case.

These results clearly show that 1-methylnaphthalene is a unique liquefaction solvent for some coals and may produce results that are not typical of all nondonor solvents. At the same time, the results suggest that some coals have a unique property or properties which promote the utilization of gaseous hydrogen through nondonor solvents, and that it may be possible to take advantage of this property to improve hydrogen usage through coal selection. Finally, 1-methylnaphthalene, as a model solvent, may have utility

in identifying those coals, such as Ireland Mine coal, that appear to be able to be converted in a low SQI recycle solvent.

ACKNOWLEDGMENT

This work was supported by the Commonwealth of Kentucky, Kentucky Energy Cabinet and DOE Contract No. DE-FC-22-85PC80009 as part of the Consortium for Fossil Fuel Liquefaction Science (administered by the University of Kentucky).

REFERENCES

1. R.C. Neavel in "Coal Science" (M.L. Gorbaty, J.W. Larson and I. Wender, Eds.) Academic Press, New York, N.Y., 1982, pp. 1-19.
2. B. Pina, D. Collins, G. Snell and B. Davis, Minerals and Metallurgical Processing, 1985, 154.
3. F.J. Derbyshire, P. Varghese and D.P. Whitehurst, ACS Fuel Division Preprints, 26, No. (1), 84, (1981).
4. K. Chiba, H. Tagaya and N. Saito, Energy & Fuels, 1, 363, (1987).
5. P.S. Maa, K.L. Trachte and R.D. Williams, in "Chemistry of Coal Conversion", (R.H. Schlosberg, Ed.) Plenum Pub. Corp., 1985, p. 317.
6. S.-C. Shin, R.M. Baldwin and R.L. Miller, 1, 377, (1987).
7. B. H. Davis, et al., Task VI. Basic Process/Resource Evaluation Task, Cooperative Research in Coal Liquefaction Infratechnology and Generic Technology Development, Final Report on DOE Contract No. DE-FC-22-85PC80009, submitted by the Consortium for Fossil Fuel Liquefaction Science, October 1, 1986 to December 31, 1987.
8. P.S. Virk, D.H. Bass, C.P. Eppig and D.J. Ekpenyong, A.C.S. Fuel Div. Preprints, 24, (No. 2), 144, (1979).

TABLE 1. Coal Properties

	<u>W. Ky. #9</u>	<u>E. Ky. Peach Orchard</u>
ASH (dry)	11.71	5.29
VM (daf)	43.21	40.11
FC (daf)	56.79	59.89
C (daf)	76.80	83.24
H (daf)	5.41	5.54
N (daf)	1.90	1.70
S (daf)	8.41	.96
O (diff, daf)	7.48	8.56
Pyritic S (daf)	5.22	.08
Organic S (daf)	2.87	.87
Sulfate S (daf)	.32	.01
Vitrinitis	90.9	65.1
Intertinites	7.1	22.5
Liptinites	2.0	12.4

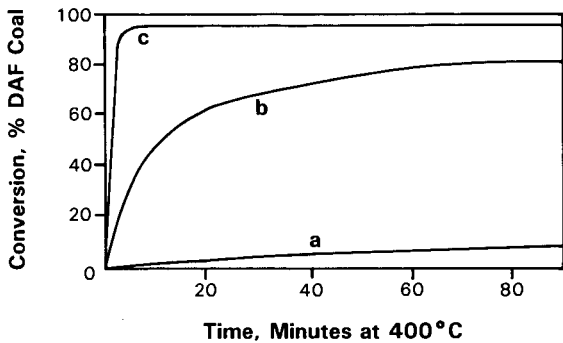


Figure 1a. Conversion of Coal reacted at 400°C in tetralin; (a) noncondensable gas; (b) benzene-soluble material + gas; (c) pyridine-soluble material + gas. DAF = dry ash-free (from Reference 1).

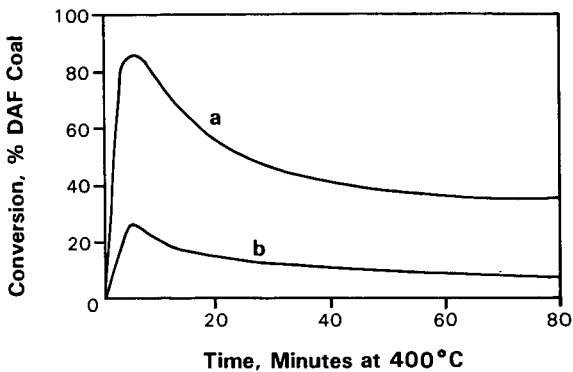


Figure 1b. Conversion of coal reacted at 400°C in naphthalene: (a) pyridine-soluble material; (b) benzene-soluble material. DAF = dry ash-free (from Reference 1).

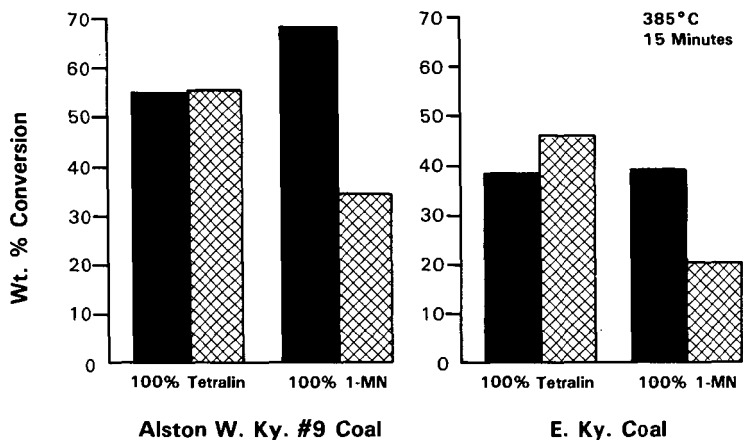


Figure 2. Conversion in a donor (tetralin) or nondonor (1-methylnaphthalene) solvent using hydrogen (■) or nitrogen (⊠) atmosphere.

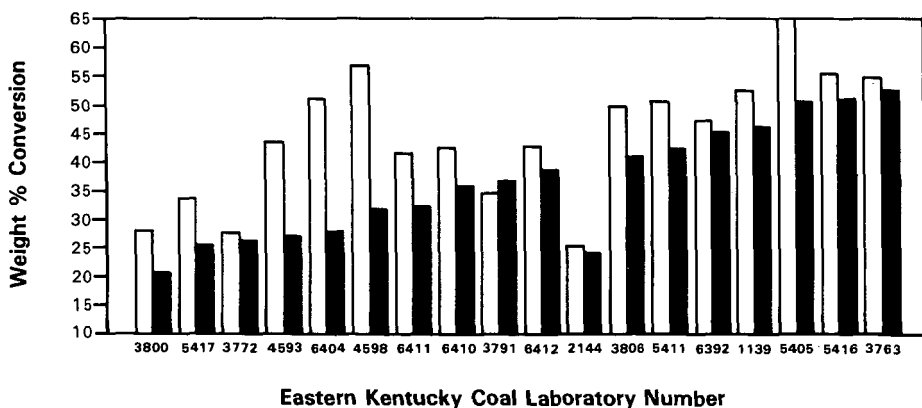


Figure 3. Comparison of conversions at 385°C and 15 minutes for eastern Kentucky channel samples in tetralin (□) and 1-methylnaphthalene (■) solvents.

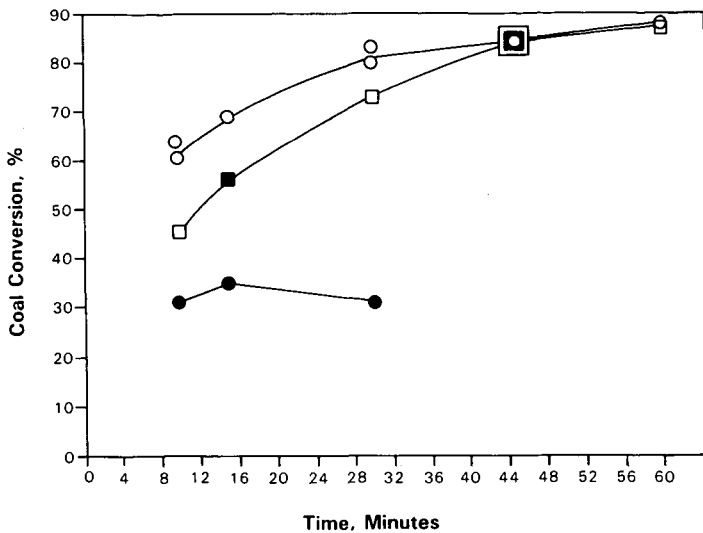


Figure 4. Time dependence of conversion of a Western Kentucky No. 9 Alston coal at 385°C utilizing (1) gaseous (□) hydrogen or (■) nitrogen with a tetralin solvent or (2) gaseous (○) hydrogen or (●) nitrogen with 1-methylnaphthalene solvent.

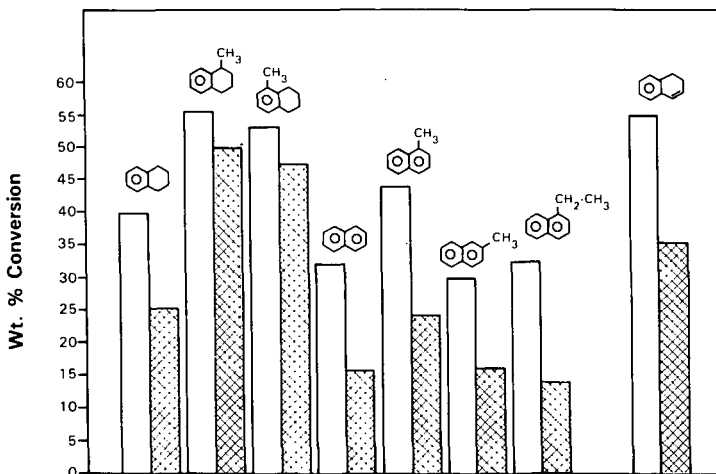


Figure 5. Coal conversion at 15 minutes at 385°C in the presence of gaseous hydrogen for a Western Kentucky No. 9 Alston coal (□) or Eastern Kentucky Peach Orchard coal (▨) and with the indicated solvent.

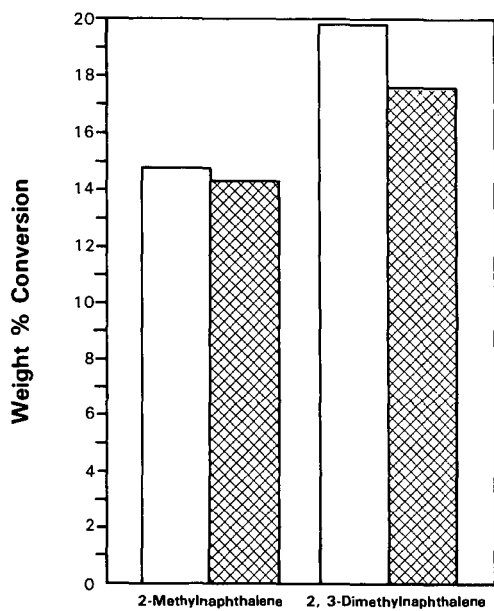


Figure 6. Comparison of the conversion of a Peach Orchard coal starting with a solid (□) or in liquid (▨) solvent.

Hydroliquefaction of Coal-Oil Agglomerates

Bao C. Ha, John A. Ruether, Dennis N. Smith, and Joseph A. Mima
U.S. Department of Energy
Pittsburgh Energy Technology Center
Pittsburgh, Pennsylvania 15236

ABSTRACT

A novel coal hydroliquefaction process has been developed at PETC that employs a low-solvent-to-coal ($S/C = 0.35$) feed with a water-soluble dispersed catalyst. The effectiveness of liquefaction catalysts, iron and molybdenum, when loaded on the outside surface of coal-oil agglomerates is compared to that of aqueous impregnation. In the presence of 1 wt% iron and 5 vol% hydrogen sulfide, the iron-impregnated coal gave higher conversions than an agglomerated feed. Iron catalyst must be in intimate contact with individual coal particles for highest reactivity. Aqueous impregnation is, therefore, the best catalyst-loading method for dispersed iron. In the presence of 0.1 wt% molybdenum, higher conversions were, however, achieved with the coal-oil agglomerates than with molybdenum-impregnated coal. Oil agglomeration of feed coal eliminated the need for impregnation of molybdenum catalyst on the coal to achieve high conversions at low solvent-to-coal ratio of 0.35. In the absence of catalyst, higher conversions were also achieved with coal-oil agglomerates compared to a simple mixture of coal and oil at $S/C = 0.35$. The improved reactivity of agglomerates is thought to be due to the complete wetting of individual coal particles by binder oil, a hydrogen donor solvent, which was effected during the oil agglomeration step.

INTRODUCTION

During the development of novel approaches to direct liquefaction, organic solvent, water, and a water-soluble transition metal salt catalyst were found to be complementary aids to increase soluble yields of coal hydrogenation.¹ The dependence of tetrahydrofuran (THF) soluble yields on the organic solvent-to-coal (S/C) ratio of the feed described a plateau in the presence of equal masses of coal and water. Conversions reached a maximum with a small amount of solvent, $S/C = 0.5$, and additional organic solvent caused no change in soluble yields. The use of small concentrations of a water-soluble molybdenum salt effectively increased the plateau value of conversion and decreased the S/C ratio for the onset of the plateau compared to uncatalyzed systems.

Subsequently it was shown that in the presence of a dispersed molybdenum salt catalyst, conversions are independent of water partial pressure.² Yields of THF solubles in excess of 90 percent were achieved at S/C as low as 0.25 in the molybdenum-impregnated systems with no added water. The combination of 1 percent iron and 5 volume percent addition of hydrogen sulfide was found to be as effective as 0.1 percent molybdenum in low-solvent-to-coal ($S/C = 0.33$) systems.³

Low-solvent-to-coal liquefaction could potentially reduce the product recycle stream and increase throughput of the coal feed for a given size of equipment. Spherical agglomeration is considered for preparation of the low-solvent-to-coal feed because of ease of handling. Our previous work had, however, been involved with only iron- and molybdenum-impregnated coals.¹⁻³ Catalyst effectiveness by another loading method, deposition on the outside of the coal-oil agglomerates during agglomeration, has to be assessed. At a low solvent-to-coal ratio ($S/C = 0.35$), an effective liquefaction catalyst is required to prevent solvent starvation and high yields of undesired products, char and hydrocarbon gases.

Previous studies have indicated that the mode of catalyst addition is important in coal liquefaction.⁴⁻⁶ Both molybdenum and iron are effective during coal hydrogenation without organic solvent when loaded on the coal particles by an aqueous-impregnation procedure. The effectiveness of ferrous sulfate improved with prolonged mechanical mixing, but it was still less than when iron was aqueously impregnated onto the coal.^{4,5} However, Schlesinger et al.⁷ indicated that impregnation with molybdenum was not needed if the ammonium heptamolybdate was thoroughly mixed in the presence of a solvent ($S/C = 1.5$). The present research investigates the effects on conversions of the mode of catalyst addition and the form of the coal-oil feed in low-solvent-to-coal systems. Results are reported for uncatalyzed systems and with use of water-soluble salts of molybdenum and iron.

EXPERIMENTAL

MATERIAL

Minus-200-mesh grind of Illinois No. 6 (Burning Star mine) bituminous coal was used (dmmf analysis: 5.3% H, 75.4% C, 1.0% N, 3.4% S, 14.9% O). In the experiments with added catalysts, molybdenum or iron, the catalyst was loaded on the coal either by aqueous impregnation or by deposition on the external surface of coal-oil agglomerates.

In the aqueous impregnation procedure, the feed coal was prepared by mixing with water containing a dissolved transition metal salt, ammonium heptamolybdate or ferrous sulfate. The mixture was then dried in a vacuum oven at 110°C, and the catalyst deposited on the coal particles.

In the oil agglomeration procedure, a coal-derived binder oil was added to an agitated mixture of coal and water, and coal-oil agglomerates were formed into spherical particles of 2- to 3-mm-diameter size. In experiments with catalyst, the water contained the dissolved molybdenum or iron. The agglomerates were then drained by sieving. The catalyst was deposited on the agglomerates by evaporation of catalyst solution in a vacuum oven at 110°C. Previous work has shown that coal-oil agglomerates have negligible internal void, so any water adhering to agglomerates after draining was on their outer surface.⁸

For each method of catalyst addition, the catalyst concentration was either 0.10% molybdenum or 1.0% iron, reported as weight percent based on coal. The amount of catalyst deposited was calculated by measuring weight loss of water on drying. Hydrogen gas containing 5 volume percent of hydrogen sulfide was used in experiments with iron catalyst. The liquefaction solvent serving as the agglomeration binder oil was SRC II heavy distillate produced in Run 2406 at the Fort Lewis, Washington, pilot plant. The solvent-to-coal ratio was 0.35 for all experiments, i.e., those employing coal-oil agglomerates and those utilizing unagglomerated coal as feed.

PROCEDURE

Liquefaction experiments were carried out in a stirred one-liter batch reactor. The standard operating conditions for all experiments were either a 400°C or 427°C reaction temperature and a 60-minute reaction time at the desired temperature. Typically, the batch autoclave was charged with 144 gm of either a simple mixture of coal and organic solvent or a charge of coal-oil agglomerates, then pressurized (cold) to 1300 psig with hydrogen gas. The stirrer was operated at 1000 to 1100 rpm. It took from one to one and one-half hours to heat the reactor system electrically from ambient temperature to reaction temperature.

ANALYSIS

The gaseous products were metered and then analyzed by gas chromatography. The yield of C₁ through C₄ was determined as hydrocarbon gases. The hydrogen consumption was calculated from the difference between the initial hydrogen gas charged and the final hydrogen gas collected. The liquefaction residues were analyzed by solvent extraction for THF, benzene, and pentane insolubles. The conversions were calculated by

$$\% \text{ conversion} = \frac{\text{dmnf coal} - \text{organic insolubles}}{\text{dmnf coal}} \times 100\%$$

The conversions were corrected for the insolubles in the SRC II heavy distillate. It was arbitrarily assumed that the organic vehicle was inert in calculating conversions, since insolubles deriving from coal or solvent could not be distinguished.

RESULTS AND DISCUSSION

There was a concern that at the same concentration of catalyst, expressed as a weight percent of coal, agglomerates would show reactivity lower than that of feed coal for which the coal particles were individually impregnated with catalyst. Agglomerates are typically 2 - 3 mm in diameter, while individual coal particles have diameters on the order of 74 microns for minus-200-mesh grind. The catalyst deposited on the external surface of agglomerates will not be as highly dispersed as it is when impregnated on individual coal particles. Indeed, in systems containing 1.0 percent iron and 5 volume percent hydrogen sulfide, agglomerates showed liquefaction reactivity lower than

that of feed coal that was previously aqueously impregnated with iron catalyst (see Figure 1). At 400°C reaction temperature, the benzene-soluble yield was lowered by 9%, and the pentane-soluble yield by 25%. Catalytic activity of iron depends strongly on close contact of iron with coal.

In the presence of 0.10% molybdenum catalyst, oil agglomeration of feed coal, however, increased liquefaction yields (see Figure 2). At 400°C, agglomerated feed coal was more reactive than molybdenum-impregnated coal and increased substantially the liquefaction yields of soluble fractions. The benzene-soluble yield was improved by 12%, and pentane-soluble yield by 28%. At 427°C, the catalytic effect became prominent and masked the contributions of oil agglomeration. High conversions to THF and benzene solubles were obtained for both agglomerated and molybdenum-impregnated coal feeds. At low solvent-to-coal ratio of 0.35, oil agglomeration eliminated the need for impregnation of molybdenum catalyst into coal.

Since agglomerated feedstock with molybdenum catalyst showed an enhancement in liquefaction reactivity, experiments were performed to investigate the effect of the reactant form in uncatalyzed reactions. Figure 3 compares yields of soluble fractions for both agglomerated coal feed and a simple mixture of coal and solvent at the same composition without any catalysts. The liquefaction reactivity was improved dramatically with the oil-agglomerated coal compared to nonagglomerated feed. At 427°C, the enhancement in the liquefaction yields was 19% for all soluble fractions. However, conversions to solubility yields were significantly lower compared to the results obtained with catalyst-impregnated coal feed (see Figures 1 and 2).

Thus an increase in liquefaction reactivity was observed in non-catalyzed systems with oil-agglomerated coal. During coal-oil agglomeration, a water slurry of coal is first contacted with oil while being agitated. Through a series of transfer steps that occur between oil droplets and coal particles during agitation, coal particles become coated individually with oil. Subsequently, the coal particles coalesce and, with further time and agitation, form spherical agglomerates. The bridging oil in coal-oil agglomerates is thought to exist in a capillary state, giving the agglomerates a unique structure.⁸ The agglomerates are noteworthy for their compactness (absence of interior air space), sphericity, and strength. Each coal particle is completely wetted and in intimate contact with a binder oil, which is also a liquefaction donor solvent, within the agglomerate. During initial dissolution, donor solvent is readily available for donating and shuttling hydrogen. The enhanced hydrogen-transferring processes caused higher hydrogen consumption in agglomerated systems with or without any catalysts (Figures 4, 5, and 6), and improved the yields of solubles.

CONCLUSIONS

Molybdenum is effective during low-solvent-to-coal liquefaction when loaded on the outside surface of coal-oil agglomerates. However, iron catalyst must be in intimate contact with in-

dividual coal particles for highest reactivity. Aqueous impregnation is the best catalyst-loading method for dispersed iron. Oil agglomeration of feed coal increased liquefaction yields in systems with no catalyst. The unique structure of coal and binder oil, which is also a hydrogen donor solvent, in the agglomerated state enhances the hydrogen-transferring processes during initial dissolution.

ACKNOWLEDGMENT

The reactions were conducted by William Staymates.

DISCLAIMER

Reference in this report to any specific commercial product, process, or service is to facilitate understanding and does not necessarily imply its endorsement or favoring by the United States Department of Energy.

REFERENCES

1. Ruether, J.A., Mima, J.A., and Kornosky, R.M., "Organic Vehicle, Catalyst, Water: Interplay of Three Aids to Coal Hydroliquefaction," presented at the U.S. D.O.E. Direct Liquefaction Contractors' Conference, Pittsburgh, Pennsylvania, November 19, 1985.
2. Ruether, J.A., Mima, J.A., Kornosky, R.M., and Ha, B.C., Energy & Fuels, 1(2), 1987, pp. 198 - 202.
3. Ha, B.C., Ruether, J.A., Smith, D.N., and Mima, J.A., Effect of Hydrogen Sulfide During Low-Solvent-to-Coal Liquefaction, in preparation, 1988.
4. Weller, S., Pelipetz, M.G., Friedman, S., and Storch, H.H., Ind. Eng. Chem., 42(2), 1950, pp. 330 - 334.
5. Weller, S., and Pelipetz, M.G., Ind. Eng. Chem., 43(5), 1951, pp. 1243 - 1246.
6. Hawk, C.O., and Hiteshue, R.W., "Hydrogenation of Coal in the Batch Autoclave," U.S. Dept. of Interior, Bureau of Mines, Bulletin No. 622, 1965.
7. Schlesinger, M.D., Frank, L.V., and Hiteshue, R.W., "Relative Activity of Impregnated and Mixed Molybdenum Catalysts for Coal Hydrogenation," U.S. Dept. of Interior, Bureau of Mines, R.I. No. 6021, 1962.
8. Capes, C.E., McIlhinney, A.E., and Sirianni, A.F., Agglomeration 77, Sastry, K.V.S., Ed., AIME, New York, 1977, pp. 910 - 930.

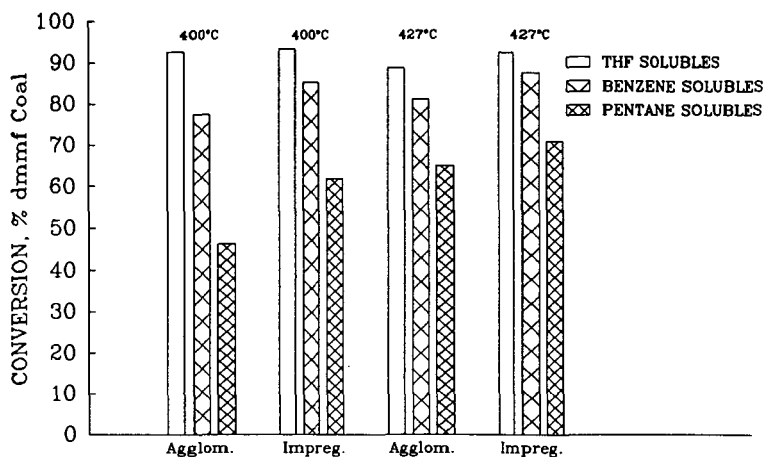


Figure 1. In Systems Containing 1.0% Iron and 5.0 Volume % Hydrogen Sulfide, Aqueous Impregnation Is a More Effective Catalyst-Loading Method than Agglomeration.

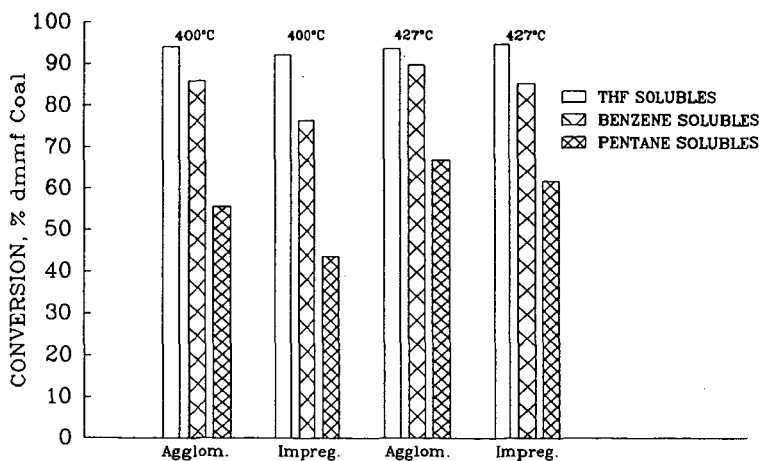


Figure 2. In Systems Containing 0.10% Molybdenum, Oil Agglomeration Improves Liquefaction Yields.

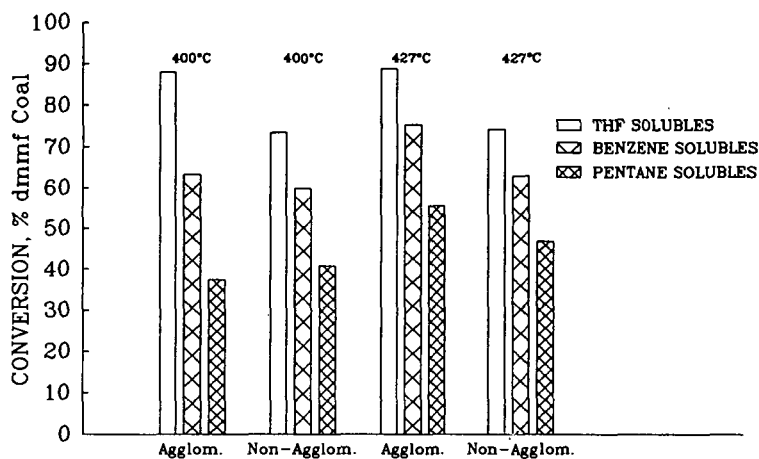


Figure 3. In Non-Catalyzed Systems, Oil Agglomeration Enhances Liquefaction Reactivity.

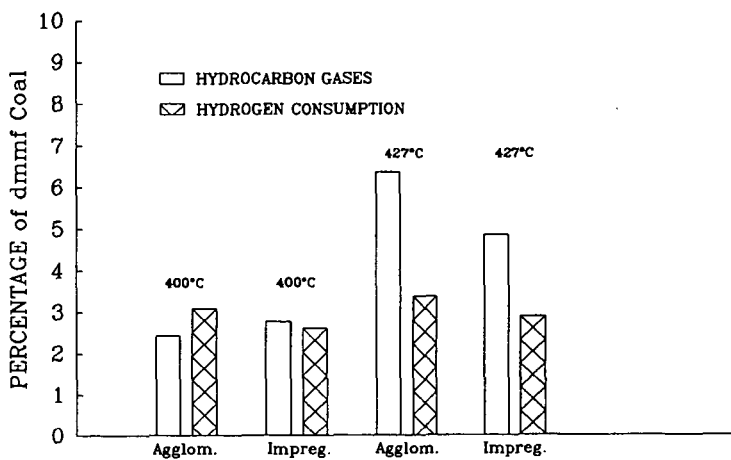


Figure 4. In Systems Containing 1.0% Iron and 5.0 Volume % Hydrogen Sulfide, Agglomerated Feed Consumes More Hydrogen.

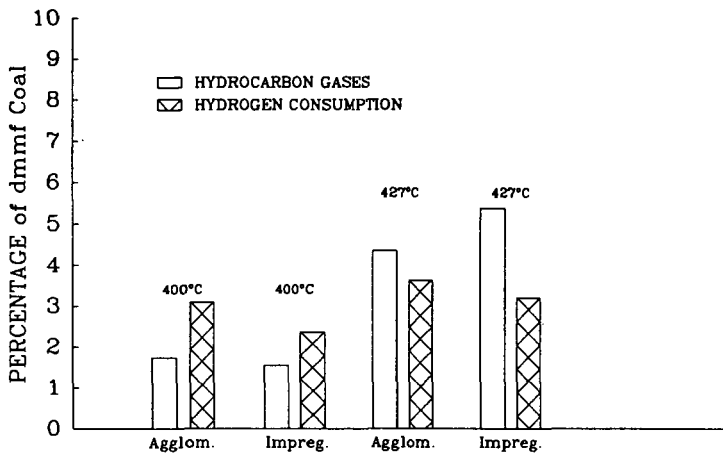


Figure 5. In Systems Containing 0.10% Molybdenum, Agglomerated Feed Consumes More Hydrogen and Produces Less Hydrocarbon Gases.

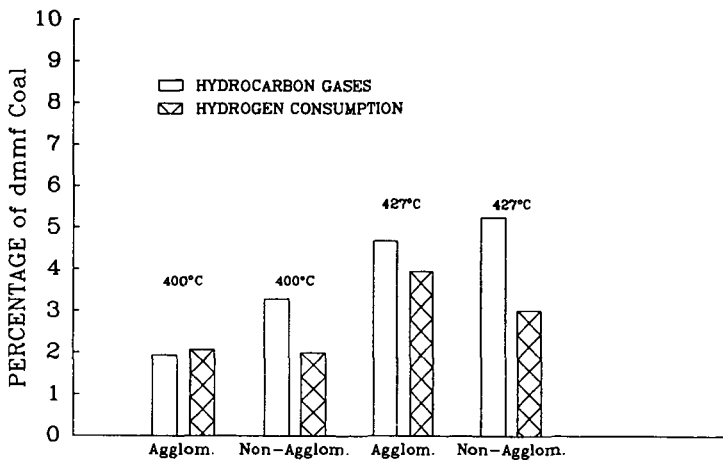


Figure 6. In Non-Catalyzed Systems, Agglomerated Feed Also Consumes More Hydrogen and Produces Less Hydrocarbon Gases.

HIGH LIQUID YIELDS FROM BITUMINOUS COAL VIA
HYDROPYROLYSIS WITH DISPERSED CATALYSTS

C. E. Snape* and C. Bolton
British Coal, Coal Research Establishment,
Stoke Orchard, Cheltenham, Glos., GL52 4RZ, UK

R. G. Dosch and H. P. Stephens
Sandia National Laboratories, Albuquerque, NM 87185

INTRODUCTION

In some respects, coal hydroxyprolysis is potentially a more attractive route for the production of liquid fuels than direct liquefaction techniques utilizing solvents. It offers a process configuration that avoids the use of a recycle solvent, which constitutes up to two-thirds of the reactor feed stream. However, historically, pyrolysis processes have been associated with low conversions of coal to liquid products (1-3), making char the principal product for which some application, apart from providing process heat and hydrogen, must be found. Moreover, large quantities of methane are usually produced during hydroxyprolysis at temperatures above 600°C which are required to achieve substantial liquid yields. Consequently, hydrogen consumptions are high. Results of two-stage hydroxyprolysis studies, in which primary tar vapors are passed through a catalyst bed, previously reported by several of the authors (4-6) have shown that daf yields of 20-25% distillate along with only 3-4% methane can be achieved if non-catalytic hydroxyprolysis of bituminous coal, carried out at a pressure of about 150 atmospheres and a temperature of 500°C, is followed by catalytic upgrading of the tar at a temperature of 400°C.

Early work (7,8) established that coals could be catalytically hydrogenated in batch reactors in the absence of a solvent to give high conversions to pyridine soluble materials. Impregnated molybdenum catalysts were among the most active studied. More recent work (9) has demonstrated that dispersed sulfided Mo is effective under mild conditions; over 50% chloroform soluble material can be generated from bituminous and subbituminous coals by reaction at 400°C and a cold-charge hydrogen pressure of 70 atmospheres. Lewis acids, such as zinc and stannous chlorides, have been shown to enhance liquid yields (10,11), but relatively large concentrations of catalyst are required. Early work has shown that Mo could be used to achieve hydroxyprolysis yields exceeding the proximate volatiles content (12,13). However, sulfided Mo, which is thought to be the most active form for coal conversion, was not used. Moreover due to the high temperatures and pressures used, secondary reactions could not be controlled giving rise to a low selectivity to liquid products.

In this paper we report the results of catalytic hydroxyprolysis experiments in which greater than 60% daf coal basis yields of tar are produced with weight ratios of tar to gases up to 80% higher than observed in an uncatalyzed reaction. The work has also shown that dispersed sulfided molybdenum and hydrous titanium oxide (HTO) catalysts coated directly on the coal are superior to Lewis acids and alumina supported hydrogenation catalysts in terms of tar yields achieved and reduction of the amount of light hydrocarbon gases produced. In addition, we have performed two-stage hydroxyprolysis tests which demonstrate that the tar produced is readily upgraded.

* Present address: University of Strathclyde, Department of Pure and Applied Chemistry, Glasgow, Scotland, G1 1XL.

EXPERIMENTAL

Coal and Catalysts

A high volatile UK bituminous coal (Linby), ground to 75 to 150 micron particle size range, was used for these tests. Analysis of the coal has been reported elsewhere (4). Catalysts used for these tests were 1) zinc and stannous chloride Lewis acids, 2) a commercial Ni-Mo/alumina, 3) bulk HTO (14,15) formulations (Pd and Co-Ni-Mo), 4) coatings of Ni and Pd HTOs and 5) dispersed sulfided Mo. Lewis acid catalysts were impregnated into the coal from aqueous solution. Powdered (-200 mesh) alumina supported and bulk HTO catalysts were physically mixed with the coal, the catalyst weight being 20% daf coal. Ni and Pd HTO catalyst coatings were dispersed by coating the coal with sodium hydrous titanium oxide (Na HTO) followed by contact of the Na HTO-coated coal with aqueous solutions of either Ni or Pd. This resulted in the active metal being incorporated into the hydrous titanate coating via ion exchange for Na⁺. Finely divided MoS₂ was dispersed by wetting the coal with solutions of (NH₄)₂MoS₄ or (NH₄)₂MoO₂S₂. The amounts of active metals in all the materials are given in Table I.

Apparatus and Procedure

The hydropyrolysis reactor and procedures used for the tests have been described previously (4,5). Most of the tests were single-stage catalytic hydropyrolysis experiments, carried out at 150 atmospheres hydrogen pressure and 500°C. The hydropyrolysis zone was heated at a rate of 5°C/s from ambient and held at temperature for 10 min. Hydrogen was passed downward through the reactor at a flow rate equivalent to 5 l/min at standard temperature and pressure and tars were collected in an ice-cooled trap. For comparison with the catalytic experiments, a single-stage test was also performed without catalyst. In addition, two two-stage experiments were performed: the first with a non-catalytic hydropyrolysis stage followed by a presulfided Ni-Mo/alumina catalytic upgrading stage (5,6) operated at 400°C, and the second with dispersed MoS₂ catalyst (0.6% Mo, daf coal basis) in the hydropyrolysis stage followed again by presulfided Ni-Mo/alumina catalyst in the second stage.

Product Recovery and Analysis

Gas exiting the reactor was collected and analyzed for C₁-C₄ hydrocarbons, CO and CO₂. Following the completion of each experiment, the post-reaction contents of the reactor tube were removed and weighed to determine the char and ash remaining. Liquid products contained in the reactor product cold trap were first weighed, then recovered with dichloromethane (DCM). Water was removed using phase separating paper and weighed, and the DCM solutions were evaporated to give tar samples for analysis. The daf coal basis percentage yield of tar for each experiment was calculated as the weight of material recovered in the cold trap less the weight of water produced. The tars were subjected to a variety of analyses to determine the elemental composition--including oxygen concentration, phenolic OH, aromatic hydrogen content, and number average molecular weight. For the two-stage experiments, the liquid products exiting the second stage of the reactor were recovered neat in order to determine the fraction of light naphtha.

RESULTS AND DISCUSSION

Single-Stage Hydropyrolysis

The products resulting from the single-stage catalytic hydropyrolysis experiments, classified as tar, methane, C₂-C₄ hydrocarbons, and char, are listed in Table I. For comparison with the catalytic experiments, the distributions for a non-catalytic experiment are included. As can be seen in Table I, all of the catalyzed

experiments produced significantly more tar than the non-catalytic case. Examination of the results for the various catalysts indicates that tar yields and product selectivity are dependent on the catalyst or active metal employed and the technique used to disperse the catalyst with the coal. The greatest tar yields, 59-64%, were achieved with well-dispersed catalysts containing metals known to be active for coal conversion.

The effect of the active metal may be seen by comparison of the experiments with Ni and Pd HTO coatings and MoS₂. As anticipated, the Pd and Mo catalysts gave higher tar yields (~60%) than the Ni catalysts (~50%). With respect to dispersion, Pd HTO catalysts coated onto the coal and the MoS₂ dispersed from aqueous solution gave higher yields than the Pd HTO and Ni-Mo/alumina finely divided catalyst powders which were physically mixed with the coal, even though the coal basis amount of active metal was significantly greater for the powdered catalysts. The Lewis acid catalysts, ZnCl₂ and SnCl₂, dispersed onto the coal from aqueous solution, produced tar yields of 36% and 54%, respectively, despite the five-fold difference in catalyst weight. This result suggests that further experiments are also needed with Ni and Pd HTO catalyst coatings to determine the minimum amount of active metal required to achieve high yields. Indeed, we have performed experiments similar to those reported here that showing that concentrations of Mo as low as 0.1% can be used without sacrificing tar yield.

In general, C₁-C₄ hydrocarbon gas formation increased with the increase in tar yield. For most of the catalytic experiments, the amount of methane formed (2-4%) was nearly equal to that for the non-catalytic experiment (3%). However, the Lewis acid catalysts produced significantly more methane (6%). The yield of C₂-C₄ hydrocarbon gases produced by the non-catalyzed case was 4%; the catalyzed experiments produced yields from 4 to 9%. Because liquids are the desired hydropyrolysis products, and gaseous hydrocarbons are not only of low value but result in wasteful consumption of hydrogen, a useful figure of merit, shown in Table I, for comparison of the efficiency of conversion is the selectivity defined in terms of the weight ratio of tar to gas yield. Compared to the selectivity for the non-catalyzed experiment, 3.7, the selectivities for the Lewis acid catalysts, 2.8 and 4.1, at best offer little improvement. However, the other catalysts show relative improvement in selectivity ranging from 35 to 80%.

Two-Stage Hydropyrolysis

The two-stage experiments were performed to demonstrate that the tar produced in greater yields from catalyzed hydropyrolysis can be hydrotreated in a second stage to produce a high quality liquid product. Table II shows the compositions of the primary tars produced by non-catalytic and catalytic hydropyrolysis, along with the compositions of the products resulting from second-stage vapor-phase hydrotreatment of the primary tars with presulfided Ni-Mo/alumina catalyst. First-stage product distributions in terms of yields of tar, hydrocarbon gases, and char are given in Table I for similar non-catalyzed and MoS₂ catalyzed experiments. As can be seen from the two tables, tar yield for the catalyzed product was double that for the uncatalyzed product in the single-stage experiments, and although the H/C ratio, aromatic hydrogen and nitrogen contents for both primary tars were similar after the first stage of the two-stage experiments, the oxygen and sulfur contents of the catalyzed hydropyrolysis tar were significantly less than those for the uncatalyzed tar. In addition, the number average molecular weight of the tar produced by the catalyzed experiment was only slightly greater than that produced by uncatalyzed hydropyrolysis.

The composition and average molecular weights of the tars described above indicate that upon hydrotreatment they should yield liquids of similar composition.

Examination of the analyses for the hydrotreated products of the tars shows this to be an accurate assumption. However, two significant differences were noted: the product resulting from the catalytically produced hydroxypropylolysis tar had a lower H/C ratio, but a greater daf coal basis yield of light naphtha.

CONCLUSION

Although hydroxypropylolysis processes have been historically associated with high yields of methane and light hydrocarbon gases, and low yields of total liquid products, the experiments described in this paper demonstrate otherwise. We have shown that with the proper choice of catalysts and reaction conditions, two-stage catalytic hydroxypropylolysis can achieve yields of high-quality liquids rivaling those for two-stage direct liquefaction processes which utilize a recycle solvent. In addition, the yield of low value hydrocarbon gases can be minimized. Use of catalytic hydroxypropylolysis to convert coal to liquid fuels may offer advantages associated with elimination of the recycle solvent, which constitutes two-thirds of the mass of the reactor feed in traditional direct liquefaction processes. However, in order to be economically feasible, processing technology must be developed to use low catalyst concentrations or to permit addition, withdrawal, regeneration and recycle of the first-stage hydroxypropylolysis catalyst. This, of course, is a task requiring a great deal of additional effort.

ACKNOWLEDGEMENTS

The authors thank the British Coal Corporation for permission to publish this paper. The views expressed are those of the authors and not necessarily those of the Corporation. This work was supported by the Corporation through an ECSC contract (The Direct Conversion of Coal to Chemical Feedstocks, 7220-EC/827). The portion of this study performed at Sandia National Laboratories was funded by the U.S. Department of Energy under contract DE-AC04-76DP00789.

REFERENCES

1. Gavalas, G. R., "Coal Pyrolysis", Elsevier (1985).
2. Chakrabartty, S. K. and du Plessis, M. P. "Modern Coal Pyrolysis", Alberta Research Council, Information Series 95 (1985).
3. Furfari, S., IEA Report No. ICTIS/TR20 (1982).
4. Snape, C. E. and Martin, T. G., Proc. of Round Table Meeting, Commission of the European Communities, Brussels, December 12, 1987, EUR 10588, p. 167.
5. Bolton, C., Snape, C. E., and Stephens, H. P., Amer. Chem. Soc., Fuel Div., Prep. of Papers 32, No. 1, 617 (1987).
6. Stephens, H. P., Bolton, C. and Snape, C. E., Coal Sci. Tech. 11, 1987 International Conf. on Coal Sci., p. 703 Elsevier, Amsterdam (1987).
7. Weller, S., Pelipetz, M. G., Friedman, S. and Storch, H. H., Ind. Eng. Chem. 42 (2), 330 (1950).
8. Hawk, C. O. and Hiteshue, R. W., U. S. Bur. Mines Bull. No. 622 (1965).
9. Derbyshire, F. J., Davis, A., Lin, R., Stansberry, P. G. and Terrer, M-T., Fuel Proc. Tech., 12, 127 (1986).
10. Wood, R. E. and Wiser, W. H., Ind. and Eng. Chem. Proc. Des. Dev., 15 (1), 144 (1976).
11. Kershaw, J. R., Barrass, G., and Gray, D., Fuel Proc. Tech., 3, 115 (1980).
12. Hiteshue, R. W., Friedman, S. and Madden, R., U. S. Bur. of Mines reports 6027 (1962), 6125 (1962), 6376 (1964) and 6470 (1964).

13. Schroeder, W. C., U. S. Patents 3,030,297 (1962), 3,152,063 (1964) and 3,926,775 (1975).
14. Dosch, R. G., Stephens, H. P. and Stohl, F. V., U. S. Patent No. 4,511,455 (1985).
15. Stephens, H. P., Dosch, R. G., and Stohl, F. V., Ind. and Engr. Chem. Prod. Res. and Dev. 24, 15 (1985).

TABLE I. Product Distributions Resulting from Single-Stage Hydropyrolysis Experiments¹

CATALYST (daf Coal Basis Wt % Active Metal)	TAR	METHANE	C ₂ -C ₄ HYDROCARBONS	CHAR	SELECTIVITY Prod. Wt. Ratio (tar/gas)
None	26	3	4	60	3.7
ZnCl ₂ (5%)	36	6	7	45	2.8
SnCl ₂ (1%)	54	6	7	30	4.1
Ni-Mo/Alumina (3.6%)	42	3	4	42	6.0
CoNiMo HTO-bulk (2.9%)	38	2	4	46	6.3
Pd HTO-bulk (2.0%)	47	3	4	35	6.7
Ni HTO coating (0.5%)	50	4	6	32	5.0
Ni HTO coating (1.0%)	53	4	6	29	5.3
Pd HTO coating (0.7%)	64	3	9	16	5.3
Pd HTO Coating (1.6%)	62	4	7	20	6.2
MoS ₂ (0.6%)	59	4	6	20	5.9

1. Products are given on a Wt.% daf coal basis and included -6% water and -2% CO + CO₂.

TABLE II. Composition of Primary Hydropyrolysis Tar and Second-Stage Product for Experiments With and Without a Catalyzed First Stage¹

<u>Primary Tar Composition</u>	<u>Uncatalyzed First Stage</u>	<u>Catalyzed First Stage²</u>
C	84.3	86.1
H	6.8	7.0
O Wt % of product	5.3	3.6
N	1.5	1.7
S	0.9	0.4
OH	4.3	3.0
H/C atomic ratio	0.97	0.98
% Aromatic H of total H	36	33.5
M _n -number ave. mol. wt.	250	270

Second-stage Product³

C	84.0	88.0
H Wt % of product	13.6	11.9
OH	0.01	0.05
ppm N	7	33
H/C atomic ratio	1.94	1.62
% Aromatic H of total H	4	7
Light Naphtha (Wt % daf coal)	8.3	11.2

1. First Stage Conditions - 500°C, 150 atm hydrogen pressure.
 Second Stage Conditions - 400°C, 150 atm hydrogen pressure.
2. First Stage Catalyst - 0.4%, coal basis, MoS₂.
3. Second Stage Catalyst - Ni-Mo/alumina.

CATALYTIC CONVERSION OF METHANE TO METHANOL,
FORMALDEHYDE AND HIGHER HYDROCARBONS

Jack H. Lunsford

Department of Chemistry
Texas A&M University
College Station, TX 77843

INTRODUCTION

By suitably choosing the catalyst and oxidant it is possible to direct the conversion of methane either to oxygenated products (HCHO and CH₃OH) or hydrocarbons (mainly C₂H₄). High selectivities to methanol and formaldehyde have been achieved only at low conversion levels and only using nitrous oxide as the oxidant (1,2). Considerably more progress, however, has been made in the oxidative coupling of methane to form ethane and ethylene (C₂ products) (3-8). The purpose of this paper is to show that both formation of oxygenates and C₂ products occur by a common intermediate, namely the CH₃· radical, which in one case reacts with the surface to form methoxide ions, and in the other reacts mainly in the gas phase to form ethane.

CONVERSION TO OXYGENATES

Molybdena supported on silica is moderately active and selective for the catalytic conversion of CH₄ to CH₃OH and HCHO when N₂O is used as the oxidant as indicated by the results of Table I (1). Up to ca. 2% conversion very high combined selectivities to CH₃OH and HCHO were obtained, but at 6% conversion the selectivities to the desired oxygenates were decreased considerably. With O₂ as the oxidant the results were considerably poorer.

Although this system holds little promise as a practical catalyst, it does provide insight into possible means of activating CH₄ and following the chemistry of surface intermediates. This study, for example, points to the role of thermally generated O⁻ ions in the activation of methane. Previous work by Bohme and Fehsenfeld (9) have shown that gas phase O⁻ ions are very effective in the abstraction of hydrogen atom from simple alkanes via the reaction



Likewise, methyl radicals are formed on Mo^{VI}/SiO₂ via the photochemical reactions



and their EPR spectra are shown in Figure 1b (1,10). Of more importance in catalysis, O⁻ may be formed by the thermal reaction of Mo^V/SiO₂ with N₂O, and CH₄ reacts with these oxygen ions at temperatures as low as 196°C. The resulting CH₃· radicals are shown in Figure 1a.

Infrared results (Figure 2) suggest that these $\text{CH}_3\cdot$ radicals react with the molybdena surface via reductive addition to form methoxide ions. It is known from extensive work on the partial oxidation of methanol over supported and unsupported molybdena that methoxide ions are intermediates in the formation of formaldehyde. In the presence of water these molybdenum alkoxide ions react to form methanol. Thus, the partial oxidation of methane to oxygenates may be understood by the catalytic cycle depicted in Scheme I. In addition to the selective cycle one must also consider the possibility of a two-electron reaction with N_2O to form oxide ions. A molecule of CH_4 would then have to be consumed in a nonselective manner to reduce Mo^{VI} back to Mo^{V} . In principle the two-electron transfer could be minimized by dispersing the Mo as a dimer on the surface and by avoiding the reduction of this molybdenum to the IV oxidation state.

OXIDATIVE COUPLING

When methyl radicals are formed on oxides which contain no reducible metal ions, then the formation of methoxide ions is limited and the radicals have adequate lifetimes either to couple on the surface or to desorb into the gas phase. Several of the more active and selective catalysts for the oxidative dimerization of methane are listed in Table II, where it is apparent that the steady state yields of C_2 products may reach 25%. The starting materials are given in the table and under reaction conditions the working catalyst are mainly metal oxides which are extensively covered by alkali metal carbonates. These carbonates probably serve, in part, to prevent the formation of methoxide ions on oxides such as ZnO and Mg_6MnO_8 .

In addition, alkali metal ions may yield specific centers which are capable of forming methyl radicals. For example, with the Li^+/MgO , and Na^+/CaO catalysts centers of the type $[\text{Li}^+\text{O}^-]$ and $[\text{Na}^+\text{O}^-]$ serve as sources of O^- ions, which activate methane as described in the previous section (3,5). There is increasing evidence that at reaction temperatures greater than 750°C , the alkali metal carbonates partially decompose to form their respective oxides and that the oxides themselves are able to activate methane. This is particularly true for Na_2O_2 , which is the most stable oxide of sodium (13).

On the crystal faces of closed shell oxides, of which MgO is an example, the bonding of $\text{CH}_3\cdot$ radicals is weak (14), and therefore it is not surprising that the radicals emanate into the gas phase where coupling occurs. It has been demonstrated that over a Li^+/MgO catalyst >40% of the C_2 products may be formed by such gas phase coupling reactions (15,16). Unfortunately, in the presence of molecular oxygen other gas phase radical reactions may occur which ultimately result in the formation of CO_2 . Similarly, C_2H_6 and C_2H_4 may be oxidized both heterogeneously and homogeneously which limits C_2 yields to ca. 25%.

ACKNOWLEDGMENTS

This work was supported mainly by the National Science Foundation under Grant No. CHE-8617436.

REFERENCES

1. Liu, H.-F., Liu, R.-S., Liew, K.Y., Johnson, R.E. and Lunsford, J.H., *J. Am. Chem. Soc.*, 106, 4117 (1984).
2. Kahn, M.M. and Somorjai, G.A., *J. Catal.*, 91 263 (1985).
3. Ito, T. and Lunsford, J.H., *Nature (London)*, 314, 721 (1985); Ito, T., Wang, J.-X., Lin, C.H. and Lunsford, J.H. *J. Am Chem. Soc.* 107, 5062 (1985).
4. Matsuura, I., Utsumi, Y. Nakai, M. and Doi, T., *Chem. Lett.*, 1981 (1986).
5. Lin, C.-H., Wang, J.-X. and Lunsford, J.H., *J. Catal.*, in press.
6. Otsuka, K., Liu, Q., Hatano, M., Morikawa, A., *Chem. Lett.* 467 (1986).
7. Moriyama, T., Takasaki, N., Iwamatsu, E. and Aika, K. *Chem. Lett.*, 1165 (1986); Iwamatsu, E., Moriyama, T., Takasaki, N. and Aika, K., *J. Chem. Soc. Chem. Commun.* 19 (1987).
8. Sofranko, J.A., Leonard, J.J., Jones, C.A., Gaffney, A.M. and Withers, H.P., *Petroleum Div. Preprint, ACS Meeting, New Orleans, Aug. 1987*, pp. 763-769.
9. Bohme, D.K. and Fehsenfeld, F.C., *Can. J. Chem.* 47, 2712 (1969).
10. Lipatkina, N.I., Shvets, V.A. and Kazansky, V.B. *Kinet. Katal.* 19, 979 (1978).
11. Cheng, W.-H., Chowdhry, U. Ferretti, A., Firment, L.E., Groff, R.P., Machiels, C.J., McCarron, E.M., Ohuchi, F., Staley, R.H. and Sleight, A.W. in "Heterogeneous Catalyst" (B.L. Shapiro, Ed.) pp. 165-181, Texas A&M Univ. Press, College Station, Texas, 1984.
12. Yang, T.J. and Lunsford, J.H., *J. Catal.* 103, 55 (1987).
13. Otsuka, K., Said, A.A., Jinno, K. and Komatsu, T., *Chem. Lett.* 77 (1987).
14. Mehandru, S.P. and Anderson, A.B., *J. Am. Chem. Soc.* 110, 1715 (1988).
15. Campbell, K.D., Morales, E. and Lunsford, J.H., *J. Am. Chem. Soc.* 109, 7900 (1987).
16. Campbell, K.D. and Lunsford, J.H., *J. Phys. Chem.*, in press.

Table I. Conversion and Selectivity during Methane Oxidation^{a,b}

T, °C	conven, %	selectivity, %			
		HCHO	CH ₃ OH	CO	CO ₂
550	1.6	79.5	20.5		
560	1.9	80.1	19.9		
570	2.9	64.3	13.8	19.1	2.8
580	4.0	58.8	10.0	27.7	3.4
594	6.0	49.5	7.8	38.1	4.6

^a1.0 g of Mo/Cab-O-Sil, P_{CH₄} = 75 torr, P_{N₂O} = 280 torr, P_{H₂O} = 260 torr, F = 1.33 mL/s.

^bRef. 1.

Table II. Oxidative Coupling of Methane Over Promoted Metal Oxide Catalysts

Catalyst	Temp, °C	CH ₄ Conv, %	C ₂ Sel, %	C ₂ Yield %	Ref.
Li ₂ CO ₃ /MgO	720	43	45	19.4	1
Li ₂ CO ₃ /Sm ₂ O ₃	750	38	54	20.7	6
NaNO ₃ /MgO	800	39	57	22.4	7
Li ₂ CO ₃ /ZnO	740	36	67	23.9	4
Na ₂ CO ₃ /CaO	725	33	45	14.8	5
NaMnO ₄ /MgO	925	22	70	15.4	8

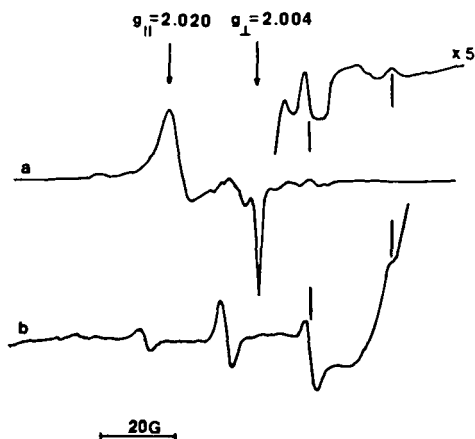


Figure 1. EPR spectra of methyl radicals: (a) after reaction of CH_4 with O^- on Mo/SiO_2 ; (b) after UV irradiation of oxidized Mo/SiO_2 in the presence of CH_4 . Reactions were carried out and spectra recorded with the sample at -196°C . (Ref. 1)

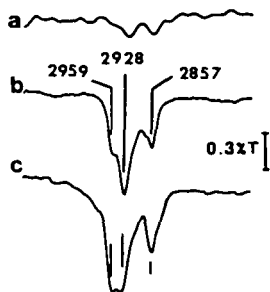
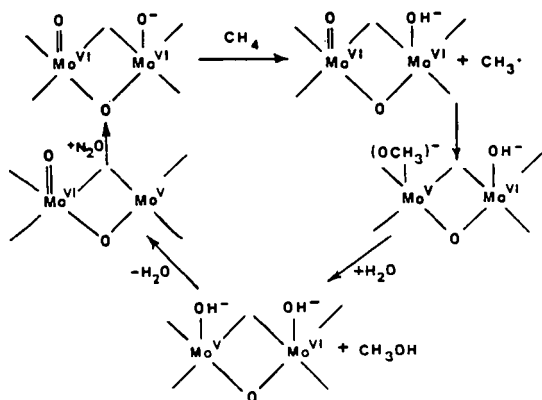
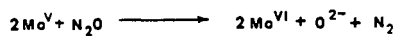
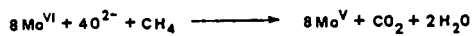


Figure 2. Infrared spectra of methoxide ions on Mo/SiO_2 : (a) background after reduction of catalyst in CO , followed by adsorption of N_2O and evacuation; (b) after subsequent adsorption of CH_4 and evacuation; (c) after adsorption of CH_3OH and evacuation. (Ref. 1)



SCHEME 1

THE ROLE OF ALKALI PROMOTERS IN SELECTIVE
CATALYTIC COUPLING OF METHANE

Jon G. McCarty and M. A. Quinlan
SRI Int'l, 333 Ravenswood Ave., Menlo Park, CA 94025

ABSTRACT

The role of alkali promoters in increasing the hydrocarbon selectivity of catalytic methane coupling is under investigation for series of unpromoted and alkali-promoted alkaline earth and rare earth oxides. Multilayer quantities of CO_2 and fractional monolayer quantities of O_2 and H_2O evolved during temperature-programmed desorption (TPD) experiments immediately following the stationary-state oxidative dimerization of methane by Na/CaO and Li/MgO . These results suggest that a relatively passive and protective layer of molten alkali carbonate with surface hydroxide and surface oxide components is formed on the promoted CaO and MgO surfaces during partial oxidation. Isotope exchange experiments with deuterium-labeled methane in the absence of gas phase oxygen showed high rates of H-D exchange on both the unpromoted and the Na-promoted CaO catalysts, indicating that the formation of methyl radicals may not limit the rate of production of higher hydrocarbons. The presence of an adsorbed species that released methane at moderate temperature, about 550 K, was also revealed in the TPD experiments following methane dimerization. Methyl (or methoxy) and hydroxyl entities coadsorbed on the carbonate layer are suggested as the source of methane observed in these TPD experiments.

INTRODUCTION

An increase in the worldwide supply of natural gas, increasing restrictions on the flaring of remote natural gas, and the high cost of synthesis gas conversion provide great incentives to develop processes that directly and economically convert methane to readily transportable and higher value products.¹⁻³ Hydrocarbon formation through the selective oxidation of only the excess hydrogen in the methane molecule is thermodynamically favorable, while direct thermal conversion of methane to higher hydrocarbons is thermodynamically unfavorable and energy intensive. However, the partial oxidation of methane is difficult because of the relatively high reactivity of useful products and the very

favorable thermodynamics for deep oxidation to carbon dioxide. Successful processes for direct methane conversion into higher hydrocarbons must therefore use highly selective catalysts that strongly inhibit total oxidation, yet retain the capability of activating the stable methane molecule.

Several classes of catalysts have significant selectivity for methane activation, including alkaline earth oxides, rare earth oxides, manganese oxide, and oxides of the soft metals such as lead, cadmium, bismuth, and antimony. Alkali promoters are widely used with methane activation catalysts,⁴⁻⁸ and often increase selectivity without a corresponding increase in the methane conversion rate. Thus, alkali may act more to suppress hydrocarbon oxidation than to promote methane conversion. In the present work we have used fixed-bed reactor kinetic studies, methane H-D exchange reaction experiments, and post-reaction temperature-programmed desorption (TPD) examination to study the mechanism of methane oxidative dimerization by a variety of unpromoted and alkali-promoted alkaline earth oxide and rare earth oxide catalysts.

EXPERIMENTAL RESULTS

Catalyst Preparation

Samples of alkali-promoted alkaline earth oxide catalysts were prepared from high-purity CaO , MgO , Ba(OH)_2 , Na_2CO_3 , K_2CO_3 and Li_2CO_3 (Johnson Matthey, Puratronic[®], > 99.99%). The preparation consisted of adding appropriate amounts of the alkali carbonate and alkaline earth oxide or hydroxide to a small quantity of distilled water and boiling for 1 hour. The resulting slurry was then air dried overnight at 423 K. Various mole fraction compositions were prepared where the mole fraction of alkali metal is defined as the ratio of moles of alkali metal to the sum of the moles of alkali metal and the moles of alkaline earth oxide. BET (N_2) surface area measurements were performed on these catalysts following a standard pretreatment. Complex rare earth oxide catalysts, such as LaAlO_3 and La_2O_3 , were prepared by precipitation of nitrate salt solutions with tetramethyl ammonium hydroxide, followed by centrifugation and drying. These catalysts were calcined in air at 873 K and characterized by x-ray diffraction and BET surface area measurements prior to the kinetic studies.

Fixed-Bed Reactor Studies of Methane Activation

Isothermal reaction kinetics for methane activation by the alkali-promoted alkaline earth oxide catalyst were examined over a period of time (15 to 72 h) sufficient to establish stationary-state conditions.

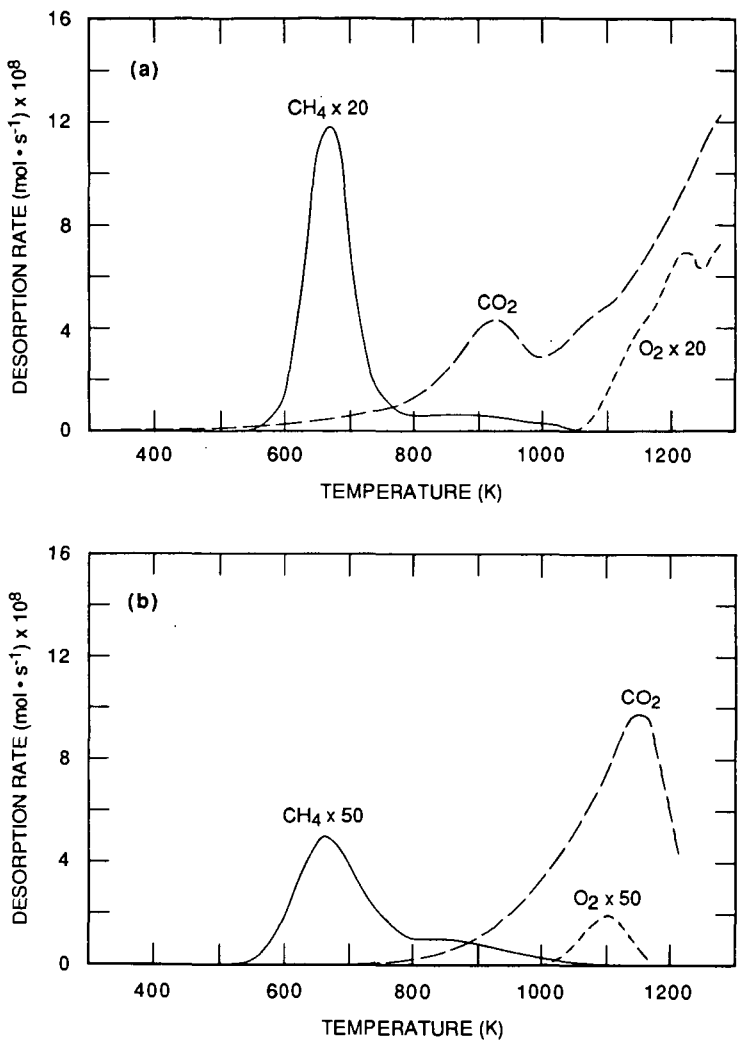
catalytic rates were measured using a fixed-bed microreactor system. Approximately 50-mg samples were loaded in 4-mm-ID quartz reactors. The reaction products were analyzed by gas chromatography using a 6-ft Carbosieve[®] column with a flame ionization detector. The chromatographs were calibrated using a certified standard blend of reactant and product gases. The methane conversion and product selectivities were based on the number of moles of carbon reacted per unit time. C₂₊ yield is defined as the product of methane conversion and selectivity. Product distributions for the series of alkali-promoted alkaline earth oxides at 1000 K ranged from total combustion (for CaO) to 74% C₂₊ (for Li/MgO). The highest methane activation rate was observed for the Na/CaO catalyst.

The results of our kinetic studies are best understood as competition between oxidative coupling of the methane and its complete oxidation to CO₂. Both reactions show a positive reaction order with respect to CH₄; however, the coupling reaction was inhibited by increasing oxygen partial pressure. Thus, with low oxygen partial pressure, methane conversion was not altered by P_{O₂}, but the selectivity for C₂H₆ and C₂H₄ decreased with increasing P_{O₂}.

Extrapolation of our results to zero oxygen partial pressure predicts that selectivities to C₂H₆ approaching 100% are inherently possible in alkali-promoted catalyst systems. Similar results in this range of low oxygen partial pressures were reported by Ito, et al.⁵ When the degree of methane conversion is high, both C₂H₄ and C₂H₆ are observed. The beneficial effect of low O₂ partial pressure on C₂₊ selectivity has long been noted, and is the basis for the redox processes involving the sequential partial oxidation of methane and regeneration of the oxide with air, as demonstrated in the work of Jones, et al.⁹ and Keller and Bhasin.¹⁰

Temperature-Programmed Desorption Studies

The temperature-programmed desorption (TPD) technique was to identify adsorbate binding states as well as bulk phases in the alkali-enriched alkaline earth oxide catalysts. After reaction at elevated temperature, the catalyst was cooled to room temperature in the reactive gas mixture. A stream of pure helium was then passed through the reactor and the catalyst was heated to 1300 K at a rate of 1 K s⁻¹. Desorption and decomposition products were continuously monitored by on-line mass spectrometry. The principal ion masses corresponding to CH₄, H₂O, C₂H_x, CO, C₃H_x, O₂, CH₃OH, and CO₂ were continuously scanned (Figure 1 and Table 1). Variable amounts of O₂, which evolve at high temperatures (>1000 K), small amounts of H₂O, and large quantities of CO₂ indicative of bulk carbonate decomposition were observed. All catalysts unexpectedly exhibited methane desorption at low temperature (650 ± 50 K) in submonolayer quantities.



RA-2614-24

Figure 1. Temperature programmed desorption from alkali-metal-promoted alkaline earth catalysts.
 (a) 30 mol % Li/MgO.
 (b) 30 mol % Na/CaO.
 ($1 \text{ K} \cdot \text{s}^{-1}$ heating rate; $0.5 \text{ ml} \cdot \text{s}^{-1}$ He flow rate)

Table 1
TEMPERATURE-PROGRAMMED PRODUCT ANALYSIS^a

Catalysts	Conc. of Sites ($\mu\text{mol g}^{-1}$)	Amount of Desorbed Product ^c ($\mu\text{mol g}^{-1}$)			
		CH ₄	H ₂ O	O ₂	CO ₂
0.01 Na/CaO	96	3.5 (600)	312 (700)	1.1 (1175)	27.9 (800)
0.30 Na/CaO	46	1.7 (675)	10.5 (400+)	0.6 (1100)	583 (1150)
0.30 Li/CaO	17	0.4 (700)	0.8 (broad)	11.0 (>1100)	3.4 (>1100)
0.30 Li/MgO	40	12.9 (675)	15.8 (broad)	12.6 (1225)	683 (925, >1300)

^aTPD conditions: $0.5 \text{ cm}^3 \text{ s}^{-1}$ He flow rate, 1 K s^{-1} heating rate, 0.04 g of catalyst.

^bNumber of surface sites estimated assuming site density of 1×10^{19} sites m^{-2} for the catalyst surface area following pretreatment at 973 K in air for 48 hours.

^cNumber in parenthesis refers to temperature of desorption peak maxima (K).

The quantities of evolved water vapor for 30 mol% Na/CaO and 30 mol% Li/MgO and oxygen for 30 mol% Li/CaO and 30 mol% Li/MgO approached the estimated surface cation density based on the BET surface area measurements, assuming 1.0×10^{19} sites m^{-2} . The CO₂ evolved for the 0.01 and 0.3 Na/CaO and 0.3 Li/MgO samples was almost equal to the quantity of carbonate expected if all alkali was converted to the carbonate during reaction. Thermodynamic calculations predict the formation of bulk carbonates under reaction conditions, despite the low CO₂ selectivity of the alkali/alkaline earth oxide catalysts. The nearly one-fourth monolayer quantities of desorbing oxygen and water vapor (the latter presumably from hydroxyl species) may arise from chemisorbed species or possibly from gas dissolved in the bulk carbonate.

Isotopic Exchange

The extent of hydrogen exchange between CD₄ and CH₄ on calcium oxide catalysts was investigated by injecting an aliquot consisting of a dilute

mixture of CD_4 and CH_4 into a stream of helium and through the catalyst bed at elevated temperatures. The degree of H-D exchange in the methane components of the effluent gas was measured by on-line mass spectrometry. Several pulses of a mixture containing 2.0 μmol CH_4 and 0.6 μmol CD_4 were injected over a temperature range from 300 to 1200 K for CaO and Na-promoted CaO catalysts and for an empty reactor containing the thermocouple assembly. Ion current for masses 15 through 20 amu corresponding to CH_3^+ , CH_4^+ , CDH_3^+ , $CD_2H_2^+$, CD_3H^+ and CD_4^+ ions respectively, were scanned during each pulse.

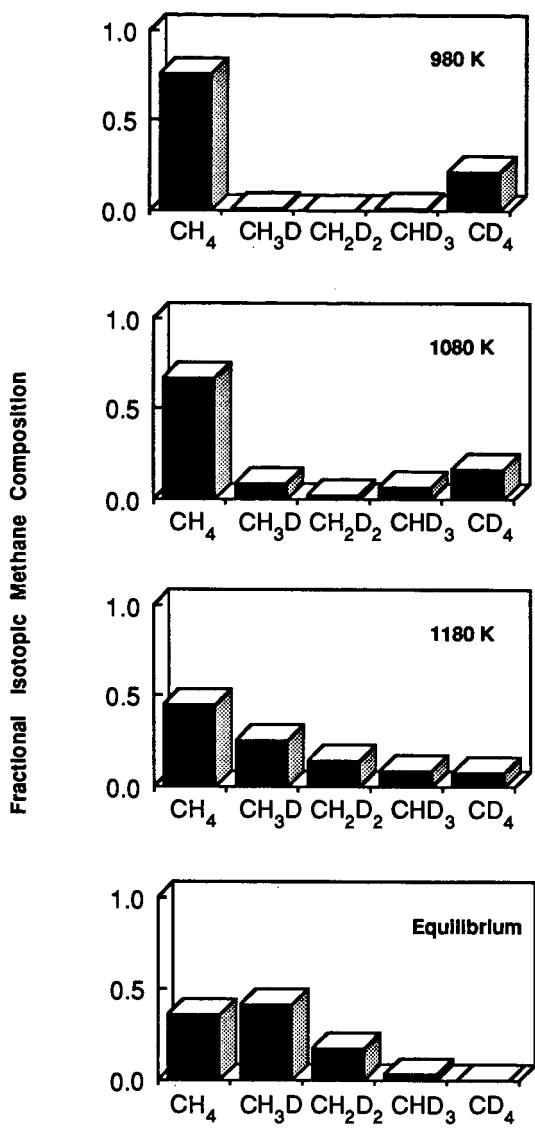
Both pure CaO and sodium promoted calcium oxide showed substantial activity for hydrogen exchange with CD_4 . The extent of H exchange between CH_4 and CD_4 was taken as the conversion of CD_4 since the equilibrated population of CD_4 would be very small ($< 1\%$ of the total methane) given the low D/H ratio ($D/H = 0.3$). At 980 K, 6% of the CD_4 was converted to $CD_{4-x}H_x$ on Na/CaO (Figure 2) while about 60% was converted on CaO. Under these conditions, stationary-state methane conversion with the Na/CaO catalyst was about 5%. Similarly exchange measurements have been reported¹¹ for MgO and Al_2O_3 . Based on CD_4 conversion in the blank reactor, less than 15% of the observed exchange with Na/CaO was attributed to homogeneous gas phase reaction or to reactions occurring on the thermocouple assembly or reactor wall surfaces.

Apparently the hydrogen exchange reaction and the coupling reaction occur simultaneously. The temperature of the onset of hydrogen exchange (800 to 900 K) is approximately the same as the appearance of C_{2+} and CO_2 reaction products during the temperature programmed oxidative coupling of methane over 0.3 Na/CaO and the onset of H_2O and CO_2 evolution during the TPD experiments.

CONCLUSIONS

The kinetics of methane activation were examined for a series of CaO catalysts promoted by lithium, sodium, and potassium oxide/carbonate salts. The methane conversion activity and higher hydrocarbon selectivity follow the order $Na > Li > K$ with respect to promoter. This result is in accord with the idea that cation size, and presumably intersolubility of alkali-alkaline earth cations, influences the nature and surface density of active sites.

The sodium-promoted CaO catalyst system showed high intrinsic C_2H_6 selectivity ($> 80\%$ mol% carbon basis in the limit of low conversion and low oxygen partial pressure), good activity (about twice the methane conversion rate per unit area relative to lithium-promoted magnesia under



RA-2614-26

Figure 2. Isotopic concentration of methane pulses over 30 mol% Na/CaO at various temperatures. (Pulse composition: 2.1 micromoles CH₄, 0.6 micromole CD₄)

identical reaction conditions), and good stability (no observable decrease in rate and selectivity after 72 hours). Our results are in substantial agreement with published work.

Detailed reaction order experiments showed that the rate of methane conversion was linear with methane partial pressure as expected and independent of oxygen partial pressures, whereas the C_2 selectivity varied as the square root of methane partial pressure and the inverse square root of oxygen partial pressure. This result shows that operation at moderate pressure (especially with fixed low oxygen partial pressure) with Na/CaO and presumably other alkali-promoted alkaline earth oxide catalyst would increase the hydrocarbon yield. Other kinetic studies showed the weak dependence of C_2 selectivity of CO_2 partial pressure and the strong correlation between ethene/ethane product ratio and methane conversion.

ESR experiments were performed in situ at temperatures up to 920 K to detect thermally induced radical oxygen anion species in the presence of oxygen, methane, or a reacting gas mixture. Signals attributable to O^- or $[A^+O^-]$ centers were photoinduced at 78 K but rapidly disappeared at higher temperatures (temperatures below 300 K). This result indicates that O^- centers are not sites for methane activation by selective dimerization catalysts.

TPD experiments indicate that the alkali components after extended reaction exist in the form of (probably molten) carbonate salts on MgO and CaO catalysts. Minor, perhaps fractional, monolayer quantities of oxygen and hydroxyl species were also shown to be present on the working catalysts. Other TPD experiments presented tantalizing evidence for an organic intermediate which was stable at temperatures below 550 K, but which decomposed into methane at 750 K in the absence of oxygen.

A picture of the working alkali-promoted alkaline earth methane dimerization catalysts and the reaction mechanism is emerging from the present work and the numerous methane activation studies under way throughout the world. Recent evidence presented by the Texas A&M group¹²⁻¹⁵ convincingly confirms that a free radical mechanism involving gas phase recombination of methyl radicals as a primary step can explain the hydrocarbon product distribution for oxidative methane dimerization. The initial step is the abstraction of a hydrogen atom by an active surface oxygen species with subsequent release of a methyl radical into the gas phase. The high exchange rates we observed between CD_4 and CH_4 suggest that the production of methyl radicals is relatively rapid. Methyl radicals are easily oxidized so that the catalyst surfaces must have a very low concentration of reducible oxygen. The working catalyst may be passivated by the formation of a molten or glassy layer of alkali

carbonate over MgO or CaO surfaces. The carbonate layer may contain surface oxygen or hydroxyl species. The location (gas/alkali carbonate interface, bulk alkali carbonate, or alkali carbonate/alkaline earth oxide interface) and the nature (O^- , O_2^- , or O^{2-}) of the active site is still uncertain. Additional research now under way should clarify both the mechanism and nature of the active site for the initial methane activation step.

ACKNOWLEDGEMENT

This work has been sponsored by a grant from the Gas Research Institute and affiliated industrial cosponsors of GRI's Methane Reaction Science program.

REFERENCES

1. R. Pitchai and K. Klier, *Catal. Rev. -Sci. Eng.* 28, 13 (1986).
2. G. Jean, V. Allenger, and M. Ternan, "Natural Gas: Alternative Sources of Liquid Fuels" in Proceedings of the 37th Canadian Chemical Engineering Conference, Montreal, Quebec, May 18-20, 1987.
3. N. W. Green and R. V. Ramanathan, "Conversion of Natural Gas to Transport Fuels," AIChE Reprint, 1988 Spring National Meeting.
4. D. J. Driscoll, W. Martir, J.-X. Wang, and J. H. Lunsford, *J. Amer. Chem. Soc.* 107, 58 (1985).
5. T. Ito, J.-X. Wang, C.-H. Lin, and J. H. Lunsford, *J. Amer. Chem. Soc.* 107, 5062 (1985).
6. C.-H. Lin and J. H. Lunsford, *J. Phys. Chem.* 90, 534 (1986).
7. T. Matsuda, Z. Minami, Y. Shibata, S. Nagano, H. Miura, and K. Sugiyama, *J. Chem. Soc., Faraday Trans. I* 82, 1357 (1986).
8. C. A. Jones, J. J. Leonard, and J. A. Sofranko, *Energy and Fuels* 1, 12 (1987).
9. C. A. Jones, J. J. Leonard, and J. A. Sofranko, numerous U.S. patents including 4443644-9, 4444984, 4523050, 4547611 assigned to Atlantic Richfield Company.
10. G. E. Keller and M. M. Bhasin, *J. Catal.* 73, 9 (1982).
11. L. Quanzhi and Y. Amenomiya, *Appl. Catal.* 23, 173 (1986).
12. T. Ito and J. H. Lunsford, *Nature* 314, 721 (1986).

13. D. J. Driscoll and J. H. Lunsford, *J. Phys. Chem.* 89, 4415 (1985).
14. J.-X. Wang and J. H. Lunsford, *J. Phys. Chem.* 90, 5883 (1986).
15. K. D. Campbell, E. Morales, and J. H. Lunsford, *J. Amer. Chem. Soc.* 109, 7900 (1987).

STUDIES OF THE GAS PHASE AND Li/TiO₂ CATALYZED OXIDATIVE COUPLING OF METHANE

G.S. Lane and E.E. Wolf

Department of Chemical Engineering
University of Notre Dame
Notre Dame, Indiana 46556

ABSTRACT

The oxidative coupling of CH₄ was studied in the absence of catalysts and using a series of lithium-promoted TiO₂ catalysts by co-feeding CH₄ and O₂. Under some operating conditions, significant gas phase oxidative coupling can occur in the absence of catalysts. The general trend dictated by the gas phase kinetics is that the hydrocarbon selectivity falls as conversion increases. In the catalytic study, the degree of promotion was studied by varying the Li loading from 0 to 31.7% on the rutile phase of TiO₂. Generally, increasing the Li loading reduces the combustion capacity of the catalyst, lowers CH₄ conversion, and increases hydrocarbon selectivity. A 16.2% Li/TiO₂ catalyst had CH₄ conversions around 15% with hydrocarbon selectivities about 75% measured after 2 hours time-on-stream. X-ray diffraction, x-ray photoelectron spectroscopy, and differential thermal analysis were used to characterize the catalyst.

INTRODUCTION

Oxidative coupling of methane has been demonstrated using cyclic feeds(1-3), and co-feeding methane and oxygen (4-9), on a variety of metal oxide catalysts. Little attention has been paid to the gas phase reactions that can occur, even though it has been established that the mechanism involves the formation of CH₃ radicals. One of the objectives of the work reported here was to establish the role of the methane oxidative coupling gas phase reactions. The second objective was to determine the effect of Li on a lithium-titania catalyst system in relation to the gas phase results. The rutile phase of titania was chosen because our previous work indicated that the support imparted special oxygen transfer capacity to Pt supported on rutile (10). Lithium has been shown to be an effective promoter for the oxidative coupling of methane (6), and for this reason it was chosen to promote the titania catalysts. Characterization techniques involving XRD, XPS, and DTA were used to relate the role of Li with the activity results.

EXPERIMENTAL

A detailed description of the experimental apparatus has been presented elsewhere (11), thus only a brief description is given here. The activity measurements were carried out in a single pass flow reactor (0.95 O.D., 15 cm long) made of fused silica. A resistive furnace was specially designed to minimize non-isothermality. Experiments were also performed in a reactor filled with quartz chips and in a stainless steel reactor. Activity measurements were conducted by co-feeding methane, O₂ and He as a diluent. Typical operating conditions were as follows: i) temperature 600-800°C, ii) contact time 0.25 to 1.05 g s/ml, and iii) feed mole ratio of methane to oxygen of 2:1 to 37:1. The reactor effluent concentrations were measured by gas chromatography using carbosphere and Hayesep Q columns in parallel. A different reactor was used for each catalyst sample due to the apparent formation of lithium silicates on the reactor walls.

The catalyst were prepared by wet impregnation using Li₂O dissolved in deionized water to give lithium loadings of 0.0, 1.0, 3.8, 6.7, 11.0 16.2, and 31% on the rutile-titania support (12). XRD analysis was conducted using a Cu K-alpha radiation, and XPS analysis were conducted on a HP-5950 ESCA spectrometer with an Al anode.

RESULTS AND DISCUSSION

Conversion and selectivity (amount of methane converted to a product) results for the gas phase studies are shown in Figs. 1a and 1b at various reactant partial pressures and in Figs. 2a and 2b at various temperatures. Depending on operating conditions; gas phase results yielded selectivities varying from 65% at 2% conversion, to 29% at 32% conversion. Results obtained when the reactor was filled with quartz chips were similar to the gas phase results, indicating that the quartz reactor walls were not responsible for the gas phase results. However, activity measurements conducted in a stainless steel reactor resulted in 100% oxygen conversion and complete combustion of methane to CO₂.

It is clear from Figs. 1a and b and 2a and b that as conversion increases, selectivity to C₂ decreases. This trend is valid when other variables, such as contact time or oxygen and methane partial pressures, are changed, and it appears to be a generic relationship. A detailed comparison of the conversion versus selectivity in the gas phase and catalytic results has been made showing that about half of the published results are below our gas phase results, whereas the other half are above (11). This indicates that in some of the catalytic studies the catalysts promoted combustion of the gas phase products to CO₂.

Results obtained with a 1% Li catalyst are shown in Figs 1c and 1d at various reactants partial pressures and in Figs. 1c and 2d at various temperatures. It can be seen that the catalyst promotes the combustion of C₂ and CO to CO₂. Under the various conditions shown in Fig. 1-2, c-d, the C₂ yield obtained in the presence of the 1% Li/TiO₂ catalyst is lower than in the gas phase.

Figures 3(a) to 3(c) display conversion, selectivity, and yield (conversion times selectivity), obtained with catalysts with different Li loadings, with a Li/MgO catalysts, and without catalysts. The results were obtained under the same operating conditions consisting of 250 mg of sample, dilution ratio of 0.4 (to minimize gas phase results), 100 cc/min total feed flow rate, methane to oxygen feed ratio of 4, 800°C, and after 2 hrs. of time-on-stream. The results in Fig. 3 show that as Li loading increases up to 11%, oxygen conversion decreases leading to an increase in selectivity. Further addition of Li results in an increase in conversion and selectivity, resulting in the highest yield for the 16.2% catalysts. Past the 16% loading the conversion decreases again lowering the yield.

XPS and XRD analysis have been conducted on the 16% catalysts at room temperature. However, DTA analysis indicates that there is a phase transition at about 750°C; consequently, the results at room temperature might not be relevant at the reaction conditions. The room temperature results indicate that increasing Li loading decreases the concentration of surface oxygen which is responsible for the oxidation of reaction intermediates. Work is underway to characterize the catalyst at reaction conditions, and ascertain the nature of the surface species responsible for the increase in selectivity.

ACKNOWLEDGEMENTS

Financial support of the Amoco Research Center, Naperville, IL, is gratefully acknowledged.

REFERENCES

1. Keller, G. E., and Bhasin, M. J., *J. Catal.* **73**, 9-19 (1982).
2. Labinger, J. A., and Ott, K. C., *J. Phys. Chem.* **91**, 2682-84 (1987).
3. (a) Sofranko, J. A., Leonard, J. J., and Jones, C. A., *J. Catal.* **103**, 302-10 (1987). (b) Jones, C. A., Leonard, J. J., and Sofranko, J. A., *J. Catal.* **103**, 311-19 (1987).
4. (a) Aika, K.-I., T. Moriyama, N. Takasaki, and E. Iwamatsu, *J. Chem. Soc., Chem. Commun.* 1210-11 (1986).
5. Hinsen, W., W. Bytyn, and M. Baerns, 8th Int. Cong. on Catal. Proc. III, 581-92 (1984).
6. Ito, T., J.-X. Wang, C.-H. Lin, and J. H. Lunsford, *J. Am. Chem. Soc.* **107**, 5062-68 (1985).
7. Kimble, J. B., and J. H. Koltz, *Energy Prog.* **6**, 226-29 (1986).
8. (a) Lin, C.-H., K. D. Campbell, J.-X. Wang, and J. H. Lunsford, *J. Phys. Chem.* **90**, 534-37 (1986). (b) Lin, C.-H., T. Ito, J.-X. Wang, and J. H. Lunsford, *J. Am. Chem. Soc.* **109**, 4808-10 (1987).
9. (a) Otsuka, K., Q. Liu, M. Hatano, and A. Morikawa, *Chem. Lett.* 467-68 (1986). (b) Otsuka, K., Q. Liu, M. Hatano, and A. Morikawa, *Chem. Lett.* 903-06 (1986). (c) Otsuka, K., K. Jinno, and A. Morikawa, *J. Catal.* **100**, 353-59 (1986).

10. Lane G. S., and E. E. Wolf, *J. Catal.* **105**, 386-404 (1987).
11. Lane G. S., and E. E. Wolf, *J. Catal.* In press.
12. Lane G. S., and E. E. Wolf, *Proc. 9th Int. Congress on Catalysis, Calgary* (1988).

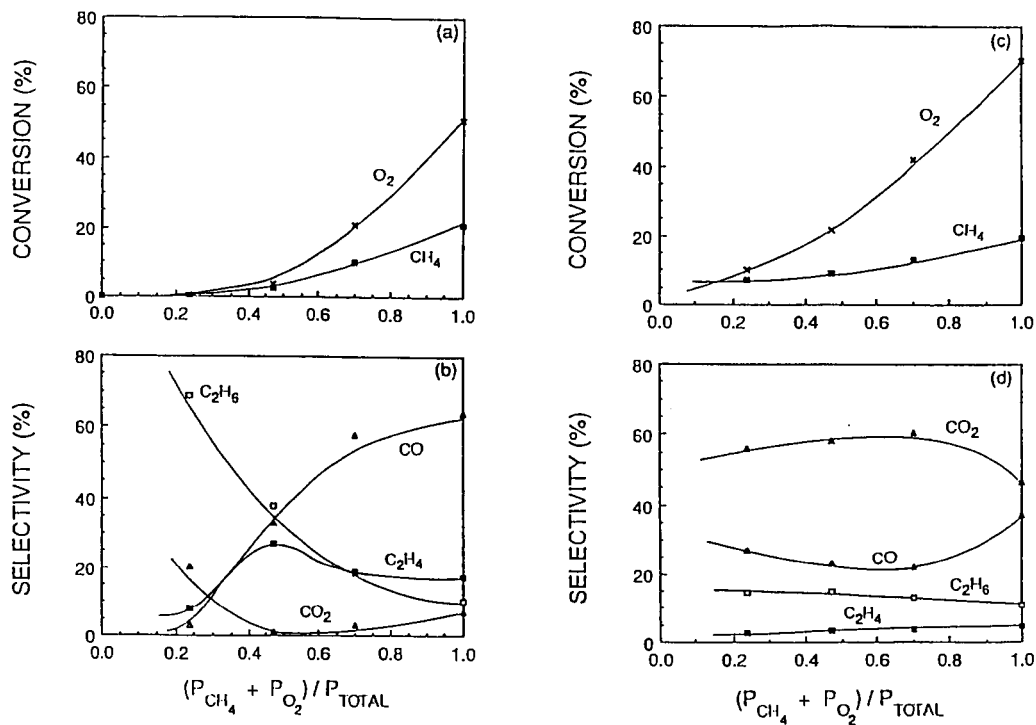


Fig. 1. Effect of dilution on conversion and selectivities at 750°C with a CH₄/O₂ feed mole ratio of 2 and a total flow rate of 50 cc/min. (a) and (b) represent results from a homogeneous study, and (c) and (d) represent results for a 1.0% Li/titania catalyst (250 mg sample).

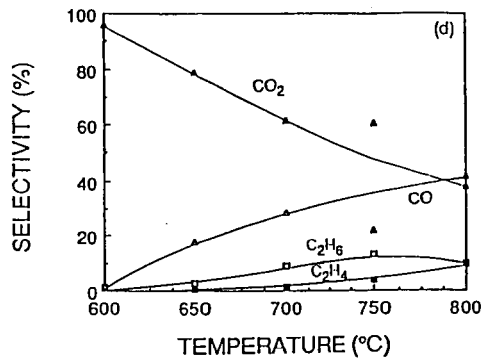
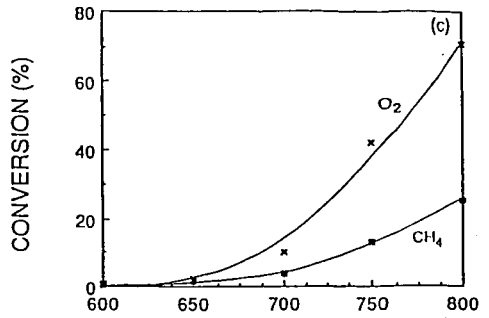
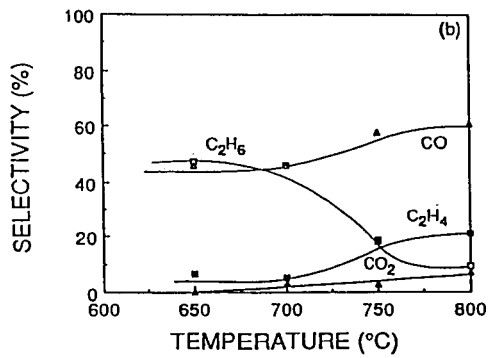
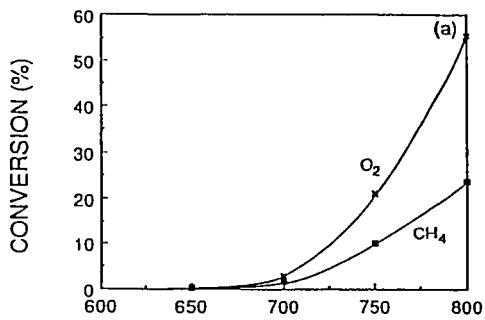


Fig. 2. Comparison of the effects of temperature on conversion and selectivity for a feed flow rate of 50 cc/min, CH₄ and O₂ partial pressures of 0.47 and 0.23, and a dilution ratio of 0.7. (a) and (b) represent results from a homogeneous study, and (c) and (d) represent results for a 1.0% Li/titania catalyst (250 mg sample).

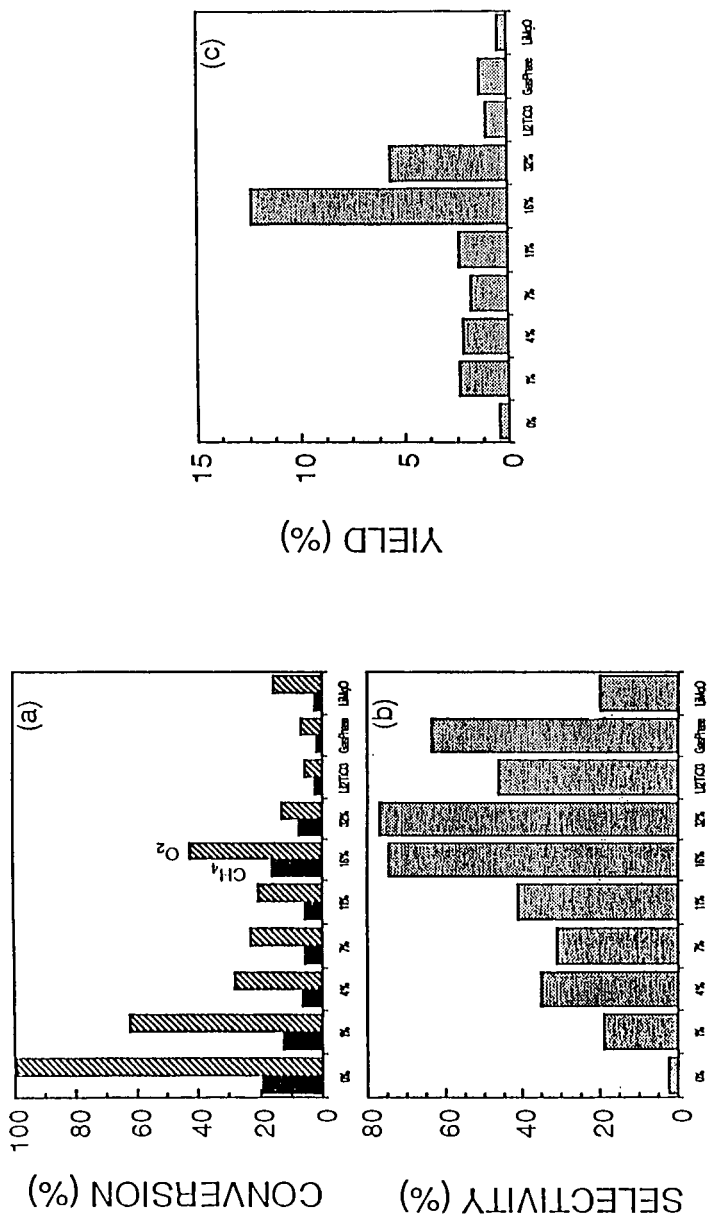


Fig. 3. Comparison of conversions, selectivities, and yields of several catalysts. The results represent samples taken at 800°C and 2 hours time-on-stream with a CH_4/O_2 feed mole ratio of 4, a total flow rate of 100 cc/min, a 250 mg catalyst sample, and a reactant partial pressure of 0.4.

"Kinetics and Mechanism of Methane
Oxidative Coupling over Samarium Oxide"

M. -Y. Lo, S. N. Kamat, and G. L. Schrader

Department of Chemical Engineering and
Ames Laboratory - USDOE
Iowa State University
Ames, Iowa 50011

Introduction

The direct conversion of methane to higher hydrocarbons is a promising process for the chemical utilization of methane, which is a major component of natural gas. Although many metal oxides (1,2) have proven to be active and selective for the direct conversion of methane to form C_2 hydrocarbons, there has been no general agreement on the mechanism of methane coupling. Lunsford and co-workers (3) studied the oxidative coupling of methane over Li/MgO and a series of rare earth oxide catalysts. Their results suggested that methyl radicals are formed during methane activation and the coupling of methyl radicals in the gas-phase is the major route for C_2 hydrocarbons formation. On the other hand, Carreiro and Baerns (4) and Asami *et al.* (5) studied the oxidative coupling of methane over lead oxo-salts and PbO/MgO catalysts, respectively. Their results suggested that ethane is formed from the coupling of adsorbed methyl radicals on the catalysts surface.

In addition, the types of oxygen species used for the activation of methane or for the subsequent reactions of activated methane are not very well defined. Lunsford and co-workers (3) suggested that O^- is responsible for the activation of methane and O^- and/or $O_2(g)$ are used for carbon oxides formation on Li/MgO catalysts. Otsuka and Nakajima (6) suggested that adsorbed O_2 is responsible for the activation of methane and $O_2(g)$ is responsible for the formation of carbon oxides over Sm_2O_3 .

Lo *et al.* (7) studied the adsorption of methanol, methyl iodide and methane over Sb_2O_4/SiO_2 using NMR spectroscopy. They observed the formation of methoxy species over the catalyst surface; this intermediate is the precursor for carbon dioxide formation.

The purpose of the present study is to use samarium oxide as a model catalyst to investigate the mechanism of methane coupling at atmospheric pressure using oxygen as the oxidant.

Experimental Procedure

Catalysts preparation

Samarium oxide (Sm_2O_3) catalysts were prepared from various samarium oxides and salts. Different calcination temperatures were employed also.

- (1) Hydrothermally (HT) treated samarium oxide was prepared by placing Sm_2O_3 (Aldrich 99.9%) in a beaker containing deionized water. Residues obtained after evaporation of the water were calcined at 800°C for 16 h and 800°C for 4 h.
- (2) Samarium oxide was heated to 1100°C for 22 h.
- (3) Samarium nitrate hexahydrate was calcined at 900°C for 1 h.

XRD was used to determine the phases present. Surface areas were determined from BET measurements using N_2 as the adsorbate at 77 K.

Reaction studies

Methane oxidation was studied using a laboratory scale fixed-bed reactor system which could be operated in either flow or pulse modes. The reactor consisted of a 7 mm ID and 19 mm length quartz tubes which act respectively as the pre-heating and catalytic zone of the reactor. The 7 mm ID tube was fused to a 6 mm OD, 1 mm ID capillary quartz tube in order to reduce the extent of post-catalytic reaction giving rise to combustion products.

Blank experiments were performed at a temperature range of 600°C to 775°C with quartz wool placed in the reactor. Catalytic tests and kinetic studies were performed using the flow mode of the reactor system at atmospheric pressure. 0.2 to 0.8 g of catalyst was used, and the flow rate ranged from 100 to 300 cc min^{-1} . Excess CH_4 was used in the reactant mixtures such that $\text{CH}_4/\text{O}_2 \geq 3$. Effluent gases were analyzed using an on-line gas chromatograph with a thermal conductivity detector. CO , O_2 , and CH_4 were analyzed using a molecular sieve 5A column and $\text{O}_2(\text{CO})$, CO_2 , CH_4 , C_2H_6 , C_2H_4 , and H_2O were analyzed using a Porapak Q column. Pulse experiments were performed using the pulse mode of the reactor system at a total flow rate of 25 cc min^{-1} with or without gas-phase oxygen. Pulse experiments using CH_3I or CH_3OH as reactants involved injection of either reactant at the reactor inlet.

Results and Discussion

The XRD powder patterns for the catalysts prepared in this study are shown in Figure 1. The catalyst prepared by hydrothermally treated Sm_2O_3 shows the presence of two phases, B (monoclinic structure) and C (cubic structure) phases (8,9). The C phase was the major component of this catalyst. The catalyst prepared by calcining Sm_2O_3 at 1100°C for 22 h shows the presence of the B phase only, and the catalyst prepared by calcining $\text{Sm}(\text{NO}_3)_2 \cdot 6\text{H}_2\text{O}$ at 900°C for 1 h shows the presence of the C phase only. These results suggested that the phase composition of the catalyst is dependent on the salt used and the calcination temperature employed.

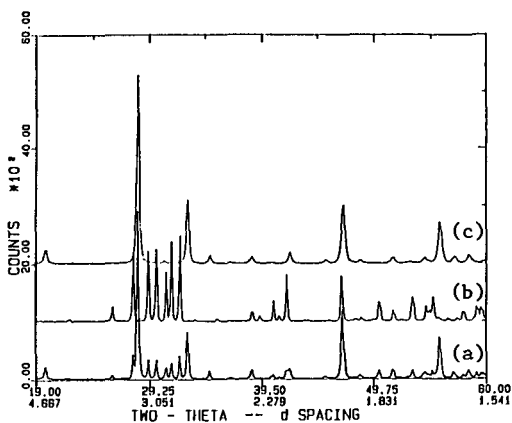


Figure 1. XRD powder patterns of samarium oxide prepared by (a) HT treatment of Sm_2O_3 (B and C phases), (b) Sm_2O_3 calcined at 1100°C for 22 h (B phase), (c) $\text{Sm}(\text{NO}_3)_3 \cdot 6\text{H}_2\text{O}$ calcined at 900°C for 1 h (C phase).

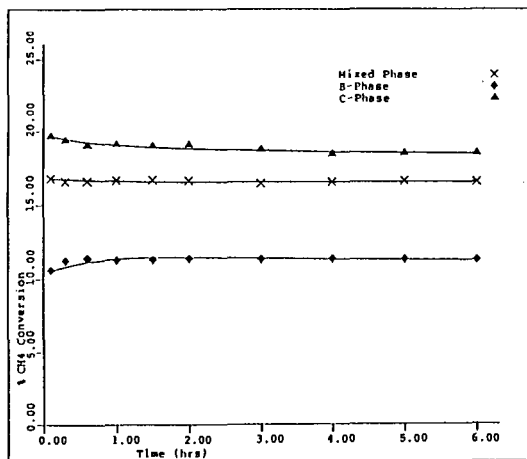


Figure 2. Time dependence on methane conversion over Sm_2O_3 catalysts prepared in this study at 750°C , $\text{CH}_4/\text{O}_2/\text{He} = 58/12/115$.

Blank experiments revealed that the conversion of methane was less than 1% with carbon oxides being the only products. This suggests that the reaction of methane over samarium oxide is surface initiated.

Table 1 shows the activity of methane coupling over untreated (used as obtained from Aldrich Chemical Co.) and hydrothermally treated Sm_2O_3 at steady state. The conversion of methane are practically the same for both catalysts. In addition, although the selectivity to CO is higher for the untreated catalyst, the total yield to carbon oxides and to C_2 hydrocarbons are constant for both catalysts. These data suggest that the two catalysts behave quite similar towards methane coupling. One possible explanation to this similarity is that the untreated catalyst has been on stream ($\text{CH}_4/\text{O}_2 = 3$) for several hours at 700°C . During this time period, the catalyst is continually exposed to water.

Figure 2 shows the conversion of methane over the three Sm_2O_3 catalysts prepared in the present study. Among the three catalysts tested, C-phase Sm_2O_3 is the most active and B-phase Sm_2O_3 is the least active for methane coupling. Figure 3 shows the selectivity to C_2 hydrocarbons over the three catalysts prepared. This figure shows that the HT-treated Sm_2O_3 catalyst gives the highest C_2 selectivity and B-phase Sm_2O_3 gives the lowest C_2 selectivity. In conclusion, C-phase Sm_2O_3 and HT-treated Sm_2O_3 catalysts show a similar C_2 yield for methane coupling. Since most methane coupling studies over Sm_2O_3 catalysts employ mixed phase Sm_2O_3 (B and C phases). The present study will employ HT-treated Sm_2O_3 , which consists of B and C phases, as the test catalyst for kinetic and mechanism study.

Figure 4 shows the effect of CH_4/O_2 ratio on methane conversion and product distribution for methane coupling over Sm_2O_3 at 750°C . High conversions of methane and high selectivity to carbon dioxide are obtained at low CH_4/O_2 ratios. On the other hand, high CH_4/O_2 ratios favor the formation of C_2H_6 in the expense of methane conversion.

Figure 5 shows the activity of methane coupling as a function of CH_4/O_2 time on stream over HT-treated Sm_2O_3 . No appreciable changes in either CH_4 conversion or product selectivities are observed after the catalyst has been used for 20 h. This suggests that the present Sm_2O_3 catalyst is much more stable than the other unpromoted low melting metal oxides (such as lead oxide) in which catalyst deactivation due to catalyst volatility is a serious problem.

Rate laws of the form:

$$\frac{d[\text{product}]}{dt} = k[\text{CH}_4]^m[\text{O}_2]^n$$

were determined for the formation of the principal products (CO , CO_2 and C_2H_6) in kinetic studies. Nonintegral reaction orders in both methane and oxygen were obtained for the formation of CO and C_2H_6 . These results suggest that the rate-determining step for C_2H_6 formation is the reaction between methane and adsorbed oxygen (0.9 order in CH_4 and 0.6 order in O_2

Table I. Activity of methane coupling over untreated and hydrothermally treated Sm_2O_3 at 700°C , $\text{CH}_4/\text{O}_2 = 3$.

Catalysts	% CH_4 Conversion	% Selectivity			
		CO	CO_2	C_2H_4	C_2H_6
Untreated Sm_2O_3	21.9	17.1	38.0	20.9	24.0
HT treated Sm_2O_3	21.2	11.7	46.2	19.9	22.2

Table II. Product distribution of methane coupling over Sm_2O_3 as a function of the # of the pulse at 800°C , $\text{O}_2/\text{CH}_4/\text{He} = 2-0/5-7/130$ with 0.4 g of catalyst.

# of pulse	Rate of product formation ($\mu\text{mole}/\text{min g}$)			
	CO	CO_2	C_2H_6	C_2H_4
1	17.2	101.1	6.8	14.6
2	19.7	90.9	6.7	14.0
3	17.2	87.7	6.4	13.8
4 ^a	--	--	--	--
5	10.7	79.9	4.5	13.1
6	9.8	56.4	3.8	11.0
7	13.5	42.2	3.2	11.0
8	23.2	38.9	2.7	10.6
9	24.9	37.2	2.2	8.9
10	21.4	27.9	3.0	8.9
reoxidation, 11 (20 cc) ^b	22.2	104.8	6.9	13.3
reoxidation, 12 (10 cc)	21.5	70.9	7.2	13.1
reoxidation, 13 (5 cc)	20.9	46.9	6.8	9.1

^aMolecular sieve 5A column was used to analyze the products formed from this pulse experiment to determine whether all O_2 are consumed during this pulse. It was found that all O_2 are consumed during all pulse experiments.

^bReoxidation was done by passing O_2 pulses through the catalyst until no O_2 uptake has taken place, the value in the parenthesis reflects the flow rate of oxygen used during pulse exit.

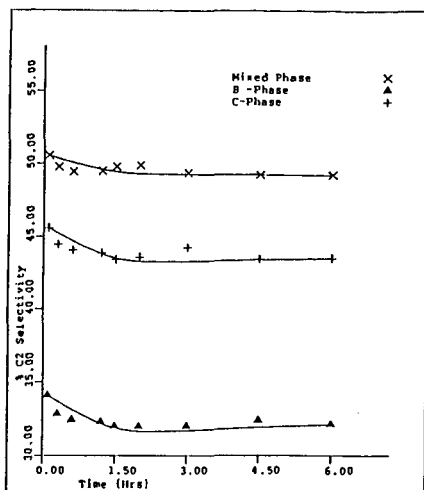


Figure 3. Time dependence on C₂ hydrocarbons selectivity over Sm₂O₃ catalysts prepared in this study at 750°C, CH₄/O₂/He = 2³ 58/12/115.

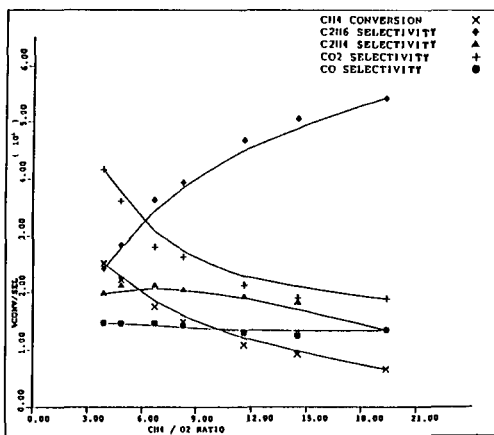


Figure 4. Effect of CH₄/O₂ ratio on methane coupling over HT treated Sm₂O₃ (B + C phases) at 750°C, total flow = 174 cc min⁻¹.

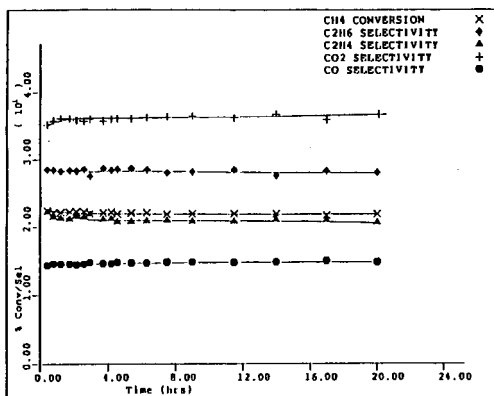


Figure 5. Time dependence on methane coupling over HT treated Sm_2O_3 (B + C phases) at 750°C , $\text{CH}_4/\text{O}_2/\text{He} = 58/12/115$.

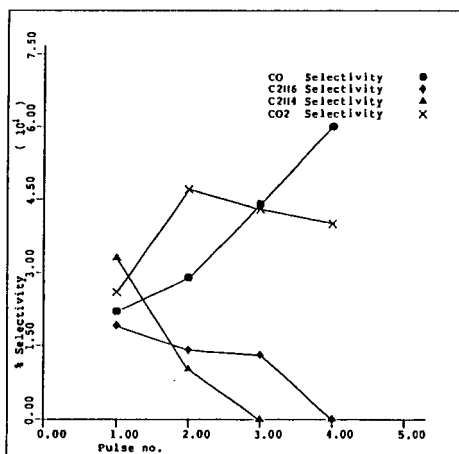


Figure 6. Product distribution in pulsed conversion of methane over HT treated Sm_2O_3 at 800°C in the absence of oxygen. Pulse size = 0.5 mL , $\text{CH}_4/\text{He} = 57/130$.

for a CH_4/O_2 ratio ranging from 4.5 to 18). Rate dependences for CO_2 formation were first order in oxygen and a negative order in methane. This suggests that gas-phase oxygen or adsorbed molecular oxygen (or both) are used for CO_2 formation. In addition, the inhibition effect of CH_4 , as indicated by the negative order, may be one reason why a 93% selectivity to C_2 hydrocarbons is obtained at very high CH_4/O_2 ratios, i.e., $\text{CH}_4/\text{O}_2 = 45$ (2).

The types of oxygen used for methane activation as well as the subsequent reactions of activated methane was investigated by using the pulse reaction studies. Figure 6 shows the product distribution obtained for the pulse reaction with CH_4 as the only reactant. Consecutive CH_4 pulses led to an immediate decrease in the formation of both C_2H_6 and C_2H_4 . No C_2H_4 is observed after the second pulse and no C_2H_6 is observed after three pulses. The total amount of oxygen used for the formation of oxygenates during the first three pulses is less than one monolayer of oxygen (assuming an oxygen packing density of 1×10^{19} atoms/ m^2). This suggests that only surface oxygen species are used for the formation of C_2 hydrocarbons. This result is in good agreement with the kinetic data in which the rate-determining step for C_2H_6 formation is found to be the reaction between gaseous methane and adsorbed monoatomic oxygen. This also suggests that the mobility of bulk oxygen to the surface is slow compared with the rate of C_2H_6 formation.

Table II provides the product distribution for the pulse experiments performed by co-feeding methane and oxygen ($\text{CH}_4/\text{O}_2/\text{He} = 5.7/2/13$) to the reactor. Despite the fact that a high O_2/CH_4 ratio was used, the rate of products formation declined as the pulse experiment progressed. This suggests that adsorbed oxygen species is involved in the formation of products. If only gas-phase oxygen were required we would expect to observe a constant rate of product formation.

The results also show that the decrease in the rate of CO_2 formation is much faster than the rate of the replenishment of oxygen species on the surface of the catalyst. This result is in good agreement with the kinetic data in which the rate of CO_2 formation is reoxidation limited.

The rate of formation of C_2H_6 and C_2H_4 also decreased as the pulse number increased, but to a lesser extent compared to the decrease in the rate of CO_2 formation. However, when the catalyst is reoxidized with O_2 prior to CH_4/O_2 pulses, the rate of C_2H_6 formation is independent to the partial pressure of oxygen in the reactant (pulses #11 to 13). This indicates that the catalyst is partially reduced at steady state since a partial dependency on O_2 partial pressure is observed in kinetic studies.

In addition, since the replenishment of oxygen species for CO_2 formation is slow and is the rate-determining step for CO_2 formation, suppression in this replenishment of oxygen species may lead to an increase in C_2 yield. This also explains why a 93% in C_2 selectivity is obtained by Otsuka *et al.* (2) when $\text{CH}_4/\text{O}_2 = 45$ was used. In such experiments, replenishment of surface oxygen for CO_2 formation is suppressed.

It is generally accepted that the breaking of a C-H bond of methane is the rate-determining step in methane coupling. As a result, methyl radical or radical-like intermediates are formed. The details on the subsequent steps of these intermediates are not very clear yet. The use of methanol or methyl iodide as reactants, in conjunction with the pulse technique, has permitted the subsequent steps following methane activation to be probed. The major products formed from methanol and methyl iodide are methane, carbon dioxide and carbon monoxide. Less than 10% of C₂ hydrocarbons are formed in both reactions. These results suggest that methoxy species is a common intermediate formed from both methanol and methyl iodide, as well as methane. This methoxy species will form either carbon oxides or methane, plus ethane in cases where methane is the reactant, depending on the availability of surface oxygen. Since less than 10% of C₂ hydrocarbon are formed, it seems reasonable to conclude that the coupling of gas-phase methyl radical is a major pathway for ethane formation during methane coupling.

References

- (1) G. E. Keller and M. M. Bhasin, J. Catal. **73**, 9 (1982).
- (2) K. Otsuka, K. Jinno and A. Morikawa, Chem. Lett., 499 (1985).
- (3) (a) K. D. Campbell, E. Morales and J. H. Lunsford, J. Am. Chem. Soc., **109**, 7900 (1987);
(b) K. D. Campbell, H. Zhang and J. H. Lunsford, J. Phys. Chem., **92**, 750 (1988).
- (4) J.A.S.P. Careiro and M. Baerns, React. Kinet. Catal. Lett., **35**, 349 (1987).
- (5) K. Asami, T. Shikada, K. Fujimoto and H. Tominaga, Ind. Eng. Chem. Res., **26**, 2348 (1987).
- (6) K. Otsuka and T. Nakajima, J. Chem. Soc., Faraday Trans., **83**, 1315 (1987).
- (7) M.-Y. Lo, S. K. Agarwal and G. Marcelin, to be published, Catal. Today.
- (8) L. Pauling, Z. Krist., **69**, 415 (1928).
- (9) R. M. Douglass and E. Staritzky, Anal. Chem., **28**, 552 (1956).

Oxidative Coupling of Methane on a Mixed Oxide Catalyst.

Ananth Annapragada and Erdogan Gulari
Department of Chemical Engineering
University of Michigan, Ann Arbor, MI-48109.

We have developed a family of catalysts for the oxidative coupling of methane which achieve high activities and selectivities at temperatures lower than those currently in the literature. Typical figures are: At 575 °C, GHSV = 28800 Hr⁻¹, CH₄/O₂ = 2, total conversion = 11%, C₂ selectivity = 43%. In this paper, we plan to present the development of the catalyst, and our results on the identification of the active components. In addition we will also discuss our steady state, pulse and TPR experiments which have lent some insight into the mechanism of the reaction.

Our steady state activity measurement experiments identified that the catalyst was active both in unsupported and supported form. In general, the unsupported catalyst was more difficult to activate than the supported catalysts. Also, the unsupported catalyst had a much lower range of active compositions than the supported catalyst. We attribute this to the possible existence of a wider distribution of crystal phases in the supported catalyst. The fact that the most active compositions in both supported and unsupported catalysts occurred at the same composition of active components led us to believe that a characterization of the active species in the unsupported catalysts would give us some information about the active species in the supported catalysts. X-ray diffraction and ESCA studies identified a unique species in the active unsupported catalysts. However, this material in pure form was not active as a methane coupling catalyst. We concluded that some complex interaction between this species and the others in the active catalyst was the cause for the activity.

One of the problems we encountered during steady state studies on the catalyst was the fact that a catalyst composition which was active on one occasion was not necessarily active on another occasion under identical conditions. In general, active compositions would achieve a high level of activity approximately 45% of the time. This indicated the existence of multiple steady states either in the in-situ preparation of the catalyst or in the reaction itself. TPR studies indicated

that temperature hysteresis and multiple steady states did indeed exist for the coupling reaction in the vicinity of our operating conditions. Surface titration experiments on the catalysts operating in each of the two steady states indicated a difference in the way oxygen was incorporated into the catalyst during operation at the higher steady state.

Steady state activation energy measurements and suitably designed pulse experiments revealed that the reaction possibly occurred by the following steps:

- (1) Hydrogen abstraction from the methane to form CH_3 - species.
- (2) Coupling of the CH_3 - species to C_2H_6 .
- (3) Pyrolysis of the Ethane to Ethylene.
- (4) Oxidation of the Ethane and Ethylene to CO and CO_2 .

At this point we can only speculate, but we believe that the first two steps occur on the surface of the catalyst, while the last two occur in the gas phase. We attribute the success of this catalyst to its ability to abstract hydrogen from methane at a temperature low enough to support reversible oxygen incorporation into the catalyst.

ELECTROCHEMICAL STUDIES OF OXYGEN ACTIVITY DURING THE OXIDATIVE COUPLING OF METHANE

By
Jeffrey W. McKown and Howard M. Saltsburg

Department of Chemical Engineering
University of Rochester, Rochester, NY 14627

When studying the kinetics of heterogeneous catalytic reactions, it is crucial to be able to measure the surface concentrations under actual reaction conditions. Unfortunately, there are virtually no techniques currently available which permit the measurement of these surface concentrations under the atmospheric pressures and high temperatures that most catalytic reactions occur. In this work we report the measurement of the thermodynamic activity of oxygen on the surface of a Li promoted MgO catalyst during the oxidative coupling of methane. This measurement provides additional information which may be utilized in the description of the different reactions responsible for the formation of the coupling and deep oxidation products.

The measurement of the thermodynamic activity of oxygen on catalytic metal films was first reported in 1976 by Vayenas and Saltsburg in a study of the oxidation of SO_2 over Pt (1,2). An electrochemical cell consisting of two porous catalytic Pt films separated by an oxide conducting solid electrolyte was utilized in these oxygen activity measurements. It has been shown that the oxygen activity on the metal films is related to the measured EMF through the Nernst equation. The surface oxygen activity is directly related to the surface oxygen concentration and its measurement subsequently provides information about reactions involving the surface oxygen.

This technique has been extended by McKown (3) so that the thermodynamic activity of oxygen on metal oxide catalysts may be measured under reaction conditions. It was demonstrated that an electrochemical based oxygen sensor similar to that utilized by Vayenas and Saltsburg was capable of measuring a mobile oxygen species on the oxide catalyst surface. In this manner, the effect that the oxidative coupling of methane reaction is having on the surface oxygen species may be monitored.

The oxygen activity on a Li promoted MgO catalyst was monitored along with overall conversion and selectivity for a variety of reaction conditions. It was found that in the presence of the coupling reaction, the measured surface oxygen activity was always lower than its equilibrium value. Furthermore, the extent of deviation from oxygen gas-surface was observed to be a function of reaction conditions. It was deduced that a reaction involving the mobile surface oxygen was responsible for the lowered steady state amount of surface oxygen. The magnitude of this deviation from equilibrium between oxygen in the gas and on the catalyst surface must then be related to the rate of reaction depleting the mobile surface oxygen.

As the selectivity for the formation of the C₂ products increased, the deviation from equilibrium between oxygen in the gas and oxygen on the catalyst surface was also observed to increase. Since an increased deviation from gas-surface equilibrium indicates an increased rate of reaction involving surface oxygen, it was concluded that the production of the C₂ products, C₂H₄ and C₂H₆, must involve a mobile surface oxygen species. Similar arguments can be employed to deduce that the C₁ products, CO and CO₂, must be formed primarily by a reaction with oxygen from the gas.

Lunsford et. al. (4,5) were able to characterize the active center responsible for the activation of the CH₄ molecule in the Li promoted MgO catalyst using ESR. We have combined their active site characterization with our oxygen activity measurements in a mechanism which is based heavily on experimental observations.

We have demonstrated the ability to measure a quantity which is directly related to the surface oxygen concentration on a metal oxide catalyst under actual reaction conditions. This technique has provided vital information about the types of reactions responsible for the selectivity in the oxidative coupling of methane.

The authors would like to thank the Petroleum Research Fund for partial support of this research.

LITERATURE CITED

1. Vayenas, C., Ph.D. Thesis, University of Rochester (1976).
2. Vayenas, C., Saltsburg H., *J. Cat.*, **57**, 296 (1979).
3. McKown, J.W., Ph.D. Thesis, University of Rochester.
4. Ito, T., Wang, J., Lin, C., Lunsford, *JACS*, **107**, 5062-5068 (1985).
5. Wang, J., Lunsford, J., *J. Phys. Chem.*, **90**, 5883-5887 (1986).

THE PARTIAL OXIDATION OF METHANE AND ETHANE ON
WELL-CHARACTERIZED VANADIUM OXIDE SURFACES

K. Lewis, T. Oyama, and G. A. Somorjai
Department of Chemistry and Materials and
Chemicals Sciences Division
Lawrence Berkeley Laboratory
University of California
Berkeley, California 94720

Vanadium oxide ordered thin films were grown by condensing vanadium metal onto gold single crystal surfaces then oxidizing it. Films of V_2O_5 could also be produced by condensing V_2O_5 onto gold. After characterization by various surface science techniques, chemisorption studies were carried out to study the bonding of CH_4 , C_2H_6 and O_2 . A high pressure cell was then used to carry out partial oxidation studies and the results were correlated with those obtained on silica supported high surface area V_2O_5 catalyst.

SYMPOSIUM ON CATALYTIC AND RELATED CHEMISTRY OF METHANE

PRESENTED BEFORE THE DIVISION OF FUEL CHEMISTRY INC.

AMERICAN CHEMICAL SOCIETY

LOS ANGELES MEETING, SEPTEMBER 25-30 1988

SELECTIVE OXIDATION OF METHANE TO FORMALDEHYDE OVER VARIOUS CATALYSTS

By

G. N. Kastanas, G. A. Tsigdinos and J. Schwank

University of Michigan, Department of Chemical Engineering, Ann Arbor, Michigan 48109

INTRODUCTION

The conversion of methane into useful intermediate oxidation products instead of complete oxidation to CO₂ or partial oxidation to CO is one of the most challenging problems for catalysis research (1). Oxidative coupling leading to the formation of ethane and ethylene from methane (2), (3), (4) and production of oxygenates as methanol and formaldehyde (5), (6), (7), (8) are the two main directions pursued so far and several promising systems have emerged although with low yields. The ultimate goal is to obtain useful intermediates as higher hydrocarbons and/or oxygenates from the main source of methane, the natural gas.

RESULTS AND DISCUSSION

Activity of Vycor- Quartz reactor tubes

Vycor glass has proven to be active in the n-butene isomerization at room temperature (9) as well as in the adsorption of ammonia at 150 °C (10). It was generally believed that the surface hydroxyl groups played an important role in the adsorption, being capable of forming hydrogen bonds with the adsorbates. Sheppard and Yates studied the interaction of various molecules with Vycor glass by infrared spectroscopy (11). In the case of methane a new band, not present in the gas phase spectrum appeared, and it was attributed to physical adsorption. Similar infrared spectroscopy results were obtained in a study of the adsorption of methane on ZSM-5 zeolites by Yamazaki et al (12). Cheaney and Walsh (13) observed a high activity of Vycor glass tubes in the combustion of methane. They attributed the activity to the deposition of a silicic acid layer on the glass

surface during the manufacture of the Vycor glass which included a treatment with HF. When silica tubes were coated with silicic acid, the high CH_4 combustion activity of the Vycor tubes could be reproduced (13).

Throughout the course of our work a small amount of ethane, from 0.14 mol % to 1.25 mol % based on methane was present in the feed stream. Table 1 summarizes the total conversion of methane and the selectivities of the various products obtained in our work over quartz and Vycor glass tubes. At a CH_4/O_2 molar ratio of about 1 and over the temperature range of 893 to 993 K both tube surfaces produced C_2H_4 , C_2H_6 , HCHO and CO_2 . The formaldehyde was identified by Gas Chromatography and Mass Spectrometry. Under the reaction conditions used here, CO was observed only over Vycor glass at temperatures > 940 K. The CO production occurred mainly at the expense of HCHO. At a given temperature, the total methane conversion, over Vycor glass was much higher than the one over quartz. At similar conversions (0.41% at 928 K for Vycor glass and 0.37% at 993 K for quartz) the CO_2 selectivity over Vycor glass was much lower than the one observed over quartz whereas the HCHO selectivity was somewhat higher. The very substantial differences in activity and selectivity between Vycor and quartz reactors despite identical flow conditions and reactor geometries imply that gas interactions sensitive to the nature of the tube surfaces occur. However, in view of the high temperatures, a contribution of gas phase reactions cannot be ruled out.

The residence time has a very significant effect on the product distribution. Fig. 1 illustrates this effect for a quartz reactor at 993 K where the residence time was increased from 3.3 s to 13.2 s by reducing the flowrates by a factor of four while keeping the CH_4/O_2 ratio close to 1. The total methane conversion increased from 0.3% to 2.52%. At a residence time of 3.3 s the formaldehyde selectivity was 60% and the combined C_2H_4 and C_2H_6 selectivity was 27%. The remaining 13% consisted of CO_2 . The short residence time quartz runs did not produce any CO. At the long residence time run of 13.2 s CO was generated at the expense primarily of HCHO. This implies that long residence times increase the probability of CO formation via the decomposition of HCHO, a reaction sequence analogous to that observed in the combustion of methane (14). Similar residence time effects were observed in the Vycor reactors.

The methane to oxygen ratio is another important factor influencing the product distribution. Oxygen rich mixtures strongly favor the overall rate of methane reaction and the rate of CO formation (at the expense of formaldehyde). In view of the blank activity of the quartz, an upper temperature limit of 893 K was imposed on runs with catalyst powders placed into quartz reactors.

Activity of silica based compounds

Various silica based compounds in powder form, including silicic acid, Cab-O-Sil, and Ludox gel exhibited similar trends of methane conversion as the empty Vycor and quartz reactors, although at much lower temperatures. Methane to oxygen ratios lower than one enhanced the activity of these catalysts, in accordance with the behavior observed in the Vycor brand and quartz tubes. Short residence times favored the selectivity of HCHO.

Table 2 compares the overall rate of methane reaction and the selectivity over the various silica compounds for a CH_4/O_2 ratio of close to 1 at a temperature of 893 K. The rate of reaction is reported in two different ways, based on the weight and the surface area of the catalysts as determined after the reaction.

TABLE 1
Conversion and selectivity achieved over Vycor and quartz U tubes at $\text{CH}_4 / \text{O}_2 = 1.14$

	T (K)	% total methane conversion	% Selectivity				
			C_2H_4	C_2H_6	HCHO	CO	CO_2
Vycor	893	0.26	2	15	81	-	2
	913	0.31	3	13	81	-	3
	928	0.41	4	17	78	-	3
	943	0.95	4	12	44	35	5
	958	1.44	4	15	40	37	4
	973	2.26	5	17	34	41	3
	993	3.93	7	19	27	45	2
quartz	963	0.13	8	13	62	-	17
	993	0.37	9	18	60	-	13

Flowrates : 10% CH_4 in Ar=29.7 cm^3 STP/min, O_2 =2.6 cm^3 STP/min. P= 205 kPa

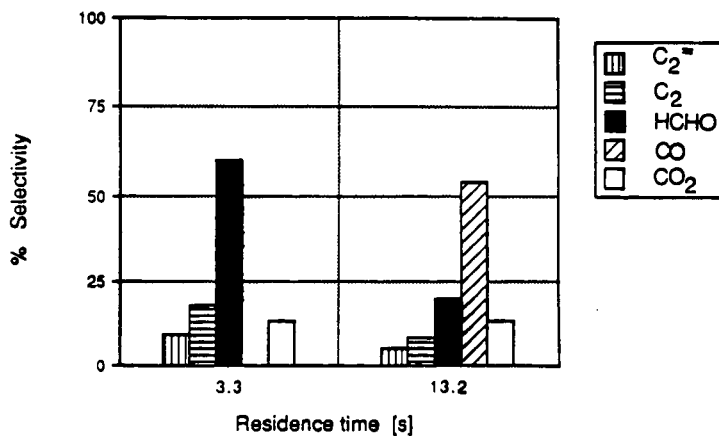


FIGURE 1 CH_4 oxidation over empty quartz reactors. Effect of the residence time on the product distribution at 993 K and CH_4 / O_2 close to 1

TABLE 2

Activity and selectivity of various silica compounds at 893 K and CH_4 / O_2 close to 1

Compound	Pressure [kPa]	Overall CH_4	Overall CH_4	Surface area after reaction [m^2/g]	% Selectivity			
		reaction rate [$\text{mol}/\text{g s}$]	reaction rate [$\text{mol}/\text{m}^2 \text{ s}$]		C_2H_4	HCHO	CO	CO_2
Silicic acid	218 ^a	1.98 E-7 ^c	0.72 E-9	274	1	23	66	10
	340 ^b	2.6 E-7	0.95 E-9	274	7	47	37	9
	515 ^b	4.2 E-7	1.53 E-9	274	1	26	63	11
Cab-O-Sil	308 ^b	2.75 E-7	1.44 E-9	191	1	30	44	24
Ludox gel	377 ^b	0.9 E-7	0.87 E-9	105	1	27	67	5

^a Flowrates: 10% CH_4 in Ar=29.7 cm^3 STP / min, O_2 =2.6 cm^3 STP / min. ^b Flowrates: 10% CH_4 in Ar= 46.8 cm^3 STP / min, O_2 =5.2 cm^3 STP / min. ^c 1.98E-7 corresponds to 1.98×10^{-7}

All three catalysts produced C_2H_4 , HCHO, CO and CO_2 . From the silicic acid runs, a trend emerged of increasing rate of methane reaction with increasing pressure. On a weight basis, silicic acid and Cab-O-Sil were more active than Ludox gel. When normalized on a surface area basis the differences in reaction rates became less pronounced. Therefore, it is very likely that the high per weight activities of silicic acid and Cab-O-Sil can be attributed to their high surface areas. A similar surface area effect could also explain the relatively high blank activity of empty Vycor glass reactors compared to the quartz reactors. Vycor glass is much more porous than quartz, and consequently, Vycor has a higher surface area.

Figure 2 shows the Arrhenius plots for the overall rate of CH_4 reaction as well as for the rates of formation of C_2H_4 , HCHO, CO and CO_2 over silicic acid at a pressure of 585 kPa. The temperatures were randomly selected within the range of 783 - 893 K. Very good linear fit of the Arrhenius plots was achieved excluding the possibility of substantial catalyst deactivation from one run to the next. In the case of formaldehyde, however, at temperatures higher than 853 K a deviation from linearity was observed in the Arrhenius plot, probably due to secondary reactions of formaldehyde to CO and CO_2 . The apparent activation energies for the overall rate of methane reaction and the formation of the various products are summarized in Table 3. For comparison, the apparent activation energy values for methane oxidation in empty Vycor glass tubes were also determined. The 95% confidence intervals used to estimate the activation energy error margin are also given in Table 3.

The apparent activation energies over silicic acid were generally lower than those over Vycor glass. On both silicic acid and Vycor glass, the apparent activation energy values for formaldehyde were very low and had within experimental error the same value.

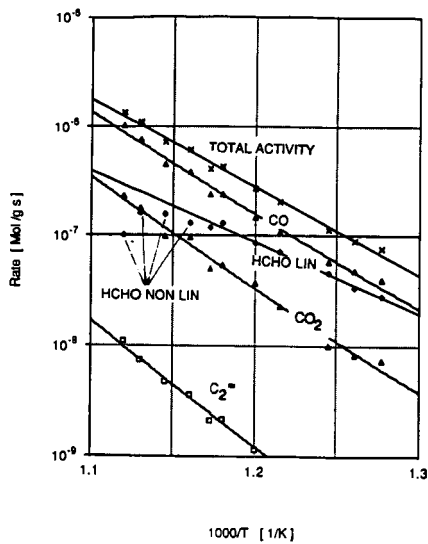


FIGURE 2 Arrhenius plots for silicic acid at 585 kPa and 783-893 K. Flowrates : 10% CH₄ in Ar=39.8 cm³ STP / min, O₂=4 cm³ STP / min . The plot for HCHO is divided into a linear (HCHO LIN) and non linear portion (HCHO NON LIN)

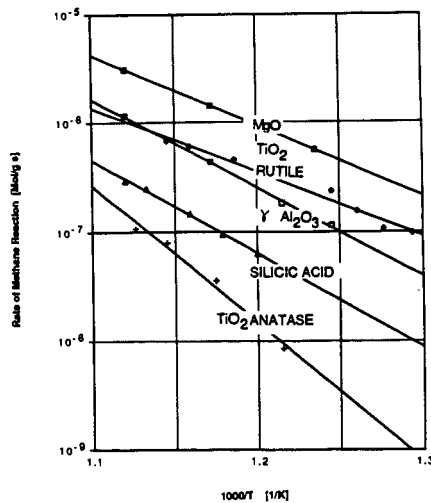


FIGURE 3 Arrhenius plots for the methane reaction rates over MgO (P=205 kPa, CH₄/O₂=1), Gamma Al₂O₃ (P=294 kPa, CH₄ / O₂=0.1), Silicic acid (P=380 kPa, CH₄/O₂=1), TiO₂ rutile (P=515 kPa, CH₄/O₂=1) and TiO₂ anatase (P=510 kPa, CH₄/O₂=1)

TABLE 3

Apparent activation energies for the rate of methane reaction and rates of product formation over silicic acid (at 585 kPa, 783-893 K) and Vycor glass (at 205 kPa, 893-993 K).

	Silicic acid [kJ/mol]	Vycor glass [kJ/mol]
Overall CH ₄ Reaction	154 ± 10	217 ± 49
C ₂ H ₄	213 ± 18	299 ± 39
C ₂ H ₆	(not formed)	236 ± 59
HCHO	125 ± 15 (linear portion of plot)	123 ± 19
CO	171 ± 15	264 ± 34
CO ₂	184 ± 18	(non linear)

This might imply that once the methane molecule is activated the formation of formaldehyde is not dependent on the nature of the catalytic surface and probably occurs in the gas phase. The difference in the activation energy for CO, however, suggests that the subsequent oxidation and/or decomposition of formaldehyde is sensitive to the nature of the catalytic surface or reactor walls.

The deactivation characteristics of silicic acid were also studied by monitoring its activity over a long time period. The methane oxidation activity maintenance was excellent over a period of 16 hrs at 863 K.

Effect of catalyst acidity

In order to investigate the effect of catalyst acidity on methane oxidation, MgO, gamma Al₂O₃ as well as two forms of TiO₂, rutile and anatase, were selected for a comparison with silicic acid. Figure 3 shows the rates of the overall methane reaction over these materials in the form of Arrhenius plots. The basic MgO was the most active catalyst. The rates over gamma alumina and rutile were of the same order of magnitude. The lowest rates were obtained over the anatase. Under our reaction conditions, only the moderately acidic silicic acid and the anatase produced formaldehyde. The formaldehyde yields over the anatase, however, were much lower than the ones over the silicic acid. Gamma Al₂O₃ and MgO do not seem to preserve formaldehyde, yielding instead deep oxidation products CO and CO₂. Rutile drives the reaction to complete oxidation, producing almost exclusively CO₂. The very substantial difference between the activity the rutile and anatase TiO₂ forms could be attributed to different oxygen adsorption characteristics, possibly induced by the open structure of the rutile (15).

In the case of the gamma Al₂O₃ and MgO, the CO₂ selectivity increased with temperature at the expense of CO, whereas for silicic acid the CO₂ selectivity remained almost unchanged at 10 to 13%. As a consequence,

silicic acid appears to be very promising for the conversion of methane into products besides CO_2 , because it suppresses the CO_2 production at higher temperatures and higher conversions

Effect of small amounts of ethane on the selective methane oxidation over silicic acid and quartz glass

Gesser et al (16) as well as Foster (17) in their reviews of early work on the oxidation of methane to methanol report that whenever natural gas or mixtures of methane and ethane were used instead of pure methane the oxidation reaction was triggered at lower temperatures. Ito et al (2) found that an increase of the ethane concentration over a methane oxidative coupling catalyst (Li^+ / MgO) improved the ethylene production. Westbrook and Pitz (18) reported that traces of ethane and propane shorten the ignition time of methane mixtures with air.

We have further investigated the effect of the ethane on the methane conversion and selectivity by varying the amount of ethane in the feed. Figure 4 shows the % selectivity of the various products versus the % CH_4 conversion for silicic acid at the temperature range of 833 to 893 K. Conditions (1) and (2) correspond respectively to 0.14 mol % and 1.25 mol % of ethane in the feed stream (based on methane). The increase in the ethane percentage in the feed enhances the ethylene, HCHO and CO_2 formation and suppresses the CO production. The most dramatic increase occurs in the ethylene selectivity and thus it would be very reasonable to attribute the ethylene formation almost exclusively to the ethane. The improvement in the formaldehyde selectivity could be due to the fact that the ethane and/or ethylene interactions with the surface inhibit the destruction of formaldehyde. At a conversion level of 5 % the increase of the ethane percentage in the feed from 0.14% to 1.25 % improves the selectivity of useful products (ethylene and formaldehyde) from 30% to 38%.

Runs of varying ethane concentration were performed over quartz tubes at 913 K and 445 kPa. The results obtained are shown on Figure 5. It is clear that the ethane in the feed has a very dramatic effect in the conversion of methane. By increasing the mol percent of ethane from 1.25% to 5.2 % based on methane, the conversion of methane nearly doubled from 1.8% to 3.2 %. The ethane conversion also increased from 10% to 40 % and always remained higher than the methane conversion. At the highest ethane mol percent of 8.9% complete conversion of ethane (90 %) and a 34.4% conversion of methane occurred. High conversions favored the CO and CO_2 formation, at the expense of formaldehyde and ethylene.

Ethylene is considered as a primary product of the ethane combustion formed via the oxidative dehydrogenation of the $\text{C}_2\text{H}_5\cdot$ radicals, in an analogous way that formaldehyde is a primary product of the methane combustion formed from the oxidation of $\text{CH}_3\cdot$ radicals (14). Therefore, the same silica surfaces that produce formaldehyde from methane can lead to the formation of ethylene from ethane. The conversion of ethane was always three to five times higher than the conversion of methane and this is in qualitative agreement with the experimental values of Bohme and Fehsenfeld (19) where it was reported that the probability for the first hydrogen abstraction increases with the size of the hydrocarbon chain. The ethane molecule apart from forming $\text{C}_2\text{H}_5\cdot$ radicals by hydrogen abstraction is also likely to act as a source of $\text{CH}_3\cdot$ radicals formed via C-C bond breakage. Experimental data show that the rate of formation of $\text{CH}_3\cdot$ radicals from ethane in this way is two orders of magnitude higher than the rate of formation of these radicals from methane (20). Therefore the $\text{C}_2\text{H}_5\cdot$, $\text{CH}_3\cdot$ as well as the H· radicals, which are generated from ethane easier than from methane could activate methane or

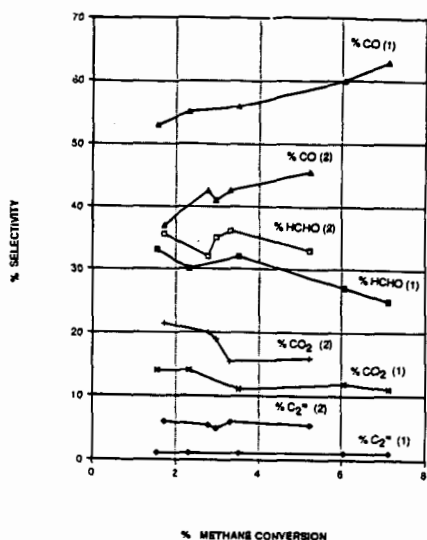


FIGURE 4 % Selectivity of the various products vs % CH₄ conversion over silicic acid. In the temperature range of 833 to 893 K as a result of the variation of the ethane concentration in the feed. (1): 0.14 mol % ethane based on methane, flowrates 10% CH₄ in Ar 31 cm³ STP/min, oxygen 3 cm³ STP/min, at 380 kPa and over 535 mg of catalyst. (2) : 1.25 mol % ethane based on methane, flowrates 10% CH₄ in Ar 50 cm³ STP/min, oxygen 5 cm³ STP/min, at 360 kPa and over 504 mg of catalyst.

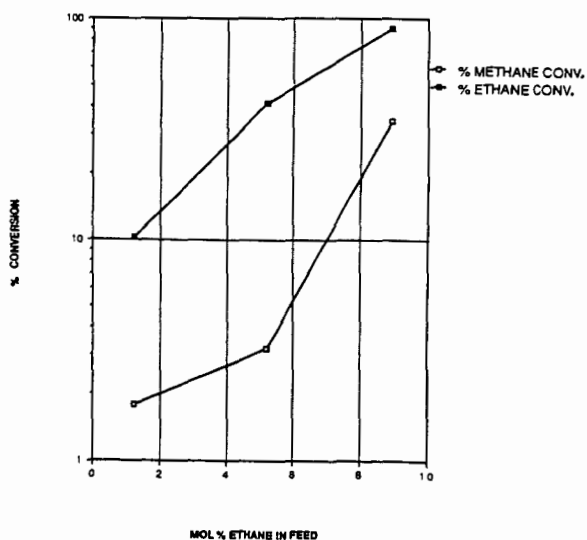


FIGURE 5 Methane and ethane conversions achieved over quartz glass at 913 K and 445 kPa as a function of the mol % ethane based on methane and ethane. Molar ratio of C to O₂ from 0.988 to 1.043.

even interfere in the process of the chain propagation occurring during the methane oxidation-combustion.

Methane oxidation over MoO₃, WO₃ and H₃BO₃ co-gels with Ludox silica

Ammonium heptamolybdate, ammonium metatungstate and H₃BO₃ were dissolved in Ludox colloidal silica. The pH was then adjusted either with nitric acid or with ammonium hydroxide and high surface area co-gels up to loadings of 12% by weight of MoO₃, WO₃ and H₃BO₃ on SiO₂ were prepared. Loadings of up to 5% by weight of MoO₃ led to complete oxidation of methane to CO₂ under an increased overall activity. Loadings of 5% by weight of WO₃ did not have any significant effect neither in the methane oxidation activity of the plain Ludox nor in the product distribution. A mechanical mixture of 5% by weight MoO₃ with Ludox exhibited almost identical activity and selectivity results as the 5% co-gel of MoO₃. This may suggest that at the high loadings used in the co-gels with Ludox MoO₃ may be present as a bulk phase.

As shown on Table 4 the boric acid co-gels dramatically improved the yields of formaldehyde over the plain silicas. It appears that while silica is responsible for the primary activation of methane, boron preserves the formaldehyde from further oxidation and / or decomposition to CO.

TABLE 4

Effect of boron in the activity and selectivity of Ludox silica at 903 K.

Compound	%Overall conversion	% Selectivity			
		HCHO	C ₂ ⁼	CO	CO ₂
Ludox silica gel	5.2	8	13	55	24
7% H ₃ BO ₃ / Ludox silica co-gel	4.9	47	12	34	7

Flowrates: 10% CH₄ in Ar=49.3 STP / min, O₂=5 cm³ STP / min. P= 480 kPa. Ethane in feed: 1.25 mol% based on methane.

ACKNOWLEDGEMENTS

Financial support of this work through the Gas Research Institute under GRI Contract 5086-260-1324 is gratefully acknowledged.

LITERATURE CITED

1. R. Pitchai and K. Klier, *Catal. Rev.-Sci. Eng.*, **28**, 13 (1986).
2. T. Ito, J.-X. Wang, C.-H. Lin, and J. H. Lunsford, *J. Am. Chem. Soc.*, **107**, 5062 (1985).
3. K. Otsuka, K. Jinno and A. Morikawa, *J. Catal.*, **100**, 353 (1986).
4. J. A. Sofranko, J. J. Leonard and C. A. Jones, *J. Catal.*, **103**, 302 (1987).
5. H.-F. Liu, R. -S. Liu, K. Y. Liew, R. E. Johnson, and J. H. Lunsford, *J. Am. Chem. Soc.*, **106**, 4117 (1984).
6. M. M. Khan and G. A. Somorjai, *J. Catal.*, **91**, 263 (1985).
7. K. Otsuka and M. Hatano, *J. Catal.*, **108**, 252 (1987).
8. N. D. Spencer, *J. Catal.*, **109**, 187 (1988).
9. L. H. Little, H. E. Klauser, and C. H. Amberg, *Can. J. Chem.*, **39**, 42 (1961).
10. N. W. Cant, and L. H. Little, *Can. J. Chem.*, **42**, 802 (1964).
11. N. Sheppard and D.J.C. Yates, *Proc. Roy. Soc. London*, **A 238**, 69 (1956).
12. T. Yamazaki, I. Watanuki, S. Ozawa and Y. Ogino, *Nippon Kagaku Kaishi*, **8**, 1535 (1987).
13. D. E. Cheaney and A.D. Walsh, *Fuel*, **35**, 238 (1956).
14. D. J. Hucknall, *Chemistry of Hydrocarbon Combustion*, Chapman and Hall, 1985.
15. A. F. Wells, *Structural Inorganic Chemistry*, 5th Ed., Oxford University Press, Oxford, 1987.
16. H. D. Gesser, N. R. Hunter and C. B. Prakash, *Chem. Revs.*, **85**, 235 (1985).
17. N. R. Foster, *Appl. Catal.*, **19**, 1 (1985).
18. C. K. Westbrook and W. I. Pitz, *Combustion Science and Technology*, **33**, 315 (1983).
19. D. K. Bohme and F. C. Fehsenfeld, *Can. J. Chem.*, **47**, 2717 (1969).
20. W. C. Gardiner, *Combustion Chemistry*, Springer-Verlag, Heidelberg, 1985.

Effect of Loading and Support on the Activity and Selectivity of Partial Oxidation of Methane, I. Lee and K. Y. Simon Ng, Department of Chemical Engineering, Wayne State University, Detroit, Michigan 48202

The major component of our vast natural gas reserves is methane. Most of the methane produced nowadays is simply used as fuel, with only a small fraction used in the water-gas process. In order to utilize our gas reserves fully, it is desirable to turn methane into more valuable oxygenated products. Even though methane is a simple molecule, it is one of the most difficult hydrocarbons to oxygenate, due to its highly symmetric character.

A number of patents have been claimed on technologies for converting methane to methanol, but there is still no commercial oxidation process utilizing the direct oxidation mechanism. Recently, a considerable amount of research has been undertaken to identify a selective catalyst system. Two recent reviews by Pitchai and Klier (1) and by Foster (2) have summarized the research on partial oxidation reported in the literature. It is to be noted that most research work (3-8) has focused on evaluating the catalytic potential of different compounds, but the role of supports, the functions of promoters, and the effect of catalyst morphology have not been studied in detail. There are indications that catalyst morphology can have a significant impact on selectivities (1). Even though Liu et al. (4) used nitrous oxide and Pitchai et al. (1) used oxygen as oxidant, they both observed that low loading catalyst showed high selectivity. Catalyst morphology has been found to depend on the metal loading, method of preparation, support, and promoter addition (9). Based on the above literature survey, we have focused our efforts on searching for a selective catalyst through support interaction, and to understand the nature of active sites for partial oxidation of methane on different supported catalysts. In this paper, we report our findings in the activity and selectivity of molybdenum- and vanadium-based catalyst on silica, silica-titania, and titania support.

EXPERIMENTAL

Supports

Three types of catalyst supports were studied. The titania oxide was P-25

from Degussa, with a surface area of $50 \pm 5 \text{ m}^2/\text{g}$. The silica was from Kodak. Both supports were used as received, without further treatment. The 1:1 ratio of titania-silica mixed oxide support was made using the method of homogeneous coprecipitation. Sodium metasilicate was first dissolved in double-distilled water and acidified to pH 1 with hydrochloric acid. Equimolar of titanium tetrachloride was then added and followed by neutralization using urea. The mixture was then heated at $90 \text{ }^\circ\text{C}$ for 6 hours. The precipitate was filtered and washed with warm distilled water. The mixed oxide was dried at $120 \text{ }^\circ\text{C}$ for 24 hours, followed by calcination at $600 \text{ }^\circ\text{C}$ for 1 hour.

Catalyst

The catalysts were prepared by the conventional impregnation method. The molybdenum-based catalysts were prepared by dissolving the desired amount of ammonium heptamolybdate in double-distilled water, and the pH was adjusted to 10 using ammonium hydroxide. For vanadium-based catalysts, the desired amount of vanadium pentoxide was dissolved in an aqueous solution of oxalic acid. The solution was then impregnated on the support. The resulting mixture was stirred thoroughly and was dried at $120 \text{ }^\circ\text{C}$ for 2 hours, followed by calcination at $500 \text{ }^\circ\text{C}$ for 24 hours.

Reactor System

A 6mm I.D. quartz U-tube reactor, with a reduction of I.D to 2mm immediately following the catalyst bed, was used. The reactor design, which allows fast removal of products from the furnace, is intended to minimize the gas phase oxidation reactions. A K-type thermocouple with an Omega temperature controller was used to control the reactor temperature to $\pm 0.1 \text{ }^\circ\text{C}$. A typical of 0.1 g of catalyst was used. The catalyst was first heated at $500 \text{ }^\circ\text{C}$ in helium for 1 hour, and with CO in helium for another 30 minutes. The reactor temperature was then lowered to $400 \text{ }^\circ\text{C}$ for 30 minutes in helium, and was subsequently increased to the reaction temperature and the reactant gases introduced. Total gas flow rate is 8 c.c./minute unless stated otherwise. The compressed gases used -- methane

(99.99%), nitrous oxide (99.0%), oxygen (99.99%), helium (99.995%), hydrogen (99.9%), nitrogen (99.9985%), and carbon monoxide (99.9%) -- were from Air Products and were used as received. The mass flow rates of reactants were controlled by Tylan mass flow controllers to $\pm 1.0\%$. Water was introduced in form of steam using a Harvard syringe pump. The whole system is heat-traced with heating wire, and insulated to prevent possible condensation of products and reactants. The products were analyzed using an HP-5890A gas chromatograph equipped with TCD and FID detectors. A 20 ft. Hayesep A column and a 5 ft. Hayesep Q column were used to separate the products.

RESULTS and DISCUSSION

Table 1 shows the conversion and selectivity of molybdenum-based catalysts with different loadings on the silica, silica-titania and titania supports using nitrous oxide as oxidant at 600 °C. On blank silica, there was a small conversion of 0.9% but no formaldehyde was observed. For the silica-supported molybdenum catalysts, both the 1% and 3% loading catalysts gave almost identical conversion (7.5%), indicating that the 3% catalyst may already contain bulk-like molybdenum species that are relatively inactive. The low loading catalyst gave a higher selectivity (42.7%) towards formaldehyde than the 3% catalyst (32.5%), which is consistent with the selectivity trends reported previously (3-5). Our results are comparable to the results of Liu et al. (14% conversion and 15% combined selectivity towards methanol and formaldehyde) and Khan et al. (2.6% conversion and 56% selectivity), taking into consideration of the conversion-selectivity relationship (7). However, the conversion-selectivity relationship is different when a different support is used. On a titania-silica support, the catalyst has a slightly higher conversion (10.2%), but the selectivity is much lower (7.2%). When supported on pure titania, the conversion of methane drops significantly, and no observable formaldehyde was detected. It is apparent from this result that on different supports, the nature of active sites is very different for partial oxidation. It is also suggested that silica plays an important role in the reaction mechanism, as evident from the fact

that mixed oxide support showed some selectivity.

Table 2 shows the effect of temperature on conversion and selectivity. For the blank silica using oxygen as oxidant, no conversion was observed at 500 °C. Conversion of 0.1% with 53.8% selectivity was observed for 600 °C, and conversion of 0.6% with 48% selectivity was observed for 650 °C. The 650 °C data was almost identical with Spencer's results (7). As we will see later, the selectivity is very different when water is added along with the reactants. When nitrous oxide was used as oxidant, a higher conversion (0.9%) was observed at 600 °C, indicating that nitrous oxide is a stronger oxidant compared to oxygen. Surprisingly, no formaldehyde was detected. For the 1.7% Mo/SiO₂ catalyst, the conversions are 0.9%, 2.3%, 7.5%, 34.6% at 500 °C, 550 °C, 600, and 650 °C respectively. The corresponding selectivities are 79.3%, 73.5%, 42.7% and 4.1%. There is a strong conversion-selectivity relationship, as reportedly previously. A similar temperature dependence was also observed for the TiSiO₂-supported catalyst. However, at comparable conversions, the selectivity is much lower compared to the silica-supported catalysts.

The performance of vanadia-based catalysts at 600 °C using nitrous oxide as oxidant was shown on Table 3. With 2% of vanadia on silica, a conversion of 31.5% and selectivity of 51.0% were observed. The yield was calculated to be 132.2 g/kgcat hr., which is significantly higher than yields reported in the literature. It should be noted that for pure silica the conversion was found to be only 0.9% and no formaldehyde could be detected. Unlike the molybdenum-based catalyst, a 15% selectivity towards formaldehyde was observed when supported on titania. Interestingly, no formaldehyde was observed for the TiSiO₂-supported catalyst, even though it showed a conversion similar to the titania-supported catalyst. It is apparent that the nature of the active site for vanadium-based catalysts is quite different from molybdenum-based catalysts, and that the effects of the support on the nature of the active site are not the same.

Table 4 shows the effect of temperature on conversion and selectivity on

vanadium-based catalysts. The conversion was found to increase, as expected, as a function of temperature; however, the selectivity did not show the same conversion-selectivity behavior as the molybdenum-based catalysts. The selectivity increases from 44% at 3% conversion (500 °C) to 51% at 31.5% conversion (600 °C). However, at 650 °C, only carbon oxides were detected. For TiSiO_2 -supported catalysts, no formaldehyde was detected for the temperature range (500-650 °C) tested. The titania-supported vanadium catalyst showed a 15% selectivity only at 600 °C, indicating that there is a narrow temperature range that can be used to produce formaldehyde.

The effect of water added as reactant and the effect of contact time on the conversion and selectivity is shown in Figures 1 and 2 for silica and vanadia-silica. The results are consistent with those reported in the literature. The conversion is generally lowered when water is added, with the exception of pure silica at 650 °C using oxygen as oxidant. The selectivity towards formaldehyde was generally improved. A more comprehensive study is continuing in this laboratory to elucidate the effect of water on product selectivity. When the contact time was reduced by 50%, the conversion was reduced from 13% to 7.5%, but the selectivity increased from 5.0% to 11.6%. With water added as reactant, a similar trend was observed. The conversion was reduced from 11.8% to 4.3% and the selectivity increased from 6.3% to 24.3%.

The effect of oxidant for vanadium-based catalysts is summarized in Table 5. For pure silica, oxygen appears to be a better oxidant, with 82% selectivity (with water as reactant) as compared to nitrous oxide (0% selectivity). However, for the vanadia catalyst, N_2O is obviously a better oxidant than oxygen, especially at a higher reaction temperature (600 °C).

CONCLUSION

The nature of the support has a dramatic effect on the catalytic activities and selectivities of molybdenum- and vanadium-based catalysts. However, the extent of support influence is different for the two catalyst systems, suggesting different

levels of support interaction and possibly different reaction mechanisms. There is a distinct conversion-selectivity relationship for the Mo/SiO₂ catalyst. However, this is not observed with the V₂O₅/SiO₂ catalysts. Thus high conversion with reasonably high selectivity seems to be possible with the vanadium catalyst to produce a high yield. Addition of water reduces conversions but improves selectivities in most cases. Nitrous oxide is found to be a better oxidant for V₂O₅/SiO₂ catalyst. However, for blank silica, oxygen gives a high selectivity towards formaldehyde, which suggests that modified silica can be a promising approach to partial oxidation of methane.

ACKNOWLEDGEMENT

Financial support of this research by American Natural Resources and by the Institute for Manufacturing Research of Wayne State University is gratefully acknowledged. The authors would like to thank Mr. Sendjaja Kao for preparing the mixed-oxide support and Miss Carolyn Parks for measuring the B.E.T. surface area.

REFERENCES

1. Pitchai, R., and Klier, K., Catal. Rev.-Sci. Eng., 28(1), 1(1986)
2. Foster., N.R., Applied Catalysis., 19, 1(1985).
3. Liu, R.S., Iwamoto, M., Lunsford, J.H., J. Chem. Soc., Chem. Commun., 78(1982).
4. Liu, H.F., Liu, R.S., Liew, K.Y., Johnson, R.E., and Lunsford, J.H., J. Am. Chem. Soc., 106, 4117(1984).
5. Khan, M.M., and Somorjai, G.A., J. Cat., 91, 263(1985).
6. Zhen, K.J., Khan, M.M., Mak, C.H., Lewis, K.B., and Somorjai, G.A., J. Cat., 94, 501(1985).
7. Spencer, N.D., Submitted to J. Cat.
8. Otsuka, Kiyoshi., and Hatano, Masahru., J.Cat., 108, 252(1987).
9. Ng, K.Y.S., and Gulari, E., J.Cat., 92, 340(1985)

Table 1

Molybdenum - Based Catalyst at 600 °C

(W / F = 0.0125 g min / cc)

CH₄:N₂O:He = 1:4:2 Total flow rate = 8 cc/ min

Catalyst	Conversion	Selectivity (%)			Yield (g/kgcat hr) (HCHO)
		HCHO	CO	CO ₂	
SiO ₂	0.9	0	50.4	49.6	0
Mo/SiO ₂ (1.7%)	7.5	42.7	43.8	13.5	20.2
Mo/SiO ₂ (3%)	7.4	32.5	54.7	12.8	15.6
Mo/TiSiO ₂ (1.7%)	10.2	7.2	65.7	27.1	5.6
Mo/TiO ₂ (3%)	2.2	0	77.7	22.3	0
Mo/TiO ₂ (5%)	1.7	0	70.2	29.8	0

Table 2

Effect of Temperature on Conversion and Selectivity

(W/F = 0.0125 g min / cc)

CH₄:N₂O:He = 1:4:2 Total flow rate = 8 cc/ min

Catalyst	Oxidant	Temp(°C)	Conversion	Selectivity(%)			Yield (g/kgcat hr) HCHO
				HCHO	CO	CO ₂	
SiO ₂	O ₂	500	0	0	0	0	0
		600	0.1	58.3	24.1	17.6	1.3
		650	0.6	48.0	45.4	6.6	5.7
	N ₂ O	600	0.9	0	50.4	49.6	0
Mo/SiO ₂ (1.7%)	N ₂ O	500	0.9	79.3	10.5	10.2	3.9
		550	2.3	73.5	19.6	7.0	9.3
		600	7.5	42.7	43.8	13.5	20.2
		650	34.6	4.1	63.5	32.4	6.8
Mo/TiSiO ₂ (1.7%)	N ₂ O	550	3.7	0	83.9	16.1	0
		600	10.2	7.2	65.7	27.1	5.6
		650	20.6	1.1	56.5	42.4	1.2

Table 3

Vanadium - Based Catalyst at 600 °C

(W/F = 0.0125 g min / cc)

CH₄:N₂O:He = 1:4:2 Total flow rate = 8 cc / min

Loading(wt %)	Conversion	Selectivity (%)			Yield (HCHO) g/kgcat hr
		HCHO	CO	CO ₂	
SiO ₂	0.9	0	50.4	49.6	0
V ₂ O ₅ /SiO ₂ (2%)	31.5	51.0	35.4	13.6	132.2
V ₂ O ₅ /TiSiO ₂ (2%)	11.4	0	73.4	26.6	0
V ₂ O ₅ /TiO ₂ (2%)	13.7	15.0	34.0	51.0	15.8

Table 4

Effect of Temperature on Conversion and Selectivity

(W/F = 0.0125 g min / cc)

CH₄:N₂O:He = 1:4:2 Total flow rate = 8 cc/ min

Catalyst	Temp (°C)	Conversion	Selectivity (%)			Yield (HCHO) (g/kgcat hr)
			HCHO	CO	CO ₂	
V ₂ O ₅ /SiO ₂ (2 %)	500	3.0	44.0	43.4	12.6	9.7
	600	31.5	51.0	35.4	13.6	132.2
	650	42.8	0	62.8	37.2	0
V ₂ O ₅ /TiSiO ₂ (2 %)	500	2.3	0	76.9	23.1	0
	600	11.4	0	73.4	26.6	0
	650	25.6	0	53.7	46.3	0
V ₂ O ₅ /TiO ₂ (2 %)	500	1.3	0	71.7	28.3	0
	600	13.7	15.0	34.0	51.0	15.8
	650	24.2	0	27.4	72.6	0

Table 5

Effect of Oxidant

(W / F = 0.0125 g min / cc)

CH₄:N₂O:He = 1:4:2 , CH₄:O₂:He = 4:1:2 Total flow rate = 8 cc/min

Loading (Wt %)	Temp (°C)	Oxidant	Conversion	Selectivity(%)			Yield(HCHO) g/kg cat hr
				HCHO	CO	CO ₂	
SiO ₂	600	O ₂	0.1	58.3	24.1	17.6	1.3
	600	N ₂ O	0.9	0	50.4	49.6	0
V ₂ O ₅ /SiO ₂ (2 %)	500	O ₂	0.2	38.5	42.5	19.0	1.4
	500	N ₂ O	3.0	44.0	43.4	12.6	9.7
	600	O ₂	13.0	5.0	69.1	25.9	14.4
	600	N ₂ O	31.5	51.0	35.5	13.5	132.2

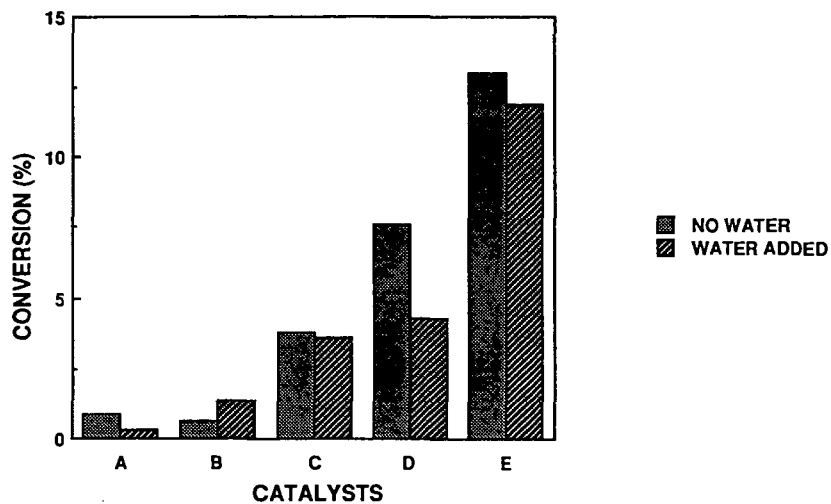


FIGURE 1. EFFECT OF WATER ON CONVERSION

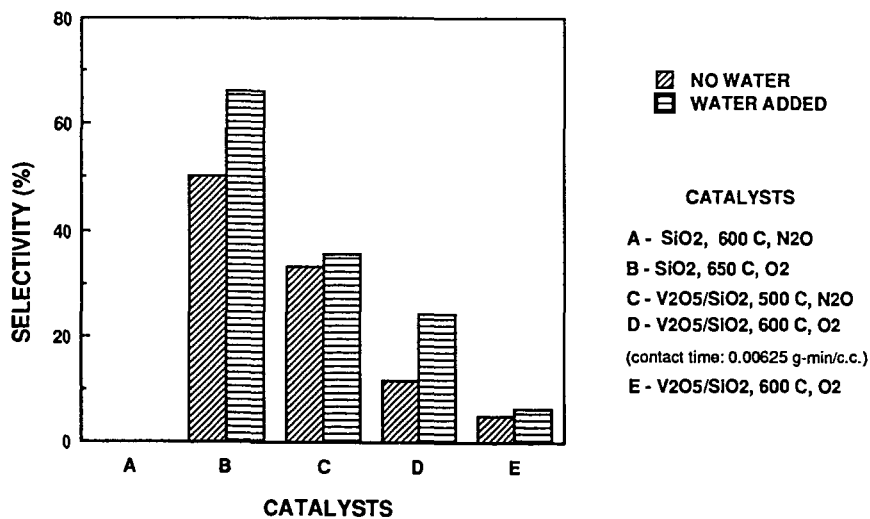


FIGURE 2. EFFECT OF WATER ON FORMALDEHYDE SELECTIVITY

Pages 413 thru 420 have intentionally been left blank.

ACS National Meeting -
Los Angeles, September 25-30, 1988
Division of Fuel Chemistry
Catalytic and Related Chemistry of Methane

Conversion of Methane into Ethylene, Acetylene and Ethane by the CCOP
Process: Control of Product Selectivities

by

S.M. Senkan*, D. Dang, M.K. Abdelaal, and M. Qun
Department of Chemical Engineering
Illinois Institute of Technology
Chicago, Illinois 60616

* To whom correspondence should be addressed.

ABSTRACT:

The oxidative pyrolysis of CH_3Cl , representing the second stage in the Chlorine-Catalyzed Oxidative-Pyrolytic (CCOP) conversion of methane into C_2 hydrocarbons have been studied in the presence of CH_4 in a flow reactor operating at 0.7 atm and 900-950 C. The effects of temperature, mixture composition, in particular the concentration of O_2 , and residence times on CH_3Cl conversion and selectivity towards the formation of C_2 products have been explored experimentally. The role of CH_4 and other operational variables in effecting rates and selectivities will be discussed in view of our current understanding of the detailed chemical kinetic aspects of the CCOP process.

INTRODUCTION:

Chlorine-Catalyzed Oxidative-Pyrolysis (CCOP) process was recently developed as a practical method to convert methane, the major component in natural gas, into more valuable products such as acetylene and ethylene (Senkan 1987a). In the CCOP process CH_4 is chlorinated to form chlorinated methanes (CM) first, followed by the oxidative pyrolysis of CM to form C_2 products such as C_2H_4 , C_2H_2 , C_2H_6 , $\text{C}_2\text{H}_3\text{Cl}$, synthesis gas (CO and H_2), and HCl in the second step. The process developed ameliorates the problem of formation of carbonaceous solid deposits inherent with the earlier chlorine-catalyzed methane conversion processes which took place in the absence of oxygen (Gorin 1943, Benson 1980, Weissman and Benson 1984). The HCl produced can either be converted back to chlorine via the well-known Deacon reaction and recycled, or can be used to oxychlorinate methane to form CMs, thus completing the catalytic cycle for

chlorine (Senkan 1987b).

In previous studies we reported experimental product distributions for the oxidative pyrolysis of isolated CH_3Cl in the presence of an inert (argon) carrier gas (Granada et al. 1987). In parallel, a detailed chemical kinetic mechanism for the oxidative pyrolysis of CH_3Cl was also developed and validated (Karra and Senkan 1988a).

As discussed in these earlier studies the selectivity for C_2H_4 can be substantially high, e.g. about 40%, at low conversions of CH_3Cl . However, it decreases rapidly with increasing conversion, rendering acetylene as the major product beyond 30% conversion of CH_3Cl . Since C_2H_4 is a more desirable product, the identification of proper process conditions that will favor its formation clearly are of interest (C&E News 1987).

Pyrolysis of CH_3Cl in the presence of CH_4 increases C_2H_4 production over C_2H_2 as demonstrated by Weissman and Benson 1984. However, in the absence of O_2 , the process also leads to the formation of significant levels of carbonaceous deposits, in particular coke, which is undesirable.

In this communication we present results on the oxidative pyrolysis of CH_3Cl conducted in the presence of CH_4 , in which coke formation is avoided. The effects of temperature, O_2 concentration and residence times on the conversion of CH_3Cl and product distributions are discussed based on experiments conducted at 0.7 atm, 900-950 C, and for a $\text{CH}_3\text{Cl}/\text{CH}_4$ ratio of about 0.25. In addition, the role of these process variables on conversion and selectivity is discussed based on our current understanding of the detailed chemical kinetic aspects of the CCO process.

EXPERIMENTAL:

The experimental facility used has been discussed in detail previously (Granada et al. 1987), thus only a brief summary will be presented here. The

experiments were conducted in a 2.1 cm ID quartz tube which was placed in a 3-zone Lindbergh furnace. The first zone of the furnace, which is about 15 cm long, was used to preheat methane which served as a reactive carrier gas. Mixtures of $\text{CH}_3\text{Cl}/\text{O}_2$ were then introduced into pre-heated methane using an air-cooled probe through radially directed injection holes. Small amounts of nitrogen (3-5%) also were introduced into the feed mixture as an internal reference gas.

Gases used were acquired either from the Matheson Co. (Joliet, IL) or from Bennet Welding Supply Co. (Bensenville, IL), and had the following reported purities: CH_3Cl :99.5% as liquid, CH_4 :99.97%, O_2 :99.6% extra dry, and N_2 :99.99%. They were used directly from the cylinders, and their flow rates were controlled by the combined use of two-stage regulators, rotameters and needle valves. The needle valves were maintained under critical flow conditions to establish uncoupled flow rates. A mechanical vacuum pump was then used to remove the reaction products from the system. The pressure in the reactor was kept slightly below atmospheric pressure (about 0.70 atm) in all the experiments to prevent toxic gases from leaking into the laboratory, and was monitored continuously by a capacitance transducer (MKS Baratron, Burlington MA).

Mean gas flow velocities in the reactor were in the range 1-10 m/s, suggesting that laminar flow conditions were present. However, the deviation from ideal plug flow behavior would be in the range 10-15%, the same order of magnitude as the other experimental errors (Cathonnet et al. 1981).

Gas samples were withdrawn continuously using a vacuum pump through a warm-water-cooled quartz sampling probe positioned centrally at the downstream end of the reactor, and then through a heated sample loop in the gas-chromatograph (Hewlett-Packard 5880A). The pressure in sampling lines and the loop was kept at about 0.25 atm to minimize the condensation of species, in particular H_2O and HCl . Following the establishment of steady sampling conditions, that were

determined in prior experiments by studying the variation of mixture composition as a function of sampling time, the sampling loop was automatically switched on-line with the helium carrier gas. Gas separation and detection were then accomplished by Porapak N (0.31 cm diameter by 1.8 m long) and by molecular sieve 5A (0.31 cm diameter by 1.8 m long) columns (both acquired from Alltech Assoc., Deerfield IL), and by the thermal conductivity detector, respectively.

Gas analysis was accomplished using standard gas chromatographic methods (GC). For reactants, i.e. CH_3Cl , CH_4 , O_2 , and N_2 , GC response factors were obtained directly by analyzing the reactor effluents in the absence of reaction, i.e. at low temperatures. For reaction products, such as C_2H_4 , C_2H_2 , C_2H_6 , $\text{C}_2\text{H}_3\text{Cl}$, and CO a certified calibration mixture (Matheson Co., Joliet IL) was used. For this calibration, a gas mixture having a composition reasonably close to those encountered in the experiments was acquired. Consequently, we estimate that the mole fractions obtained in this study should be accurate within $\pm 5\%$. Species mole fraction profiles were then obtained by moving the sampling probe relative to the stationary injection probe.

Carbon balances for each measurement were made by using the following definition:

$$\% \text{ Carbon balance} = \frac{(\text{gas-phase carbon}/\text{N}_2)_{\text{reaction mixture}}}{(\text{gas-phase carbon}/\text{N}_2)_{\text{feed mixture}}} * 100$$

and they were better than 95% for all the experiments.

RESULTS:

The major species quantified directly by GC were the reactants CH_3Cl , CH_4 , O_2 , and N_2 as the tracer gas, and the major carbon-containing products C_2H_4 , C_2H_2 , C_2H_6 and CO. Since only trace levels of CO_2 form in the CCOP process, it was neglected in the final product analysis. Unlike the oxidative pyrolysis of CH_3Cl , which leads to substantial $\text{C}_2\text{H}_3\text{Cl}$ formation, very little $\text{C}_2\text{H}_3\text{Cl}$ formed in

the current experiments when an excess CH_4 was present.

Before presenting any results a number of issues must be discussed concerning the experiments. First, as we noted previously even small amounts of O_2 in the mixture suppresses the extent of formation of carbon in the system, and this effect is most dramatic with regard to coke formation. On the other hand, when O_2 feed was deliberately cut off, rapid coking, manifested by the formation of black deposits on the inner surface of the reactor walls, was observed.

Second, although CH_4 actively participates in the process, and dramatically increases the concentration of C_2H_4 relative to C_2H_2 , the precise quantification of the extent by which CH_4 contributes to this phenomena was rendered difficult in the present studies because of CH_4 reformation from CH_3Cl and experimental errors. For example, the absolute concentrations of C_2 products formed in the experiments were of the same order of magnitude as the uncertainties in the measurements of CH_4 concentrations. Consequently, we report selectivities based on the amount of CH_3Cl reacted. This appears reasonable because CH_4 is expected to form as a major product in the oxidative pyrolysis of CH_3Cl even in the presence of excess methane based on detailed chemical kinetic calculations (Senkan 1988).

In order to systematically explore the effects of each of the process variables on CH_3Cl conversion and on product selectivities, we conducted experiments in which independently adjustable variables were changed one at a time. In Figure 1 the influence of temperature on carbon containing product concentrations in the CCOP process are illustrated for a mixture with the following pre-reaction composition: CH_3Cl 15.9%, CH_4 75.9%, O_2 4.12%, and N_2 3.98%. Nominal residence times were about 330 ms. In this and subsequent figures lines have been drawn through experimental data points (indicated by symbols) to indicate trends.

The compositions shown in this figure represent conditions at a fixed position near the exit of the reactor, and therefore do not precisely correspond to identical residence times. However, since the differences in temperatures between these experiments were at most 50 K, residence times are expected to be different by at most 5% due to temperature effects, well within normal experimental error limits. Product (carbon) selectivities, determined relative to CH_3Cl reacted, similarly are presented in Figure 2, together with the percent conversion of CH_3Cl .

As seen in Figure 1, temperature has the most dramatic effect on the concentration of CO, with CO mole percent increasing exponentially with reaction temperature. In contrast, the concentrations of all the C_2 products varied more gradually with temperature. These results can be explained in view of the detailed chemical kinetic mechanism for the CCOP process developed recently (Karra and Senkan 1988a), and will be discussed in a future publication (Senkan 1988).

The effects of O_2 concentration on rates and selectivities are presented in Figures 3 and 4, respectively. These results similarly were obtained by sampling gases near the exit of the reactor corresponding to a nominal residence time of about 330 ms. The reaction temperature was 920 C, and the following O_2 -free pre-reaction composition was used: CH_3Cl 20.6%, CH_4 74.8%, and N_2 4.56%. The concentration of O_2 in these experiments were changed by changing the flow rate of O_2 entering the reactor, while maintaining the flow rates of other gases constant. Consequently, the data points presented in Figures 3 and 4 also do not precisely correspond to same residence times. However, since O_2 represents at most 7% of the reaction mixture, differences in residence times are not expected to be different by more than this amount, again within experimental error limits. As evident from Figures 3 and 4, O_2 concentration directly effects the

level of CO formed in the system, while its impact on C₂ products is more subtle.

Since the CCOP process must proceed under non-flame conditions, the levels of O₂ in the mixture must be selected carefully (1987a). In this regard it is important to recognize that although the presence of some O₂ in the mixture is essential to prevent coke formation, an excess O₂ concentration is also undesirable because of the onset of flame reactions. The onset of flame reactions are characterized by the formation of excessive levels of CO, CO₂, H₂O and soot. The formation of excessive H₂O, in particular, causes operational problems because of its condensation together with HCl on cold surfaces at the exit of the reactor.

In Figures 5 and 6 the concentration and selectivity profiles along the reactor are presented for a mixture with the following pre-reaction composition: CH₃Cl 19.78%, CH₄ 71.62%, O₂ 4.23%, and N₂ 4.37%. These profiles were obtained at 920 C, and by moving the sampling probe along the reactor. The distance along the reactor was measured relative to the point of injection of the CH₃Cl/O₂ mixture into preheated CH₄. In this experiment, the total number of moles in the system remained essentially the same, i.e. the absolute concentration of N₂ measured by GC was constant, thus residence times were directly proportional to distance along the reactor. Since the mean gas velocity in the reactor was 1.15 m/s, the data presented in Figures 5 and 6 correspond to residence times ranging from 173 to 312 ms at the exit of the reactor.

ACKNOWLEDGEMENT:

This research was supported, in part, by funds from the U.S. Environmental Protection Agency, Grant No:R812544-01-0, and IIT IWERC Project No:8605.

REFERENCES:

Cathonnet, M., Boettner, J.C., James, H., "Experimental Study and Numerical Modeling of High Temperature Oxidation of Propane and n-Butane", 18th Symp. (Int'l) on Combustion, p.903, The Combustion Institute, Pittsburgh (1981).

Benson, S.W., "Conversion of Methane", US Patent 4,199,533, 1980.

Chemical and Engineering News, December 13, p.28, 1987.

Colket, M.B., "The Pyrolysis of Acetylene and Vinylacetylene in a Single-Pulse Shock Tube", Twenty First Symposium (International) on Combustion, p.851, The Combustion Institute, Pittsburgh 1988.

Dean, A.M., "Predictions of pressure and temperature effects upon radical addition and recombination reactions", J. Phys. Chem., v.89, p.4600 (1985).

Frenklach, M., Clary, D.W., Gardiner, W.C., and Stein, S.E., "Detailed Kinetic Modeling of Soot Formation in Shock-Tube Pyrolysis of Acetylene", Twentieth Symposium (International) on Combustion, p.887, The Combustion Institute, Pittsburgh (1984).

Granada, A., Karra, S.B., and Senkan, S.M., "Conversion of CH_4 into C_2H_2 and C_2H_4 by the Chlorine-Catalyzed Oxidative-Pyrolysis (CCOP) process: Oxidative pyrolysis of CH_3Cl ", Ind. Chem. Eng. Res., 1987, 26, 1901.

Gorin, E., "Conversion of normally gaseous hydrocarbons", US Patent 2,320,274, 1943.

Karra, S., and Senkan, S.M., "A Detailed Chemical Kinetic Mechanism for the Oxidative Pyrolysis of CH_3Cl ", Ind. Eng. Chem. Research, in press 1988a.

Karra, S.B., and Senkan, S.M., "Analysis of the Chemically Activated $\text{CH}_2\text{Cl}/\text{CH}_2\text{Cl}$ and $\text{CH}_3/\text{CH}_2\text{Cl}$ Recombination Reactions at Elevated Temperatures using the Quantum-Ricé-Rampspberger-Kassel (QRRK) Method", Ind. Eng. Chem. Research, v.27, p.447 (1988b).

Senkan, S.M. "Production of Higher Molecular Weight Hydrocarbons from Methane", US Patent 4,714,796, 1987a.

Senkan, S.M., "Conversion of methane into higher molecular weight hydrocarbons by the Chlorine-Catalyzed Oxidative-Pyrolysis (CCOP) process", Chem. Eng. Prog., 1987b, 12, 58.

Senkan, S.M., "Detailed Chemical Kinetic Modeling of the CCOP Process: Formation of C_3 and C_4 Species", in preparation (1988).

Weissman, M., and Benson, S., "Pyrolysis of Methyl Chloride, a Pathway in the Chlorine-Catalyzed Polymerization of Methane", Int. J. Chem. Kinetics, v.16, p.307 (1984).

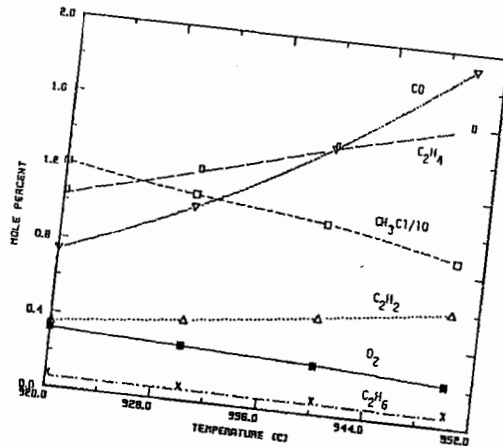


Figure 1. The effects of temperature on the concentration of species at a nominal residence time of 330 ms.

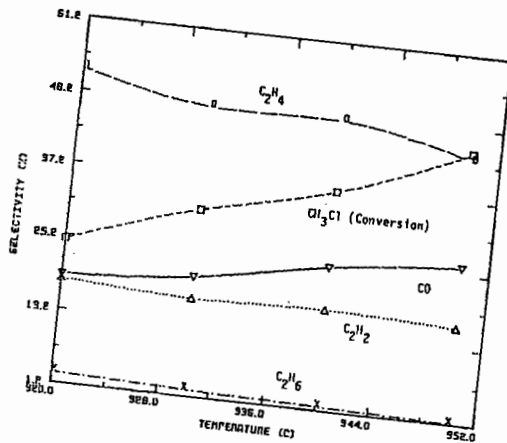


Figure 2. The effects of temperature on conversion and product selectivities at a nominal residence time of 330 ms.

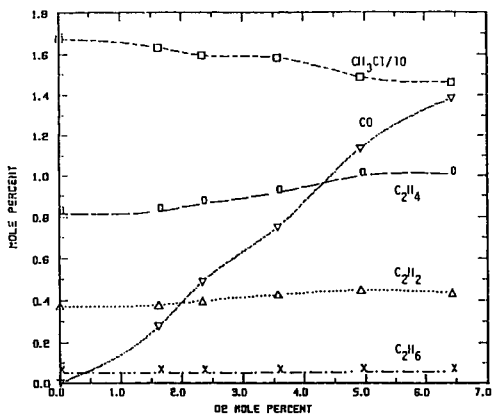


Figure 3. The effects of O₂ concentration on the concentration of species at 920 C and a nominal residence time of 330 ms.

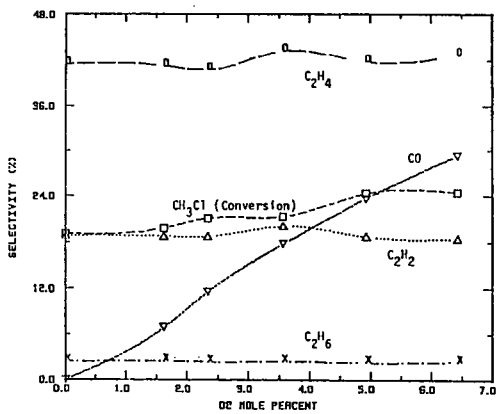


Figure 4. The effects of O₂ concentration on conversion and product selectivities at 920 C and a nominal residence time of 330 ms.

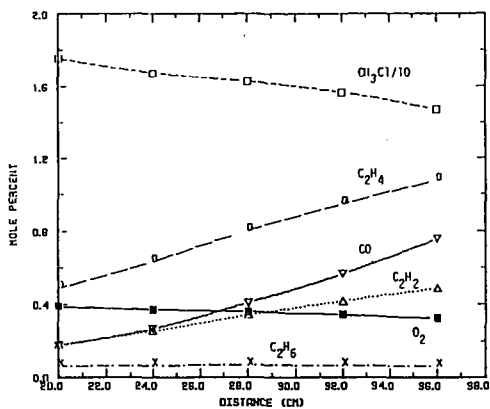


Figure 5. The effects of residence time on the concentration of species at 920 C.

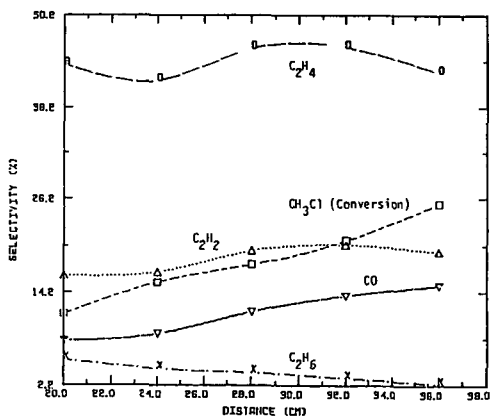


Figure 6. The effects of residence time on conversion and product selectivities at 920 C.

DIRECT METHANE CONVERSION - AN ASSESSMENT

David Gray and Glen Tomlinson
The MITRE Corporation
McLean, VA

and

John Shen
U.S. Department of Energy
Washington, D.C.

Worldwide proven reserves of natural gas are estimated to be approximately 3500 trillion cubic feet of which the U.S. has approximately 6 percent⁽¹⁾. Gas production and consumption worldwide are about 63 trillion cubic feet annually. In 1985 the U.S. produced about 27 percent of this (i.e., about 17 trillion cubic feet)⁽¹⁾. In terms of energy, natural gas consumption represents about half of the total petroleum consumed and natural gas reserves are being discovered at twice the rate of petroleum. This trend indicates the increasingly important role that gas will play in the future energy supplies of the world.

Large quantities of this natural gas are located in remote areas, isolated from centers of commerce and population. No distribution network exists for its transportation. In fact, gas associated with petroleum is often flared rather than utilized. Transportation costs of remote natural gas are a relatively expensive part of the final delivered price. Therefore, most natural gas is consumed in the country where it is produced. Liquefied natural gas (LNG) terminals and vessels can bring remote gas to market. In 1985, 30 percent (1.7 trillion cubic feet) of natural gas traded internationally was transported as LNG and this percentage is growing⁽²⁾. For shorter distances, remote gas can be compressed (CNG) and transported using tankers with pressurized containers. Alternatively, depending on the economic conditions, on-land and subsea pipelines can be constructed to transport the remote gas.

A potentially attractive option, currently being practiced in New Zealand, is to convert the gas on-site to readily transportable liquids like methanol or liquid hydrocarbons. These liquids can then be transported using conventional tankers. The New Zealand plant produces 14,500 barrels per day of gasoline, which are shipped to a refinery for blending into the New Zealand gasoline pool⁽³⁾. The option of on-site conversion of gas to liquids not only allows for easier transportation but also produces a more valuable energy commodity, i.e. a liquid transportation fuel in the case of higher hydrocarbons, or a petrochemical feedstock, gasoline additive or turbine fuel in the case of methanol. In a world where requirements for liquid transportation fuels are paramount, natural gas will increasingly be used to fulfill this role.

Methane, the major constituent of natural gas, is also a by-product of Fischer-Tropsch and other synthesis processes for the production of liquid fuels and chemicals from synthesis gas. This methane must be reformed back to synthesis gas if only liquid products are required; this process is both thermally inefficient and expensive. Thus, alternative processes for converting this methane by-product into liquids will also be a benefit to indirect liquefaction technology.

Conventional transformation of natural gas to methanol and liquid hydrocarbons involves the reforming of the natural gas to synthesis gas followed by catalytic synthesis to produce methanol. If hydrocarbons are required, the methanol can be

further processed using Mobil's Methanol-to-Gasoline (MTG) technology to produce high octane gasoline⁽⁴⁾. This conventional process is a complex processing sequence involving the highly endothermic steam reforming reaction followed by exothermic methanol synthesis.

If it were possible to convert methane directly to methanol or higher hydrocarbons with high conversion and selectivity, both the steam reforming and methanol synthesis steps could be eliminated. This direct conversion approach has the potential for considerable savings in cost if technically sound processes can be developed. Interest in direct methane or natural gas conversion has recently intensified worldwide. Several approaches to this are being researched at oil companies and in programs funded by the Department of Energy or the Gas Research Institute. The more technically advanced processes are those that operate in the temperature range 600-800°C.

This paper assesses the technical potential of some of these high temperature direct methane conversion approaches being researched by various groups. These new approaches are then compared to the conventional technology for converting methane to gasoline by utilizing steam reforming, methanol synthesis and Mobil's Methanol-to-Gasoline (MTG) technology⁽⁵⁾. The direct methane conversion approaches analyzed in this report are Oxidative Coupling, Partial Oxidation, and Oxyhydrochlorination. Computer simulation has been used to model the technical performance of conceptual commercial plants that utilize these direct methane conversion approaches. In addition, the conventional technology has been simulated with the same size plant to provide a baseline to which the new approaches could be compared. These analyses were based on the thermodynamics of the reactions and the reported yields and selectivities for each process. Results are reported on the basis of the efficiency of the lower heating value (LHV) of the product. LHV of the product is the heating value of the product divided by the heating value of the reactant. Sensitivity studies have been conducted for some of the new approaches to identify the levels of performance necessary for these direct conversion techniques to be technically as efficient as the baseline conventional technology.

Data on Oxidative Coupling have been obtained from open literature sources that document the results from Atlantic Richfield (ARCO)⁽⁶⁻⁸⁾. Partial oxidation data have been obtained from published results of H. Gesser et al. of the University of Manitoba⁽⁹⁻¹⁴⁾. Preliminary results of the Oxyhydrochlorination of methane have been obtained from the Pittsburgh Energy Technology Center (PETC)⁽¹⁵⁾.

In the analysis of Oxidative Coupling, the system used was the redox mode. In this approach, methane is contacted with a solid oxidant, in this case manganese oxide on silica. This oxidant provides lattice oxygen for the oxidative coupling of the methane and the manganese is reduced to a lower oxidation state. The solid is then transferred to a regeneration reactor where it is reoxidized. The reoxidized solid is then transferred back to the oxidative coupling reactor where it reacts again with the methane. The products from the oxidative coupling reactor, which are predominantly C₂+ olefins, are then sent to a ZSM-5 polymerization reactor where they undergo oligomerization to form gasoline.

For analysis of Partial Oxidation, methane is reacted with pure oxygen at pressures of 65 bar in a glass-lined, non-catalytic reactor to produce methanol and carbon oxides. The methanol is then sent to an MTG unit, as in the baseline case, to give high octane gasoline as a final product.

In Oxyhydrochlorination, methane is reacted with oxygen and hydrogen chloride over a copper chloride catalyst⁽¹⁶⁾. The analysis assumes a process in which the

products formed are cooled to remove water and hydrogen chloride, and the methyl chlorides produced are sent to a ZSM-5 reactor where they undergo polymerization to form gasoline and liberate hydrogen chloride. The first stage data used gave a 25 percent conversion of methane per pass and a selectivity to mono- and dimethyl chlorides of 81 percent with a molar ratio of mono- to dichloride of approximately 4 to 1. Complete oligomerization of the mono- and dichlorides was assumed to occur over the second stage ZSM-5 reactor to give a stoichiometric mixture of C₈ hydrocarbons and toluene.

Table I summarizes the known process parameters and calculated conversion efficiencies for the new direct methane conversion approaches and the baseline technology considered in this analysis. Using the preliminary data available, the computer simulations of the new approaches all show overall system efficiencies that are not greatly different from the conventional technology. Using ARCO data for the 15 percent Mn/SiO₂ system that gave a methane conversion per pass of 26 percent for a C₂+ selectivity of 60 percent, an LHV product efficiency of 56 percent was obtained for the Oxidative Coupling approach. ARCO showed that promotion of this system with sodium pyrophosphate increased C₂+ selectivity to about 70 percent. Our analysis shows that LHV product efficiency increases to 64 percent at this higher selectivity level. For Partial Oxidation, using the best available data⁽⁹⁻¹⁴⁾, an overall product efficiency of 59 percent was obtained. It was assumed that a product selectivity to methanol of 83 percent was obtained at a per pass methane conversion of 8 percent. For Oxyhydrochlorination, using the assumptions mentioned above, the overall product efficiency was estimated to be 65 percent.

Oxidative Coupling looks promising provided that the selectivity to CO and CO₂ can be maintained at a level of about 25 percent. The design of a practical high pressure redox reactor system needs to be addressed. The excess waste heat from the system, which is of good quality, also needs to be effectively utilized. If this can be done with the current selectivities, then the overall system efficiency including the potentially recoverable heat would be around 70 percent.

Partial Oxidation would appear to be a potentially attractive alternative, based on our estimates of efficiency, provided that high methanol selectivities can be achieved. However, the results from the University of Manitoba are considerably better than have been achieved elsewhere; they may be a function of the particular reactor dimensions used in the experiments. This requires further investigation.

Based on efficiency, Oxyhydrochlorination looks very attractive. However, this analysis has assumed very favorable polymerization potential for the methyl chlorides over ZSM-5, which has yet to be demonstrated in practice. Of greater potential concern for this technology, however, is the severe materials corrosion problems that exist with the handling and recovery of wet hydrogen chloride.

To further evaluate the process potential of these new technologies, additional research and development is needed together with economic analyses to quantify the expected cost savings associated with the elimination of steam reforming and methanol synthesis.

Acknowledgement:

This work was funded by Sandia National Laboratories, which is supported by the U.S. Department of Energy under Contract DE-AC04-76DP00789.

References:

1. Oil and Gas Journal, December 30, 1985, p. 66.
2. Leibson, I., S. T. Davenport and M. H. Muenzier, "Costs to Transport Natural Gas," Hydrocarbon Processing, April 1987, p. 47.
3. Fox, Joseph M., "The Fixed-Bed Methanol-to-Gasoline Process Proposed for New Zealand," paper presented at the Australian Institute of Petroleum, Coal Gasification Conference, Adelaide, March 2, 1982.
4. Haggin, J., "Methane-to-Gasoline Plant Adds to New Zealand Liquid Fuel Resources," Chemical and Engineering News, June 22, 1987, p. 22.
5. Kuo, J. C. W., Gasification and Indirect Liquefaction. Chapter 5 from The Science and Technology of Coal and Coal Utilization, edited by B. R. Cooper and W. A. Ellingson, Plenum Publishing Corp., 1984.
6. Jones, A. C., J. J. Leonard and J. A. Sofranko, "The Oxidative Conversion of Methane to Higher Hydrocarbons Over Alkali-Promoted Mn/SiO₂," Journal of Catalysis, 103, 311-319, 1987.
7. Jones, A. C., J. J. Leonard and J. A. Sofranko, "Fuels for the Future: Remote Gas Conversion," Energy and Fuels 1, 12-16, 1987.
8. Sofranko, J. A., J. J. Leonard and C. A. Jones, "The Oxidative Conversion of Methane to Higher Hydrocarbons," Journal of Catalysis, 103, 302-310, 1987.
9. Gesser, H. D. and N. Hunter, "The Direct Conversion of Methane to Methanol by Controlled Oxidation," Chemical Reviews 85 (4), August 1985, p. 235.
10. Gesser, H. D., N. R. Hunter, L. A. Morton, P. S. Yarlagadda and D. P. C. Fung, "The Direct Conversion of Methane to Methanol by a High Pressure Partial Oxidation Reaction," American Chemical Society, Division of Fuel Chemistry, Preprints 32 (3), 255, 1987.
11. Hunter, N. R., et al., "The Direct Conversion of Methane to Methanol," Proceedings of the VI International Symposium on Alcohol Fuels Technology, Ottawa, May 21-25, C-14, Vol. 11-147, 1984.
12. Hunter, N. R., et al., "The Direct Conversion of Natural Gas to Methanol by Controlled Oxidation at High Pressure," Proceedings of the 35th Canadian Chemical Engineering Conference Category, Oct. 6-9, 1985.
13. Hunter, N. R., et al., "The Direct Conversion of Natural Gas to Alcohols," presented at the VII International Symposium on Alcohol Fuels, Paris, Oct. 20-23, 1986.
14. Yarlagadda, P. S., et al., "Direct Catalytic Conversion of Methane to Higher Hydrocarbons," Fuel Science and Technology Int. 5(2), 169-183, 1987.
15. Taylor, C. E. and R. P. Noceti, "Conversion of Methane to Gasoline-Range Hydrocarbons," American Chemical Society, Division of Fuel Chemistry, Preprints 32 (3), 307, 1987.
16. Pieters, W. J. M., E. J. Carlson, E. Gates and W. C. Conner, U.S. Patent, 4,123,389 (1978).

TABLE 1
SUMMARY OF DIRECT METHANE CONVERSION APPROACHES
FOR PRODUCTION OF GASOLINE

	Number of Stages	3	2	2	2
		BASELINE TECHNOLOGY	OXIDATIVE COUPLING	PARTIAL OXIDATION	OXHYDRO-CHLORINATION
Stage 1		Steam Reforming	Oxidative Coupling	Partial Oxidation	Oxyhydrochlorination
Catalyst		Nickel	Mn/SiO ₂	None	CuCl/KCl on Silica
Temperature (°C)		800-900	815	458	340
Pressure (Bar)		7-20	35	65	15
CH ₄ Conversion Per Pass		---	26	8	25
Overall CH ₄ Conversion %		90	99	95	93
Selectivity		---	50% to C ₂ ⁺	83% to CH ₃ OH	77% to CH ₃ Cl
Stage 2		Methanol Synthesis	Olefin Oligomerization	Methanol-to-Gasoline	Methyl Chloride Oligomerization
Catalyst		Cu/Zn	ZSM-5	ZSM-5	ZSM-5
Temperature (°C)		250-300	370	320	400
Pressure (Bar)		80-100	27	22	12
Stage 3		Methanol-to-Gasoline	None	None	None
Catalyst		ZSM-5			
Temperature (°C)		320			
Pressure (Bar)		22			
Overall LHV Efficiency %		59	56	59	65

The Oxidation of Methane on Silica-Supported Heteropoly Oxometalates

S. Ahmed, S. Kasztelan and J.B. Moffat
Department of Chemistry and
Guelph-Waterloo Centre for
Graduate Work in Chemistry
University of Waterloo
Waterloo, Ontario, Canada
N2L 3G1

Abstract

The conversion of methane with nitrous oxide is shown to be catalyzed by silica-supported heteropoly oxometalates of Keggin structure, in particular 12-molybdophosphoric acid (HPMo). The activity of the HPMo catalysts is related to the presence of a thermally sensitive species whose degradation products are considerably less active in the oxidation of methane. The thermally sensitive species are identified as the heteropoly anions which are stabilized on the silica support.

Introduction

In many countries, supplies of natural gas are more plentiful than those of crude oil, often necessitating the importation of crude oil while, at least in some cases, natural gas is exported. While the heat released per carbon atom in oxidation is higher with methane than with any other hydrocarbon, methane suffers from the disadvantage of its gaseous state under ambient conditions. Further, although decreases in free energy are observed for the successive elimination of hydrogen atoms, the complete oxidation of methane is thermodynamically more spontaneous than any processes associated with the partial elimination of hydrogen. Consequently, while natural gas, whose predominant component is methane, has found considerable use as a fuel in stationary applications, it has seen relatively little use in motorized vehicles, nor as a feedstock in the production of chemicals.

Interest in the conversion of methane to more amenable substances has resulted in research efforts on the partial oxidation and oligomerization of the gas. A number of excellent recent reviews are available (1-4). The studies of partial oxidation by Lunsford and co-workers on Mo/SiO₂ (5) and Somorjai and co-workers on Mo/SiO₂ and V/SiO₂ (6) and that on oxidative coupling with transition metal oxides by Sofranko and coworkers (7-8) are particularly noteworthy. In this laboratory studies of the surface, structural and catalytic properties of heteropoly oxometalates have been in progress for a number of years. Heteropoly oxometalates are ionic solids with discrete anions of cage-like structure. The anions of Keggin structure have a central atom such as, for example, phosphorus or silicon, surrounded by four oxygen atoms arranged tetrahedrally. Twelve octahedra with, for example, tungsten or molybdenum at their centres envelope the central tetrahedron and share oxygen atoms with each other and with the former (Fig. 1).

Semiempirical extended Huckel calculations have predicted that the solid heteropoly acid containing tungsten as peripheral metal element has more acidic protons than that with molybdenum (9). In addition, the oxygen atoms in the latter anions should be more labile than those in the former anions. Indeed, methanol is converted to hydrocarbons on tungsten-containing heteropoly oxometalates but to CO and CO₂ on those containing molybdenum (10). Photoacoustic FTIR studies have shown that polar molecules such as ammonia (11), pyridine (12) and methanol (13) are able to enter the bulk structure of the heteropoly oxometalates but nonpolar species apparently cannot do so. The acidic proton has been shown to protonate the methanol molecule and at elevated temperatures the C-O bond undergoes a scission and the heteropoly anions are methylated apparently at the terminal oxygen atoms (14).

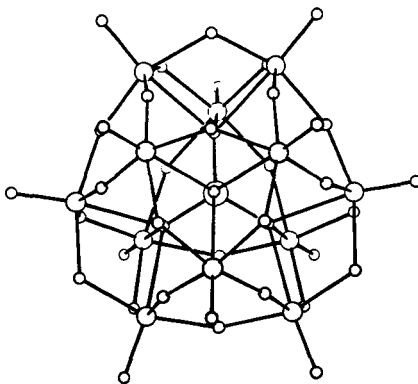


Fig. 1 Heteropoly Oxometalate Anion of Keggin Structure

In the present work the oxidative conversion of methane with nitrous oxide is studied on various heteropoly oxometalates, but primarily 12-molybdophosphoric acid ($H_3PMo_{12}O_{40}$, abbreviated to HPMo).

Experimental

Since methane cannot enter the bulk structure of the heteropoly oxometalates and the parent heteropoly acids have low surface areas, it is necessary to support the acids on a high area solid, in the present case silica (Davison Grade 407). An incipient wetness technique is employed to load the solid. A fixed-bed continuous flow reactor with on-line gas chromatograph (HP 5890) was employed for the catalytic studies (15-17).

Results

Table 1 provides a comparison of the results for various supported heteropoly oxometalates as well as supported molybdenum and vanadium catalysts. It is evident that the molybdenum-containing heteropoly oxometalates produce higher conversions and better selectivities to partial oxidation products than those containing tungsten. For comparison samples of molybdenum and of vanadium on silica have been prepared by the method of Liu (5) and the results are included in Table 1.

Table 1
Conversion and Selectivity^a

Catalyst ^b	Conversion			Selectivity		
	CH ₄	N ₂ O	CO	CO ₂	CH ₂ O	CH ₃ OH
HPMo (20.0)	5.1	36.4	65.0	22.5	12.0	0.5
HPW (26.2)	0.4	3.2	56.0	44.0	τ	nd
HSiMo (19.9)	2.5	17.0	58.6	32.3	8.7	0.4
HSiW (26.2)	0.4	2.8	44.0	56.0	τ	nd
V (1.66)	8.9	59.1	81.8	14.5	3.5	0.2
Mo (3)	0.4	3.3	57.0	31.0	12.0	τ

a Reaction Conditions: $T_R = 843$ K, $W = 0.35$ g, $F = 30$ ml min^{-1} CH₄ (67%), N₂O (33%)

b Figures in brackets refer to loading of the silica support in wt%.

The remaining of the results reported here pertain to silica-supported HPMo. As expected the selectivity to partial oxidation products increases with decreasing contact time until a maximum is reached. A maximum is also observed for the selectivity to CO while the CO₂ selectivity shows a minimum. The production of CO₂ is found to increase with reaction temperature while that of CO and formaldehyde decreases. The selectivity to partial oxidation products and the conversion have been shown to be inversely related.

It is of interest to consider the evidence for the participation of the heteropoly oxometalate in the conversion process. The conversion and selectivity in the oxidation of methane with nitrous oxide on silica-supported HPMo remain relatively unchanged for pretreatment temperatures up to approximately 773 K (Figures 2A and 2B). However at higher temperatures the conversion decreases markedly while the production of CO and CO₂ remains constant up to approximately 900 K. For temperatures higher than 900 K the production of H₂CO and CO decreases while that of CO₂ increases with all three apparently approaching that found with the support above.

Experiments in which the pretreatment temperature was held at that for which thermal degradation is occurring (823 K) and the duration of pretreatment varied (Fig. 2C and 2D) show a relatively gradual decrease in the conversion of methane and a small loss of HPMo while CO increases slightly in quantity and the production of CO₂ and H₂O decreases slowly. It is evident that the activity of the HPMo catalysts is related to the presence of a thermally sensitive species whose degradation products are considerably less active in the oxidation of methane.

The rates of reaction are found to be strongly dependent on the loading of HPMo on silica (Fig. 3). The rates increase approximately linearly (except for that of methanol) and reach maxima at a loading of approximately 120 μ mol of heteropoly anions per gram of support. This corresponds to a coverage of approximately 1000 \AA^2 /anion, to be compared with an estimate of 100 \AA^2 for the cross-sectional area of the heteropoly anion. It seems reasonable to assume, at least tentatively, that each anion is isolated on the silica support surface.

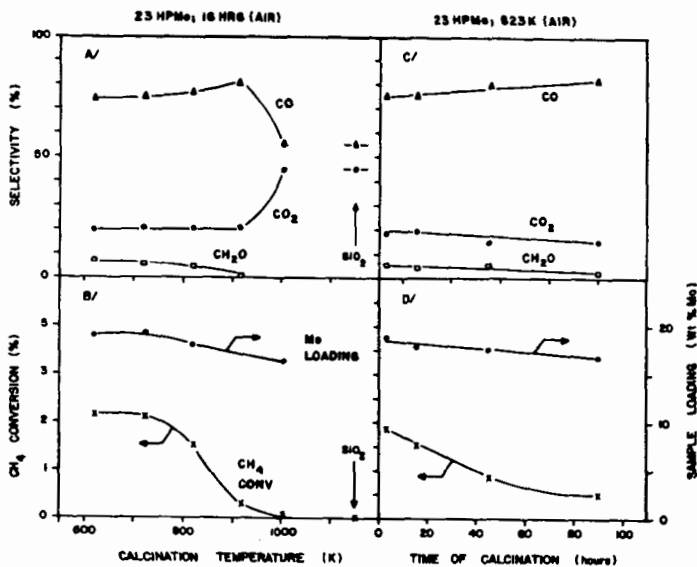


Fig.2 Effect of the temperature of pretreatment during 16 h (left) and of the time of calcination at 823 K under air (right) on the CH₄ conversion, selectivity, and Mo loading of the 23-HPMo catalyst. Reaction conditions: CH₄ (67%), N₂O (33%), T_R = 843 K, W = 0.5 g, F = 30 ml min⁻¹. Symbols: (Δ) CO, (○) CO₂, (□) CH₂O, (X) CH₄ conversion, (●) Mo loading.

Infrared spectra show that the supported HPMo retains the heteropoly anion structure up to temperatures as high as 973 K, suggesting that the silica is, in addition to providing a high area support for the HPMo, also acting to provide a thermal stabilization for the HPMo.

Acknowledgements

Part of this work was done under contract to Energy, Mines and Resources (Canada). The financial support of the Natural Sciences and Engineering Research Council of Canada is also gratefully acknowledged.

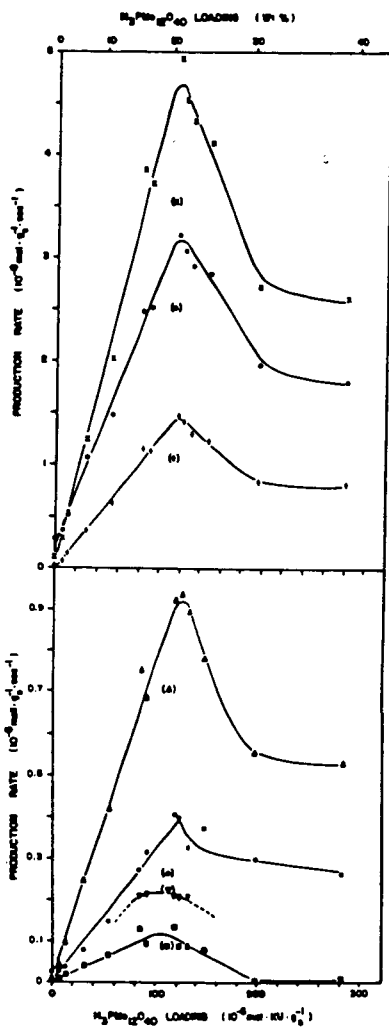


Fig. 3 Effect of the HPMo loading of the support on the production rate of the different products of the $\text{CH}_4 + \text{N}_2\text{O}$ reaction at 843 K. Reaction conditions: CH_4 (67%), N_2O (33%), W - 0.5 g, F = 30 ml min⁻¹. Symbols: (X) N_2 , (+) total carbon detected, (●) H_2O , (V) CH_3OH , (Δ) CO, (○) CO_2 , (□) CH_2O .

References

1. C.A. Jones, J.J. Leonard and J.A. Sofranko, *Energy and Fuels*, 1 (1987) 12.
2. R. Pitchai and K. Klier, *Catal. Rev.-Sci. Eng.*, 28 (1986) 13.
3. H.D. Gesser, N.R. Hunter and C.B. Prakash, *Chem. Rev.*, 85 (1985) 235.
4. N.R. Foster, *Appl. Catal.*, 19 (1985) 1.
- 5a) H.F. Liu, R.S. Liu, K.Y. Liew, R.E. Johnson and J.H. Lunsford, *J. Amer. Chem. Soc.* 106 (1984) 4117.
- b) L. Mendelovici and J.H. Lunsford, *J. Catal.*, 94 (1985) 37, and references contained therein.
6. K.J. Zhen, M.M. Khan, C.H. Mak, K.B. Lewis and G.A. Somorjai, *J. Catal.*, 94 (1985) 501.
7. J.A. Sofranko, J.J. Leonard and C.A. Jones, *J. Catal.*, 103 (1987) 302.
8. C.A. Jones, J.J. Leonard and J.A. Sofranko, *J. Catal.*, 103 (1987) 311.
9. J. B. Moffat, *J. Molec. Catal.*, 26 (1984) 385; *Proc. 8th Iberoamerican Sympos. Catalysis*, 1984, p. 349, Lisbon; *Catalysis on the Energy Scene, Studies in Surface Science and Catalysis*, S. Kallaguine and A. Mabay (Eds.), 1984, Vol. 19, p. 77, Elsevier, Amsterdam; *Catalysis by Acids and Bases*, Imelik et al (Eds.), 1985, p. 157, Elsevier, Amsterdam.
10. H. Hayashi and J.B. Moffat in *Catalytic Conversion of Synthesis Gas and Alcohols to Chemicals*, (R.G. Herman, Ed.), Plenum, N.Y., 1984, and references contained therein.
11. J.G. Highfield and J.B. Moffat, *J. Catal.*, 88 (1984) 177.
12. J.G. Highfield and J.B. Moffat, *J. Catal.*, 89 (1984) 185.
13. J.G. Highfield and J.B. Moffat, *J. Catal.*, 95 (1985) 108.
14. J.G. Highfield and J.B. Moffat, *J. Catal.*, 98 (1986) 245.
15. S. Kasztelan and J.B. Moffat, *J. Catal.*, 106 (1987) 512.
16. S. Kasztelan and J.B. Moffat, *J. Catal.*, (in press).
17. S. Ahmed and J.B. Moffat, *Applied Catal.*, (in press).

CONVERSION OF METHANE TO HIGHER HYDROCARBONS
BY SUPPORTED ORGANOMETALLIC COMPLEXES

Robert B. Wilson, Jr. and Yee-Wai Chan
Inorganic and Organometallic Program
SRI International
Menlo Park, CA 94025

ABSTRACT

Novel highly dispersed metal catalysts were prepared by attaching metal clusters to inorganic oxides. The hydridoruthenium complexes (containing one, four or six ruthenium atoms) were first reacted with triethylaluminum, which releases one equivalent of ethane per hydride to give a novel aluminum-containing complex. These complexes were then anchored to the support (alumina, zeolite 5A, or Y-zeolite) by reaction with acidic sites, in which another equivalent of ethane was released. These catalysts were active in the conversion of methane to C₂ and higher hydrocarbons at 750°C using a fixed-bed down-flow reactor under anaerobic condition. Up to 50% selectivity for higher hydrocarbons was observed with the alumina supported hexameric ruthenium clusters. The zeolite supported tetrameric cluster produced less coke than the other catalysts apparently due to the cluster being located inside the zeolite supercage.

INTRODUCTION

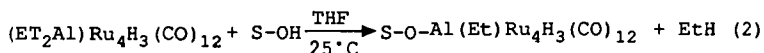
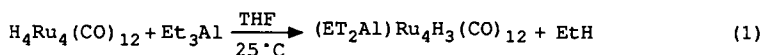
Research on the technique of surface confinement to produce novel catalysts for a wide variety of processes is continuing in many laboratories.¹⁻⁴ We have been working on the development of novel catalysts for converting methane to higher hydrocarbons. The catalysts are prepared by reacting organometallic complexes of transition metals with inorganic oxide supports to produce surface-confined metal complexes.⁵ The metal complex is then decomposed to obtain very stable, highly dispersed catalysts. The increased activity of highly dispersed catalysts is desirable for activating the relatively inert methane and because highly dispersed catalysts are resistant to coking. The use of zeolitic supports will stabilize the highly dispersed catalysts which are confined inside the zeolite pores. The variables we studied include cluster size, supporting materials, and reaction conditions.

EXPERIMENTAL DETAILS

Synthesis of catalysts

The synthesis of these catalysts involves three steps. The first step is to synthesize the ruthenium cluster precursors. The second step is a novel approach developed in our laboratory that involves the reaction of the organometallic clusters with alkyl aluminum. The final step is to anchor these catalysts on supports by a chemical reaction between the hydroxy group of the support and the alkyl groups of the organometallic cluster to give a covalent chemical bond.

The organometallic complexes include a monoruthenium complex, $\text{Ru}(\text{allyl})_2(\text{CO})_2$; a tetrameric ruthenium cluster, $\text{H}_4\text{Ru}_4(\text{CO})_{12}$; a hexameric ruthenium cluster, $\text{H}_2\text{Ru}_6(\text{CO})_{18}$; and a mixed metal cluster, $\text{H}_2\text{FeRu}_3(\text{CO})_{13}$; all were prepared according to literature procedures.^{6,7} The hydrido clusters reacted with triethyl aluminum at room temperature (eq. 1). The reaction stoichiometries were determined by measuring the quantity of ethane produced.⁵ These alkyl aluminum carbonyl ruthenium clusters were then used to react with acidic supports: -alumina, 5A molecular sieves, and LZ-Y 52 zeolite. The reaction stoichiometries were again determined by measuring the quantity of ethane produced (eq. 2).



The monomeric ruthenium complex reacted directly with the acidic support to release one equivalent of propylene. The tetraruthenium and the mixed iron-ruthenium clusters were also supported on magnesium oxide by the reaction of acidic hydride with the basic oxide. All support materials were in powder form except for the 5A molecular sieves which was 60-80 mesh.

General Procedure for testing catalysts

The activity of the catalysts were tested using a conventional fixed-bed down-flow reactor. In a typical run, the catalyst (0.5 g) was loaded into a stainless steel reactor (0.22 inch ID) under an inert atmosphere. The reactor was connected to the reactor system and purged with helium for 15 min. A helium diluted methane gas (contains 20% methane) was introduced through a mass flow controller to the reactor. A back pressure regulator was set at 50 psig and the methane flow rate was controlled by the mass flow controller. A thermocouple was immersed in the catalyst bed and connected to a temperature controller. The outlet gases were fed to a Carle 500 gas chromatography for sample analysis. The GC was programmed to separate light gases including hydrogen and hydrocarbons up to C₅. The C₆ and higher hydrocarbons and other polar compounds (C₆+) were back flushed from the column to the detector. The calibration of C₆+ was based on the area integration and referenced to the methane peak. Other components were calibrated with standard sample mixtures. Initial methane concentration was measured before and after each run at ambient temperature under the same conditions. Each sample run lasted for at least 15 h and the products were analyzed every hour. During the first 2 h of the reactions, we detected small amounts of CO, which was released from the decomposition of the metal complexes. The analytical data from the first 3 h of reactions were discarded and the subsequent 12 h data were averaged.

RESULTS AND DISCUSSION

The ruthenium catalysts were tested at 750°C under 50 psig pressure. Three different sizes of ruthenium clusters: monomer (Ru), tetramer (Ru₄), and hexamer (Ru₆) were supported on three different supports: γ -alumina, 5A molecular sieve, and Y-zeolite. The results are summarized in Table 1. We used a commercial ruthenium catalyst which is supported on alumina (obtained from Engelhard) for comparison. The amount of metal loading were based on elemental analyses (Galbraith Laboratory).

Effects of cluster size

The commercial ruthenium catalyst gave a very high conversion of methane (71.2%) but no hydrocarbon product was detected. Methane conversion on the monoruthenium catalysts were considerably lower than the ruthenium clusters (Ru_4 and Ru_6). In general, methane conversions depend on the type of support and decreased in the order of alumina, 5A molecular sieve, and zeolite. These results suggested that the methane conversion was related to the amount of surface bonded metal. On alumina, the metals are located on the surface while on 5A molecular sieves and on zeolite, increased amount of metal were located inside the zeolite pore. The differences of methane conversions were more obvious for the Ru_4 catalyst where the conversion decreased from 10.1 to 4.9 and to 1.7% on alumina, 5A molecular sieve, and Y-zeolite, respectively.

Our intention in using different supports is to confine the ruthenium cluster at different locations on or within the support. Hence, the Ru_4 and Ru_6 clusters are dispersed on the alumina surface but are partly confined inside the pores of zeolite supports. The pore size of 5A molecular sieve is too small for the Ru_6 cluster but should be large enough for the Ru_4 cluster after decomposition. Since the Y-zeolite has the largest pore (~ 17), most of the Ru_4 are located inside the zeolite pore.

Product selectivity

All the ruthenium catalysts produced ethane and ethylene. The selectivity of C_2 hydrocarbons for Ru_4 clusters increased as the percent conversion of methane decreased. The Ru_6AL has the highest total hydrocarbon yield which probably due to the higher metal loading. The total hydrocarbon yield on Ru_6MS and Ru_6ZL are about the same but the Ru_6ZL has a higher selectivity for C_2 product. Confining the metal cluster inside the zeolite cage may also limit the propagation of methane polymerization. The ruthenium monomers gave relatively low hydrocarbon yields indicating that polymerization of methane required more than one metal atom.

Table 1

ACTIVITY OF RUTHENIUM CATALYSTS ON METHANE DEHYDROGENATION^a

Catalyst ^b	Ru(wt%)	Flow Rate (mL/min)	Methane Conver(%)	Selectivity ^c to		
				H ₂ (%)	C ₂ (%)	C ₆₊ (%)
Ru-com	0.50	50	71.2	151.0	-- ^d	--
RuAL	0.35	10	3.0	139.9	2.8	--
RuMS	0.31	10	2.3	147.5	1.2	--
RuZL	0.37	10	1.7	177.5	2.6	--
Ru ₄ AL	0.61	100	10.1	78.6	1.62	--
Ru ₄ MS	0.49	100	4.9	146.6	3.52	--
Ru ₄ ZL	0.61	50	1.7	25.3	6.9	28.9
Ru ₆ AL	1.26	50	6.1	113.4	6.9	41.4
Ru ₆ MS	0.19	50	5.6	192.8	1.0	14.8
Ru ₆ ZL	0.20	50	3.6	161.9	3.6	10.0

^aReaction condition: temperature=750C, pressure=150 psig.

^bAbbreviation: Ru-com=commercial ruthenium catalyst from Engelhard;

Ru₄=(C₂H₅)₂AlRu₄H₃(CO)₁₂; Ru₆=(C₂H₅)₂AlRu₆H(CO)₁₈;

Ru=Ru(Allyl)(CO)₂; AL--alumina; MS=5A molecular sieve; ZL=LZ-Y-zeolite.

^cSelectivities were calculated on converted methane. Selectivity to hydrocarbons are based on carbon number.

^dNot detected.

Coking

The results listed in Table 1 show that more than one equivalent of hydrogen was produced per methane input, which suggests that some of the methane turned to coke. The elemental analyses listed in Table 2 showed that the Ru₄AL, Ru₄MS, Ru₆AL and Ru₆MS contained more carbon after reaction with methane. In contrast, the carbon content of the Ru₄ZL decreased after reaction. Thus, those catalysts having metal dispersed on the support surface (and therefore larger particle size) promote coke formation while the metals confined inside the zeolite cages have much reduced coking. For the Ru₄MS, the carbon content only increased slightly to 4.38% as compared to more than 20% for the Ru₄AL suggesting that at least a portion of the metal clusters are located inside the

cages of the molecular sieve. On Y-zeolite, the Ru₄ cluster in fact showed a decrease in carbon content indicating very low coking. The decrease is due to the decomposition of the ruthenium complexes, i.e. release of carbon monoxide.

Table 2

ELEMENTAL ANALYSES OF RUTHENIUM CATALYSIS FOR METHANE DEHYDROGENATION^A

Catalyst	Before Reaction			After Reaction		
	%C	%H	%Ru	%C	%H	%Ru
Ru ₄ AL	5.09	1.04	0.61	26.50	0.40	0.57
Ru ₄ MS	1.46	1.13	0.49	4.38	0.46	0.64
Ru ₄ ZL	5.25	1.53	0.61	0.58	0.22	1.26
Ru ₆ AL	9.77	1.84	1.26	23.24	0.67	0.55
Ru ₆ MS	0.95	1.68	0.19	22.29	0.19	0.32

^aReaction with methane at 750C for 15 h.

Effect of reaction conditions

The effect of reaction temperature is similar for every catalyst. Higher methane conversion and product yield are obtained at higher temperature. These results are expected because polymerization of methane is thermodynamically unfavored process.⁸ Increasing the reaction pressure has a similar effect on the methane conversion. However, the product selectivities for hydrogen and C2 hydrocarbons decrease but increases for C6+ hydrocarbons (Table 3). Highest selectivity is observed at 150 psig. As expected, increasing the space velocity lowers the methane conversion but increase the selectivity of hydrocarbon products.

Basic support and mixed metal cluster

Methane conversion on the magnesia supported ruthenium monomer and the FeRu₃ cluster are much higher than the zeolite supported analogs (Table 4). However, the product selectivities to hydrocarbons are lower.

Table 3

EFFECT OF REACTION PRESURE AND SPACE VELOCITY TO
THE ACTIVITY OF Ru₆ZL^a AT 750°C

Pressure (psig)	Flow rate mL/min	%CH ₄ Conversion	%Selectivity ^b of		
			H ₂	C ₂	C ₆₊
50	50	3.18	164.16	6.04	6.6
150	50	5.19	91.33	4.48	10.70
250	50	8.64	82.41	2.46	7.38
250	100	2.62	177.10	9.24	20.64

^aRu₆ZL = zeolite supported Ru₆ cluster, C₂H₅AlRu₆H(CO)₁₈.

^bSelectivity was based on carbon number of hydrocarbon and the amount of methane reacted.

Table 4

CATALYTIC REACTIVITY OF ZEOLITE AND MAGNESIA
SUPPORTED CATALYSTS FOR METHANE DEHYDROGENATION^a

Catalysts	Temp(°C)	Methane Conversion(%)	Selectivity ^b	
			C ₂ (%)	C ₆₊ (%)
RuMgO	600	21.044	0.1	0.5
Ru ₄ MgO	750	4.04	6.9	49.2
FeRu ₃ ZL	600	3.07	1.9	18.5
FeRu ₃ MgO	600	8.87	0.1	--

^aReaction conditions: pressure=150psig, flow rate=20 mL/min, weight of catalyst=2 g, reactor O.D.-3/8in (S.S.).

^bSelectivity to hydrocarbon is based on carbon number.

^cNot detected.

For the mixed iron-ruthenium catalysts, magnesia support also increased the methane conversion. At 600°C, the methane conversion was 8.87% for FeRu₃MgO and was 3.07% for FeRu₃ZL. At 750°C, methane conversion increased to 41.5% and 23.05% for FeRu₃MgO and FeRu₃ZL, respectively. These catalysts behave similarly to the ruthenium monomers in that the hydrocarbon yields were lower on the magnesia supported catalyst.

Increased temperature has a similar effect on the methane conversion over FeRu_3ZL , but the methane conversion was lower than the MgO supported catalysts. At 750°C , the methane conversion was 23.05%. Hydrocarbon yields increased as the reaction temperature increased from 500° to 600°C and then declined at higher temperature. The maximum yield of C_2 was 0.06% of the input methane and was 0.57% for C_6+ . Since the Ru_4ZL was essentially not active at 600°C , this low temperature reactivity of FeRu_3ZL is obviously due to an effect of the mixed metal. Introduction of the iron to the metal cluster is advantageous to methane dehydrogenation activity. Figure 3 shows the effect of increasing temperature on methane conversion and on hydrocarbon yield. Highest hydrocarbon yield was obtained at 600°C . However, the hydrogen selectivity was 170% at this temperature which suggests coke formation.

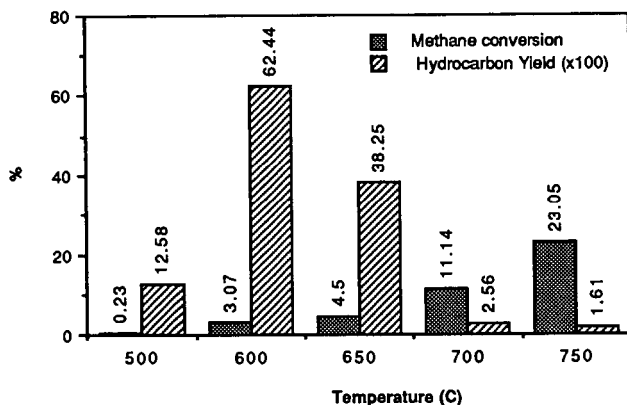


Figure 1. Activity of FeRu_3ZL for methane reforming at various temperatures.

CONCLUSION

Most of the reports on catalytic conversion of methane to higher hydrocarbons are based on metal oxides by the oxidative coupling pathway. Few examples have been reported of direct methane dehydrogenation. Table 5 lists some of the literature results on both oxidative coupling and dehydrogenation together with our results.

It is difficult to truly compare the catalytic activities of the catalysts because the experimental conditions are so different. However, based on the methane conversion and the selectivities of higher hydrocarbons, our catalysts are comparable. Interestingly, we have not detected any mid-ranged hydrocarbons (C₃-C₅). Mitchell and Waghorne reported the major product of alumina supported CaCrPt catalyst under anaerobic condition was benzene.⁹ Jones et al. also observed small amounts of benzene produced from methane dehydrogenation over silica support GeO₂.¹⁰ We have not yet identified our C₆₊ product, but it is possible that it contains benzene.

Table 5

COMPARISON OF THE ACTIVITIES OF CATALYSTS FOR METHANE DEHYDROGENATION

Catalyst	CH ₄ /O ₂	Temp. (°C)	Press (atm)	GHSV (h ⁻¹)	CH ₄ conv(%)	Selectivity to	
						C ₂	C ₆
Li/MgO ^a	2	720	1	2754	37.8	50.3	N.R. ^h
CaCrPt/AL ^b	>200 ^j	705	1	N.R.	27.64 ⁱ	31.4	68.3
PbO/MgO ^c	6	750	1	8000	10.0	65.5	N.R.
Sm ₂ O ₃ ^d	6	750	1	3.8x10 ⁷	6.5	60.0	N.R.
Sb ₂ O ₃ /SiO ₂ ^e	>200	800	1	600	0.25 ⁱ	82.9	N.R.
GeO ₂ /SiO ₂ ^f	>200	700	1	860	0.22	57.1	3.3 ^k
Ru ₆ AL ^g	>200	750	4.5	16000	6.06	6.9	41.4
Ru ₄ ZL ^g	>200	750	4.5	16000	1.74	6.9	28.9
Ru ₄ MgO ^g	>200	750	4.5	6200	4.04	6.9	49.2
FeRu ₃ ZL ^g	>200	600	4.5	6200	3.07	1.9	18.5

^aT. Ito; J-X Wang; C-H, Lin; J.H. Lunsford, J. Am. Chem. Soc., 107, 5062 (1986).

^bH.L. Mitchell, III; R.H. Waghorne; U.S. Patent No. 4239658 (1980).

^cK. Asami; S. Hashimoto; T. Shikada; Chem. Letter 1233 (1986).

^dK. Otsuka, T. Komatsu; Chem. Lett. 483 (1987).

^eC.A. Jones, J.J. Leonard; J.A. Sofranko; U.S. Patent 4,443,644 (1984).

^fC.A. Jones, J.J. Leonard; J.A. Sofranko; U.S. Patent 4,554,395 (1985).

^gThis work.

^hNot reported.

ⁱCumulative result.

^jNo oxygen added.

^kbenzene.

References

1. M.E. Dry and J.C. Hoogendoorn, *Catal. Rev.*, 23, 265 (1981).
2. D.L. King, J.A. Cusumano, and R.L. Garten, *Catal. Rev.*, 23, 203 (1981).
3. H.C. Foley, S.J. D-Cani, K.D. Tau, K.J. Chao, J.H. Onuferko, C. Dybowski, and B.C. Gates, *J. Am. Chem. Soc.*, 105, 3074 (1983).
4. J.P. Candlin and H. Thomas, "Supported Organometallic Catalysis", in *Homogeneous Catalysis II*, D. Forster and J.F. Roth, eds., *Adv. Chem. Series*, 132, 212-239 (1974).
5. Y.I. Yermakov, B.N. Kuznetsov, and V.A. Zakharou, "Catalysis by Supported Complexes," Vol.8, *Studies in Surface Science and Catalysis*, Elsevier, Amsterdam, (1981).
6. A.A. Bhattacharyya, C.L. Nagel, and S.G. Shore, *Organometallics*, 2, 1187 (1983).
7. G.L. Geoffroy and W.L. Gladfelter, *J. Am. Chem. Soc.*, 99, 7565 (1977).
8. D.R. Stull, E.F. Westrum Jr., and G.C. Sinke, *The Chemical Thermodynamic of Organic Compounds*, Wiley, New York, (1969).
9. H.L. Mitchell, III; R.H. Waghorne; U.S. Patent No. 4239658 (1980).
10. C.A. Jones, J.J. Leonard; J.A. Sofranko; U.S. Patent 4,554,395 (1985).

PARTIAL OXIDATION OF METHANE USING SUPPORTED PORPHYRIN
AND PHTHALOCYANINE COMPLEXES

Yee-Wai Chan and Robert B. Wilson, Jr.
Inorganic and Organometallic Program
SRI International
Menlo Park, California 94025

ABSTRACT

The catalytic oxidation of methane with molecular oxygen was investigated in a fixed-bed flow reactor with various anchored metal phthalocyanine (PC) and porphyrins (TPP) as the catalysts. These support organometallic species were stable at temperatures as high as 400°C. Methanol was formed from zeolite encaged RuPC, CoTPP, and MnTPP at 375°C. In contrast, a PdPC complex attached to magnesia produced ethane rather than methanol. The other surface-supported catalysts gave carbon dioxide and water as the sole observable products (by GC).

INTRODUCTION

Conversion of methane to useful chemicals by partial oxidation and oxidative dehydrogenation has received the attention of many researchers.¹ Our first approach to the goal of selective partial oxidation of methane was to synthesize zeolite encapsulated porphyrin and phthalocyanine complexes that mimic the oxygenase enzyme: Cytochrome P-450.²⁻⁵ Porphyrins and phthalocyanines are potent oxidants that also allow control of the active form of oxygen, thereby leading to control of activity and selectivity. The use of zeolitic supports will enhance the stability and reactivity of the catalysts, and will discourage the secondary reactions that always pose problems in the oxidation of methane because the primary products are more easily oxidized than methane.

Our second approach to stabilize the phthalocyanine complex is by anchoring the complex on the surface of a support. Magnesium oxide is

known to generate methyl radicals from methane,⁶ lithium promoted MgO has shown high selectivity to C₂ hydrocarbons on methane oxidation.^{8,9} The metal oxo intermediate generated from the phthalocyanine and oxygen should react with methyl radicals faster than with methane. We prepared magnesium oxide supported catalysts by reacting the basic support with the acid form of tetrasulfophtha-locyanine (TSPC) complexes. The TSPC complexes were anchored to the MgO surface by ionic interaction between the sulfonate groups of the metal complex and the basic sites of MgO.

EXPERIMENTAL DETAILS

Preparation of Metal Ion Exchanged Zeolite

To a slurry of 500 g zeolite (LZ-Y52, Unioncarbide) and water (500 mL), a 1M aqueous solution of metal salt (500 mL, FeCl₂, CoCl₂, MnSO₄, or Ru(DMSO)₂Cl₂) was added dropwise. The zeolite slurry was stirred at a constant speed. The total addition time was approximately 1 h. The mixture was allowed to stir for 24 h. The exchanged powder was filtered, washed with water until the washing were free of chloride or sulfate and then dried at 150°C under vacuum for 48 h. Elemental analysis of Co-zeolite: C, 0.27; H, 0.91; Co, 4.76; Fe-zeolite: C, 0.26; H, 1.20; Fe, 4.89; Ru-zeolite: C, 1.16; H, 1.08, Ru, 0.95.

Preparation of zeolite encapsulated metallophthalocyanine

Metal exchanged zeolite (100 g) and 8 equivalent of 1,2-dicyanobenzene were added to 200 mL of nitrobenzene in a round bottom flask fitted with a reflux condenser and a mechanical stirrer. The mixture was heated to 180°C for 4 h under nitrogen until the solution changed color (dark green for Fe, dark blue for Co, brown for Mn and Ru). The zeolite was filtered, washed with methanol to remove nitrobenzene, and Soxhlet extracted with pyridine until the solution was clear. Excess pyridine was removed by Soxhlet extraction with methanol. The zeolite powder was then boiled in a 1 M solution of NaCl (reverse metal exchange) for 4 h, washed with water and acetone. The product was dried at 150°C under vacuum for 24 h.

Preparation of zeolite encapsulated tetraphenylporphyrin

Zeolite powder (200 g) was added to 1.8 L of acetic acid in a 2 L round bottom flask equipped with mechanical stirrer and an addition funnel which contained 46.5 mL pyrrol and 66.5 mL of benzaldehyde. The acetic acid was heated to boil. The pyrrol and benzaldehyde were added slowly. The reaction mixture was boiled for 0.5 h under air. The dark purple solid was filtered while the solution was still warm. It was then washed with large amount of acetone until the washing was colorless. The product was dried at 150°C under vacuum for 24 h.

Metal insertion of tetraphenylporphyrin in zeolite

A mixture of TPP zeolite (50 g) and metal salt (0.12 mole of CoCl_2 , FeCl_2 , MnSO_4 , or $\text{Ru}_3(\text{CO})_{12}$) was added to 200 mL of dimethyl sulfoxide in a three necked round bottom flask equipped with a mechanical stirrer, a reflux condenser, and a gas inlet adaptor. The reaction mixture was heated to reflux for 3 h. The product was washed with water and methanol. Excess metal salt was removed by boiling in a 1 M aqueous solution of NaCl for 2 h. The product was washed again with water and methanol and then dried at 150°C for 24 h.

Preparation of magnesia supported tetrasulfothalocyanines

The tetrasulphthalocyanine complexes were prepared via the reaction of monosodium salt of 4-sulfophthalic acid, urea, and metal salt in the presence of catalytic amounts of ammonium molybdate, and ammonium chloride at 180°C. The acid form of the complexes were obtained by acidification of the aqueous solutions with 2 N HCl. The resulting metal complex (0.5 g) was then dissolved in DMF (500 mL), added to MgO powder (10 g), and stirred for 2 h. After washing with DMF and acetone, the catalysts were dried at 60° under vacuum overnight. Five catalysts: PdTSPCMgO, FeTSPCMgO, CuTSPCMgO, RuTSPCMgO, CoTSPCMgO, were prepared by this method.

General procedure for testing methane oxidation catalysts

The catalyst (3 g) was loaded into a stainless steel reactor (3/8" OD). The reactor was connected to the reactor system and purged with helium for 15 min. It was heated to 200°C under a slow flow of hydrogen for 2 h. Methane (10.3% in helium) and oxygen (5.2% in helium) were introduced to the reactor and the temperature was increased to 300°C or higher. Methane and oxygen were individually controlled by mass flow controllers. The reactor pressure was set at 50 psig via a back pressure regulator. A thermocouple was immersed in the catalyst bed and connected to a temperature controller that controls the furnace. The outlet gases were fed to a GC sampling valve through heated stainless steel tubing (110°C).

RESULTS AND DISCUSSION

Phthalocyanine complexes are synthesized within the zeolite pore by first exchanging the metal ion into the pore, followed by template condensation.¹⁰ We used Na-Y zeolite because it has large pores that allows the phthalocyanine complexes to fit in and contains exchangeable ions. Some of the phthalocyanines that adsorbed on the zeolite surface were removed by extraction with pyridine and acetone. Excess metal ions were then back exchanged with sodium ions. Surface reflectance UV-Vis and FT-IR of the non-extracted catalysts evidenced the presence of phthalocyanine.

The zeolite encapsulated metalloporphyrins was synthesized by a modified method. The metal free ligand was first synthesized inside the zeolite cage by refluxing benzaldehyde, pyrrol, and the Na-Y zeolite (without metal exchange) in acetic acid. The surface attached porphyrin was extracted with methanol. The washings contain tetraphenylporphyrin as indicated by its UV-Vis spectrum.

The desired metal ion was inserted into the porphyrin by boiling the metal salt and the zeolite containing the porphyrin in dimethyl-

sulfoxide solution. The product was washed with water and then Soxhlet extracted with methanol to remove surface-bound TPP complex. Uncomplexed metal ions are removed by reverse ion-exchange with sodium chloride. However, the excess iron ions were not exchangeable by sodium ions and we have not attempted to remove the excess iron by another method. The FePCZL and the ReTPPZL thus contained excess iron ions. The metal loading (by weight) and the percent of super cages occupied by the metal complexes (calculated based on the results from elemental analyses) are listed in Table 1.

Table 1

METAL AND COMPLEX LOADING OF ZEOLITE ENCAPSULATED COMPLEXES

<u>Catalyst</u> ^a	<u>Wt. % metal Loading</u>	<u>% Supercages Occupied</u>
CoPCZL	1.53	60
FePCZL	4.15 ^b	50
RuPCZL	0.97	20
MnPCZL	1.62	68
CoTPPZL	0.15	5
FeTPPZL	4.04 ^b	8
RuTPPZL	0.13	2.5
MnTPPZL	0.12	4.3

^aPc = phthalocyanine, TPP = Tetraphenylporphyrin, ZL = zeolite.

^bThe iron complexes contained excess iron ions which can not be exchanged by sodium ions.

These zeolite catalysts were tested for methane oxidation at 375°C under 50 psig pressure. The results are averaged from data taken during the 15 to 20 h of the runs and are summarized in table 2. Three catalysts including RuPcZL, CoTPPZL, and MnTPPZL showed some reactivity toward the formation of methanol. As shown in table 5, the RuPcZL gave the highest selectivity of methanol. The methane conversions were generally below 10%. Carbon dioxide and water were always the major products.

Three control experiments were run using the blank zeolite, ruthenium exchanged zeolite (with triruthenium dodecacarbonyl), and ruthenium tetracarboxyphthalocyanine. The blank zeolite gave essentially no reactivity toward methane oxidation. Less than 0.5% of methane was oxidized to carbon dioxide. The ruthenium zeolite produced hydrogen, carbon dioxide and water with approximate 16% methane conversion. The RuTPPZL and FePcZL also gave hydrogen which suggest that these two catalysts behaved like the simple metal exchanged zeolite, because the excess metal ion in these two catalysts was not removed by the reverse ion exchange process. The productions of hydrogen were due to the catalytic ability of the zeolite adsorbed metal particles.

Table 2

ACTIVITY OF METHANE OXIDATION CATALYSTS

Catalyst	% Conv. of CH ₄	H ₂	% Selectivity of		
			CO ₂	H ₂ O	CH ₃ OH
Zeolite	0.5	---	100	---	---
RuZL	15.9	45	100	100	---
CoPcZL	6.3	---	100	100	---
FePcZL	18.2	1.2	100	42	---
RuPcZl	4.8	---	87	1	11.3
MnPcZL	9.6	---	80	65	---
CoTPPZL	1.9	---	94	120	5.8
FeTPPZL	1.9	---	100	73	---
RuTPPZL	8.4	50	99	146	---
MnTPPZL	1.8	---	95	126	3.5

Reaction conditions: Temperature=375C, Pressure=50psig, CH₄/O₂=4, GHSV=2600 h⁻¹.

Some of the catalysts were also tested at higher temperature under the same condition. The results were summarized in Table 3. Methane conversions were generally increased at higher temperature. Again, only

RuPcZL and CoTPPZL showed some activity toward methanol formation, but the yields were significantly decreased. These results indicated that the metal complexes decomposed at high temperature and therefore lost their activity. The characteristic blue green color of the phthalocyanines and the purple color of the porphyrins disappeared after the high temperature reactions. The decomposition of catalysts were confirmed by elemental analyses.

Table 3

ACTIVITY OF METHANE OXIDATION CATALYST AT HIGH TEMPERATURE

Catalyst	Temp. (°C)	% Conversion		% Selectivity			
		CH ₄	O ₂	H ₂	CO ₂	H ₂ O	CH ₃ OH
RuZL	500	20.8	99.0	110.0	89.3	---	---
FePcZL	500	22.7	87.2	15.9	100.0	45.0	---
RuPcZL	450	9.0	99.6	---	96.7	0.5	3.3
CoTPPZL	450	3.3	56.1	---	98.0	126.2	2.0
FeTPPZL	450	6.1	32.8	---	100.0	65.1	---

Reaction conditions: Pressure=50 psig, CH₄/O₂ = 4, GHSV = 2600 h⁻¹.

It has been noted that high levels of complex loading results in blocking the access of substrate to the metal center.¹¹ The zeolite encapsulated phthalocyanines prepared in this work contained relatively high complex loading. About half of the super cages in the zeolite were filled with metal complex in the CoPCZL, FePCZL, and MnPCZL. The RuPCZL was the only catalyst that showed activity and it contained less metal complex than the others. We are not certain whether the lack of catalytic activity was due to the accessibility of methane to the active site of the catalyst or was truly an inactive metal complex since methane is a rather small molecule. In contrast, the TPP analog of RuPCZL was not active in converting methane to methanol but the CoTPPZL

and the MnTPPZL were active. Since all the zeolite encapsulated TPP complexes contained low complex loading, the nature of the metal complex should be responsible for the catalytic activity.

We tested four metal complexes of tetrasulfophthalocyanine supported on magnesium oxide (Pd, Fe, Ru, Cu). The metal loading and complex loading are listed in Table 4. Interestingly, the palladium catalyst (PdTSPCMgO) produced ethane from the oxidation of methane at 375°C instead of methanol (Table 5). Although the selectivity was low (2.8%), oxidative coupling of methane to ethane at such low temperature is unusual. Increasing the reaction temperature to 400°C, increased methane conversion and decreased ethane selectivity. Further increases of the temperature to 450°C decomposed the complex. All other catalysts tested gave only products of complete oxidation, ie. CO₂ and H₂O.

Table 4

METAL LOADING AND COMPLEX LOADING OF THE MAGNESIUM OXIDE SUPPORTED CATALYSTS

Catalyst	Metal loading (Wt%) ^a	Complex loading (mol/100g) ^b
FeTSPCMgO	0.24	0.052
RuTSPCMgO	0.45	0.047
PdTSPCMgO	0.18	0.026
CuTSPCMgO	0.37	0.054

^aBased on elemental analysis.

^bMole of complex were calculated based on the carbon weight from the elemental analyses.

Table 5

ACTIVITY OF MgO SUPPORTED METHANE OXIDATION CATALYSTS^a

Catalysts	Temp. (°C)	%Conversion of Methane	%Selectivity ^b	
			CO ₂	C ₂ H ₆
PdTSPCMgO	375	1.4	97.2	2.8
	400	2.6	97.8	2.2
	450	5.7	99.7	0.3

^aCondition: Pressure = 1 atm, CH₄/O₂ = 10, GHSV = 5000 h⁻¹.

^bSelectivity was calculated based on carbon number.

CONCLUSION

To the best of our knowledge, this is the first observation of methanol production from partial oxidation of methane using cytochrome-P450 mimic. Encapsulating the porphyrin and phthalocyanine complexes inside the zeolite cages precludes the intermolecular reactions which leads to the problem of catalyst deactivation. Anchoring the metal complexes on the support surface also prevents such bimolecular self destruction. Oxidative coupling of methane is usually observed at temperature much higher ($>700^{\circ}\text{C}$) than what we observed for PdTSPCMgO (375°C). Many questions remained to be answered including improving product selectivity.

References

1. R. Pitchai and K. Klier, *Catal. Rev.-Sci. Eng.*, 28(1), 13-88 (1986).
2. J. T. Groves and D. V. Subramanian, *J. Am. Chem. Soc.*, 106, 2177 (1984).
3. J. P. Collman, T. Kodadek, S. A. Raybuck, and B. Meunier, *Proc. Natl. Acad. Sci. USA*, 80, 7039 (1983).
4. D. Mansuy, P. Battioni, and J-P. Renaud, *J.C.S. Chem. Commun.*, 1255 (1984).
5. A. M. Khenkin and A. A. Shteinman, *J.C.S. Chem. Commun.*, 1219 (1984).
6. T. Ito, T. Tashiro, T. Watanabe, K. Toi, and I. Ikenmoto, *Chem. Lett.*, 1723 (1987).
7. D. L. Driscoll, W. Martir, J.-X. Wang, and J. H. Lunsford, *J. Am. Chem. Soc.*, 107, 58 (1985).
8. E. Iwamatsu, T. Moriyama, N. Takasaki, and K.-I. Aika, *J.C.S. Chem. Commun.*, 19 (1987).
9. T. Ito, J.-X. Wang, C.-H., Lin, J. H. Lunsford, *J. Am. Chem. Soc.*, 107, 5062 (1986).
10. G. Meyer, D. Wohrle, M. Mohl, and G. Schulz-Ekloff, *Zeolites*, 4, 30 (1984).
11. N. Herron, G. D. Stucky, and C. A. Tolman, *J.C.S. Chem. Commun.*, 1521 (1986).

BIOCONVERSION OF METHANE TO METHANOL BY METHYLOBACTERIUM ORGANOPHILUM.

LORI E. PATRAS AND ALICE TANG

UNOCAL
SCIENCE AND TECHNOLOGY DIVISION
BREA, CALIFORNIA

INTRODUCTION

Large reserves of natural gas have stimulated the development of processes that can convert methane to more valuable chemicals such as methanol. Commercial routes to methanol involve three steps. First synthesis gas is generated from natural gas or naphtha at 15-30 atmospheres and 840-900 °C. The synthesis gas is converted to methanol using a copper catalyst which requires the process condition of 300-350 psig and 250-270 °C. The methanol is then distilled to desired purity. Many bacteria and fungi grow on methane at ambient temperature and pressure. In this study we attempt to develop a low severity route from methane to methanol, involving a biochemical catalyst.

Methylobacterium organophilum was grown in a methane-oxygen controlled atmosphere water bath shaker apparatus to study the bioconversion of methane to more valuable chemicals such as methanol. To optimize production of methanol from the metabolism of methane by Methylobacterium organophilum, we tested the effects of culture enrichment and inhibitors.

EXPERIMENTAL

Methylobacterium organophilum was purchased from the American Type Culture Collection (ATCC #27886). For all studies, excepted when noted, ammonium mineral salts (AMS) medium was used.

All growth experiments were conducted under a methane atmosphere, in a controlled atmosphere water bath shaker apparatus. Liquid cultures were grown in 250 ml Erlenmeyer flasks at 30 °C on the rotary shaker (150-200 rpm) at pH 6.8 with methane as the only carbon source for growth (unless otherwise stated). The atmosphere of the incubator shaker was normally continuously gassed with 65% methane, 20% oxygen, and 15% nitrogen.

Cell densities were measured by monitoring the absorbance at 660nm by Sargent-Welch model SM spectrophotometer. The cells were harvested by centrifugation and dry cell weights were determined after drying the cell paste in a vacuum oven.

Cell free culture broth was analyzed for methanol by gas chromatography. The cells were removed by centrifugation followed by filtration.

RESULTS AND DISCUSSION

Methylobacterium organophilum is a facultative methylotroph; it can grow not only on C-1 compounds but also on multicarbon compounds as the sole sources of carbon and energy. Figure 1 shows the growth of M. organophilum on one-carbon and multicarbon substrates.

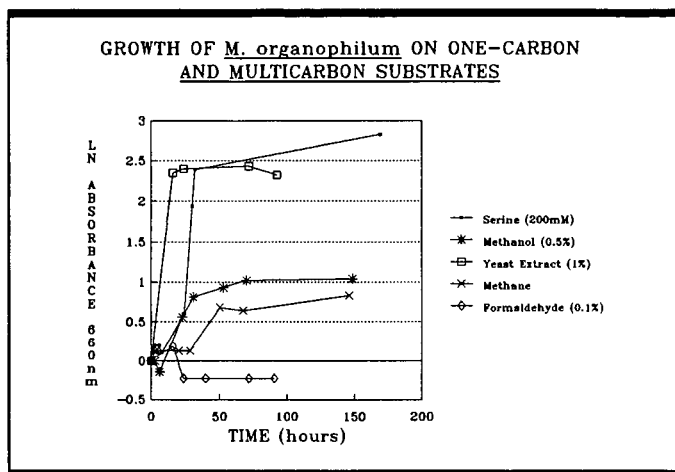


Figure 1

The specific growth rate on methane is lower than the other substrates. This is expected since the solubilities in water of the other substrates are higher than the solubility of methane in water.

Another important characteristic of M. organophilum is the type II intracytoplasmic membrane. Cultures previously grown on a multicarbon substrate for growth and energy required several transfers grown on methane before accumulating methanol. This "inactive" state of the microbe may be explained by the fact that it is necessary for the bacterium to possess an intracytoplasmic membrane for methane metabolism to occur. The literature reports that M. organophilum contains an intracytoplasmic membrane when grown on methane but this membrane is not present during growth on higher substrates such as methanol and glucose (1).

Methylobacterium organophilum oxidizes methane by a special C-1 oxidation pathway (see below).

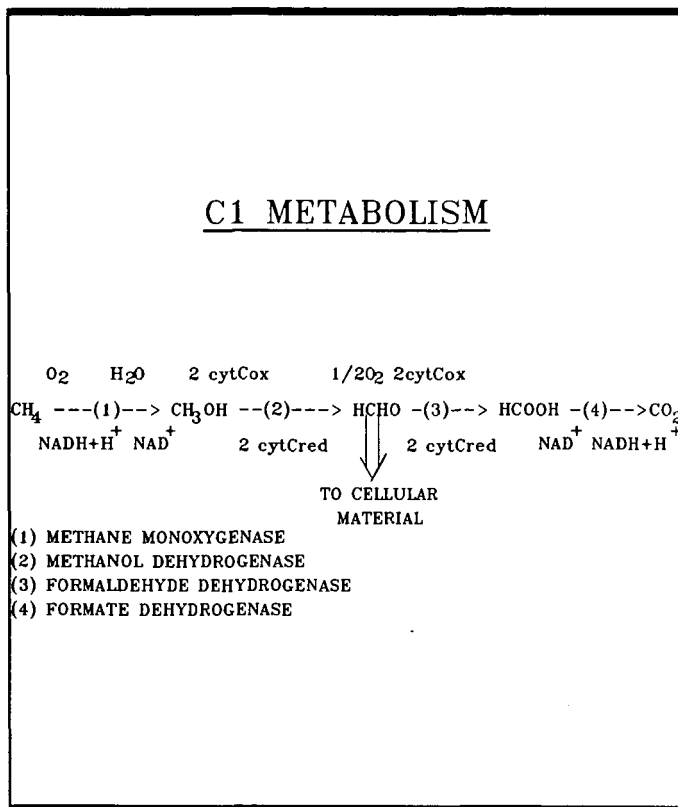


Figure 2

Biomass is produced through formaldehyde assimilation. The mechanism of the reaction $\text{CH}_4 \text{ ----> CH}_3\text{OH}$ involves atmospheric oxygen incorporated directly into the methane molecule with the aid the enzyme, monooxygenase. The hydrogen requirement is supplied by the conversion of formic acid to carbon dioxide implying that methane oxidation is a function of successive oxidations. This presents a problem if methane oxidation is stopped at methanol because the regeneration of NAD^+ would be lost.

High biomass cultures of *M. organophilum* were tested for methanol accumulation while growth was monitored (see below).

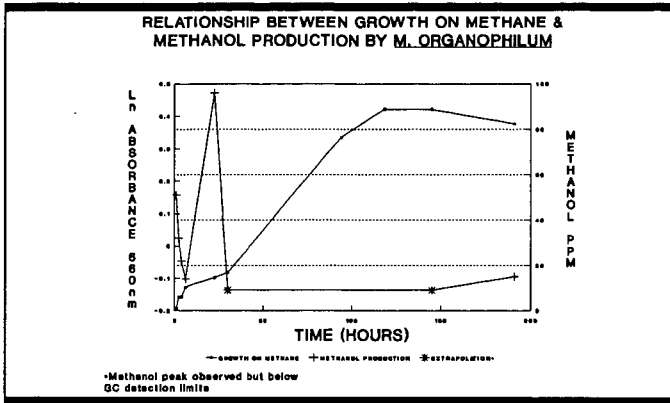


Figure 3

It appears that methanol accumulates during non-growth periods from methane oxidation. This is expected since during growth, the methanol is further metabolized for cell growth and energy. During initial incubation, methanol production was low (1.1 mmoles/gDCW.Hr).

The effect of iodoacetic acid on methanol production was studied. Cultures of *M. organophilum* were tested for methanol accumulation during growth on methane in the presence of iodoacetic acid (see below).

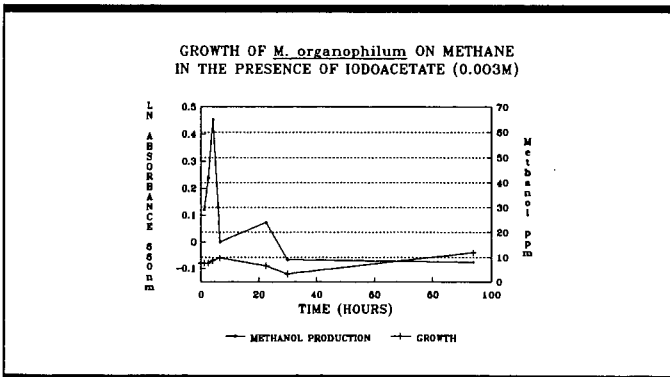


Figure 4

Figure 6 shows that regulation in M. organophilum is obvious during growth on more than one carbon substrate in the medium.

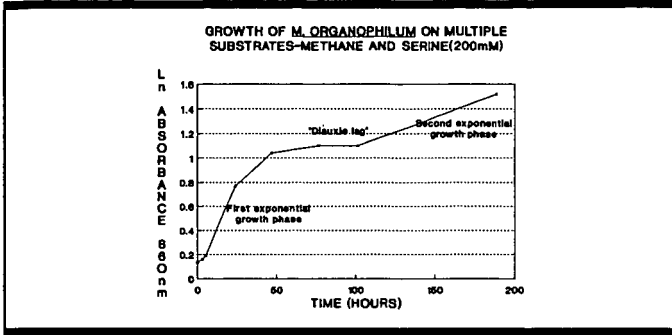


Figure 6

Growth of M. organophilum on methane and serine shows the diauxic phenomenon discovered by Monod(2). The substrates are utilized in two exponential growth cycles. The growth cycles are separated by an intermediate lag phase.

Formic acid could be a product produced by a metabolic block created by the addition of serine since the following part of the pathway precedes serine.



However, formic and acetic acid are also produced by M. organophilum during serine fermentation void of methane (see below).

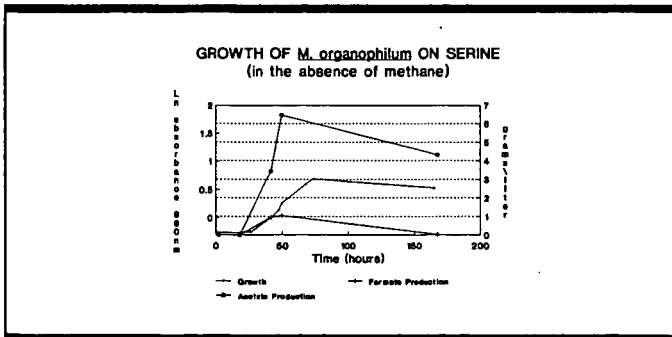


Figure 7

Waber et al (3) have shown the conversion of serine to pyruvate, which is decarboxylated to form acetate by Clostridium acidiurici. Kobota (4) found that serine generated formic acid from a cell-free preparation from Bacillus brevis in the presence of a cofactor, tetrahydrofolic acid. Tetrahydrofolate is present in M. organophilum and is used for 1-carbon group transfer and reduction.

CONCLUSIONS

Methanol accumulated during non-growth periods of methane metabolism by M. organophilum in the presences and absence of inhibitors under the conditions described. The production rate was increased by varying experimental conditions. For example, methanol accumulation increased by a factor of ca. 4 by pregrowing the culture in the presence of an inhibitor. When compared to commercial processes of methanol production, the bioconversion of methanol is ca. 90 times less active. Increasing methanol yields by optimizing culture medium and growth condition is limited by the natural isolate of Methylobacterium organophilum ability to synthesize methanol. Successful exploitation of Methylobacterium organophilum requires the application of genetic techniques for the optimization of methanol production.

Formic acid and acetic acid were growth associated products of serine fermentation by Methylobacterium organophilum.

REFERENCES

1. Patt, T. E., Cole, G. C. and Hanson, R. S., "Methylobacterium, a New Genus of Facultatively Methylophilic Bacteria," International Journal of Systematic Bacteriology, Apr. 1976, Vol. 26., No. 2, p. 226-229.
2. Monod, J., "Recherches sur la Croissance des Cultures," Bacteriennes Hermann et Cie, Paris, 1942.
3. Waber, Lewis J. and Harland G. Wood, "Mechanism of Acetate Synthesis from CO₂ Clostridium acidiurici," Journal of Bacteriology, Nov. 1979, p. 468.
4. Kubota, Kou, "Generation of Formic Acid and Ehtanolamine from Serine in Biosynthesis of Linear Gramicidin by a Cell-Free Preparation of Bacillus brevis (ATCC #8185)," Biochem. and Biophys. Res. Comm., 1982, Vol. 105, No. 2, p. 688,

Biological Production of Methanol from Methane

R. E. Corder, E. R. Johnson, J. L. Vega, E. C. Clausen, and J. L. Gaddy
Department of Chemical Engineering, University of Arkansas
Fayetteville, Arkansas 72701

Cultures of methanotrophs have been isolated that convert methane into methanol. Biocatalytic conversion offers the advantages of good thermal efficiency and low capital cost, since ordinary temperatures and pressures are employed. High product yield in a single-step reaction and simplified purification technology are possible, since methanol is the only product.

These unusual bacteria usually metabolize methane completely to CO₂, with methanol as an intracellular intermediate. Therefore, methanol production requires manipulation of the ordinary enzymatic reactions by regulation of the electron transport and environmental conditions to favor the methane monooxygenase pathway. This paper presents preliminary results of the culture isolation techniques and procedures to manipulate the cultures to produce methanol. These procedures have been successfully demonstrated with two isolates producing up to 1 g/L methanol extracellularly.

INTRODUCTION

Methanol is a major raw material for petrochemical production and is currently under consideration as a liquid fuel. Methanol is produced catalytically by the reaction of hydrogen and carbon monoxide at high pressure (300 psia) and moderate temperature (Strelzoff, 1970). H₂ and CO are obtained from methane by reforming with steam to yield synthesis gas. A second step, involving a water-gas shift reaction, is used to increase the H₂/CO ratio. The reforming step is generally carried out at 800-1000°C and 300 psig, whereas the water gas shift reaction utilizes metal oxide catalysts at 400-500°C and 300 psig (Shah and Stillman, 1970; and Shreve, 1967). These severe conditions result in high capital and operating costs and poor thermal efficiencies. Simpler, more efficient processes are necessary.

Natural gas demand and production declined to less than 17 trillion cu. ft. last year, with reserves dropping below eight years (Oil Gas J., 1986a; Beck, 1987). By 1990, gas imports are expected to be up 300 percent over present levels, despite a continuing decline in demand (Oil Gas J., 1986b). While flaring of natural gas has been substantially reduced in recent years, the U.S. presently wastes about 10 x 10¹⁰ cu. ft. annually (Hillard, 1980), or the equivalent of 1.4 billion gallons of methanol (40 percent of our liquid fuel requirement). Also, in many areas, gas wells remain shut-in because potential gas production is too remote or too dilute to justify pipelines and transportation. If simple conversion technology were available to produce liquid fuels on-site, flared and remote gas could be utilized.

Catalytic conversion of coal synthesis gas, using Fischer-Tropsch reactions, has been found to produce methanol and higher alcohols with sustained catalyst activity (Klier *et al.*, 1986; Dombek, 1986). By-products of the Fischer-Tropsch reactions include light hydrocarbon gases, predominantly methane. Methane is also a by-product from some gasification

processes (Mills, 1982). Methane is very stable in the subsequent processing steps to produce liquid fuels. Therefore, a technology or catalyst for converting methane directly into liquid fuels would substantially enhance the efficiency and yields of these processes.

A simple and efficient process for producing methanol from methane would save significant quantities of energy in industrial processes. Also, technology for conversion of small volumes or dilute mixtures of methane would enable production from remote gas and oil wells, saving wasted energy and reducing imports of crude oil. Furthermore, this technology would enhance the application of coal conversion technologies. Methanol production from methane is a mature technology and substantial advances or breakthroughs in catalytic processes are not likely. Therefore, innovative approaches to this problem are necessary.

Biological Conversion of Methane

Of the many biological species and microbiological reactions possible, only the methanotrophs are capable of converting methane. The usual sequence of methane metabolism proceeds to cell biomass and CO₂ with methanol as an intracellular intermediate. The interruption of the enzymatic reactions, by manipulation of the environmental conditions or mutation, could result in a culture that produces an excess of methanol that accumulates extracellularly.

Such a biocatalytic process has substantial economic potential for application to Fischer-Tropsch products, coal synthesis gas and natural gas conversion. Methane, in the gas stream following the Fischer-Tropsch synthesis, would be passed through the biological reactor for conversion to methanol. Similarly, methane in synthesis gas could be converted to methanol prior to or following Fischer-Tropsch synthesis. The conversion would take place in a single step at ordinary temperatures and at atmospheric or elevated pressures, if desirable. No products, other than methanol, are produced by these cultures. Complete methane conversion, with near stoichiometric yields, should be possible. Methanol recovery from the fermentation media could be accomplished by stripping or liquid extraction (extractive fermentation).

Purpose

The purpose of this paper is to present the results from preliminary laboratory experiments aimed at isolating a methanotroph culture that is capable of accumulating methanol as a product. Two isolates have been obtained that are capable of producing up to 1 g/L extracellularly.

MICROBIOLOGY OF METHYLOTROPHS

The biological conversion of methane to methanol by the reaction:



is carried out by a very specialized group of organisms that are also able to utilize methanol, methylamine or formate (in addition to methane) as sole carbon and energy sources. This class of organisms is called methylootrophs. Organisms that utilize primarily methane are called methanotrophs.

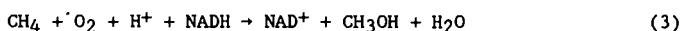
Organisms such as Methylococcus capsulatus and Methylomonas sp. are considered obligate methylotrophs and cannot grow on carbon sources other than methane, methanol, or formate. Energy is derived from the oxidation of these compounds to carbon dioxide, and most of the carbon is obtained from the fixation of formaldehyde by condensation with a pentose phosphate. Microorganisms that cannot utilize methane but can utilize methanol, methylamine and formate (e.g. Hyphomicrobium and a few Pseudomonas species) are generally also considered to be methylotrophs. Two types of methylotrophs have been established on the basis of the type of complex membranous organelles. Type I exhibits a system of paired membranes running throughout the cell or aggregated at its periphery. Type II exhibits a series of bundles composed of disc-shaped membrane vesicles distributed throughout the cell.

Type I methylotrophs utilize the ribulose monophosphate pathway for the assimilation of formaldehyde and have an incomplete tricarboxylic acid cycle. These organisms lack alpha-ketoglutarate dehydrogenase (Patel, 1984). Type II methylotrophs utilize the serine pathway for the assimilation of formaldehyde and have a complete tricarboxylic acid cycle (Large, 1983).

The methane molecule can only be attacked by a substitution mechanism. It was shown in 1970 that growth on methane is accompanied by the incorporation of an oxygen atom from gaseous oxygen into the molecule to give methanol, as was shown in Equation (1). Methane is actually oxidized finally to CO₂, with methanol, formaldehyde, and formate formed as intermediates (Anthony, 1982; and Higgins et al., 1981a):



This series of reactions occurs intracellularly and no methanol is produced extracellularly. In order for the methanotroph to produce methanol, conditions for the subsequent enzymatic reactions must be made unfavorable. The enzyme, methane monooxygenase, catalyzes the reaction:



The enzyme occurs in both soluble and particulate form. The physical location of the enzyme as a cytoplasmic or extracytoplasmic enzyme has not been determined. Noting that NADH is a substrate, it is generally assumed that the reactions are cytoplasmic. This assumption is also consistent with the fact that they are proton utilizing (Hooper and DiSpirito, 1985). Reducing equivalents from the formaldehyde, formate, and perhaps methanol dehydrogenase reactions are utilized in methane monooxygenase, in the reduction of NAD⁺ for biosynthetic reactions, or in electron transport leading to ATP synthesis.

Although the prosthetic group of methanol dehydrogenase is a novel quinone coenzyme (pyrroloquinoline quinone) the enzyme utilizes a soluble cytochrome c as an electron acceptor and is therefore a proton-yielding dehydrogenase (Beardmore-Gray et al., 1983). Localization studies have shown that methanol dehydrogenase (Alefounder and Ferguson, 1981; Burton et al., 1983; and Kasprzak and Steenkamp, 1983; 1984) and the electron acceptors cytochromes C_L, and possibly cytochrome C_H (Beardmore-Gray et al., 1983; Burton et al., 1983;

Jones *et al.*, 1982; and Quilter and Jones, 1984), are in the periplasm (Alefounder and Ferguson, 1981; and Kasprzak and Steenkamp, 1983). Thus, methanol oxidation clearly fits the generalization described in Equation (3) by Hooper and DiSpirito (1985).

Formaldehyde and formate dehydrogenase occur in forms which use either NAD⁺ or dyes as electron acceptors (Johnson and Quayle, 1964; and Marison and Wood, 1980). Substrate oxidation is proton yielding and could logically be periplasmic:



and



Depositing cross-membrane translocation of electrons to the proton-utilizing reduction of NAD⁺:

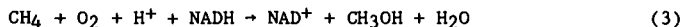


the action of a dehydrogenase located in the periplasm would generate a proton gradient in both reactions. This seems not to be the case with the NAD-linked formaldehyde (Kasprzak and Steenkamp, 1983) and formate (Jones *et al.*, 1982) dehydrogenases; since they are soluble and use NAD, they are probably cytoplasmic. The topological location of the dye-linked enzymes is unknown.

In summary, in the methylotrophs, the proton-utilizing methane monooxygenase may be cytoplasmic and the energy-linked proton-yielding oxidation of methanol is periplasmic. Thus, CH₃OH functions as a transmembrane hydrogen transporter. In contrast, NAD-linked oxidations of formaldehyde and formate, which produce reductant for methane monooxygenase, biosynthesis, or electron transport, leading to ATP synthesis and CO₂ for carbon assimilation, are apparently cytoplasmic. Therefore, mechanisms for control of these separate enzyme systems to allow methanol production is feasible and likely. Furthermore, the potential to control electron flow and block specific enzyme sites with inhibitors to increase methanol yields is substantial.

THE PRODUCTION OF CHEMICALS USING METHYLOTROPHS

It is possible to biologically convert methane to methanol using whole cell systems or cell-free enzyme systems. Cell-free systems require an external source of reducing energy supplied by NADH for substrate oxidation. The methylotrophic enzyme which is of greatest interest is methane-monooxygenase which catalyzes the reaction:



This enzyme, although of fundamental importance for bacterial growth on methane, may become industrially important for quite a different reason. Since it is such a non-specific enzyme, it will oxidize a wide number of compounds in addition to methane (Large, 1983), some of which cannot be transformed by traditional industrial chemical methods.

Methane monooxygenase enzyme involved in catalyzing the hydroxylation of methane also catalyzes the oxygenation of various hydrocarbons and cyclic, alicyclic and aromatic compounds (Colby and Dalton, 1976; Colby *et al.*, 1977; Dalton, 1980; Dalton and Colby, 1982; Higgins *et al.*, 1981b; and Patel *et al.*, 1979). Thus, it is possible to convert methane to methanol or other short-chain hydrocarbons to their alcohols using whole cell systems. Patel (1984) reported that in using the soluble enzyme, methane monooxygenase, extracted from Methylobacterium sp. strain CRL-26, he was able to oxidize methane to methanol, ethane to ethanol, propane to 1-propanol and 2-propanol, butane to 1-butanol and 2-butanol and pentane to 1-pentanol and 2-pentanol, etc.

However, unlike simple hydrolases or oxidases, mixed-function oxidases, such as methane monooxygenase, need reduced nicotinamide nucleotides in addition to oxygen in order to function. Cell free systems, such as an immobilized enzyme system, are thus considered costly and impractical to use for the conversion of methane to methanol.

As an alternative to cell free systems, it is also possible to convert methane to methanol using whole cell systems, which supply their own reducing equivalents by substrate oxidation. Methane-utilizing organisms, grown on methane or methanol, have the ability to oxidize and transform a variety of non-growth substrates to commercially useful chemicals. This is due to the broad specificity of enzymes involved in the oxidation of methane to carbon dioxide. The isolation of such organisms, particularly those that might produce methanol from methane, would have broad application.

RESULTS AND DISCUSSION

CULTURE ISOLATION

Experimental studies were carried out in an effort to isolate methanotrophs from anaerobic digester sludge. This source of inoculum was chosen since the sludge contains significant quantities of methane in the liquid phase, and should, therefore, contain methanotrophs capable of using the methane.

Digester sludge was inoculated into a mineral salts medium, shown in Table 1, using a 10 percent by volume inoculum. As noted, the medium was essentially a salts medium, but also contained vitamins found essential for methanogen growth. The gas phase above the liquid media was maintained at 1 atm, and contained 20 volume percent methane and 80 percent air.

A mixed culture developed from this initial seeding was enriched by successive transfer to new media and gas every 72 hours. The enrichment procedure lasted a total of approximately 8 weeks. The enrichment was then

Table 1

Medium for Methylotroph Isolation

	<u>g/L</u>
KNO ₃	2.5
Na ₂ HPO ₄	0.21
KH ₂ PO ₄	0.29
MgSO ₄ ·7H ₂ O	0.20
FeSO ₄ ·7H ₂ O	0.001
Trace elements ^a	1ml/L
Vitamins ^b	10ml/L

^a The trace elements stock solution, shown below, were diluted 1000 times prior to use.

	<u>mg/L</u>
CuSO ₄	50
H ₃ BO ₃	10
MnSO ₄ ·4H ₂ O	10
ZnSO ₄ ·7H ₂ O	70
MoO ₃	10

^b A methanogen minimal medium, shown below, was diluted 100 times prior to use.

Biotin	2
Folic acid	2
Pyridoxine HCl	10
Thiamine HCl	5
Riboflavin	5
Nicotinic Acid	5
Ca-pantothenate	5
Vitamin B ₁₂	0.1
p-amino benzoic acid	5
Thioctic acid	5

streaked onto agar plates utilizing the same media as in Table 1, and incubated under an atmosphere of 20 percent methane, 80 percent air until colonies appeared.

Individual colonies were picked, inoculated into fresh liquid media, and examined for purity. Two of the isolates that were obtained were obligate methanotrophs, and thus were selected for further testing.

CONVERSION OF METHANE TO METHANOL

Utilizing the obligate methanotrophs isolated from digester sludge, experiments were initiated to determine the feasibility of producing methanol from methane. Stoppered 250-ml Erlenmeyer flasks were used as batch reactors. The liquid media utilized in the experiments was identical to the media of Table 1.

To facilitate mass transfer of methane from the gas phase to the liquid phase for reaction, gentle agitation (approximately 150 rpm) was employed, using a shaker incubator. The organisms were again grown under an atmosphere of 20 percent methane and 80 percent air at one atmosphere total pressure. Two obligate methanotroph isolates were compared in the study, along with the enrichment culture obtained after successive transfer from the digester sludge.

After obtaining growth in the reactors, the gas phase was switched to 100 percent methane in place of the 20:80 methane/air mixture. This substitution was made in order to prevent complete oxidation of methane to CO₂ as was shown in Equation (2). Incubation with gentle agitation occurred for 24 hours.

The results of these preliminary studies is shown in Table 2. Liquid phase analysis for methanol was performed using gas-solid chromatography. As noted, the two pure culture methanotrophs showed an accumulation of methanol, producing 0.5 and 1.0 g/L methanol in 24 hours. These levels of methanol production in 24 hours indicate the potential for good reaction rates in continuous culture. The enrichment, which contained methanotrophs and

Table 2

Biological Conversion of Methane to Methanol
(Preliminary Studies)

	Methanol Produced After 24 hours <u>(g/L)</u>
Isolate #1	0.5
Isolate #2	1.0
Enrichment	0

methanol-utilizing methylotrophs, showed no accumulation of methanol. The differences in the methanol production by the methanotrophs can be contributed to sensitivity to the presence of methanol, activity of the culture, and the ability of the cultures to utilize methanol as a substrate.

The results of these preliminary experiments are quite encouraging and demonstrate that the organisms are capable of producing methanol extracellularly at fast rates. Low cell densities and gentle agitation were used and, consequently, low methanol concentrations were obtained in the short reaction time. A measurement of the cell density in the flask showed a very low cell concentration of 0.3 g/L on a dry weight basis. A higher cell mass concentration (analogous to a higher catalyst concentration) would increase reaction rate to yield more product in the 24 hour period.

The experimental conditions can undoubtedly be improved to maximize methanol yields. Also reaction rates would be increased by providing better mass transfer of methane and oxygen from the bulk gas phase to the organisms in the liquid phase. The total pressure in the experiments was only 1 atmosphere. Higher pressures would be expected to significantly enhance reaction rate. Significantly higher methanol concentrations should be possible under improved conditions of cell density, reaction conditions and system design.

REFERENCES

- Alefounder, P. R. and S. J. Ferguson. 1981. A periplasmic location for methanol dehydrogenase from Paracoccus denitrificans, implications for proton pumping by cytochrome aa₃. Biochem. Biophys. Res. Commun. 98: 778-784.
- Anthony, C. 1982. The Biochemistry of Methylotrophs. Academic Press, Inc., New York.
- Beardmore-Gray, M., D. T. O'Keefe, and C. Anthony. 1983. The methanol: cytochrome C. oxidoreductase activity of methylotrophs. J. Gen. Microbiol. 129: 923-933.
- Beck, R. J., Oil and Gas J., 42 (Jan 26, 1987).
- Burton, S. M., D. Byrom, M. Carrer, G.D.D. Jones and C. W. Jones. 1983. The oxidation of methylated amines by the methylotrophic bacterium Methylophilus methylotrophus. FEMS Microbiol. Lett. 17: 185-190
- Colby, J. and H. Dalton. 1976. Some properties of a soluble methane monooxygenase from Methylococcus capsulatus strain Bath. Biochem. J. 157: 495-497.
- Colby, J., D. I. Stirling and H. Dalton. 1977. The soluble methane monooxygenase of Methylococcus capsulatus (Bath.). Its ability to oxygenate n-alkanes, n-alkenes, ethers and alicyclic, aromatic and heterocyclic compounds. Biochem. J. 165: 395-402.

- Dalton, H. 1980. Oxidation of hydrocarbons by methane monooxygenase from a variety of microbes. Adv. Appl. Microbiol. 26:71-87.
- Dalton, H., and J. Colby. 1982. Methane monooxygenase: an iron-sulfur flavoprotein complex. p. 763-767. In V. Massey and C. H. Williams (ed.) Flavins and Flavoprotein. Elsevier/North-Holland Pub. Co., N.Y.
- Dombek, D. B. 1986. Optimum Fuel Alcohol Mixtures from Syngas Oxygenate Synthesis, Proceedings Indirect Liquefaction Review, PETC.
- Higgins, I. J., D. Best, R. C. Hammond, and D. Scott. 1981a. Methane-oxidizing microorganisms. Microbiol. Rev. 45:556-590.
- Higgins, I. J., D. Best and D. Scott. 1981b. Hydrocarbon oxidation by Methylosinus trichosporium: Metabolic implication of the lack of substrate specificity of methane monooxygenase. p. 11-20. In H. Dalton (ed.) Microbial Growth on C₁ Compounds. Hayden Publishing Co., London.
- Hillard, J. H., Natural Gas, Kirk-Othmer Encycl. of Chem. Tech., 11, 630, Wiley (1980).
- Hooper, A. B. and A. A. DiSpirito. 1985. In bacteria which grow on simple reductants, generation of a proton gradient involves extracytoplasmic oxidation of substrate. Microbiol. Rev. 49: 140-157.
- Johnson, P. A., and J. R. Quayle. 1964. Microbial growth on C₁ compounds. Oxidation of methanol, formaldehyde and formate by methane-grown Pseudomonas AMI. Biochem. J. 93: 281-290.
- Jones, C. W., S. A. Kingsbury, and M. J. Dawson. 1982. The partial resolution and dye mediated reconstitution of methanol oxidase activity in Methylophilus methylotrophus. FEMS Microbiol Lett. 13: 195-200
- Kasprzak, A. A. and D. J. Steenkamp. 1983. Localization of the major dehydrogenases in two methylotrophs by radiochemical labeling. J. Bacteriol. 156:348-353.
- Klier, K., K. J. Smith and J. G. Nunan. 1986. Direct Synthesis of Methanol ls, Oxygenate Synthesis - F-T Products, Proceedings Indirect Liquefaction Review, PETC.
- Large, P. J. 1983. Methylotrophy and methanogenesis. American Society for Microbiology, Washington, D.C.
- Marison, I. W., and A. H. Wood. 1980. Partial purification and characterization of a dye-linked formaldehyde dehydrogenase from Hyphomicrobium X. J. Gen. Microbiol. 117:305-313.
- Mills, G. A. Synfuels from Coal Progress in USA. 1982. Energy Progress, (57).

- Patel, R. N. 1984. Methane Monooxygenase from *Methylobacterium* sp. ain CRI-26, in *Microbial Growth on C₁ Compounds*. (R. L. Crawford and R. S. Hanson eds.) pp 83-90.
- Patel, R. N., C. T. Hou, A. I. Laskin, A. Felix, and P. Derelanko. 1979. Microbial oxidation of gaseous hydrocarbons: hydroxylation of n-alkanes and epoxidation of n-alkenes by cell-free particulate fractions of methane utilizing bacteria. *J. Bacteriol.* 139:675-679
- Quilter, J. A. and C. W. Jones. 1984. The organization of methanol dehydrogenase and C-type cytochromes on the respiratory membrane of *Methylophilus methylotrophus*. *FEBS Lett.* 174:167-172.
- Shah, M. and J. Stillman. 1970. *Ind. Engr. Chem. Proc. Des. and Dev.* 62 (12) p. 59.
- Shreve, R. N. 1967. *Chemical Process Industries*, McGraw-Hill, New York.
- Strelzoff, S., *Chem. Engr. Symp. Ser.*, 66, 98 (1970).
- _____, *Oil & Gas J.*, 29 (Oct. 6, 1986a).
- _____, *Oil & Gas J.*, 36 (Sept. 29, 1986b).

COMPUTER-AIDED MOLECULAR DESIGN OF ALKANE-ACTIVATION CATALYSTS

John A. Shelnut, Frances V. Stohl, Barry Granoff

Sandia National Laboratories, Albuquerque, NM 87185

Introduction

Methane can provide an abundant source of liquid fuels if an efficient method of conversion can be found. Direct conversion, without an initial steam reforming step to carbon monoxide and hydrogen, offers several significant advantages. These include improved efficiency, reduced capital costs, and more effective resource utilization. The key to success lies in the development of a catalyst that will activate the relatively inert carbon-hydrogen bond in methane. Several approaches are under active investigation, including oxidative coupling, partial oxidation by molecular oxygen at high temperature, photochemical conversion, and biomimetic processes.¹⁻³ Our work focuses on a novel biomimetic approach to the development of catalysts for activation of methane, using computer-aided molecular design (CAMD) techniques.

The biomimetic CAMD methodology consists of several elements: (1) Design activities are guided by the structural and chemical information about naturally occurring biological catalysts that carry out alkane oxidation to alcohols. The macromolecular biological catalysts are investigated to determine the features that need to be designed into a synthetic catalyst in order to mimic the alkane-oxidation function. (2) Molecular mechanics calculations are used to evaluate possible designs for catalysts based on synthetic metalloporphyrins. The metalloporphyrins have been chosen because they occur at the active site of many monooxygenases and other enzymes that catalyze C₁ chemistry. Also, the porphyrin macrocycle provides a platform upon which additional molecular architecture is erected to provide the structural features required to mimic the enzymes. Recent Russian work⁴ has demonstrated methane-to-methanol conversion using an iron-porphyrin catalyst; thus, methane-activation catalysts based on the metalloporphyrins are feasible. (3) The computer designed catalysts are then synthesized. (4) The synthetic catalysts are characterized by various spectroscopic techniques including Raman-difference, transient Raman, FTIR, NMR, and UV-visible absorption spectroscopies. We are also using these spectroscopic probes to further structurally characterize some of the enzymes of interest (methylreductase⁵⁻⁷ and heme proteins⁸). (5) The designed catalysts are tested in alkane-oxidation reactions. The activity test results and results of the structural studies are evaluated to obtain structure-activity relationships that form a basis for making further improvements in the catalyst. This feedback procedure gives an iterative method for optimizing catalytic properties.

The reaction catalyzed by the monooxygenase cytochrome P₄₅₀ uses molecular oxygen to oxidize alkanes at ambient temperatures. The reaction may be amenable to molecular engineering techniques that will result in a synthetic methane-oxidation catalyst. The active site of cytochrome P₄₅₀ contains an iron-porphyrin (heme) prosthetic group. Cytochrome P₄₅₀ uses two equivalents of reduced nicotinamide adenine dinucleotide (NADH) to activate molecular oxygen; the resulting high oxidation-state Fe-oxo intermediate then attacks a C-H bond of the alkane by inserting an oxygen atom.

The protein matrix surrounding the iron porphyrin serves to protect and control access to the catalytic site. Because the X-ray crystal structure of cytochrome P₄₅₀ is known, we can use the structure of the active site of the enzyme to guide the design of a synthetic analog specifically engineered for methane activation rather than oxidation of biological substrate molecules. The

X-ray crystal structure of cytochrome P₄₅₀ of *Pseudomonas putida*⁹ shows several features of the active site that might be engineered into a synthetic porphyrin. First, the enzyme has a hydrophobic pocket of the same size and shape as the substrate (camphor). The pocket promotes selective binding of the substrate molecule without axial coordination to the metal. The pocket also orients the camphor molecule so that only a specific carbon atom of camphor is (regioselectively) hydroxylated. Second, the pocket is rigid, thus maintaining its size and shape in the absence of substrate. The pocket's rigidity prevents the enzyme from self oxidation and probably self destruction. Finally, the asymmetric environment of the iron porphyrin in the protein provides a mercapto-sulfur ligand opposite the substrate binding pocket. The electron donating thiolate ligand is thought to facilitate cleavage of the O-O bond, thus, promoting formation of the active oxo intermediate.

To design a homogeneous metalloporphyrin-based catalyst for methane activation, two major problems must be addressed. First, a catalytic center capable of hydroxylating methane with high catalyst-turnover rates is required. This property is determined by the choice of metal, axial ligands, and electronic properties of the porphyrin macrocycle. We are addressing this problem by examining a variety of metalloporphyrin catalysts with a range of alkanes of decreasing molecular weights. The idea is to identify the porphyrins with high activity for the harder-to-oxidize gaseous hydrocarbons, methane in particular. The second major problem is to control which species have access to the active site. Because alkanes bind only via weak van der Waals interactions, detection of alkane binding itself presents a formidable obstacle to experimental studies aimed at determining what species can enter the cavity. One approach is to use comparative studies of the hydroxylation of various alkanes to determine which alkanes can enter the pocket. These studies also provide information about such properties as the size and shape of the pocket and the ability to select the carbon atom at which hydroxylation occurs (regioselectivity).

Here, we report on recent efforts to design, synthesize and test a regioselective alkane-to-alcohol catalyst based on the carboranyl porphyrins. The bulky carboranyl units attached to porphyrins like the one shown in Figure 1 provide a means of controlling the chemistry at the site of O₂ activation and C-H bond addition. By varying the structure of the porphyrin macrocycle and the nature of the connectors between the carborane units and the phenyl rings, a cavity was designed that controls access of various substrates, oxidants, products, and solvents to the reactive metal center. In this way, these porphyrins are being engineered to mimic the active site of cytochrome P₄₅₀.

Experimental Procedures

Materials. The catalysts used in this work include manganese(III) tetra(pentafluorophenyl) porphyrin (MnTpFPPX), where X represents an axial ligand, manganese(III) tetra(2'-carboranylphenyl-anilide) porphyrin chloride (MnTCBPpCl), and the manganese(III)-chloride derivative (MnTDNPPCl) of tetra(2',6'-dinitrophenyl) porphyrin free base (H₂TDNPP). H₂TpFPPCl was obtained from Porphyrin Products and converted to the Mn(III) derivative. The icosahedral carboranyl porphyrin, which was synthesized at the University of California at San Francisco by Stephen Kahl¹⁰ using the Rothmund condensation, was converted anaerobically to the Mn(III)Cl derivative by dissolving it in methanol containing MnCl₂ at room temperature. Isomerization of the carboranylphenyl substituents is not expected under these conditions. H₂TDNPP was synthesized¹¹ using a modification of the method recently reported by Lindsey.¹² Methylene chloride (99+%) was used as the solvent in the activity tests. Methylene bromide or methylene chloride were used in imidazole titration experiments. The oxidant was either O₂ or iodosylbenzene (IOB) prepared from the reaction of iodosobenzene

diacetate with NaOH.¹³ The alkanes used for various tests were cyclohexane (99+%), and n-hexane (99%). Sodium borohydride (NaBH₄) was used as a reductant (analogous to NADH in the cytochrome P₄₅₀ reaction) when O₂ was used as the oxidant. NaBH₄ was obtained commercially and used without further purification. Imidazole (Im) was obtained commercially and purified by distillation.

Reaction Conditions. Reactions with cyclohexane and hexane were performed in the solution phase in an argon atmosphere glove box. Methylene chloride was the solvent. The ratio of reactant:oxidant:catalyst was 1100:20:1 on a mole basis. These reactions were carried out at ambient temperatures (about 30° C) and at atmospheric pressure. Reactants were stirred at 1000 rpm. Reaction times were 2 h. For the run with MnTDNPP, a solution of 3.98 μmoles of the porphyrin and 17.57 mg of iodobenzene in 1.1 ml of methylene chloride and 0.5 ml of cyclohexane was stirred in a glove box for two hours. Product yields were 2 and 9 μmoles of cyclohexanone and cyclohexanol, respectively.

Product Analysis. Oxidation products were identified using gas chromatography/mass spectrometry techniques and quantified using capillary column gas chromatographic techniques with commercially available compounds as standards. Product yields are reported as the number of catalyst turn-overs during the 2 h run. Typically, however, the reaction stops after only 30 min, because the supply of oxidant is exhausted.

Molecular Modeling. CAMD was carried out on an Evans&Sutherland PS390 graphics work station using a MicroVAX II host computer. Three dimensional graphical display and molecular energy-optimization and dynamics calculations were performed using BIOGRAF software (BioDesign).

Results and Discussion

A Mn(III)-carboranyl porphyrin that has some of the structural features of cytochrome P₄₅₀ is shown in Figure 1. The porphyrin (α⁴-MnTCBPP) has all four ortho substituents on the phenyl rings oriented toward the same side of the porphyrin plane (α⁴ isomer). For the α⁴ isomer, the bulky carborane groups at the ends of the 3-atom chain, which links them to the phenyl rings, form a pocket adjacent to the Mn atom in the macrocycle. A possible cavity can be seen in the graphical display of the carboranyl porphyrin (Figure 1). The energy-minimized structure with van der Waals surfaces displayed (not shown) best shows that the pocket exists and is large enough to contain methane and molecular oxygen. Further, the cavity is small enough to prevent other test-system components (e. g. solvent, promoters) from reaching the reactive center. Thus, the carboranyl porphyrin shows potential for providing the size-recognition features required for selective substrate binding. Moreover, molecular dynamics calculations in the presence of model organic solvents (e. g. pentane) show that it is energetically favorable for methane to bind in the pocket of the oxo intermediate. Two features that we would like to tailor into the porphyrin are not yet incorporated. First, the dynamics calculation shows that the carboranyl-porphyrin pocket is not as rigid as we think is required based on the enzyme's X-ray crystal structures.⁹ And, second, P₄₅₀'s thiolate ligand has not been provided, although we have been able to mimic the thiolate ligand with a nitrogenous base (imidazole). Although these two features are not incorporated in an optimum way into the catalyst, nevertheless, experimental studies of the catalyst provide information on how well the cavity controls reactions occurring at the protected site, and, the experimental results obtained using the carboranyl porphyrin can be compared to predictions of the molecular modeling.

One prediction of the molecular modeling studies is that a nitrogenous ligand such as imidazole is too large to coordinate to the metal on the hindered

side of the porphyrin because it sterically cannot fit into the methane binding pocket. Imidazole can still coordinate at the open face of the α^4 isomer, however. In contrast, for porphyrins that are not sterically hindered, such as Mn(III) tetraphenyl porphyrin (MnTPP) and MnTpFPP, both faces of the macrocycle are available for axial ligation of imidazole. Indeed, changes in the uv-visible absorption spectrum of MnTPP and MnTpFPP, obtained as a function of imidazole concentration, show that two imidazole molecules successively coordinate (equilibrium association constants for MnTpFPP with Im in methylene bromide, $\log K_1 = 2.0$; $\log K_2 = 3.1$). On the other hand, the spectral changes for the Mn(III) α^4 -carboranyl porphyrin indicate that only one imidazole molecule binds and that this one-to-one complex is completely formed at 0.1 M imidazole (in methylene chloride, $\log K = 2.5$). For the unhindered porphyrins very little (~20%) of the 1:1 complex is formed before subsequent formation of the 2:1 complex.

One consequence of the lack of coordination of imidazole on the hindered face of the carboranyl porphyrin is that we have successfully mimicked the single axial ligand of the iron in cytochrome P₄₅₀. In the protein, only one thiolate ligand binds because only one ligand is available from the heme's asymmetric protein environment; in the carboranyl porphyrin case only one ligand can bind because of imidazole's lack of access to the small cavity formed by the carborane units. The mimicry of the thiolate ligand of cytochrome P₄₅₀ by an imidazole is good since a single imidazole ligand is known from our work and that of others^{14,15} to promote the catalytic activity of manganese porphyrins.

We can also exploit the formation of the 1:1 imidazole complex with the carboranyl porphyrin to block alkane-activation reactions at the open face of the porphyrin and force the reaction to occur in the cavity. We wish to block the open face because the reaction at this site is not expected to show significant regioselectivity for primary carbons. The bars in Figure 2 illustrate the relative yields of alcohols under various reaction conditions. The first bar on the left shows the yield of hexanols for an unhindered porphyrin, in this case MnTpFPP. The MnTpFPP result is shown for comparison with the α^4 -MnTCBPP tests. (In this case, we have circumvented the use of molecular oxygen as the oxidant by using a single oxygen donor (iodosylbenzene) to generate the active intermediate directly without the use of reductants. The iodosylbenzene oxidant system is more stable and chemically less harsh than the reductant-O₂ system.) When imidazole is absent (second bar in Figure 2), the open face of α^4 -MnTCBPP is available to cyclohexane, which is hydroxylated with a yield comparable to the unhindered porphyrin. The molecular modeling work indicates that the reaction primarily occurs on the open face because neither cyclohexane nor iodosylbenzene have access to the metal site on the sterically blocked face of the carboranyl porphyrin.

The third bar in Figure 2 illustrates that when imidazole is added (0.1 M) the yield is greatly reduced demonstrating that the coordination of imidazole effectively blocks the alkane-oxidation reaction. This result is consistent with our studies of the yield as a function of imidazole concentration for unhindered porphyrins. Such studies show that the complex with imidazole blocking both axial ligand sites is inactive. In the case of the carboranyl porphyrin, one axial position is sterically blocked and the other has imidazole bound; therefore, little activity is observed. A small amount of substrate oxidation might still occur at the open face because of rapid equilibrium of imidazole association and dissociation at the manganese.

The fourth bar illustrates that when hexane rather than cyclohexane is used as the substrate only a trace amount of hexanol is produced. Less hexane is oxidized than cyclohexane (third bar, Figure 2) partly because hexane has two

primary carbons, which are harder to oxidize than the carbons of cyclohexane. However, it is not clear why so little hexanol is produced relative to cyclohexanol. One might have expected some hexane oxidation since CAMD techniques show that the end of the hexane molecule could reach the protected metal site. However, molecular modeling also suggests that the oxo intermediate cannot be formed in the pocket because iodocyclohexane cannot readily reach the manganese atom.

Finally, if molecular oxygen, which can enter the pocket, is used as the oxidant, then we might expect some hydroxylation of hexane with regioselectivity for the primary alcohol. The fifth bar in Figure 2 shows the yield of hexanols obtained when O_2 is used as the oxidant. In this test sodium borohydride is used to reduce the catalyst, which then binds O_2 . This species is subsequently reduced again yielding the active manganese-oxo intermediate. The total yield of hexanols is minute primarily because the $NaBH_4-O_2$ system rapidly destroys the catalyst,¹⁶ as shown by the rapid bleaching of the porphyrin absorbance during the reaction. Another reason for the low yield is that it is statistically unlikely for the end of the hexane molecule to work its way into the cavity. Nevertheless, some activity is observed. Preliminary results (not shown) indicate that the yield of primary alcohol (1-ol) increases relative to the secondary alcohols (2-ol and 3-ol) when compared to an unhindered porphyrin (first bar). A less harsh O_2 activation reaction than the $NaBH_4$ system is necessary to increase the yield. Preliminary estimates of the primary regioselectivity for the $MnTCBPP$ -imidazole- $NaBH_4-O_2$ system appears to compare favorably with hydroxylation of hexane by the bis-pocket porphyrin, $Mn(III)$ tetra(triphenylphenyl) porphyrin,¹⁷ also a size selective catalyst. The primary regioselectivity of the latter porphyrin is better than for some cytochromes P_{450} ,¹⁸⁻²⁰ showing that a synthetic catalyst can be as regioselective as the enzyme itself.

One way to solve the problem of protecting the open face of the carboranyl porphyrins is to synthesize a porphyrin having no open faces. One possibility is the *di-ortho-phenyl* analog of the carboranyl porphyrin, which is shown in Figure 3. Recently, we have succeeded in synthesizing the precursor of this class of bis-deep-pocket porphyrins, namely H_2TDNPP and its diamino derivative.¹¹ Efforts are underway to synthesize several bis-deep-pocket porphyrins based on H_2TDNPP .

The manganese(III) derivative of $H_2TDNPPCl$ is interesting in its own right as a potential methane-activation catalyst because (1) it provides shallow cavities at the metal on both faces of the macrocycle and (2) the iron derivative of the related mono-nitro-phenyl-porphyrin has recently been reported to activate methane.⁴ We have not yet tried to oxidize methane with $MnTDNPP$, but we have demonstrated that $MnTDNPPCl$ has catalytic activity for converting alkanes to alcohols as demonstrated by the oxidation of cyclohexane. Turnover numbers for the 2-h run were 0.5 for cyclohexanone and 2.2 for cyclohexanol. Uv-visible absorption spectra at the end of the run showed the presence of a $Mn(IV)$ or $Mn(V)$ porphyrin intermediate species, thus, indicating that the reaction had probably not run to completion.

Conclusions

We have shown that the chemistry occurring at the open face of the deep-pocket porphyrin can be controlled by axial ligation, which forces the reaction to take place in the cavity. Preliminary tests indicate regioselectivity of alkane oxidation by a manganese(III) deep-pocket porphyrin in a reaction using O_2 as the oxidant.

MnTDNPP, a precursor in the synthesis of deep-pocket porphyrins with the pockets on both faces of the porphyrin, has been synthesized and its manganese derivative was shown to be active in alkane oxidation. MnTDNPP may also be interesting from the point of view of methane and ethane activation.

Acknowledgements

We thank Stephen Kahl for kindly providing the carboranyl porphyrin, Dan Trudell and Carlos Quintana for technical assistance. This work performed at Sandia National Laboratories and supported by the U. S. Department of Energy Contract DE-AC04-76DP00789.

References

1. Gesser, H. D.; Hunter, N., *Chem. Rev.* **1985**, *85*, 235.
2. Jones, A. C.; Leonard, J. J.; Sofranko, J. A., *J. Catal.* **1987**, *103*, 311.
3. Groves, J. T. in *Metal Ion Activation of Dioxygen*, Ed. Spiro, T. G. (Wiley: New York), Chpt. 3, 1980.
4. Belova, V. S.; Khenkin, A. M.; Shilov, A. E., *Kinet. Katal.* **1987**, *28*, 1016.
5. Shelnutt, J. A.; Shiemke, A. K.; Scott, R. A., *Div. Fuel Chem. Preprints*, Vol. 32, Eds. Ratcliffe, C. T.; Suuberg, E. M. American Chemical Society: Washington) **1987**, pg. 272.
6. Shiemke, A. K.; Scott, R. A.; Shelnutt, J. A., *J. Am. Chem. Soc.* **1988**, *110*, 1645.
7. Shelnutt, J. A., *J. Am. Chem. Soc.* **1987**, *109*, 4169.
8. Muhoberac, B. B.; Shelnutt, J. A.; Ondrias, M. R., *FEBS Lett.* **1988**, in press.
9. Poulos, T. L.; Finzel, B. C.; Gunsalus, I. C.; Wagner, G. C.; Kraut, J., *J. Biol. Chem.* **1985**, *260*, 16122.
10. Kahl, S. B., in *Neutron Capture Therapy*, Ed. Hatanaka, H. (Mishimura Co.) **1986**.
11. Quintana, C. A.; Assink, R. A.; Shelnutt, J. A., *J. Am. Chem. Soc.* submitted.
12. Lindsey, J. S.; Schreiman, I. C.; Hsu, H. C.; Kearney, P. C.; Marguerettaz, A. M., *J. Org. Chem.* **1987**, *52*, 827.
13. Saltzman, H.; Sharefkin, J. G., *Organ. Synth.* **1963**, *43*, 60.
14. Battioni, P.; Renaud, J.-P.; Bartoli, J. F.; Mansuy, D., *J. Chem. Commun.* **1986**, 341.
15. Meunier, B.; de Carvalho, M.-E.; Bortolini, O.; Momenteau, M., *Inorg. Chem.* **1988**, *27*, 161.
16. Tabushi, I.; Koga, N., *J. Am. Chem. Soc.* **1979**, *101*, 6456.
17. Cook, B. R.; Reinhert, T. J.; Suslick, K. S., *J. Am. Chem. Soc.* **1986**, *108*, 7281.
18. Frommer, U.; Ullrich, V.; Staudinder, H.; Orrenius, S., *Biochem. Biophys. Acta* **1972**, *280*, 487.
19. Ellin, A.; Orrenius, S., *Molec. Cell Biochem.* **1975**, *8*, 69.
20. Morohashi, K.; Sanano, H.; Okada, Y., Omura, T., *J. Biochem.* **1983**, *93*, 413.

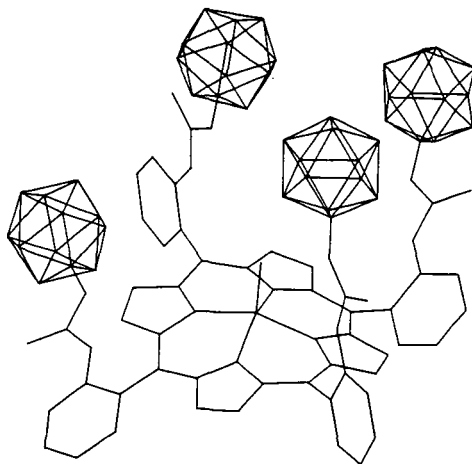


Figure 1. Oxo-metallo- α^4 -tetra(2'-carboranylphenyl-anilide) porphyrin. Energy minimized BIOGRAF structure (not global minimum).

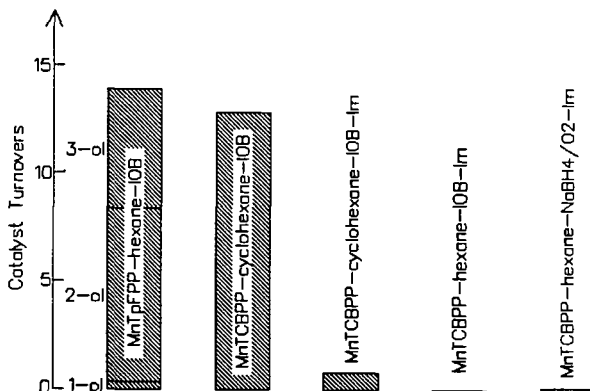


Figure 2. Alkane hydroxylation by designed Mn(III)- α^4 -tetra(2'-carboranylphenyl-anilide) porphyrin catalyst.

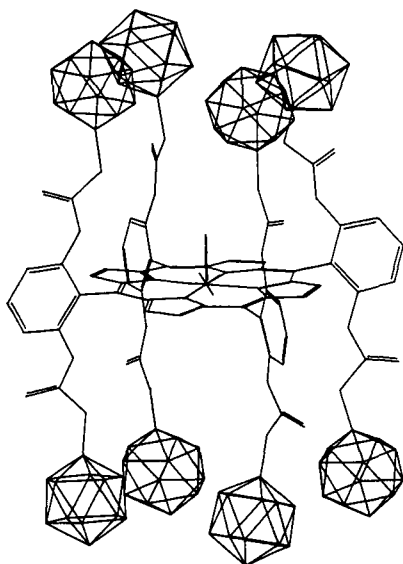


Figure 3. Example of a bis-deep-pocket carboranyl porphyrin that can be synthesized from tetra(2',6'-dinitrophenyl) porphyrin. BIOGRAF structure not fully energy minimized.